Terms and Conditions of Use of Digitised Theses from Trinity College Library Dublin

Copyright statement

All material supplied by Trinity College Library is protected by copyright (under the Copyright and Related Rights Act, 2000 as amended) and other relevant Intellectual Property Rights. By accessing and using a Digitised Thesis from Trinity College Library you acknowledge that all Intellectual Property Rights in any Works supplied are the sole and exclusive property of the copyright and/or other IPR holder. Specific copyright holders may not be explicitly identified. Use of materials from other sources within a thesis should not be construed as a claim over them.

A non-exclusive, non-transferable licence is hereby granted to those using or reproducing, in whole or in part, the material for valid purposes, providing the copyright owners are acknowledged using the normal conventions. Where specific permission to use material is required, this is identified and such permission must be sought from the copyright holder or agency cited.

Liability statement

By using a Digitised Thesis, I accept that Trinity College Dublin bears no legal responsibility for the accuracy, legality or comprehensiveness of materials contained within the thesis, and that Trinity College Dublin accepts no liability for indirect, consequential, or incidental, damages or losses arising from use of the thesis for whatever reason. Information located in a thesis may be subject to specific use constraints, details of which may not be explicitly described. It is the responsibility of potential and actual users to be aware of such constraints and to abide by them. By making use of material from a digitised thesis, you accept these copyright and disclaimer provisions. Where it is brought to the attention of Trinity College Library that there may be a breach of copyright or other restraint, it is the policy to withdraw or take down access to a thesis while the issue is being resolved.

Access Agreement

By using a Digitised Thesis from Trinity College Library you are bound by the following Terms & Conditions. Please read them carefully.

I have read and I understand the following statement: All material supplied via a Digitised Thesis from Trinity College Library is protected by copyright and other intellectual property rights, and duplication or sale of all or part of any of a thesis is not permitted, except that material may be duplicated by you for your research use or for educational purposes in electronic or print form providing the copyright owners are acknowledged using the normal conventions. You must obtain permission for any other use. Electronic or print copies may not be offered, whether for sale or otherwise to anyone. This copy has been supplied on the understanding that it is copyright material and that no quotation from the thesis may be published without proper acknowledgement.

School of Pharmacy and Pharmaceutical Sciences, Trinity College Dublin

FORMULATION AND CHARACTERISATION OF POLYELECTROLYTE COMPLEX NANOPARTICLES FOR THE DELIVERY OF SALMON CALCITONIN

by

Anita Monika Umerska, M.Sc. (Pharm.)

being a thesis submitted for the degree of
Doctor of Philosophy in Pharmacy and Pharmaceutical Sciences

at
University of Dublin
Trinity College

under the supervision and direction of
Lidia Tajber, M.Sc. (Pharm.), Ph.D.,
and
Professor Owen I. Corrigan,
B.Sc. (Pharm.) (N.U.I.), M.A., Ph.D. (N.U.I.), F.T.C.D., F.P.S.I.

March 2013

DECLARATION

I declare that this thesis has not been submitted as an exercise for a degree at this or any other university. I have carried out all the practical work except where duly acknowledged. The thesis includes the unpublished and published work of Dr. Sinéad Ryan, carried out jointly as a part of an SFI strategic research cluster "Irish Drug Delivery Network" (IDDN).

I agree to deposit this thesis in the University's open access institutional repository or allow the library to do so on my behalf, subject to Irish Copyright Legislation and Trinity College Library conditions of use and acknowledgment.

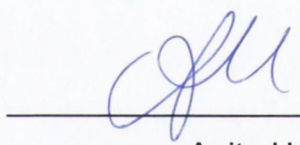

Anita Umerska

TABLE OF CONTENTS

RESULTS AND DISCUSSION

ACKNOWLEDGEMENTS

First of all I would like to thank my supervisors, Dr. Lidia Tajber and Prof. Owen Corrigan for giving me this opportunity for doing a Ph.D. at Trinity College Dublin. I am very grateful for your guidance and support throughout my studies and in the preparation of this thesis, for useful advices an fruitful discussions, which greatly helped me in developing wider perception of the studied subject.

I would also like to thank Dr. Sinéad Ryan (UCD, DIT) and Prof. David Brayden (UCD) for *in vitro* and *in vivo* work done on my nanoparticles.

Special thanks to Dr. Krzysztof Paluch for his help with SEM, NMR and other experimental techniques and to Dr. Iwona Inkielewicz-Stępniak for introducing me to the world of cell culture. I would also like to thank to Dr. Maria Jose Santos-Martinez and Dr. Carlos Medina for their help in cell culture experiments.

Many thanks to academic and technical staff of the School of Pharmacy for their assistance in technical matters. Thanks to Neal Leddy, Clodagh Dooley, Heath Bagshaw and Leaona O'Connor for the help with TEM and SEM.

I wish to thank the Trinity Trust for travel grant which allowed me to attend an international conference in Istanbul.

Warm thanks to all the former and current members of the School of Pharmacy research groups for their advices, assistance and friendship.

I am very grateful to my family for their encouragement, love and support.

Finally, I would also like to express my gratitude to the Science Foundation of Ireland for funding my project.

This study was funded by the Irish Drug Delivery Research Network, a Strategic Research Cluster grant (07/SRC/B1154) under the National Development Plan co-funded by EU Structural Funds and Science Foundation Ireland.

PRESENTATIONS AND PUBLICATIONS ASSOCIATED WITH THIS THESIS

Poster Presentations

"Preparation and characterisation of hyaluronate-based nanoparticulate carriers suitable for oral peptide delivery", at 2009 AAPS Annual Meeting and Exposition, 8-12.11.2009, Los Angeles, CA, USA. [Anita Umerska, Owen I. Corrigan and Lidia Tajber]

"Formulation and characterisation of polymeric chitosan and hyaluronate nanoparticulate carriers", at Joint Schools of Pharmacy Conference, 29-30.03.2010, Belfast, UK. [Anita Umerska, Owen I. Corrigan and Lidia Tajber]

"Formulation and characterisation of polymeric chitsan and hyaluronate nanoparticulate carriers", at ESF-UB Conference on Nanomedicine Reality Now and Soon, 23-28.10.2010, Sant Feliu de Guixols, Spain. [Anita Umerska, Owen I. Corrigan and Lidia Tajber]

"Redispersibility studies on freeze-dried hyaluronic acid/chitosan nanoparticles", at 8th World Meeting on Pharmaceutics, Biopharmaceutics and Pharmaceutical Technology, 19-22.03.2012, Istanbul, Turkey. [Anita Umerska, Iwona Inkielewicz-Stępniak, Owen I. Corrigan, Carlos Medina and Lidia Tajber]

Publication

"Exploring the assembly process and properties of novel crosslinker-free hyaluronate-based polyelectrolyte complex nanocarriers", International Journal of Pharmaceutics, 436 (2012) 75-87. [Anita Umerska, Krzysztof J. Paluch, Iwona Inkielewicz-Stępniak, Maria Jose Santos-Martinez, Owen I. Corrigan, Carlos Medina and Lidia Tajber]

Patent Application

"A polymeric nanoparticle", PCT/EP2011/068561; WO/2012/052565; Filled on 24.10.2011; Published on 26.04.2012; Inventors: Lidia Tajber, Owen I. Corrigan, Sinéad Ryan, David Brayden, Anita Umerska,

ABBREVIATIONS AND SYMBOLS

-	to
%	percent
°	degree
°C	degree Celsius
~	approximately
®	registered trademark
µg	micrograms
µm	micrometer
µM	micromoles per litre
µl	microlitre
^{1}H NMR	^{1}H Nuclear Magnetic Resonance spectroscopy
Å	Angstrom
AB	acetate buffer
AE	association efficiency
AFM	Atomic Force Microscopy
ANOVA	analysis of variance
APC-Annexin V	Annexin V, allophycocyanin conjugate
BSA	bovine serum albumin
Caco-2	human colon adenocarcinoma cells
$CaCl_2$	calcium chloride
CHMP	EMEA's Committee for Medicinal Products for Human Use
CHON	chondroitine
cDNA	complementary deoxyribonucleic acid
CH_3COOH	acetic acid
CH_3COONa	sodium acetate
CIA	collagen-induced arthritis
Cl^-	chloride anion
CL113	chitosan chloride Protasan UP CL113
CL213	chitosan chloride Protasan UP CL213
CL42	chitosan chloride Chitoceuticals

cm	centimetre
cm^{-1}	frequency
cm^2	square centimetre
CMA	Centre for Microscopy and Analysis at TCD
CMR	charge mixing ratio
CO_2	carbon dioxide
conc.	concentration
CS	chitosan
Cu	copper
DD	degree of deacetylation
Dex	dexamethasone 21-phosphate, disodium salt
DL	drug loading
DLS	Dynamic Light Scaterring
DMARDs	disease-modifying anti-rheumatoid drugs
DNA	deoxyribonucleic acid
DSC	differential scanning calorimetry
e.g.	exempli gratia
EDTA	ethylenediaminetetraacetic acid
EMEA	European Medicines Agency
ESE	emulsification solvent evaporation
et al.	et alli or et aliae
FITC-BSA	BSA, fluorescein isothiocyanate conjugate
FTIR	Fourier transform infrared spectroscopy
g	gram
g	gravitational acceleration constant
G	chitosan glutamateG113 chitosan glutamate Protasan UP G113
G213	chitosan glutamate Protasan UP G213
GADPH	glyceraldehyde 3-phosphate dehydrogenase
GI	gastro-intestinal
GPC	Gel Permeation Chromatography
GPI	glucose-6-phosphate isomerase
H	enthalpy
h	hour

H	hydrogen
H_20	water
H_2O_2	hydrogen peroxide
H-bond	hydrogen bond
HA	hyaluronic acid
HA176	hyaluronic acid 176 kDa
HA201	hyaluronic acid 201 kDa
HA257	hyaluronic acid 257 kDa
HA292	hyaluronic acid 292 kDa
HA343	hyaluronic acid 343 kDa
HA590	hyaluronic acid 590 kDa
HA1161	hyaluronic acid 1161 kDa
HA2882	hyaluronic acid 2882 kDa
HCl	hydrochloric acid
HEPES acid	4-(2-hydroxyethyl)-1-piperazineethanesulfonic
HNO_3	nitric acid
HPLC	high performance liquid chromatography
I.A.	intra-articular
I.P.	intra-peritoneal
i.e.	id est
IC_{50}	half maximal inhibitory concentration
ICP-MS	Inductively Coupled Plasma-Mass Spectrometry
IEP	isoelectric point
IL	interleukin
IL-1	interleukin 1
IL-1β	interleukin 1 beta
IL-6	interleukin 6
J/g	joules per gram
k	release rate constant
K/BxN arthritis	serum transfer murine model of inflammatory
KBr	potassium bromide
KCl	potassium chloride

kDa	kilodalton
kV	kilovolt
LDV	Laser Doppler Velocimetry
LPS	lipopolysaccharides
M	moles per litre
mA	milliampere
MEM	Eagle's minimal essential medium
mg	milligram
MHC	major histocompatibility complex
min	minute
ml	millilitre
mm	millimetre
mM	millimolar
MMP	matrix metalloproteinase
MMP1	matrix metalloproteinase-1, interstitial collagenase
MMP2	matrix metalloproteinase-2, gelatinase A
MMP3	matrix metalloproteinase-3, stromelysin 1
MMP9	matrix metalloproteinase-9, gelatinase B
MMP13	matrix metalloproteinase-13, collagenase 3
MMR	mass mixing ratio
Mn	number average molecular weight
mPa	millipascal
mRNA	messenger ribonucleic acid
MTS	3-(4,5-dimethylthiazol-2-yl)-5-(3-carboxymethoxyphenyl)-2-(4-sulfophenyl)-2H-tetrazolinum
MTX	methotrexate
mV	millivolt
Mw	weigh average molecular weight
Mw/Mn	polydispersity index
MWCO	molecular weight cut off
n^-/n^+	the ratio of number of moles of negative charges to number of mols of positive charges
N/A	not applicable

Na^+	sodium cation
NaCl	sodium chloride
NaH_2PO_4	sodium dihydrogen phosphate
Na_2HPO_4	disodium hydrogen phosphate
$NaNO_3$	sodium nitrate
NaOH	sodium hydroxide
ng	nanograms
Ni	nickel
nm	nanometre
nM	nanomoles per litre
NMR	Nuclear Magnetic Resonance
NP	nanoparticles
NPs	nanoparticles
NR4A	nuclear receptor subfamily 4, group A
NR4A1	nerve growth factor IB
NR4A2	nuclear receptor related 1 protein, NURR1
NR4A3	neuron-derived orphan receptor 1
NSAIDs	non-steroidal anti-inflammatory drugs
NURR1	nuclear receptor related 1 protein, NR4A2
OA	ostheoarthritis
O/W	oil in water
p	p-value
P	protamine
PBS	phosphate buffered saline
PCR	polymerase chain reaction
PDI	polydispersity index
PEG	polyethylene glycol
PGE_2	prostaglandin E2
pH	minus log of hydrogen ion concentration
PI	propidium iodide
pK_a	acid ionization constant
PLA	poly(lactic acid)
PLGA	poly(lactic-co-glycolic acid)
PM	physical mixture

PMA	phorbol-12-myristate-13-acetate
PROT	protamine
PS	particle size
PVA	poly(vinyl alcohol)
qRT-PCR	quantitative real-time polymerase chain reaction
R^2	correlation coefficient
RA	rheumatoid arthritis
RI	refractive index
RNA	ribonucleic acid
rpm	revolutions per minute
RT	room temperature
s	second
sCT	salmon calcitonin
SDS	sodium dodecylsulfate
SEM	scanning electron microscopy
siRNA	small interfering ribonucleic acid
SW1353	human chondrosarcoma cells
TCD	Trinity College Dublin
TEM	transmission electron microscopy
TFA	trifluoroacetic acid
THP-1	human acute monocytic leukemia cell line
T_g	glass transition temperature
T_m	melting pointTIMPs tissue inhibitors of metalloproteinases
TM	trademark
TNFα	tumor necrosis factor alpha
TPC	total polymer/polysaccharide concentration
TPP	tripolyphosphate
TR	trehalose
U937	human cell line established from a diffuse histiocytic lymphoma of a 37 years old male
UCD	University College Dublin
UV	ultraviolet
UV-VIS	ultraviolet-visible

v/v	volume in volume
w/v	weight in volume
w/w	weight in weight
W	Watt
W/O	water in oil
W/O/W	water in oil in water
XRD	X-ray diffraction (powder)
ZP	zeta potential
λ	wavelength
ΔH	change in enthalpy

SUMMARY

The studies in this thesis explored the formulation of various polyelectrolyte complex nanoparticles as potential carriers for the delivery of macromolecules. The complexes were formed between a polyanion (hyaluroninc acid, HA or chondroitin, CHON) and a polycation (chitosan, CS, or protamine, PROT). Salmon calcitonin (sCT) was selected as a macromolecule to be encapsulated in the nanoparticles due to its clinical use in bone diseases and potential application in arthritis. Different factors influencing the formation and properties of the nanoparticles (NPs) were examined, e.g. concentration of the polymers, polyanion/polycation mixing ratio, molecular weight of polymers. The molecular weight of the polymers was determined by GPC (Gel Permeation Chromatography). The properties of the NPs were characterised with the use of different techniques. Particle size and size distribution were analysed with the employment of dynamic light scattering (DLS), zeta potential was measured with the use of laser Doppler velocimetry (LDV), while morphology was investigated by transmission electron microscopy (TEM) and scanning electron microscopy (SEM). Physical stability of the nanoparticle suspensions upon storage at room temperature were performed for a period up to 4 weeks. sCT was loaded into each type of NPs: HA/CS, CHON/CS, HA/PROT and CHON/PROT, and the possibility of formation of NPs between sCT and polyanions:HA and CHON was also examined. Non-associated sCT was separated from NPs by a combined ultrafiltration-centrifugation technique, and concentration of sCT was analysed by HPLC (high performance liquid chromatography). The release of sCT from the polyelectrolyte complex nanoparticles was also examined. Selected formulations were converted into solid state forms by freeze-drying with the employment of trehalose and poly(ethylene glycol) polymers (PEGs) as cryoprotectants. The toxicity of the NPs, polymers and cryoprotectants was examined on Caco-2 cells with the use of MTS assay and flow cytometry. The *in vitro* (cell culture) and *in vivo* (in rats) performance of HA/CS/sCT NPs was also examined.
Uncomplicated, organic solvent and surfactant-free production method by simply mixing aqueous solutions of polylelctrolytes at room temperature was successfully employed to fabricate novel, cross-linker-free and non-sedimenting nanoparticles. It was possible to obtain NPs with good physical properties (i.e. small and homogenously dispersed) for all of the polyelectrolyte pairs tested: HA/CS, HA/PROT, CHON/CS, CHON/PROT. The physicochemical properties of the NPs were found to

be conveniently adjusted by changing the formulation conditions: polymer mixing ratio, polymer concentration, type and molecular weight of the polymers. The example of HA/CS NPs showed that the type of counterion in chitosan salt also plays a role- the glutamate salt is not recommended as the glutamate residue interacts and is incorporated into the NPs. The influence of the molecular weight of the polymer was especially pronounced in the range of higher molecular weights, leading to the formation of aggregates or a substantial increase in particle size. However, the main factor determining particle formation and properties was the mixing ratio of the polyelectrolytes. A change in the polyanion/polycation mixing ratio considerably altered the physicochemical properties of the particles, especially zeta potential. When CS was used as a polycation, stable particles with either a positive or with a negative surface charge were acquired. On the other hand, complexation of polyanions to PROT yielded stable NPs with negative zeta potential values, while positively charged particles increased their size systematically within first hours of storage. NPs were stable after short-term storage at room temperature and the solid state form was successfully obtained by freeze-drying.

sCT was successfully loaded into all types of NPs tested with association efficiency values close to 100% and a high drug loading. Moreover, CHON/sCT NPs were successfully produced. NPs were capable to provide a prolonged release of sCT and the release was markedly slower in the case of CHON-based NPs.

NPs were found to be well tolerated by Caco-2 cells and PROT-based NPs were found to be more toxic than CS-based NPs. Complexation to polyanions and formation of NPs decreased the toxic effects exerted by the polycation.

Moreover, it was shown (collaboration with Dr. Sinéad Ryan, UCD) that in human chondrocyte and macrophage cell lines HA/CS/sCT NPs produced markedly higher reduction in inflammatory biomarker (NR4As and MMPs) mRNA expression than HA or sCT alone with the efficacy comparable to dexamethasone commonly used in the treatment of rheumatoid arthritis. In the K/BxN mouse model of inflammatory arthritis, HA/CL113/sCT NPs delivered by the IA (intra-articular) route reduced knee diameter over time, preserved both bone and cartilage and reduced synovitis infiltration damage compared to controls. sCT formulated into a NP was superior to free sCT in cartilage preservation showing that formulation of the peptide into NPs improved the therapeutic effect and sustained release of sCT.

ORIGIN AND SCOPE

Salmon calcitonin (sCT), commercially available as injectable and nasal spray forms (Guggi et al., 2003), and indicated for the treatment of bone diseases, e.g. osteoporosis, Paget's disease and bone metastasis (Guggi et al., 2003) is also a promising candidate to be used in osteoarthritis (Manicourt et al., 2005). However, the full market potential of this peptide has not yet been reached due to the low patient compliance associated with the injectable dosage forms (Guggi et al., 2003) and poor bioavailability from the commercial nasal spray, Miacalcin® (Hinchcliffe et al., 2005). Therefore the development of a new, more compliant delivery system for sCT is of a vital importance. Polymeric nanoparticles represent an interesting strategy because of their abilities to entrap macromolecules, protect them against degradation and enhance their transmucosal transport (de la Fuente et al., 2008a).

Several approaches have been attempted to produce calcitonin or elcatonin-loaded polymeric nanoparticles, among them poly(lactic-co-glycolic acid) (PLGA)-based nanoparticles being one of the most common (Mehta et al., 1994, Jeyanti et al., 1996, Calis et al., 1995, Kawashima et al., 2000). Although the peptide was very efficiently associated with the particles, a very low drug loading, up to 1.55 % by Kawashima et al. (2000), is one of the main disadvantages of PLGA nanoparticles. Drug loading higher than 10% has not been achieved so far for sCT.

Other common disadvantage of PLGA-based or similar nanoparticles is the involvement of surfactants and organic solvents in their fabrication. Water-soluble, biodegradable, polyelectrolyte complex nanoparticles have been shown to overcome these problems. Polyelectrolyte complex NPs have also evolved because of the limitations, in terms of toxicity, of the currently available systems (Hartig et al., 2007). The employment of naturally occurring polymers already approved for the use in drug delivery provides an attractive option, as the use of novel polymer would raise a need for complicated toxicity studies. Moreover, some of the naturally occurring polyelectrolytes (e.g. hyaluronic acid, chondroitin) have biological properties (e.g. anti-inflammatory and structure protection in arthritis) complementary to pharmacological action of sCT, therefore combining these polysaccharides in the same delivery system as sCT seems to be particularly attractive not only in terms of the facilitation of the delivery of sCT.

The scope of this thesis was:

- to develop and characterise polyelectrolyte complex nanoparticles composed of naturally occurring, biocompatible polymers: hyaluronic acid, chondroitin, chitosan or protamine
- to investigate and characterise the influence of different formulation variables (e.g. polymers mixing ratio, concentration and molecular weight) on the formation and properties of the nanoparticles
- to load sCT into selected nanocarriers, characterise them and optimise the formulation variables in order to achieve maximum association efficiency and drug loading possible
- to assess *in vitro* cytotoxicity of nanoparticles
- to obtain the solid state form of the particles by freeze-drying
- to examine selected formulation *in vitro* for the eventual reduction of inflammatory biomarkers and *in vivo* in order to verify the performance of the nanoparticles in mouse model of inflammatory arthritis

1. Introduction

1.1 Definition and classification of nanoparticles

By a general definition, nanoparticles are particulate dispersions or solid particles that vary in size from 1 to 1000 nm.

Different classes of nanoparticles can be distinguished (Medina et al., 2007):

- Ceramic nanoparticles are composed of inorganic systems with porous characteristics (e.g. silica, titania and alumina).
- Metallic nanoparticles (e.g. iron oxide nanoparticles) comprise a class of superparamagnetic agents that can be coated with phospholipids, dextran or other compounds to enhance stability and prevent aggregation.
- Gold shell nanoparticles are spherical particles consisting of a dielectric core covered by a thin metallic shell, which is typically gold.
- Carbon nanomaterials include fullerenes and single or multi-walled nanotubes.
- Quantum dots are nanoparticles made of semiconductor materials with fluorescent properties.
- Liposomes are composed of lipid bilayer membranes surrounding an aqueous interior.
- Nanoemulsions comprise oil in water dispersions stabilised with surfactants in order to maintain their shape and size.
- Polymeric nanoparticles are composed of different polymers e.g. polysaccharides (Boddohi et al., 2009), poly(lactic-co-glycolic acid) (PLGA) (des Rieux et al., 2006).

1.2 Investigations into application of nanoparticles in drug delivery

Nanoparticles are being extensively investigated for their applications in medicine such as drug delivery systems, molecular diagnosis, medical imaging and tissue engineering (Emerich et al., 2003). Since the nanotechnology offers a suitable means of controlled and/or site specific delivery of low and high molecular weight drugs and bioactive agents, significant efforts have been devoted to potential use of nanotechnology in drug delivery (Hamidi et al., 2008). Pharmaceutical nanotechnology focuses on formulating active ingredients into biocompatible nanoparticles. These systems may offer many advantages as they focus on improved safety, efficacy of the drug (e.g. by providing a targeted delivery of the active, improving its bioavailability, extending its effect in target tissue and improving stability against chemical or enzymatic degradation). The submicron size is the basis for the advantages of nanoparticle-based drug delivery systems (Alonso, 2004; Hamidi et al., 2008). Nanoparticles have been considered as potential drug carriers intended for various transmucosal routes of administration, e.g. oral, nasal, pulmonary and ocular (Alonso, 2004).

Nanoparticles may have the form of nanocapsules or nanospheres (Hamidi et al., 2008). Nanospheres are matrix spherical systems, while nanocapsules are vesicular systems composed of a cavity surrounded by a boundary structure, e.g. polymeric. The drug may be dissolved, entrapped, encapsulated or attached to nanoparticles (Hamidi et al., 2008).

Polymeric nanoparticles have a range of advantages compared to other carriers. They are characterised by much better stability in the GI tract than for example liposomes and thus can protect the encapsulated drug. Their physicochemical properties such as size, zeta potential and hydrophobic/hydrophilic characteristics, release properties of the encapsulated drug (typically sustained or triggered by different factors) as well as behaviour in the biological systems (bioadhesion, targeting, uptake by cells) can be adapted by the appropriate choice of various polymeric materials (de la Fuente et al., 2008a). Nanoparticulates have better absorption properties compared to larger carriers due to their very small, submicron sizes and therefore enormous surface area. Some molecules, especially polymers, for instance polyethylene glycol (PEG) and molecules exhibiting bioactive properties e.g. lectins can be adsorbed or chemically grafted to particle surface (des Rieux et al., 2006).

Polymeric nanoparticles can entrap macromolecules and protect them against chemical and physical degradation (Sánchez et al., 2003). Nanoparticles can also enhance transmucosal transport of the associated macromolecules, thus acting as nanocarriers (Alonso, 2004). Incorporation of drug into delivery systems in the form of nanoparticulate polymer matrices offers many benefits, e.g. controlled drug release and protection, prolonged blood circulation and many other adjustable characteristics (Hartig et al., 2007).

It is very important for medical applications that nanoparticles are biocompatible and biodegradable. Serious issues with respect to biocompatibility and toxicity are disadvantages of nanoparticles such as carbon nanotubes (Jain et al., 2007), fullerenes (Isakovic et al., 2006), quantum dots (Pelley et al., 2009) and other metal based nanoparticles (Schrand et al., 2010). The lack of biodegradability or toxicity of the degradation products of some synthetic polymers used for nanoparticles fabrication may also be a problem. Specifically, alkylcyanoacrylate nanostructures suffer from toxic breakdown products (Hartig et al., 2007). Recently there is an increased interest in nanoparticles composed of naturally occurring polymers such as polysaccharides or their derivatives due to their diverse structures, a large number of reactive groups, low toxicity, safe, biodegradability and stability (Liu et al., 2008). Indeed, water-soluble, biodegradable polyelectrolytes degrade at a slow rate, do not alter normal cell function and use water as a solvent in their fabrication, what is an important advantage for products that potentially may be applied as drug delivery systems in humans (Hartig et al., 2007). Such polymers are generally intended to be used solely as carriers for the delivery of bioactive substances (Janes et al., 2001), however some of the polymers are known to possess pharmacological and functional properties as well. Examples of those polymers include chitosan, hyaluronic acid, chondroitin and their application in nanomedicine could be multifold.

1.3 Polymers used in the formulation of nanoparticles and their physicochemical properties

There are many polymers at disposal for developing nanoparticles for drug delivery. A few criteria determine whether a given polymer is deemed suitable for delivery of drugs, they are: biocompatibility and bioavailability (they have a crucial impact on elimination properties of the systems), cytotoxicity, degradation rate that

determines the rate of drug release and easiness of production. The choice of materials also depends on the size and morphology of the particles, the surface charge, drug loading and desired release profile (des Rieux et al., 2006; Sundar et al., 2010). The polymers may generally be classified as biodegradable and non-biodegradable. The term biodegradable is used in a broad meaning that the polymer will eventually disappear after introduction in the body. This may be due to hydrolytic or oxidative enzymatic degradation, however e.g. polylactides are hydrolysed at a relatively high rate even at room temperature at neutral pH without any help of hydrolytic enzymes. The polymers may also be classified as natural or synthetic (Ikada and Tsuji, 2000).

Initially polymeric nanoparticles were designed using albumin and synthetic non-biodegradable polymers, e.g. poly(methylacrylate) and polyacrylamide. However the systemic administration of non-biodegradable nanoparticles in humans is limited due to the risks of chronic toxicity as a result of overloading tissues with the non-degradable polymers (Sundar et al., 2010). Also, purified polyethylene and silicone do not have toxic effects on cells but are not blood compatible, because after implantation thrombus formation and encapsulation by collagenous fibrous tissues takes place at their surface (Ikada and Tsuji, 2000). As a consequence, nanoparticles composed of synthetic biodegradable polymers (e.g. polyanhydride, poly(lactic-co-glycolic acid) and polyalkylcyanoacrylate) were designed (Sundar et al., 2010). Polymers that are insoluble in water generally do not interact physically or chemically with living cells unless the surface of the material has very sharp projections or a high density of a cationic moiety. However, as a result of the degradation, biodegradable polymers always release low molecular weight compounds into the outer environment, and in some cases the normal condition of the cell is disturbed by such foreign compounds (Ikada and Tsuji, 2000). For instance, alkylcyanoacrylate nanostructures suffer from toxic breakdown products: alcohol, acrylic acid and formaldehyde (Müller et al., 1991). The most commonly used polymers are polyesters, either alone or in combination with other polymers. PLGA and PLA, employed for numerous *in vivo* applications are highly biocompatible and biodegradable (des Rieux et al., 2006). PLGA and poly(ε-caprolactone) (PCL) are both aliphatic polyesters synthesized by ring-opening polymerisation. PLGA is degraded non-enzymatically in both earth environments and human body, while PCL is enzymatically degraded in earth environments, but non-enzymatically in the body. As polylactides, especially polyglycolide, are hydrolysed in living organisms to the respective monomers and

oligomers soluble in aqueous media, the whole mass of the polymer disappears without any trace of the remnants, therefore they are referred to as absorbable (resorbable) polymers (Ikada and Tsuji, 2000). However, the limitation of biodegradable water-insoluble polymers is that they are mostly hydrophobic, whereas nucleic acids, many of peptides and proteins, which are recognised to have a great potential in therapeutics, are hydrophilic. This leads to difficulties for the drug to be efficiently encapsulated (Sundar et al., 2010). Hence, the preparation of nanoparticles with the employment of more hydrophilic and naturally occurring polymers has been explored.

Nanoparticles composed of biodegradable polymers like polysaccharides and proteins have the potential to be used as efficient drug delivery systems for sustained, controlled and targeted release, aiming to improve the therapeutic effects as well as to reduce the side effects of the formulated active ingredients (Sundar et al., 2010). To date the most appreciated natural polymer employed for nanoparticles production is CS due to its mucoadhesive abilities and being a permeability enhancer and also thanks to the chemical properties (presence of charged groups) which allows the formulation of particles free of organic solvent at relatively mild conditions of preparation (des Rieux et al., 2006). The examples of macromolecules efficiently associated to CS nanoparticles are proteins such as bovine serum albumin (BSA), tetanus toxoid, diphtheria toxoid (Janes et al., 2001) and the peptides: insulin (Janes et al., 2001, Bayat et al., 2008, Aktas et al., 2005), cyclosporine and caspase inhibitor (Aktas et al., 2005). For a particular protein, the greatest loading efficiency was obtained when the protein was dissolved at a pH above the isoelectric point of the compound, so that the macromolecule was primarily negatively charged to bind to the positively charged CS (Janes et al., 2001). Alonso's group has shown on rats and rabbits that chitosan nanoparticles have the potential to enhance absorption through mucosa (Vila et al., 2004; Prego et al., 2005). Among cationic polymers used in the formation of polyelectrolyte complex nanoparticles, undoubtedly chitosan is the most extensively investigated within the current scientific literature (Andrews et al., 2009). There are many anionic polymers complexed with chitosan to produce polyelectrolyte complex nanoparticles. Some of the examples are hyaluronic acid (de la Fuente et al., 2008a, Boddohi et al., 2009), chondroitin sulphate (Yeh et al., 2011), carboxymethylcellulose, dextran sulphate, alginate and polyaspartic acid (Liu et al., 2008). Interestingly, heparin has been used in order to produce polyelectrolyte complex NPs with chitosan (Liu et al., 2008, Boddohi et al., 2009), but it was also

loaded as an active into CS/HA NPs (Oyarzun-Ampuyero et al., 2009). Chitosan has also been chemically modified in order to obtain forms soluble at neutral pH either as a cationic form (N-trimethylchitosan) or amphoteric or negatively charged form (carboxymethylchitosan) (Liu et al., 2008). Other polycations used in the formation of polyelectrolyte complex nanoparticles are protamine (Mori et al., 2010), polyarginine (Oyarzun-Ampuyero et al., 2011) and polyethylenimine (Pathak et al., 2009). Proteins have also been used in drug delivery systems. For instance, gelatin has been used in the synthesis of nanoparticles for drug delivery during last thirty years. Gelatin is a natural water soluble macromolecule obtained from the heat dissolution and partial hydrolysis of collagen. Type A gelatin, produced via acid hydrolysis of collagen, has the isoelectric point between 7 and 9, while type B gelatin, obtained by alkaline hydrolysis of collagen has the isoelectric point between 4.8-5.0 (Sundar et al., 2010). Interestingly, albumins, e.g. bovine serum albumin, with the isoelectric point of 4.7-4.9 (Hopwood, 1970) can be used as a nanocarrier for the delivery of bioactive molecules, e.g. siRNA (Yogasundaram et al., 2012) as well as the active ingredient encapsulated into the nanoparticles (de la Fuente et al., 2008a). Human serum albumin was used as a protective colloid in albumin/protamine/oligonucleotide nanoparticles, overcoming the disadvantages of protamine/oligonucleotide nanoparticles, e.g. improving the stability and preventing aggregation under isotonic conditions (Lochmann et al., 2005).

Polyelectrolyte complex nanoparticles have been investigated as a potential delivery system for low molecular weight drugs, e.g timolol maleate (Wadhwa et al., 2010), doxorubicin (Tsai et al., 2011) as well as biological macromolecules, e.g. previously mentioned heparin (Oyarzun-Ampuyero et al., 2009), growth factors (Parajó et al., 2010), bovine serum albumin and cyclosporine A (de la Fuente et al., 2008a), and nucleic acids (de la Fuente et al., 2008b).

1.4 Methods used in the preparation of polymeric nanoparticles

There is a considerable number of techniques that are used to produce nanoparticles, which allows for a broad differentiation of their internal and external structure as well as composition and biological properties. The choice of the method is influenced by the solubility of the active compound to be associated/complexed with the nanoparticles as well as the solubility, chemical structure, characteristic chemical groups, molecular weight, crystallinity/amorphicity of the polymer (des Rieux et al., 2006).

In general, polymeric nanoparticles may be prepared either by polymerisation of dispersed monomers or by dispersion of preformed polymers (Soppimath et al., 2001). The use of particles obtained by polymerization may be limited because of the presence of residual monomers, oligomers, catalysts as well as possible cross-reaction with drug (Quintar-Guerrero et al., 1996). Therefore preparation of nanoparticles from synthetic polymers is usually done by dispersion of polymers. There are a few preparation methods, the choice of which is mainly dependant on the hydrophobic/hydrophilic characteristics of actives to be incorporated (des Rieux et al; 2006).

The nanoprecipitation technique developed by Fessi and co-workers was used for encapsulation of lipophilic drugs (Fessi et al., 1989). In this process nanospheres are formed. Nanoprecipitation requires two miscible solvents. Both, the encapsulated molecule and the polymer should dissolve in one of them (referred to as a solvent), but not in the second system (referred to as a non-solvent). When the polymer solution is added to the non-solvent, nanoprecipitation occurs by a rapid desolvation of the polymer as a result of diffusion of polymer-containing solvent into the dispersing medium. In the classical approach acetone or ethanol are used as solvents for the polymer and a lipophilic drug. By extending this classical approach to a more versatile drug/polymer/solvent/non-solvent scheme (e.g. by using different alcohols as non-solvents, and different chemical families like ketones and esters as solvents) Bilati et al., (2005) have adapted the nanoprecipitation method for encapsulation of hydrophilic compounds into PLA and PLGA nanoparticles. Nanoprecipitation enables to obtain nanoparticles with small polydispersity indices.

The classic emulsification solvent evaporation technique (ESE) described by Bodmeier and McGinity (1987) and its different variations were initially used to obtain microparticles composed of synthetic polymers, e.g. PLGA. The ESE process is composed of two steps: the emulsification of a polymer solution in a suitable water immiscible and volatile organic solvent (e.g. dichloromethane, chloroform or ethyl acetate) containing the encapsulated substance into an aqueous phase followed by hardening of the particles through solvent evaporation (either by increased temperature/decreased pressure or by continuous stirring) and polymer precipitation (Bodmeier and McGinity, 1987; Soppimath et al., 2001; Rosca et al., 2004). The shear stress produced by homogenizer, sonicator or whirl mixer applied during emulsification process leads to breaking up the polymer solution into microdroplets. It is mainly this step where the particle size and size

distribution are determined (Rosca et al., 2004). The ESE method is known to work best for water-insoluble drugs (Bodmeier and McGinity, 1987). The use of conventional O/W ESE method for the encapsulation of water soluble ingredients will generally lead to rapid partitioning of the drug from the organic phase into the aqueous phase, resulting in the formation of particles with a very low drug loading (Bodmeier and McGinity, 1987; O'Donnel and McGinity, 1997). Therefore innovative modifications to the conventional O/W ESE method have been developed to evade this problem. One of them is an ESE method based on the formation of a multiple W/O/W emulsion as reported by Herrmann and Bodmeier (1995). In this method a primary W/O emulsion containing an aqueous solution of the active ingredient emulsified into a solution of the polymer in a water-immiscible solvent is emulsified into an external aqueous phase to form a W/O/W emulsion. The microspheres are formed after diffusion and evaporation of the solvent and precipitation (hardening) of the polymer in the emulsified droplets (Hermann and Bodmeier, 1995). By conveniently adjusting the formulation process (e.g. by the use of ultrasounds in the emulsification step) the size of the dispersed particles may be reduced markedly and nanoparticles may be obtained (Blanco and Alonso, 1997).

The emulsification-diffusion method is a variant, in which an O/W emulsion is formed with a solvent that is only partially soluble in water, e.g. benzyl alcohol, propylene carbonate (Quintanar-Guerrero et al., 1996). The organic solvent containing the polymer and a stabiliser (e.g. polyvinyl alcohol, poloxamer 188, gelatin) is added to the aqueous phase, similar to the previous method. Following mutual saturation of the two phases (organic solvent and water), both liquids are in a state of thermodynamic equilibrium. After stirring the organic solvent solution is dispersed as globules in the equilibrium with continuous phase and the stabiliser is adsorbed on the large interfacial area created. In the next step a large amount of water is added to such emulsion. As a result, the diffusion of the partially water miscible organic solvent to the external phase occurs and after some time the nanoparticles come out of solution (Quintanar-Guerrero et al., 1996).

Another modification is so called "salting-out/solvent displacement" technique which draws on aspects of both methods described earlier (i.e. ESE and nanoprecipitation). The polymer and drug are dissolved in an organic solvent (acetone) miscible with water and emulsified into an aqueous continuous phase loaded with both, a salting-out agent (e.g. magnesium chloride) and a suitable stabiliser (e.g. PVA). The presence of sufficient quantities of polyelectrolyte is

necessary to effect the separation of an organic phase from an aqueous phase, the two being fully miscible otherwise. Controlled dilution of the electrolyte by addition of aqueous solution of the stabiliser gives rise to particle formation as acetone diffuses from organic droplets (McCarron et al., 2006).

Other than the commonly used synthetic hydrophobic polymers, research activity is now focused on the preparation of nanoparticles composed of hydrophilic polymers like chitosan, alginate, etc. (Soppimath et al., 2001). Nanoparticles composed of natural polymers are usually obtained by mild methods presenting the benefit of producing organic solvent-free formulations. The techniques employed are ionic gelation (e.g. chitosan cross-linked with sodium tripolyphospahte anions) (Calvo et al., 1997) or coacervation (chitosan, gelatine nanoparticles) (Borges et al., 2005, Leo et al., 1997). Coacervation is the separation into two liquid phases in colloidal systems. Coacervate is the phase more concentrated in colloid component and the other phase is the equilibrium solution (de Kruif et al., 2004). Nanoparticles composed of gelatin or albumin may be obtained by the slow addition of protein precipitating agent, like neutral salt (sodium or ammonium sulphate) or alcohol (ethanol) to the solution of protein. The process is often followed by chemical cross-linking with glutaraldehyde to stabilise the nanoparticles. The disadvantage of the stabilising agents is the possibility of their reaction with the drug and possible increase in toxicity of the formulation. Also, this method is not appropriate for very hydrophilic drugs as they are readily washed out of the particles (Grabnar et Kristl, 2011).

Coacervation caused by the interaction of two oppositely charged colloids is referred to as a complex coacervation. However, in many cases, the complexes are solid-like (precipitate) in nature (de Kruif et al., 2004). Polyelectrolyte complex formation is mainly caused by strong Coulomb interactions between oppositely charged polyelectrolytes, whereby the gain in enthropy due to the release of the low molecular weight counterions initially bound to polyelectrolytes plays a decisive part (Dautzenberg et al., 2002; Schatz et al., 2004). Other intermacromolecular interactions, e.g. hydrogen bonding, van deer Waals forces, hydrophobic interactions or dipole-charge transfer may also be involved in the formation of polyelectrolyte complexes (Schatz et al., 2004), nevertheless they are considerably weaker than Coulombic interactions and therefore would have to occur in a great number in order to exert a more significant effect. At certain conditions, polyelectrolyte complexes can precipitate in the form of colloidal size particles. Usually, there is a narrow window of physicochemical conditions where the

complexes are formed and stay in the form of colloidal dispersion (de Kruif et al., 2004). The process of NP formation should be conducted in diluted solutions in order to prevent macroscopic gelation that leads to bulk hydrogels (Oh et al., 2009). Some of the factors determining the formation and properties of polyelectrolyte complexes are the strength and location of ionic sites, polymer chain rigidity, pH, temperature, ionic strength and mixing intensity (Hartig et al., 2007). The stability of polyelectrolyte complex nanoparticles depends on the repulsion between similarly charged nanoparticles. When the charge is neutralised, aggregation occurs. Therefore the net charge of the system must be either strongly positive or strongly negative if the system is to be colloidally stable. Polyelectrolyte complexes are known to aggregate when polycation and polyanion charge mixing ratio is close to 1 (Boddohi et al., 2009). In an ionic gelation process nanoparticles are formed as a result of inter- and intramolecular cross-links between the polyelectrolyte (e.g. chitosan) and the counterion (e.g. sodium tripolyphosphate, TPP), as described by Calvo et al., (1997). In contrast to polyelectrolyte complexation, where the complex is formed between two oppositely charged polyelectrolytes, the ionic gelation process involves the interactions between a polyelectrolyte and a small molecular weight counterion. Similarly to polyelectrolyte complexation, ionic gelation is a very mild process useful for association of macromolecules like nucleic acids, proteins and peptides. It can be performed at room temperature and no special equipment is required. It is essential to identify the cross-linking conditions that will yield the formation of nanoparticles (Grabnar et Kristl, 2011). Both methods, polyelectrolyte complexation and ionic gelation are very often combined. For instance, polyelectrolyte complexation between CS and HA as well as ionic gelification of CS by TPP were employed in the production of CS/TPP/HA nanoparticles described by de la Fuente et al., (2008a, b and c) and HA-coated CS/TPP NPs by Nasti et al., (2009).

1.5 Physicochemical properties of polymeric nanoparticles

The critical determinant of the fate of orally administered nanoparticles is the particle size and size distribution, as particle transport by the intestinal epithelium is size-dependant (Alonso, 2004; des Rieux et al., 2006). The particle size may be influenced by the concentration and nature of the surfactant used. High concentrations of surfactant decrease the size of particles. The particle size is also influenced by the polymer molecular weight and the trend is that smaller and less polydispersed nanoparticles are typically obtained when the PLGA with higher molecular weight is employed (Zambaux et al., 1998). The processing parameters

can also influence the micromeritic properties such as size of nanos. A few examples of such parameters include the number of homogenization cycles if a microniser is used, sonication time, type and properties of excipients, drug concentration and oily/aqueous phase ratio in the case of PLGA nanoparticles (des Rieux et al., 2006). Mainardes and Evangelista (2005) showed that sonication time, PLGA and drug amounts, the concentration of PVA, ratio between aqueous and organic phases and the method of solvent evaporation had a significant influence on the size distribution of PLGA nanoparticles containing praziquantel.

The extent of nanoparticle uptake is also governed by their surface properties. Firm assumptions regarding the most advantageous nanoparticle surface properties still remain controversial and this depends on the type of intestinal cell (enterocytes versus M cells). Surface charge and hydrophobicity of the nanoparticles are greatly influenced by the nature of polymer(s) and their composition. The surface charge of polyelectrolyte complex nanoparticles depends on the mass mixing ratio of the oppositely charged polyelectrolytes, as shown for CS/HA NPs (de la Fuente et al., 2008b, Boddohi et al., 2009) and HA/polyarginine NPs (Oyarzun-Ampuero et al., 2011). It is possible to modify the particle surface by coating or attaching a molecule hoping that the diverse properties of such molecules will alter the characteristics of the nanoparticle surface. These modifications mainly aim to change the zeta potential of the particle and their hydrophobicity as well. This way the colloidal stability, mucoadhesive properties of the nanoparticles as well as ability to bind/adsorb protein molecules to their surface are influenced, and in turn, altering oral absorption of the nanoparticles (des Rieux et al., 2006).

The most frequent polymers employed in coating of nanoparticles are PEG and chitosan. Kawashima et al., (2000) have shown that the formation of mucoadhesive CS coating around PLGA nanopartilces improved the oral absorption of elcatonin. PEG coating around the nanocarrier helped to improve their stability in biological fluids and, as a consequence, facilitated the transport of the associated macromolecules across the intestinal and nasal epithelia (Tobio et al., 1998; Tobio et al., 2000; Vila et al., 2002). In order to combine the benefits of chitosan and PEG, Prego et al., (2006) designed a new type of nanocapsules with the use of chitosan chemically modified with PEG. They showed that by the use of PEGylated chitosan and modification of the PEGylation degree it was possible to obtain chitosan coated nanocapsules with a good stability, a low cytotoxicity and with absorption enhancing properties.

Recently, coating nanoparticles with HA has attracted the attention of scientists (de la Fuente et al., 2008a, b and c; Nasti et al., 2009). HA could potentially favour targeting of the nanoparticles to cell types that express HA surface receptors, since several receptors have been related with the cellular uptake of HA, e.g. CD44 receptor (Knudson et al., 2002). Nasti et al., (2009) coated CS/TPP nanoparticles with HA by adsorption of the polyanion on positively charged nanoparticles as a result of electrostatic interactions. They also showed the beneficial character of HA-coating in the reduction of toxicity (IC_{50} in J774 macrophages increased from 0.7-0.8 mg/ml to 1.8 mg/ml for uncoated and HA-coated nanoparticles, respectively).

It is also possible to attach a ligand to the particle surface to achieve target specificity for receptors present on the surface of enterocyte or M cell. Various molecules have been tested for their use as ligands (targeting molecules) and one of the examples could be lectins (des Rieux et al., 2006).

A successful nanocarrier may be the one, which is characterised by a high loading capacity, as that would reduce the dose of the nanoparticles required for administration (Soppimath et al., 2001). Generally, the active ingredient may be loaded into the particles either by incorporation of the drug at the time of production of the nanoparticles or by adsorption of the drug after nanoparticle formation by incubating NPs in the drug solution. An alternative method is the chemical conjugation of the drug into nanoparticles (Soppimath et al., 2001). While encapsulating an active, one has to keep in mind its activity after the process i.e. integrity of the compound. It is one of the most important parameters influencing the bioavailability and pharmacological efficiency of that active (des Rieux et al., 2006). As many biomolecules, e.g. proteins, are heat sensitive, and some of the operations in the preparation of the particles, e.g. sonication or solvent evaporation may result in the exposure of the drug to high temperature, it may be necessary to modify the process parameters in order to preserve their activity. It has been shown e.g. that for the double emulsion technique the process temperature, the use of a rotating evaporator and duration of the organic solvent evaporation did not affect the properties of formed nanostructures, but were in favour of an increased loading efficiency of therapeutically active protein (Zambaux et al., 1998). For the nanoprecipitation technique Govender et al., (1999) showed that the encapsulation efficiency of a water soluble drug (procaine hydrochloride) into PLGA nanoparticles was improved either by increasing the pH of the aqueous phase from 5.8 to 9.3, or

by replacement procaine hydrochloride by procaine base, thereby reducing aqueous solubility of the drug.

The release profile is influenced by the character of polymers comprising the formulation. Polymers from natural sources usually provide a relatively quick release of the drug, while synthetic polymers are characterised by a more sustained release of the drug ranging from days up to weeks, even month (des Rieux et al., 2006). The nature (e.g. hydrophilic/hydrophobic) and the physicochemical characteristics will determine and significantly impact on the mechanism of drug release and overall profile.

1.6 Routes of administration of nanoparticles

Dosage forms, including nanoparticles, can be designed for administration by different delivery routes in order to achieve the most optimum therapeutic response. When designing dosage forms, factors governing choice of administration route and the specific requirements of that route should be taken into account. Dosage forms may be administered to exert local or systemic effects and this factor may be of importance for the choice of the delivery route.

The most common and convenient methods for drug administration are the transmucosal routes, which among others include oral, pulmonary and nasal route. Although each of them has its biological specificity and particular requirements, the mucus layer is a common element of all mucosal surfaces (de la Fuente et al., 2008a). Mucus is a complex, viscous and adherent secretion which is synthesised by specialised goblet cells in the columnar epithelium lining all organs exposed to the external environment (Bansil and Turner, 2006; Andrews et al., 2009). It is a mixture containing more than 95% of water, 0.5-5% of glycoproteins mucins (Mw of 1-40 million Da), 1% of mineral salts, 0.5-1% of free proteins as well as lipids and mucopolysaccharides (Madsen et al., 1998; Edsman and Hagerstrom, 2005). The glycoprotein mucin is the principal structural component responsible for the viscoelastic properties of mucus forming a highly entangled system of macromolecular chains with physical interactions including electrostatic interactions and hydrogen bonding (Madsen et al., 1998). Mucus performs many functions, such as maintenance of a hydrated layer over the epithelium and lubrication for the passage of objects. It also serves as a barrier to noxious substances (e.g. HCl in the stomach) and pathogens and enables the exchange of gases and nutrients with the underlying epithelium. Mucus is the first barrier with which dosage forms or active ingredients must interact and diffuse through, in

order to be absorbed and get access to the circulatory system and target end organs (Bansil and Turner, 2006; Andrews et al., 2009).

Two major problems for drugs administered via transmucosal routes (e.g. oral) in reaching the suitable biological compartments are poor drug stability and limited transport across ephitelia. These difficulties are particularly important in case of biotech compounds such as nucleic acids, peptides and proteins, for which they represent limiting steps for their adequate clinical exploitation. Consequently, these molecules require appropriate delivery systems capable of protecting them from biological environments and facilitating their transport through biological barriers (Alonso, 2004). In 1988 Damge and co-workers showed, for the first time, that polyalkylcyanoacrylate nanocapsules protected insulin from degradation and facilitated its transport across the intestinal barrier (Damge et al., 1988). The ability of colloidal carriers to enhance the transport of associated molecules has been attributed to different mechanisms depending on the nanocarrier composition, namely: (i) mucoadhesion, (ii) particle internalization phenomenon and (iii) permeation enhancing effect (Garcia-Fuentes, 2005). The use of mucoadhesive polymers (i.e. polymers having the ability of attaching to mucosal surfaces) is generally accepted as a promising strategy because they prolong the residence time and to improve the specific localization of drug delivery systems on various membranes (Grabovac et al., 2005). A number of reports have made it clear that the particle size, surface charge, hydrophobicity and the presence or absence of surface ligands are critical for the interaction of delivery carrier with the absorptive site, and also that the biological behaviour of the material forming the nanocarrier is a determining factor for its efficacy (Desai et al., 1996; Florence, 1997; des Rieux et al., 2006; Prego et al., 2006).

Polymers exhibiting mucoadhesive properties (e.g. chitosan (CS)) were found to be very good candidates for the design of a transmucosal drug nanocarrier, e.g. for elcatonin or calcitonin (Kawashima et al., 2000; Prego et al., 2006). Colloidal particles containing CS, either in the form of a coating or as a nanomatrix, were demonstrated to improve the transport of drugs across the intestinal and nasal (Vila et al., 2002) and the ocular (de Campos et al., 2003) mucosa. Chitosan has mucoadhesive properties, but it can also have a penetration enhancing effect by partial disruption of the tight junction between cells that restricts the paracellular route of transport for hydrophilic compounds. It has been shown that coating lipid nanocapsules either with PEG or with CS resulted in similar association with Caco-2 cells, but only CS-coated nanocapsules reduced

transepithelial electric resistance in a dose-dependent manner. Also, only sCT-loaded CS-coated NPs had a significantly better hypocalcemic response than the control (sCT solution) after oral administration to rats in contrast to sCT-loaded PEG-coated nanoparticles, which did not differ significantly from the control (Garcia-Fuentes et al., 2005).

1.6.1 Intraarticular delivery of nanoparticles

Intraarticular (I.A.) administration of drugs (i.e. administration directly into the affected joint) is an attractive approach for the treatment of joint diseases like osteoarthritis (OA) (Morgen et al;, 2013). OA is locally restricted to one or a few joints, therefore providing a unique opportunity for local I.A. treatment without the risk of systemic side effects. The formulations for I.A. applications should be sterile and compatible with the physiological conditions at the application site (i.e. isotonic and pH ideally close to 7.4, but not below 5.5) (Gerwin et al., 2006). I.A. delivery may offer several advantages over oral dosing, especially for drugs that have systemic toxicity, are poorly absorbed or have undesirable pharmacokinetic profiles (Morgen et al., 2013). Indeed, direct delivery of the drug to the affected joint offers the possibility to achieve appropriate drug concentrations at the site of action by applying low amounts of drug. Also, I.A. administration enables employment of drugs which have good efficacy, but low oral bioavailability, which is an issue for many of the novel drug candidates in development (Gerwin et al., 2006).

Since many compounds are rapidly cleared from the joint after intra-articular injection, increasing the retention time of the therapeutic agent in the joint is the biggest challenge in developing an intraarticular delivery system (Morgen et al., 2013). A longer duration of action would be desirable to limit the number of I.A. injections due to the discomfort and pain associated with administration as well as possible risk of infection (Gerwin et al., 2006). Many types of particulate carriers have been investigated in order to achieve this goal, including liposomes, microparticles and nanoparticles (Morgen et al., 2013). The use of micro and nanoparticles, e.g. albumin or PLGA has been investigated (Gerwin et al., 2006). Horisawa et al., (2002) described that PLGA nanoparticles should be more suitable for delivery into the inflamed synovial tissue than microparticles due to their ability to penetrate synovium. PLGA-based particles can provide local therapy actions in joint diseases in a different manner depending on the particle size (Horisawa et al., 2002). HA is administered via I.A. route in order to help in restoring of viscoelastic properties of synovial fluid (e.g. Synvisc injections), but HA has also been

demonstrated to have a multiplicity of biological actions on cells *in vitro*, e.g. anti-inflammatory effects (Gerwin et al., 2006). HA is also an ingredient of synovial fluid. HA is known to interact with CD44 receptors of the cells, especially chondrocytes. One of the attempts to increase the retention time of drugs within the knee cavity and to improve the interactions between cells and particles is the use of HA-functionalized PLA/PLGA particles (Zille et al., 2010).

1.7 Nanoparticulates as potential delivery systems for peptides and proteins

Many drugs derived by biotechnology, including peptides and proteins have become a central focus of pharmaceutical research efforts in recent years. From a therapeutic perspective, proteins offer the distinct advantage of specific mechanisms of action and are highly potent. In contrast to the small molecular weight drugs, peptides and proteins need special formulation strategies to become viable therapeutic products (Pisal et al., 2009). Major limitations in the use of peptides and proteins are their low bioavailability and the ratio of drug accumulation at its site of action to the amount delivered to the body (Hartig et al., 2007). Typically, these molecules are characterised by a short half-life in biological fluids and a high probability of off-target effects (Hartig et al., 2007). They also have high molecular weights, are unstable and immunogenic (Pisal et al., 2009). As a consequence, the use of naked macromolecules is limited and advanced delivery systems that act locally are needed (Hartig et al., 2007). In order to improve the current limitations of therapeutic peptides and proteins, most efforts are focused around one of the two approaches - either the change in the agent itself (e.g. by covalent attachments of moieties like PEG or by mutations in protein structure) or by a change in the formulation. Different formulation systems, such as polymeric microparticles, nanoparticles and liposomes have been examined. PLA and PLGA-based biodegradable microparticles are currently available on the market as delivery systems for leuprolide acetate, growth hormone, octreotide acetate, lanreotide and triptorelin pamoate. However, the favorable characteristics of the carrier itself must be balanced against the negative effects on protein stability during preparation and storage, and further research is needed to resolve issues with protein stability, degradation and loading (Pisal et al., 2009).

In the late 80's, Damgé et al., (1988) showed that polyalkylcyanoacrylate nanocapsules were able to protect insulin against degradation and facilitate its transport through the intestinal barrier. Following this study, nanoparticles have been extensively examined as carriers for oral peptide and protein delivery, e.g.

luteinizing hormone releasing hormone (LHRH) (Hillery et al., 1996 a and b; Allèman etal., 1998), salmon calcitonin (sCT) (Prego et al., 2005, Gracia-fuentes et al., 2005), insulin (Prego et al., 2005,26), immunodominant peptides for collagen induced arthritis (CIA) (Lee et al., 2005), dalargin (Schroeder et al., 2000), and helodermin (Chalasani et al., 2007). A number of animal studies have demonstrated their ability to improve the oral absorption of loaded peptides and proteins, for example calcitonin or insulin (Hartig et al., 2007). However they have not been followed by scaling-up industrial experiments or clinical trials. It is difficult to draw conclusions from animal studies to human applications. Therapeutic applications of these described peptide formulations have been shown as limited due to some variability of the delivered dose and problems with bioavailability. Still, nearly all published work described studies in early stages of development. Nanoparticulate drug delivery systems are still of very high interest to researchers especially for formulations containing highly potent drugs with a low dose response as well as for local drug delivery (des Rieux et al., 2006). The key requirements for an ideal nanoparticle carrier are small size (50-200 nm), high loading and entrapment efficiency, slow complex dissociation *in vivo* and optimized targeting to the desired tissue with limited non-specific uptake by other tissues. The development of nanoparticle formulation which can combine these benefits with low costs and simple design are of vital importance for a highly efficient delivery system (Hartig et al., 2007).

1.7.1 Salmon calcitonin

Calcitonin is a polypeptide hormone comprised of 32 amino acids. It has been found that salmon and eel calcitonins are more potent in mammals, especially in man, than human or other mammalian calcitonin types (Torres-Lugo et al., 2000). The amino acid sequence of salmon calcitonin is shown in Fig. 1.4. The estimated isoelectric point of sCT is 10.4 (Maier et al., 1977) and at pH 7.4 it is expected to carry an overall charge of approximately 3+ (Epand et al., 1983).

Salmon calcitonin (sCT) has been used for more than 30 years and is licenced to treat hypercalcaemia, Paget's disease and as a second-line treatment for post-menopausal osteoporosis (Guggi et al., 2003). sCT is also a promising candidate to be used in osteoarthritis (Manicourt et al., 2005) and in combined therapy with alendronate in patients with rheumatoid arthritis (Ozoran et al., 2007). Interest in sCT as a potential treatment for OA has increased due to the discovery of beneficial metabolic actions on cartilage and bone turnover (Sondergaard et al.,

2006). The 32-amino-acid peptide hormone exerts a potent anti-resorptive effect by direct binding to osteoclasts (Mancini et al., 2007, Karsdal et al., 2011) and directly affects chondrocyte (Conrazier et Chevalier 2008; Burt et al., 2009). sCT has the also the added benefit in its analgesic effects. The majority of evidence of the analgesic activity is derived from clinical studies in tumour metastasis (Edwards 2011), Paget's disease (Horisawa et al., 2002), osteoporosis fracture (Liang et al., 2005) and several controlled prospective double-blind studies to improve pain (Ralph et al., 2005; Wang et Wan, 2008). There is published *in vitro* evidence that calcitonin can directly inhibit MMPs and block collagen degradation in articular chondrocytes exposed to TNFα/oncostatin M to induce an OA. *In vitro* and *ex vivo* studies have found that calcitonin has both anti-catabolic and anabolic effects in cartilage, by attenuating proteoglycan and collagen type II degradation as well as by inducing their syntheses. A small phase II randomized, double-blind, placebo-controlled trial assessing the efficacy of oral salmon calcitonin in knee OA was also conducted (Sondergaard et al., 2006). Results showed an improvement in Lequesne's function scores as well as a reduction of biomarker levels of urinary CTXII, MMP-3 and 13. Intriguingly, while oral formulations of sCT have reached Phase III clinical trials for both osteoporosis and OA (e.g. Karsdal et al., 2011), direct evidence of local anti-inflammatory effects of sCT is scant. An indirect benefit of sCT however was detected in the collagen-induced arthritis (CIA) rat where intra-peritoneal (I.P.) injections of sCT permitted enabled sub-therapeutic doses of prednisolone to achieve adequate reduced paw swelling, thus potentially negating potential systemic side effects associated with prolonged use of high dose steroids (Mancini et al., 2007).

Although sCT was commercially available as an injectable format and nasal spray (Guggi et al., 2003), its short half-life has always posed as a problem in that that frequent dosing is required by patients. Its short half-life is mainly due to multiple peptidase cleavage sites and is therefore susceptible to proteolytic degradation. The stability of sCT was improved and the half-life extended when administration by I.V. injection *in vivo* by site specific cysteine-1 conjugation of sCT to a comb-shaped end-functionalised (poly(PEG) methyl ether methacrylate) (Ryan et al., 2009).

The full market potential of calcitonin has not yet been reached due to the low patient compliance associated with the injectable dosage forms (Guggi et al., 2003). Also, the absorption of sCT from the commercial nasal spray, Miacalcin® shows a great variability in the range 0.3-30.6%, with an average bioavailability of

3% compared to intramuscular injection (Hinchcliffe et al., 2005). The systemic delivery of sCT via routes other than by injection and nasal presents an attractive therapeutic option (Paton et al., 2000).

However there have been reports that calcitonin contributes to an increased invasiveness of prostate cancer cells (Sabbisetti et al., 2005). On the 19th July 2012, EMEA (European Medicines Agency) completed a review of the benefits and risks of calcitonin-containing medicines, concluding that the risk of cancer is slightly increased as a result of long term use of these medicines. Therefore CHMP (the Agency's Committee for Medicinal Products for Human Use) recommended that calcitonin-containing medicines should only be authorised for a short-term use in Paget's disease, acute bone loss due to sudden immobilisation and hypercalcaemia caused by cancer. They should no longer be used for osteoporosis (EMA/476001/2012).

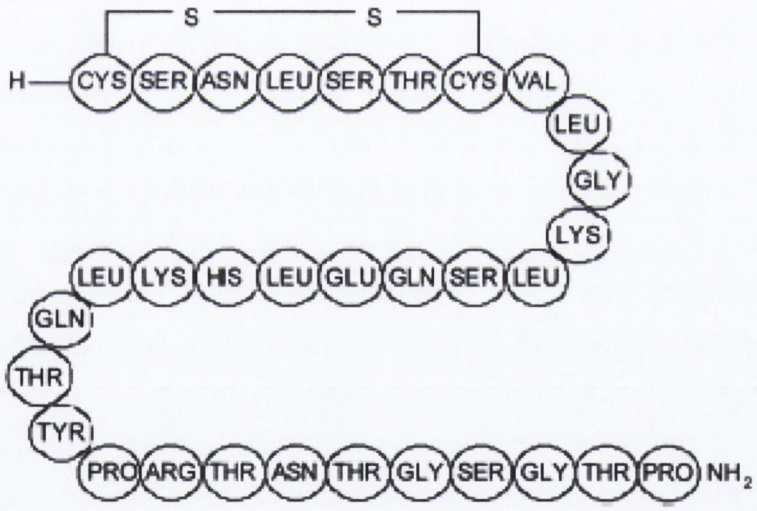

Fig. 1.1 Amino acid sequence of salmon calcitonin (Torres-Lugo and Peppas, 2000).

Several approaches have been attempted to produce calcitonin or elcatonin-loaded polymeric nanoparticles.

For instance, Lowe and Temple (1994) formulated human calcitonin-loaded polyacrylamide nanospheres for the oral delivery with the aim to decelerate enzymatic decomposition of the peptide in the guts by polymerisation in an inverse emulsion (water-in-oil). This method employed a large amount of an organic solvent (e.g. hexane) and several washings of obtained nanospheres with ethanol. Although the NPs had the size below 50 nm, the loading efficiency was very low

(below 5%) and calcitonin was immediately released after hydration. The studies concluded that the nanocapsules gave no significant overall enhancement of peptide absorption.

Vranckx et al., (1996) loaded sCT into butylcyanoacrylate nanocapsules using the interfacial polymerisation technique. Besides the monomer, no potentially toxic compounds were used, therefore no purification method was considered. The method involved the use of an organic solvent (ethanol) and a surfactant (sodium lauryl sulphate and Span® 80). The NP size ranged from 200-300 nm and the encapsulation efficiencies reached 50%. The addition of Brij® 35 to the aqueous phase decreased the particle size to 50 nm, however the encapsulation efficiency was also decreased (30%). The effectiveness of the NPs after an oral administration was estimated at 45% of the activity after an i.v. administration of the same dose in conscious fasted rats.

Garcia-Fuentes et al., (2005) prepared calcitonin-loaded chitosan-coated lipid NPs by the double emulsion solvent emulsification method. This method involved the use of sonication, organic solvents (methylene chloride) and a surfactant (Poloxamer 188). The size of the particles was 509 nm, but the coating with chitosan caused the decrease in encapsulation efficiency from 90% to 30%. In another study, Prego et al., (2006) have shown that chitosan nanocapsules performed successfully as oral carriers for sCT, as they reduced significantly the serum calcium levels after oral administration to rats. The nanoemulsion prepared by solvent displacement technique was incubated with chitosan solution leading to the formation of chitosan nanocapsules. Chitosan nanocapsules had the size between 250 and 344 nm, and were characterised by a positive surface charge (approximately 30 mV). However, the sCT encapsulation efficiency was of 40%, and was markedly reduced compared to the control nanoemulsion (~98%). The performance of the chitosan nanocapsules was not affected by the characteristics of chitosan (i.e. the counterion in chitosan salt and the molecular weight of chitosan).

PLGA-based nanoparticles are one of the most common candidates for calcitonin or elcatonin nanocarriers (Kawashima et al., 2000; Glowka et al., 2010; Yang et al., 2012). For instance, Glowka et al., (2010) formulated calcitonin-loaded NPs composed of PLGA, Eudragit® RS or a blend of both polymers with the use of the double emulsion solvent evaporation method. This technique involved the use of organic solvents (methylene chloride), sonication and surfactants (polyvinyl

alcohol). The size of the particles ranged between 441 and 609 nm. The encapsulation efficiencies were 69-83%, however drug loading was very low (0.2%). *In vivo* studies conducted in Wistar rats showed that increased serum sCT levels were sustained for 3 days after subcutaneous administration of PLGA nanoparticles and the achieved bioavailability was increased compared to sCT solution.

Makhlof et al., (2010) synthesized a thiomer derivative of glycol chitosan and obtained the NPs by ionic gelation with TPP. This method did not involve the use of organic solvents or surfactants. The NPs obtained had the size of 230-330 nm and the efficiency of association of sCT with the NPs was 54-64%. Calcitonin-loaded NPs resulted in a pronounced hypocalcemic effect for at least 12 and 24 h via pulmonary delivery and a corresponding pharmacological availability varied between 27 and 40% depending on the formulation.

1.8 Backgrounds to polymers used in the current work

1.8.1 Chitosan

Chitosan (CS), commercially obtained by the deacetylation of chitin, is a polysaccharide composed of randomly distributed D-glucosamine (deacetylated unit) and N-acetyl-D-glucosamine (acetylated unit) linked by β-(1→4) glycosidic bonds (Fig. 1.1). The pKa value of the amino group of chitosan is approximately 6.5, therefore in acidic media these amino groups undergo protonation and chitosan becomes a polycation. However, chitosan is insoluble at neutral and alkaline pH (Leane et al., 2004). The solubility of chitosan salts with inorganic and organic acids and the charge density of chitosan depend on pH and the polymer deacetylation degree. The solubility of chitosan is also affected by others anions present in the solution. In the presence of acetate, lactate or glutamate CS shows good solubility, whereas phosphate, polyphosphates and sulphate decrease the solubility (Berthold et al., 1996). The positive charge of chitosan influences its reactivity with negatively charged surfaces, e.g. cell and mucosal membranes; thus chitosan is a mucoadhesive polymer. The mucoadhesivity in combination with biocompatibility, non-toxicity and permeability enhancing properties render chitosan an interesting biomaterial favourable for promoting absorption across mucosal membranes. Indeed, chitosan nanoparticles have been shown to improve the oral bioavailability of peptide and protein formulations (Agnihotri et al., 2004).

The formation of chitosan microparticles by a coacervation/precipitation process with sodium sulphate has been described by Berthold et al., (1996). As shown by Borges et al., (2005), the use of ultrasounds for homogenisation led to the formation of chitosan particles in the nanoscale size (643±172 nm), however one of the major drawbacks of this technique was the high polydispersity (PDI of 0.379±0.178).

Other anions were used to decrease the solubility of chitosan, among them TPP being the most common. Calvo et al., (1997) developed chitosan/TPP nanoparticles in a mild ionic gelation process by mixing two aqueous phases at room temperature. The size of the smallest NPs was 264 nm, and it was possible to achieve it by simply optimising the concentrations of TPP and CS, without the employment of sonication. Therefore TPP is a more effective cross-linker than sulphate.

The ability of chitosan to form polyelectrolyte complexes has been demonstrated (Denuziere et al., 1996), and numerous attempts were made to obtain CS/HA NPs (de la Fuente et al., 2008 a, b and c; Oyarzun-Ampuyero et al., 2009). In many of the published investigations the use of a cross-linker (such as TPP) was essential to obtain NPs. However, high concentrations of TPP have been found to be unfavourable as TPP neutralises the positive charge of chitosan, which may lead to aggregation of such NPs (Wadhwa et al., 2010). Boddohi et al., (2009) on the other hand, managed to obtain HA/CS NPs without TPP, however aggregation of the particles was observed and NPs were recovered only after leaving the suspensions to settle overnight.

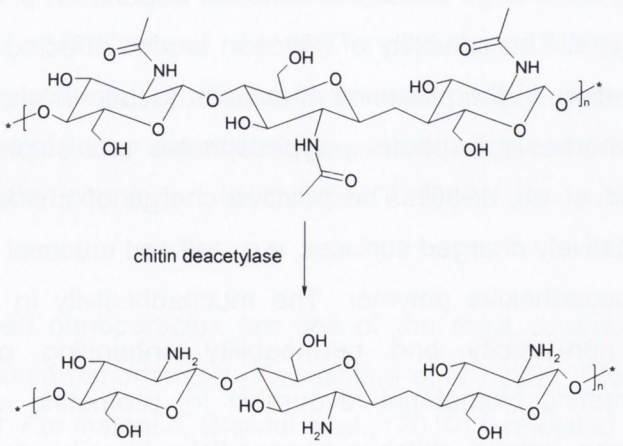

Fig. 1.2 The deacetylation of chitin to chitosan (Liu et al., 2008).

1.8.2 Hyaluronic acid

There are a few negatively charged polysaccharides that form polyelectrolyte complexes with chitosan. Among them hyaluronic acid (HA) seems particularly interesting due to its physicochemical and biological properties. Hyaluronic acid is a naturally occurring, mucoadhesive, biocompatible and biodegradable polysaccharide present in the components of extra-cellular matrix of connective tissues and is particularly concentrated in the vitreous fluid of the eye, synovial fluid, umbilical cords and chicken combs. HA is an anionic, nonsulfated glycosaminoglycan composed of repeating disaccharide units containing D-glucuronic acid and D-N-acetylglucosamine linked via alternating β (1→4) and β (1→3) glycosidic bonds. The chemical structure of HA is shown in Fig. 1.2. The charges of carboxylic groups in glucuronic acid, which are dependent on pH and ionic strength of the environment, influence the shape of chains and their interactions with surrounding molecules. The pK of the D-glucuronic acid is 3.23, while the pK of the polymer was estimated as 2.9 (Lapčík et al., 1998).

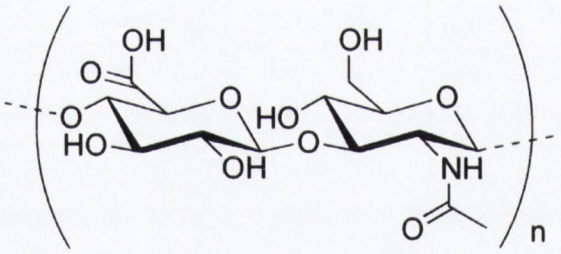

Fig. 1.3 Chemical structure of hyaluronic acid (Liu et al., 2008)

In vivo the polymers of HA can vary in size from 5 to 20000 kDa. The action of hyaluronic acid depends on its molecular weight. The function of large polymers is space-filling, immunosuppression, suppression of angiogenesis, inhibition of phagocytosis. It also suppresses the synthesis of HA. Smaller hyaluronan fragments (oligomers) are angiogenic, immuno-stimulatory and inflammatory (Stern et al., 2006). Hyaluronic acid interacts specifically with cell-surface receptors, e.g. CD44. Thus, it has previously been used in the treatment of cancer cells over-expressing CD44 (Choi et al., 2010). The second generation mucoadhesion property of HA is the result of CD44 receptor mediated binding. Moreover, hyaluronic acid acts in synergy with chitosan to enhance mucoadhesion (Wadhwa et al., 2010).

It has been demonstrated that it is possible to form HA-based polyelectrolyte complex NPs, nonetheless most of the work conducted so far has

focused on HA/CS NPs (e.g. de la Fuente et al., a, b and c; Boddohi et al., 2009). However, being a polyanion, HA has the ability to form polyelectrolyte complexes with other polycations. Among them, polypeptides and proteins are particularly interesting because of their biodegradability, biocompatibility and many other potential applications. For instance, complexes of HA based on electrostatic interaction with poly-L-lysine (Hahn and Hoffmann, 2005) and lysozyme (van Damme et al., 1994; Morfin et al., 2011) have been formulated and examined. Hahn and Hoffamnn (2005) used the electrostatic attractions between HA and lysine to obtain a biocompatible polyelectrolyte complex multilayer for surface modification of various biomaterials. Morfin et al., (2011), who examined the lysozyme-HA complexes, managed to obtain different systems appearing as one or two phased systems, transparent or turbid depending on the experimental conditions used. As the macroscopically homogenous turbid or opalescent liquid is likely to contain nanoparticles (Calvo et al., 1997), it is thus possible that some of the systems described by Morfin et al., (2011) were nanosuspensions. There also have been reports on complexation of HA to polyarginine (Kim et al., 2009; Oyarzun-Ampuyero et al., 2011) and polyelectrolyte complex NPs have successfully been obtained. Both research groups managed to obtain small NPs with sizes of 90-170 nm, being either positively (Kim et al., 2009, Oyarzun-Ampuyero et al., 2011) or negatively charged (Oyarzun-Ampuyero et al., 2011). Kim et al., (2009) used HA/polyarginine complex as a carrier for siRNA. Although Oyarzun-Ampuyero et al., (2011) suggested that incorporation of hydrophilic macromolecular drugs, e.g. peptides into HA/polyarginine nanocarriers might be possible, no such studies have been published so far.

1.8.3 Protamine

Protamine (PROT) is a mixture of positively charged proteins extracted from salmon roe. It is rich in arginine, similarly to some viral proteins which utilise arginine-rich sequences of amino acids (Reynolds et al., 2005). The molecular weight of the major component of salmine is approximately 5.1 kDa (manufacturer's data, Sigma). Protamine is capable to bind and precipitate DNA. It may be employed in the purification of DNA binding proteins or in the removal of DNA from protein samples. Protamine sulphate also has antibacterial properties and inhibits the activity of pepsin. Similarly to other polycations, it has been demonstrated to inhibit the classical pathway of the complement. Protamine also inhibits the turnover of lipoproteins by lipoprotein lipase and neutralises the anticoagulant effect of heparin. Reynolds et al., (2005) have shown that protamine

has a membrane translocating activity, which could be used in pharmaceutical applications.

PROT is already used in formulations containing insulin (Hagedorn, 1937). Being a natural product, its cost is substantially less than synthetic peptides, e.g. polyarginine. It has a long history of use establishing its biological effects and general safety in humans (Reynolds et al., 2005).

Junghans et al., (2000) have shown that PROT is capable to spontaneously form complexes with oligonucleotides. These complexes had the form of 150-170 nm nanoparticles, which doubled their size after 3 days. It was possible to reduce the particle size even to 46 nm by changing the mixing ratios of both components. These particles were characterised by either positive or negative surface charge, however in cell culture medium all dispersions contained negatively charged particles. Complexation to PROT protected the oligonucleotides from enzymatic degradation. Moreover, the complexes of oligonucleotides with PROT were characterised by a higher cellular uptake than oligonucleotides on their own (Junghans et al., 2000). Mayer et al., (2005) reported that substitution of protamine free base by protamine sulphate greatly reduced the size of oligonucleotide-protamine-albumin nanoparticles from 200 to 40 nm. However, no information about surface charge of these particles is available.

Apart from nucleic acids, PROT has been shown to form polyelectrolyte complex with heparin, a glycosaminoglycan with a high charge density. Mori et al., (2010) produced polyelectrolyte complex micro and nanoparticles containing heparin and protamine as a carrier for FGF-2.

It has also been demonstrated that covalent conjugation of HA to antisense oligodeoxynucleotide formed more stable polyelectrolyte complexes with protamine than naked nucleotide.

1.8.4 Chondroitin

Chondroitins are heteropolysaccharides purified from various tissues composed of alternate sequences of uronic acids (D-glucuronic or L-iduronic) and differently sulphated residues of N-acetyl-D-galactosamine linked by β(1→3) glycosidic bonds. The structure of CHON is shown in Fig. 1.3. The regular disaccharide sequence of chondroitin-4-sulphate (CHON), also referred to as chondroitin sulphate A, is composed of [(1→4)-O-(D-glucopyranosyluronic acid)-

(1→3)-O-(2-N-acetamido-2-deoxy-D-galactopyranosyl-4-sulphate)]. Chondroitin-6-sulphate, also referred to as chondroitin sulphate C, is mainly constituted by the following disaccharide unit: [(1→4)-O-(D-glucopyranosyluronic acid)- (1→3)-O-(2-N-acetamido-2-deoxy-D-galactopyranosyl-6-sulphate)]. Inside the chains of the polysaccharide it is possible to locate disaccharides with a different number and position of sulphate groups in varying percentages, e.g. non-sulphated or disulphated disaccharide where two sulphate groups are O-linked in position 2 of D-glucuronic acid and 6 of N-acetyl-D-galactosamine (disaccharide D) or in position 4 and 6 of N-acetyl-D-galactosamine (disaccharide E). The sulphation of N-acetylgalactosamine residues makes CHON a strongly charged polyanion (Montfort et al., 2008). Different heterogenous structure of chondroitins, in terms of a degree of sulphation, molecular weight, percentage of differently sulphated disaccharides, relative amounts of glucuronate and iduronic acid depending on the tissue of origin are responsible for diverse and specialised functions of these polysaccharides (Volpi et al., 2003).

Chondroitin sulphate is present in many connective tissues; it is very abundant in cartilage, skin, corpus vitreum and blood vessels. Most CHON is present as the sugar chains of aggrecan in the cartilage, and a proper hydration of the cartilage is ensured by its high water retaining ability. Therefore, CHON plays a part in the visco-elastic property of the cartilage. Reduced level of CHON in the cartilage is one of the risk factors for arthritis in elderly people. CHON is a popular dietary supplement for joint pain and is well recognised as a symptomatic slow-acting drug for osteoarthritis. However, its mechanism of action still remains unclear (Imada et al., 2010). Both, chodroitin-6-sulphate and chondroitin-4-sulphate were found to prevent cartilage destruction as a result of the suppression of the expression of ADAMTS-4 and -5 and MMP-13 genes. They also promoted cartilage remodelling due to the up-regulation of aggrecan core protein expression. Furthermore, chondroitin-4-sulphate was shown to increase the TIMP-1 production and TIMP-3 mRNA, leading to further inhibitory effect of MMPs and aggrecanase activities. CHON was able to modulate the function of chondrocytes as well as synovial fibroblasts, and thereby exerted multifunctional chondroprotective effect in degenerative arthritis diseases (Imada et al., 2010). The *in vitro* and *in vivo* studies in rabbits showed the ability of CHON to inhibit the nuclear translocation of nuclear factor κB, a central component in sustaining the inflammatory reaction in many diseases. Therefore CHON may potentially treat other autoimmune and inflammatory diseases apart from osteoarthritis ad may become an additional

option in anti-inflammatory therapy. Moreover, CHON appears to have a favourable safety profile, with no interactions with other drugs observed and adverse effects comparable to placebo (du Souich, 2009). CHON has been shown to be absorbed after oral administration in humans as a high molecular weight polysaccharide (Volpi, 2002).

CHON sulphates have both, weak (carboxylate) and strong (sulphate) acid residues. Due to its acidic nature CHON is able to produce ionic complexes with positively charged molecules, e.g. chitosan (Denuziere et al., 1996). Examples of such complexes include nanoparticles (Yeh et al., 2011, Hou et al., 2012, da Silva et al., 2012). All above mentioned CHON/CS NPs were characterised by a positive surface charge, which may be attributed to the amino groups of chitosan. They were used to associate FITC-BSA (Yeh et al., 2011) or Nell-1 like molecule (Hou et al., 2012). CHON/CS nanoparticles were obtained by mixing aqueous solutions of oppositely charged polyelectrolytes (Yeh et al., 2011), however in some cases sonication was employed (da Silva et al., 2012). The incorporation of TPP as a cross-linker seemed to have a negative impact on the particle size, as the CHON/CS/TPP NPs produced by Hou et al., (2012) were markedly larger than cross-linker free NPs obtained by Yeh et al., (2011) (550-850 nm compared to 178-370 nm, respectively). On the contrary, the incorporation of TPP was beneficial for HA/CS NPs (de la Fuente et al., 2008a).

Apart from CS, CHON has been shown to form polyelectrolyte complexes with other polycations, e.g. lysozyme (van Damme et al., 1994) and polyethylenimine (Pathak et al., 2009). Complexation to CHON has been reported to significantly decrease the cytotoxicity of polyethylenimine in HepG2 and HeLa cells (Pathak et al., 2009).

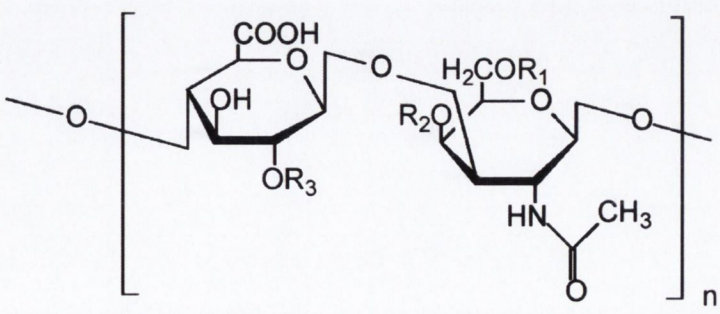

Fig.1.4 Chemical structure of one unit in chondroitin sulphate chain. Chondroitin-4-sulphate: R_1=H, R_2=SO_3H, R_3=H. Chondroitin-6-sulphate: R_1=SO_3H, R2 and R_3=H (Liu et al., 2008).

2. Materials and methods

2.1 Materials

4-(2-hydroxyethyl)-1-piperazineethanesulfonic acid (HEPES)	Sigma
Acetic acid (glacial) 100%	Merck, Germany
Acetonitrile, HPLC grade	Sigma
APC-Annexin V	BD Biosciences, USA
Buffer solution pH 4	Fluka, Germany
Buffer solution pH 7	Fluka, Germany
Buffer solution pH 10	Fluka, Germany
Calcium chloride dihydrate	Sigma
Chitosan chloride salt (CL213, high molecular weight)	NovaMatrix, Norway
Chitosan chloride salt (CL113, low molecular weight)	NovaMatrix, Norway
Chitosan chloride salt(CL42)	Chitoceuticals, Germany
Chitosan glutamate salt (G213, high molecular weight)	NovaMatrix, Norway
Chitosan glutamate salt (G113, low molecular weight)	NovaMatrix, Norway
Chondroitin 4-sulphate sodium salt (CHON)	Sigma
Deuterium oxide	Sigma
Dexamethasone 21-phosphate disodium salt	Sigma
Disodium hydrogen phosphate dodecahydrate	Merck, Germany
E-Toxate ™ kit	Sigma
Fetal Bovine Serum	Sigma
Gentamycin sulphate	Sigma
L-Glutamic acid	Sigma
Hydrochloric acid	Sigma
Minimal Essential Medium Eagle	Sigma
Non-Radioactive Cell Proliferation Assay	Promega Corporation USA
Poly(ethylene glycol) (PEG) 2000	Aldrich, England
Poly(ethylene glycol) (PEG) 4000	BDH Limited, England
Poly(ethylene glycol) (PEG) 10000 linear	Fluka, Germany
Poly(ethylene glycol) (PEG) 10000 branched (four-armed)	JenKemTechnology,USA
Penicillin G sodium salt	Sigma
Potassium bromide	Sigma

Potassium chloride	Sigma
Propidium iodide	BD Biosciences, USA
Protamine sulphate salt	Sigma
Pullulan GPC polysaccharides standards	Polymer Laboratories, UK
Salmon calcitonin (sCT)	Polypeptide Laboratories AB, Sweden
Sodium acetate trihydrate	Sigma
Sodium bicarbonate	Sigma
Sodium chloride	Sigma
Sodium dihydrogen phosphate dihydrate	Merck, Germany
Sodium dodecylsulphate	Sigma
Sodium hyaluronate (HA)	Sigma
Sodium hydroxide	Sigma
Sodium pyruvate solution	Sigma
Sodium sulphate anhydrous	Fluka, Germany
Streptomycin sulphate	Sigma
Tetrahydrofuran	Sigma
Trehalose dihydrate	Sigma
Trehalose dihydrate suitable for cell culture	Sigma
Trehalose dihydrate endotoxin-free	Carbosynth, UK
Trifluoroacetic acid	Sigma
Tripolyposphate (TPP)	Fluka, Germany
Trypsin-EDTA solution	Sigma
Water (sterile-filtered, endotoxin tested)	Sigma

2.2 Methods

2.2.1 Ultrasonication

Ultrasonication of sodium hyaluronate (HA) solutions was performed with the aid of a 130 Watt ultrasonic processor (SONICS VC130PB, Sonics and Materials Inc., USA) equipped with the probe with diameter of 3 mm. Sonication was carried out at an amplitude of 80, which corresponds to power of 13W. Solutions of HA were transferred into a beaker immersed in an ice bath and processed with the ultrasonic probe. The duration of the ultrasonic treatment was 10, 30 minutes, 1, 1.5, 2, 4 and 6 hours. HA was optionally recovered by lyophilisation for gel permeation and cell culture experiments.

2.2.2 Gel Permeation Chromatography (GPC)

GPC studies were performed using an analytical system composed of LC-10 AT VD liquid chromatograph pump system, SIL-10 AD VP autoinjector, FCV-10 AL VP low pressure gradient flow-control valve, DGU-14A degasser, a Waters 410 refractive index (RI) detector with GPC for class VP (Version 1.02) and SCL-10A VP system controller (Shimadzu). The column used was Plaquagel –OH mixed 8 μm 300 × 7.5 mm (Polymer Laboratories Ltd., UK).

For HA samples, the composition of the mobile phase was similar to that recommended by column's manufacturer (Varian). The mobile phase was composed of 0.2 M NaCl (substitution for $NaNO_3$) and 0.01 M NaH_2PO_4 brought to pH 7.4 with NaOH solution. For chitosan, the mobile phase was composed of 0.33 M acetic acid and 0.2 M sodium acetate (adapted from Boryniec et al., 1997). The mobile phase flow rate in each case was 1 ml/min and the column and detector temperatures were set to 35 °C. Pullulan standards (PL Polymer Laboratoires, Germany), were used to construct the calibration curve. Standards and samples were prepared as 0.5-1 mg/ml solutions in the mobile phase and 100μl of samples or standards were injected in triplicate.

Data collection and integration were accomplished using Shimadzu CLASS-VP software (version 6.10) with GPC for Class VP (version 1.02).

2.2.3 ^{1}H- Nuclear Magnetic Resonance Spectroscopy (^{1}H-NMR)

For NMR experiments, HA and chitosan samples were dissolved in deuterium oxide at concentration of 1% w/v and analysed with the use of a Bruker Avance 400 NMR spectrometer. The chemical shifts are presented in parts per million (ppm). The degree of deacetylation of chitosan samples was determined by equation 2.1 (Hirai et al., 1991) using the integral intensity, ICH_3, of the CH_3

residue and the sum of integral intensities IH_2-H_6 of the H_2, H_3, H_4, H_5, H_6' and H_6 protons.

Degree of deacetylation (%) = $\{1-(\frac{1}{3}ICH_3 / \frac{1}{6}ICH_2 - H_6)\} \times 100$ Equation 2.1

2.2.4 Quantification of glutamic acid

The method for glutamic acid (glutamate) analysis was adapted from Afzal et al., (2002) and it was performed using a HPLC system as described in Section 2.3 using a SPD-10A VP photodiode array UV-VIS detector (Shimadzu) instead the RI detector. Samples and stock standard solution were prepared in 0.15% v/v aqueous solution of trifluoroacetic acid (TFA). Chitosan chloride solution prepared at the same concentration as chitosan glutamate was used as a control. 50 µl of the standard or sample were injected onto the Luna 5µ C18 (2) 250 × 4.6 mm column (Phenomenex). The flow rate of 1 ml/min using the mobile phase composed of 65% v/v of the aqueous phase (0.15% w/w TFA) and 35% v/v of tetrahydrofuran was employed. UV detection was carried out at 220 nm. The glutamate peak had a retention time of ~2.3 min. Data collection and integration were accomplished using Shimadzu CLASS-VP software (version 6.10).

2.2.5 Chloride determination (done by CMA)

Determination of the chloride ions was performed with a Dr Lange LCK 311 test. The test is based on the photometric determination (λ=468 nm, Dr Lange Lasa 100 spectrophotometer, Dr. Bruno Lange GmbH, Germany) of iron(III) thiocynate concentration formed by thiocynate ions released from mercury thiocynate reacting with the chloride ions.

2.2.6 Sodium content determination (done by CMA)

Inductively coupled plasma–mass spectrometry (ICP-MS) was used for sodium quantification in HA. A known weight of the sample was placed in a digestion vessels and reacted with 69% HNO_3 and 30% H_2O_2. The vessel was sealed and heated in a microwave digester operating at 1000 W for 20 minutes at 200 °C. The sample was then diluted with deionised water and the digest analysed by ICP-MS Varian 820.

2.2.7 Preparation of nanoparticles

2.2.7.1 Preparation of HA/CS carriers and HA/CS/sCT NPs

Solutions of HA with different molecular weights were first prepared at a concentration of 0.1 or 0.2% w/v in deionised water as described in Section 2.2.1. sCT was optionally dissolved in HA solution. Those solutions were then mixed with chitosan (CS) solution (CL113 0.1% or 0.2%, CL213, G113, G213 0.1% w/v in deionised water) at room temperature under magnetic stirring. A predefined aliquot of CS solution was added to a known volume of HA solution (the total polymer concentration (TPC) was either 0.1% w/v or 0.2% w/v) and stirring was maintained for 10 minutes to allow stabilisation of the system. A suspension of particles was instantaneously obtained upon mixing of polymer solutions, however in samples containing HA2882, HA1161, CL213 or G213 precipitation was also observed. The amount of precipitating flocs was estimated gravimetrically. The supernatant was carefully separated from the flocs by aspiration using a plastic dropper, while the remaining residue was dried overnight in a vacuum oven at room temperature and weighed.

Due to the dissimilar charge mixing ratio of polymers caused by the presence of different amounts of the counterion and deacetylation degree of chitosan, all figures presenting results pertinent to the above studies show the chitosan fraction and mass mixing ratio (HA/CS) on the horizontal axes. Samples were analysed in triplicate.

2.2.7.2 Preparation of HA/PROT carriers and HA/PROT/sCT NPs

The solution of HA prepared at concentration of 0.1 or 0.2% w/v in deionised water was sonicated for 0.5, 2 or 6 hours. sCT was optionally dissolved in HA solution.

4 ml of protamine sulphate aqueous solution of various concentrations (0.2-4.4 mg/ml) was added to 10 ml of HA solution at room temperature under magnetic stirring. The stirring was maintained for 10 minutes to allow stabilisation of the system. A suspension of particles was instantaneously obtained upon mixing of polymer solutions. Samples were analysed in triplicate.

2.2.7.3 Preparation of CHON-based NPs

CHON, PROT, CS and sCT were dissolved in deionised water at appropriate concentrations. Optionally, sCT solution was first added to CHON solution (to produce sCT-loaded NPs). CS or PROT solution was then added to CHON or CHON/sCT solutions/dispersions. A predefined aliquot of CS or PROT

solution was added to a known volume of CHON solution and stirring was maintained for 10 minutes to allow stabilisation of the system. A suspension of particles was instantaneously obtained upon mixing of polymer solutions. Samples were analysed in triplicate.

2.2.8 Separation of non-associated sCT

Non-associated sCT was separated from nanoparticles by a combined ultrafiltration-centrifugation technique (Centriplus YM-50, MWCO of 50 kDa for HA-based NPs or Amicon Ultra-15, MWCO of 30 kDa for CHON-based NPs; Millipore, USA). 5 ml of sample were placed in the sample reservoir (donor phase) of the centrifugal filter device and centrifuged for 1 hour at 3000 rpm for HA-based NPs, or in three cycles of 20 minutes at 3000 rpm for CHON-based NPs. After centrifugation the volume of the solution in the filtrate vial (acceptor phase) was measured with the use of an automatic pipette (X61319M, Gilson, France) and the filtrate was assayed for the content of sCT by HPLC as described in Section 2.2.10. This quantity of sCT was referred to as the non-associated sCT.

The nanoparticle suspension from the sample reservoir was made up to 5 ml with deionised water. 0.75 ml of the nanoparticle suspension from the sample reservoir was mixed with a predefined volume of 0.0001M NaOH to break up the nanoparticles and release sCT and centrifuged for 30 minutes at 13000 rpm. The supernatant was assayed for sCT content by HPLC (as described in Section 2.2.10) and this portion of the peptide was referred to as the extracted sCT. The rest of dispersion from the sample reservoir was analysed for particle size, zeta potential and transmittance as described in Sections 2.2.14 and 2.2.16, respectively. The particle size, zeta potential and transmittance as well as the pH (Section 2.2.18) and viscosity of nanoparticles (Section 2.2.15) before separation of the non-associated sCT was also measured.

Association efficiency (AE) and drug loading (DL) were calculated with the use of the following equations:

$$AE=[(A-B)/A]*100\% \qquad \text{(Eqn. 2.2)}$$

where A is the total amount (mass) of sCT and B is the mass of non-associated sCT

$$DL=[(A-B)/C]*100\% \qquad \text{(Eqn. 2.3)}$$

where C is the total weight of all the components of NPs.

2.2.9 Release studies

250 µl of NPs were added to 2.25 ml of PBS (HA-based NPs) or to 2.25 ml PBS or acetate buffer or diluted PBS or diluted acetate buffer (1:10 dilutions for both buffers were made) or 0.25M HCl or water (CHON-based NPs).

The composition of PBS was as follows: 137 mM NaCl, 2.7 mM KCl, 1.4 mM NaH_2PO_4, 1.3 mM Na_2HPO_4 were adjusted to pH 7.4 with NaOH solution.

The composition of acetate buffer (pH 5) was as follows: 1.48 mM CH_3COOH and 35.2 mM of CH_3COONa.

Samples were incubated at 37 °C at 100 rpm in a reciprocal shaking water bath model 25 (Precision Scientific, India). After 1, 2, 4, 6 and optionally 24 hours 2.5 ml samples were withdrawn and released sCT was separated a combined ultrafiltration-centrifugation technique as described in Section 2.2.8. The samples were centrifuged at 4500 rpm for 15 minutes. After centrifugation the volume of the solution from the filtrate vial (acceptor phase) was measured with the use of an automatic pipette (X61319M, Gilson, France) and the filtrate was assayed for the content of sCT by HPLC (released sCT, the HPLC method is described in Section 2.2.10).

The nanoparticle suspension from the sample reservoir was made up to 2.5 ml with PBS or other release medium and returned to the water bath to continue the release studies.

Release studies data was fitted to the first order equation:

$W=W_\infty(1-e^{-kt})$ (Eqn. 2.4)

where W is weight released at time t, W_∞ is the weight released at infinity, and k is the release rate constant using Origin ver. 7.5 software (Corrigan et al., 2006).

2.2.10 Quantification of sCT

The analysis of sCT content was performed using an HPLC system as described in Section 2.2.4. Standard solutions of sCT with appropriate concentrations were prepared in deionised water. 50 µl of the standard or sample were injected onto the Jones Chromatography Genesis 4µ C18 150 × 4.6 mm column. The flow rate of 1 ml/min using the mobile phase composed of 0.116% w/v NaCl, 0.032% v/v TFA, and 34% v/v acetonitrile was employed. UV detection was carried out at 215 nm. The sCT peak had a retention time of ~5 min. The calibration curve was linear in the concentration range of 1.5-50 µg/ml. Data collection and integration were accomplished using Shimadzu CLASS-VP software (version 6.10).

2.2.11 Physical stability of nanoparticles

Physical stability studies of the nanoparticle suspensions upon storage at room temperature were performed for a period of up to 4 weeks. Samples from each formulation were withdrawn periodically during studies and the particle size, zeta potential and transmittance (as described in Sections 2.2.14 and 2.2.16, respectively) were measured. In the case of CHON-based NPs, the results are shown as %, taking the initial value of a parameter as 100%. Samples were analysed in triplicate.

2.2.12 Stability studies of sCT-loaded HA/CL113 NPs

The formulation containing TPC of 1 mg/ml, HA/CL113 MMR of 5 and 0.1 mg/ml of sCT was prepared as described in section 2.2.7.1. Aliquots of the sample stored at 4 °C, room temperature (22 °C) and 37 °C were withdrawn after 1, 2 or 3 days of storage and analysed for AE, particle size (PS), polydispersity index (PDI), zeta potential (ZP) and transmittance (as described in Sections 2.2.8, 2.2.10, 2.2.14, and 2.2.16 respectively). The results are presented as the ratio of values measured after 1, 2 or 3 day-period of storage to the initial value of that parameter. Samples were analysed in triplicate.

2.2.13 Stability studies of CHON-based NPs in different buffers

The physical stability of NPs was examined in the following buffers/solutions: PBS, diluted PBS, acetate buffer, diluted acetate buffer, HCl solution (see Section 2.2.9). An aqueous suspension of CHON-based NPs was diluted with the appropriate buffer or solution in the ratio of 1:10 v/v (NPs:buffer/solution). Samples were characterised for PS, PDI, ZP (as described in Section 2.2.16) immediately after mixing and after 1 day of storage at room temperature. Samples were analysed in triplicate.

2.2.14 UV-Vis spectroscopy

2.2.14.1 Transmittance measurements

Transmittance of polymer solutions and nanoparticle formulations were measured using an UV-1700 PharmaSpec UV-Visible spectrophotometer (Shimadzu) at an operating wavelength of 500 nm in optically homogenous quartz cuvettes (Hellma) with the light path of 10 mm.

2.2.14.2 UV spectra of HA, sCT and HA/sCT solutions

For HA structural investigations UV spectra of 0.1% w/v HA solutions were recorded using the same spectrophotometer and cuvettes as above. For HA/sCT interactions, the spectra were recorded at 0.03 mg/ml of sCT and the HA/sCT MMR was 5. The absorbance values were measured at wavelengths range between 200 and 280 nm with a sampling interval of 1 nm.

2.2.15 Viscosity

Low frequency vibration viscometer (SV-10 Vibro Viscometer, A&D Company Limited) was employed to measure the viscosity of polymer solutions and nanoparticles suspensions at 25±0.2 °C. Samples were equilibrated at 25 °C in the water bath (Precision Scientific Reciprocal Shaking Bath Model 25, India) prior to the measurement. Three separate aliquots were prepared for each sample and at least three measurements were carried out for every aliquot. The mean value was taken as a result.

In order to examine potential HA/sCT or CL113/sCT interactions, Huggins' constant values were calculated based on dynamic viscosity measurements of three different concentrations of HA, CL113, and HA/sCT and CL113/sCT solutions. At first the relative viscosity (η_r) was calculated with the use of equation 2.5:

$$\eta_r=\eta/\eta_0 \qquad \text{(Eqn. 2.5)}$$

where η is the dynamic viscosity of the polymer solution, and η_0 is the dynamic viscosity of the solvent, i.e. water (0.89 mPa*s). Then the specific viscosity (η_{sp}) was determined based on equation 2.6;

$$\eta_{sp}=\eta_r-1 \qquad \text{(Eqn. 2.6)}$$

The concentration of the polysaccharide expressed in g/dL was plotted against the viscosity number, also referred to as reduced viscosity (η_{sp}/C), determined at a range of polymer concentrations and the intercept produced on extrapolation of the line to the ordinate yielded the constant- intrinsic viscosity (limiting viscosity number). The slope was the Huggins' constant.

2.2.16 Particle size and zeta potential analysis

The intensity-averaged mean particle size (particle size diameter) and the polydispersity index of the nanoparticles were determined by Dynamic Light Scattering (DLS) with the use of 173° backscatter detection and the electrophoretic mobility values measured by Laser Doppler Velocimetry (LDV) were converted to

zeta potential by the Smoluchowski equation. Both DLS and LDV measurements were done on a Zetasizer Nano series Nano-ZS ZEN3600 fitted with a 633 nm laser (Malvern Instruments Ltd., UK). Samples were placed directly into the folded capillary cells without dilutions. Each analysis was carried out at 25°C with the equilibration time set to 5 minutes. The readings were carried out at least three times for each batch and the average values of at least three batches are presented. The results obtained were corrected for sample viscosity. Particle size and zeta potential of sedimenting samples were measured in the supernatant after allowing the sample to equilibrate for 24 hours.

2.2.17 Morphology of nanoparticles

2.2.17.1 Transmission electron microscopy (TEM)

TEM was performed with the use of Jeol 2100 (Japan). Liquid samples were immobilised on copper grids and stained with either 1% w/v ammonium molybdate solution for 60 seconds or 1% w/v uranyl acetate solution for 30 seconds and dried overnight for viewing by TEM. The accelerating voltage was 200 kV.

2.2.17.2 Scanning electron microscopy (SEM)

SEM was carried out with a Zeiss Supra Variable Pressure Field Emission Scanning Electron Microscope (Germany) equipped with a secondary electron detector at 2 kV. Liquid samples were directly placed onto aluminium stubs, dried for 24 hours at ambient temperature in a desiccator over silica gel and sputter-coated with gold under vacuum prior to analysis.

2.2.18 pH measurements

An Orion pH meter (model 520A) equipped with an Orion Ross™ 8103SC glass body pH semi-micro electrode was used for pH measurements. The pH meter was calibrated using standard buffer solutions (Orion) of pH 4.00, 7.00 and 10.00 (±0.01).

2.2.19 Determination of the isoelectric point of nanoparticles

Particle sizer Zetasizer Nano series Nano-ZS ZEN3600 fitted with a 633 nm laser together with a MPT-2 autotitrator (Malvern Instruments Ltd., UK) were used to determine the isoelectric point of the nanoparticles. 0.25M HCl and 0.25M NaOH were used as titrants. 12 ml of nanoparticles suspension was added initially to the sample container. Each analysis was carried out at room temperature in automatic

regime using the target pH tolerance of 0.2 units. Three particle size and three zeta potential measurements were carried out for each pH value and the sample was recirculated between repeat measurements.

2.2.20 Freeze-drying of NPs

An appropriate amount of trehalose dihydrate, poly(ethylene glycol) (PEG, with molecular weight of 2,000 or 4,000 or 10,000 linear or 10,000 branched) or trehalose and PEG was added to nanoparticle suspension and dissolved. Aliquots of the formulation (4 ml) were dispensed into 15 ml Greiner plastic centrifuge tubes and frozen in liquid nitrogen. Tubes with frozen samples were placed in a VirTis wide mouth filter seal glass flasks and attached to one of the ports of manifold of a benchtop VirTis 6K freeze-dryer model EL (SP Scientific, USA). Vacuum of 29-31 mtorr was obtained by the use of an Edwards 5 RV5 rotary vane dual stage mechanical vacuum pump (Edwards, England). After 48 hours of freeze drying the tubes were removed and capped. Freeze drying was performed with at least three independent samples of each formulation. Sample reconstitution was performed by adding 4 ml of water (or serum-free medium for cell culture experiments) and manual, moderate shaking. Samples were analysed in triplicate.

The concentrations of trehalose presented in the thesis refer to trehalose dihydrate. They correspond to concentrations of anhydrous trehalose as shown in Table 2.1.

Table 2.1 Conversion of trehalose dihydrate to anhydrous trehalose concentrations.

Trehalose dihydrate [%, w/v]	Anhydrous trehalose [%, w/v]
0.1	0.09
0.2	0.18
0.5	0.45
1.0	0.91
2.0	1.81
3.0	2.72
4.0	3.62
5.0	4.53
7.0	6.35
11.0	9.96

2.2.21 Freeze-drying of HA solutions

Approximately 25 ml of solution of sonicated HA was transferred to 50 ml Greiner plastic centrifuge tubes and frozen in the freezer (Tricity, Denmark) at -20°. Tubes were then placed in a VirTis wide mouth filter seal glass flasks and freeze-dried as described in Section 2.2.20. Samples were analysed in triplicate.

2.2.22 Fourier transform infrared spectroscopy (FTIR)

Infrared spectra of HA or HA/CL113 NPs recovered by lyophilisation were recorded on a Nicolet Magna IR 560 E.S.P. spectrophotometer equipped with MCT/A detector, working under Omnic software version 4.1. A spectral range of 650-4000 cm^{-1}, resolution 2 cm^{-1} and accumulation of 64 scans were used in order to obtain good quality spectra. KBr disks method was used with 0.5-1% sample loading. KBr disks were prepared by direct compression under 8 bar pressure for 2 minutes.

2.2.23 Differential Scanning Calorimetry (DSC)

DSC experiments were conducted using a Mettler Toledo DSC 821^e with a refrigerated cooling system (LabPlant RP-100, UK). Nitrogen was used as the purge gas. Hermetically sealed aluminium pans with three vent holes were used throughout the study and sample weights varied between 2 and 7 mg. DSC measurements were carried out at a heating/cooling rate of 10°C/min. The DSC system was controlled by Mettler Toledo $STAR^e$ software (version 6.10) working on a Windows NT operating system.

2.2.24 Powder X-ray diffraction (XRD)

Powder X-ray diffraction analysis was conducted using a Rigaku Miniflex II desktop X-ray diffractometer (Rigaku, Japan) operating at 30 kV and 15 mA and fitted with a Haskris cooling unit. Ni-filtered Cu Kα radiation (λ=1.5408 Å) was used. Room temperature measurements were recorded for the range 5-40 2theta degrees at a step size of 0.05°/sec. A low background silicon mount (Rigaku, Japan) was used to support the sample during measurements.

2.2.25 Cell culture studies

Human colon adenocarcinoma cells (Caco-2) were obtained from European Collection of Cell Cultures. Cells were cultured in 75 cm^2 cell culture flasks in Eagle's Minimal Essential Medium (MEM), supplemented with 20% foetal bovine

serum, penicillin (0.006 mg/ml), streptomycin (0.01 mg/ml), gentamicin (0.005 mg/ml), sodium bicarbonate (2.2 g/l), sodium pyruvate (0.11 g/l), pH 7.4 (adjusted with NaOH or HCl solution if necessary) at 5% CO_2 and 37° humidified atmosphere (CO_2 incubator series 8000DH, ThermoScientific). Cells were supplied with fresh medium every second day and split after detaching with ethylenediaminetetraacetic acid (EDTA)-trypsin twice a week. For experimental purposes the passage number range was maintained between 20 and 30.

2.2.26 MTS assay

Caco-2 cells were seeded into flat-bottom 96-well plates in 100 µl of 20% MEM at a density of 25000 cells per well (cells were previously counted with the aid of Z1 Coulter Particle Counter, Beckman Coulter) and incubated at 37 °C for one day. The medium was then replaced with 100 µl of the sample dispersed or dissolved in serum-free media. After 72 hours of incubation, or 24 h when a serum-free medium at pH-5 was used, the supernatant was removed from the wells and replaced with serum-free media. 20 µl of the MTS reagent prepared according to the manufacturer protocol was then added into each well; in case of positive control (0% viability) the media was replaced by 10% SDS solution in serum-free media 30 min before the addition of MTS reagent. After 4 hours the UV absorbance of the formazan product was measured spectrophotometrically (FLUOstar Optima microplate reader, BMG Labtech) at 492 nm. Positive control was treated as a blank and its absorbance was subtracted from each reading. The cells viability was expressed as the ratio of the absorbance reading of the cells treated with different samples and for negative control (cells treated with serum-free (0%) MEM at pH=5.0 or pH=7.4), which was assumed to have 100% of the cells viability. IC_{50} values (concentrations required to reduce the viability of cells by 50% as compared with the control cells) were calculated by fitting the experimental points to the Hill equation (Goutelle et al., 2008). At least three different batches of samples were tested in cells with at least three different passage numbers.

2.2.27 Flow cytometry

The content of one 75 cm^2 flask of confluent Caco-2 cells was seeded into eight 25 cm^2 flasks, each containing Caco-2 cells suspended in 4 ml of 20% MEM. Cells were allowed to attach for 24-48 hours. The medium was then replaced with 3 ml of sample (sonicated HA). After 72 hours of incubation the supernatant was removed and cells were harvested with trypsin/EDTA. After neutralisation, the cells were combined with the previously removed supernatant and centrifuged (300 g, 5

minutes); the supernatant from centrifugation was discarded, and cells were washed with binding buffer (0.14M NaCl, 0.0025M $CaCl_2$ and 0.01M 4-(2-hydroxyethyl)-1-piperazineethanesulfonic acid (HEPES), pH 7.4 adjusted with NaOH solution). 20 µl of the cells suspension were stained with 5µl of APC-Annexin V, 5 µl of propidium iodide and diluted with 70 µl of binding buffer and incubated in dark at room temperature for 15 minutes. Then the cell suspension was further diluted with binding buffer, transferred to a flat bottom 96-wells plate and applied to flow cytometric analysis. All analyses were performed by a BD FACSArray™ bioanalyser (Becton Dickinson, UK). The instrument was set up to measure the size (forward scatter), granularity (side scatter) and cell fluorescence. Antibody binding was measured by analysing individual cells for fluorescence. The mean fluorescence intensity was determined after correction for cell autofluorescence. Fluorescence histograms were obtained for 10000 individual events. Data was analysed using BD FACSArray™ system software and expressed as a percentage of control fluorescence in arbitrary units. At least three different batches of samples were tested in cells with at least three different passage numbers.

2.2.28 Statistical analysis

All samples were analysed in at least in triplicate. The statistical significance of the differences between samples was determined using one-way analysis of variance (ANOVA) followed by posthoc Tukey's test. Minitab software was employed for all analyses. Differences were considered significant at $p<0.05$.

2.2.29 *In vitro* and *in vivo* studies of anti-inflammatory effects of HA/CL113/sCT NPs (chapter 9)

Experiments performed at UCD by Dr Sinéad Ryan

2.2.29.1 Sample preparation

HA (Mw of 257 kDa) was obtained by ultrasonicating a solution of native HA in deionised water, as described in section 2.2.1. Briefly, a predefined aliquot of CL113 solution made up in deionised water was added to a known volume of HA and sCT solution with stirring. A dispersion of NP was obtained instantly after adding CL113 solution to the HA/sCT liquid phase. The TPC was 1 mg/ml, HA/CL113 MMR was 5 and the final sCT concentration in the NP dispersion was 0.1 mg/ml. NPs were then freeze-dried with endotoxin free trehalose dihydrate dissolved in NPs dispersion at concentration of 4% (equivalent to 3.62% of anhydrous trehalose). Freeze-drying was performed as described in section 2.2.20.

2.2.29.2 Detection of endotoxins

The absence/quantification of endotoxins in samples administered to animals was performed with the aid of E-Toxate ^{TM} kit (*Limulus* amebocyte lysate, Sigma, catalogue number ET0200) following the manufacturer's protocol. The sensitivity limit of the kit was 0.05–0.1 endotoxin units (EU) per ml.

2.2.29.3 Tissue Culture and Reagents

Tissue culture reagents were obtained from BioSciences, Ireland. The sample composed of TPC of 1 mg/ml, HA/CL113 MMR of 5 and sCT of 0.1 mg/ml prepared at TCD according to Section 2.2.7.1 and freeze-dried with 4% of trehalose (Section 2.2.20) was tested. The cell lines SW1353, THP-1 and U937 were obtained from ATCC (USA). Human chondrosarcoma cells (SW1353), human macrophage cells (U937) and human monocytes (THP-1) were maintained in Roswell Park Memorial Institute (RPMI) 1640 medium containing 10% fetal calf serum, HEPES, and penicillin/streptomycin (Invitrogen, UK) at 37°C and 5% CO_2 in air. Cells were passaged with 0.25% trypsin/EDTA (Invitrogen, UK) and seeded on 6 well plates.

2.2.29.4 Effects of sCT, HA and HA/CL113/sCT NPs on mRNA expression of NR4As and MMPs in human chondrocytes, monocytes and macrophages

SW1353 chondrocytes, THP-1 monocytes and U937 macrophages were seeded on 6-well plates in serum-containing RPMI media. Phorbol-12-myristate-13-acetate (PMA) (20 ng/ml) was added to activate the THP-1 and U937 cells. After 24 hours, media was replaced with serum-free RPMI medium for overnight incubation. sCT (100 nM), HA (2.8 µg/ml) or HA/CL113/sCT NPs, as well as either of the stimulating agents, PGE_2 (1 µM) or IL-1β (10 ng/ml), were then added contemporaneously to cells in serum-free medium. The incubation lasted from 1-6 hours in order to capture the peak expression of NR4As and MMPs. Dexamethasone 21-phosphate disodium salt (Dex, 100 nM), was used as a positive control for down-regulation of NR4A2 and MMPs, while negative controls received serum-free medium. mRNA was then isolated from SW1353 cells using TRIzol® solution (Invitrogen, UK) according to the manufacturer's protocol. mRNA levels were determined by UV spectroscopy at wavelength of 260 nm. NR4A1, 2 and 3 and MMP1, 3 and 13 mRNA expression levels were measured by quantitative real time (qRT)-PCR and normalised to glyceraldehyde 3-phosphate dehydrogenase (GAPDH) expression.

2.2.29.5 Quantitative real-time reverse transcription (qRT)-PCR

2 µg of RNA were reverse-transcribed into cDNA using an oligo(dT) primer and Moloney murine leukemia virus reverse transcriptase (Invitrogen). qRT-PCR was conducted using SYBR Green Master Mix and an ABI PRISM 7900HT thermocycler (Applied Biosystems, UK). Duplicate reactions were analysed in 10 µl volumes containing 40 ng of cDNA and 0.2 µM primers. The real-time primers have been described previously: NR4A1, 2 and 3 (Bonta et al., 2006) MMP-1 (Wyatt et al., 2002) MMP-3 and -13 (Koshy et al., 2002) and glyceraldehyde-3-phosphate dehydrogenase(GAPDH) (Wyatt et al., 2002). Pre-designed TaqMan® primers for NR4A receptors were obtained from Applied Biosystems, UK. Relative mRNA expression levels were calculated using the $2^{-(ddc(t))}$ method with GAPDH as a control.

2.2.29.6 I.A. administration and assay of sCT formulations to K/BxN serum transfer murine model of inflammatory arthritis

Animal work was approved and performed under the guidelines of the Ethical Committee for the Use of Animals, Barts and the London School of Medicine and the UK Home Office in accordance with the UK Animals (Scientific Procedures) Act, 1986. 6-8 week old male BALB/c mice were injected intra-peritoneally (I.P.) with 150 µl serum and PBS from K/BxN mice to induce arthritis at day 0 (Monach et al., 2008; Christianson et al., 2012). The arthritis index was assessed on a scale of 0–3 with the following designations: 0 = no swelling or erythema; 1 = slight swelling or erythema; 2 = moderate erythema and swelling in multiple digits or entire paw; 3 = pronounced erythema and swelling of entire paw; 12 = maximum score per mouse. Mice that developed a clinical score >1 were administered test treatments. On day 1, mice were anaesthetized with isoflurane (3%) in nitrous oxide ($0.4\ l\ min^{-1}$) and oxygen ($0.2\ l\ min^{-1}$) using an IMS anaesthetic unit (Harvard Apparatus, Kent, UK). 5 µl of test treatment was administered by single I.A. injection to the left knee using a Hamilton syringe fitted with a 30-gauge needle. Treatments were: Control serum (negative control); sCT (0.2µg), sCT (0.2µg)-HA NP; Dex (0.2µg); K/BxN serum (positive control). The right knee of each mouse was injected with PBS (internal control). The arthritis index was assessed daily by knee diameter using dial calipers and all four paws were clinically scored using an established scoring system (Monach et al., 2010). Mice were sacrificed on day 4 after serum transfer and hind paws above the knee joint were harvested for histology to assess the effects of drug treatments on

inflammation, bone and cartilage degradation. Tissue samples from each hind paw were snap-frozen for RNA analysis and stored at -80°C.

2.2.29.7 Histology analysis

Hind paws or whole knee joints from sacrificed mice were harvested, dissected and fixed in 4% paraformaldehyde for 12 hours at 4 °C. Fixed tissues were de-calcified for 72 hours with agitation in formic acid and washed in water for 12 hours, followed by immersion in 4% paraformaldehyde and embedding in paraffin. 5 µm sections were mounted on slides and stained with hematoxylin and eosin (H&E) or Saffarin O. Histological sections were scored by an observer blinded to the treatment using different criteria (i) inflammation (synovitis infiltration and pannus formation), (ii) cartilage erosion and (iii) bone erosion on a scale of 0-3 (0, none; 1, minimal invasion of meniscus; 2, partial invasion of meniscus; 3, severe invasion of meniscus).

2.2.29.8 RNA extraction from mouse tissue and qRT-PCR analysis

Hind paw ankle joints were isolated and treated with RNA*later*®, flash frozen in liquid nitrogen and stored at -80 °C. 30mg of frozen ankle tissue was homogenised using Precellys® 24 ceramic bead technology (Bertin Technologies, Montigny-le-Bretonneux, France). RNA was isolated using the RNAeasy Plus® Mini kit (Qiagen, UK). Generation of cDNA and PCR were performed as described above. The oligonucleotide primers used for NR4A1, NR4A2 and NR4A3 and GAPDH were previously published (Bonta et al., 2006; Wyatt et al., 2002).

2.2.29.9 Statistical analysis

One-way ANOVA followed by Dunnet's post test was used for *in vitro* studies with $P < 0.05$ set as the limit of significance. For *in vivo* studies, two-way ANOVA with Bonferroni post tests were performed.

Experiments described in Sections 2.2.29.4 – 2.2.29.8 as well as statistical analysis described in section 2.2.29.9 were performed at UCD (Ireland) or Queen Mary University of London (UK) by Dr Sinéad Ryan.

3. Hyaluronic acid-chitosan nanoparticles

3.1 Introduction

Nanoparticles (NPs) are being extensively investigated for medical applications such as drug delivery systems, molecular diagnosis, medical imaging and tissue engineering (Emerich and Thanos, 2003). Recently, there is an increased interest in NPs composed of naturally occurring polymers such as polysaccharides or their derivatives due to their diverse structures, a large number of reactive groups, low toxicity, biodegradability and satisfactory stability (Liu et al., 2008). Such polymers are generally intended to be used solely as carriers for the delivery of bioactive substances (Janes et al., 2001), however some of the polysaccharides are known to possess pharmacological and functional properties as well. Examples of those polymers include chitosan (CS) and hyaluronic acid (HA) and their applications in nanomedicine could be multifold.

CS nanoparticles have been shown to improve the oral bioavailability of peptide and protein formulations as the positive charge of CS influences its reactivity with negatively charged surfaces, e.g. cell and mucosal membranes and it has permeability enhancing properties (Agnihotri et al., 2004). HA is present in the components of extra-cellular matrix of connective tissues and its action *in vivo* depends on the polymer size. Large (400-20,000 kDa) HA chains suppress angiogenesis and inhibit phagocytosis, while oligomeric hyaluronan fragments are angiogenic, immuno-stimulatory and inflammatory (Stern et al., 2006). Hyaluronic acid also interacts specifically with cell-surface receptors, e.g. CD44 and it has previously been used in the treatment of cancer cells over-expressing CD44 (Choi et al., 2010). Also, HA acts in synergy with CS to enhance mucoadhesion (Wadhwa et al., 2009). Thus combining HA and CS into a nanoparticle may be a useful approach to form functional and also targeted delivery systems.

Although NPs containing HA and CS have been studied (Boddohi et al., 2009; de la Fuente et al., 2008 a, b), further research is required, as to the best of our knowledge, no systematic screening of factors leading to the formation of such NPs with predictable properties has been published to date.

In many of the published investigations the use of a crosslinker (tripolyphosphate, TPP) was essential to obtain NPs (de la Fuente et al., 2008a, Oyarzun-Ampuero et al., 2009). However, high concentrations of TPP have been found to be unfavourable as TPP neutralises the positive charge of chitosan, which may lead to aggregation of such NPs (Wadhwa et al., 2009). Boddohi et al. (2009)

on the other hand, managed to obtain HA/CS NPs without TPP, however aggregation of the particles was observed and NPs were recovered only after leaving the suspensions to settle overnight.

In this work we attempted to manufacture cross-linker free and stable NPs composed of only HA and CS. To achieve this goal, we comprehensively investigated the manufacturing process of HA/CS NPs including examination of polymer molecular weights, the type of chitosan salt, polymer mixing ratio and total polymer concentration. The physical stability of the nanoparticle dispersion on storage at room temperature and upon the exposure to different pH values was also examined. Cytotoxicity of selected HA/CS NPs was evaluated in the Caco-2 cell line. With the recent advent of the quality by design approach adopted by the pharma industry (ICH guideline Q8, 2009), such methodical studies will become a necessity if any nanoparticulate system is to reach to the manufacturing stage.

3.2 The physicochemical properties of polymers and the influence of ultrasound on physicochemical properties of HA

The physicochemical properties of the various types of chitosan and hyaluronic acid 'as received' are presented in Table 3.1. All chitosan salts were characterised by a degree of deacetylation higher than 80%. The molecular weight of G113 and CL113 was lower compared to G213 and CL213 (approximately 100 kDa and 350-400 kDa, respectively). The content of counterion was 15% in chloride salts and 30% in glutamate salts.

Hyaluronic acid, on the other hand, had a high molecular weight (2882 kDa) and low counerion content (3.6%).

Table 3.1 Physicochemical characteristics of chitosan salts and native HA used in the studies. DD – degree of deacetylation according to manufacturer's data, DD NMR - degree of deacetylation calculated from nuclear magnetic resonance data, Mn - number average molecular weight, Mw - weight average molecular weight

Polymer	Counter ion	Counter ion content	DD	DD NMR	Mn [kDa]	Mw [kDa]	Mw/Mn
HA	Na^+	3.6%	N/A	N/A	772±9.77	2882±24.50	3.73±0.064
CL113	Cl^-	15.5%	83%	83.5 %	33 ±7.33	110±6.78	3.38±0.544
CL213	Cl^-	14.0%	86%	79.8 %	113±1.81	340±13.62	3.01±0.169
G113	glutamate	30.6±3.08 %	86%	N/A	35±1.93	115±14.16	3.27±0.224
G213	glutamate	30.4±2.94 %	86%	N/A	227±21.9	398±37.29	1.75±0.004

The viscosity and GPC results showed that HA with initially high molecular weight (2882±24.50 kDa) was effectively depolymerised even after a relatively short exposure (i.e. 10 minutes) to ultrasound (Table 3.2). The viscosity of 0.1% w/v solution of native HA was about 17 times higher than the viscosity of water at 25 °C (Table 3.2). Ultrasonication resulted in a reduction of the viscosity of HA solution depending on the duration of exposure (Table 3.2). The decrease in viscosity of HA was very rapid during the first 30 min and decelerated when sonication was maintained for longer times (1-6 hours). Ultrasonic treatment also resulted in the reduction of the molecular weight of HA (Mn and Mw) as a result of depolymerisation (Table 3.2).

The native HA was heterogeneous in terms of molecular weight distribution and had a high polydispersity of approximately 3.73 (Table 3.2), however even a short sonication time (10 minutes) caused a significant drop in the polydispersity index (Mw/Mn) leading to an increase in the polymer molecular weight homogeneity. After 30 minutes of sonication the decrease in Mw/Mn values was still noticeable, however with a further increase in the sonication treatment the decrease in heterogeneity of the polymer became less pronounced (Table 3.2).

Table 3.2 Physicochemical parameters of native and sonicated HA. Symbols as in Table 3.1.

Sonication time of HA [hrs]	Sample name	Dynamic viscosity [mPa*s]	Mn [kDa]	Mw [kDa]	Mw/Mn
0	HA2882	15.49±0.815	772±9.77	2882±24.50	3.73±0.064
0.17	HA1161	8.33±0.434	409±9.45	1161±35.99	2.84±0.125
0.5	HA590	4.13±0.225	238±9.45	590±20.44	2.43±0.043
1	HA343	2.91±0.179	145±6.93	343±14.40	2.36±0.044
1.5	HA292	2.37±0.133	128±4.89	292±6.68	2.28±0.039
2	HA257	2.14±0.162	118±4.89	257±8.43	2.18±0.042
4	HA201	1.72±0.025	96±2.51	201±3.40	2.08±0.019
6	HA176	1.49±0.233	86±1.09	176±4.32	2.05±0.028

Ultrasonication has been reported as a simple and efficient method of obtaining HA of lower molecular weight from the original high molecular weight compound (Lapčík et al., 1998). It is generally accepted that mechanical force is the factor causing depolymerisation of HA during a sonication process. Depolymerisation by ultrasonication depends on the process parameters and it is characterised by a limiting molecular weight (Miyzaki et al., 2001). Indeed, we

observed that after 4 and 6 hours of sonication the reduction in the molecular weight, although significant (p-value=0.0014), was less apparent than compared with the first 30 minutes of sonication. Drimalova et al. (2005) reported that prolonged sonication of HA results in a gradual depolymerisation levelled to a limiting molecular weight of 100 kDa. Based on those findings, it can be assumed that applying the current sonication conditions, the molecular weight of 176 kDa for HA obtained after 6 hours of sonication is close to the limiting molecular weight value and a further increase in sonication time would not decrease the molecular weight markedly.

Structural changes in sonicated HA were investigated by H^1NMR, FTIR and UV. H^1NMR showed viscosity dependent intensities of the spectra (data not shown), consistent with the report of Alkrad at el. (2003), however no peak shifts were observed. FTIR spectra of HA, pre- and post- sonication, were very similar indicating no other than molecular weight changes in the polymer structure (Fig. 3.1). No shifts of the asymmetric COO^- stretching band at 1616 cm^{-1} nor the amide I vibration at 1653 cm^{-1} (Bezakova et al., 2008) were discerned, however the originally broad and asymmetric absorption at 3100-3600 cm^{-1} assigned to the hydrogen bonding amine and hydroxyl groups of HA appeared to broaden even more when the HA was subjected to sonication. This in contrast to observations of (Bezakova et al., 2008), where narrowing of the H-bond band, assigned to a decrease in hydrogen-bond strength, was noticed as a result of depolymerisation by microwave irradiation. The increase in strength of H-bonds observed in this work can perhaps be explained by increased entropy of the system resulting from shortening the polymer chains, thus enabling better mutual accessibility of H-bond donor and acceptor groups. UV analysis also suggested minor structural differences when comparing native and sonicated HA, visible as slight differences in slopes of the spectra (data not shown), nevertheless no extra absorption bands appeared suggesting decomposition (Drimalova et al., 2005). Therefore it was concluded that sonication only decreased the molecular weight of HA without introducing structural damage to the polymer.

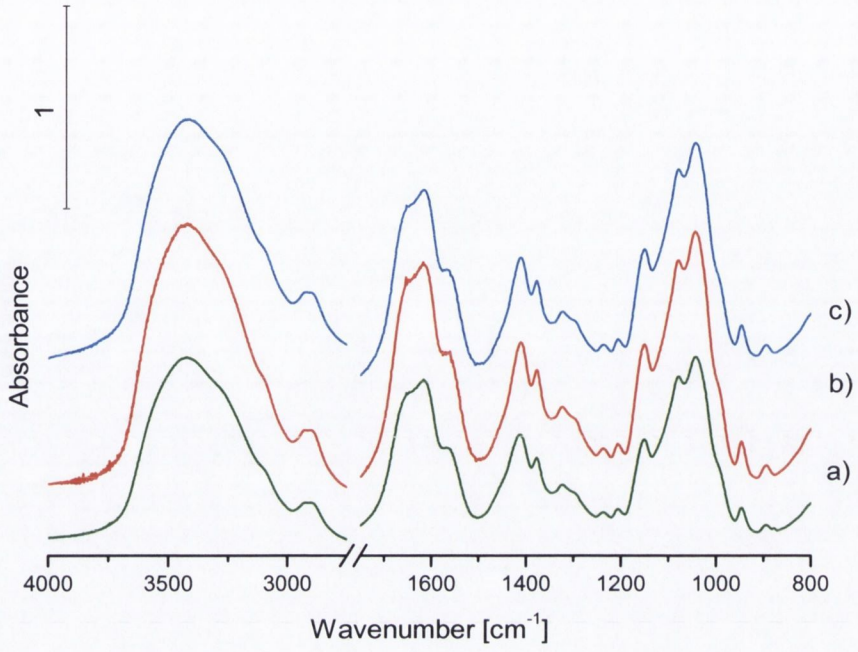

Fig.3.1 FTIR spectra of a) native HA and HA sonicated for b) 2h and c) 6h.

3.3 HA/chitosan nanoparticles – formation and formulation variables

3.3.1 Impact of HA molecular weight

To examine the influence of the molecular weight of HA on the formation and properties of HA/CS nanoparticles, HA polymers with different molecular weights obtained by the sonication process (Section 3.2) were used. Three different HA/CL113 mass mixing ratios with total polymer content (TPC) of 1 mg/ml were selected. The HA/CL113 mass mixing ratio (MMR) of 1 resulted in the formation of positively charged NPs, while ratios of 2.5 and 5 resulted in negatively charged NPs (Fig. 3.2). NPs with an MMR of 5 were observed to have generally lower zeta potential values compared to those based on an MMR of 2.5 for all molecular weights of HA studied.

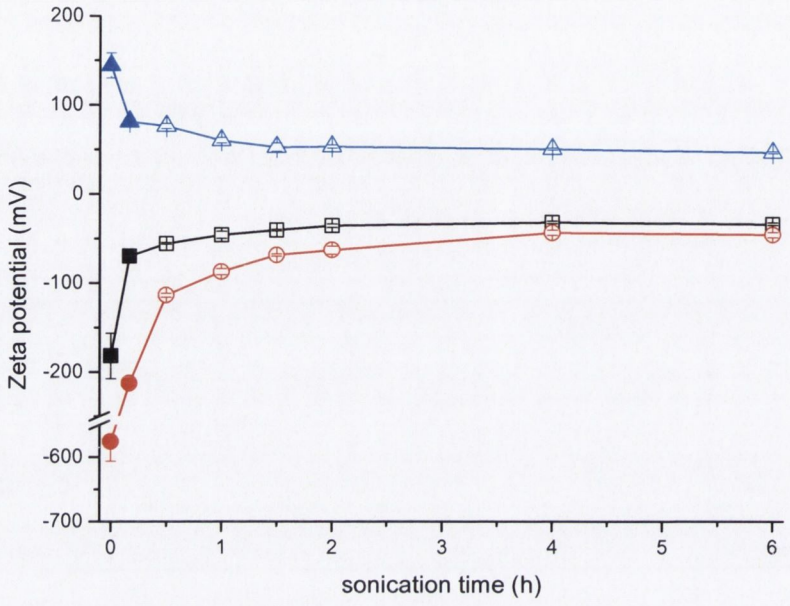

Fig.3.2 Zeta potential of NPs formulated with HA sonicated for various time periods and CL113. TPC was 1 mg/ml. Circles – HA/CL113 with MMR of 5, squares - HA/CL113 with MMR of 2.5 and triangles - HA/CL113 with MMR of 1. Filled symbols indicate flocculating and sedimenting samples, while empty symbols indicate neat NP dispersions.

When either native HA (HA2882) or HA sonicated for 10 minutes (HA1161) was used, the formation of NPs was accompanied by the presence of visually large flocs for all three MMRs (Fig. 3.3).

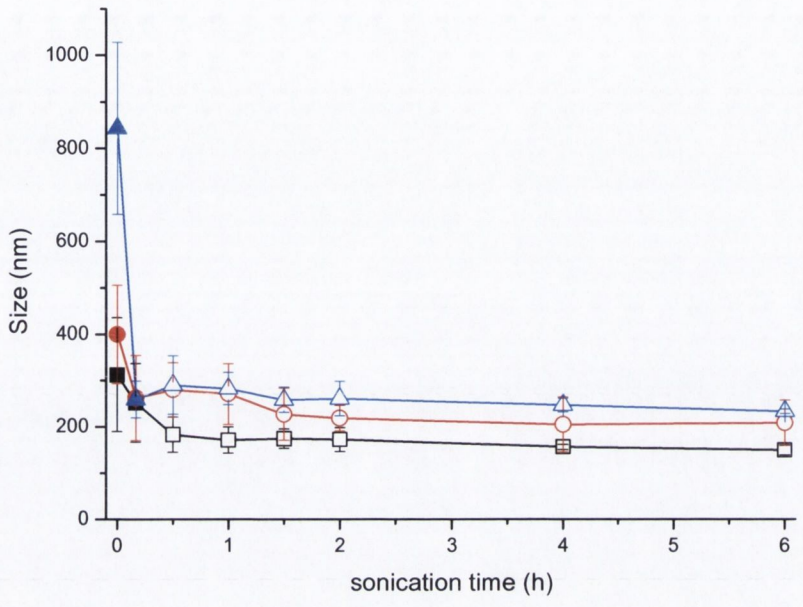

Fig.3.3 Particle size of NPs formulated with HA sonicated for various time periods and CL113. TPC was 1 mg/ml. Circles – HA/CL113 with MMR of 5, squares - HA/CL113 with MMR of 2.5 and triangles - HA/CL113 with MMR of 1. Filled symbols indicate flocculating and sedimenting samples, while empty symbols indicate neat NP dispersions.

SEM analysis of the precipitate revealed that those flocs were not composed of discreet nanoparticles or even microparticles, but rather formed a bed of material with a rough surface (Fig. 3.4 a). The amount of precipitating flocs was 26.5±3.0% and 24.2±0.6% of the overall particulates formed when native HA was used to prepare NPs with MMR=5 and MMR=1, respectively, while for HA1161 it was 27.1±10.7% and 29.0±0.5% for MMR=5 and MMR=1, respectively.

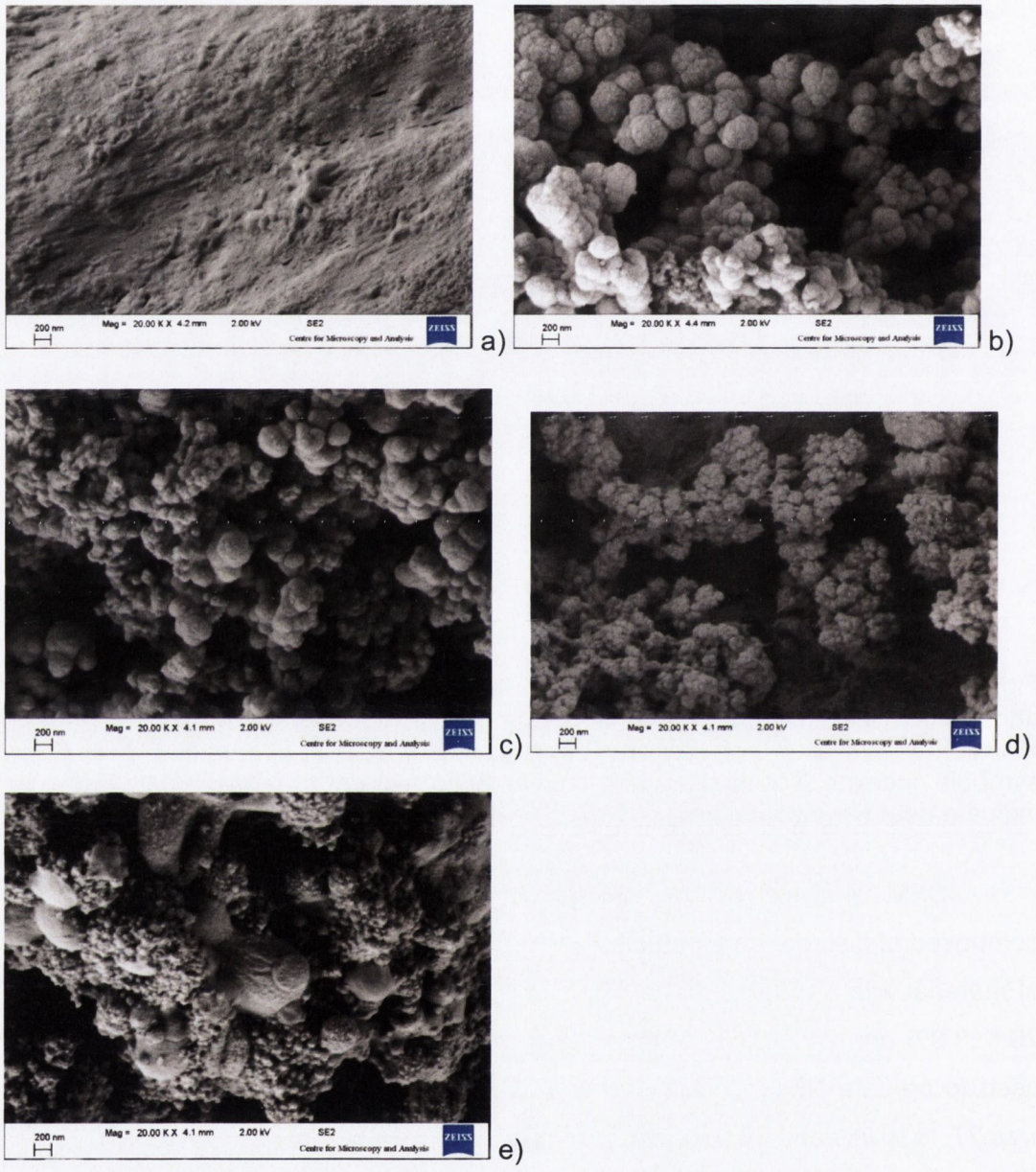

Fig. 3.4 Scanning electron micrographs of: a) HA2882/CL113 MMR=2.5, b) HA257/CL113 MMR=2.5, c) HA257/CL213 MMR=2.5, d) HA257/G213 MMR=2.5 and e) HA257/CL113 MMR=1.7 (CMR=1). TPC of 1 mg/ml was used in all cases.

Formulations with HA sonicated for shorter periods (especially 30 minutes, HA590) were more turbid compared to formulations with HA of lower molecular weights (Fig. 3.5). Since the theoretical yields of NPs formed using HA sonicated for different times should be the same, as identical amounts of HA were used, the differences in transmittance may be related to changes in particle size due to the higher molecular weight of HA used. As both HA and chitosan are polymers with

high molecular weight, and their solutions in water are viscous, the high viscosity may impair the mixing process and so favour the formation of aggregates (Mackay et al., 2006). The sonication process, and thus the reduction of the molecular weight of HA, renders the solution less viscous (Table 3.2). The formulation with a HA/CL113 MMR of 5 was more transparent than those with MMRs of 2.5 and 1 for the whole range of molecular weights of HA examined.

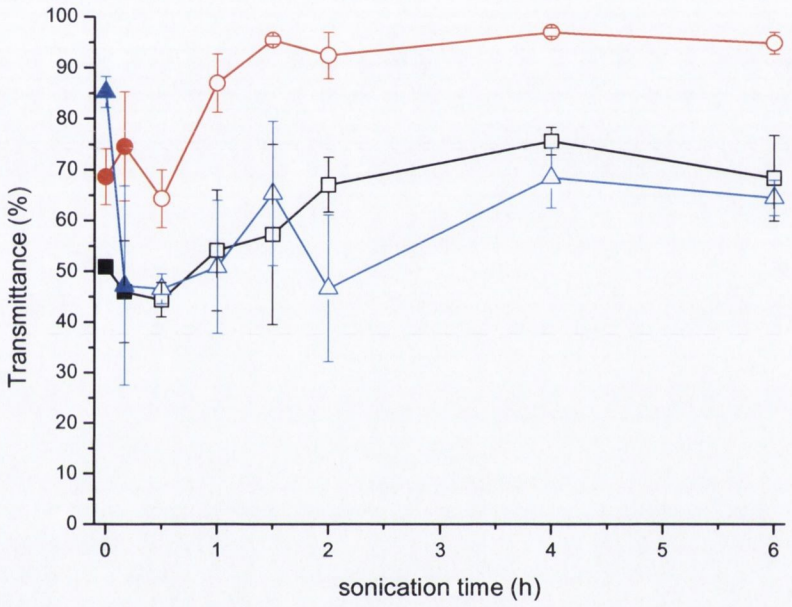

Fig.3.5 Transmittance of NPs formulated with HA sonicated for various time periods and CL113. TPC was 1 mg/ml. Circles – HA/CL113 with MMR of 5, squares - HA/CL113 with MMR of 2.5 and triangles - HA/CL113 with MMR of 1. Filled symbols indicate flocculating and sedimenting samples, while empty symbols indicate neat NP dispersions.

For all the HA/CL113 MMRs tested (5, 2.5 and 1) sonication of HA used for preparation of the NPs for at least 30 minutes resulted in a decrease in the particle size (Fig. 3.3) and no aggregation was seen to occur (Fig. 3.5). SEM showed well-developed nanostructures when HA257 was used (Fig. 3.4 b). No further change in the particle size was observed when HA was sonicated for up to 6 h (HA176). Generally, PDI values (Fig. 3.6) and zeta potential (Fig. 3.2) also decreased with the increase of the duration of sonication of HA. The reduction in the absolute values of zeta potential is more pronounced when HA solutions sonicated for shorter periods were used and this can be observed in negatively as well as positively charged particles. Since the pH of the formulations was not seen to be affected by the molecular weight of HA and was approximately 5.8 and 4.4 for all negatively and positively charged samples, respectively, variations in zeta potential

values could be explained by a limited ability of the polymer chains to mix effectively due to high viscosity, thus forming large entities having different arrangement of polymers on the surface compared with NPs.

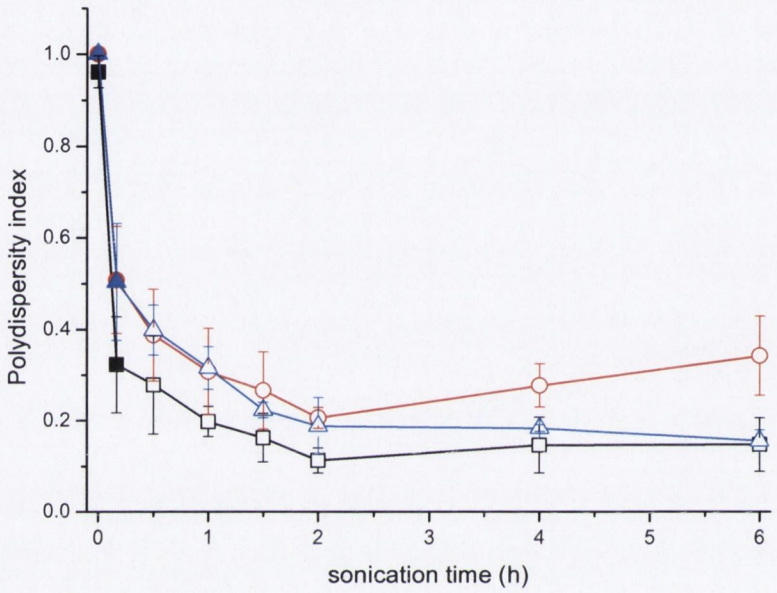

Fig.3.6 Polydispersity index of NPs formulated with HA sonicated for various time periods and CL113. TPC was 1 mg/ml. Circles – HA/CL113 with MMR of 5, squares - HA/CL113 with MMR of 2.5 and triangles - HA/CL113 with MMR of 1. Filled symbols indicate flocculating and sedimenting samples, while empty symbols indicate neat NP dispersions.

When the duration of ultrasound treatment was increased to 30 minutes and more, it was possible to obtain nanoparticles without the tendency to sediment for at least 24 hours. HA with a molecular weight of 257 kDa, obtained by sonication of native HA for 2h, was used in subsequent studies since its molecular weight appeared to provide the optimum balance between the viscosity of HA solution, leading to the production of non-sedimenting NPs, as well as sonication time.

3.3.2 Impact of chitosan molecular weight and type of counterion

Formation of particles of different sizes including large, fast sedimenting flocs and NPs was observed when high molecular weight salts of chitosan were used (CL213 and G213). It appeared that the flocculating structures in both cases were made of NPs (Fig. 3.4 c and d), but the particulates formed by HA/G213 were irregular and formed cauliflower-like assemblies. The samples were allowed to

settle overnight to remove aggregated particles and any NPs remaining in the liquid after 24 h were subsequently characterised. CL113 and G113 produced stable NP dispersions with the exception of MMRs corresponding to charge mixing ratios (CMR) of approximately 1 (see Section 3.3.3).

It was noticed that, even after sedimentation of aggregates, transmittance of CL213 NPs was smaller than CL113 NPs, which did not form sedimenting particles (Fig. 3.7). That may suggest that when chitosan with a higher molecular weight was used, more particles were formed. When the polymer chain is longer, there are more amino groups to interact with carboxyl groups of HA leading to precipitation of the interacting polymer chains as nanoparticles or aggregates.

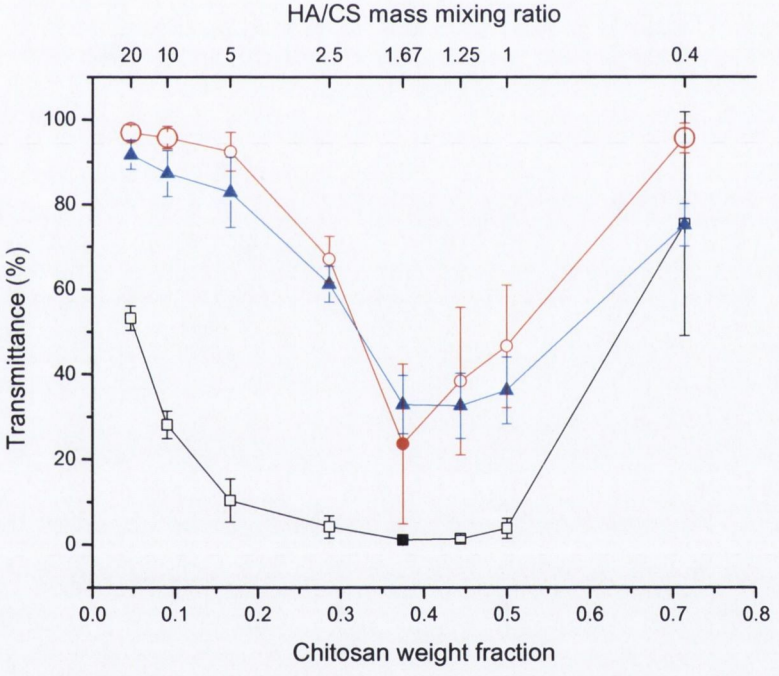

Fig. 3.7 Transmittance of HA/CS chloride NP systems. HA molecular weight was 257 kDa. Squares – HA/CL113 with TPC of 2 mg/ml, circles - HA/CL113 with TPC of 1 mg/ml, upward triangles - HA/CL213 with TPC of 1 mg/ml. All lines are for visual guidance only. Filled symbols indicate data for flocculating and sedimenting samples obtained after standing samples for 24 h, while empty symbols indicate data obtained immediately after preparing the dispersions. Small empty symbols indicate visually opalescent NP dispersions and large empty symbols indicate dispersions visually transparent.

The transmittance values were similar when G213 (after sedimentation) and G113 were studied and for cationic G213 NPs the transmittance was lower than for G113 NPs, consistent with reduced concentration of NPs due to removal of particles (Fig. 3.8).

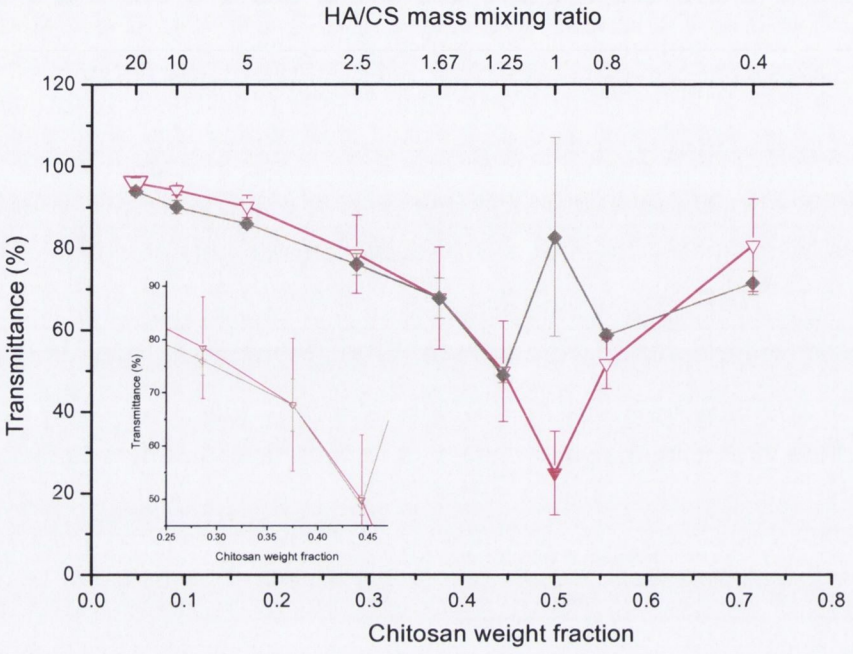

Fig. 3.8. Transmittance of HA/CS glutamate NP systems. HA molecular weight was 257 kDa. Downward triangles - HA/G113 with TPC of 1 mg/ml and diamonds - HA/G213 with TPC of 1 mg/ml. All lines are for visual guidance only. Filled symbols indicate data for flocculating and sedimenting samples obtained after standing samples for 24 h, while empty symbols indicate data obtained immediately after preparing the dispersions. Small empty symbols indicate visually opalescent NP dispersions and large empty symbols indicate dispersions visually transparent. Inset is for clarity purposes.

Comparing chitosan glutamate and chloride NPs, it was observed that the glutamate NPs were more negatively charged (Fig. 3.9). Since the glutamate contains two carboxylic and one amino residues with pKa values of 2.19, 4.25 and 9.67 (Stahl, Wermuth, 2008), respectively, it exists as a negatively charged deprotonated carboxylate at pH above 5. Hence it can be assumed that not only the chitosan chains, but also the counterion can be involved in the formation of NPs and become incorporated into the particulate. The amount of the glutamate counterion entrapped in the NPs was quantified to be 10.35±0.29% w/w for HA/G113 NPs with MMR=1.67 and 12.50±0.38% w/w for HA/G113 NPs with MMR=0.8. A careful selection of the polymer salt is therefore advised.

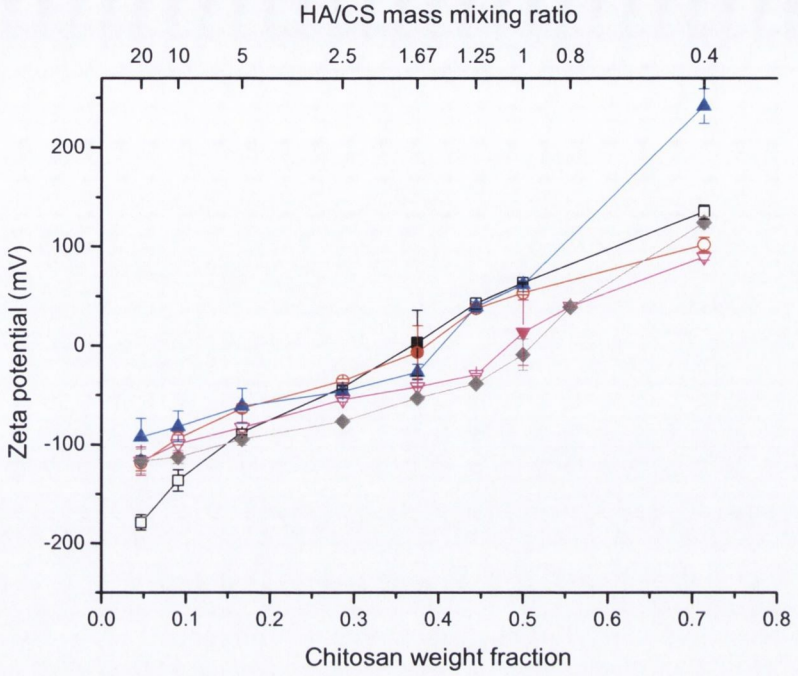

Fig.3.9 Zeta potential of various HA/CS NP systems. HA molecular weight was 257 kDa. Squares – HA/CL113 with total polymer concentration (TPC) of 2 mg/ml, circles - HA/CL113 with TPC of 1 mg/ml, upward triangles - HA/CL213 with TPC of 1 mg/ml, downward triangles - HA/G113 with TPC of 1 mg/ml and diamonds - HA/G213 with TPC of 1 mg/ml. All lines are for visual guidance only. Filled symbols indicate data for flocculating and sedimenting samples obtained after standing samples for 24 h, while empty symbols indicate data obtained immediately after preparing the dispersions.

Even after sedimentation of aggregates, the particle size (Fig. 3.10) and polydispersity indices (Fig. 3.11) of CL213 and G213 NPs were greater than CL113 and G113 NPs, suggesting unsuitability of polymers with high molecular weight for the manufacture of stable NP carriers.

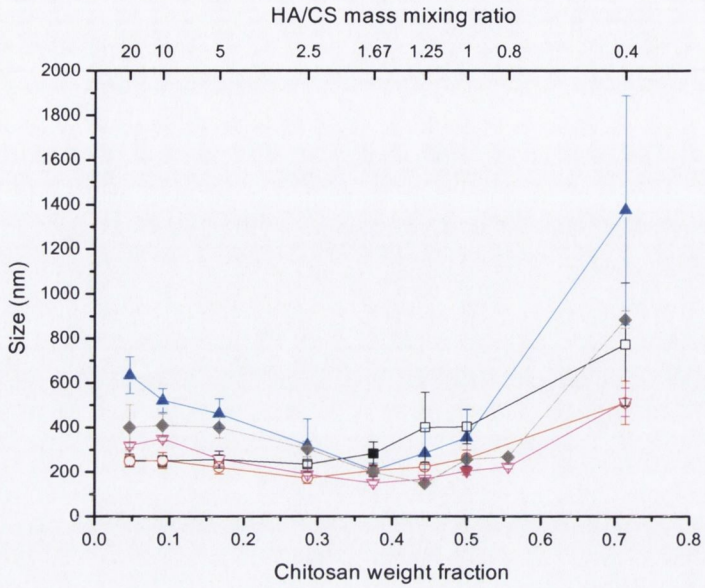

Fig.3.10 Particle size of various HA/CS NP systems. HA molecular weight was 257 kDa. Squares – HA/CL113 with total polymer concentration (TPC) of 2 mg/ml, circles - HA/CL113 with TPC of 1 mg/ml, upward triangles - HA/CL213 with TPC of 1 mg/ml, downward triangles - HA/G113 with TPC of 1 mg/ml and diamonds - HA/G213 with TPC of 1 mg/ml. All lines are for visual guidance only. Filled symbols indicate data for flocculating and sedimenting samples obtained after standing samples for 24 h, while empty symbols indicate data obtained immediately after preparing the dispersions.

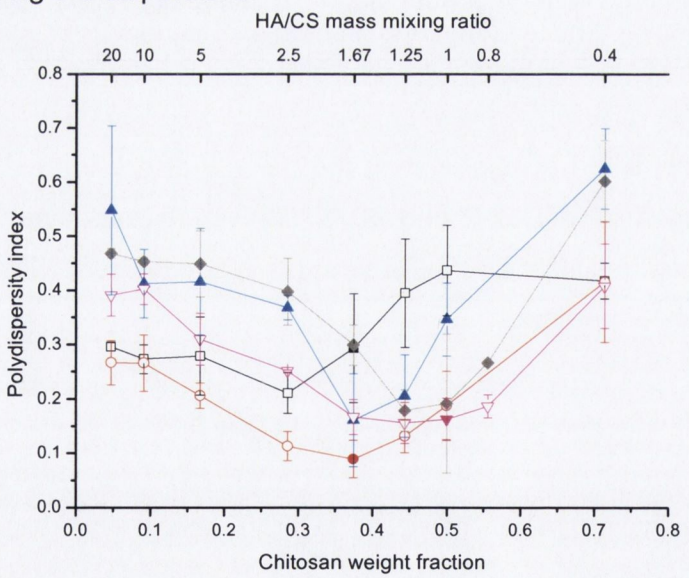

Fig.3.11 Polydispersity index of various HA/CS NP systems. HA molecular weight was 257 kDa. Squares – HA/CL113 with total polymer concentration (TPC) of 2 mg/ml, circles - HA/CL113 with TPC of 1 mg/ml, upward triangles - HA/CL213 with TPC of 1 mg/ml, downward triangles - HA/G113 with TPC of 1 mg/ml and diamonds - HA/G213 with TPC of 1 mg/ml. All lines are for visual guidance only. Filled symbols indicate data for flocculating and sedimenting samples obtained after standing samples for 24 h, while empty symbols indicate data obtained immediately after preparing the dispersions.

3.3.3 Impact of polymer mixing ratio

Generally, negatively charged particles (Fig. 3.9) were obtained at high HA contents and their sizes at first decreased slightly or did not change significantly with decreasing HA/CS ratio, however when the polymer's MMR was approaching the charge equivalence point ($n^-/n^+=1$), the particle size rapidly increased and large aggregates were formed consistent with a decrease in particle repulsion as the net surface charge decreased. It was impossible to measure the properties of such systems immediately after preparation, thus the sedimenting samples were characterised after standing for 24h and removing the precipitate (data for those samples is presented as filled symbols in Figs. 3.9 and 3.10). With a further decrease in MMR the particles formed had positive zeta potential values (Fig. 3.9). A similar tendency as that for the size was observed for PDI values (Fig. 3.11); generally they decreased with increasing content of chitosan (but for formulations with high excess of HA the changes are not significant), then reached the minimum just before the inversion of the particle charge, when the charge mixing ratio was close to 1, to increase again with a further increase in the chitosan content.

HA and CS are polyelectrolytes which are able to dissociate in aqueous solutions, resulting in charged polymer chains. For HA, the charge is produced upon dissociation of the carboxylic groups in D-glucuronic acid (pKa of 3.23) and the pKa of HA was estimated to be 2.9 (Lapčik et al., 1998). The pKa value of the amino group of CS is approximately 6.5, therefore in acidic media these amino groups undergo protonation and chitosan becomes a polycation. Furthermore, the charge density (number of charged groups per gram of polymer) of chitosan depends also on its deacetylation degree (Boddohi et al., 2008). It is known that when the polymer charge mixing ratio (CMR) is 1, opposite charges are neutralised and aggregation as well as phase separation is expected to occur (Nizri et al., 2004). The MMR values were hence converted into the equivalent CMRs considering the counterion content, the degree of deacetylation for chitosan and environmental pH.

Based on experimental values, the CMR corresponding to complete polymer charge neutralisation for HA/CL113, HA/CL213, HA/G113 and HA/G213 were 1.05, 1.02, 0.80 and 0.71, respectively, corresponding to MMRs of 1.56, 1.41, 1.02 and 0.94, respectively. Thus only the NPs based on chitosan chloride, but not the glutamate salt, had CMRs close to 1. That deviation of CMR from 1 for HA/G is supportive of the proposed above hypothesis that the glutamate residue is in fact incorporated into the particles and does not act as a counterion only. Distinct zones of NP formation and phase separation and aggregation were also determined

visually. When a large excess (in terms of CMR) of one of the polymers was used, the sample had an appearance of a solution. With the quantities of polymers approaching the CMR of 1, the systems first became opalescent, then turbid and finally the NPs were seen to aggregate. Visual observations were confirmed by transmittance measurement (Fig. 3.7 and 3.8). SEM revealed that at CMR=1 the particle size of formed NPs was very broad and microparticles as well as NPs were formed (Fig. 3.4 e).

The type of interactions between the NP constituents was investigated by infrared spectroscopy. FTIR spectra of pure HA and CS showed characteristic bands of ionised polymers, as the polymers used to prepare NPs were sodium and chloride salts, respectively. CS spectrum (Fig. 3.12) presented bands at 3418 cm^{-1} of –OH and –NH stretching, 1634 cm^{-1} of amide I, 1521 cm^{-1} of $-NH_3^+$, 1414 cm^{-1} of $-CH_2$ bending and 1154 cm^{-1} of antisymmetric C–O–C stretching (Peniche et al., 2007; Lawrie et al., 2007). FTIR spectrum of HA (Fig. 3.12) showed peaks at 3407 cm^{-1} of –OH and –NH stretching, 1653 cm^{-1}, 1616 cm^{-1} as well as 1567 cm^{-1} of amide I and $-COO^-$ (as described in section 3.1), 1412 cm^{-1} of $-CH_2$ bending and 1154 cm^{-1} and 1079 cm^{-1} of antisymmetric C–O–C stretching (Denuziere et al., 1996). The infrared spectrum of the 1:1 w/w CS:HA physical mixture (PM) was dominated by the characteristic vibrations of HA (Fig. 3.12), however small differences in the position and appearance of some of the absorption bands of PM were seen in comparison to NPs. The latter had a characteristic broad band at 1629 cm^{-1} of amide I and $-COO^-$, while the band at 1562 cm^{-1} was shifted and less prominent compared to that of pure HA (Fig. 3.12). Therefore it can be concluded that the polymers retained their ionic character in the NPs and that the type of intermolecular interaction is mainly of electrostatic nature.

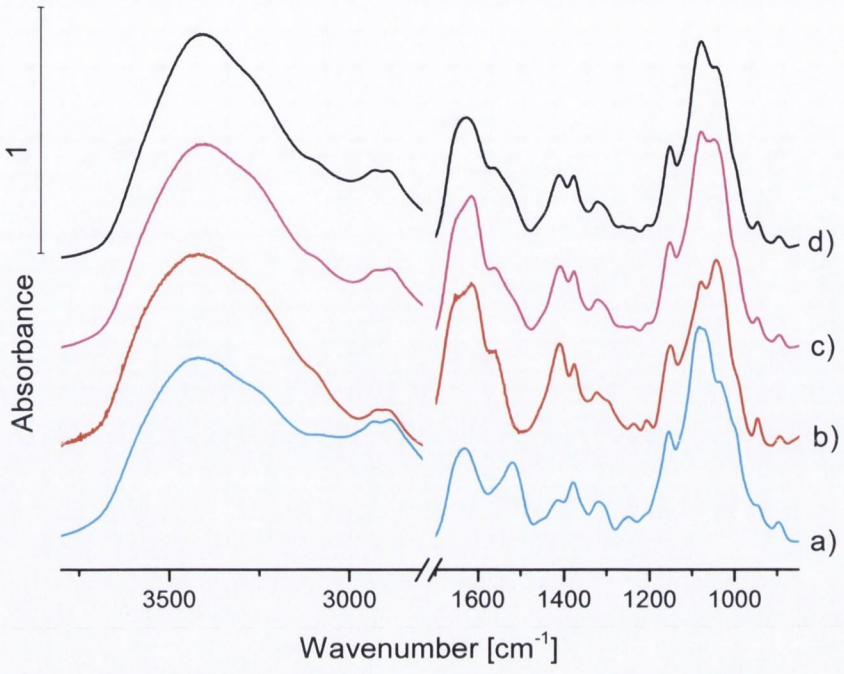

Fig.3.12 FTIR spectra of a) CL113, b) HA257, c) 1:1 w/w physical mixture of CL113 and HA257 and d) HA257/CL113 NPs (1:1 w/w).

Apart from the formulations with amounts of polymers close to charge neutralisation, all NP dispersions had an absolute value of zeta potential above 30 mV (Fig. 3.9), indicating their good physical stability. The dispersions had pH values between 4.2 and 6.1 with lower values corresponding to higher chitosan contents.

Fig. 3.13 shows that the polymer mixing ratio had a considerable influence on the viscosity of NP suspensions and lower viscosity values were measured for lower CMRs. It has been reported that the particulates themselves barely influence the viscosity (Philip et al., 1989). Our results showed that viscosity may be a useful tool for the estimation of non-complexed residual polymer in the system. When one of the polymers is used in excess, there are still molecules of that polymer which do not participate in the formation of NPs or which only weakly interact with the NPs; these polymer molecules are responsible for the increase in viscosity of the continuous phase.

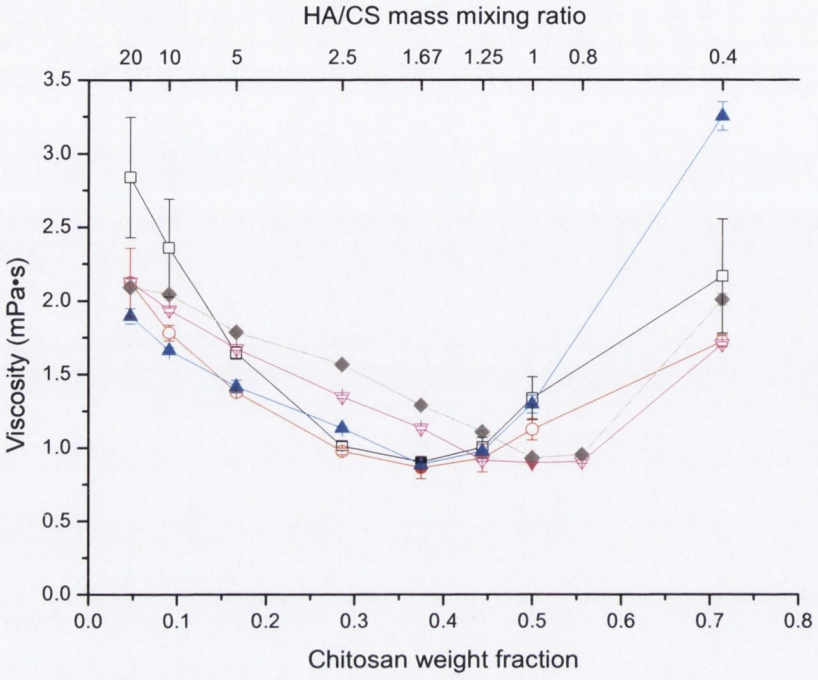

Fig.3.13 Viscosity of various HA/CS NP systems. HA molecular weight was 257 kDa. Squares – HA/CL113 with total polymer concentration (TPC) of 2 mg/ml, circles - HA/CL113 with TPC of 1 mg/ml, upward triangles - HA/CL213 with TPC of 1 mg/ml, downward triangles - HA/G113 with TPC of 1 mg/ml and diamonds - HA/G213 with TPC of 1 mg/ml. All lines are for visual guidance only. Filled symbols indicate data for flocculating and sedimenting samples obtained after standing samples for 24 h, while empty symbols indicate data obtained immediately after preparing the dispersions.

3.3.4 Impact of total polymer concentration

Generally, the yield of particles formed was higher for the higher polymer concentration (transmittance measurements in Figure 3.7 shows that 2 mg/ml formulations are more turbid compared to 1 mg/ml). For anionic NPs, when a high excess of HA was used, the particle size of 1 and 2 mg/ml formulations did not differ significantly, however at an MMR of 1, the 1 mg/ml NPs were statistically significantly smaller compared to the 2 mg/ml formulations (Fig. 3.10). All 2 mg/ml samples had moderate PDI values (between 0.2 and 0.5), while for the 1 mg/ml formulations the PDI values were low (below 0.2), which suggests homogenous size distributions (Fig. 3.11).

It was observed that when an excess of one of the polymers was used, viscosity of the 2 mg/ml NP dispersion was greater than that of the 1 mg/ml, however the viscosities of NPs with the MMRs of 1-2.5 (corresponding to the CMRs close to 1) were comparable (Fig. 3.13).

3.4 TEM of NPs

TEM micrographs show that the particles are approximately spherical, but in some cases deformations can be observed (Fig. 3.14). When the HA/CL113 mass MMR was 2.5, the particles appeared to be compact and well defined. The NPs with the HA/CL113 MMR of 5 were composed of a relatively dense core surrounded by a less solid and diffused polymer corona making the NPs less spherical in shape. Similar types of morphologies for HA/CS NPs were deduced, but not observed directly, by Boddohi et al., (2009), who noticed that as the charge mixing ratio was farther from 1, the relative size of the polymer corona was increased. Fig. 3.14 A may suggest that the polymer used in insufficient quantity in terms of charge neutralisation is localised mainly in core, while the polymer in excess is present in the core as well as in the corona, being the dominant constituent and responsible for surface charge of the particle.

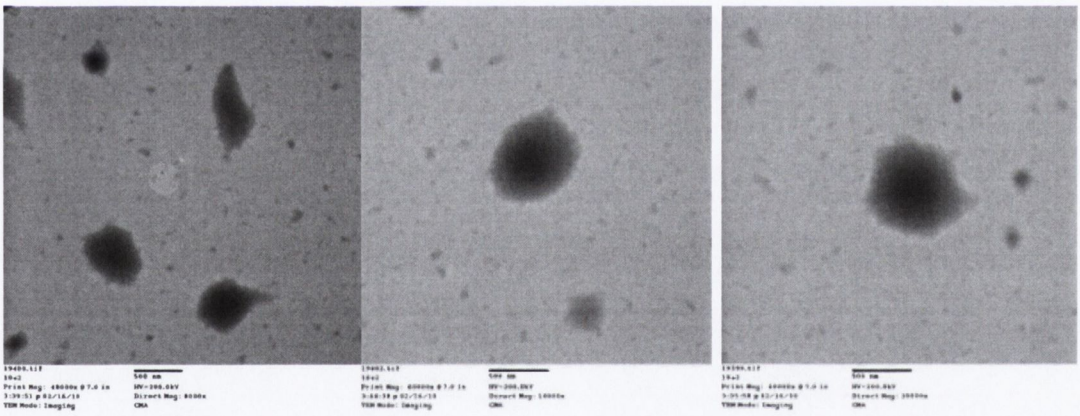

A)

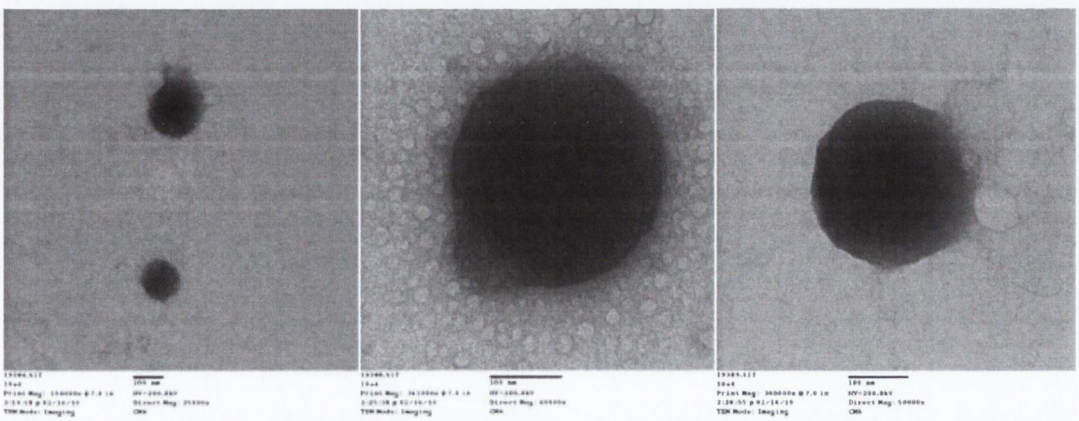

B)

Figure 3.14. TEM micrographs of HA/CL113 NPs with MMR of A) 5 and B) 2.5. HA molecular weight was 257 kDa and TPC was 1 mg/ml

3.5 Isoelectric points of NPs

Table 3.3 shows the isoelectric points (IEPs) of selected HA/chitosan NPs. Most of the negatively charged formulations tested (MMRs of 2.5 and 5) had IEPs close to 3. The IEP shifted to more acidic pH values with increasing content of HA in the systems (2.83 for the HA/CL113 MMR of 2.5 and 2.47 for the MMR of 5). When the HA/CL113 mass mixing ratio was 1, the IEP of this formulation was 7. When the total polymer concentration was increased to 2 mg/ml, or when glutamate salt was used instead of chloride, the isoelectric point was not affected (p-value of 0.8678 and 0.9006, respectively). A change in the molecular weight slightly affected the values of IEP, however the differences between the IEPs of nanoparticles composed of 257 kDa HA were not significantly different (p-value of 0.0784 and 0.2864) from either 590 kDa HA or 176 kDa HA. Thus, the HA/CS mass mixing ratio appears to be the most important factor influencing the IEP.

The surface of NPs becomes more negatively charged with increasing pH, and the increase in hydrogen ion concentration leads to an increase in positive charge of the particles. However, aggregation of NPs was observed even when the surface charge of the particles decreased to about ±10 mV.

Table 3.3 Isoelectric points of HA/CS nanoparticles. TPC – total polymer concentration.

HA type	Type of CS salt	TPC (mg/ml)	HA/CS mass mixing ratio	Isoelectric point
HA590	CL113	1	2.5	3.76±0.57
HA257	CL113	1	2.5	2.83±0.38
HA176	CL113	1	2.5	3.10±0.02
HA257	CL113	1	1	6.98±0.54
HA257	CL113	1	5	2.47±0.25
HA257	G113	1	2.5	2.87±0.09
HA257	CL113	2	2.5	2.86±0.09

Depending on the route of administration, NPs may be exposed to different environmental pH values. Thus the IEP (the pH at which a particular molecule or surface carries no net electrical charge) is a very important property of NPs as at a pH near the isoelectric point colloids are usually unstable and flocculation is likely to occur. Thus is appears that the NPs with MMRs of 2.5 and 5 will be stable at physiological pH values of 7.35-7.45, while those with the MMR of 1 should be preferred when used in acidic environments. We found no statistical difference (p-value of 0.0760) in the particle size of the HA/CL113 NPs with an MMR of 2.5 in the pH range of 5.9-7.4 (the size range was 170-215 nm), while the NPs with an

MMR of 1 remained stable as nanoparticulate dispersions within the pH range of 2-5.9 (the mean NP size was 194-260 nm), whereas at pH of 7.4 the particles flocculated within a few hours.

3.6 Stability of HA/CL113 nanoparticles after storage at room temperature

For the evaluation of dispersion stability of NPs upon storage at RT two negatively charged (HA/CL113 the MMRs of 2.5 and 5) and one positively charged formulation were selected (MMR of 1). Fig. 3.15-3.17 show changes in the particle size, zeta potential and PDI, respectively for the two formulations over 28 days storage at RT.

Positively charged NPs (MMR of 1) were the least stable formulation. First signs of sedimentation were visually observed after two weeks of storage, while for both formulations containing negatively charged NPs (MMRs of 2.5 and 5) the first signs of sedimentation were noticeable after 3 weeks. After 4 weeks it was possible to observe sediment at the bottom of the vial for all samples, especially for positively charged.

The particle size of positively charged NPs decreased systematically from 239 (day 0) to 152 nm (day 28) (p-value < 0.0001) (Fig. 3.15).

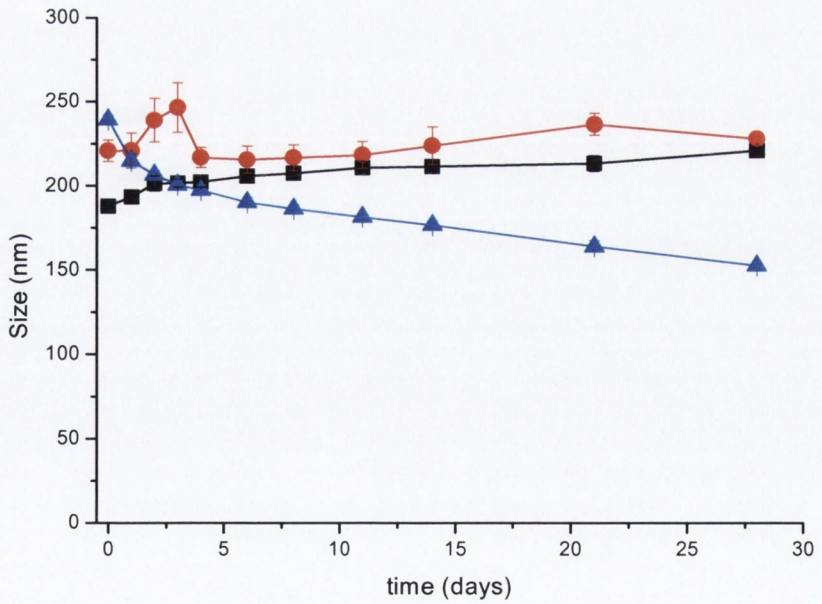

Fig. 3.15. Stability studies of NPs dispersions at room temperature: particle size. Triangles - HA/CL113 NPs with MMR of 1, circles - HA/CL113 NPs with MMR of 5 and squares - HA/CL113 NPs with MMR of 2.5. HA molecular weight was 257 kDa and the total polymer concentration was 1 mg/ml. All lines are for visual guidance only.

A similar trend was observed for PDI, which decreased from the initial value of 0.270 to 0.150 after 28 days (p-value < 0.0001) (Fig. 3.16).

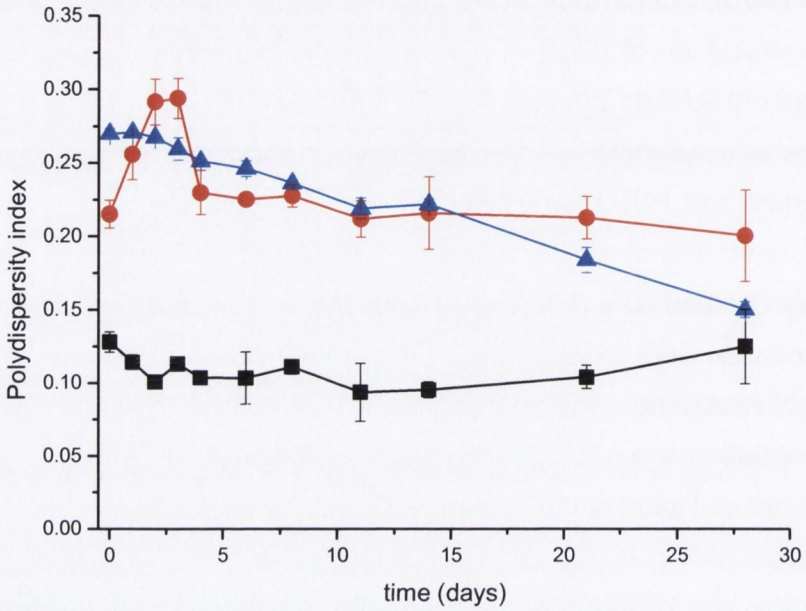

Fig. 3.16. Stability studies of NPs dispersions at room temperature: polydispersity index. Triangles - HA/CL113 NPs with MMR of 1, circles - HA/CL113 NPs with MMR of 5 and squares - HA/CL113 NPs with MMR of 2.5. HA molecular weight was 257 kDa and the total polymer concentration was 1 mg/ml. All lines are for visual guidance only.

The zeta potential remained steady for 21 days (51-52 mV), and in the fourth week of storage it slightly decreased to 47 mV (Fig. 3.17).

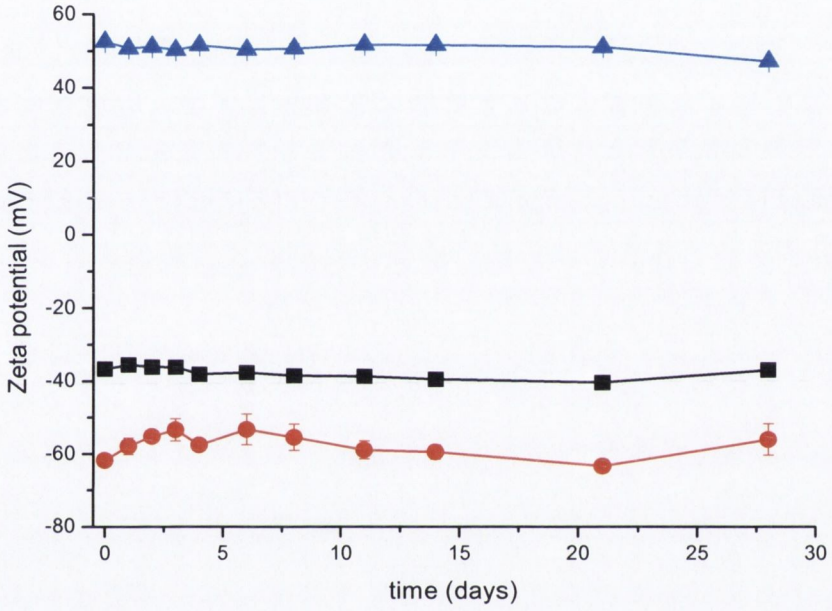

Fig. 3.17. Stability studies of NPs dispersions at room temperature: zeta potential. Triangles - HA/CL113 NPs with MMR of 1, circles - HA/CL113 NPs with MMR of 5 and squares - HA/CL113 NPs with MMR of 2.5. HA molecular weight was 257 kDa and the total polymer concentration was 1 mg/ml. All lines are for visual guidance only.

The samples became more transparent during storage (the transmittance increases from 58% initially to 70% after 3 weeks, data not shown).

In contrast, the size of negatively charged NPs with the HA/CL113 MMR of 2.5 systematically increased during storage from 188 to 221 nm (p-value = 0.0003) and the PDI values remained low (Fig. 3.17). The transmittance values decreases from 68% to 54% after 3 weeks (data not shown), so they became more turbid. For both negatively charged formulations the initial value of the zeta potential did not differ significantly (p-value of 0.0938 and 0.7856 for MMR 5 and 2.5, respectively) from the zeta potential value after 4 weeks of storage, and slight fluctuations of zeta potential could be observed (Fig. 3.17). Interestingly, there was an initial increase in particle size and polydispersity of the formulation with the HA/CL113 MMR of 5 - the hydrodynamic diameter and PDI reached its peak values after the third day of storage and then decreased to values which did not differ significantly

(p-value of 0.1692 for size; p-value of 0.4691 for PDI) from the initial values (Fig. 3.15 and 3.16). That increase in the particle size was however minor as the size increased only by about 10%.

3.7 Cytotoxicity studies

3.7.1. HA post-sonication

The cytotoxicity of sonicated HA used for the production of the nanoparticles was examined. HA with three molecular weights were tested (590, 257 and 176 kDa obtained by sonication of native HA for 0.5h, 2h and 6h, respectively) at a concentration of 5 mg/ml (which is much higher than the mass of HA in NPs) by MTS assay and flow cytometry (FC). It can be observed from MTS results (Fig. 3.18), that the HA samples tested not only exhibited a lack of negative effects on cellular viability, but instead the number of living cells was approximately 10-20% higher than the control. This may suggest that HA either has a cytoprotective effect on cells, or may increase their proliferation rate (Kawasaki et al., 1999). Moreover, the molecular weight of HA did not have an effect on cell viability.

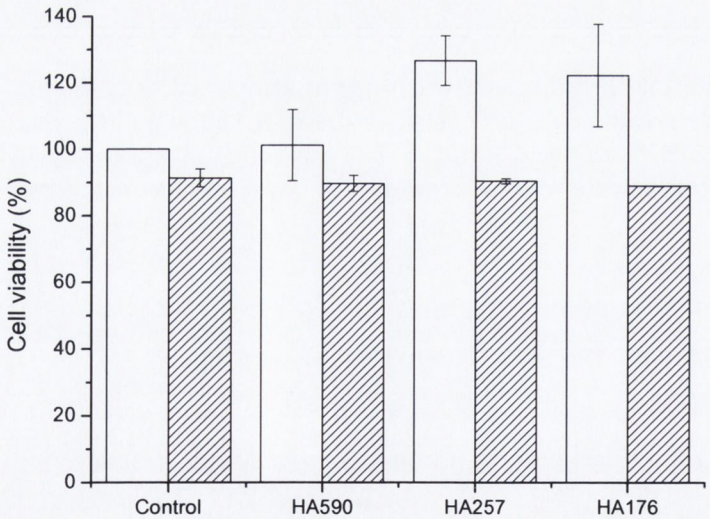

Fig. 3.18 Cell viability (MTS assay, empty bars) and apoptosis (flow cytometry, hashed bars) in Caco-2 cells after 72 h treatment with HA 5 mg/ml solutions of the polymer with molecular weight of 590, 257 and 176 kDa. B) C) and D) Scatter plots for apoptosis assay – control, HA with molecular weight of 590 and 176 kDa, respectively. HA sonicated induced similar apoptosis/necrosis events in Caco-2 cells compared to the control. Representative recordings of 3 similar experiments. Q1: necrotic cell zone, Q2: late apoptosis or dead cell zone Q3: living cell zone Q4: viable apoptotic cell zone.

The above HA samples were also analysed for apoptotic/necrotic incidence using FC. This assay showed that the viability of control cells and cells treated with all HA samples was comparable (there was no significant difference between any of them, Fig. 3.19 A, B and C), thus it can be stated that sonication did not result in formation of HA with adverse toxicological effects on the cells.

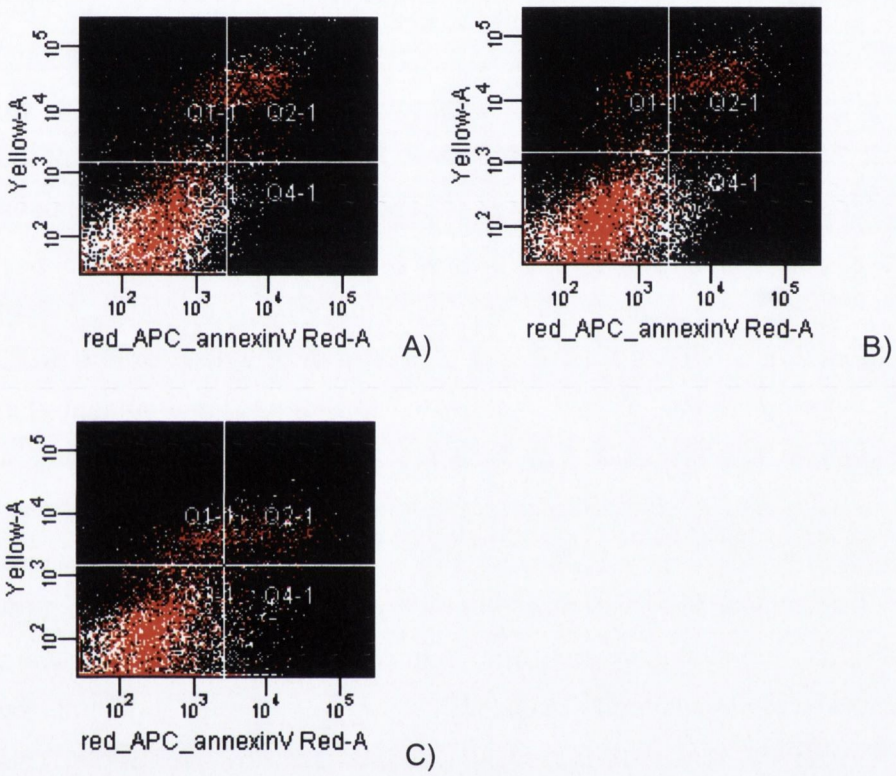

Fig. 3.19 A) B) and C) Scatter plots for apoptosis assay – control, HA with molecular weight of 590 and 176 kDa, respectively. HA sonicated induced similar apoptosis/necrosis events in Caco-2 cells compared to the control. Representative recordings of 3 similar experiments. Q1: necrotic cell zone, Q2: late apoptosis or dead cell zone Q3: living cell zone Q4: viable apoptotic cell zone.

3.7.2 Nanoparticles

For the evaluation of NP cytotoxicity, one negatively charged (HA/CL113 with an MMR of 5) and one positively charged formulation (with an MMR of 1) were chosen. The zeta potential of NPs with an MMR of 1 in serum-free media (pH=7.4) inverted and was measured to be -17.2±1.25 mV, consistent with the IEP of the formulation of approximately 7. The % of viable Caco-2 cells measured by MTS assay in serum-free media at pH 7.4 for the NP concentrations 20-500 μg/ml and chitosan (CL113) concentrations 125-5000 μg/ml was not significantly different from the control. A change in the colour of medium to orange followed by

precipitation was observed upon dissolving chitosan in serum free media. As mentioned earlier, the pKa of amino group of chitosan is 6.5, so at pH 7.4 only about 10% of amino groups of chitosan would be dissociated. Since chitosan is poorly soluble in aqueous solutions with neutral or basic pH (Kudsiova, Lawrence, 2008), the concentration of chitosan remaining in solution will be much smaller due to precipitation of non-ionised chitosan chains. That may explain why the viability of Caco-2 cells is not affected by chitosan at pH 7.4. Also, it has been shown that the degree of chitosan toxicity depends on the charge density, configurational arrangements of the cationic residues and degree of deacetylation (Kudsiova, Lawrence, 2008; Schipper et al., 1996). Also, Loretz et al. (2007) reported that the zeta potential is the key feature that contributes most to the toxicity of chitosan NPs, while the size of the particles only slightly affects their toxicity.

Considering the impact of pH on the toxicity of NPs formulations, serum free media without sodium bicarbonate (pH 5.0) was also used for the MTS experiments. The zeta potential values for the HA/CL113 formulations measured in this modified medium were 20.3±0.314 and -18.7±0.247 mV for NPs with MMR=1 and MMR=5, respectively. A concentration-dependent cytotoxicity was observed for chitosan on its own (CL113) and NPs with MMR=1 (Fig. 3.20). The IC_{50} values calculated from the cell viability-concentration graph were significantly different (p-value < 0.0001) for the chitosan solutions and NPs with MMR=1 and were 25.9±1.02 μg/ml for chitosan and 83.9±2.66 μg/ml for the NPs. Thus, by formulating CL113 as HA-based NPs, the IC_{50} was increased by over 3-fold. This suggests that positively charged HA/CL113 NPs can be used as a less toxic alternative to chitosan formulations. HA/CL113 with MMR=5 were found be non-toxic in the whole range of concentration studied and furthermore, cytoprotective effects were seen, similar to those when HA on its own was used as described above, at higher HA concentrations (Fig. 3.20). It can be concluded that HA present in the NPs seems to play a protective role neutralising the toxic effects of chitosan. This is in agreement with the work of Nasti et al., (2009), who showed that coating of CS/TPP nanoparticles with HA decreased their toxicity in J774 macrophages- the IC_{50} increased from 0.7-0.8 mg/ml to 1.8 mg/ml.

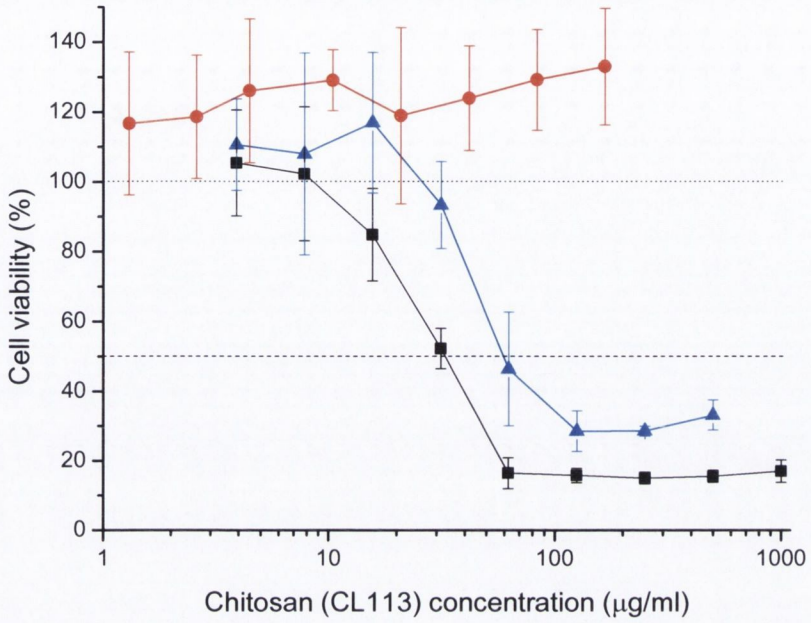

Fig.3.20 Cell viability (MTS assay) for Caco-2 cells as a function of chitosan concentration. Squares indicate chitosan (CL113), triangles HA/CL113 NPs with MMR of 1 and circles HA/CL113 NPs with MMR of 5. The treatment time was 24 h using medium at pH=5.0. The dashed line indicates 50% cell viability. Viability of the control group was 100% (dotted line).

3.8 Conclusions

A production method aimed at fabrication of novel, cross linker-free and non-sedimenting NPs was successfully developed. The physicochemical properties of the NPs were found to be conveniently adjusted by changing the formulation conditions: polymer mixing ratio, total polymer concentration, the molecular weight of the polymers and the type of the counterion in the chitosan salt. The main factor determining particle formation and properties was the mixing ratio of the polymers. However, other parameters, e.g. the salt of chitosan used and the total polymer concentration also played a role. The influence of molecular weight of the polymers was especially pronounced in the range of higher molecular weights causing NP instability and/or formation of microparticles. A change in HA/CS mass ratio considerably changed the physicochemical properties of the nanoparticles, especially the zeta potential. A decrease in the HA content was accompanied by an increase in zeta potential and its inversion from negative to positive values. Fine-tuning of the HA/CS ratio allowed for non-toxic NPs at pH=5 and 7.4 to be produced, a vital property when NPs are formulated for e.g. the oral route of administration.

Overall, the HA/CS NPs obtained can be considered as viable and non-toxic carriers for formulating bioactive compounds due to their favourable physicochemical and biopharmaceutical properties.

4. Calcitonin-loaded hyaluronic acid-chitosan nanoparticles

4.1 Introduction

Salmon calcitonin (sCT) is commercially available as injectable and nasal spray form (Guggi et al., 2003). It is indicated for the treatment of bone diseases, e.g. osteoporosis, Paget's disease and bone metastasis (Guggi et al., 2003; Makhlof et al., 2010). sCT is also a promising candidate to be used in osteoarthritis (Manicourt et al., 2005) and in combined therapy with alendronate in patients with rheumatoid arthritis (Ozoran et al., 2007). However, the full market potential of this peptide has not yet been reached due to the low patient compliance associated with the injectable dosage forms (Guggi et al., 2003). Also, the absorption of sCT from the commercial nasal spray, Miacalcin® shows great variability in the range 0.3-30.6%, with an average bioavailability of 3% compared to intramuscular injection (Hinchcliffe et al., 2005). Therefore the development of a new, more compliant delivery system for sCT is of a vital importance. The systemic delivery of sCT via routes other than by injection and nasal presents an attractive therapeutic option (Paton et al., 2000). However, the bioavailability of sCT may be compromised by certain barriers when e.g. oral or pulmonary administration is envisaged. Polymeric nanoparticles represent an interesting strategy because of their abilities to entrap macromolecules, protect them against degradation and enhance their transmucosal transport (de la Fuente et al., 2008a).

Several approaches have been attempted to produce calcitonin or elcatonin-loaded polymeric nanoparticles, among them PLGA-based nanoparticles being one of the most common (Kawashima et al., 2000, Glowka et al., 2010, Yang et al., 2012). Although the peptide was very efficiently associated with the particles, for instance Yang et al. (2012) managed to achieve up to 96.7% of loading efficiency, a very low drug loading, up to 1.55% by Kawashima et al. (2000), 0.1 and 0.2% by Yang et al. (2012) and Glowka et al. (2010), respectively, is one of the main disadvantages of PLGA-based nanoparticles. Garcia-Fuentes et al., (2005) and Prego et al., (2006) developed lipid-based nanocarriers for the delivery of sCT, however the drug loading was not stated, nevertheless is expected to be low as the lipids and other ingredients are used in significantly higher quantities than sCT. Other common disadvantages of lipid or PLGA-based nanoparticles are the use of surfactants and organic solvents. Cetin et al., (2012) managed to obtain Eudragit® and Eudragit®-PLGA NPs with a considerably higher sCT loading (up to 9.9%), but

the association efficiency values, although high (up to 69.13%), still could have been improved; also surfactant and organic solvents were used in their production.

Polyelectrolyte complex nanoparticles offer an attractive alternative, as they do not require organic solvents or surfactants in their manufacturing process. Makhlof et al., (2010) developed calcitonin-loaded NPs by the method of ionic gelation of chitosan-thioglycolic acid polymer conjugate with TPP. Although the process of particle preparation is simple and organic solvent free, the use of novel polymer would raise a need for complicated toxicity studies. Therefore employment of naturally occurring polymers already approved for the use in drug delivery provides an attractive option.

As mentioned earlier (see Chapters 2 and 3), HA is a naturally occurring, biocompatible, biodegradable, non-immunogenic and mucoadhesive polymer, and specifically interacts with cell-surface receptors, e.g. CD44. Apart from those interesting features useful for the potential application in a drug delivery system, HA also has many interesting biological properties (Stern et al., 2006). HA has been proven to be a safe and symptom-modifying treatment for osteoarthritis of the knee, in terms of significantly reducing pain and improving function (Huang et al., 2011). Some of the properties of HA (e.g. anti-inflammatory and structure protection in arthritis) may be complementary to pharmacological action of sCT, therefore combining these two compounds (HA and sCT) in one drug delivery system seems to be particularly attractive not only in terms of facilitation of the delivery of sCT. To our best knowledge, no delivery system containing HA and sCT has been developed so far.

4.2 Investigations into HA/sCT interactions

The estimated isoelectric point of sCT is 10.4 (Maier et al., 1977). At pH 7.4 it is expected to carry an overall charge of approximately 3+ (Epand et al., 1983). HA on the other hand, with pKa of its carboxylic groups of 2.9 (Lapčik et al., 1998), bears a negative charge. The protonated amino groups of protein are believed to associate with the de-protonated groups of anionic polysaccharides (de Kruif et al., 2004). Therefore both compounds, HA and sCT, are expected to interact by electrostatic forces at neutral and slightly acidic pH.

In order to examine the HA/sCT complexes, both compound solutions were mixed at different mass ratios. The concentration of HA (molecular weight of 257 kDa, used for the preparation of most of HA/chitosan NPs described in Chapter 3) was kept constant (0.71 mg/ml) and different concentrations of sCT were used (0.54, 1.09, 1.63, and 2.17 mg/ml, producing HA/sCT with MMRs of 1.3, 0.65, 0.44

and 0.33, respectively). Mixtures with HA/sCT MMRs of 1.3 and 0.65 had the appearance of solutions, while mixtures containing HA and sCT at MMRs of 0.44 and 0.33 were turbid (transmittance values of 77.8±0.5 and 62.2±2.3%, respectively) due to the formation of large particulates, visible to the naked eye. Transmittance of HA/sCT mixtures decreased with an increasing sCT/HA MMR (Fig. 4.1). Based on these observations it can be concluded that sCT may interact with HA. It was observed that a precipitate was formed when sCT was used in relatively large quantities compared to HA (e.g. in HA/sCT mixtures with an MMR of 0.44 and lower). Thus this precipitate is very likely to contain a HA/sCT complex.

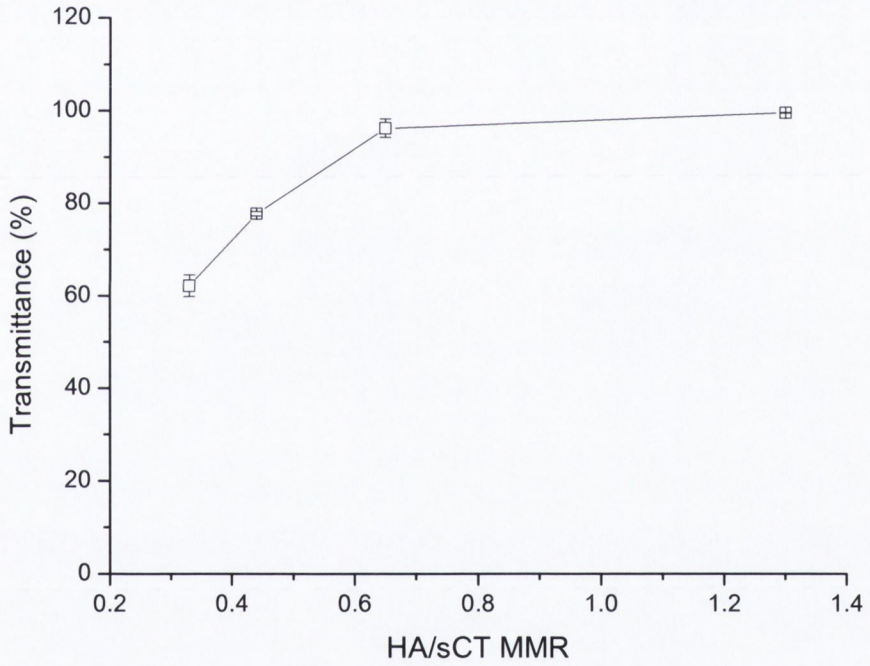

Fig.4.1 Transmittance of the dispersions of HA/sCT complexes.

In order to further examine the solubility of HA/sCT complex(s), two most turbid mixtures containing HA/sCT at MMRs of 0.44 and 0.33 were diluted 1:1 (v/v) with water or with 1 mg/ml HA aqueous solution. Changes in absorbance at 500 nm upon dilution of the HA/sCT complex are shown in Fig. 4.2. There was a dramatic decrease in absorbance for both samples upon dilution with HA solution; for the sample with HA/sCT MMR of 0.44, absorbance was close to 0, therefore indicating that the HA/sCT complex dissolved. Following 1:1 (v/v) dilution of the complex with water the absorbance of HA/sCT mixtures with MMRs of 0.44 and 0.33 decreased 4 and 3.2-fold, respectively.

In conclusion, the solubility of the HA/sCT complex depends mainly on the HA/sCT MMR, however the concentration of the complex also plays a role. Also, the HA/sCT complex may be considered as highly soluble when compared to HA/chitosan complexes (see chapter 3).

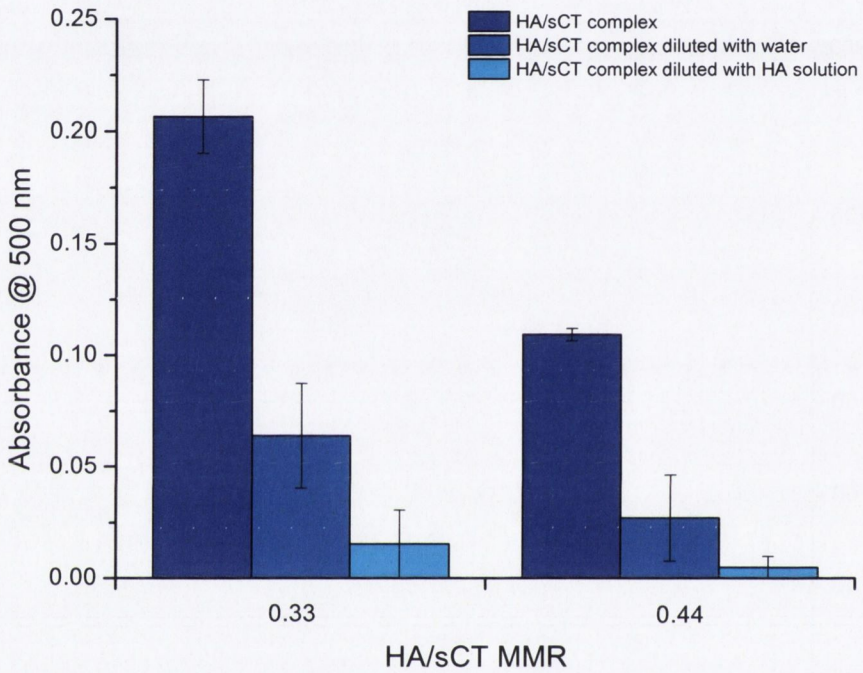

Fig.4.2 Absorbance of the HA/sCT complex with MMRs of 0.44 and 0.33 diluted 1:1 (v/v) with water or with 1 mg/ml aqueous solution of HA.

Since the precipitate formed by HA and sCT at high MMR values was soluble in water, a possibility of a soluble complex formation was also investigated. The dynamic viscosity of HA solution was compared to that of HA solution containing sCT dissolved while maintaining the same concentration of HA. After dissolving sCT in the HA solution (the MMR of HA/sCT was 2) the viscosity decreased markedly ($p<0.05$) compared to the control (HA solution without sCT) by 0.48, 0.51 and 1.41 mPa*s for 0.05, 0.1 and 0.2% of HA257, respectively (Table 4.1). It is known that a change in the value of the Huggins' constant can be used to evaluate the interaction of drug molecules in solution with polymers (Molyneux et Frank, 1961). Huggins' constant values were therefore calculated based on dynamic viscosity measurements of three different concentrations of HA and HA/sCT solutions.

Table 4.1 Dynamic viscosity [mPa*s] of HA, HA/sCT, CL113, CL113/sCT aqueous solutions

Polysaccharide concentration [%]	HA	HA/sCT MMR=2	CL113	CL113/sCT MMR=2
0.05	1.80±0.046	1.32±0.010	1.45±0.017	1.43±0.017
0.1	2.14±0.162	1.63±0.019	1.76±0.023	1.75±0.008
0.2	3.37±0.638	1.96±0.008	2.21±0.090	2.21±0.013

It can be observed that the plot of reduced viscosity against HA concentration was linear in the case of both HA and HA/sCT solutions (Fig.4.3, Table 4.2). When both lines were extrapolated to the vertical axis, where c=0, the intrinsic viscosity values were similar (0.30 and 0.33). However, the slope (or Huggins' constant) was significantly lower (2.6-fold) for sCT dissolved in the HA solution. The change in the Huggins' constant value provides a confirmation that a soluble complex between HA and sCT is indeed formed.

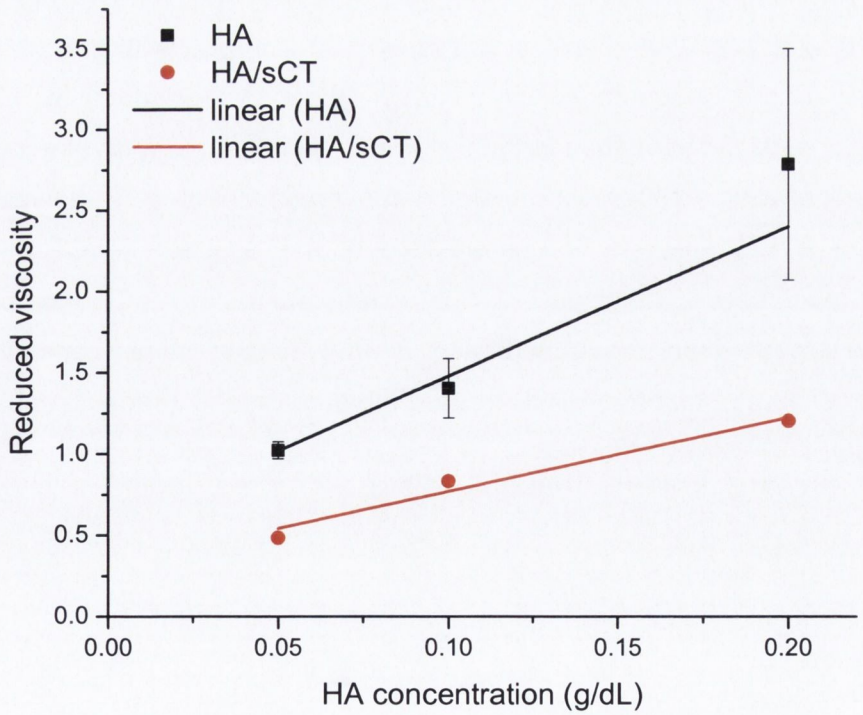

Fig. 4.3 Reduced viscosity of HA and HA/sCT solutions plotted against polysaccharide concentration.

Table 4.2 Intrinsic viscosity, Huggins' constant and linearity (R^2) of reduced viscosity plotted against concentration of the polysaccharides HA or CL113.

	Intrinsic viscosity	Huggins' constant	R^2
HA	0.3309	12.063	0.9841
HA/sCT	0.2978	4.6388	0.9707
CL113	0.3539	5.6902	0.9923
CL113/sCT	0.3702	5.6421	0.9923

As the dispersion containing HA/sCT at MMR of 0.65 with transmittance of 96.2±2.0% is slightly more turbid than a solution, DLS and LDV measurements were performed in order to examine if NPs were formed. Although the particle size and polydispersity index measured by DLS were 88±25 nm and 0.651±0.190, respectively, the sample was too polydisperse and the quality of the data was too poor for cumulant analysis. Also, the surface charge of the particles seems to be low (zeta potential of -11.6±2.17 mV), indicating that although NPs were probably formed, they did not have good physical characteristics.

Interactions between HA and sCT were also confirmed by UV analysis. The spectra of two soluble HA/sCT complexes were measured in the wavelength range between 200-280 nm. The spectrum of the HA/sCT complex with the MMR of 5 was similar to the spectrum of HA solution (Fig.4.4). The complex absorbs markedly more UV radiation than HA at the same concentration within the range of wavelength between ~200-240 nm due to the presence of sCT, however the spectrum of the complex is not an additive of the spectra of sCT and HA. Moreover, absorbance between ~215-240 nm of the HA/sCT complex is considerably lower than the absorbance of sCT at the same concentration. Therefore, the complexation to HA decreases the amount of UV radiation absorbed in this range.

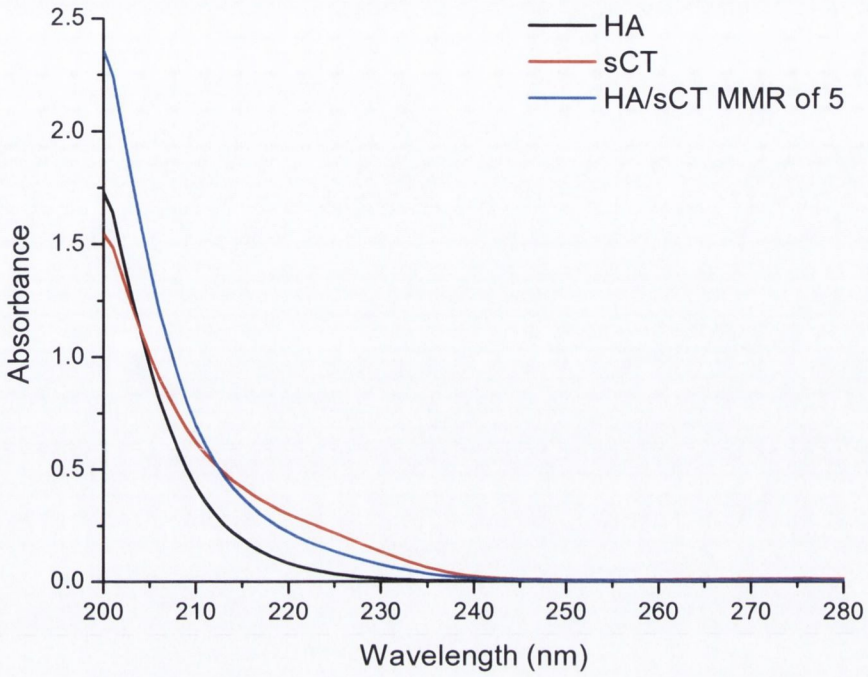

Fig.4.4 UV spectra of HA/sCT MMR of 5 complex; spectra of HA solution and sCT solution of the same concentration as in the complex are also shown in both cases. sCT concentration was kept constant at 0.03 mg/ml.

A decrease in absorbance is even more pronounced for the HA/sCT complex with MMR of 1 (Fig.4.5) as absorbance of the complex is markedly lower over the wavelength range 200-~240 nm.

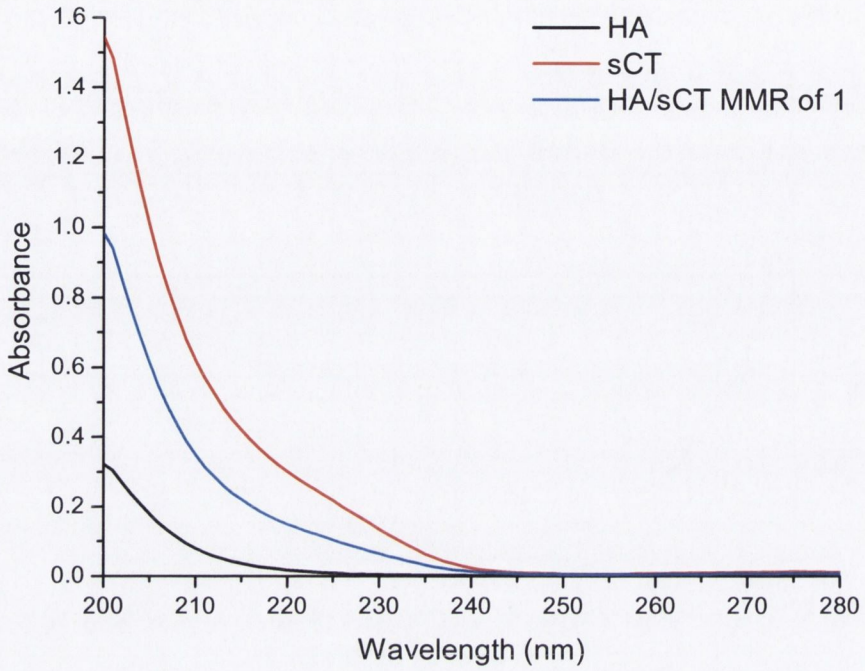

Fig. 4.5 UV spectra of HA/sCT of 1 complex; spectra of HA solution and sCT solution of the same concentration as in the complex are also shown in both cases. sCT concentration was kept constant at 0.03 mg/ml.

4.3 Investigations into CS/sCT interactions

Interestingly, when sCT was dissolved in CL113 solution at CL113/sCT MMR of 2, the appearance of the system did not change and the viscosity of CL113/sCT solution did not differ from the control (CL113 solution without sCT) (Table 4.1) for all CL113 concentrations tested. Therefore the plot of reduced viscosity against CL113 concentration was linear for both CL113 and CL113/sCT solutions and the values of intrinsic viscosity and Huggins constant were practically the same for both systems (Fig. 4.6). As both, sCT and CL113, are expected to be positively charged in a solution, an electrostatic interaction or salt formation is very unlikely to occur between these two polyelectrolytes.

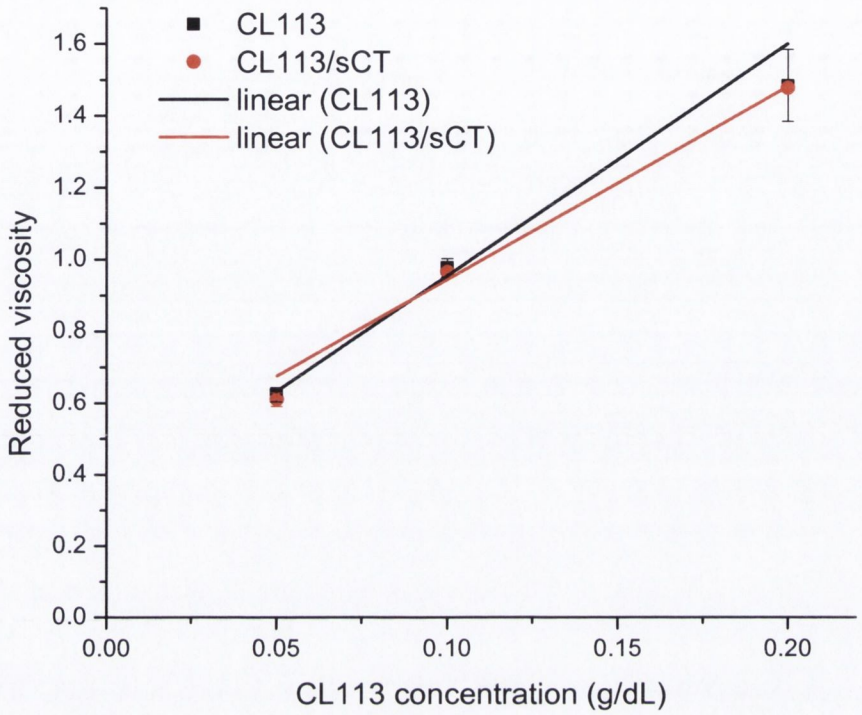

Fig. 4.6 Reduced viscosity CL113 and CL113/sCT solutions plotted against polysaccharide concentration

4.4 Characterisation of HA/CL113/sCT complexes: formulation variables. Impact of HA/CL113 MMR, TPC and sCT concentration

Observing that the HA/sCT complex is highly soluble and even at high HA/sCT MMRs no particles with desirable physical properties were formed, an attempt was made to add another polycation in order to produce polyelectrolyte complex NPs containing sCT and HA. Chitosan has been shown to form an insoluble complex with HA (Chapter 3, Denuziere et al., 2005) and it is expected that in certain conditions the HA/CS complex may be precipitated in the form of nanoparticles (Boddohi et al., 2009, Chapter 3). Since the interactions between sCT and HA are mainly electrostatic in nature, the negatively charged NPs with high absolute values of zeta potential well above 30 mV, as described in Chapter 3, seem to be promising candidates as the carriers of sCT. Indeed, the addition of chitosan has been shown to markedly decrease (from >90% to ~30%) the encapsulation efficiency of sCT by lipid NPs (Garcia-Fuentes et al., 2005).

At first, attempts were made to incorporate different amounts of sCT (0.1, 0.2, 0.35, 0.5 and 1.0 mg/ml) into the HA257/CL113 NPs with TPC of 1 mg/ml and MMRs of 2.5, 5 and 10. In most cases stable, non-sedimenting (within 24 hours or

longer) nanoparticles were formed, however in formulations containing the highest concentration of sCT (1 mg/ml) and HA/CL113 MMRs of 2.5 and 5 an immediate aggregation was observed. Furthermore, in the formulation with sCT concentration of 0.5 mg/ml and HA/CL113 MMR of 2.5 precipitation was observed after a few hours of storage at room temperature.

Next step was incorporation of the highest amounts of sCT used previously (0.5 and 1.0 mg/ml) with TPC of 1 mg/ml into NPs with 2 mg/ml TPC and the same HA/CL113 MMRs (2.5, 5 and 10) as used above. All formulations based on HA/CL113 MMRs of 5 and 10 were physically stable, no sedimentation was observed up to 24 hours. In contrast to 1 mg/ml TPC NPs, the 2 mg/ml TPC-based formulation with HA/CL113 MMR of 2.5 was physically stable and it was necessary to increase the concentration of sCT to 1 mg/ml to cause aggregation. Therefore it seems that the main factor determining the physical stability of HA/CL113/sCT NPs is not just the HA/CL113 ratio and the dose of sCT, but the mixing ratio of all these three substances (HA/CL113/sCT). For instance, for HA/CL113 NPs with MMR of 2.5 (TPC of 1 mg/ml), aggregation was observed for the HA/CL113/sCT formulation with MMR of 2.5/1/1.75, while the formulation with TPC of 2 mg/ml and sCT of 0.5 mg/ml (HA/CL113/sCT MMR of 2.5/1/0.87) was stable.

The above experiments indicate that HA interacts with chitosan and sCT mainly by electrostatic forces and, as the negative charges of HA are neutralised by chitosan and sCT, the net charge of the particles decreases and aggregation occurs. Being positively charged in all the formulation conditions tested (pH of the NP dispersions containing sCT varies between 5.1 and 5.7), sCT and chitosan compete for binding with negatively charged carboxylic groups of HA. The interaction of chitosan with HA is expected to be stronger than the interaction between sCT and HA as chitosan is capable of precipitating HA at lower concentrations and has higher charge density than sCT.

It can be seen that transmittance of all TPC 1 mg/ml-based formulations decreased gradually with an increase in the amount of sCT used (Fig. 4.7). The difference was especially pronounced in nano-formulations with HA/CL113 MMR of 2.5. Employing 0.1 mg/ml of sCT had no significant impact on transmittance compared to sCT-free NPs. However, using higher amounts of sCT: 0.2 mg/ml and 0.35 mg/ml led to a marked, statistically significant ($p=0.014$ and 0.007 for sCT of 0.2 and 0.35 mg/ml, respectively) decrease in transmittance values in comparison to the empty NPs. The decrease in transmittance values can also be seen for formulations of HA/CL113 with MMRs of 5 and 10; for HA/CL113 with MMR of 5 it was more substantial compared to HA/CL113 with MMR of 10, however much

smaller than for HA/CL113 with MMR of 2.5. For HA/CL113 formulations with MMR of 5, 0.2 mg/ml of sCT was needed to decrease transmittance significantly ($p=0.043$) compared to the control nano-formulation without sCT, and in case of HA/CL113 with MMR of 10, 0.35 mg/ml of sCT reduced transmittance significantly ($p=0.024$) to the control. The HA/CL113 formulation with MMR of 10 and sCT of 1.0 mg/ml was significantly more turbid than other HA/CL113 NPs with MMR of 10 containing smaller amount of sCT.

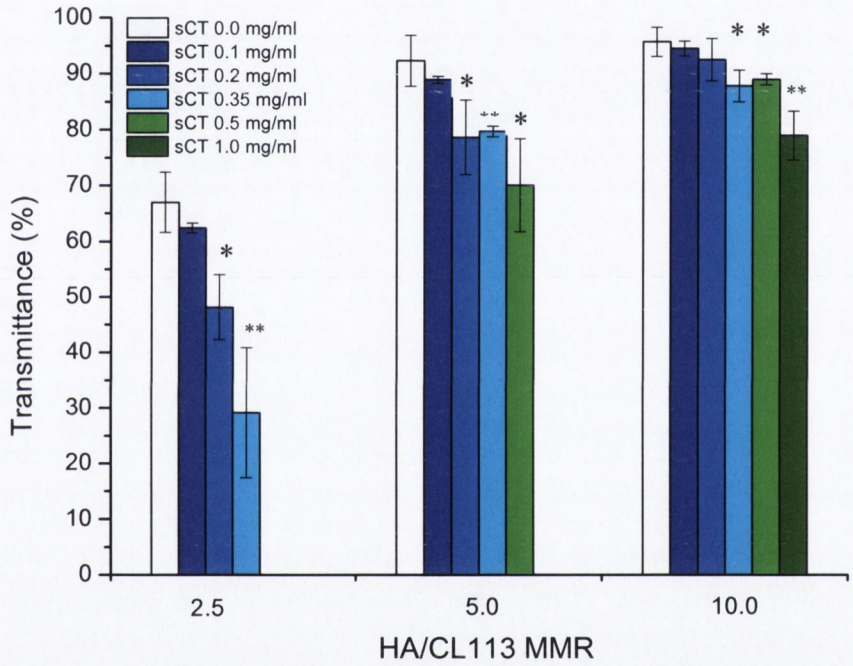

Fig.4.7 Transmittance of sCT-containing HA/CL113 NPs based on TPC of 1 mg/ml.*$p<0.05$ and **$p<0.01$ versus sCT 0.0 mg/ml.

In contrast to TPC of 1 mg/ml NPs, it was seen that when TPC was increased to 2 mg/ml, a small, but not statistically significant ($p<0.05$) increase in transmittance values was observed for formulations with MMRs of 5 and 10 (Fig. 4.8). This may be attributed to a decrease in the particle size due to incorporation of sCT. The transmittance of 0.5 mg/ml sCT–containing NPs with MMR of 2.5 was almost the same as transmittance of the control (HA/CL113 NPs with MMR of 2.5 without sCT).

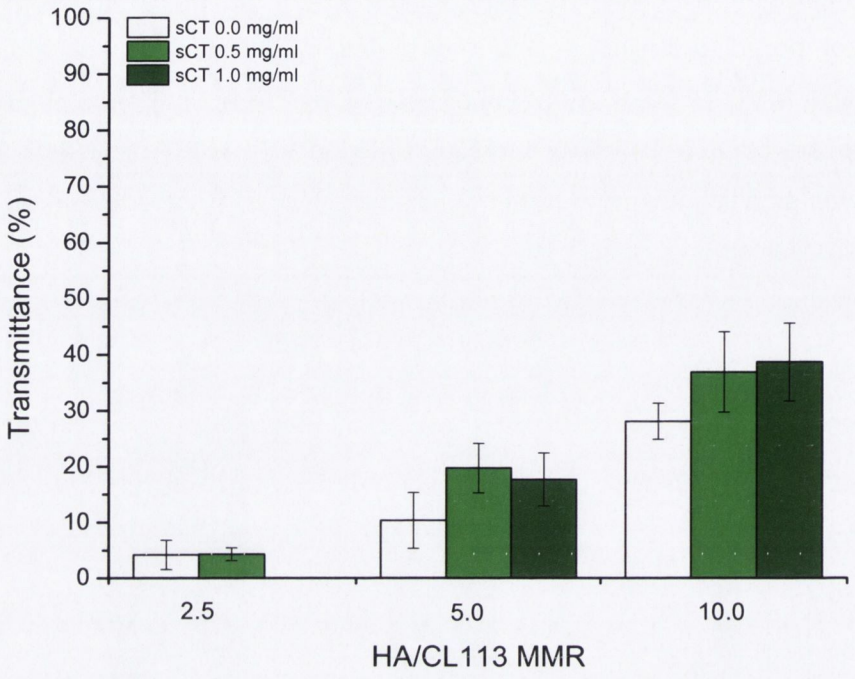

Fig.4.8 Transmittance of sCT-containing HA/CL113 NPs based on TPC of 2 mg/ml.

Similarly to HA/CL113 NPs without sCT (see Chapter 3), a marked, statistically significant decrease in transmittance was observed for sCT-containing NPs for each concentration of sCT and TPC tested when HA/CL113 MMR was decreasing. Also, 1 mg/ml TPC-based formulations were more transparent compared to similar 2 mg/ml-based formulations (with the same HA/CL113 MMR and sCT concentration). It can be concluded, that although sCT has an influence on transmittance of the NP suspension, HA/CL113 MMR and TPC remain the main factors influencing turbidity of the nano-formulations.

It was seen for each HA/CL113 MMR and TPC tested that inclusion of sCT decreased the dynamic viscosity of the nano-suspensions considerably (Fig. 4.9). The higher the dose of sCT, the lower the dynamic viscosity of the suspension was measured. This decrease in viscosity was the greatest for formulations with HA/CL113 MMR of 10, and the smallest for HA/CL113 MMR of 2.5- based formulations for both TPCs tested. As mentioned in Chapter 3, the increased viscosity of nano-suspensions compared to water may be attributed to free polymer chains present in excess which are loosely bound to the nanoparticles. In all formulations tested here HA is believed to be in excess, which is confirmed by the negative zeta potential of these NPs. As the nanoparticles themselves are not expected to increase the viscosity (Philip et al., 1989), and the component present

in deficiency is supposed to be fully bound in the complex (Dautzenberg and Jaeger, 2002), HA appears to be the main factor determining the viscosity of the examined nano-suspensions. As presented above, the interaction between HA and sCT resulted in a decrease in the viscosity and it may, to a degree, be a reason for the decreased viscosity of the HA/CL113 nano-suspensions. Still, it can be observed that the concentration of sCT is not the only factor influencing the viscosity.

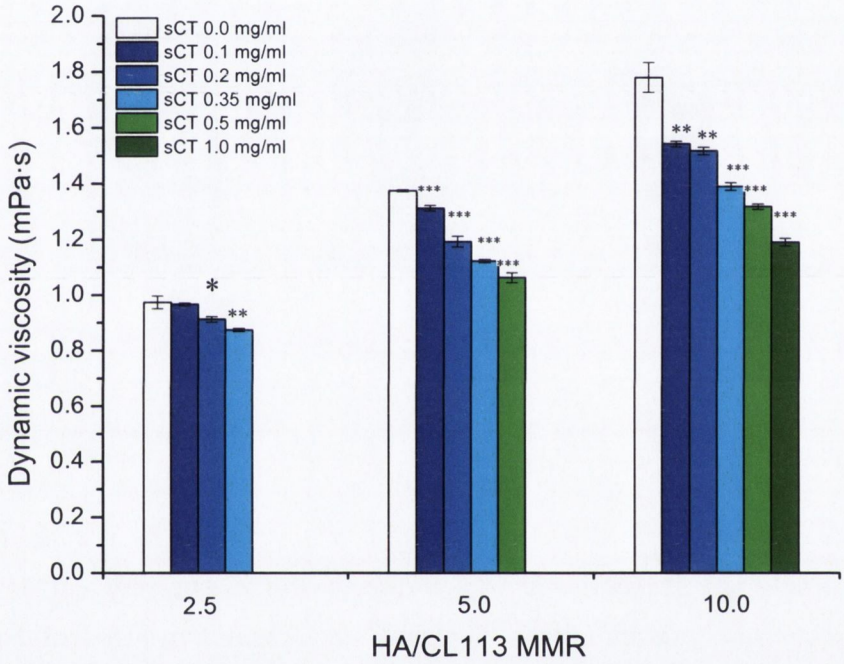

Fig.4.9 Dynamic viscosity of sCT-loaded HA/CL113 NPs based on TPC of 1 mg/ml. *p<0.05, **p<0.01 and ***p<0.001 versus sCT 0.0 mg/ml.

The viscosity increase correlated with an increase in HA/CL113 MMR, and 2 mg/ml-based formulations (Fig.4.10) are more viscous compared to those 1 mg/ml. These two tendencies are the same as for HA/CL113 NPs which do not contain sCT.

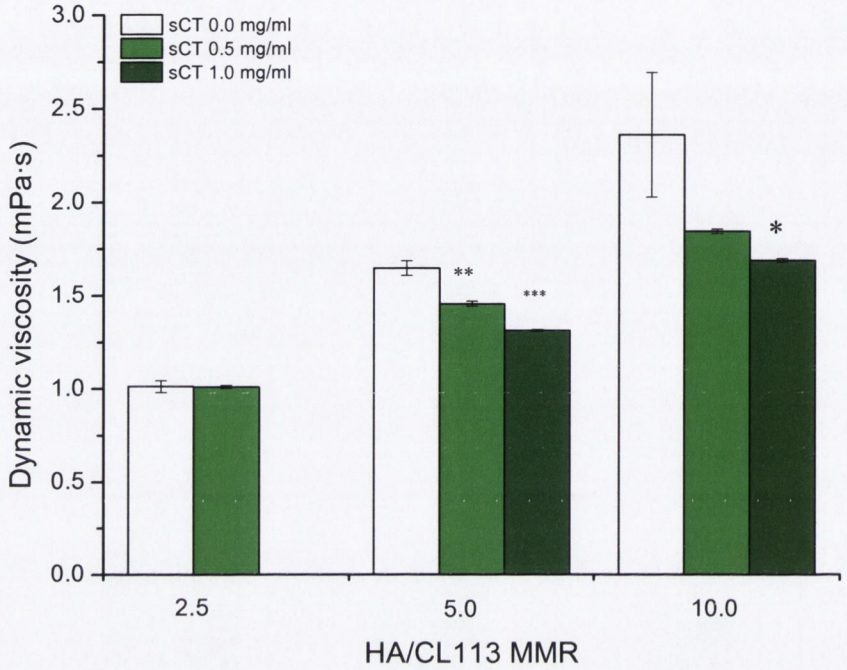

Fig.4.10 Dynamic viscosity of sCT-loaded HA/CL113 NPs based on TPC of 2 mg/ml. *p<0.05, **p<0.01 and ***p<0.001 versus sCT 0.0 mg/ml.

All HA/CL113 NPs containing sCT were characterised by a small particle size, the diameter of the particles was between 148±4 nm (TPC of 1 mg/ml; HA/CL113 MMR of 5 and sCT of 0.35 mg/ml) and 229±28nm (TPC of 1 mg/ml; HA/CL113 MMR of 2.5 and sCT of 0.35 mg/ml) (Fig.4.11). To our best knowledge, the former are one of the smallest, if not the smallest sCT-loaded particles produced so far. Other ionic-complexation based sCT containing nanoparticles reported so far are well over 200 nm in diameter. For example, Makhlof et al., (2010) produced 245 nm glycol chitosan based NPs, and Le et al., (2009) made TPP-sCT ionic complex with the diameter of 225 nm. The lipid (Garcia-Fuentes et al, 2005) or PLGA nanoparticles (Yung et al., 2009) were also characterised by the particle size greater than 200 nm. However, Cetin et al., (2012) obtained sCT-loaded Eudragit®-PLGA and Eudragit® nanoparticles smaller than 200 nm (the smallest had a diameter of 157.4±1 nm).

When TPC was 1 mg/ml and HA/CL113 MMR was 10, even using one of the lowest dose of sCT (0.2 mg/ml) decreased the particle diameter significantly ($p=0.020$). A further increase in the concentration of sCT led to a decrease and fluctuations in the particle size, but no statistically significant differences between them was found and all of them differed significantly from the control sample

without sCT. A gradual decrease and then slight variations were also observed for NPs with TPC of 1 mg/ml and HA/CL113 of 5, however only two samples with the highest doses of sCT (0.35 and 0.5 mg/ml) were statistically significantly smaller that the control sample without sCT ($p=0.013$ and 0.041 for 0.35 and 0.5 mg/ml of sCT, respectively). Different tendency can be observed for formulations with TPC of 1 mg/ml and HA/CL113 MMR of 2.5 - employing up to 0.2 mg/ml of sCT did not change the particle size statistically significantly ($p=0.675$), however an increase in the concentration of sCT to 0.35 mg/ml led to a statistically significant ($p=0.027$) increase in the particle diameter compared to the sample without sCT.

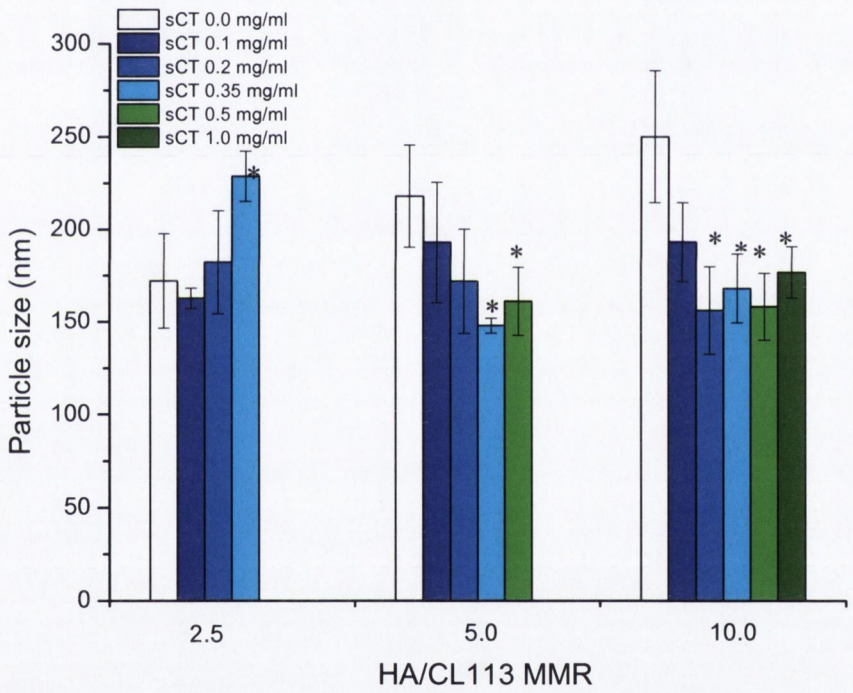

Fig. 4.11 Mean particle size of sCT loaded HA/CL113 NPs TPC of 1 mg/ml. *$p<0.05$ versus sCT 0.0 mg/ml.

The particle size of sCT-loaded NPs with TPC of 2 mg/ml tested was statistically significantly ($p<0.05$) lower than the size of the control sample without sCT with the exception of sCT of 0.5 mg/ml and HA/CL113 MMRs of 10 and 2.5, where p values were of 0.051 and 0.053, respectively. There were no statistically significant differences between the particle size of NPs with sCT concentration of 0.5 or 1 mg/ml, TPC of 2 mg/ml and HA/CL113 MMR of 5 and 10. Also, the HA/CL113 MMR did not seem to have a significant influence on the particle size of 2 mg/ml TPC NPs.

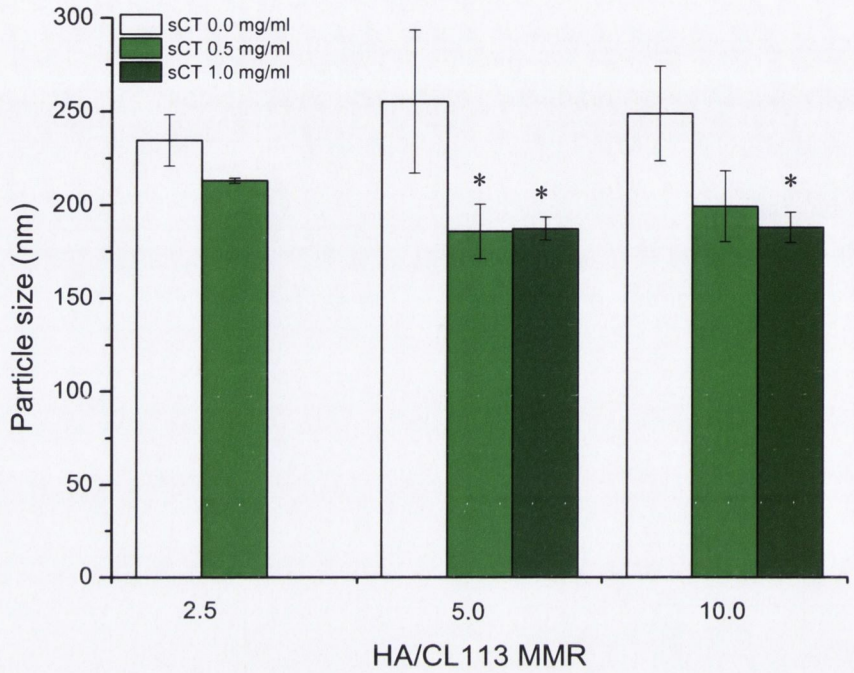

Fig. 4.12 Mean particle size of sCT loaded HA/CL113 NPs TPC of 2 mg/ml. *$p<0.05$ versus sCT 0.0 mg/ml.

All sCT-loaded NPs tested were characterised by a narrow size distribution as the PDI values were in the range between 0.072±0.035 (TPC of 1 mg/ml, HA/CL113 MMR of 2.5, sCT of 0.35 mg/ml) (Fig. 4.13) and 0.246±0.037 (TPC of 2 mg/ml, HA/CL113 MMR of 10, sCT of 0.5 mg/ml) (Fig. 4.14). Generally, loading of sCT into the NPs caused a gradual decrease in PDI values and some slight variations in this parameter can be observed. Samples with the highest sCT concentrations (e.g. TPC of 1 mg/ml, HA/CL113 MMR of 5 and sCT of 0.5 mg/ml; TPC of 1 mg/ml, HA/CL113 MMR of 10 and sCT of 1 mg/ml as well as TPC of 2 mg/ml, HA/CL113 MMR of 5 and sCT of 1 mg/ml) were characterised by PDI values significantly lower ($p<0.05$) than those of control samples without sCT. The particles were more homogenously dispersed in formulations containing higher amounts of CS also, samples with a lower concentration of polysaccharides were more homogenously dispersed, but the difference was not significant compared to the samples with higher polymer concentrations.

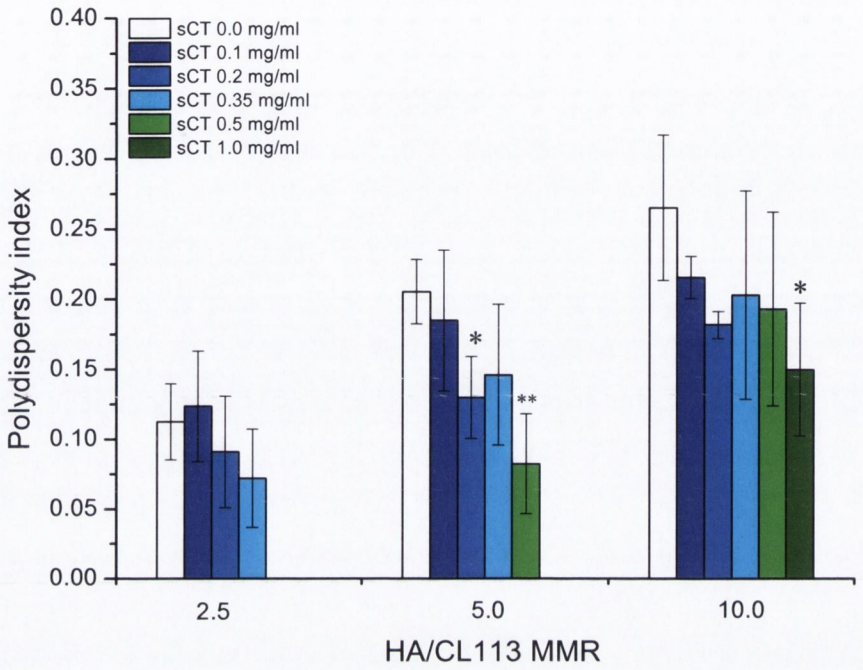

Fig. 4.13 Polydispersity indices of sCT-loaded HA/CL113 NPs TPC of 1 mg/ml. *p<0.05 and **p<0.01 versus sCT 0.0 mg/ml.

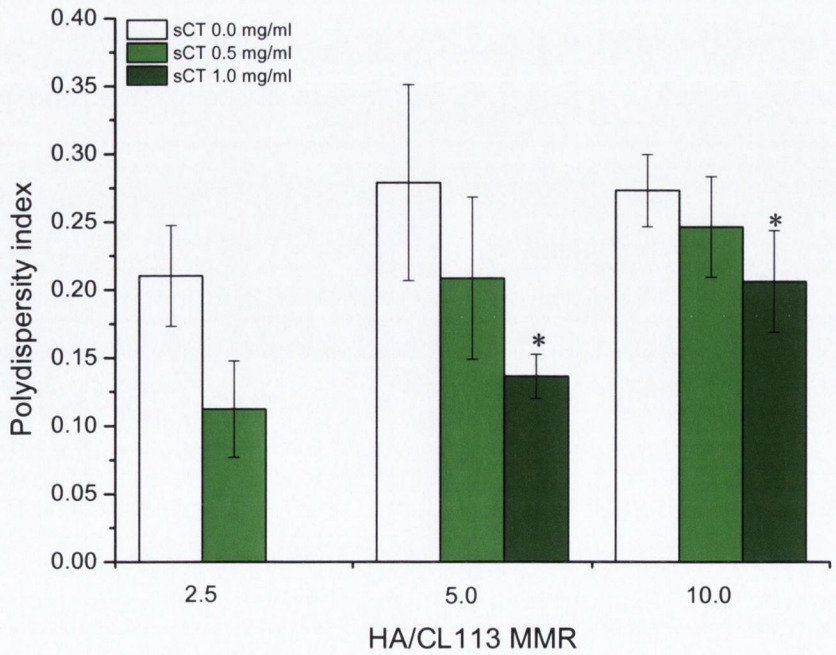

Fig. 4.14 Polydispersity indices of sCT-loaded HA/CL113 NPs TPC of 2 mg/ml. *p<0.05 versus sCT 0.0 mg/ml.

sCT forms a complex with HA and the solubility of this complex depends on MMR of both species. As mentioned earlier, when CS is added to HA/sCT complex dispersion, a competition between CS and sCT for binding with carboxylic groups of HA occurs. CS binds to HA much stronger than sCT- it has a higher charge density and molecular weight and it is capable to precipitate with HA at much lower concentrations. Therefore sCT is expected to be displaced from its HA binding places by CS. However, when HA is used in a high excess, it is expected to bind to both macromolecules. Nevertheless, due to the binding of HA to CS, many carboxylic groups of HA are not available for binding with sCT and the actual sCT/HA mixing ratio may be increased. As the solubility of the complex formed between sCT and HA decreases with increasing sCT concentration, it may possible that insoluble sCT/HA complexes are formed in the particles, and the presence of CS further decreases the solubility of the complexes. . Indeed, the increase in turbidity of NPs with TPC of 1 mg/ml containing larger amounts of sCT, despite a decrease in the particle size, suggests than more particles are formed. Also, 2 mg/ml-based formulations are markedly more turbid and are likely to contain more particles that the 1 mg/ml-based formulations, therefore the decrease in the particle size due to the presence of sCT may exert a stronger effect on the transmittance values than the possible formation of more particles. An increase in the particle size of NPs with TPC of 1 mg/ml, HA/CL113 MMR of 2.5 and sCT of 0.35 mg/ml formulation was observed. This formulation contains a relatively small excess of HA in relation to CL113 and sCT, and it is possible that the repulsion between positive charges of those species present in the particle due to their relatively smaller degree of neutralisation by negative charges of HA may be responsible for the increased particle size. Furthermore, NPs with larger amounts of sCT are generally characterised by lower polydispersity than HA/CL113 NPs without sCT and HA/sCT nanoparticles, therefore indicating that it is unlikely that two populations of particles, HA/sCT and HA/CL113, are formed. Hence, most of the particles formed are expected to contain both polycations: CS and sCT.

All nano-formulations tested maintained their negative surface charge despite loading sCT into the particles (Fig. 4.15 and 4.16). However a gradual, considerable decrease in the surface charge that correlated with the increase in sCT concentration was observed. Nevertheless, most of the nano-suspensions were characterised by the absolute values of zeta potential of close to 30 or more, therefore indicating their good physical stability. A statistically significant decrease in the surface charge can also be correlated with a decrease in HA/CL113 MMR and TPC.

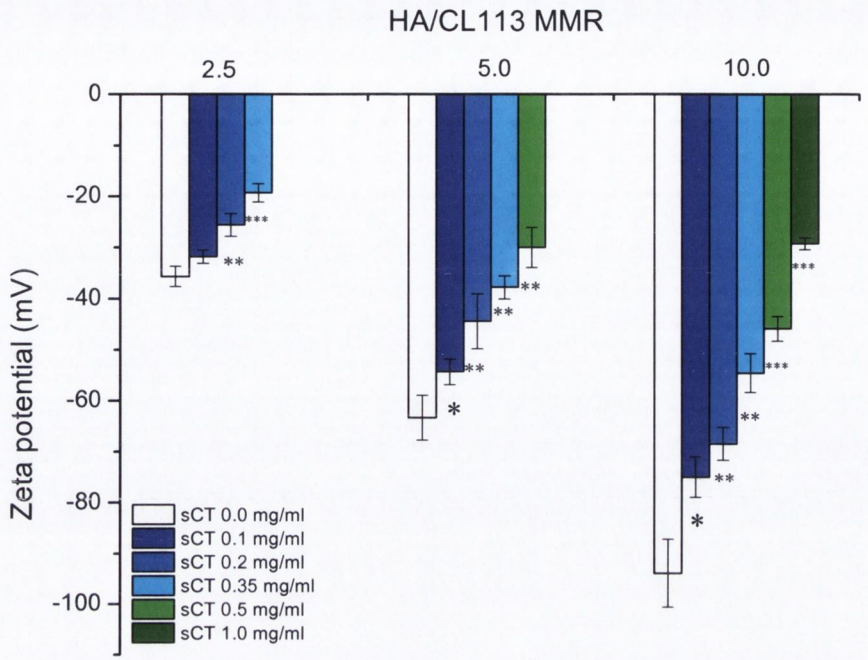

Fig. 4.15 The zeta potential of sCT-loaded HA/CL113 NPs TPC of 1 mg/ml. *p<0.05, **p<0.01 and ***p<0.001 versus sCT 0.0 mg/ml.

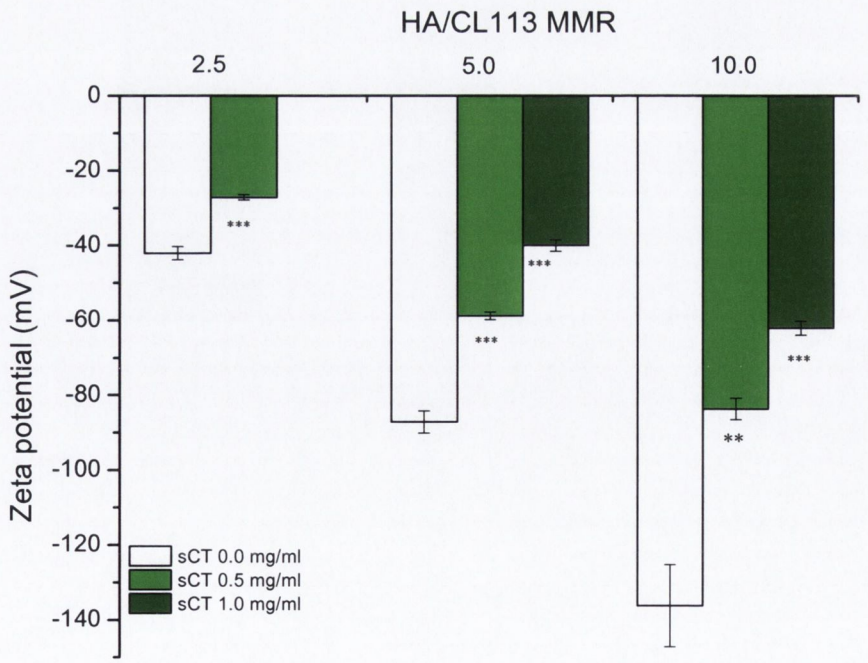

Fig. 4.16 The zeta potential of sCT-loaded HA/CL113 NPs TPC of 2 mg/ml. **p<0.01 and ***p<0.001 versus sCT 0.0 mg/ml.

pH of all sCT-containing samples varied between 5.1 and 5.7 and therefore may be considered as relatively similar (Fig. 4.17 and 4.18). An increase in the concentration of $[H^+]$ corresponding to an increasing concentration of sCT may be observed. Apart from incorporation of sCT into the NPs, a decrease in pH may also be partially responsible for the decrease in the negative surface charge of the nanoparticles. Neither the HA/CL113 MMR nor the concentration of the polysaccharides had a significant influence on the pH of the nano-suspensions. Although high amounts of chitosan decreased considerably the pH of HA/CS nanoparticles (see chapter 3), for sCT studies only formulations with a high excess of HA in relation to CL113 (high HA/CL113 MMR) with similar pH values were selected, and this may explain why no considerable influence of HA/CL113 MMR on pH was observed.

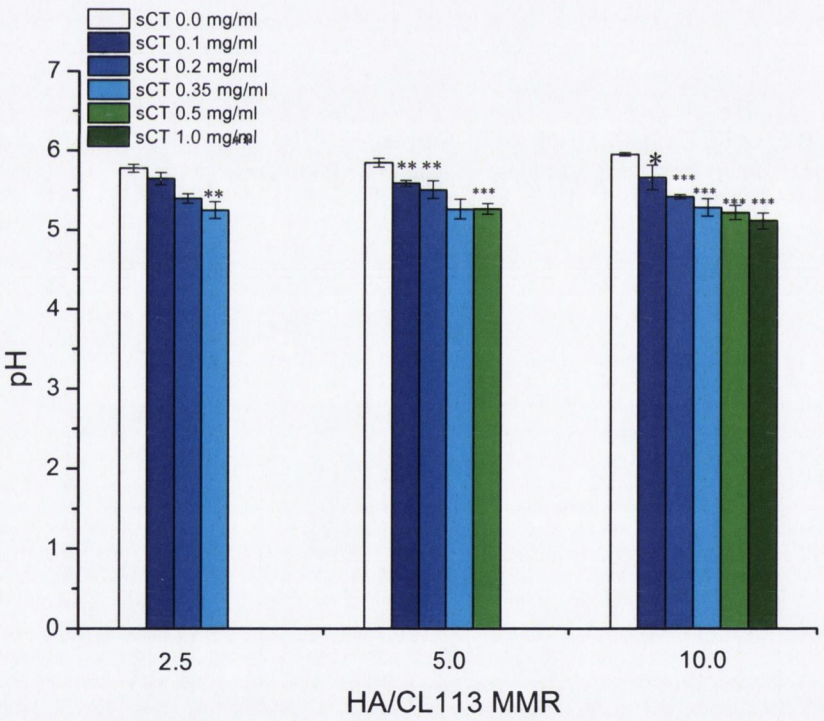

Fig. 4.17 pH of sCT-loaded HA/CL113 nanosuspensions TPC of 1 mg/ml. *p<0.05, **p<0.01 and ***p<0.001 versus sCT 0.0 mg/ml.

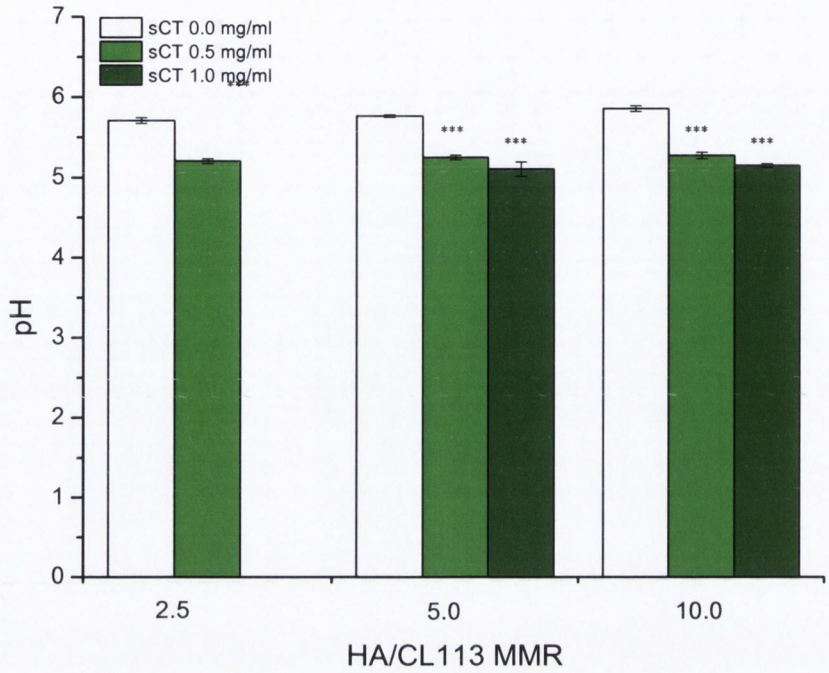

Fig. 4.18 pH of sCT-loaded HA/CL113 nanosuspensions TPC of 2 mg/ml. ***p<0.001 versus sCT 0.0 mg/ml.

4.5 Characterisation of HA/CL113/sCT nanoparticles: Impact of the molecular weight of HA

As described in Chapter 3, the molecular weight of HA had a considerable influence on the properties of HA/CL113 NPs. In order to verify the influence of the molecular weight of HA on the properties of sCT-loaded NPs, formulation of HA/CL113 MMR of 5, TPC of 1 mg/ml and sCT of 0.5 mg/ml was selected due to its good physical stability, micrometric properties (PS, ZP) and high sCT loading (for loading see Section 4.8 below). Three molecular weights of HA were tested: 176 kDa, 257 kDa and 590 kDa. HA with higher molecular weight was not considered due to formation of macroscopic aggregates with chitosan (Chapter 3).

It can be seen that incorporation of sCT did not influence the turbidity of 590 kDa HA based formulation, however the transmittance of sCT-loaded formulations with HA of 257 and 176 kDa was significantly lower than their controls without sCT containing the same type and amount of the other polymer (Fig. 4.19). Also, sCT-loaded formulation based on 176 kDa HA was significantly more transparent than the formulation containing 590 kDa HA.

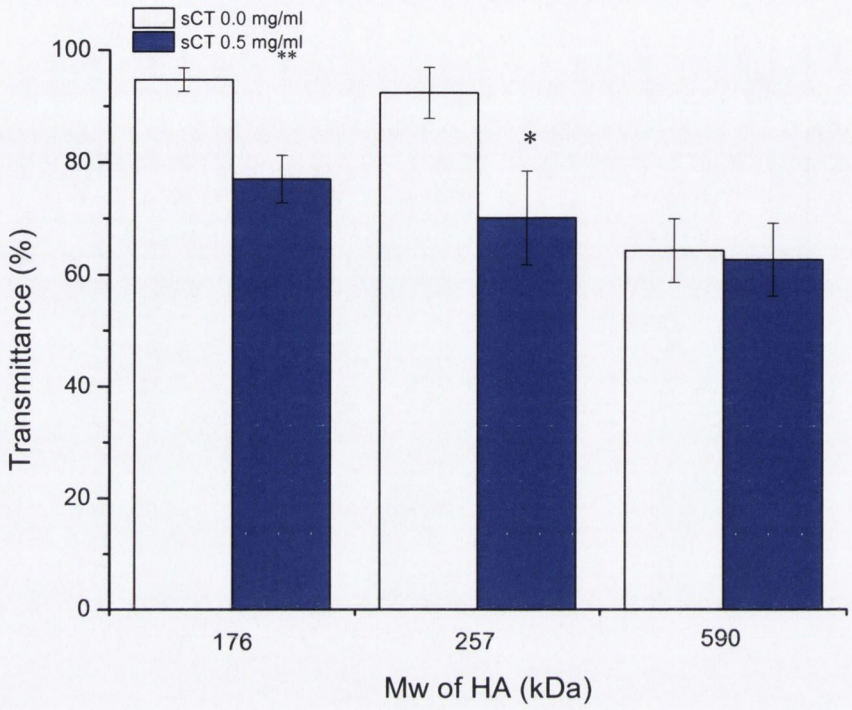

Fig. 4.19 Transmittance of sCT-loaded HA/CL113 NPs containing HA with different molecular weights. *p<0.05 and **p<0.01 versus sCT 0.0 mg/ml.

The dynamic viscosity of sCT-loaded nano-suspensions was statistically significantly lower than nano-suspensions without sCT for all three HA tested. 590 kDa HA-based nano-suspension containing sCT was significantly more viscous that other two formulations containing 176 and 257 kDa HA (Fig. 4.20).

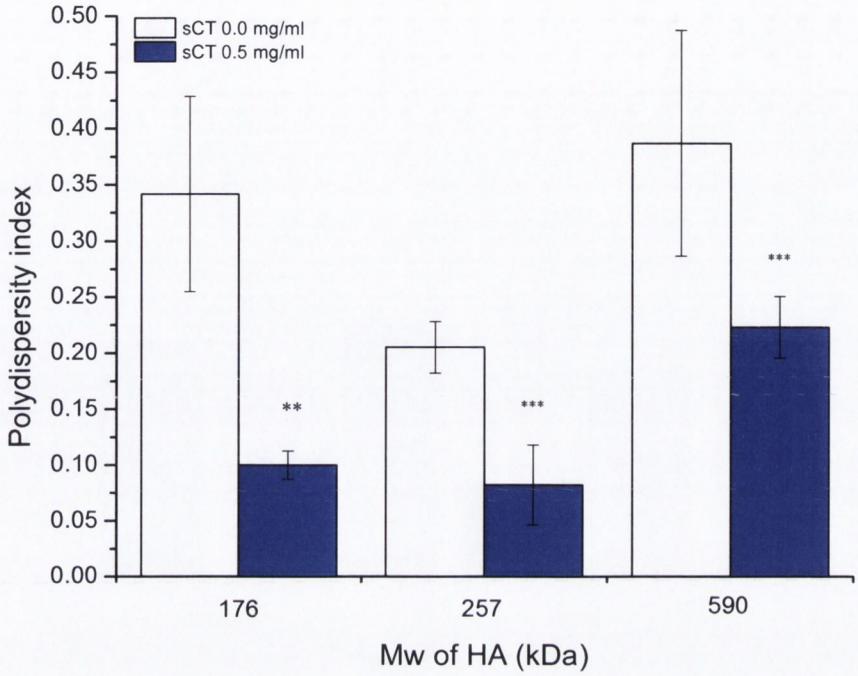

Fig. 4.20 Viscosity of sCT-loaded HA/CL113 NPs containing HA with different molecular weights. **p<0.01 and ***p<0.001 versus sCT 0.0 mg/ml.

After loading of 0.5 mg/ml sCT into NPs containing HA at different Mw, a statistically significant decrease in the particle size was observed compared to the controls without sCT (p=0.019 and 0.041 for HA590 and HA257-based samples, respectively) with the exception of HA176-based sample, where p=0.055 (Fig. 4.21). All sCT-loaded formulations with different Mw HA tested had a similar particle size between 131-161 nm, therefore it can be concluded that the molecular weight of HA in the range of ~150-600 kDa does not influence the particle size of sCT-loaded NPs.

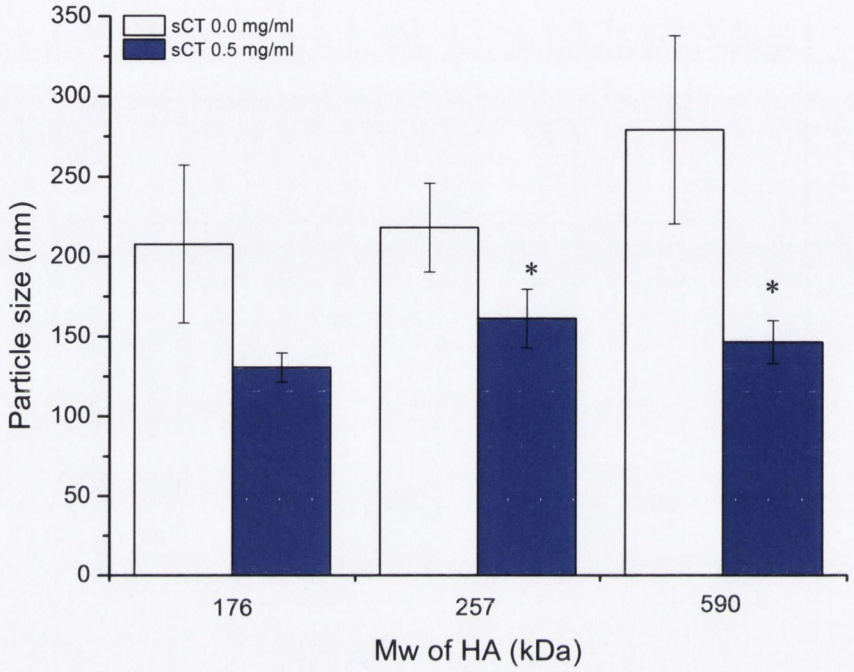

Fig. 4.21 Particle size of sCT-loaded HA/CL113 NPs containing HA with different molecular weights. *p<0.05 versus sCT 0.0 mg/ml.

Loading of sCT also statistically significantly decreased the polydispersity index of the nanoparticles compared to control samples without sCT (Fig. 4.22). NPs containing 590 kDa HA were characterised by a significantly broader size distribution that NPs with 257 or 176 kDa HA.

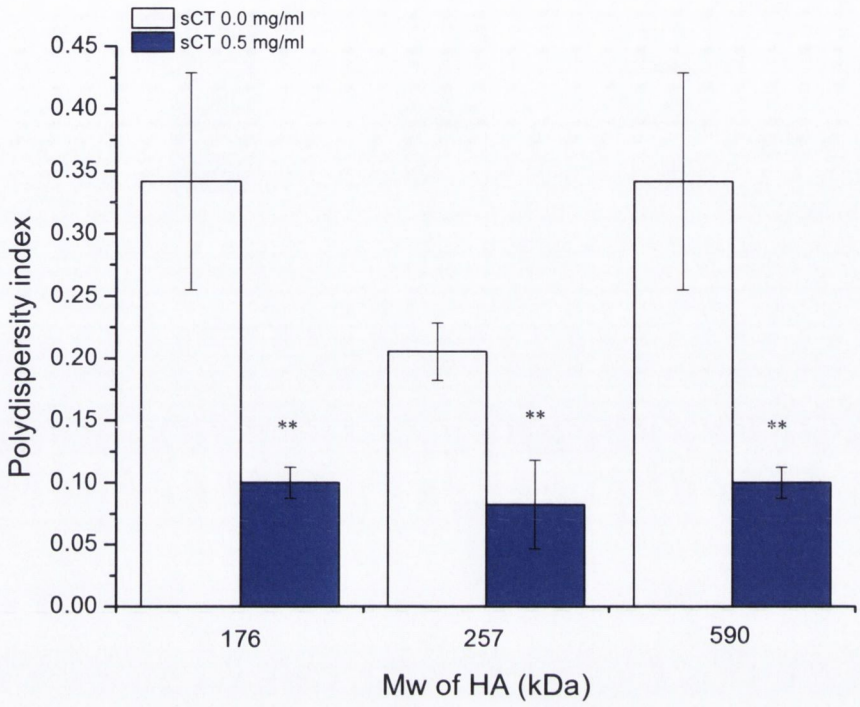

Fig. 4.22 Polydispersity index of sCT-loaded HA/CL113 NPs containing HA with different molecular weights. **p<0.01 versus sCT 0.0 mg/ml.

The negative surface charge of the NPs was markedly decreased upon incorporation of sCT into the NPs (Fig. 4.23). The difference in the zeta potential value between sCT-loaded NPs and control without sCT was the highest for 590 kDa HA-based NPs as the surface charge decreased by 74 mV. However even after incorporation of 0.5 mg/ml sCT, the particles maintained a highly negative surface charge of -30 mV in the case of 176 and 257 kDa HA NPs, and -45.4 mV in the case of 590 kDa HA NPs.

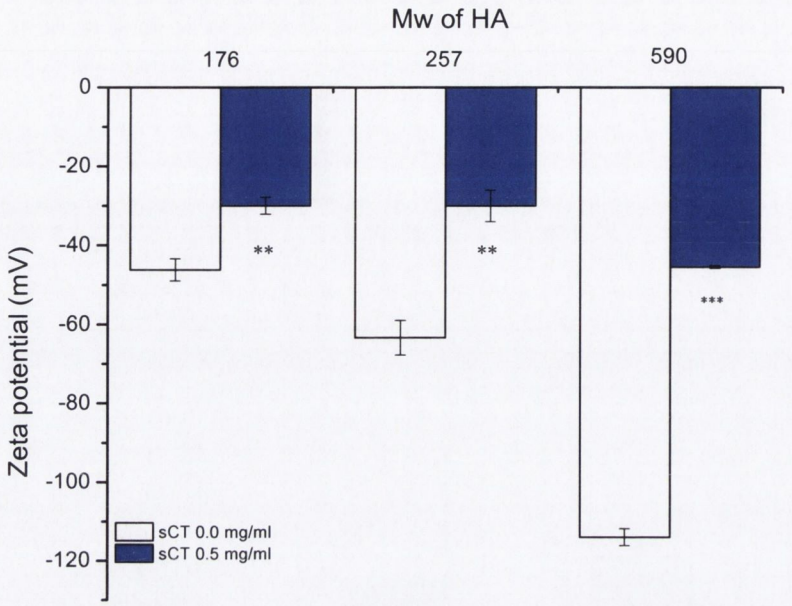

Fig. 4.23 Zeta potential of sCT-loaded HA/CL113 NPs containing HA with different molecular weights. **p<0.01 and ***p<0.001 versus sCT 0.0 mg/ml.

The molecular weight of HA did not have any influence on the pH of sCT-loaded nanoparticles- there were no statistically significant differences between pH of sCT-loaded different Mw HA-based NPs (Fig. 4.24). Loading of 0.5 mg/ml of sCT decreased the pH by ~0.4 unit in the case of all three molecular weights of HA tested.

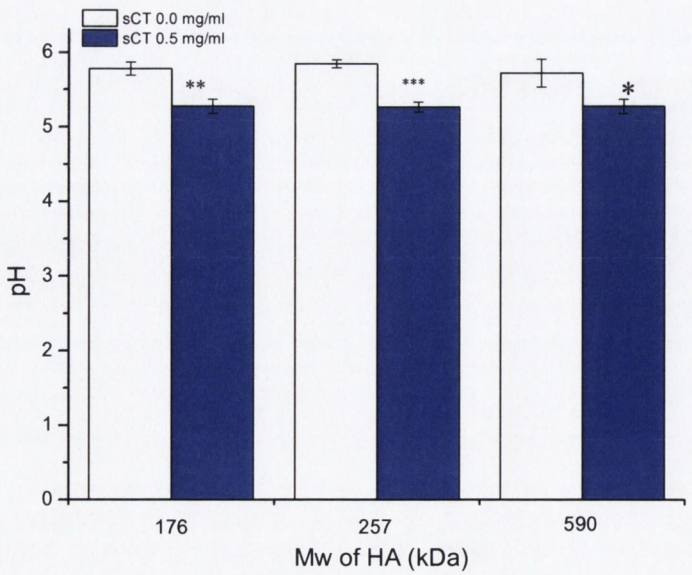

Fig. 4.24 pH of sCT-loaded HA/CL113 NPs containing HA with different molecular weights. *p<0.05, **p<0.01 and ***p<0.001 versus sCT 0.0 mg/ml.

4.6 TEM and SEM of HA/CL113/sCT NPs

TEM (Fig.4.25) and SEM (Fig.4.26) micrographs show that HA/CL113/sCT NPs were spherical in shape. Similarly to the previously described HA/CL113 NPs (Chapter 3), sCT-loaded NPs with HA/CL113 MMR of 5 are composed of a relatively dense core surrounded by diffused corona (Fig. 4.25 A and B). The size of the particles in TE micrographs was comparable to size determined by DLS, but some of the NPs seen in TE micrographs were slightly smaller- possibly due to removal of water (HA is known to swell in water). Interestingly, the corona was not observable for sCT-loaded HA/CL113 MMR of 2.5 NPs (Fig. 4.25 C). This is in agreement with the previous studies about HA/CL113 NPs without sCT, where the size of corona decreased when the charge mixing ratio of polymers was approaching 1 (Chapter 3). The size of most of sCT-loaded HA/CL113 MMR of 2.5 NPs observed in TE micrographs (Fig. 4.25 C) was also similar to size determined by DLS (163±5 nm), however a few larger particles were present (the size of approximately 300 nm), what may be the result of aggregation of some of the particles.

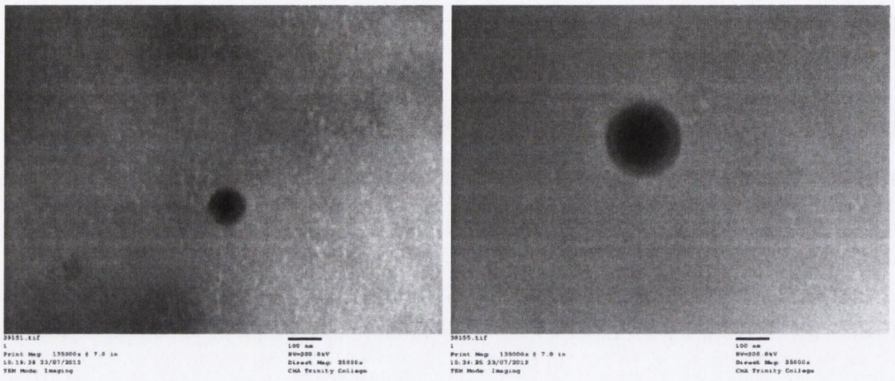

A)

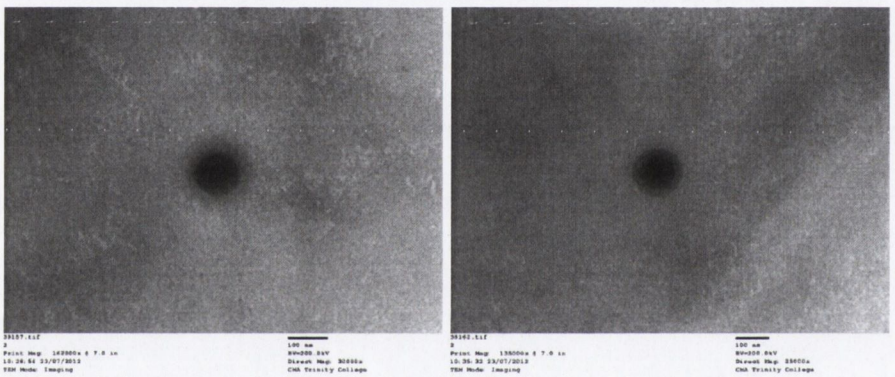

B)

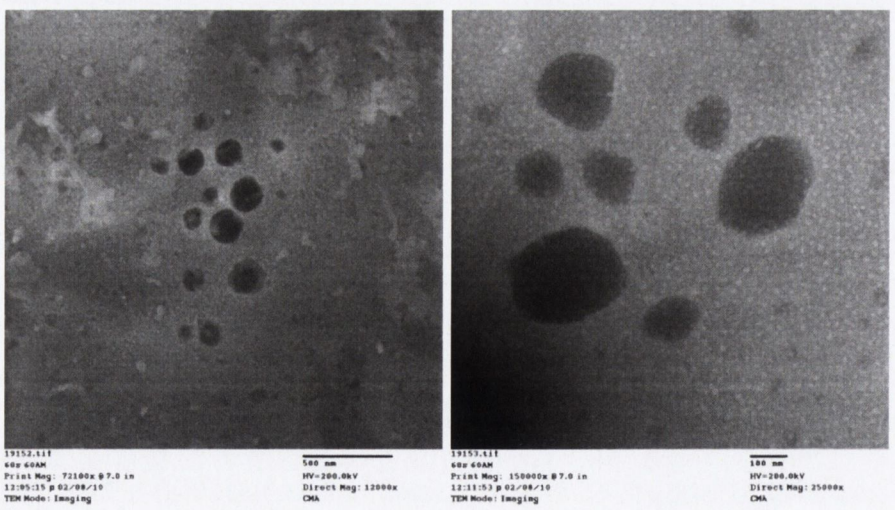

C)

Fig.4.25 TEM micrographs of A) HA/CL113 MMR of 5, sCT of 0.1 mg/ml (S2- DLS: 193±33 nm); B) HA/CL113 MMR of 5, sCT of 0.5 mg/ml (S11- DLS: 161±18 nm); C) HA/CL113 MMR of 2.5, sCT of 0.1 mg/ml (S3- DLS: 163±5 nm). TPC was of 1 mg/ml in all cases. Scale bars: A, B and C right- 100 nm; C left- 500 nm.

SEM micrographs show that HA/CL113/sCT NPs formed cauliflower-like assemblies. The formation of assembles and bridges may be the result of sample coating and processing. The size of samples observed in SE micrographs was smaller than the size determined by DLS or TEM perhaps due to water removal. In HA/CL113 MMR of 2.5 NPs the presence of larger aggregates was also observed, which is consistent with TEM results.

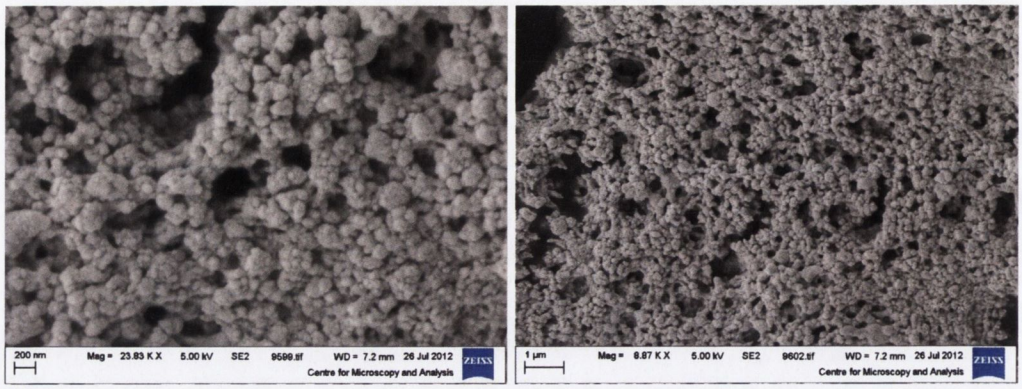

A)

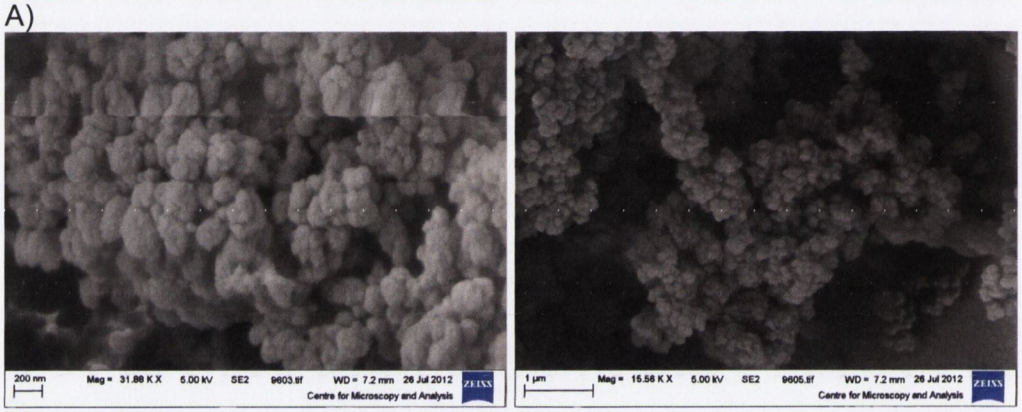

B)

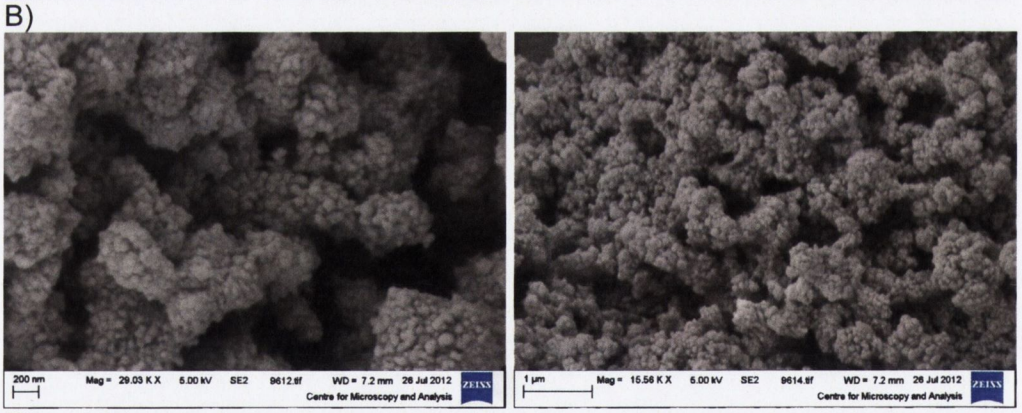

C)

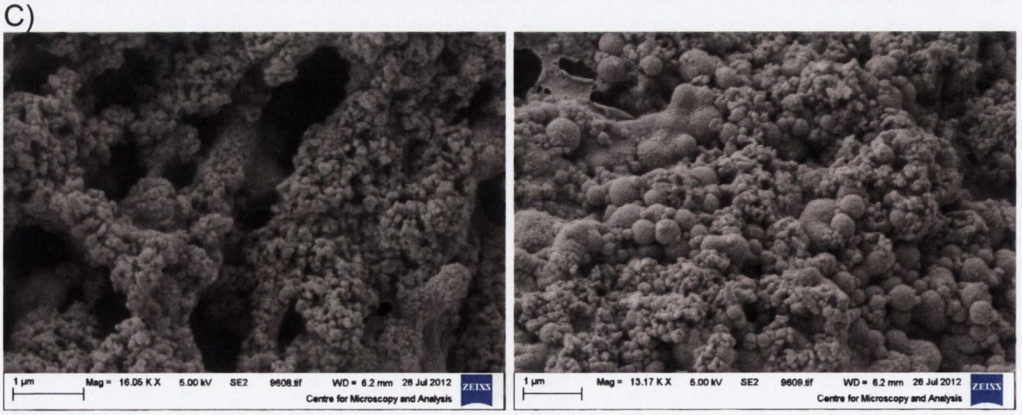

D)

Fig.4.26 Scanning electron micrographs of A) TPC of 1 mg/ml, HA/CL113 MMR of 5, sCT of 0.1 mg/ml (S2- DLS: 193±33 nm); B) TPC of 1 mg/ml, HA/CL113 MMR of 5, sCT of 0.5 mg/ml (S11- DLS: 161±18 nm); C) TPC of 2 mg/ml, HA/CL113 MMR of 5, sCT of 0.5 mg/ml (S18- DLS: 186±14 nm); D) TPC of 1 mg/ml, HA/CL113 MMR of 2.5, sCT of 0.35 mg/ml (S9- DLS: 229±13).

4.7 Isoelectric point of sCT-loaded HA/CL113 NPs

As previously shown, sCT decreased significantly the surface charge of the particles. HA/CL113 MMR has been shown to be the main factor determining the isoelectric point of the particles. As sCT is also positively charged at neutral and acidic pH values, it is important to examine if the isoelectric point, and therefore the sign of the surface charge of the particles at different pH is affected by sCT. Table 4.3 shows the values of the isoelectric points of HA/CL113 MMR of 5 and TPC of 1 mg/ml NPs loaded with different amounts of sCT.

Table 4.3 The isoelectric point values of sCT-loaded HA/CL113 NPs.

TPC [mg/ml]	HA/CL113 MMR	sCT [mg/ml]	IEP
1	5	0.1	2.42±0.07
1	5	0.2	2.56±0.42
1	5	0.5	2.52±0.54

The value of isoelectric point was not affected by the presence of sCT and all formulations tested had the isoelectric point values between 2.42-2.56.The values did not differ significantly from the isoelectric point of the control formulation without sCT (2.47- see Chapter 3). It may be due to the fact that the pKa of HA is 2.9 and therefore at low acidic pH values most of the carboxylic groups of HA are not ionised anymore, the interactions between HA and sCT may be considerably weaker and the HA-sCT complex is likely to dissociate. Also, there is a competition between chitosan and sCT for the few carboxylic groups of HA which remain ionised and, as chitosan binds to HA stronger than sCT, chitosan is most likely to be bound to HA. As the charge density of sCT is much lower than that of chitosan, it may not have a significant effect on the net particle surface charge at low pH values where the system is close to charge neutralisation point.

In conclusion, similarly to HA/CL113 MMR of 5 NPs without sCT, sCT-loaded NPs are not expected to be stable at low acidic pH values, e.g. in the stomach juice, therefore a protection (e.g. enteric-coated capsules) would be needed if they are to be administered orally.

4.8 Binding of sCT by HA/CL113 NPs: isolation of non-associated sCT, association efficiency and drug loading

When preparing drug-loaded carriers, it is necessary to determine the association efficiency (AE) and the drug loading (DL), as they are two important nanoparticle quality control key parameters with substantial impact in their application (Lu et al., 2011). Successful polymeric nanocarriers should be

characterised by a high loading capacity in order to reduce the amount of the particles required for administration. To determine the AE and DL, non-associated drug must be isolated from the carrier and carrier-associated drug. High speed centrifugation (15,000 g, 30 min) caused aggregation of negatively charged HA-based NPs. That is in agreement with studies of Oyarzun-Ampuero et al., (2009) who observed that if the amount of polyanions in CS-HA-TPP-heparin NPs was too high, it was impossible to isolate the particles due to particle aggregation or lack of resuspendability.

An alternative to high speed centrifugation is a combined ultrafiltration-centrifugation technique, already used e.g. for the separation of non-encapsulated sCT from chitosan-PEG nanocapsules (Prego et al., 2006). Another challenge is to isolate associated sCT from the nanoparticles. Difficulties in the extraction of nano-encapsulated sCT have already been reported (Prego et al., 2006), therefore many authors (e.g. Prego et al., 2006, Garcia-Fuentes et al., 2005, Cetin et al., 2012) used an indirect method to determine the amount of sCT bound with NPs, which is calculated as the difference between the total amount of sCT used to prepare the loaded systems and the non-encapsulated sCT.

Combined ultrafiltration-centrifugation technique was successfully used in the separation of sCT from the NPs and sCT was extracted from its complexes with HA with the employment of 0.0001 M NaOH solution. The validation of these methods is described in Appendix 1.

As shown in Table 4.4, sCT associated with HA/CL113 NPs very efficiently. In all formulations tested the association efficiency (AE) values were well over 90%, nearly 100% in most cases. Although there were statistically significant differences in the groups of formulations with HA/CL113 MMR of 5 and 10 when different concentrations of sCT were used (e.g. the AE of sCT 0.5 mg/ml was significantly smaller ($p=0.041$) than AE of other HA/CL113 based samples containing a smaller quantity of sCT), the differences were smaller than 2%. All the AE values of the group with HA/CL113 MMR=2.5 were significantly different ($p=0.006$), however the difference, again, is very small and less than 4%. It is worth mentioning that the formulations with the lowest AE for each HA/CL113 mass ratio tested contained the highest dose of sCT for that particular HA and CL113 particle composition. It can be observed that the HA/CL113 MMR also had an effect on the AE of sCT in HA/CL113 NPs. Although the difference was small, NPs with HA/CL113 MMR of 2.5 always had the AE value significantly lower than two other MMRs for all doses of sCT tested $p=0.022$, 0.001 and $p<0.001$ for 0.1, 0.2 and 0.35 mg/ml of sCT), and when the dose of sCT was increased to at least

0.35 mg/ml, the difference between the AE of all MMRs tested were significant ($p=0.043$ and 0.036 for sCT of 0.35 and 0.5 mg/ml, respectively, when HA/CL113 MMR of 5 was compared to MMR of 10).

Table 4.4 The association efficiency and drug loading of TPC 1 mg/ml-based HA/CL113/sCT NPs. Samples 12, 14 and 15 aggregated and as they were not usable they were not further analysed.

Sample	Initial sCT concentration [mg/ml]	HA/CL113 MMR	Extracted sCT [%]	AE [%]	Drug loading [%]
1	0.1	10	99.32±1.34	99.52±0.09	9.05±0.01
2	0.1	5	93.84±4.39	99.47±0.32	9.05±0.03
3	0.1	2.5	89.44±2.72	98.09±0.81	8.93±0.07
4	0.2	10	95.01±1.90	99.49±0.30	16.60±0.05
5	0.2	5	95.13±3.22	99.40±0.35	16.58±0.06
6	0.2	2.5	90.51±4.17	96.02±0.96	16.11±0.16
7	0.35	10	93.02±1.38	99.86±0.05	25.90±0.01
8	0.35	5	93.97±5.23	99.64±0.12	25.86±0.03
9	0.35	2.5	85.91±3.09	94.57±0.70	24.87±0.18
10	0.5	10	92.22±1.12	99.85±0.05	33.30±0.02
11	0.5	5	93.91±2.57	98.34±0.84	32.97±0.28
12	0.5	2.5	N/A	N/A	N/A
13	1.0	10	88.10±1.12	98.29±0.37	49.57±0.19
14	1.0	5	N/A	N/A	N/A
15	1.0	2.5	N/A	N/A	N/A

As the amount of the polysaccharides used was the same in all formulations tested (TPC = 1 mg/ml), only the proportions between HA and CL113 were changed. sCT was very efficiently associated with the particles and the main factor determining the sCT loading of the particles was the dose of sCT used in their preparation. The maximum dose of sCT which could be loaded into the particles was determined by their composition- the more HA in the particles, the more of sCT they were capable to associate before aggregation occurred.

A similar behaviour of NPs was observed when TPC was increased to 2 mg/ml (Table 4.5). Only two highest doses of sCT were tested: 0.5 and 1 mg/ml. An increase in the dose of sCT loaded resulted in a slight, barely noticeable decrease in the AE, easier to observe when extracted sCT was taken into account, however the differences were generally not significant. Similarly to the 1 mg/ml TPC-based NPs, the lowest HA/CL113 MMR tested for a particular dose of sCT had AE and drug loading significantly lower than other MMRs.

Table 4.5 The association efficiency and drug loading of TPC 2 mg/ml-based HA/CL113/sCT NPs. Sample 22 aggregated and as it was not usable it was not further analysed.

Sample	Initial sCT concentration [mg/ml]	HA/CL113 MMR	Extracted sCT [%]	AE [%]	Drug loading [%]
17	0.5	10	96.93±2.52	99.62±0.09	19.94±0.02
18	0.5	5	97.50±3.76	99.19±0.38	19.87±0.08
19	0.5	2.5	90.61±1.78	94.20±1.88	19.06±0.38
20	1.0	10	95.21±1.78	99.21±0.14	32.82±0.13
21	1.0	5	92.94±3.41	97.71±0.38	33.26±0.05
22	1.0	2.5	N/A	N/A	N/A

It can be seen, that the molecular weight of HA used for the preparation of the particles did not have an influence on binding of sCT to the particles. There was no significant difference in the AE or drug loading between NPs composed of 590, 257 or 176 kDa HA (Table 4.6).

Table 4.6 Association efficiency and drug loading of HA/CL113/sCT NPs containing HA590 and HA176).

Sample	Initial sCT concentration [mg/ml]	Mw of HA [kDa]	Extracted sCT [%]	AE [%]	Drug loading [%]
23	0.5	590	96.11±1.53	98.37±0.21	32.97±0.07
24	0.5	176	94.26±2.37	98.74±0.23	33.05±0.08

In conclusion, sCT-loaded HA/CL113 nanoparticles were characterised by an excellent association efficiency and very high drug loading. To our best knowledge, this is the highest loading of sCT reported so far, and one of the highest association efficiencies. This is undoubtedly one of the main advantages of HA/CL113 NPs over other nanoparticle-based delivery systems described so far.

4.9 *In vitro* release of sCT

The results of *in vitro* release studies of sCT from NPs showed that an initial quick release of the peptide occurred upon dilution of NPs in PBS (Fig.4.27).

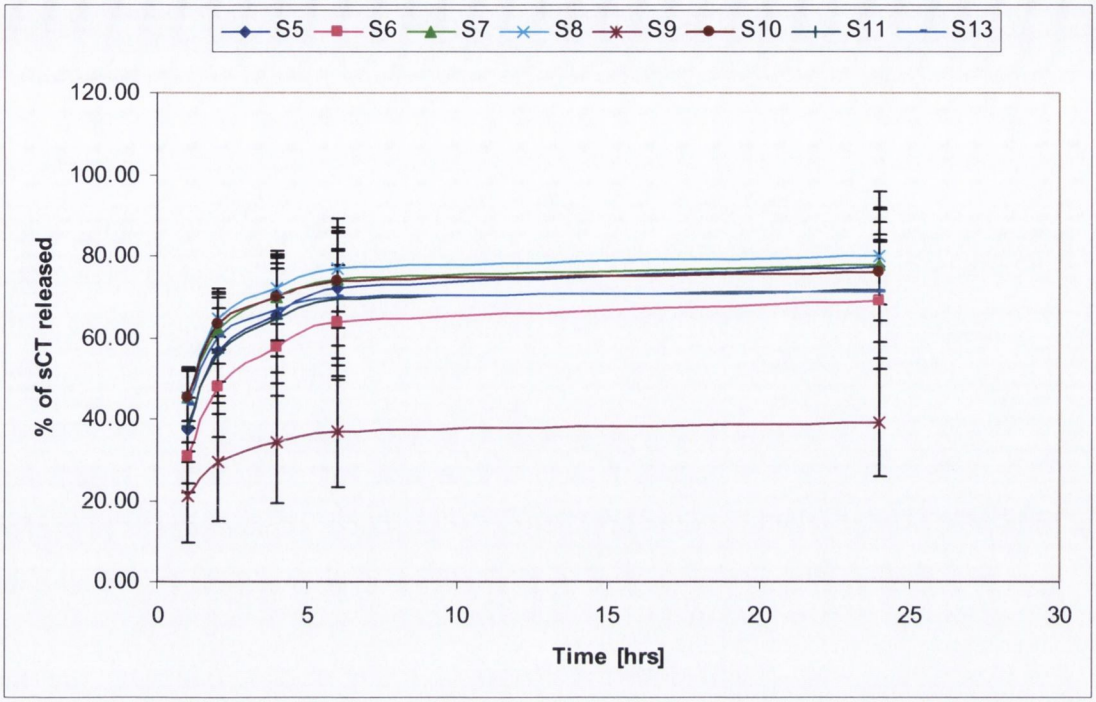

Fig.4.27 *In vitro* sCT release studies from sCT-loaded HA/CL113 NPs.

The amount of sCT released within the first hour ranged between 21±11 and 45±7%, depending on the formulation. The interactions between polymers within the NPs are expected to be mainly electrostatic, therefore if the ionic strength of the dispersant increases, the charges of the polymers in particles may be shielded and Coulombic interactions will be weaker. Also, as the pH of PBS (7.4) is higher than that of nano-suspensions, the positive charge of sCT is decreased and therefore its interactions with HA may be weaker, even though the negative charge of HA is supposed to increase. A dilution, which may increase the solubility of HA/sCT complex, may also be a factor which facilitates the dissociation of sCT from the nanoparticles.

This initial quick release phase (1-2 hours) was followed by a prolonged release phase within next 4 hours. The rate of sCT release decreased considerably over time. After 6 hours of release a plateau was achieved.

All formulations had similar release profiles with the exception of sample containing 0.35 mg/ml of sCT and HA/CL113 MMR of 2.5, which was characterised by a markedly lower release than other formulations and in which only 40% of sCT was released after 24 hours. In other formulations the amount of sCT released after 24 hours varied between 71 and 80%.

As described in Chapter 3, HA/CL113 NPs are composed of a relatively dense hydrophobic core, which is composed of HA and chitosan, and a corona

with smaller density, which is supposed to contain mainly HA. Although a complex between sCT and HA is formed before addition of chitosan, the chitosan is supposed to have much stronger interactions with HA than sCT and therefore upon its incorporation into the system it may replace sCT. As the corona contains the excess of HA, it is likely that this is where sCT is primarily localized in the particle. Indeed, particles with higher HA/CL113 MMRs, which are expected to have bigger coronas, are capable to load more sCT. The incorporation of sCT may increase the density and cause the contraction of the corona due to reduction of repulsion between HA chains and cross-linking the HA chains by sCT. This may be responsible for the decrease in the particle size of sCT-loaded NPs when compared to equivalent, unloaded systems. The release studies appear to confirm this hypothesis. The initial burst and quick release phase may be due to the dissolution of sCT localized on the particle surface and in the outer layers of corona, which due to its looser structure is more easily penetrated by the dispersant. However, as some of sCT may be localized in the hydrophobic, dense core, it is more difficult to extract it from there and that fraction of sCT may be released in a final, slow released phase.

Interestingly, the formulation with the lowest amount of sCT released (sample 9) was made of HA and CL113 at MMR of 2.5 and samples with the lowest HA/CL113 MMR are characterised by the smallest corona layer. Two samples with HA/CL113 MMR of 2.5 were tested for release of sCT- one of them had 0.2 mg/ml of sCT (sample 6), and the release profile of that formulation was similar to formulations with higher HA/CL113 MMRs, although the amount of sCT released was slightly lower. Another HA/CL113 MMR of 2.5 sample had the sCT concentration increased to 0.35 mg/ml (sample 9), and this formulation had a considerably lower amount of sCT released. It is possible, that when the amount of sCT is lower, it is localized in the corona layer, however due to relatively small size or lack of the corona in HA/CL113 MMR of 2.5 NPs, the carboxylic groups of HA in corona may be instantaneously saturated, and relatively high fraction of sCT is localized in the hydrophobic core. This may explain why only 40% of sCT was released from the HA/CL113 of 2.5 and sCT of 0.35 mg/ml formulation (sample 9). Indeed, when the amount of sCT released per mg of NPs was taken into account instead of % of sCT released (Fig.4.28), it can be observed that both HA/CL113 of 2.5 formulations released similar doses despite the fact that the loading of those two formulations differed considerably. For other formulations tested the amount of sCT released was determined by the drug loading- samples with similar drug loading released similar quantities of sCT irrespective of the HA/CL113 MMRs.

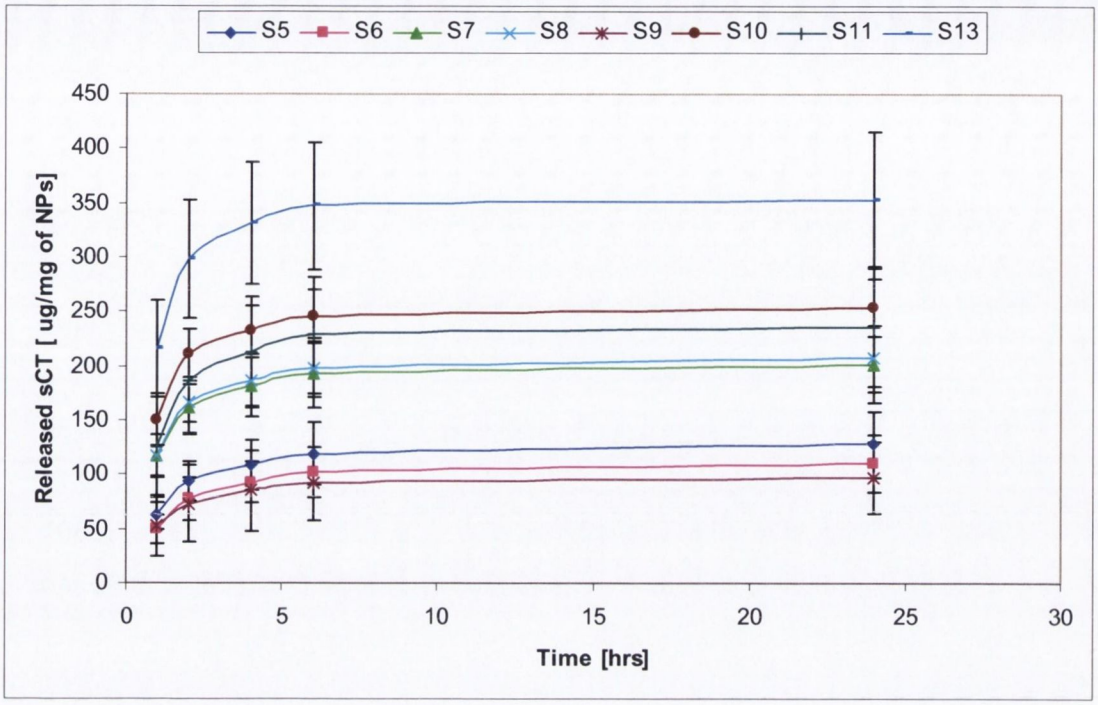

Fig.4.28 The dose of sCT released from sCT-loaded HA/CL113 NPs.

The data from the release studies was fitted to the first order equation (see Chapter 2, Section 2.2.9, Equation 2.4). The parameter estimates and related statistics are summarised in Table 4.7. Examples of the fitting curves of average values of the amount of sCT released from the different formulations are shown in Appendix 2. It can be observed that some samples with higher HA/CL113 MMR generally release more sCT than samples with lower MMRs. This difference is especially pronounced in the 0.35 mg/ml sCT based samples- 1 mg of S7 or S8 (HA/CL113 MMRs of 10 and 5, respectively) releases 100 μg of sCT more than 1 mg of S9 (HA/CL113 MMR of 2.5). The release rate constant k is also lower for the samples with HA/CL113 MMR of 2.5 compared to higher HA/CL113 MMRs (5 and 10).

Table 4.7 Model parameter estimates and related goodness of fit statistics for sCT release data fitted to the first order model. The composition of samples is shown in Table 4.4

Sample	k [min^{-1}]	W_∞ [µg/mg of NPs]	Red. Chi-Sq.	R Sq.
S5	0.6778±0.0607	135±3.3	22.70	0.99176
S6	0.6034±0.0471	124±2.8	14.70	0.99366
S7	0.8958±0.0679	217±4.0	39.43	0.99448
S8	0.8624±0.0565	217±0.9	30.05	0.99538
S9	0.7642±0.0644	108±0.8	12.71	0.99285
S10	0.9349±0.0520	259±3.4	29.83	0.99710
S11	0.7832±0.0431	245±3.5	27.78	0.99697
S13	0.9644±0.0386	390±3.7	36.38	0.99844

Although the release of sCT from HA/CL113 NPs is markedly prolonged, most sCT is released within 6 hours. The release may be relatively rapid compared with other delivery systems capable of providing the release of proteins for days (Corrigan and Li, 2009). The rate of protein release from ionic hydrogels is influenced by various structural parameters of the protein and polyelectrolyte as well as by the environmental conditions inside hydrogel (Cooper et al., 2005). Proteins with low molecular weights are generally characterised by faster release rates. Also, Kamiya and Klibanov (2002) examined the release of lysozyme from its complexes with different polyanions. They confirmed that a protein is gradually released from its non-covalent, water-insoluble complex with oppositely charged polyion over the period of hours and days, and the rate of in vitro release markedly depends on the nature of the polyion. Polymers with higher linear charge density were found to provide slower release of lysozyme. Since HA has a very low charge density and sCT is a peptide with low molecular weight, most of sCT release is expected to occur within a few hours.

4.10 Stability studies of sCT-loaded HA/CL113 NPs

It is of a vital importance to ensure that the association of the drug with the NPs is unchanging upon storage and that degradation of the active does not occur. The formulation containing TPC of 1 mg/ml, HA/CL113 MMR of 5 and 0.1 mg/ml of sCT, which was also tested *in vivo* as described in Chapter 9, was selected for stability studies. No presence of the non-associated/released sCT was observed

after 1, 2 or 3 days of incubation, neither at 4 °C, nor at room temperature or 37 °C. Therefore it can be concluded that the sCT-loaded NPs were stable in terms of drug association. sCT was then extracted from the NPs with the use of 0.0001 M NaOH solution. The amount of sCT extracted on the day of preparation of NPs was treated as 100%. There was no statistically significant difference in the amount of sCT extracted from the NPs upon storage at 4 °C for at least 3 days (See Appendix 3, Fig. 12.3.1). The amount of sCT extracted from the particles after 3 days of storage at room temperature was only by 4% lower than the amount extracted on the day of preparation of NPs, however the difference was statistically significant. When the NPs were stored at 37 °C, the amount of sCT isolated from the particles decreased statistically significantly by 2% after first day, and by another 2% after third day. Therefore the stability of association can be considered as satisfactory, and it is recommended that the particles are to be refrigerated during storage. Also, as a control the stability studies of sCT with incubated with water, HA solution and CL113 solution were carried out. It was possible to recover all sCT from all samples tested after 3 days regardless of the temperature of storage (See Appendix 3, Fig. 12.3.2-12.3.4).

The physical stability of sCT-loaded NPs was also evaluated over 3 days in order to verify if the loading of sCT has any effect on the particle size, PDI, zeta potential and transmittance and the results are presented in Fig. 4.29-4.32. No major changes in those parameters were observed upon three days of storage- only the particle size increased significantly by ~4% for the particles stored at room temperature and at 37 °C (Fig. 4.29), and a transmittance of the particles stored at this temperature decreased on average by 11% (Fig.4.30). All these changes may be considered as small and therefore it may be concluded that the particles are physically stable on short term storage.

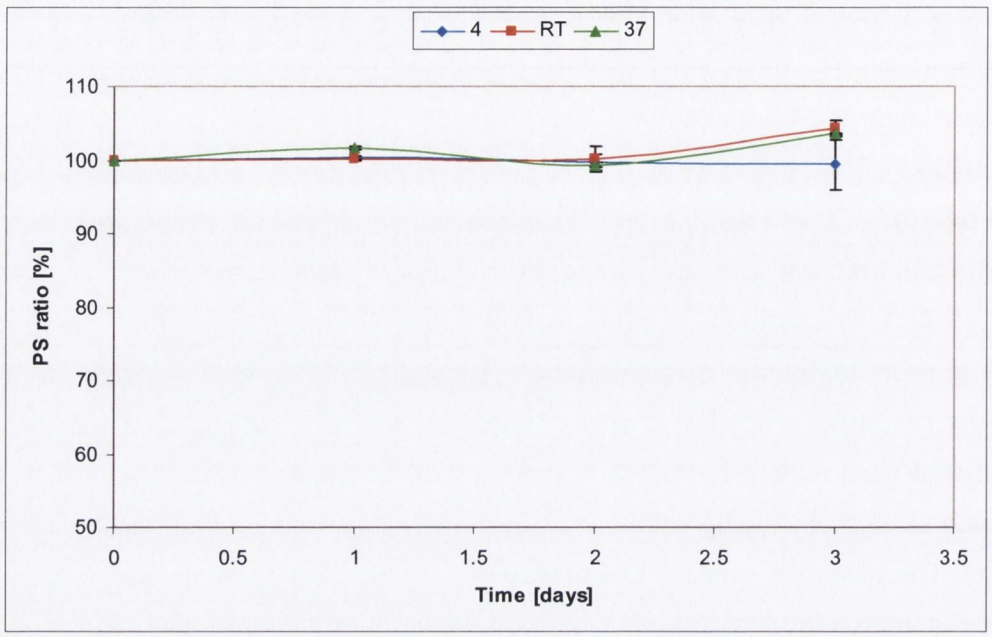

Fig.4.29 Stability studies of HA/CL113/sCT NP dispersions upon storage at 4 °C, room temperature and 37 °C for 3 days: particle size. The changes in PS are presented as percentage ratio after storage in relation to an initial value treated as 100%.

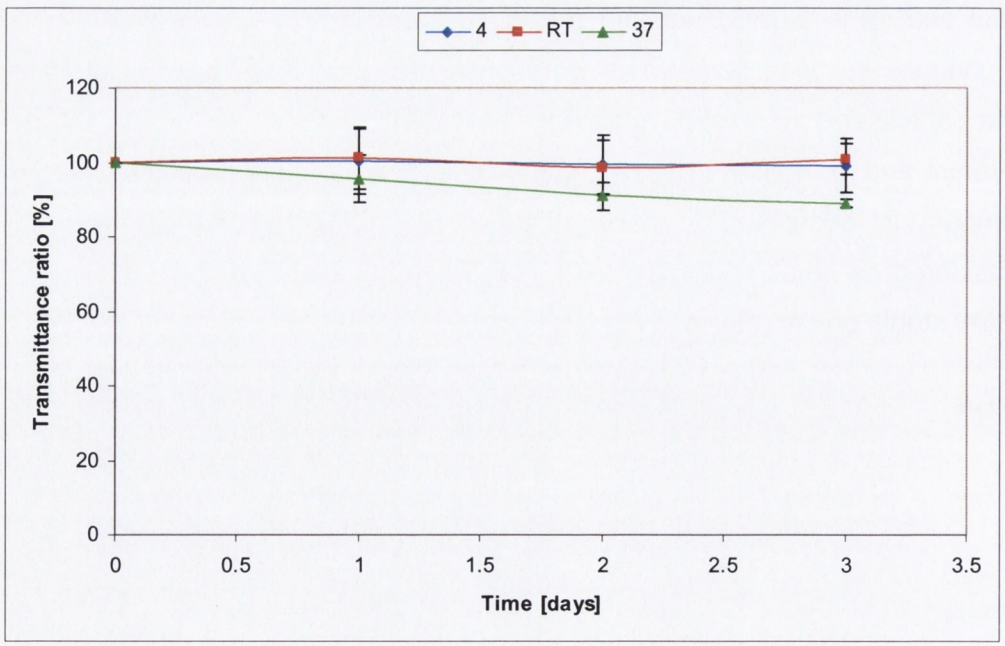

Fig.4.30 Stability studies of HA/CL113/sCT NP dispersions upon storage at 4 °C, room temperature and 37 °C for 3 days: transmittance. The changes in transmittance are presented as percentage ratio after storage in relation to an initial value treated as 100%.

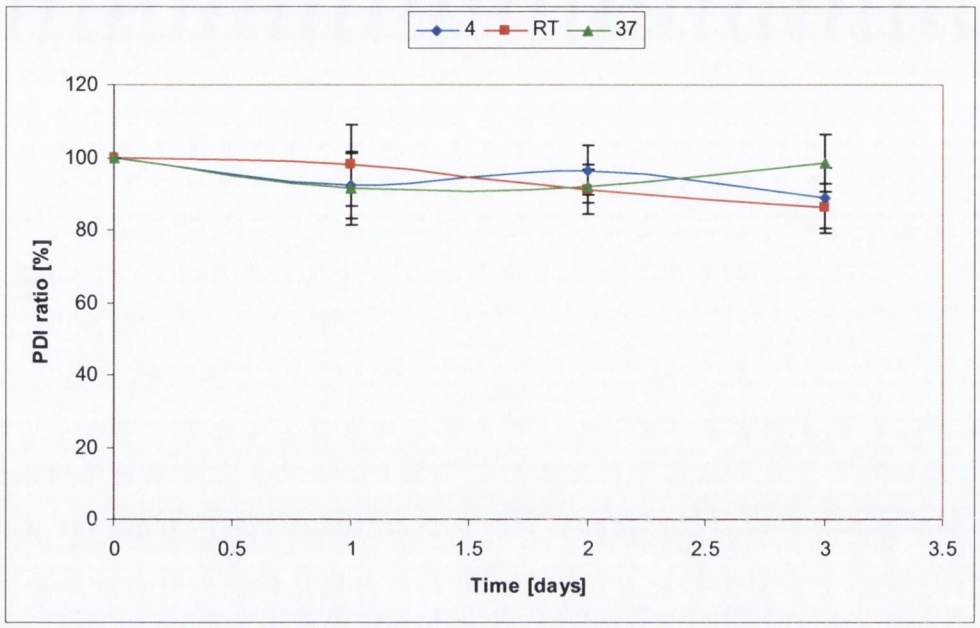

Fig.4.31 Stability studies of HA/CL113/sCT NP dispersions upon storage at 4 °C, room temperature and 37 °C for 3 days: polydispersity index. The changes in PDI are presented as percentage ratio after storage in relation to an initial value treated as 100%.

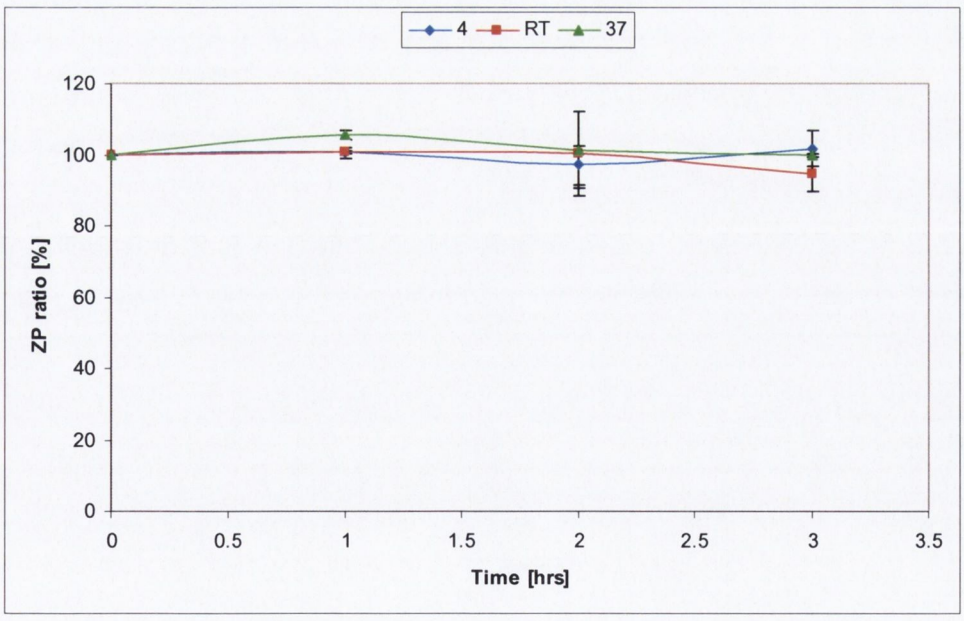

Fig.4.32 Stability studies of HA/CL113/sCT NP dispersions upon storage at 4 °C, room temperature and 37 °C for 3 days: zeta potential. The changes in ZP are presented as percentage ratio after storage in relation to an initial value treated as 100%.

4.11 Summary and conclusions

Salmon calcitonin was found to form a soluble complex with HA. It is likely that complexation between the two species occurs via electrostatic interactions.

sCT-loaded HA/CL113 nanoparticles were successfully developed and characterised. The NPs were spontaneously formed in mild conditions in a simple process of mixing aqueous polyelectrolyte solutions at room temperature, without any organic solvents or surfactants. Negatively charged HA/CL113 NPs have an excellent ability to associate sCT with AE values ~95-100% being one of the highest reported up to now. Very high sCT loading up to 50% (the highest described to date) may be achieved. The loading capacity depends on the composition of the nanoparticles and increases with the increase of HA content. Also, the NPs are capable to provide a sustained release pattern of sCT in comparison to free drug solution. sCT loading changes the physical properties of the nanoparticles.

Although the surface charge of the particles decreases due to the presence of sCT, other properties of the particles were improved: sCT-loaded particles are usually smaller and more homogenously dispersed than HA/CL113 NPs without sCT. HA/CL113/sCT NPs had the hydrodynamic diameter 150-230 nm, what makes them one of the smallest sCT NPs described so far. Moreover, short-term storage stability studies showed that the physical properties of the particles do not change and no release of sCT was observed.

HA/CL113/sCT NPs described in this chapter are the first drug delivery system which combines two important biomacromolecules working in a synergistic way: HA and sCT.

In summary, the HA/CL113 NPs may be considered as a promising carrier for the delivery of sCT.

5. Hyaluronic acid-protamine nanoparticles

5.1 Introduction

It has been demonstrated that it is possible to form HA-based polyelectrolyte complex NPs, nonetheless most of the work conducted so far has focused on HA/chitosan NPs (Boddohi et al., 2009, de la Fuente et al., 2008, Chapter 3). However, being a polyanion, HA has the ability to form polyelectrolyte complexes with other polycations. Among them, polypeptides and proteins are particularly interesting because of their biodegradability, biocompatibility and many other potential applications. For instance, complexes of HA based on electrostatic attraction with poly-L-lysine (Hahn et Hoffman, 2005) and lysozyme (Van Damme et al., 1994; Morfin et al., 2011) have been formulated and examined. Hahn and Hoffman (2005) used the electrostatic interactions between HA and lysine to obtain a biocompatible polyelectrolyte complex multilayer for surface modification of various biomaterials. Morfin et al., (2011), who examined the lysozyme-hyaluronic acid complexes, managed to obtain different systems appearing as one or two phased systems, transparent or turbid depending on the experimental conditions used. As the macroscopically homogenous turbid or opalescent liquid is likely to contain nanoparticles (Calvo et al., 1997), it is thus possible that some of the systems described by Morfin et al., 2011 were nanosuspensions. There also have been reports on complexation of HA to polyarginine (Kim et al., 2009, Oyarzun-Ampuero et al., 2011) and polyelectrolyte complex NPs have been successfully obtained. Both research groups managed to obtain small NPs with sizes of ~90-170 nm, positively (Kim et al., 2009, Oyarzun-Ampuyero et al., 2011) or negatively charged (Oyarzun-Ampuyero et al., 2011). Kim et al. (2009) used the HA/ polyarginine NPs as carriers for siRNA. Oyarzun-Ampuyero et al., (2009) managed to obtain NPs by simple mixing of polycation and polyanion solution and no cross-linker was used. Although these authors suggested that incorporation of hydrophilic macromolecular drugs, e.g. peptides into the nanocarriers might be possible, no such studies have been published so far. Also, the high price of polyarginine may be one of the disadvantages of its use in the drug delivery. Therefore, clearly there is a need to produce other polyelectrolyte-complex based delivery systems composed of nano-complexed HA.

Hence, another polycation, which could be complexed to HA in order to produce NPs, is required. Ideally, such a compound should be reasonably cheap, naturally occurring and already used in drug delivery, as that would minimise the

need for additional biodegradability and toxicity studies. Protamine (PROT) would be an ideal candidate, as it is a strongly charged cationic protein, naturally occurring and is already used in formulations containing insulin (Hagedorn, 1937). Additionally, PROT is used as a drug itself being applied as an antagonist for heparin. Protamine is a mixture of positively charged proteins extracted from salmon roe. It is rich in arginine, similarly to some viral proteins, which utilise arginine-rich sequences of amino acids to provide membrane-translocating activities. Indeed, Reynolds et al., (2005) have shown that protamine has a membrane translocating activity, which could be used in pharmaceutical applications. Being a natural product, its cost is substantially less than synthetic peptides, e.g. polyarginine. It has a long history of use establishing its biological effects and general safety in humans (Reynolds et al., 2005).

Junghans et al., (2000) have shown that PROT is capable to spontaneously form complexes with oligonucleotides. These complexes had the form of 150-170 nm nanoparticles, which doubled their size after 3 days. It was possible to reduce the particle size even to 46 nm by changing the mixing ratios of both components. These particles were characterised by either positive or negative surface charge, however in cell culture medium all dispersions contained negatively charged nanoparticles. Complexation to PROT protected the oligonucleotides from enzymatic degradation. Moreover, the complexes of oligonucleotides with protamine were characterised by a higher cellular uptake than oligonucleotides on their own (Junghans et al., 2000). Mayer et al., (2005) reported that substitution of protamine free base by protamine sulphate greatly reduced the size of oligonucleotide-protamine-albumin nanoparticles from 200 to 40 nm. However, no information about the surface charge of these particles is available.

PROT has already been shown to form polyelectrolyte complexes NPs not only with nucleic acids, but also with a glycosaminoglycan with high charge density, heparin. Mori et al. (2010), produced polyelectrolyte complex micro and nanoparticles containing heparin and protamine as a carrier for FGF-2. Mok et al., (2007) demonstrated that covalent conjugation of HA to antisense oligodeoxynucleotide formed more stable polyelectrolyte complexes with protamine than naked nucleotide. However, to our best knowledge, no delivery system based on HA/PROT interactions have been developed so far. Due to the mentioned earlier interesting properties of HA and PROT such hybrid HA/PROT nanoparticles may have the potential to become interesting carriers for the delivery of peptides.

5.2 HA/PROT nanoparticles: formation and formulation variables. Impact of the molecular weight of HA, HA and PROT concentration and HA/PROT mass mixing ratio

At first, preliminary experiments were performed in order to screen conditions of potential formation of NPs. The concentration of HA was kept constant at 0.71 or 1.43 mg/ml (similar to the previously used for the preparation of HA/CS NPs) and a specified volume of protamine solution with different concentrations varying from 0.2 to 3.2 mg/ml was added to HA solution (corresponding to 0.06 and 0.91 mg/ml of PROT in the final dispersion, respectively). Depending on the concentration of PROT solution added, a few types of dispersions were observed: solution, opalescent or turbid dispersion and phase separation.

Generally, higher concentrations of PROT resulted in the formation of more turbid systems (Fig.5.1). Samples made using higher concentration of HA (1.43 mg/ml) were generally less transparent than those with lower HA concentration (0.71 mg/ml). This tendency was changed only when the concentration of PROT was approaching 0.51 mg/ml. The concentration of PROT equal to 0.51 mg/ml was sufficient for the phase separation to occur for NPs based on 0.71 mg/ml HA, however it was necessary to increase the concentration of PROT to 0.91 mg/ml to cause aggregation of formulations based on 1.43 mg/ml HA. On the other hand, the molecular weight of HA did not seem to have an influence on the appearance of formulations. Transmittance of 0.71 mg/ml HA-based formulations did not differ significantly for NPs based on HA with molecular weights of 590, 257 and 176 kDa. However, when native HA with molecular weight of 2882±24.50 kDa was used, NP aggregation occurred even at lower concentrations (e.g. 0.06 or 0.11 mg/ml) of PROT. As previously shown (Chapter 3) native HA formed aggregates with other polycation, chitosan, due to its high molecular weight and high viscosity of its solution. Therefore systems containing native HA were not further examined as potential nanocarriers.

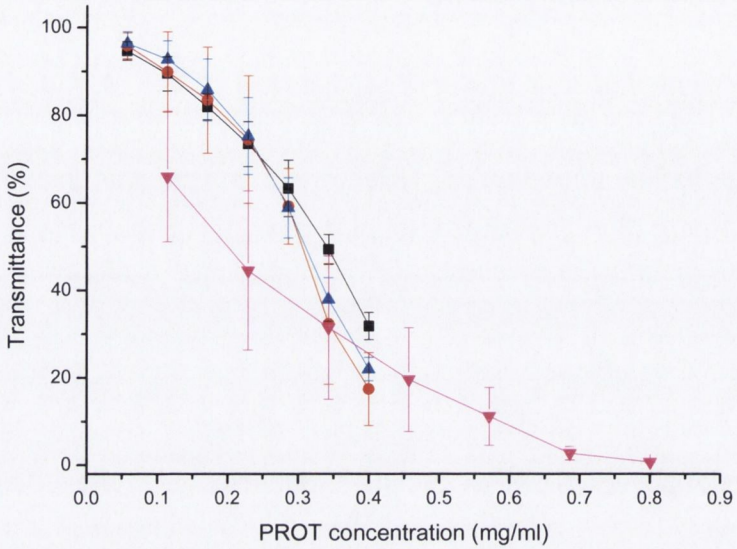

Fig.5.1 Physicochemical properties of HA/PROT NPs: transmittance. Black squares indicate NPs made of HA 176 kDa (conc. 0.7 mg/ml), red circles - HA 257 kDa (conc. 0.7 mg/ml), blue triangles - HA 590 kDa (conc. 0.7 mg/ml) and magenta inverted triangles - HA 257 kDa (conc. 1.4 mg/ml).

As shown in Fig.5.2, the viscosity of the formulations was greatly affected by the molecular weight of HA and thus the viscosity of HA solution used. Only for highest concentrations of PROT this effect becomes negligible. The amount of PROT in the formulation also had a considerable effect on that parameter. The higher the amount of PROT added, the lower was the viscosity of the formulation. Another parameter that influenced the viscosity of HA/PROT formulations was the concentration of HA used as the viscosity of 1.43 mg/ml HA-based formulations was always significantly higher than the viscosity of 0.71 mg/ml HA-based systems for the same PROT concentration used.

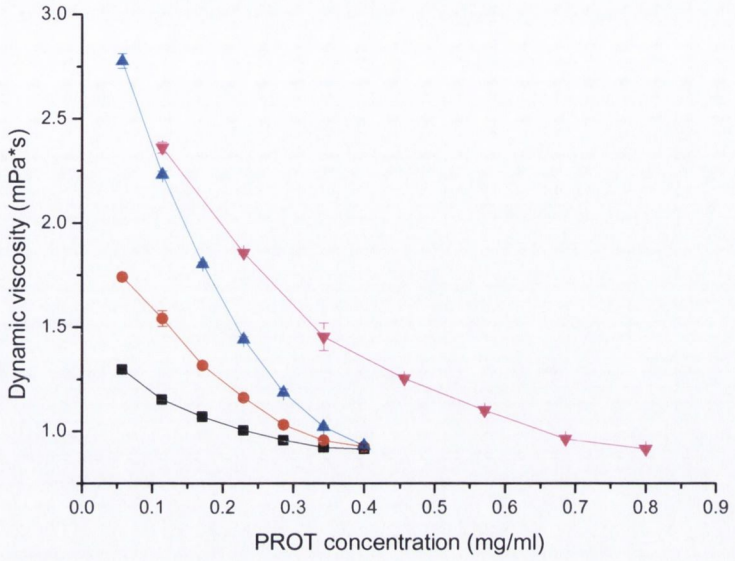

Fig.5.2 Physicochemical properties of HA/PROT NPs: viscosity. Black squares indicate NPs made of HA 176 kDa (conc. 0.7 mg/ml), red circles - HA 257 kDa (conc. 0.7 mg/ml), blue triangles - HA 590 kDa (conc. 0.7 mg/ml) and magenta inverted triangles - HA 257 kDa (conc. 1.4 mg/ml).

The hydrodynamic diameter of HA/PROT NPs increased gradually with the increasing amount of PROT added (Fig. 5.3). Neither the molecular weight (between 590 and 176 kDa) nor the concentration of HA (0.71 or 1.43 mg/ml) seemed to have a strong effect on the size of the particles formed. It is noteworthy that HA/PROT NPs are indeed very small polyelectrolyte complex NPs with some of them well below 100 nm. To the best of our knowledge, complexation to PROT resulted in the formation of one of the smallest, if not the smallest ever reported, HA based polyelectrolyte complex NPs. Only Kim et al., (2009) managed to produce HA-containing NPs smaller than 100 nm (88.5±11.5 nm) by complexation to polyarginine. Other reported HA complexes with polyarginine (Oyarzun-Ampuyero et al., 2011) and chitosan (de la Fuente et al., 2008, Chapter 3) are significantly bigger than 100 nm in diameter.

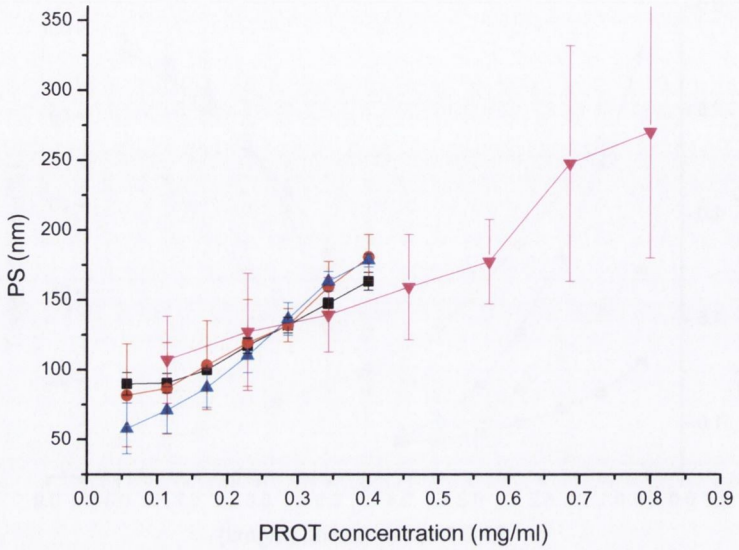

Fig.5.3 Physicochemical properties of HA/PROT NPs: particle size. Black squares indicate NPs made of HA 176 kDa (conc. 0.7 mg/ml), red circles - HA 257 kDa (conc. 0.7 mg/ml), blue triangles - HA 590 kDa (conc. 0.7 mg/ml) and magenta inverted triangles - HA 257 kDa (conc. 1.4 mg/ml).

Most of the tested formulations were homogenously dispersed with the PDI values below 0.2 (Fig. 5.4). The molecular weight of HA had a significant influence on the size distribution. The 590 kDa HA-based formulations had the highest PDI values, which decreased gradually from 0.348 to 0.129 with an increasing amount of added PROT. The 257 and 176 kDa HA-based formulations were generally more homogenously dispersed. The PDI values at first decreased rapidly and then remained constant or fluctuated slightly for PROT concentrations higher than 0.29 mg/ml. The PDI values of 1.43 mg/ml HA-based formulations at first decreased slightly, however not significantly, reached the minimum at a PROT concentration of 0.46 mg/ml and then increased.

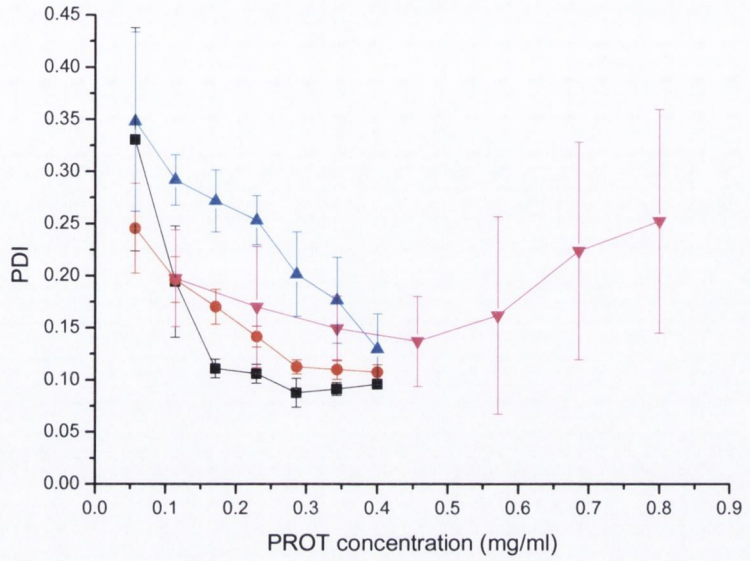

Fig.5.4 Physicochemical properties of HA/PROT NPs: polydispersity index. Black squares indicate NPs made of HA 176 kDa (conc. 0.7 mg/ml), red circles - HA 257 kDa (conc. 0.7 mg/ml), blue triangles - HA 590 kDa (conc. 0.7 mg/ml) and magenta inverted triangles - HA 257 kDa (conc. 1.4 mg/ml).

Stable (non-sedimenting and non-aggregating) NPs were characterised by negative values of zeta potential. In contrast to the particle size, the surface charge of particles decreased with increasing amount of protamine added (Fig. 5.5). Also, the molecular weight of HA and its concentration considerably impacted on the zeta potential values of the particles. The negative values surface charge increased with increasing molecular weight and concentration of HA.

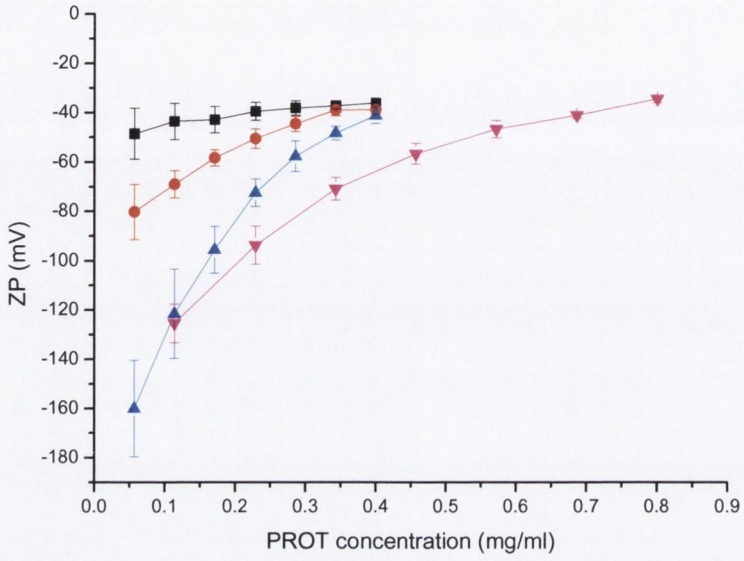

Fig.5.5 Physicochemical properties of HA/PROT NPs: zeta potential. Black squares indicate NPs made of HA 176 kDa (conc. 0.7 mg/ml), red circles - HA 257 kDa (conc. 0.7 mg/ml), blue triangles - HA 590 kDa (conc. 0.7 mg/ml) and magenta inverted triangles - HA 257 kDa (conc. 1.4 mg/ml).

Despite the changes in zeta potential, all formulations had similar pH values, ranging between 5.57 and 6.25; the pH decreased slightly with the increasing amount of PROT in the formulations (Fig. 5.6).

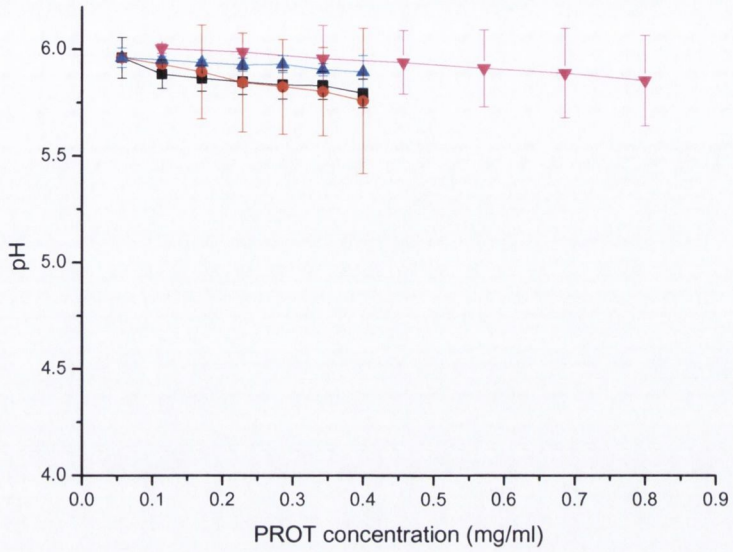

Fig.5.6 Physicochemical properties of HA/PROT NPs: pH. Black squares indicate NPs made of HA 176 kDa (conc. 0.7 mg/ml), red circles - HA 257 kDa (conc. 0.7 mg/ml), blue triangles - HA 590 kDa (conc. 0.7 mg/ml) and magenta inverted triangles - HA 257 kDa (conc. 1.4 mg/ml).

All the formulations showed in Figures 5.1-5.6 contained negatively charged particles. Attempts were also made to obtain positively charged particles, as they could be promising carriers for encapsulation/adsorption of negatively charged macromolecules. After mixing PROT and 176 kDa HA solutions (PROT conc. = 0.3 mg/ml, HA conc. = 0.16 mg/ml) at the PROT/HA MMR of 5 it was possible to obtain small and homogenously dispersed nanoparticles (initial values of PS and PDI of 252±2.3nm, 0.065±0.003, respectively), however their surface charge was very low (5.5-7 mV) and sedimentation could be noticed within a few hours. Figures 5.7-5.9 show the kinetics of aggregation of those particles; the particle size increased at first rapidly within first ~2 hours and then reached a plateau up to 20 hours of storage (Fig. 5.7). After 22 hours of storage the presence of micron-size aggregates was evident from DLS measurements.

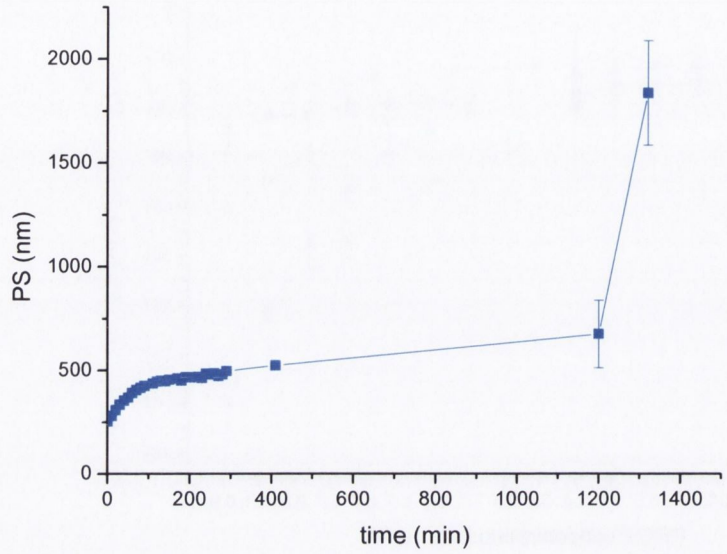

Fig. 5.7 Kinetics of particle size (PS) changes of positively charged PROT/HA NPs (PROT/HA MMR=5) over 22 hours of storage at 25 °C.

PDI value on the other hand increased rapidly from 0.065±0.003 to 0.187±0.006 after 30 minutes, then fluctuations were observed for the next ~2.5 hours, followed by a dramatic increase to 0.592±0.099 after another 17 hours of storage, accompanied by noticeable aggregation of the particles (Fig. 5.8).

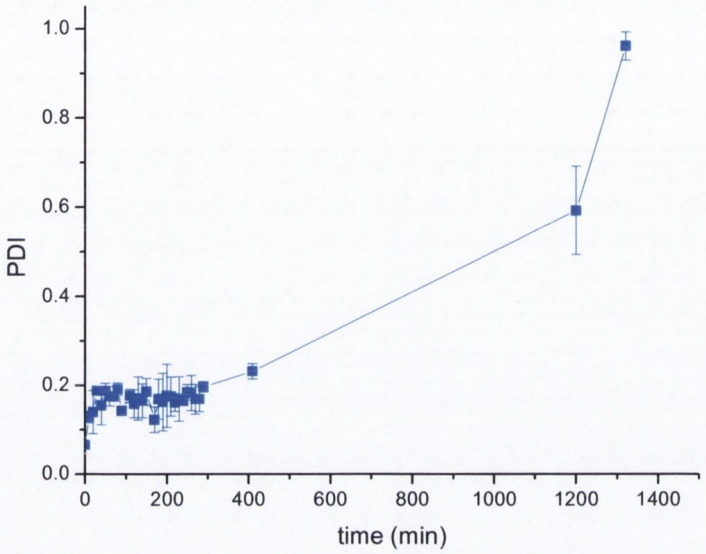

Fig. 5.8 Kinetics of polydispersity index changes of positively charged PROT/HA NPs (PROT/HA MMR=5) over 22 hours of storage at 25 °C.

The values of zeta potential fluctuated between ~7.3 and 5.5 mV during the first hours of storage, however a substantial increase up to ~ 11.5 mV after 20 hours was measured, followed by a decrease to 7.9 mV after 22 hours.

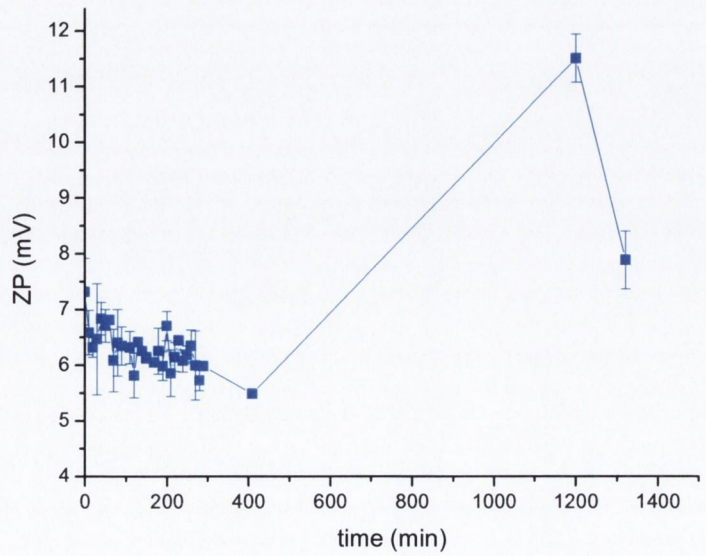

Fig. 5.9 Kinetics of zeta potential changes of positively charged PROT/HA NPs (PROT/HA MMR=5) over 22 hours of storage at 25 °C.

In contrast to the results presented above, stable, positively charged NPs were formed when HA and polyarginine (Kim et al., 2009, Oyarzun-Ampuyero et al., 2011) as well as HA and chitosan (Chapter 3) were used. Thus, the behaviour of the HA/PROT pair is different than the above polyelectrolyte complexes. A possible explanation can lie in the severely different molecular weights of the components used, as the molecular weight of HA used in the positively charged NPs was ~35 times higher than the molecular weight of the major component of protamine (5.1 kDa; manufacturer's data). According to Boddohi et al., 2010, when the polyelectrolyte in excess (PROT in this case) has a much lower molecular weight than the other polymer (HA), a more compact morphology results leading in some cases to flocculation of the NPs and poor colloidal stability. However the difference in charge density along with the difference in molecular weight may also be an important factor which causes the poor stability of positively charged HA/PROT NPs. Schatz et al., (2004) examined polyelectrolyte complexes composed of chitosan and dextran sulphate. When they mixed a high Mw chitosan (365 kDa) and a low Mw dextran sulphate (5 kDa), the situation was analogical to that described above: the polyelectrolyte pair was composed of long molecules with a low charge density and small molecules with a high charge density, only the charges were distributed in the opposite way. When chitosan was used in excess, stable positively charged particles were obtained, however when dextran sulphate was used in excess, the negatively charged polyelectrolyte complexes had poor colloidal stability. However, positively charged polyelectrolyte complexes between HA and polyarginine obtained by Oyarzun-Ampuyero et al. (2011) were stable even despite the differences in charge density and chain length of both molecules. The ratio between the molecular weight of the components used by Schatz et al., (2004) was 73, that used by Oyarzun-Ampuyero et al. (2011) was 11-33, while that to form the HA/PROT NPs as described in this work was 35. Therefore one must be careful if the NPs are formed by complexation between two polyelectrolytes having significantly different molecular weights and charge densities.

Another difference between the HA/PROT complex and other polyelectrolyte complexes such as e.g. HA/chitosan (Boddohi et al., 2008, Chapter 3), heparin/chitosan (Boddohi et al., 2008) and chitosan/dextran (Schatz et al., 2004) is the decrease in the hydrodynamic diameter of the latter complexes during the titration with the oppositely charged polyelectrolyte until a secondary aggregation was obtained preceding the irreversible flocculation. Boddohi et al., (2008) deducted that this behaviour indicates that the particles are composed of

relatively dense hydrophobic core and less defined hydrophilic corona, the latter being compacted upon the addition of oppositely charged polyelectrolyte. However the size of HA/PROT particles gradually increases with higher protamine concentrations, possibly indicating different mechanism of complex formation and maybe different structure.

It is known that the polyelectrolyte complex formation process is usually entropically driven by the release in small counterions, initially bound to polyelectrolytes and release of water from the hydrated polyelectrolyte molecules (Boddohi et al., 2011). In some cases, van der Waals forces and dipole-charge transfer may be involved in the formation of complexes between polyelectrolytes as well (Boddohi et al., 2011).

5.3 TEM of HA/PROT NPs

TE micrographs show that the HA/PROT NPs (Fig.5.10) were approximately spherical, compact and well defined, similar to the previously described HA/CL113 NPs (see Chapter 3). In some cases deformations were observed however, in contrast to the HA/CL113 NPs, no core and corona structure was observed in HA/PROT NPs. The particle size determined by TEM was observed to be smaller than that determined by DLS. The difference is especially pronounced in HA of 0.7 mg/ml, PROT of 0.11 mg/ml sample as the particles seen in TEM micrographs had the size approximately between 30 and 80 nm, compared to 86 nm by DLS (Fig.5.10A). Differences in particle size between DLS and TEM may be due to possible modification of some of the properties of particles during sample preparation for TEM: drying and staining of the particles. The nanoparticles analysed by TEM contain mainly HA, which is known to swell upon hydration (Lapčík et al., 1998). Therefore it is likely that the size of the particles decreases due to the removal of water during the drying process. Vogel et al., (2005) also reported some changes in the particle properties during preparation for TEM analysis, e.g. disintegration of the particles and considerable variability in size distribution between similarly treated samples. In the sample containing more PROT (0.34 mg/ml) and therefore a smaller ratio of HA to the polycation the particles observed in TEM micrographs were approximately between 100-200 nm, which is in agreement with DLS data.

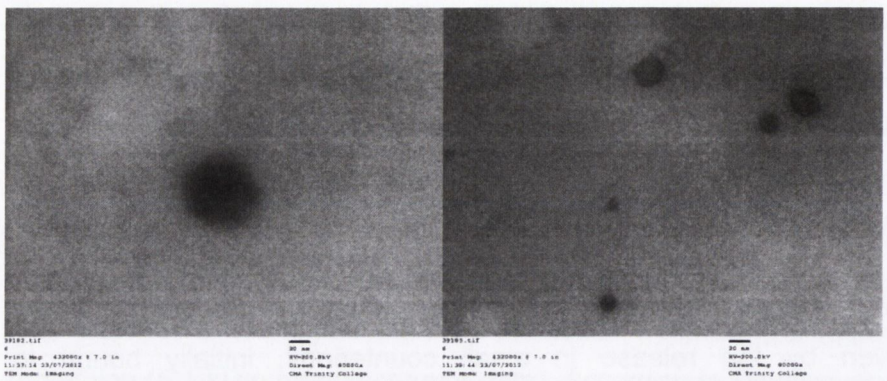

A)

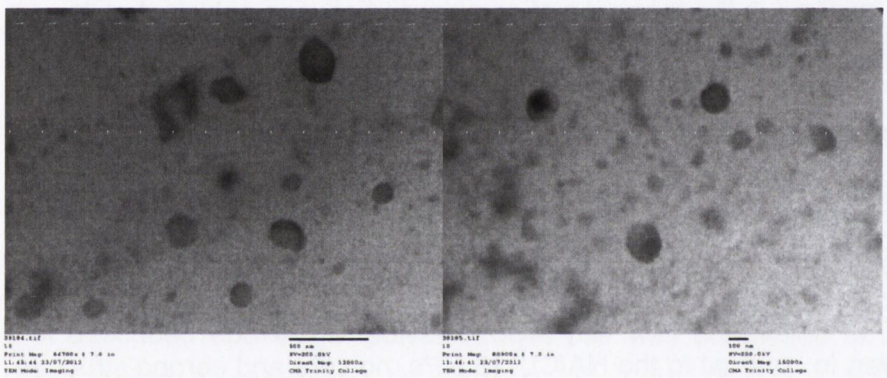

B)

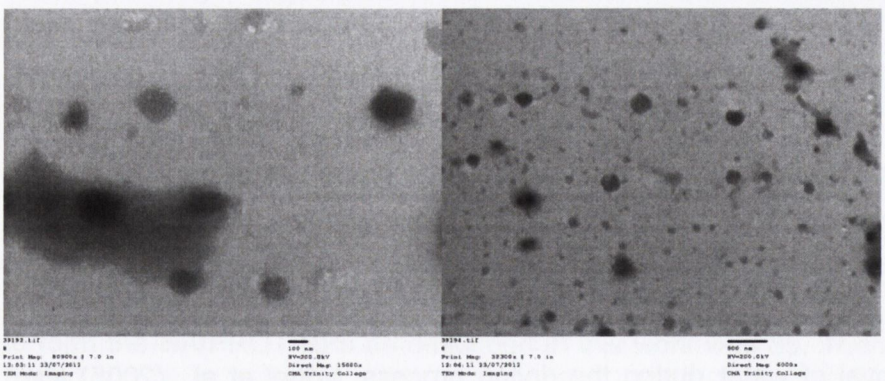

C)

Fig. 5.10 TE micrographs of HA/PROT and HA/PROT/sCT NPs; A) HA of 0.7 mg/ml, PROT of 0.11 mg/ml (86 nm by DLS); B) HA of 0.7 mg/ml, PROT of 0.11 mg/ml, sCT of 0.5 mg/ml (140 nm by DLS); C) HA of 0.7 mg/ml, PROT of 0.34 mg/ml (160 nm by DLS). Scale bars: A-20 nm; B left- 500 nm, right- 100 nm; C left- 100 nm, right- 500 nm

5.4 Isoelectric point of HA/PROT nanoparticles

The IEP values of selected HA/PROT NPs are shown in Table 5.1 Both formulations with the HA/PROT mass mixing ratio of 6.3 did not show the isoelectric point at pH above 2, therefore it is likely that their negative charge would be maintained upon exposure to low pH values in the gastro-intestinal tract. When the concentration of PROT was increased and the HA/PROT MMR was decreased to 3.1, the charge of the particles became neutralised at pH 2.61±0.63 and 1.95±0.34 for formulations with PROT of 0.457 and 0.229 mg/ml, respectively, however the difference between those two values is not statistically significant ($p=0.186$). As it can be shown on the example of formulations based on 0.71 mg/ml HA, a further decrease in HA/PROT MMR to 2.1 resulted in an increase in the IEP value to 2.90±0.05. Therefore it can be concluded that the IEP of HA/PROT NPs depends mainly on the HA/PROT mass mixing ratio, however the quantity of protamine in the formulation may also play a role. On the other hand, the IEP values with the HA/PROT MMR of 3.1 based on HA with different molecular weights did not differ significantly ($p=0.461$), therefore the molecular weight of HA used does not seem to affect the pH at which the charge of the NPs is neutralised.

Table 5.1 Isoelectric point values of HA/PROT NPs.

Mw of HA [kDa]	HA [mg/ml]	PROT [mg/ml]	sCT [mg/ml]	Isoelectric point
257	0.714	0.114	-	1.83±0.29
257	0.714	0.114	0.5	1.66±0.37
257	0.714	0.229	-	1.95±0.34
257	1.429	0.229	-	1.83
257	0.714	0.343	-	2.90±0.05
257	1.429	0.457	-	2.61±0.63
176	0.714	0.229	-	2.26±0.28
590	0.714	0.229	-	2.25±0.35

5.5 Stability studies of negatively charged HA/PROT nanoparticles after storage at room temperature

Three water dispersions of NPs based on 0.71 mg/ml HA 257 kDa were selected for stability studies upon storage at room temperature (formulations FA,

FB and FC with PROT of 0.11, 0.23 and 0.34 mg/ml, respectively). First signs of sedimentation were seen after 2 weeks of storage and after 4 weeks sedimentation was easy to notice for each formulation tested. The changes in transparency of the systems are shown in Fig. 5.11. Transmittance of FC, which is the most turbid of all the formulations tested, did not change significantly during 4 weeks of storage, and transmittance of other formulations systematically decreased over the first two weeks of storage. After 4 weeks of storage, however, FA became more transparent and a significant increase in the transmittance values between weeks 3 and 4 was observed, which may be attributed to sedimentation of aggregating particles.

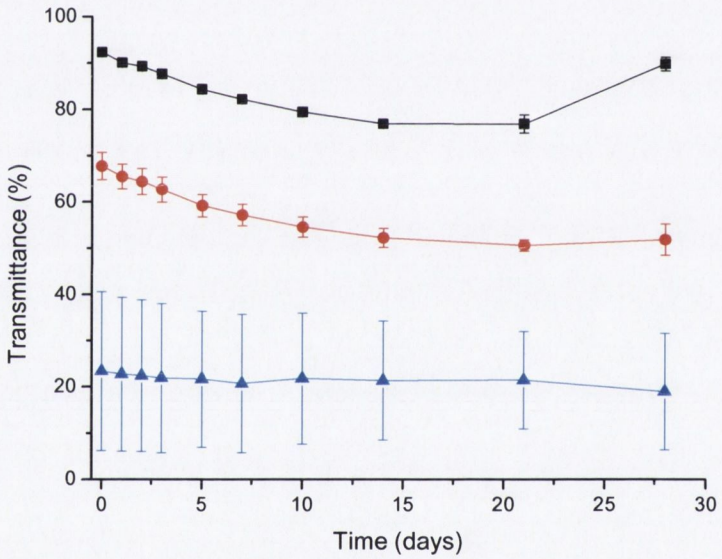

Fig.5.11 Stability studies of negatively charged HA/PROT NP dispersions at room temperature: transmittance. NPs were made of 0.71 mg/ml 257 kDa HA and the concentration of PROT was 0.11, 0.23, 0.34 mg/ml, respectively for FA (black squares), FB (red circles) and FC (blue triangles).

The particle size of FA and FB increased gradually and significantly for the first three weeks of storage, while the size of particles in formulation FC remained steady (Fig. 5.12). The increase in the particle size occurred earlier in case of FA in comparison to FB, however even after 3 weeks of storage the particles of FA were still smaller than FB (162±5 and 178±5 nm for FA and FB, respectively; $p=0.017$). After 4 weeks of storage a significant increase in the particle size can be observed in all formulations tested, especially pronounced in FA.

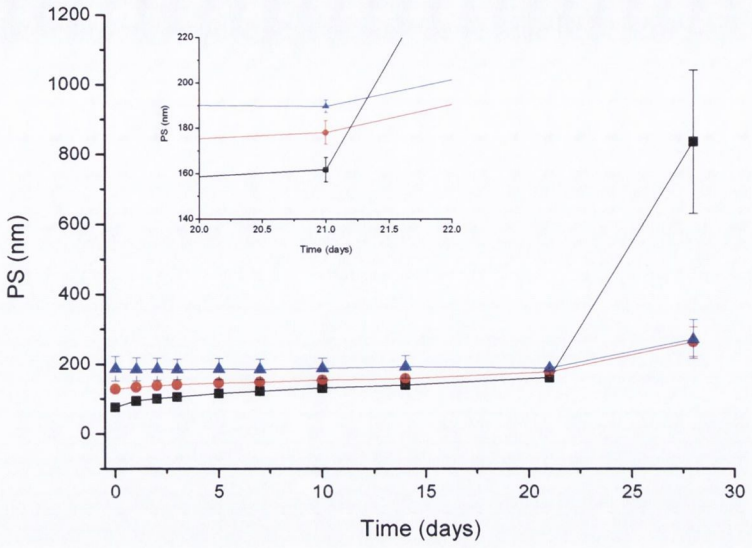

Fig.5.12 Stability studies of negatively charged HA/PROT NP dispersions at room temperature: particle size (PS). NPs were made of 0.71 mg/ml 257 kDa HA and the concentration of PROT was 0.11, 0.23, 0.34 mg/ml, respectively for FA (black squares), FB (red circles) and FC (blue triangles). Insert is for clarity purposes.

PDI of FA and FB decreased noticeably in the first days of storage, while PDI of FC generally remained steady up to 3 weeks of storage. However, after fourth week of storage a significant decrease in homogeneity of the FA NPs may be observed, which corresponds to the increase in particle size (Fig. 5.13).

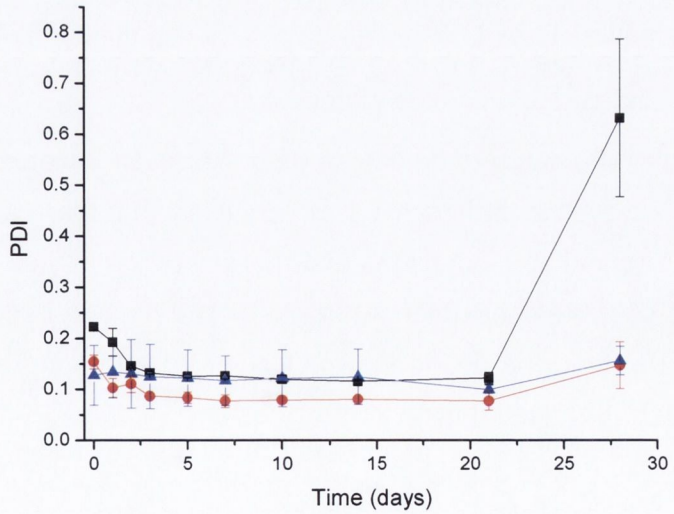

Fig.5.13 Stability studies of negatively charged HA/PROT NP dispersions at room temperature: polydispersity index (PDI). NPs were made of 0.71 mg/ml 257 kDa HA and the concentration of PROT was 0.11, 0.23, 0.34 mg/ml, respectively for FA (black squares), FB (red circles) and FC (blue triangles).

The charge of the particles becomes less negative during storage, and the decrease is most pronounced in formulation FA. After 2 weeks of storage the zeta potential values of FA, FB and FC were all significantly different from one another, however there is no statistically significant difference between FA and FB after 3 weeks. After 4 weeks there is no significant difference between all three formulations (Fig. 5.14).

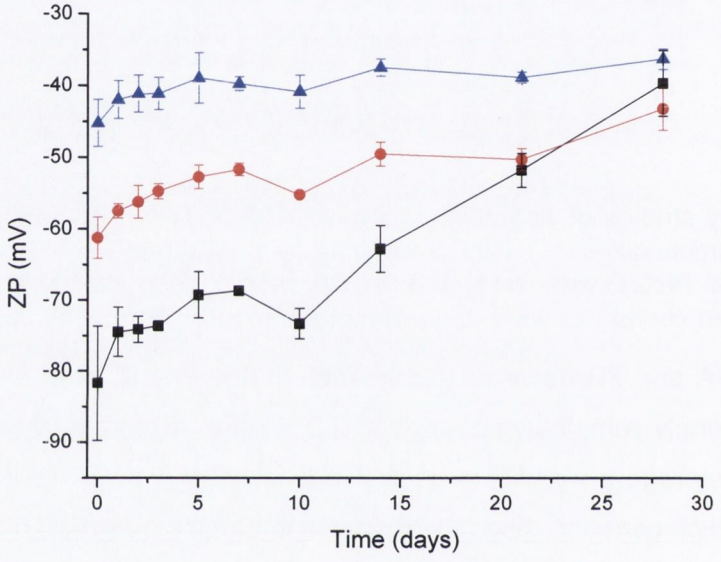

Fig.5.14 Stability studies of negatively charged HA/PROT NP dispersions at room temperature: zeta potential. NPs were made of 0.71 mg/ml 257 kDa HA and the concentration of PROT was 0.11, 0.23, 0.34 mg/ml, respectively for FA (black squares), FB (red circles) and FC (blue triangles).

Although the NPs seem to be usable after 1 or even 2 weeks of storage, it can be seen that the system is dynamic. It is very likely that there are interactions between the particles and some changes and reorganisation in their structure may occur. One of the possible consequences could be the change in the interactions between the particles and the associated molecules of active ingredient, leading either to its release or stronger binding to the particles.

5.6 Physicochemical characterisation of sCT-loaded HA/PROT nanoparticles

Table 5.2 shows the composition of sCT-loaded HA/PROT nanoformulations tested. Formulations containing different concentrations of HA and PROT were selected in order to examine the influence of HA and PROT concentration and their mixing ratio on the properties of sCT NPs. Also, different concentrations of sCT were used, since (as shown in Chapter 4) the amount of sCT exerted a considerable effect on the formation and properties of the NPs. Dispersions containing the highest amounts of protamine (i.e. 0.8 mg/ml of PROT for 1.43 mg/ml of HA and 0.4 mg/ml of PROT for 0.71 mg/ml of HA) were not considered as viable delivery systems, because dispersions containing high HA/PROT MMRs were not stable and were characterised by lowest surface charge.

Table 5.2 The composition, association efficiency (AE) and drug loading of sCT-loaded HA/PROT formulations tested.

Sample	Initial sCT conc. [mg/ml]	HA conc. [mg/ml]	PROT conc. [mg/ml]	Extracted sCT [%]	AE sCT [%]	sCT loading [%]
F1	1.0	1.429	0.343	88.92±1.84	93.8±2.84	34.86±1.04
F2	1.0	1.429	0.457	83.53±3.50	90.6±5.03	32.44±1.80
F3	0.5	1.429	0.457	89.79±1.99	95.6±2.03	20.23±0.43
F4	0.5	1.429	0.686	75.14±3.47	84.7±8.82	16.69±1.74
F5	1.0	0.714	0.114	81.11±3.36	89.6±2.78	51.97±1.61
F6	0.5	0.714	0.114	91.88±2.80	98.4±0.22	37.27±0.08
F7	0.5	0.714	0.229	80.98±4.48	91.4±3.07	32.65±1.10
F8	0.5	0.714	0.343	64.07±11.64	85.4±4.55	28.77±1.53
F9	0.1	0.714	0.114	94.67±0.82	99.8±0.02	10.75±0.00
F10	0.1	0.714	0.229	92.37±0.26	99.7±0.05	9.56±0.00
F11	1.0	1.429	0.114	98.11±0.70	98.8±0.04	39.03±0.02

The properties of sCT-loaded HA/PROT NPs are illustrated in Figures 5.15-5.20.

As described in Chapter 4, a complex was formed between sCT and HA after dissolving the peptide in HA solution during one of the first steps of preparation of NPs. This complex had the appearance of a solution. The addition of

PROT solution to the above HA/sCT solution resulted in a noticeable increase in turbidity of the dispersion (Fig.5.15). Similarly to HA/PROT NPs without sCT, the higher the concentration of PROT, the lower was the transmittance. Low concentrations of sCT (0.1 mg/ml) did not have a significant influence on the turbidity of the nano-suspensions, however when the concentration of sCT was increased to 0.5 or 1 mg/ml, it was evident that the formulations became less transparent. Also, the increase in the HA concentration led to the formation of more turbid HA/PROT/sCT systems and the formulations based on 1.43 mg/ml HA solutions are characterised by lower transmittance values compared to equivalent 0.71 mg/ml HA-based formulations (Fig.5.15).

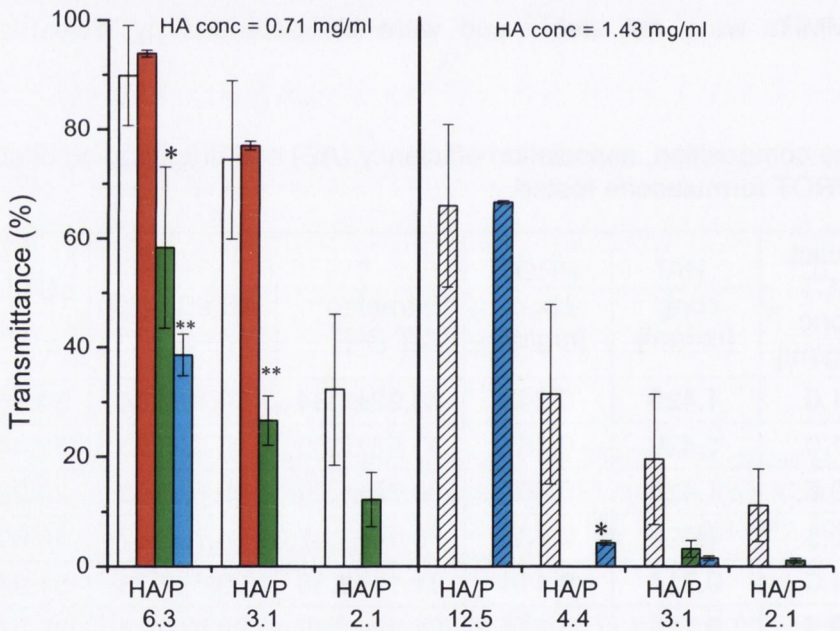

Fig.5.15 Transmittance of sCT-loaded HA/PROT NPs. Empty bars indicate unloaded NPs, red bars – 0.1 mg/ml sCT, green bars – 0.5 mg/ml sCT and blue bars – 1 mg/ml sCT. Hashed bars indicate that HA at the concentration of 1.43 mg/ml was used to formulate the NPs. P=PROT *$p<0.05$ and **$p<0.01$ versus unloaded NPs (empty bars).

The loading of sCT into particles had a considerable impact on their properties. Generally, an increase in the quantity of sCT caused a decrease in viscosity of the nano-suspensions in samples containing the same amount of HA and PROT (Fig.5.16). The difference could be seen especially in formulations containing lower amounts of PROT, which are more viscous compared to

formulations with more PROT. For example, viscosity of the formulation containing 1 mg/ml of sCT, 1.43 mg/ml HA and 0.11 mg/ml PROT (sample F11) is of 1.61±0.03 mPa*s, is by 0.75 mPa*s smaller than the viscosity of the equivalent formulation without sCT. As the particulates themselves are not expected to influence the viscosity (Philip et al., 1989), and the increased viscosity of nano-suspension (compared to water) may be attributed to the presence of residual, non-complexed polymer (HA in this case). A drop in the dynamic viscosity value due to the presence of sCT in the system may be a confirmation that sCT indeed interacts with HA possibly enabling the incorporation of more HA into the particles. The marked increase in the particle size caused by sCT seems to confirm that a higher amount of HA may be bound in the nanoparticles containing sCT compared to dispersions with the same composition without sCT. On the other hand, formulations containing more PROT and characterised by lower HA/PROT MMR have the quantities of both polymers closer to stoichiometric and negligible amount of excess HA non-associated with the particles, therefore their viscosity is not affected to a large degree by inclusion of sCT.

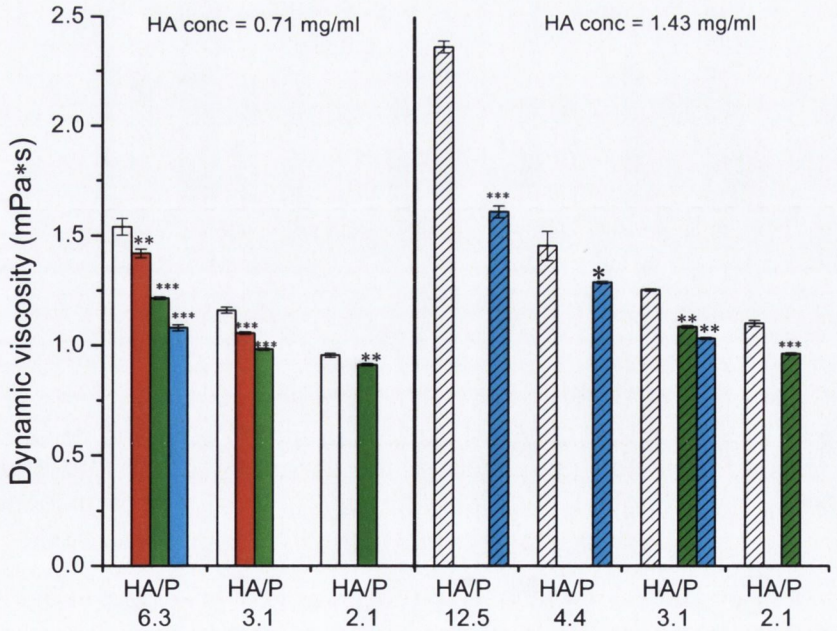

Fig.5.16 Viscosity of sCT-loaded HA/PROT NPs. Empty bars indicate unloaded NPs, red bars – 0.1 mg/ml sCT, green bars – 0.5 mg/ml sCT and blue bars – 1 mg/ml sCT. Hashed bars indicate that HA at the concentration of 1.43 mg/ml was used to formulate the NPs. P=PROT *p<0.05, **p<0.01 and ***p<0.001 versus unloaded NPs (empty bars).

An increase in the amount of sCT loaded into the particles increased the size of the particles markedly (Fig. 5.17) The more sCT the formulation contained, the larger were the particles. It may be that the repulsion between positive charges of protamine and sCT may be responsible for the increase in the size of sCT loaded NPs however, as mentioned earlier, a possible incorporation of higher amounts of HA into the particles indicated by a decrease in viscosity may also take place. Decrease in transmittance values may be also attributed to increasing size of the particles, however it is also possible that more particles were formed. An example of TE micrographs of NPs containing sCT is shown in Fig. 5.10C.

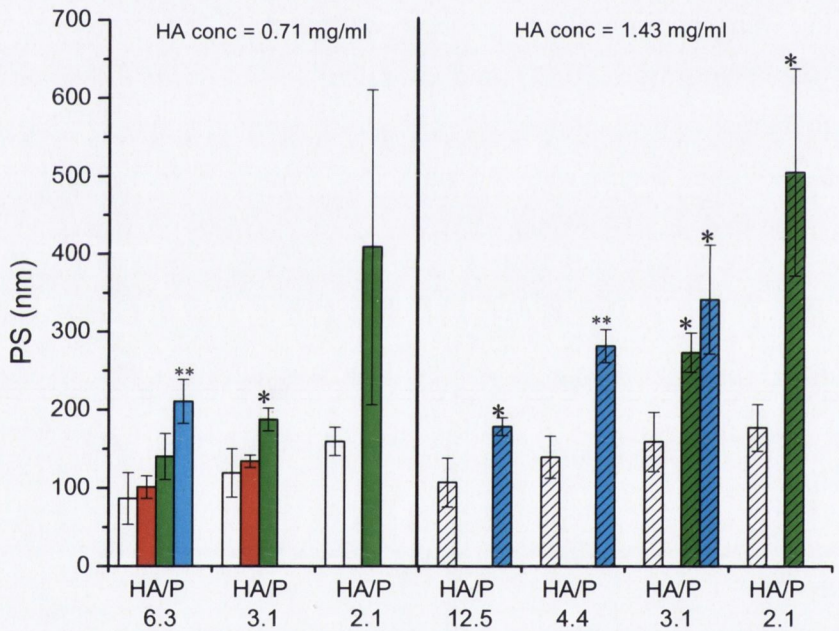

Fig.5.17 Particle size of sCT-loaded HA/PROT NPs. Empty bars indicate unloaded NPs, red bars – 0.1 mg/ml sCT, green bars – 0.5 mg/ml sCT and blue bars – 1 mg/ml sCT. Hashed bars indicate that HA at the concentration of 1.43 mg/ml was used to formulate the NPs. P=PROT *$p<0.05$ and **$p<0.01$ versus unloaded NPs (empty bars).

Most of sCT-loaded formulations (i.e. F1, F3, F5-7 and F9-11) were homogenous dispersion of the particles (majority of them had PDI smaller than 0.25, Fig. 5.18), however no clear relationship between the amount of sCT present and PDI values could be observed. Only the least stable formulations (F2, F4 and F8) had the PDI values significantly increased. That increase in PDI value was accompanied by an increase in particle size and after a few hours precipitation could be observed.

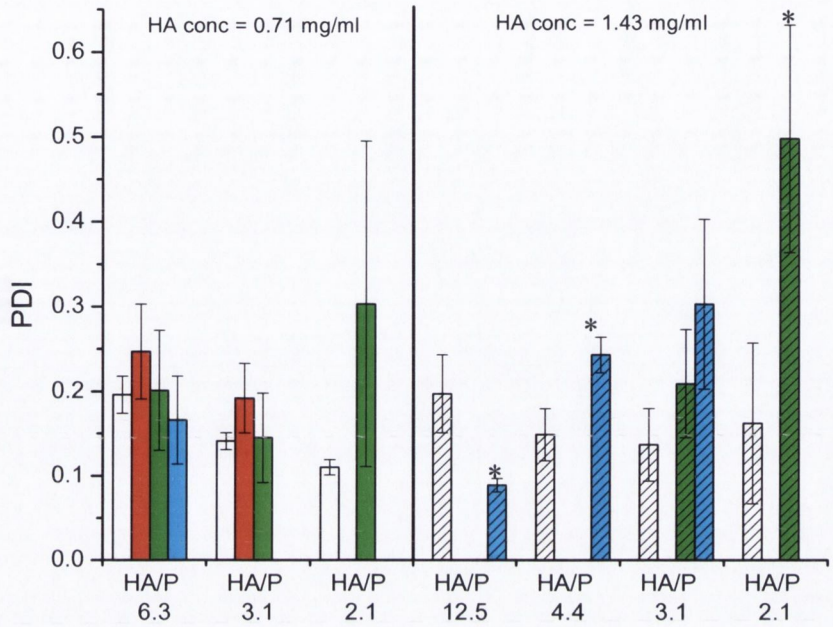

Fig.5.18 Polydispersity index of sCT-loaded HA/PROT NPs. Empty bars indicate unloaded NPs, red bars – 0.1 mg/ml sCT, green bars – 0.5 mg/ml sCT and blue bars – 1 mg/ml sCT. Hashed bars indicate that HA at the concentration of 1.43 mg/ml was used to formulate the NPs. P=PROT *$p<0.05$ versus unloaded NPs (empty bars).

Loading of sCT decreased the charge of the particles in a concentration-dependent manner, however all formulations remained negatively charged (Fig. 5.19). This may indicate that some sCT was deposited on the surface of the particles. Many formulations (i.e. F1, F3, F6 and F9-11) even after incorporation of sCT into the NPs were still characterised by a highly negative surface charge. In some cases loading of sCT led to a decrease in ZP to values close to -20 mV (F5 and F8); this decrease was especially pronounced in formulations containing higher amounts of PROT.

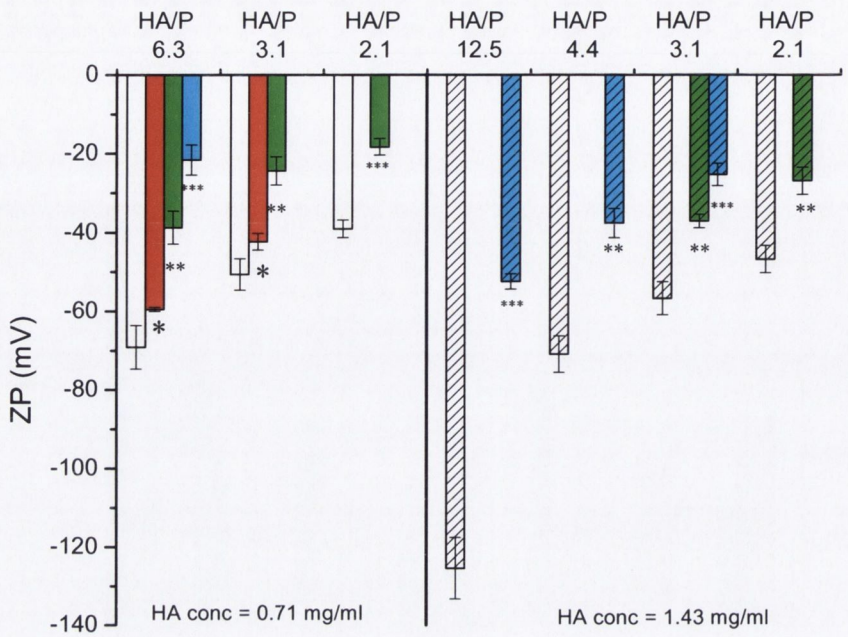

Fig.5.19 Zeta potential of sCT-loaded HA/PROT NPs. Empty bars indicate unloaded NPs, red bars – 0.1 mg/ml sCT, green bars – 0.5 mg/ml sCT and blue bars – 1 mg/ml sCT. Hashed bars indicate that HA at the concentration of 1.43 mg/ml was used to formulate the NPs. P=PROT *p<0.05, **p<0.01 and ***p<0.001 versus unloaded NPs (empty bars).

It may be observed, that loading of sCT slightly decreased pH of HA/PROT nano-suspensions (Fig.5.20). Similar trend was observed in HA/CL113/sCT NPs (Chapter 4).

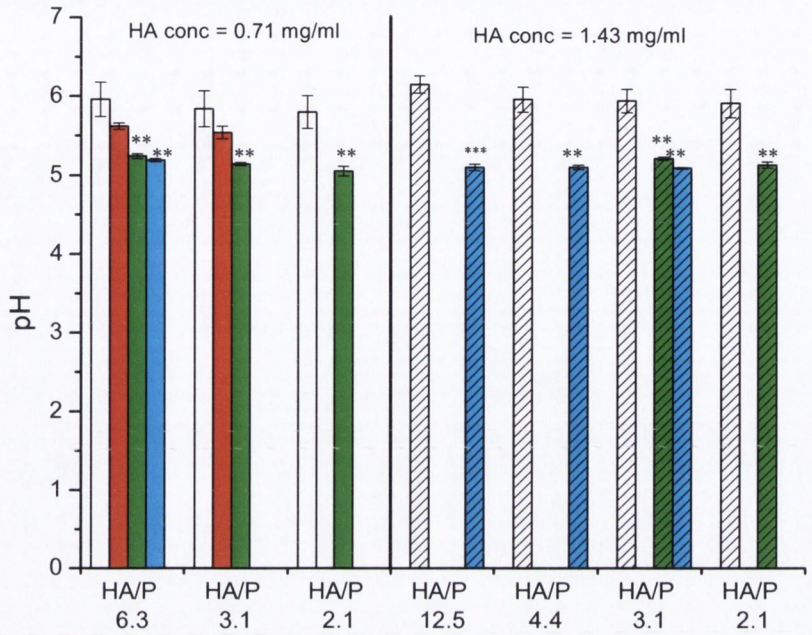

Fig.5.20 pH of sCT-loaded HA/PROT NPs. Empty bars indicate unloaded NPs, red bars – 0.1 mg/ml sCT, green bars – 0.5 mg/ml sCT and blue bars – 1 mg/ml sCT. Hashed bars indicate that HA at the concentration of 1.43 mg/ml was used to formulate the NPs. P=PROT **$p<0.01$ and ***$p<0.001$ versus unloaded NPs (empty bars).

Table 5.1 shows that loading of 0.5 mg/ml of sCT did not affect the isoeletric point of the 0.71 mg/ml HA-based formulation with HA/PROT mass mixing ratio of 6.26. This finding is in agreement with the properties of the HA-based sCT-loaded NPs described in chapter 4. Therefore sCT could be safely loaded into the NPs which contain low amount of protamine, without significantly changing their behaviour in acidic environments.

Association efficiency is a very important parameter, as it is vital to minimise the amount of the non-encapsulated active. As shown in Table 5.2, sCT was successfully associated with HA/PROT nanoparticles. The association efficiency values were very high (most of them were over 90%). Although those values are slightly lower than for HA/CL113/sCT NPs, they can be considered as one of the highest reported so far. Some authors managed to obtain AE values higher than 90% (e.g. Yang et al., 2012), however many authors reported much

lower values (e.g. Cetin et al., 2012: 69%, Makhlof et al., 2010: 64%). Only the formulations with a higher amount of PROT in relation to HA (i.e. F4 and F8) were characterised by slightly lower AEs. Formulations with higher HA content and higher HA/PROT mass mixing ratio were capable to associate more sCT (e.g. F11, where more than 98% of sCT was effectively associated with the particles despite the fact that the concentration of sCT of 1 mg/ml was the highest which was tested).

Another important parameter complementary to AE is the drug loading that is defined as the mass of sCT to the total mass of NPs. High drug loading values are desired if the therapeutic concentrations are to be achieved and the toxic effects minimised. HA/PROT NPs are characterised by very high sCT loading values, even approaching 52% w/w. That is undoubtedly one of the key advantages of HA/PROT NPs over other sCT containing NPs, such as PLGA-based, where it is necessary to use high polymer concentrations to successfully bind the active. For instance, Glowka et al., (2010) achieved only 0.2% w/w loading of sCT in PLGA NPs despite high encapsulation efficiency values (up to 83%). High loading capacities of polyelectrolyte complex NPs have previously been reported for other compounds, e.g. Oyarzun-Ampuyero et al., (2009) managed to load ~60% w/w of heparin into chitosan-based NPs containing also HA.

It appears that the amount of sCT which could be loaded into HA/PROT NPs is not unlimited - if this amount is exceeded aggregation is likely to occur. Due to the high cost of sCT it was impractical to establish the maximum dose of sCT which could be loaded into all tested HA/PROT NPs, but it is evident that formulations with higher concentration of PROT or lower HA/PROT MMR were capable to load smaller amounts of sCT. For example F4 and F8 were characterised by the least favourable properties (i.e. highest particle size and PDI, low surface charge and the lowest AE values from all formulations tested), therefore it is likely that the amount of sCT used for their preparation is close to the maximum dose of sCT that the HA/PROT NPs are able to associate.

sCT had the IEP of 10.2 and therefore it is expected to bear a positive charge under all formulation conditions tested. As described in Chapter 4, sCT is bound to HA by electrostatic interactions. Indeed, the formation of protein/polysaccharide complexes is dominated by electrostatic interaction (Ganzevles et al., 2007). Van Damme et al., (1994), who examined the interactions between HA and lysozyme (which has the IEP similar to sCT), confirmed the

electrostatic nature of the interaction. Protamine, which is an arginine-rich protein with IEP of ~12, bears a stronger positive charge than sCT. Therefore after incorporation of PROT into the HA/sCT dispersion a competition between these two positively charged macromolecules for binding with negatively charged carboxylic groups of HA is likely to take place. The interaction of PROT with HA should be much stronger that of sCT according to the Coulomb's law, thus it is not recommended to have too much PROT in the formulation, as it limits the amount of sCT which may be loaded into the particles (e.g F4 and F8). However, the presence of PROT (or other polycation, e.g. chitosan, see Chapter 4) is necessary to cross-link the sCT-HA soluble complex, so that NPs can be formed. When too much PROT is added into the formulation, sCT is probably released from its complex with HA and is deposited on the negatively charged surface of the particles, being responsible for a decrease in surface charge and aggregation of particles. This may happen in formulations F4, F2 and F8, which were deemed unstable and in which precipitation was observed after a few hours of storage. The same formulations were susceptible to precipitation during separation of non-associated sCT by ultrafiltration-centrifugation.

In conclusion, as sCT, especially when used at high concentrations (e.g. 1 mg/ml), has a destabilising effect on the NPs, it is necessary to compromise that effect with the need to have a high loading of sCT necessary to produce a desired pharmacological effect. Formulations with low PROT content seem to be the best carriers for sCT as they are characterised by good stability and high loading efficiency.

5.7 sCT release studies from HA/PROT nanoparticles

The results of the *in vitro* release studies are shown in Fig.5.21

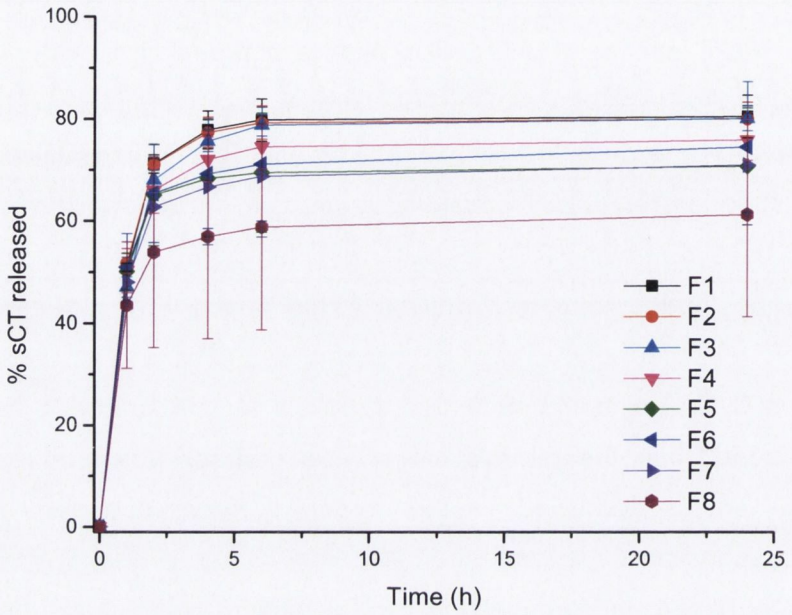

Fig. 5.21 Release profiles of sCT from the different HA/PROT nanoparticles.

The release profiles of sCT may be considered as similar for all the formulations tested. Although the percentage of sCT released from F8 is slightly lower, even in this case the difference is not statistically significant. F8 is one of the most unstable formulations (particles aggregated quickly into larger agglomerates) and it is possible that some sCT was irreversibly bound to the aggregated fraction.

In all formulations tested the initial quick release of sCT was followed by a prolonged release phase. Approximately half of the sCT dose loaded into the NPs was released immediately and up to ~70-80% of sCT was released after 6 hours. The release profiles of sCT-loaded HA/PROT NPs were similar to HA/CL113/sCT NPs (presented in Chapter 4), with the latter generally characterised by slightly smaller (by a few %) amount of sCT released during an initial quick release phase. As sCT is believed to interact mainly with HA by electrostatic forces, the initial quick release may be due to the dilution in PBS, which is characterised by a higher pH and ionic strength than the initial NP dispersion, what leads to weakening of HA/sCT interactions. The release profile may also be dependent on the localisation of sCT in the nanoparticles, similarly to the HA/CL113/sCT NPs. Therefore, initially sCT localised close to the particle surface is released, followed by sCT molecules placed deeper inside the particles. Although the release of sCT from HA/PROT NPs is notably prolonged, most of sCT was released within 6 hours.

The release of sCT may be relatively rapid compared with other delivery systems which are capable provide the release of proteins for days (Corrigan and Li, 2009). The rate of protein release from ionic hydrogels is influenced by the various structural parameters of the protein and polyelectrolyte as well as by the environmental conditions inside hydrogel (Cooper et al., 2005). Proteins with low molecular weights are generally characterised by faster release rates (Cooper et al., 2005). Also, Kamiya and Klibanov (2002) examined the release of lysozyme from its complexes with different polyanions. They confirmed that a protein is gradually released from its non-covalent, water-insoluble complex with oppositely charged polyion over the period of hours and days and the rate of *in vitro* release was markedly dependent on the nature of the polyion. Polymers with higher charge density were found to provide slower release of lysozyme. Since HA has very low charge density and sCT is a peptide with low molecular weight, it is expected that most of sCT release would occur within a few hours.

Table 5.3 Model parameter estimates and related goodness of fit statistics for sCT release data fitted to the first order model. The composition of samples is shown in Table 5.2

Sample	k [min^{-1}]	W_∞ [µg/mg of NPs]	Red. Chi-Sq.	R Sq.
F1	1.03686±0.03087	279±1.9	9.38	0.99922
F2	1.06966±0.02814	258±1.5	6.12	0.99940
F3	0.92326±0.03594	160±1.5	5.61	0.99858
F4	1.10763±0.04434	124±1.1	3.21	0.99865
F5	1.27921±0.04219	363±2.3	16.40	0.99920
F6	1.21897±0.08332	268±3.7	40.19	0.99637
F7	1.18087±0.06321	226±2.5	18.00	0.99771
F8	1.30142±0.09905	170±2.5	18.80	0.99579

The release data was fitted to the first order equation (see Chapter 2, Section 2.2.9, Equation 2.4). The parameter estimates obtained and related statistics are summarised in Table 5.2. It can be observed, that formulations containing smaller quantity of PROT are capable to release markedly higher amount of sCT than formulations with lower amount of PROT. Interestingly, it has been shown (see Section 5.6) that NPs with higher content of PROT were considerably larger, and possibly it is more difficult for the molecules of dispersant to penetrate inside the NPs, therefore it is likely that some of sCT molecules remain entrapped in the NPs.

The release rate constant was markedly higher in HA/PROT NPs compared to HA/CL113 NPs described in previous chapter. Therefore HA/CL113 NPs are capable to provide a slightly slower release of sCT compared to HA/PROT NPs.

5.8 Cytotoxicity studies

Cytotoxicity of PROT and NPs was examined on Caco-2 cells to assess any potential toxic interactions with cells. As mentioned earlier, HA is not toxic to Caco-2 cells even at 5 mg/ml (see Chapter 3).

MTS assay and flow cytometry showed that protamine exerts toxic effects in Caco-2 cells, depending on concentration (Fig.5.22-5.24). The MTS assay appeared to be more sensitive than flow cytometry (IC_{50} of 0.24±0.01 and 0.52±0.03 mg/ml, respectively) (Fig.5.22).

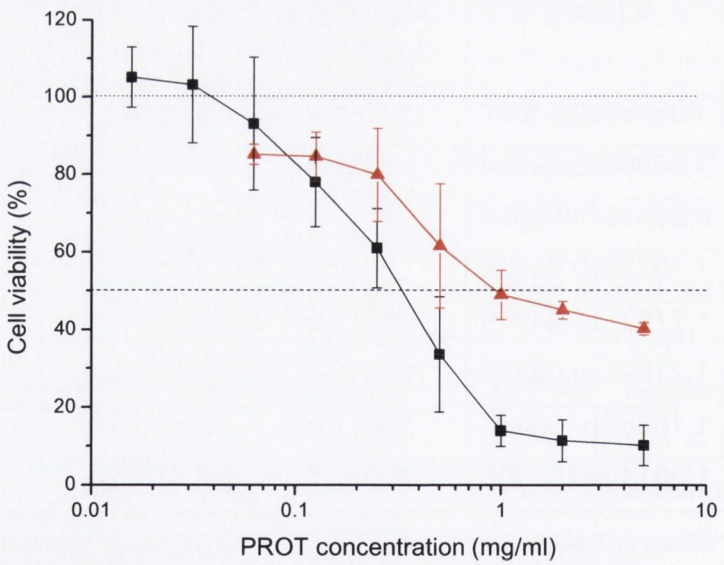

Fig.5.22 The cytotoxicity of protamine on Caco-2 cells after 72 h of exposure to protamine solution in medium. Cell viability determined by flow cytometry (red symbols) and the MTS assay (black symbols), the dashed line indicates 50% cell viability. Viability of the control group was 100% (dotted line).

It can be seen from the scatter plots (Fig. 5.23) and apoptosis assay results (Fig. 5.24) that higher concentrations of PROT considerably increased the number of cells in Q2 zone (late apoptosis or dead cells). Also, exposure to higher concentrations of PROT (0.5 mg/ml and higher) significantly ($p=0.020$) increased the number of viable apoptotic cells in the population compared to the control (7.00±3.11% and 1.83±1.03% of viable apoptotic cells, respectively).

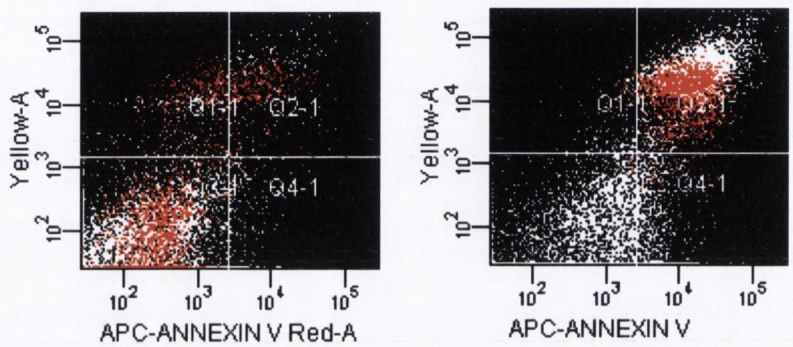

Fig.5.23 The cytotoxicity of protamine on Caco-2 cells after 72 h of exposure to protamine solution in medium. Scatter plots of apoptosis assay: control (left) and PROT 5 mg/ml (right). (Q1 (red). PI positive, Annexin V negative: necrotic cell zone; Q2 (blue). PI positive, Annexin V positive: late apoptosis or dead cell zone; Q3 (green). PI negative, Annexin V positive: living cell zone; Q4 (orange). PI negative, Annexin V negative: viable apoptotic cell zone). Representative recordings of 3 similar experiments are presented.

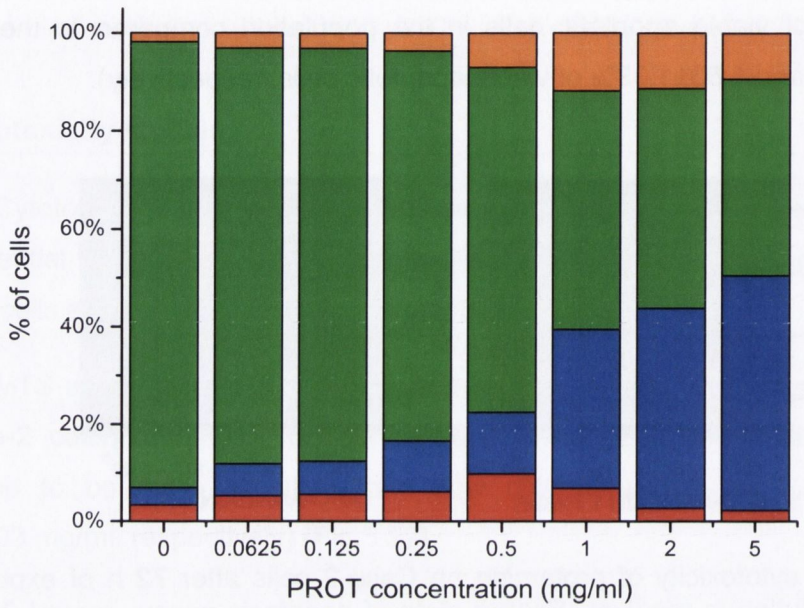

Fig.5.24 The cytotoxicity of protamine on Caco-2 cells after 72 h of exposure to protamine solution in medium. The results of apoptosis assay by flow cytometry (Q1 (red). PI positive, Annexin V negative: necrotic cell zone; Q2 (blue). PI positive, Annexin V positive: late apoptosis or dead cell zone; Q3 (green). PI negative, Annexin V positive: living cell zone; Q4 (orange). PI negative, Annexin V negative: viable apoptotic cell zone).

The NPs selected for cytotoxicity studies by MTS assay had HA/PROT MMR of 3.1. This dispersion was stable and even after dilutions with the medium contained the concentration of PROT high enough to produce a toxic effect to Caco-2 cells, so that the comparison of effects of PROT and HA/PROT NPs could be made. At the highest concentration possible to achieve for this formulation, i.e. 1 mg/ml of NPs (which contains 0.25 mg/ml of PROT), the viability of the cells was decreased significantly (70.31±15.65% of viable cells) when compared to the serum-free medium (100%) (Fig.5.25).

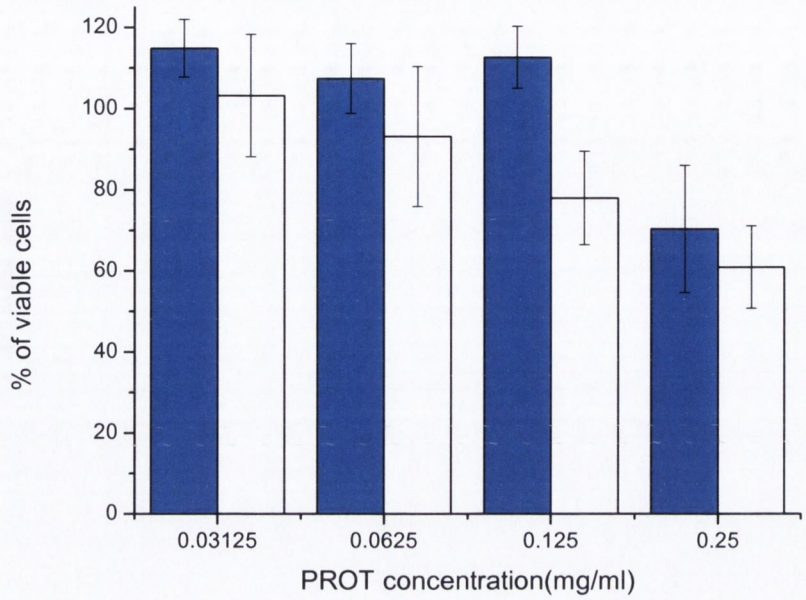

Fig.5.25 The viability of Caco-2 cells by MTS assay after 72 h of incubation with HA/PROT NPs (HA/PROT MMR=3.13) and PROT. Blue bars indicate NPs and open bars indicate PROT solution.

The cell viability after the treatment with 0.25 mg/ml of PROT and NPs containing 0.25 mg/ml PROT was comparable (Fig. 5.25). Further 1:1 dilutions of the above NPs (with the serum-free medium) did not show any toxic effects even at 0.5 mg/ml of NPs (containing 0.125 mg/ml of PROT) in contrast to PROT on its own, which at 0.125 mg/ml decreased the amount of living cells by ~20% compared to the serum-free medium. Therefore, it can be concluded that HA present in the NPs has a protective effect on Caco-2 cells against the negative influence of PROT.

5.9 Summary and conclusions

A new type of nanoparticle carrier that incorporates in its structure HA and PROT was successfully developed. The formation and characteristics of the particles depend on the conditions used, e.g. the concentration of both polyelectrolytes and their MMR, and also on the molecular weight of HA used. Positively charged nanoparticles were not stable upon storage at room temperature, in contrast to dispersions containing negatively charged particles, which is usable after up to two weeks in the liquid form. By modulation of formulation conditions it was possible to produce NPs with good micromeritic properties, i.e monodispersed and with a very small size. Some of the nano-suspensions were characterised by a particle size below 100 nm, which can be considered as very small for polymeric nanoparticles. Indeed, the smallest particles containing HA590 and PROT at HA/PROT MMR of 13 were characterised by an average hydrodynamic diameter of 58±18nm, which is the smallest reported so far for HA nanoparticles.

Also, most of HA/PROT dispersions tested had the isoelectric point close to pH of 2, therefore is appears that they will be stable and will maintain their negative charge at neutral and slightly acidic pH in the intestines. HA/PROT NPs showed low toxicity to Caco-2 cells. Moreover, binding to HA seems to protect Caco-2 cells against toxic effects exerted by protamine.

HA/PROT NPs appear to be an interesting candidate for the delivery of sCT, as they are characterised by excellent capacity to load high doses of sCT and provide prolonged release of this peptide. By optimising the composition of the nanoparticles, it was possible to obtain sCT-loaded NPs which maintained good micrometric properties. HA/PROT NPs may also be considered as a promising system for the delivery of other compounds than sCT.

6. Chondroitin/calcitonin, chondrotin/chitosan and chondrotin/chitosan/calcitonin nanoparticles

6.1 Introduction

Chondrotin sulphate (CHON) is an abundant glycosaminoglycan found in cartilage, bone and connective mammalian tissue. CHON exhibits a wide variety of biological functions and is currently used as an anti-inflammatory, chondroprotective and antirheumatic drug. It has been shown to be absorbed after oral administration in humans as a high molecular weight polysaccharide (Volpi, 2002).

Chondroitin sulphates have both, weak (carboxylate) and strong (sulphate) residues. Due to its acidic nature CHON is able to produce ionic complexes with positively charged molecules (Denuziere et al., 1996). Indeed, similarly to HA, CHON has been shown to form polyelectrolyte complex with chitosan (Denuziere et al., 1996). Examples of such complexes include NPs composed of CHON and CS. Yeh et al.,(2011) prepared and characterised FITC-BSA loaded CHON/CS NPs. The encapsulation efficiency of FITC-BSA was as high as 90% and the NPs were able to provide a prolonged release of this protein (over four days and longer). Some of the NP process formation parameters were examined (e.g. pH, weight ratio and concentration), however all formulations described by Yeh et al. were characterised by a positive surface charge. Hou et al., (2012) produced CS/TPP/CHON NPs as carriers for Nell-1 like molecule (a novel osteoinductive protein with an isoelectric point of 5.66). Although the particles were capable to provide a prolonged release of this protein, the particle size was relatively high (550-850 μm). Also, all prepared NPs showed a positive zeta potential. Da Silva et al., (2012) prepared cross-linker free CS/CHON NPs; the particles obtained showed small sizes (the smallest were ~150 nm), narrow size distribution, but again only positively charged systems were acquired.

As positively charged NPs are generally more toxic than those negatively charged (see Chapter 3) and negatively charged NPs are more promising candidates for the encapsulation of positively charged macromolecules (e.g. sCT), it would be interesting to examine if stable, negatively charged CHON/CS NPs can also be obtained. Negatively charged CHON/CS NPs, which would be good carriers for positively charged macromolecules, have not been described so far. CHON-based NPs would make particularly attractive carrier for sCT due to complementary pharmacological action of both molecules and their use in e.g.

arthritis. To our best knowledge, no delivery system containing CHON and sCT have been described so far.

Previously presented sCT loaded HA-based NPs (see Chapter 4 and 5) offer an attractive formulation format for the delivery of sCT, nevertheless the electrostatic interactions between HA and sCT are relatively week due to the weak charge and low charge density of the former, and as a result ~50% of sCT was released within one hour. Development of another delivery system characterised by a more prolonged release of sCT would provide a therapeutic alternative to HA/CS/sCT NPs. Since CHON molecules contain both, weak and strong acid moieties, it is expected that electrostatic interactions of this polysaccharide with positively charged molecules e.g. sCT and CS may be stronger than those in HA/CS systems.

6.2 Characterisation of polymers

CHON is characterised by a markedly lower molecular weight than HA obtained by ultrasonication. As shown in Table 6.1, the weight average molecular weight of CHON determined by GPC was 58.6±0.23 kDa. This value was 3 times smaller than the lowest Mw of HA obtained by sonication and 49 smaller than the Mw of native HA (see Chapter 3).

Table 6.1 Physicochemical properties of chondroitin. Mn- number average molecular weight, Mw-weight average molecular weight, Mw/Mn- polydispersity index

Polymer	Mn [kDa]	Mw [kDa]	Mw/Mn
CHON	33.4±0.41	58.6±0.23	1.76±0.011

In Chapter 3 CL213 was found to cause precipitation of HA/CS NPs because of its high molecular weight, therefore CL113 and another chitosan chloride with smaller molecular weight (CL42) was used to produce CHON/CS NPs. The molecular weight values of CL42 are shown in Table 6.2, and the properties of CL113 are presented in Chapter 3. CL42 had an evidently smaller molecular weight than CL113 (Mw of 41.9±0.87 and 110±6.78 kDa, respectively). The degree of deacetylation (DD) determined by NMR was similar for both chitosan types (~83%).

Table 6.2 Physicochemical properties of CL42. Mn- number average molecular weight, Mw-weight average molecular weight, Mw/Mn- polydispersity index.

Polymer	Mn [kDa]	Mw [kDa]	Mw/Mn	DD
CHIT	14.2±0.12	41.9±0.87	3.96±0.037	83.5%

6.3 CHON/sCT nanoparticles

As presented in Chapter 4, sCT with its isoelectric point of 10.4 is expected to carry a positive charge at neutral and acidic pH. CHON on the other hand carries a negative charge due to the presence of covalently bound to the pyranose ring sulphate and carboxylic acid groups. Similarly to HA, CHON is expected to interact with sCT by Coulombic forces at neutral and slightly acidic pH.

Therefore CHON/sCT complexes obtained by mixing solutions of the polymer and peptide at different concentrations and different mixing ratios (see Table 6.3) were first examined. Upon mixing the solutions different phenomena were observed: formation of a solution, opalescent and turbid dispersion and in one case (CHON of 0.35 mg/ml, sCT of 2 mg/ml) - an unstable sample resulted and formation of aggregates were seen.

Transmittance values of the dispersions are shown in Fig.6.1; the sample where the phase separation occurred was not suitable for UV analysis due to the rapid sedimentation of the particles. It can be seen that the turbidity of the dispersions increased correspondingly to a decrease in CHON/sCT MMR. Samples with MMR of 0.35 were very turbid with the transmittance values of 12% (sCT of 1 mg/ml) or close to 0% (sCT of 2 mg/ml). Dispersions containing higher concentration of sCT (2 mg/ml) were significantly more turbid than samples with 1 mg/ml of sCT with the same amount of CHON. CHON/sCT dispersions were also more turbid than the previously described HA/sCT dispersions (see Chapter 3).

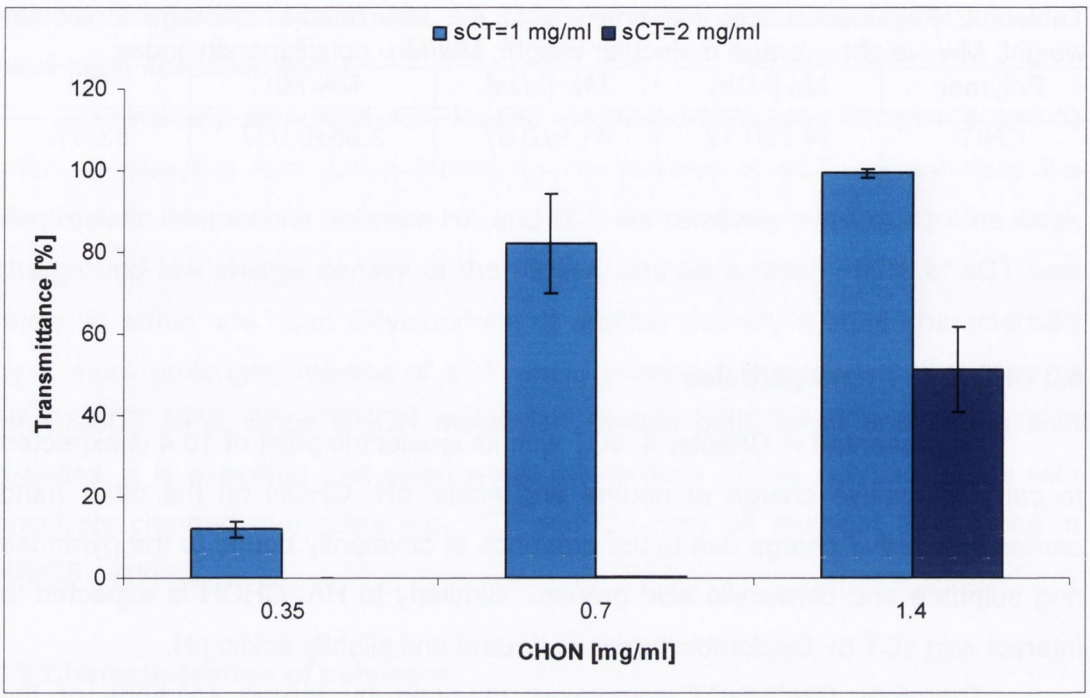

Fig.6.1 Transmittance of CHON/sCT dispersions.

Dynamic viscosity of CHON/sCT dispersions is shown in Fig 6.2. It can be observed that the viscosity depends on CHON/sCT MMR. The viscosity of dispersions containing CHON and sCT at MMRs of 0.175 and 0.35 was similar to the viscosity of water (0.89 mPa*s) and therefore it is likely that most of CHON molecules was bound to sCT. Mixtures with higher MMRs (0.7 and 1.4) were more viscous than water probably due to the presence of excess of CHON in relation to sCT. Both dispersions with MMR of 0.35 (with sCT of 1 mg/ml and 2 mg/ml) were characterised by the same viscosity (0.91 mPa*s), however when CHON/sCT MMR was increased to 0.7, the sample with higher concentration of both species (CHON of 1.4 mg/ml, sCT of 2 mg/ml) was significantly more viscous than the dispersion containing 0.35 mg/ml CHON and 1 mg/ml sCT. Therefore the influence of concentration of CHON and sCT on the viscosity was more pronounced at higher CHON/sCT mixing ratios, which again may be attributed to the presence of excess of CHON.

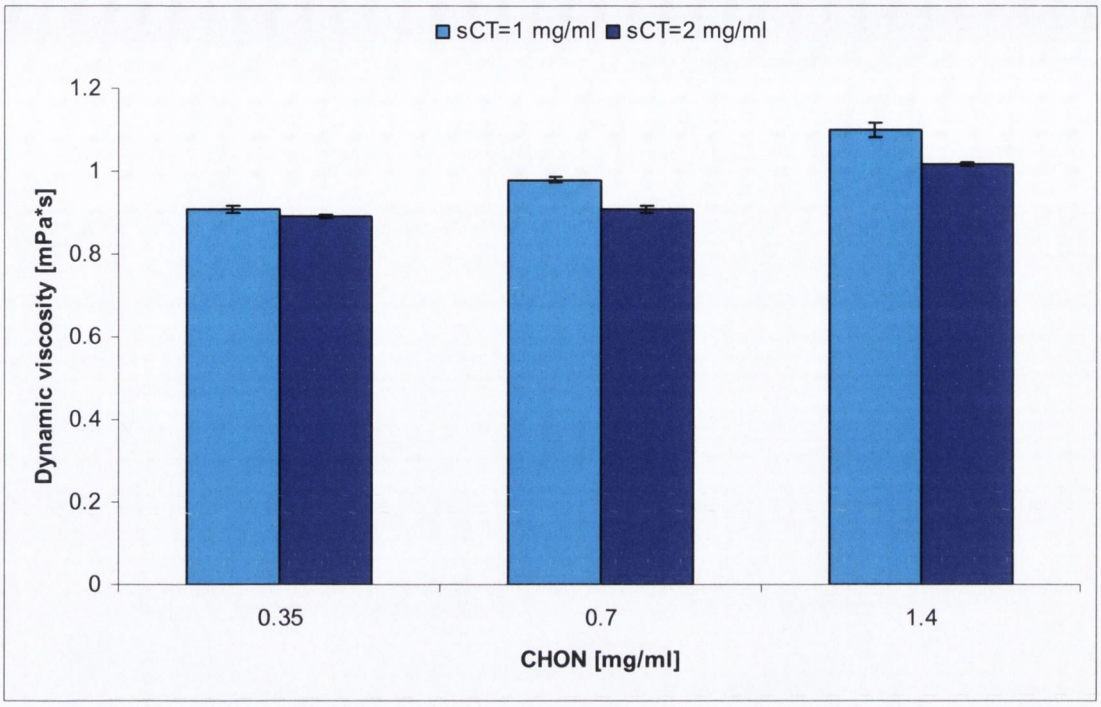

Fig.6.2 Dynamic viscosity of CHON/sCT dispersions

Figure 6.3 shows the hydrodynamic diameter of CHON/sCT NPs. Most of CHON/sCT dispersions, with the exception of CHON/sCT of MMR of 0.175 (which was not shown in the figure 6.3 as it was unsuitable for DLS analysis), were characterised by particles with sizes in the nano-range. CHON of 0.7 mg/ml and sCT of 2 mg/ml NP dispersion contained relatively large nanoparticles with the size of 830±145 nm. Interestingly, the dispersion containing CHON and sCT at the same MMR of 0.35 and the concentration of both ingredients two times lower was composed of markedly smaller NPs with the average size below 200 nm. However, when CHON/sCT MMR increased to 0.7, both dispersions (i.e. CHON of 0.7 mg/ml, sCT of 1 mg/ml and CHON of 1.4 mg/ml, sCT of 2 mg/ml) tested were characterised by similar particles with sizes of 100-120 nm, without a statistically significant difference ($p=0.210$). Based on absorbance calculated from the transmittance values, it appears that the amount of particles in the dispersion containing 1.4 mg/ml of CHON and 2 mg/ml of sCT was approximately two times higher compared to the dispersion containing 0.35 mg/ml of CHON and 1 mg/ml of sCT. Although the average size of the system with particles made of CHON/sCT MMR of 1.4 (163±13 nm) was statistically significantly ($p=0.007$) greater than that of both CHON/sCT MMR of 0.7 dispersions, no conclusions can be made as the quality of the sample was not satisfactory for DLS measurements. Similarly to

HA/sCT complexes, the excess of the anionic polysaccharide increases the solubility of its complexes with sCT.

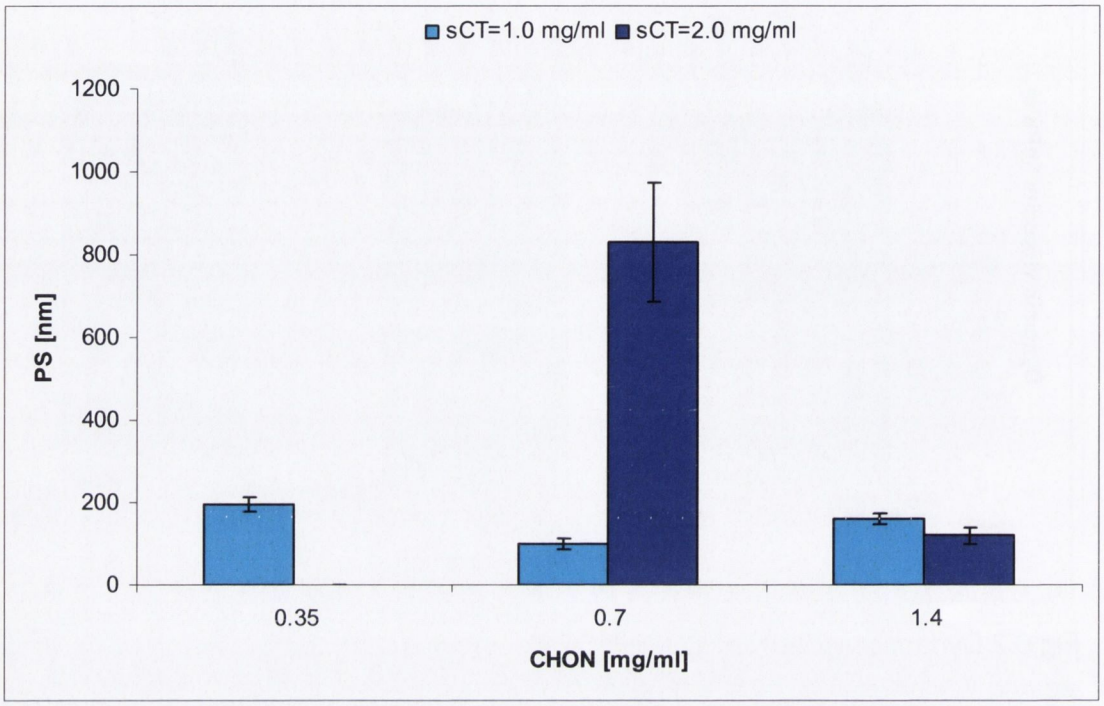

Fig. 6.3 The hydrodynamic diameter of CHON/sCT NPs.

As shown in Fig.6.4, most of CHON/sCT nano-suspensions tested was homogenously dispersed with PDI values below 0.25. However, the dispersion containing CHON and sCT at MMR of 1.4 (CHON of 1.4 mg/ml, sCT of 1 mg/ml) was characterised by a markedly higher PDI of ~0.5. As mentioned above, this dispersion did not meet the quality criteria for DLS measurements possibly due to the lack of homogenous size distribution. As the sample contained a relatively high quantity of CHON compared to sCT, it is possible that the excess of CHON was responsible for the increase in the solubility of the CHON/sCT complex and the decrease in the amount of the particles. Also, as the amount of sCT was relatively low, the competition between CHON molecules for binding with positively charged groups of sCT may have resulted in the formation of highly disordered nanoparticles with relatively low density.

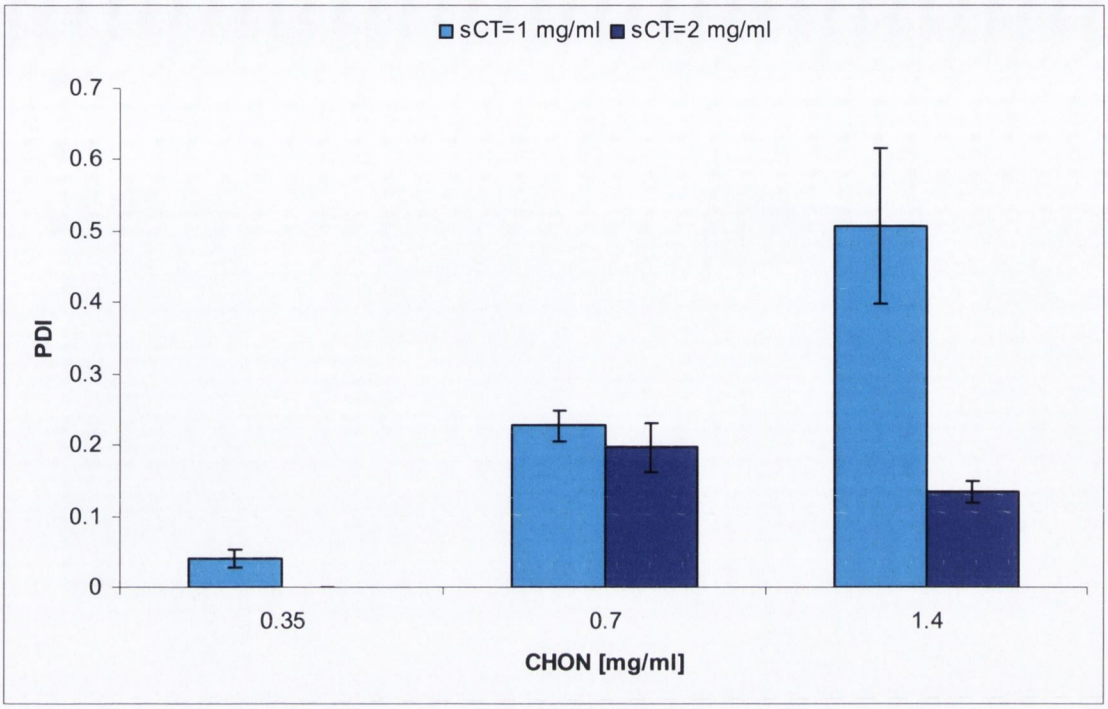

Fig. 6.4 Polydispersity indices of CHON/sCT nanocomplexes.

The zeta potential of CHON/sCT particles is shown in Fig.6.5. Surface charge of the particles depended on the composition of the dispersions and all dispersions tested contained negatively charged particles. The negative surface charge can be attributed to the dominant presence of CHON molecules on the particle surface. The value of zeta potential was markedly affected by the MMR of both polymers. The lower CHON/sCT MMR, the lower was the absolute value of zeta potential. The dispersion containing CHON/sCT at MMR of 0.175, where aggregation was observed, was characterised by a slightly negative surface charge of ~-7 mV. The nano-suspensions with CHON/sCT MMR of 0.35 contained particles bearing more negative charge of -14.4±0.22 and -15.7±0.51 mV for samples containing 0.35 mg of CHON and 1 mg of sCT/1ml and 0.7 mg of CHON and 2 mg of sCT/1ml, respectively. The difference between these two values was statistically significant ($p=0.0154$). When CHON/sCT MMR increased to 0.7, the particles became markedly more negatively charged with zeta potential values of approximately -35 mV and a further increase in CHON/sCT MMR to 1.4 led to another significant increase in surface charge to approximately -45 mV.

The absolute value of zeta potential decreased correspondingly to an increase in sCT and a decrease in CHON concentration. When the negative charge of CHON was neutralised by sCT an increase in the particle size was observed (as in the case of the dispersion containing 0.7 mg/ml of CHON and 2

mg/ml of sCT) or even aggregation may have taken place (the sample with MMR of 0.175).

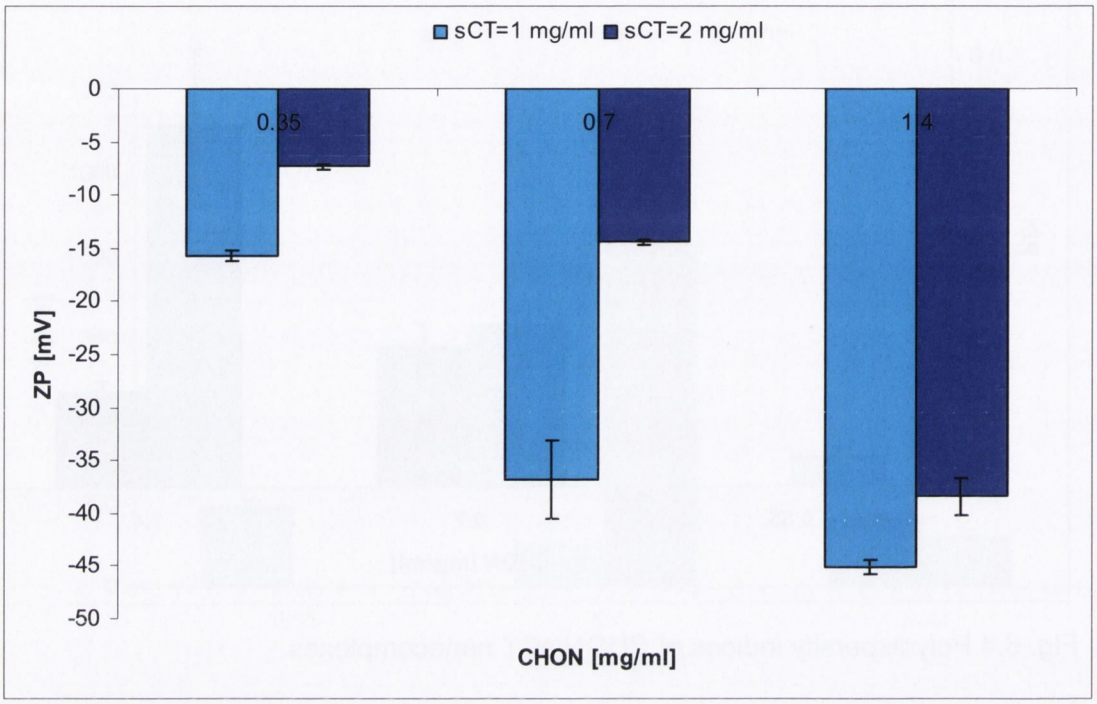

Fig. 6.5 The zeta potential of CHON/sCT dispersions.

Fig. 6.6 shows pH of CHON/sCT nano-suspensions. pH of the CHON/sCT dispersions tested was slightly acidic and varied between 3.7 and 5.3. The concentration of hydrogen ions was affected by the concentration of sCT. An increase in sCT concentration from 1 to 2 mg/ml led to a significant decrease of pH for all nano-suspensions tested. An increase in CHON concentration and CHON/sCT MMR increased pH of dispersions.

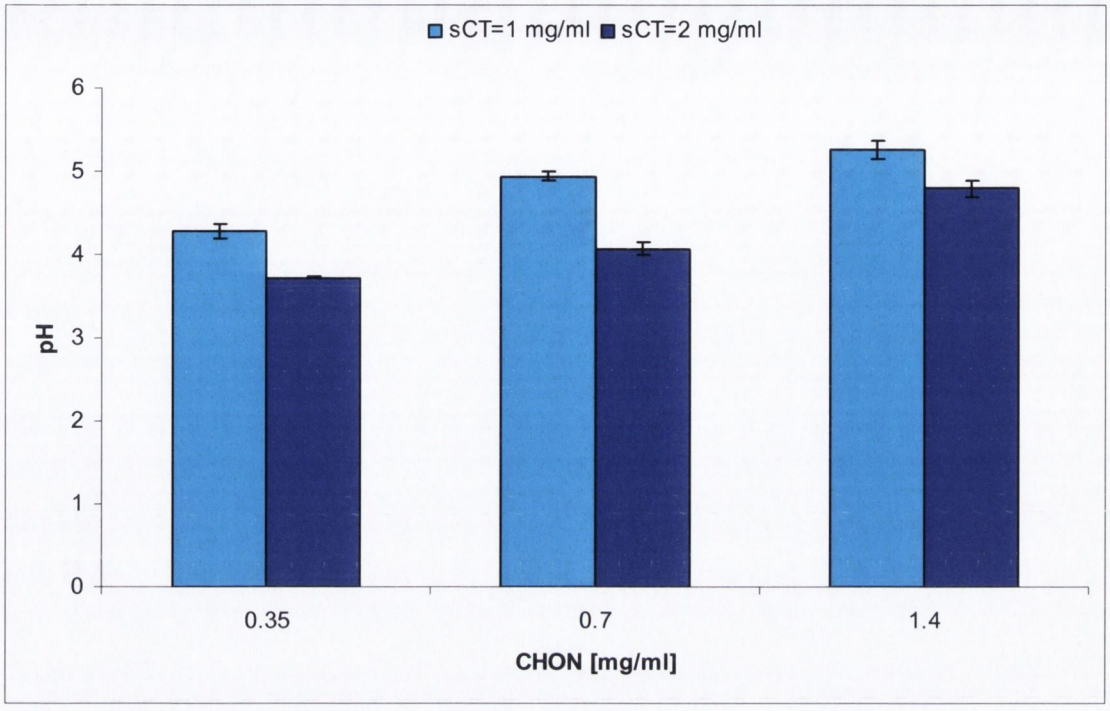

Fig. 6.6 pH of CHON/sCT dispersions.

Table 6.3 Association efficiency (AE) and drug loading (DL) of CHON/sCT complexes.

CHON [mg/ml]	sCT [mg/ml]	CHON/sCT MMR	AE [%]	Extracted sCT [%]	DL [%]
0.35	1	0.35	94.4±3.96	10.6±2.93	73.0±3.06
0.35	2	0.175	44.1±14.41	0.7±0.03	71.6±23.4
0.7	1	0.7	99.7±0.23	80.0±1.27	58.8±0.14
0.7	2	0.35	95.1±2.39	10.2±0.57	73.1±1.84
1.4	1	1.4	99.9±0.12	76.3±4.85	41.6±0.05
1.4	2	0.7	99.8±0.16	81.9±0.51	58.8±0.10

sCT non-associated with CHON was separated by a combined ultrafiltration-centrifugation technique as described in Chapter 4. Similarly to the HA-based sCT loaded NPs, 0.0001 M NaOH solution was added in order to dissolve the CHON/sCT complex, however mass balance was not achieved (Table 6.3). It was found that no adsorption of sCT in the centrifugal filter unit occurred, therefore the lack of mass balance may be attributed mainly to incomplete extraction of sCT from its complexes with CHON. This is in contrast to sCT-loaded HA NPs described in Chapters 4 and 5, where the mass balance was obtained in all cases. The difficulty in the complete extraction of sCT from its complexes with

CHON may be another indication that the interactions between CHON and sCT are stronger than HA-sCT interactions.

As shown in Table 6.3, sCT was bound very efficiently to CHON in the nanoparticles. Nearly 100% of sCT was associated with CHON when CHON/sCT MMR was 1.4 or 0.7. Also, comparable AE was obtained for MMR of 0.35 (at 1 mg/ml sCT). Therefore, in diluted dispersions such as that containing 0.35 mg/ml of CHON the mass of sCT which the polysaccharide was able to efficiently bind was 3 times higher than the mass of CHON. However when CHON/sCT MMR was further decreased to 0.175, phase separation occurred immediately after mixing the sCT and CHON solutions and 56% of sCT was found in non-associated fraction. Therefore, at CHON/sCT MMR of 0.35 and higher, CHON was able to efficiently bind sCT, however with a further decrease in CHON/sCT MMR the binding places in CHON molecules became saturated and sCT molecules not involved in the interactions with CHON were separated from the CHON/sCT complex by ultrafiltration-centrifugation.

CHON/sCT dispersions were characterised by an excellent loading capacity and stable CHON/sCT NPs contained up to 73% (w/w) of sCT.

The amount of sCT extracted from the associated fraction depended on CHON/sCT MMR. Less than 1% of sCT was extracted from the system containing CHON and sCT at MMR of 0.175. When CHON/sCT MMR was increased to 0.35 the amount of sCT extracted was ~10%. In the case of these samples 85% sCT was not recovered. That may be due to the high insolubility of the CHON/sCT complex with MMR of 0.35, as samples with this MMR were the most turbid and after mixing with 0.0001 M NaOH solution followed by high speed centrifugation (13,000 rpm) the presence of sediment was observed. Up to ~80% sCT was successfully extracted when CHON/sCT MMR was of 0.7 or 1.4.

Samples with CHON/sCT MMR of 0.7 were found to preserve their physical properties (i.e. PS, PDI, ZP and transmittance) after the application of ultrafiltration-centrifugation technique markedly better than CHON/sCT NPs with lower CHON/sCT MMRs (see Appendix 4).

6.4 CHON/CS nanoparticles - formulation and formation variables

As previously described (Schatz et al., 2004; Chapter 3), the molecular weight of the polymers is one of the main factors influencing the formation and properties of the nanoparticles. Due to the relatively small molecular weight of CHON compared to HA, there was no need to further reduce it by sonication.

When CL113 was used with HA, the total polymer concentration (TPC) was kept at 1 and 2 mg/ml due to the high viscosity of the polymer solutions. However, as the molecular weight of CHON and CL42 is lower (Table 6.1 and 6.2), and consequently the viscosity of their solutions is also lower (see Appendix 5), CHON/CL42 dispersions with higher TPCs (3 and 5 mg/ml) were also investigated. Similarly to the previously tested HA/CS systems, it was possible to observe either solutions or opalescent or turbid macroscopically homogenous systems or even phase separation depending on the polymer mixing ratio and concentration used.

The phase separation was observed only when CHON/CS MMR was 1.25, regardless of TPC or the molecular weight of chitosan used. As mentioned in the introduction, CHON/CS complexes and NPs were previously described. It has been shown that the complexation between CHON and CS occurs due to strong electrostatic interactions between positively charged amino groups of chitosan and both, sulphate and carboxylic groups of CHON (Denuziere et al., 1996).

Turbidity of CHON/CS dispersions is illustrated in Fig.6.7. It can be observed, that dispersions with TPC of 5 mg/ml were markedly more turbid than other dispersions even at the highest CHON/CS MMR of 20. Generally, the higher TPC, the lower was the transmittance value. The differences in the transparency of the samples were especially pronounced at MMR values of 1, 1.7 and 2.5, and became insignificant at highest (10, 20) and lowest (0.4) MMRs with the exception of TPC 3 mg/ml MMR 0.4 and TPC 5 mg/ml-based dispersions. The molecular weight of chitosan also was found to have an impact on transmittance of CHON/CS dispersions. Samples where CL113 was used were in general less transparent than CL42-based samples.

Another important parameter affecting turbidity of CHON/CS dispersions was the mixing ratio of the polysaccharides. Transmittance of CHON/CS dispersions with the MMR of 1.25 was not measured due to the formation of large, quickly sedimenting aggregates, which made the samples unsuitable for the spectrophotometric analysis. Dispersions became increasingly turbid when the MMR approached 1.25. The influence of CHON/CS MMR on turbidity of the dispersions was found to be affected by TPC and molecular weight of chitosan. For example, in the case of 1 mg/ml TPC-based samples the decrease in CHON/CL42 MMR from 20 to 5 did not affect transmittance of the dispersions (the system had the appearance of a solution with transmittance values of ~99%), while for the samples with TPC of 5 mg/ml, transmittance decreased from 85% to 46% with the decrease of CHON/CL42 MMR from 20 to 5.

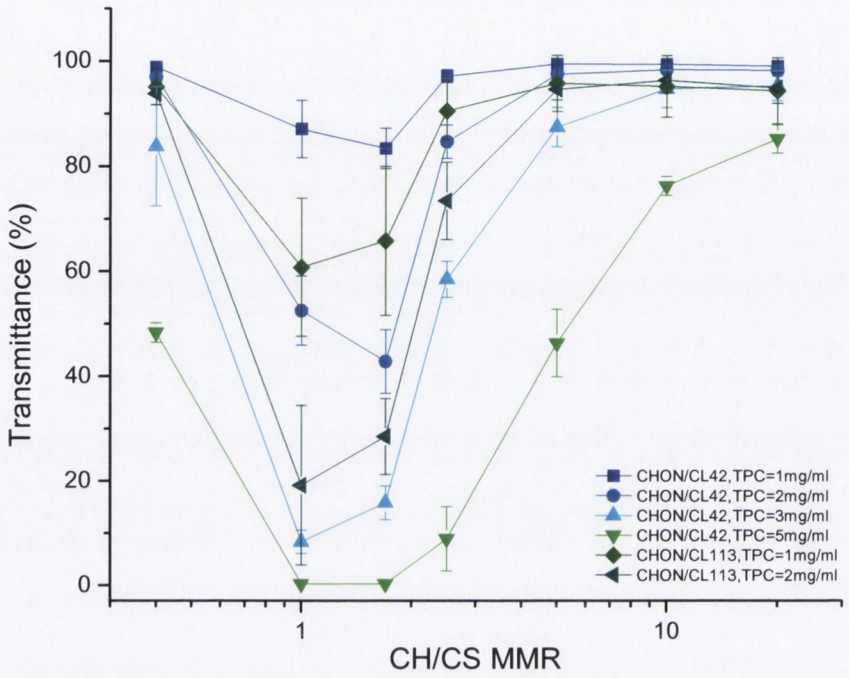

Fig.6.7 Transmittance of CHON/CS dispersions.

Fig.6.8 shows the dynamic viscosity of different CHON/CS dispersions. Generally, the viscosity decreased when the CHON/CS MMR decreased reaching the minimum at MMR of 1.25 and then increased with a further decrease in CHON/CS MMR. TPC also had an influence on the viscosity of CHON/CS dispersions. As expected, an increase in TPC led to an increase in the viscosity of the dispersion.

The molecular weight of chitosan did not seem to have an effect on the viscosity of dispersions with CHON/CS MMRs of 20-1.25, however when CHON/CS MMR decreased to 0.4, dispersions containing chitosan with higher molecular weight (CL113) were markedly more viscous than CL42-based dispersions. Furthermore, the viscosity of 2 mg/ml CHON/CL113 MMR of 0.4 dispersion was comparable to the viscosity of 5 mg/ml CHON/CL42 MMR of 0.4 dispersion (the dynamic viscosity values, being of 1.498±0.039 and 1.435±0.019 mPa*s, respectively), but the dynamic viscosity of 1 mg/ml TPC CHON/CL113 MMR of 0.4 (1.208±0.022 mPa*s) was significantly higher than the viscosity of 3 mg/ml TPC CHON/CL42 MMR of 0.4 dispersion (1.16±0.008 mPa*s). As the samples with CHON/CS MMR of 0.4 contain the highest amounts of chitosan for all MMRs tested, and chitosan is expected to be in the highest excess in relation to

CHON, its impact on the viscosity of dispersions is likely to be enhanced in case of the lowest CHON/CS MMR.

In summary, at MMRs of 20-1.17, the viscosity of NP dispersions was mainly influenced by TPC and not by the molecular weight of chitosan.

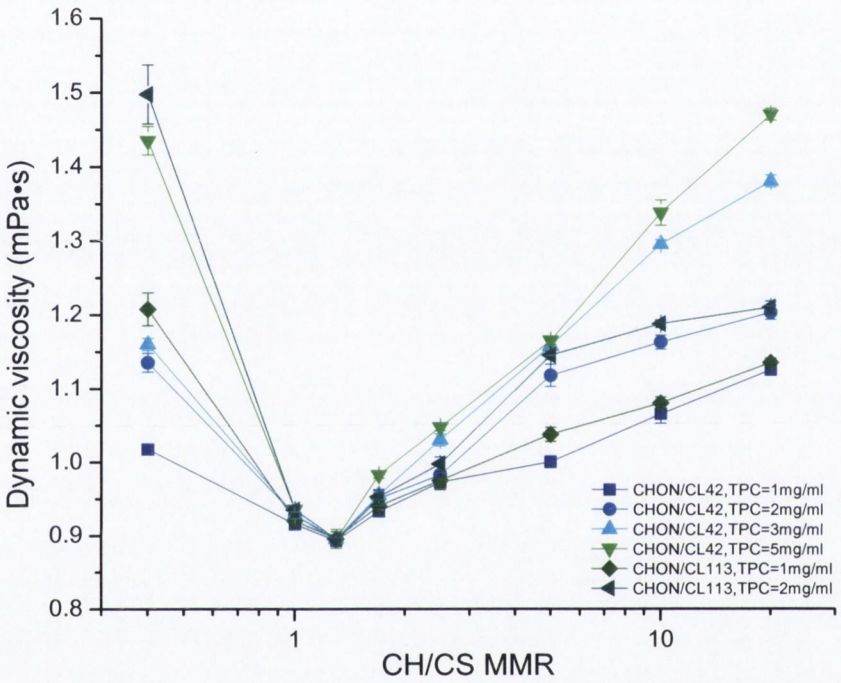

Fig.6.8 Dynamic viscosity of CHON/CS dispersions.

Fig.6.9 shows the hydrodynamic diameter of CHON/CS particles. As previously mentioned, aggregation was observed for dispersions containing CHON/CS MMR of 1.25. Apart from these systems, all dispersions were characterised by particles with small sizes that varied between 78±6 and 269±12 nm (TPC of 1 mg/ml, CHON/CL42 MMR of 2.5 and TPC of 2 mg/ml, CHON/CL113 MMR of 0.4, respectively).

All three parameters: TPC, CHON/CS MMR and the molecular weight of chitosan were found to have an impact on the particle size. Nano-suspensions containing CL113 had a markedly higher particle sizes than suspensions with CL42 for both TPCs tested: 1 and 2 mg/ml. The smallest particle sizes for each TPC and chitosan tested were: 77±6, 85±4, 99±5, 147±4, 128±8 and 152±5 nm for TPC of 1 mg/ml with CHON/CL42 MMR of 2.5, TPC 2 mg/ml with CHON/CL42 MMR of 5, TPCs of 3 and 5 mg/ml with CHON/CL42 MMR of 10, TPC of 1 mg/ml with

CHON/CL113 MMR of 1.7 and TPC of 2 mg/ml with CHON/CL113 MMR of 1.7, respectively.

The particle size was also influenced by CHON/CS MMR, and the effect exerted by MMR was affected by TPC and the molecular weight of chitosan. When CL113 was used, the particle size at first decreased with decreasing MMR, then reached the minimum at CHON/CL113 MMR of 1.7 and increased again remaining steady with a further decrease in CHON/CL113 MMR. For CL42-based NPs with TPC of 1 mg/ml, the particle size decreased significantly from 147±14 nm at CHON/CS MMR of 20, through 116±11 nm at MMR of 10, to 90±9 nm and 78±6 nm for MMRs of 5 and 2.5, respectively, and then increased significantly to 99±8 nm at MMR of 1.7. There was no statistically significant difference between the sizes at MMR of 1.7, 1 and 0.4 and at MMR of 1.25 aggregation occurred due to the particle charge neutralisation.

The particle size was also affected by TPC. Generally, the higher TPC, the larger was the hydrodynamic diameter of the nanoparticles, however some deviations from this trend may be observed.

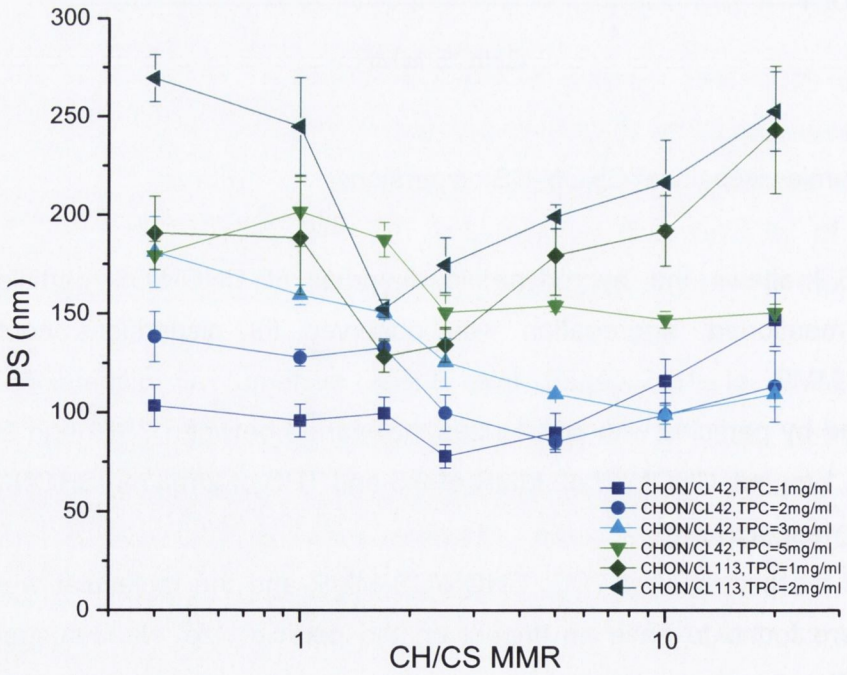

Fig. 6.9 Hydrodynamic diameter of CHON/CS particles.

Fig. 6.10 shows the polydispersity indices of CHON/CS NPs. The PDI values varied between 0.098±0.014 and 0.372±0.009 for TPCs of 1 mg/ml, and

CHON/CL113 MMR of 1 and CHON/CL42 MMR of 20, respectively. Most of the nano-suspensions had homogenous size distributions with PDI values below 0.25. For TPC of 1 mg/ml, the molecular weight of chitosan did not have a significant influence on the PDI of the NPs and only when CHON/CS MMR was 1 the difference between PDI of CL113 and CL42-based samples was statistically significant. Dispersions with TPC of 1 mg/ml and the highest CHON/CS MMRs were characterised by the highest PDI values amongst all CHON/CS NPs tested. Similar trends (i.e. a marked decrease, the minimum and slight increase of PDI with the decrease in CHON/CL42 MMR) were observed for TPC of 2 and 3 mg/ml CHON/CL42 nano-suspensions. No major changes in PDI values were observed for dispersions with TPC of 5 mg/ml and most of the systems had a homogenous size distribution with PDI ~0.200, only for MMRs of 5 and 2.5 a slight decrease to 0.158±0.012 and 0.155±0.006, respectively, was seen.

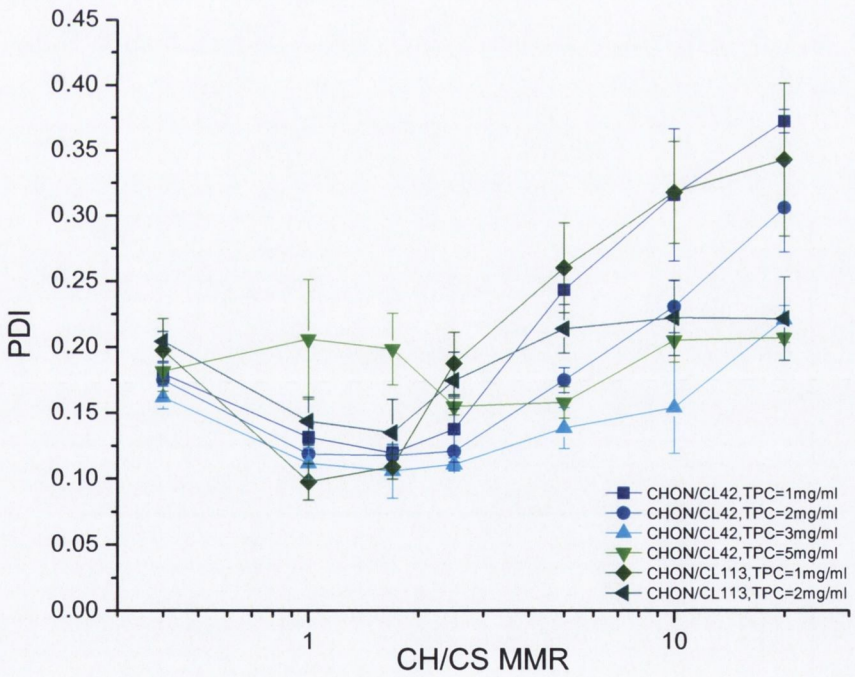

Fig. 6.10 Polydispersity indices of CHON/CS NPs.

Fig 6.11 presents the zeta potential of CHON/CS dispersions. The main factor determining the zeta potential was the MMR of the polymers, similar to HA/CS systems described in Chapter 3. The higher CHON/CS MMR, the smaller was the zeta potential. The surface charge was highly negative for CHON/CS MMRs between 1.7 and 20, and at CHON/CS MMRs of 1 and 0.4 the charge was

highly positive. The charge inversion occurs close to CHON/CS MMR of 1.25, therefore aggregation at this MMR may be attributed to charge neutralisation. For some CHON/CS MMRs tested neither TPC, nor the molecular weight of chitosan had an impact on the zeta potential values and no statistically significant differences were observed for CHON/CS particles with MMRs of 1.7, 2.5 and 5. For CHON/CL42 MMRs of 10 and 20, samples with TPCs of 3 and 5 mg/ml were characterised by a significantly stronger negative charge than TPCs of 1 and 2 mg/ml and no significant difference between CL42 and CL113-based NPs was observed for those MMRs. On the other hand, for CHON/CS MMR of 1, TPC did not have any effect on the zeta potential (the ZP values did not differ significantly), however dispersions containing CL113 were characterised by statistically significantly higher zeta potential values than CL42-based dispersions. The zeta potential values of CHON/CS MMR of 0.4 were found to be influenced by the molecular weight of chitosan (dispersions with CL113 were characterised by markedly higher positive zeta potential values than dispersions with CL42 at the same TPC) and by TPC (the positive charge increased correspondingly to an increase in TPC).

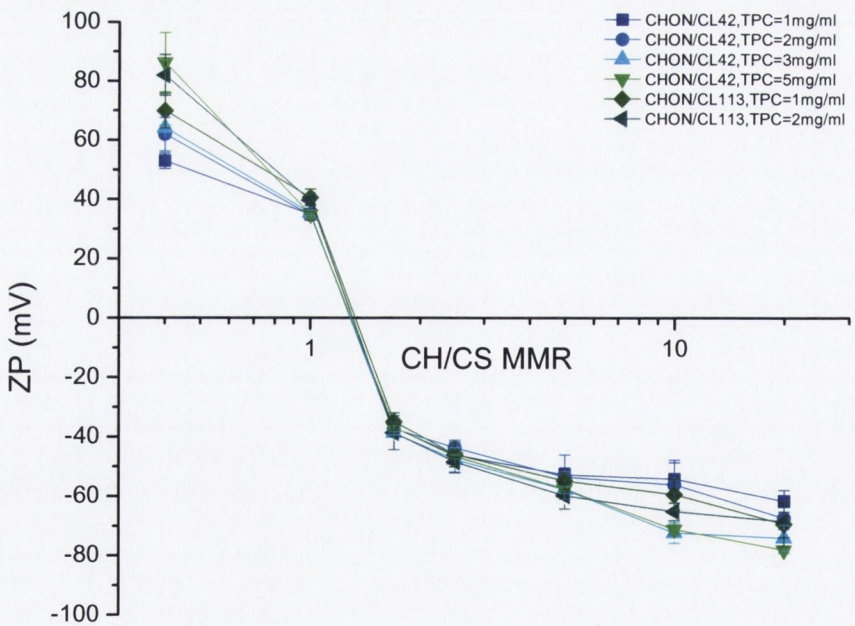

Fig. 6.11 Zeta potential of CHON/CS NPs.

Fig. 6.12 shows the pH of CHON/CS dispersions. The dispersions can be considered as slightly acidic or close to neutral with pH values ranging from 3.99 to 6.54. The concentration of hydrogen ions increased correspondingly to a decreasing CHON/CS MMR. The decrease was initially slow, however between CHON/CS MMRs of 1.7 and 1 a pronounced sudden decrease was observed. Interestingly, between these two MMRs an inversion in zeta potential also took place. Positively charged samples had slightly acidic pH values ~4-4.5, while negatively charged samples were characterised by pH closer to neutral (~5.5-6.5). TPC did not have an important influence on pH of CHON/CS dispersions.

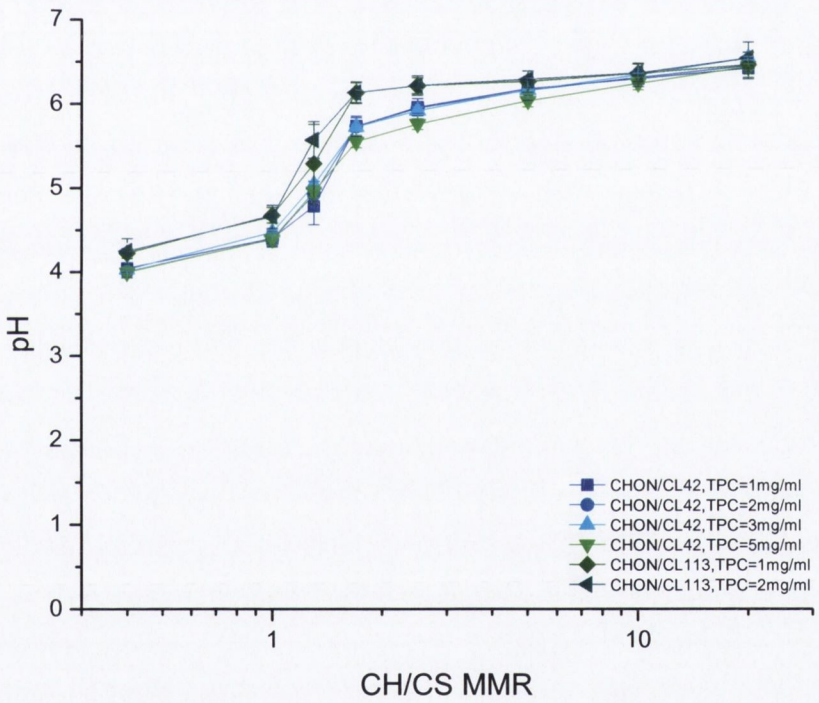

Fig. 6.12 pH of CHON/CS dispersions.

CHON/CS NPs have previously been described by Yeh et al., (2011). The complexes obtained by Yeh et al., (2011) using simple mixing of aqueous solutions of both polyelectrolytes can be classified as nanoparticles, however their particle sizes were considerably larger than those described in this chapter (between 178 and 370 nm). They observed that at a fixed MMR of the polymers, the size increased with increasing polymer concentration, which is in agreement with our observation that the increase in TPC generally produces larger particles. The zeta potential of particles manufactured by Yeh and co-workers (2011) was positive in all cases (approximately between 30-50 mV), however they did not make samples

with higher CHON/CS MMR, which could produce negatively charged particles. They also observed, that at a fixed pH aggregation occurred at a certain polymer MMR, e.g. at pH 6, 5 and 4 aggregation was seen at CHON/CS MMRs of 1.09, 1.36 and 1.42, respectively. Although our experimental design was slightly different (the MMR of the polymers was modified, but the pH of the complex was not adjusted to a fixed value), the published results are in agreement with the present observations of aggregation at CHON/CS MMR of 1.25. Below this value chitosan is the dominant element of the surface of the NPs and determines their surface charge, which is positive in both, our and Yeh et al. works. However, Yeh et al. (2011) did not describe the systems with higher CHON/CS MMR than those determined at the aggregation point. It is shown here that when CHON/CS MMR is markedly higher than the MMR of the aggregation point (e.g. 2.5, 5 or 10), small, monodispersed, negatively charged NPs can be obtained. In these formulations CHON is the dominant component of the surface of the particles and determines their zeta potential. These NPs would make particularly attractive carriers for positively charged molecules.

Similarly to HA/CS NPs, the surface charge of CHON/CS NPs was also determined mainly by the MMR of the polysaccharides and it is possible to obtain both, positively and negatively charged NPs with suitable properties as carriers for negatively and positively charged macromolecules, respectively (Chapter 3).

In relation to the particle size of NPs, da Silva et al., (2012) also obtained small (154 nm) CHON/CS NPs, however only positively charged formulations were made. Also, they employed sonication of NPs for 1 hour; our results show that this step is not necessary to obtain CHON/CS NPs with desirable characteristics.

The incorporation of a cross-linker (TPP), commonly used for HA/CS NPs (de la Fuente et al., 2008a, b and c), into CHON/CS NPs had a negative impact on the particle size (Hou et al., 2012). All NPs obtained by this group had diameters of 550-850 nm, therefore can be considered as relatively large when compared to other polyelectrolyte NPs. Also, bearing a strong negative charge, TPP competes with CHON for the binding sites of positively charged CS molecules. Indeed, high concentrations of TPP have been found unfavourable in chitosan-based NPs (Wadhwa et al., 2010).

6.5 Isoelectric point of CHON/CS NPs

Table 6.4 presents the isoelectric points of selected CHON/CL NPs. None of the formulations with CHON/CS MMR of 5 or 2.5 showed a sign of the isoelectric point after titration with 0.25 M HCl down to pH of 1.6-1.7. The CHON/CS NPs with

MMR of 5 and 2.5 were negatively charged above pH 1.6-1.7. In contrast, the previously examined HA/CL113 NPs showed IEPs close to 3, shifted to more acidic pH (2.5) at higher HA/CL113 MMR of 5 (Chapter 3). Therefore negatively charged CHON/CS NPs with CHON/CS MMR of 2.5 and higher appear to be more stable in acidic environments than HA/CL113 NPs and the charge inversion from negative to positive at pH ~2 does not occur.

CHON/CL42 NPs with MMR of 1, on the other hand, were characterised by isoelectric points close to neutral. The IEPs were of ~6.2, regardless of TPC tested. This IEP was more acidic than that of HA/CL113 MMR of 1 NPs (Chapter 3). Similarly to HA/CL113 NPs, CHON/CS NPs are expected to be stable and carry a positive charge at acidic pH (e.g. in stomach), but they are not good candidates for carriers used at neutral pH values due to the possibility of aggregation or inversion of the surface charge to negative at physiological pH of 7.4. This inversion of the surface charge could markedly change the interactions of the NPs with the associated macromolecules, as these interactions very often are via electrostatic forces.

Table 6.4 Isoelectric point of CHON/CL42 NPs. N/D: not detectable

TPC	CS	CHON/CS MMR	sCT [mg/ml]	IEP
2	CL113	5	-	N/D
2	CL42	5	-	N/D
1	CL42	5	-	N/D
1	CL42	5	0.5	N/D
1	CL42	2.5	-	N/D
2	CL42	1	-	6.2±0.18
1	CL42	1	-	6.19±0.01

6.6 sCT-loaded CHON/CS NPs

Negatively charged CHON/CL42 MMRs of 2.5, 5 and 10 mg/ml NPs were selected to be tested as potential carriers for sCT. As TPC of 5 mg/ml rendered most viscous nano-suspensions with largest particles, TPCs of 1, 2 and 3 mg/ml were only used in sCT loading studies.

Incorporation of sCT produced an increase in the turbidity of the dispersions (Fig. 6.13). Samples containing 0.5 mg/ml of sCT were significantly

more turbid that samples with the same CHON and CL42 content without sCT, the only exception was dispersions with TPC of 1 mg/ml and 2 mg/ml and CHON/CL42 MMR of 10, where the increase in turbidity was not statistically significant. The decrease in transmittance of the dispersions due to the incorporation of sCT was more pronounced for samples with lower CHON/CL42 MMRs (especially 2.5) and higher TPCs (2 and 3 mg/ml). Further increase in sCT content (to 1 mg/ml) did not change significantly the turbidity of 3 mg/ml-based dispersions compared to samples containing 0.5 mg/ml of sCT. On the contrary, a statistically significant decrease in transmittance of TPC of 2 mg/ml-based samples with CHON/CL42 MMRs of 2.5 and 5 containing 1 mg/ml of sCT was observed compared to samples with 0.5 mg/ml of sCT. Nevertheless, similarly to HA/CL113 NPs, sCT concentration was not the only factor that influenced turbidity of nano-dispersions. TPC and MMR also had an impact on the transmittance values and the higher the TPC and lower CHON/CL42 MMR, the lower was transmittance.

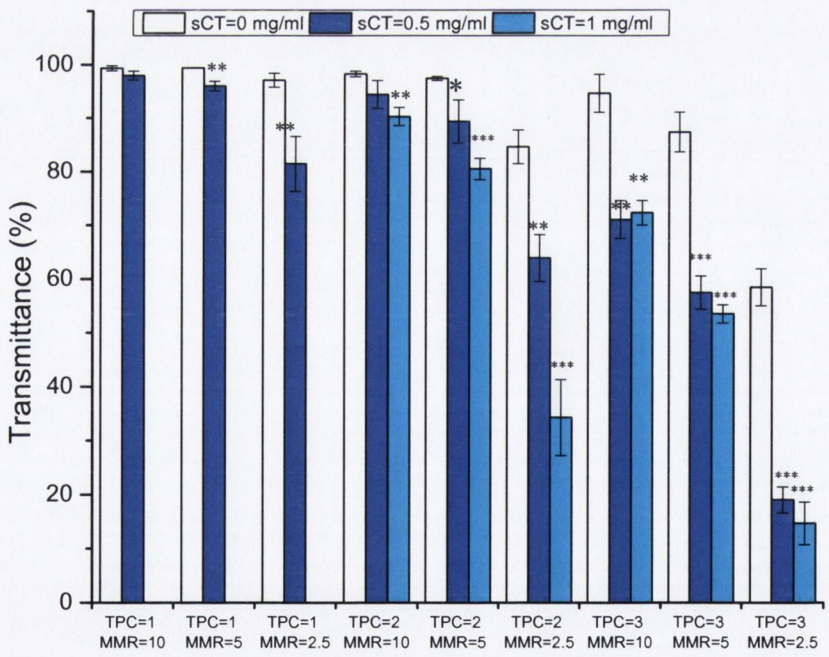

Fig. 6.13 Transmittance of sCT-loaded CHON/CL42 dispersions. *p<0.05, **p<0.01 and ***p<0.001 versus sCT=0 mg/ml (empty bars)

CHON/CL42 dispersions containing sCT had lower viscosity than dispersions without sCT (Fig. 6.14). Incorporation of 0.5 mg/ml of sCT decreased significantly the viscosity of CHON/CL42 dispersions; the only exceptions were two dispersions with TPC of 1 mg/ml containing CHON/CL42 with MMRs of 10 and 5,

where the decrease in viscosity due to the incorporation of sCT was not statistically significant (p=0.094 and 0.210 for MMRs of 10 and 5, respectively). A further increase in sCT concentration to 1 mg/ml decreased significantly the viscosity of TPCs of 2 and 3 mg/ml CHON/CL42 MMR of 5 and TPC=2 mg/ml CHON/CL42 MMR of 10 dispersions; the viscosity of other dispersions containing 1 mg/ml of sCT did not differ significantly from equivalent dispersions containing 0.5 mg/ml of sCT. Nonetheless, CHON/CL42 MMR and TPC remained the main factors influencing the viscosity of CHON/CL42/sCT dispersions.

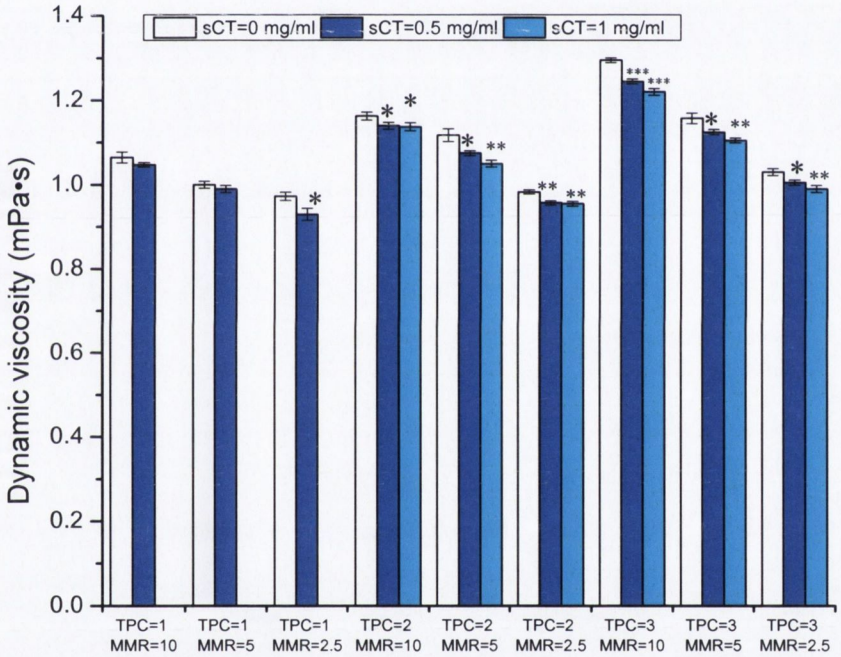

Fig.6.14 The dynamic viscosity of sCT-loaded CHON/CL42 dispersions. *p<0.05, **p<0.01 and ***p<0.001 versus sCT=0 mg/ml (empty bars)

Fig. 6.15 shows the particle size of sCT-loaded CHON/CL42 NPs. All CHON/CL42/sCT dispersions tested contained small NPs with the average hydrodynamic diameter ranging from 95±26 to 249±15 nm (TPC=1 mg/ml, CHON/CL42 MMR=5, sCT=0.5 mg/ml and TPC=3 mg/ml, CHON/CL42 MMR=10, sCT=1 mg/ml, respectively). Incorporation of sCT did not change significantly the size of particles containing TPC of 1 mg/ml CHON/CL42 MMRs of 2.5, 5 and 10 (p=0.050, 0.771 and 0.323, respectively), but in all other dispersions a statistically significant increase in particle size was observed. Interestingly, a further increase in sCT concentration to 1 mg/ml did not change the particle size significantly when compared to similar dispersions containing 0.5 mg/ml sCT (p values between

0.223-0.930). The particle size of sCT-loaded CHON/CL42 NPs also was affected by TPC and MMR. Generally, the higher TPC, the larger was the particle size. There was no significant difference in the particle size between TPC of 1 and 2 mg/ml with the exception of CHON/CL42 MMR of 2.5 (p= 0.057, 0.090 and 0.034 for MMRs 10, 5 and 2.5, respectively); however dispersions with TPC of 3 mg/ml had a significantly larger particle size than TPC of 2 mg/ml-based dispersions for both sCT concentrations (0.5 and 1 mg/ml) (p values ranged from 0.014 to 0.025 for MMRs of 10 and 2.5, respectively for sCT 0.5 mg/ml-based samples and between 0.000 and 0.010 for MMRs 2.5 and 5, respectively for sCT 1 mg/ml-based samples). When sCT concentration was 0.5 mg/ml, and TPCs of 1 or 2 mg/ml, no statistically significant difference was found for the particle size of all CHON/CL42 MMRs tested (2.5, 5 and 10) (p=0.933 and 0.675 for TPC of 1 and 2 mg/ml, respectively), however either an increase in TPC to 3 mg/ml or an increase in sCT concentration to 1 mg/ml or both together led to statistically significant differences in particle size for different CHON/CL42 MMRs (p=0.001 or less). Systems with CHON/CL42 MMR of 2.5 NPs had the smallest particle sizes, while CHON/CL42 MMR of 2.5 NPs had the largest particle sizes.

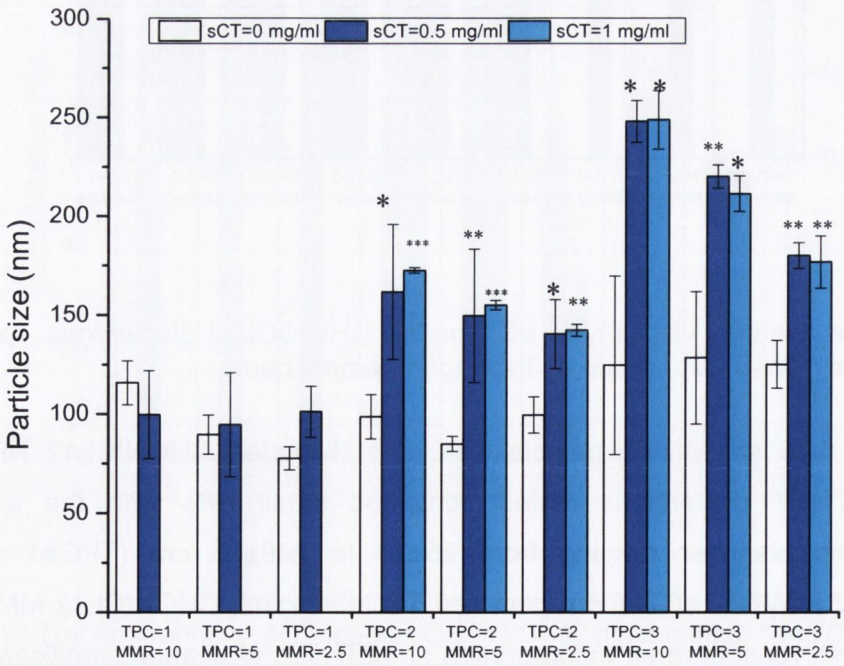

Fig.6.15 The particle size of sCT-loaded CHON/CL42 NPs *p<0.05, **p<0.01 and ***p<0.001 versus sCT=0 mg/ml (empty bars)

Fig. 6.16 displays PDI values of sCT-loaded CHON/CL42 NPs. When TPCs were 1 or 2 mg/ml, loading of sCT did not change the PDI values significantly, however when TPC was 3 mg/ml, a statistically significant increase in PDI in sCT-loaded dispersions was observed compared to similar CHON/CL42 dispersions without sCT. Many CHON/CL42/sCT dispersions with PDI values below 0.25 (all dispersions with CHON/CL42 MMR of 2.5 and TPCs of 1 and 2 mg/ml CHON/CL42 MMR of 5) remained homogenously dispersed. In some samples, especially with TPC of 3 mg/ml and CHON/CL42 MMR of 10, PDI values were increased to moderate values (up to 0.355). Neither TPC nor sCT concentration (0.5 or 1 mg/ml) was found to have a significant influence on the PDI values of CHON/CL42/sCT dispersions. CHON/CL42 MMR, on the other hand had a noticeable influence on PDI values and the higher CHON/CL42 MMR, the higher was PDI value. Dispersions with lower CHON/CL42 MMR (i.e. 2.5) were usually more homogenously dispersed than dispersions with higher content of CHON in relation to CL42 (MMRs of 5 and 10), however only in case of TPC of 3 mg/ml (sCT of 0.5 and 1 mg/ml) and TPC of 2 mg/ml, sCT of 1 mg/ml this difference was statistically significant.

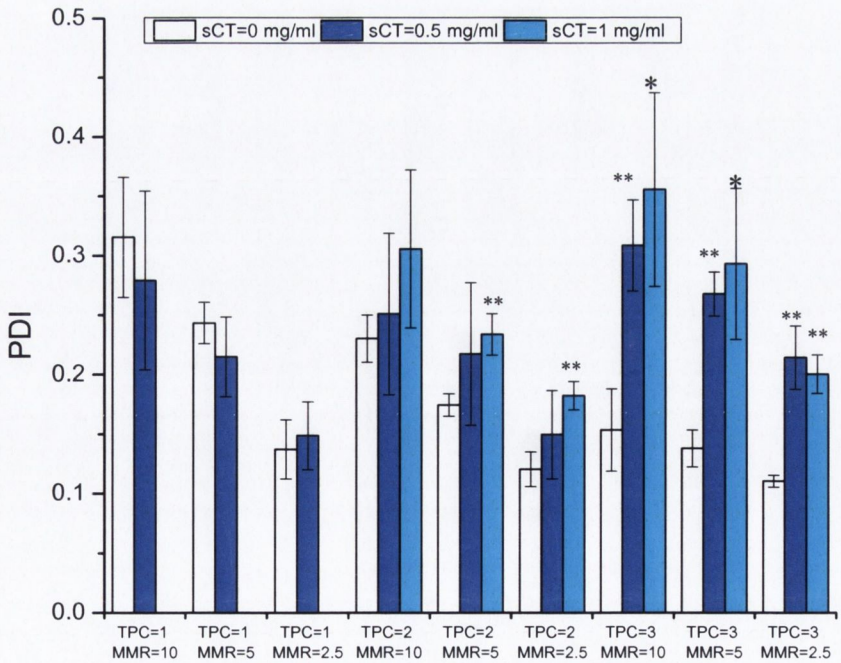

Fig.6.16 The polydispersity index of sCT-loaded CHON/CL42 NPs. *p<0.05 and **p<0.01 versus sCT=0 mg/ml (empty bars)

Fig. 6.17 illustrates the zeta potential values of CHON/CL42/sCT NPs. Despite loading of positively charged sCT, all formulations tested were characterised by a strong negative surface charge ranging from -31.4±2.32 to -72.4±3.43 mV. Loading of 0.5 mg/ml of sCT significantly decreased the surface charge of TPC of 1 mg/ml-based formulations, with the exception of CHON/CL42 MMR of 10. A decrease in absolute value of zeta potential corresponding to an increase in sCT concentration was also observed for TPC of 2 mg/ml-based dispersions with CHON/CL42 MMRs of 2.5. For 3 mg/ml of TPC-based dispersions the surface charge also decreased with an increasing sCT content, but only samples with the highest sCT concentration of 1 mg/ml bore a significantly smaller surface charge. TPC had a significant influence on the zeta potential of all sCT-loaded formulations tested- the higher the TPC, the higher was the absolute value of zeta potential for all MMRs and sCT concentrations tested. CHON/CL42 MMR also had a marked influence on the zeta potential of CHON/CL42/sCT NPs: surface charge of the particles increased correspondingly to an increasing content of CHON in the formulation.

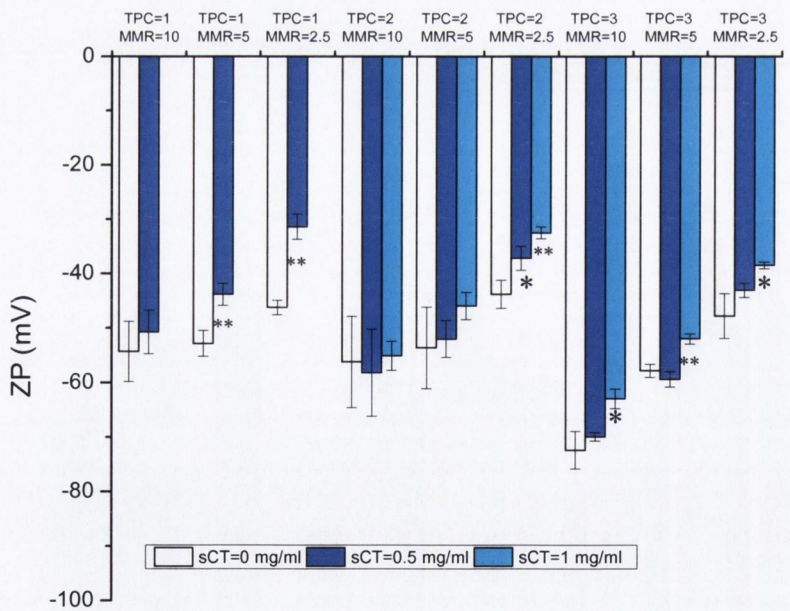

Fig.6.17 The zeta potential of sCT-loaded CHON/CL42 NPs *p<0.05 and **p<0.01 versus sCT=0 mg/ml (empty bars)

All CHON/CL42/sCT formulations tested were characterised by slightly acidic pH values between 5.65 and 4.82. Loading of sCT noticeably decreased the pH of CHON/CL42 dispersions (Fig.6.18).

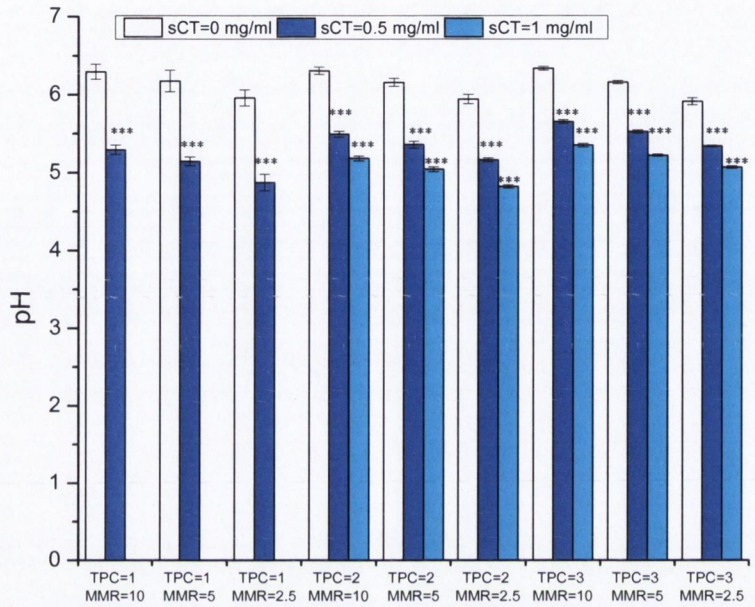

Fig.6.18 pH of CHON/CL42/sCT dispersions. ***p<0.001 versus sCT=0 mg/ml (empty bars)

Table 6.5 shows the AE and drug loading of CHON/CL42/sCT NPs. sCT was very efficiently (~100%) associated with CHON/CL42 NPs. High AE values may be attributed to interactions between negatively charged CHON and positively charged sCT, as described in section 6.2. A competition between positively charged groups of chitosan and sCT for binding with negatively charged groups of CHON is likely to occur, however incorporation of chitosan into the formulation did not decrease the AE in the range of sCT (0.5 and 1 mg/ml) and CL42 (0.1-0.21 mg/ml) concentrations tested probably because CHON was used in much higher quantities than CL42 (CHON/CL42 MMRs of 2.5, 5 and 10). It was possible to extract most of sCT (73-96%) from CHON/CL42/sCT NPs after dilution with 0.0001 M NaOH solution (Table 6.5). High drug loading (14-33%) was achieved when sCT was incorporated into CHON/CL42 NPs. Similar drug loading was accomplished for the previously described HA-based sCT-containing nanocarriers (Chapter 4 and 5). Nevertheless the loading of sCT was markedly smaller in CHON/CL42/sCT NPs when compared to CHON/sCT nano-complexes (42-72%). It may be due to the

fact that incorporation of positively charged CS neutralises some of the negatively charged groups in CHON molecules, and therefore CHON/CS NPs are capable to associate smaller quantities of sCT compared to CHON on its own before the charge neutralisation and flocculation processes occur.

Table 6.5 The association efficiency and drug loading of sCT-loaded CHON/CL42 NPs.

TPC [mg/ml]	CHON/CL42 mass ratio	Initial sCT [mg/ml]	Extracted sCT [%]	AE [%]	Drug loading [%]
3	2.5	0.5	74.8±4.3	99.8±0.03	14.26±0.004
3	5	0.5	76.9±4.0	99.9±0.02	14.27±0.003
3	10	0.5	72.8±3.7	99.8±0.01	14.26±0.001
3	2.5	1.0	80.2±1.8	99.5±0.27	24.91±0.068
3	5	1.0	81.8±2.6	99.8±0.04	24.96±0.010
3	10	1.0	83.4±1.9	99.7±0.17	24.94±0.043
2	2.5	0.5	86.8±5.0	99.4±0.23	19.90±0.046
2	5	0.5	86.6±7.6	99.7±0.07	19.95±0.014
2	10	0.5	86.3±7.3	99.8±0.04	19.97±0.008
2	2.5	1.0	80.3±2.1	98.9±0.61	33.09±0.204
2	5	1.0	89.8±0.7	99.6±0.16	33.24±0.053
2	10	1.0	88.8±2.0	99.7±0.15	33.27±0.050
1	2.5	0.5	91.0±5.0	99.3±0.29	33.18±0.097
1	5	0.5	91.9±2.9	99.5±0.08	33.22±0.027
1	10	0.5	96.3±4.5	99.7±0.08	33.27±0.027

All the formulations preserved their properties satisfactorily after centrifugation-ultrafiltration with the exception of TPC of 3 mg/ml, CHON/CL42 MMR of 2.5-based samples (see Appendix 6).

6.7 Stability of CHON/CL42 NPs after storage at room temperature

To evaluate the physical stability of CHON/CL42 nano-suspensions, two formulations with negatively charged (CHON/CL42 MMRs of 5 and 2.5) and one with positively charged (CHON/CL42 MMR of 1) NPs were selected. First signs of sedimentation were noticeable after 3 weeks of storage of nano-suspension with positively charged particles and after 4 weeks in both negatively charged

formulations. Figures 6.19-6.22 show changes in transmittance, particle size, polydispersity index and zeta potential of the NPs. No major change in turbidity of both formulations containing negatively charged NPs was observed, however transmittance of CHON/CL42 MMR of 2.5 increased statistically significantly to 105.5±3% of the initial value after 4 weeks (Fig.6.19).

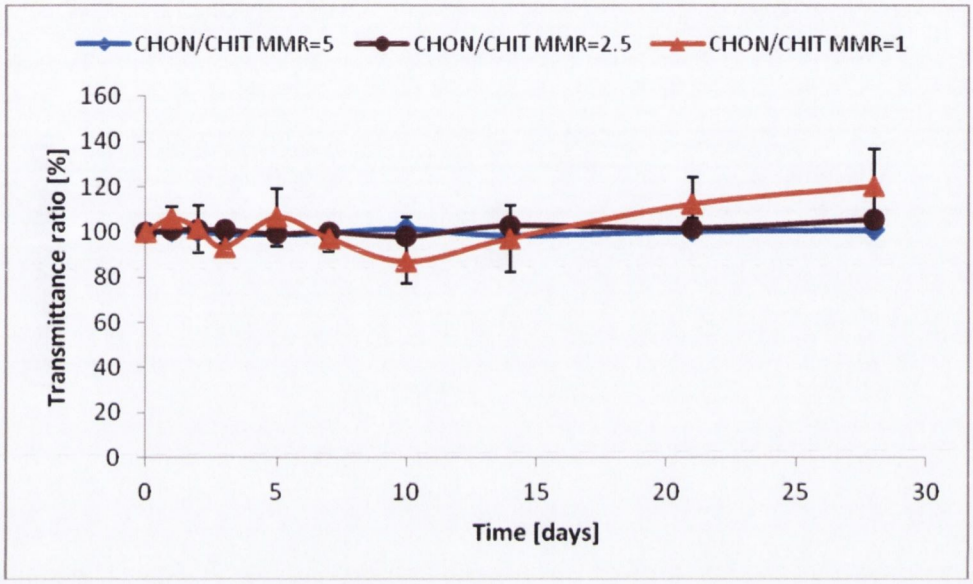

Fig.6.19 Stability of CHON/CL42 nano-suspensions at room temperature: transmittance. The changes in transmittance are presented as a ratio of the values after defined time of storage (e.g.1 day) to initial value (0 days) and are expressed in %. TPC was of 2 mg/ml in all samples tested.

The particle size (Fig. 6.20) and polydispersity index (Fig. 6.21) of the formulations remained practically the same over 4 weeks of storage. The value for any of these parameters after 28 days did not differ more than 6% from the original value and none of the differences were statistically significant.

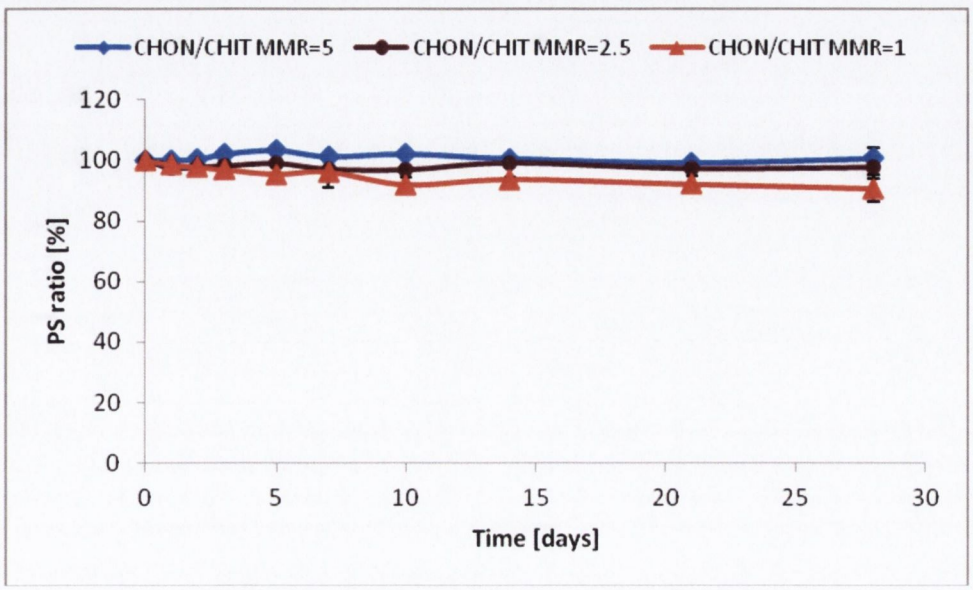

Fig.6.20 Stability of CHON/CL42 nano-suspensions at room temperature: particle size. The changes in particle size are presented as a ratio of the values after defined time of storage (e.g.1 day) to initial value (0 days) and are expressed in %. TPC was of 2 mg/ml in all samples tested.

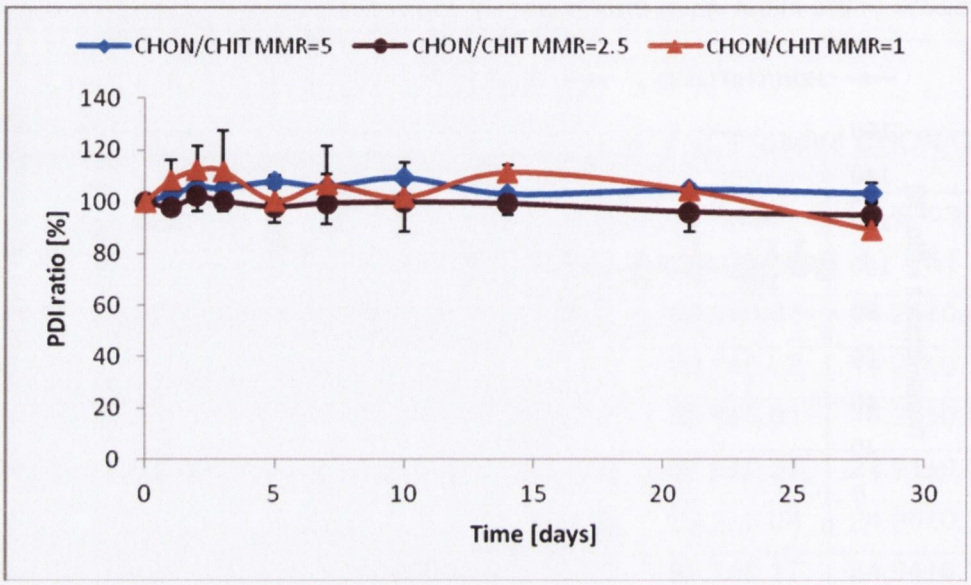

Fig.6.21 Stability of CHON/CL42 nano-suspensions at room temperature: polydispersity index. The changes in PDI are presented as a ratio of the values after defined time of storage (e.g.1 day) to initial value (0 days) and are expressed in %. TPC was of 2 mg/ml in all samples tested.

Although the surface charge after 4 weeks was significantly lower (by 20-25%, which corresponds to ~10 mV) compared to the initial value, the particles remained strongly negatively charged with the zeta potential values well below -30 mV, what indicates their good colloidal stability. A similar decrease in the surface charge (by 25%) was observed for the positively charged formulation. No increase but a decrease in particle size and polydispersity index (by 10%, statistically significant) was also observed for positively charged CHON/CL42 NPs.

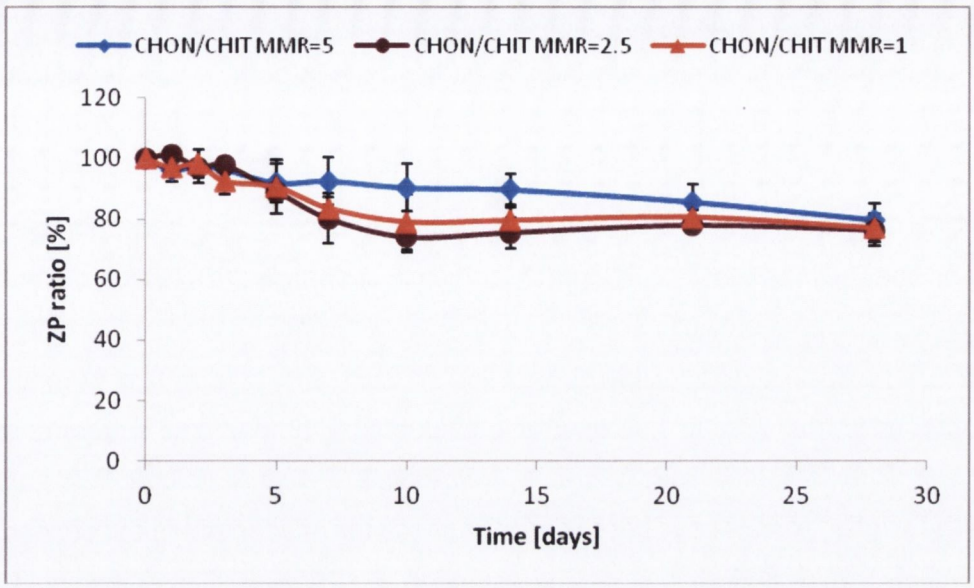

Fig.6.22 Stability of CHON/CL42 nano-suspensions at room temperature: zeta potential. The changes in ZP are presented as a ratio of the values after defined time of storage (e.g.1 day) to initial value (0 days) and are expressed in %. TPC was of 2 mg/ml in all samples tested.

In summary, CHON/CL42 NPs may generally be considered as physically stable after short-time storage at room temperature without any major change in their physical properties.

6.8 Stability of CHON/sCT and CHON/CL42/sCT NPs in different media

It is commonly known that the properties of polyelectrolyte complex NPs depend on many parameters, also on the properties of the dispersant such as its ionic strength and pH (Boddohi et al., 2009). Therefore it is expected that the properties of polyelectrolyte complexes can be modified depending on the medium.

In order to examine the influence of different formulation variables (i.e. the presence of CS in the particles, TPC and CHON/CL42 MMR) three formulations with the following composition: CHON of 1.4 mg/ml, sCT of 2.0 mg/ml; TPC of 2 mg/ml, CHON/CL42 MMR of 5, sCT of 1.0 mg/ml and CHON/CL42 MMR of 2.5, TPC of 3 mg/ml, sCT of 1 mg/ml were selected for stability studies in different media. Figures 6.23-6.25 show the stability of CHON/sCT and CHON/CL42/sCT NPs in different environments: 0.25 M HCl (pH 1.2), acetate buffer (AB) (pH 5), PBS (pH 7.4) and diluted (1:10) buffers (pH 5 and 7.4, respectively).

It can be observed that the initial size of 120±20 nm of CHON/sCT NPs was, in general, increased after dilution with different dispersants. No increase in

the particle size was seen when diluted AB was used. However, when AB or PBS were used, a marked, statistically significant increase in particle size up to 230 nm (diluted PBS) or 280 nm (AB or PBS) was observed. Furthermore, a significant increase in the average particle diameter was observed after 1 day of storage in AB or diluted AB, but after 24 hours in PBS or diluted PBS the initial particle size did not change markedly. CHON/sCT particles suspended in AB or diluted AB remained homogenously dispersed. In addition, strong negative surface charge (~-25-27 mV) was retained in the non-diluted AB. On the contrary, a pronounced increase in PDI values was observed upon dispersing the particles either in diluted PBS or in PBS. Also, the surface charge decreased to -16 mV (diluted PBS) or -8.8 mV (PBS). An increase in the ionic strength of the dispersant may be partially responsible for the decrease in the surface charge. CHON/sCT complex could also be partially destabilised or dissolved after an increase in pH to 7.4. CHON/sCT complexes may be considered as unstable in acidic environments as a dramatic increase in particle size to 760 nm was observed in HCl solution and a further increase in particle size upon storage was observed. The particles were characterised by a significantly broader size distribution, which was increased after 24 hours of storage at room temperature. However, the negative surface charge was retained in HCl solution.

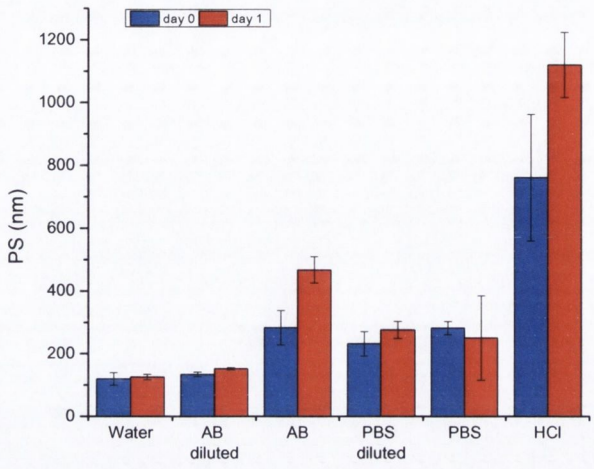

A)

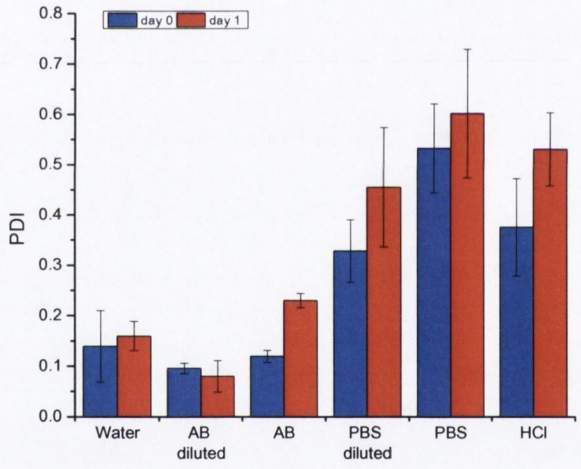

B)

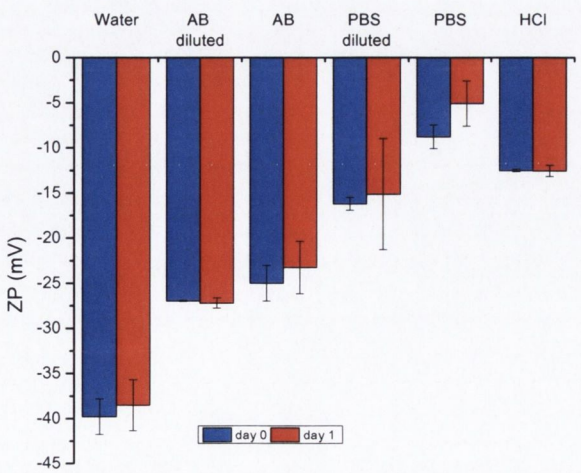

C)

Fig. 6.23. Characterisation, i.e. particle size (A), polydispersity index (B) and zeta potential (C) CHON/sCT NPs (CHON of 1.4 mg/ml, sCT of 2.0 mg/ml).

The particle size of sCT-loaded CHON/CL42 NPs did not change significantly in diluted PBS (compared to water), however when PBS with higher ionic strength was used the particle size was doubled to 350 nm and further increased by 100 nm after 24 hours of storage (Fig. 6.24). The particle size in both ABs was increased from 155±2 nm in water to 188 and 206 nm in diluted AB and AB, respectively. A further, statistically significant increase in particle size by 18 nm after 24 hours of storage was observed only in case of non-diluted AB. An increase in the particle size to 400 nm was observed in HCl solution. In all media tested the NPs remained homogenously dispersed with PDI values varying from 0.144 (HCl solution) to 0.265 (diluted AB). Only in PBS a significant increase in PDI was observed after 24 hours. The particles maintained highly negative surface charge of -26 - -32 mV in all buffers (diluted and non-diluted AB and PBS). Only in HCl solution the surface charge became markedly decreased (-2.5±2.1 mV).

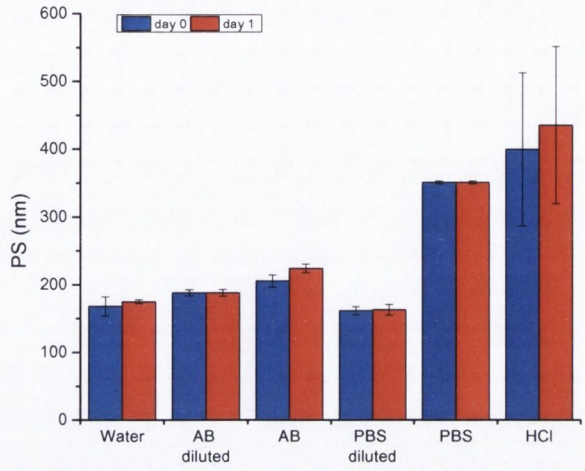

A)

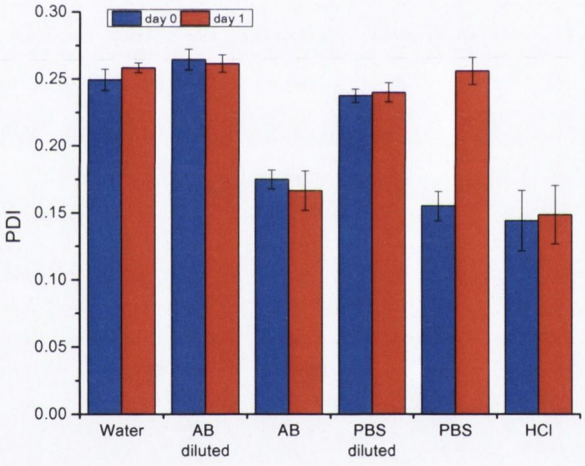

B)

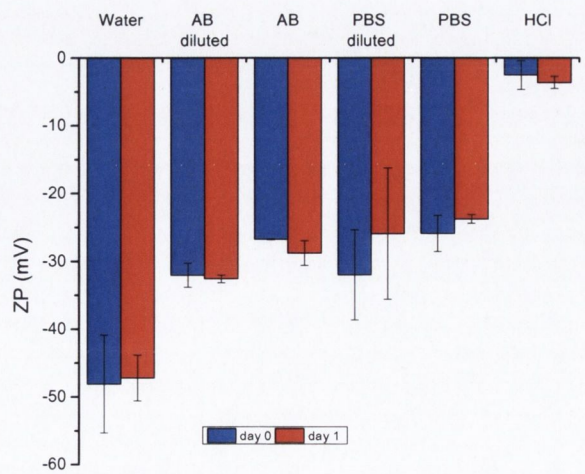

C)

Fig. 6.24 Characterisation, i.e. particle size (A), polydispersity index (B) and zeta potential (C) TPC of 2 mg/ml, CHON/CL42 MMR of 5, sCT of 1 mg/ml NPs.

Another CHON/CL42/sCT formulation with TPC of 3 mg/ml and CHON/CL42 MMR of 2.5 was tested for the stability in different environments (Fig. 6.25). Immediate aggregation was observed in PBS. However, the particle size in diluted PBS remained the same as in water, no statistically significant difference was observed. Similarly to the previous CHON/CL42/sCT formulation, the particle size in ABs remained close to 200 nm (190 and 228 nm in diluted AB and AB, respectively) and only in non-diluted AB a further, significant increase in particle size by 22 nm was observed. However, these NPs became markedly bigger (683 nm) in HCl solution. Apart from PBS, NPs with TPC of 3 mg/ml and CHON/CL42 MMR of 2.5, sCT of 1 mg/ml remained homogenously dispersed in all media tested with PDI values between 0.101 (AB) to 0.192 (HCl). In diluted PBS and both ABs highly negative surface charge -25 - -31.4 mV was maintained. Interestingly, in HCl solution an inversion of the surface charge from negative (-38.5 mV in water) to positive (+5 mV) was observed. This inversion of the surface charge at highly acidic pH was not observed in the previous formulation, which was characterised by a lower CL42 concentration and higher CHON/CL42 MMR.

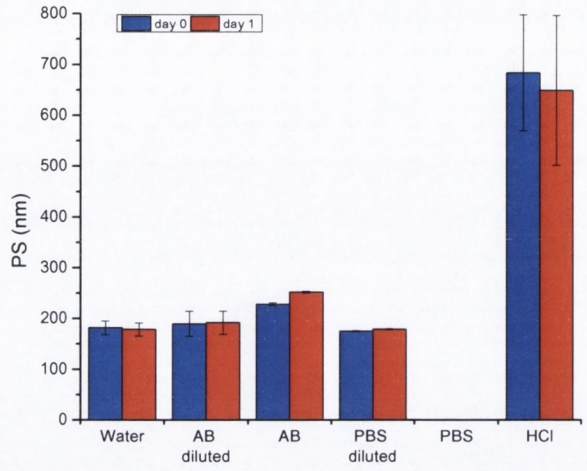

A)

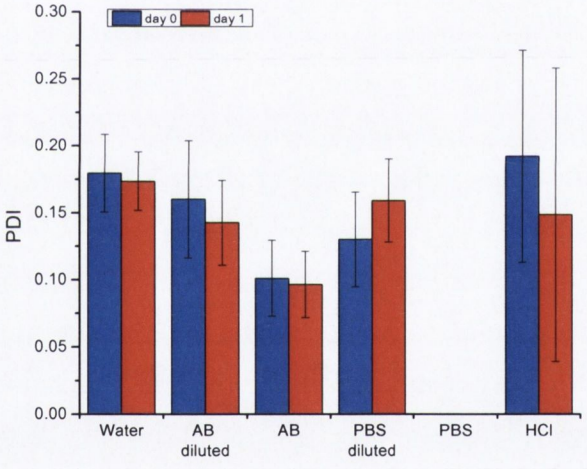

B)

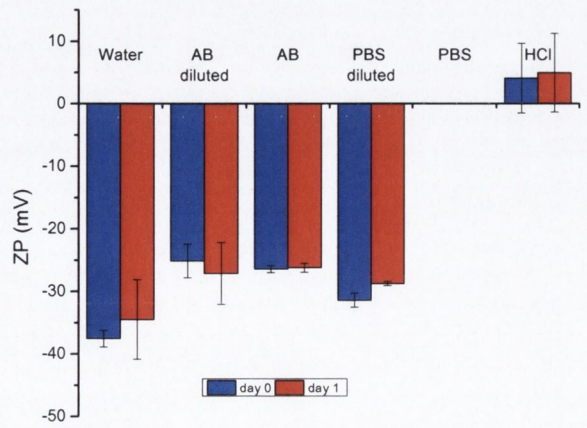

C)

Fig. 6.25 Characterisation, i.e. particle size (A), polydispersity index (B) and zeta potential (C) TPC of 3 mg/ml, CHON/CL42 MMR of 2.5, sCT of 1 mg/ml NPs.

In summary, the physical stability of CHON-based sCT-loaded NPs in most of the environments tested may be considered as acceptable. Apart from a few exceptions (e.g. CHON/CL42 MMR of 2.5 in PBS) extensive aggregation was not observed and the size remained in the submicron range. The properties of the NPs, although altered, remained satisfactory. The maintenance of the negative surface charge by CHON/sCT and CHON/CL42 MMR of 5 NPs is in agreement with titration studies (Section 6.6).

6.9 *In vitro* release of sCT

Fig. 6.26 shows the cumulative release of sCT from CHON/sCT and CHON/CL42/sCT nanocomplexes. It can be seen that almost no sCT was released either to water or to diluted acetate buffer from all the formulations tested. Apart from these two media, in other cases an initial relatively quick release phase was followed by a slow, prolonged release phase. A similar trend was observed for HA-based sCT-containing NPs, but the fraction of sCT initially released was markedly smaller in CHON-bases nano-formulations. Only 26±11, 17±1 and 8±3.6% of sCT was released into PBS from CHON/sCT, CHON/sCT MMRs of 5 and 2.5 formulations during the first hour, compared to ~50% in HA-based formulations.

The release of sCT from its nano-complex with CHON was influenced by the dispersant. The quickest release was observed for PBS solutions, regardless of their ionic strength. 45% was released within first two hours and after that the release rate was markedly decreased (~10% within the next 2 hours, and ~5% within last 2 hours). The % of sCT released into AB from CHON/sCT nanocomplexes was smaller as only 23±3% of sCT was released after 6 hours. The amount of sCT released into HCl solution was higher than the amount released into AB, but smaller than PBS. 23±5% of sCT was released into HCl solution within first two hours, and another 15% within next 4 hours.

This pH-dependent sCT release from sCT/CHON complexes may be an indication that at pH 5 the interactions between CHON and sCT are stronger that at 7.4 or 1.2. The negative charge of CHON increases, but the positive charge of sCT decreases correspondingly to increasing pH. In an acidic pH the opposite occurs: the positive charge of sCT increases, while CHON decreases its negative charge. It seems that at pH 5 the attractive Coulombic forces between these two oppositely charged molecules are maximal. Interestingly, pH of CHON/sCT nano-complex dispersion in water is very close to 5 (4.8±0.1). Apart from pH, the ionic strength of the dispersant also plays a very important role: dilution of AB 10 times prevented the release of sCT from its complex with CHON.

The differences in the sCT release profiles depending on the dispersant (HCl solution, AB, diluted PBS, PBS) used were less pronounced for sCT-loaded CHON/CL42 MMR of 5 NPs and in sCT-loaded CHON/CL42 MMR of 2.5 NPs these differences were not statistically significant (p=0.960) with 31±16, 31±15, 26±11 and 30±10% of sCT released after 6 hours from the latter formulation into PBS, diluted PBS, AB and HCl, respectively.

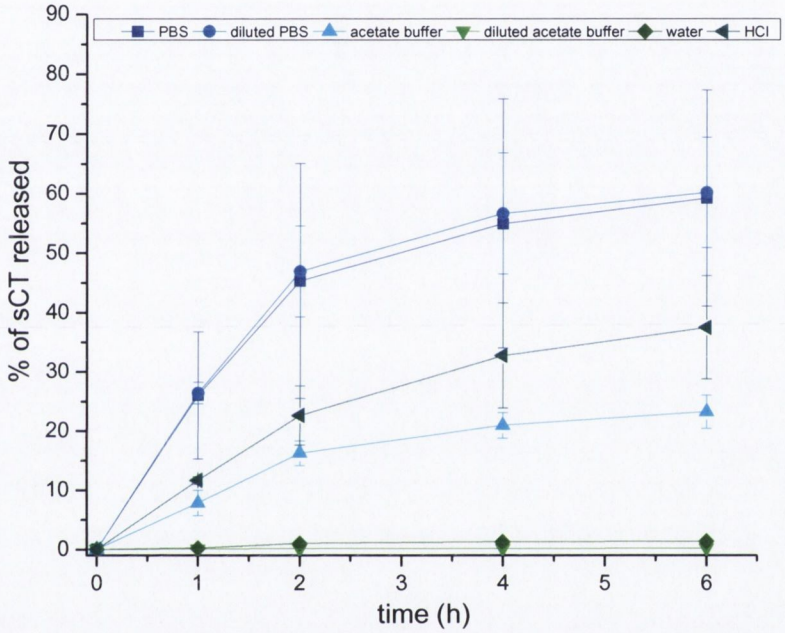

A)

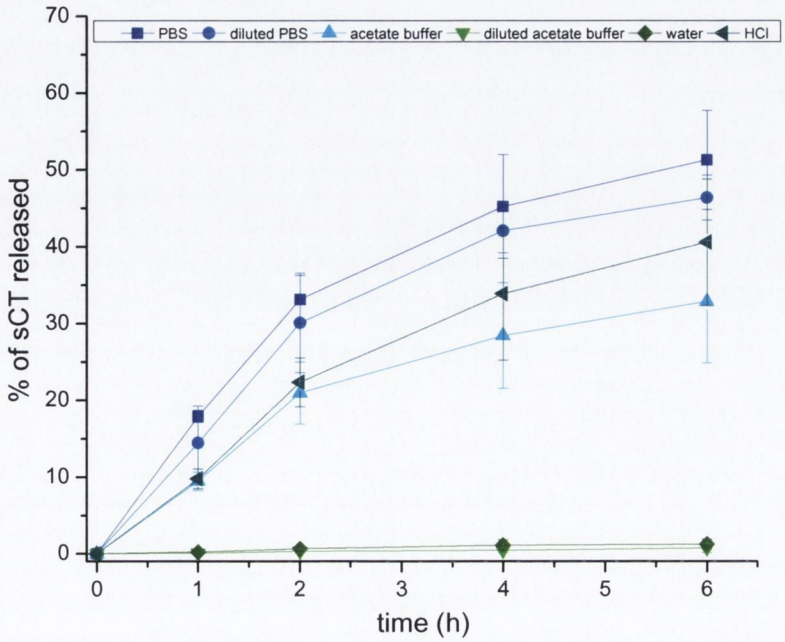

B)

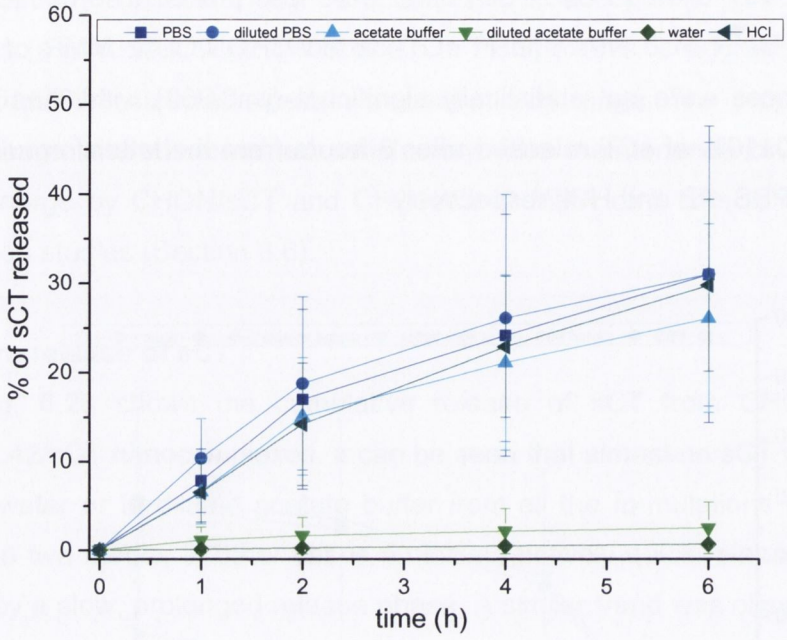

C)

Fig.6.26 Cumulative release of sCT from A) CHON/sCT NPs (CHON of 1.4 mg/ml, sCT of 2.0 mg/ml); B) TPC of 2 mg/ml, CHON/CL42 MMR of 5, sCT of 1 mg/ml NPs, C) TPC of 3 mg/ml, CHON/CL42 MMR of 2.5, sCT of 1 mg/ml NPs into different media.

The release data was fitted to the first order equation (see Chapter 2, Section 2.2.9, Equation 2.4) for AB, PBS, diluted PBS and HCl solutions. The parameter estimates obtained and related statistics are summarised in Tables 6.6-6.8. It can be observed, that the amount of sCT released from CHON/sCT NPs depended on the media. The lowest amount was released to acetate buffer (pH 5), while the amount of sCT released into PBS or HCl solution was markedly higher (Table 6.6).

Table 6.6 Model parameter estimates and related goodness of fit statistics for sCT release from CHON/sCT NPs (CHON of 1.4 mg/ml, sCT of 2.0 mg/ml) data fitted to the first order model.

Buffer/Solution	k [min^{-1}]	W_∞ [µg/mg of NPs]	Red. Chi-Sq.	R Sq.
Acetate buffer	0.4556±0.05040	147±12.5	26.02	0.99288
HCl	0.3637±0.04724	252±72.0	8.71	0.99837
PBS	0.5870±0.14554	360±108.0	41.87	0.99646
PBS diluted	0.6309±0.04352	365±64.0	60.9	0.99632

Similarly to CHON/sCT NPs, the amount of sCT released from CHON/CL42 MMR of 5 NPs into acetate buffer was smaller compared to PBS or HCl (Table 6.7).

Table 6.7 Model parameter estimates and related goodness of fit statistics for sCT release from TPC of 2 mg/ml, CHON/CL42 MMR of 5, sCT of 1 mg/ml NPs data fitted to the first order model.

Buffer/Solution	k [min^{-1}]	W_∞ [µg/mg of NPs]	Red. Chi-Sq.	R Sq.
Acetate buffer	0.3867±0.11489	125±42	4.35	0.99670
HCl	0.2721±0.0.0714	174±58	11.47	0.99454
PBS	0.4273±0.04263	186±29.7	13.1	0.99665
PBS diluted	0.3982±0.14381	177±8.5	39.18	0.99119

On the other hand, the quantity of sCT released into HCl from CHON/CL42 MMR of 2.5 NPs was higher compared to acetate buffer or PBS (Table 6.8). That may be the result of inversion of the surface charge to slightly positive in strongly acidic environments (see Section 6.9), and therefore weakening the electrostatic interactions between sCT and CHON compared to media with higher pH, where negative surface charge was maintained. Also, the amount of sCT released from CHON/CL42 MMR of 2.5 NPs was smaller compared to CHON/CL42 MMR of 5 NPs.

Table 6.8 Model parameter estimates and related goodness of fit statistics for sCT release from TPC of 3 mg/ml, CHON/CHIT MMR of 2.5, sCT of 1 mg/ml NPs data fitted to the first order model.

Buffer/Solution	k [min^{-1}]	W_∞ [µg/mg of NPs]	Red. Chi-Sq.	R Sq.
Acetate buffer	0.2725±0.05502	80±26.9	6.78	0.99275
HCl	0.2257±0.03588	127±7.1	6.38	0.99742
PBS	0.2489±0.02003	97±50.0	1.67	0.99529
PBS diluted	0.3697±0.01450	86±41	4.84	0.99246

Overall, CHON-based NPs were characterised by a markedly slower release rate of sCT than HA-based NPs.

6.10 Cytotoxicity of CHON/CS NPs

CHON did not decrease the viability of Caco-2 cells even after 72 hours of exposure (Tab. 6.9). The amount of viable cells determined by flow cytometry (88.5±1.74%) did not differ significantly from the control, i.e. serum-free medium (91.27±2.70%). The number of viable cells after 72 hours of exposure to CHON determined by MTS assay was significantly higher than control. Therefore it can be concluded that CHON does not have toxic effects on Caco-2 cells. This non-toxic character of CHON is comparable to that of another glycosaminoglycan, HA (Chapter 3). It is possible, that CHON also has a protective effect on Caco-2 cells (similar to HA) or increases their proliferation rate. The effect of chitosan on the viability of Caco-2 cells is described in chapter 3.

Table 6.8 The viability of Caco-2 cells after 72 hours of exposure to CHON in serum-free medium)

CHON [mg/ml]	% of viable cells by flow cytometry	% of viable cells by MTS assay
5	88.5±1.74	125.1±10.1

Similarly to HA/CL113 NPs, CHON/CL113 NPs dispersed in the serum-free medium (pH 7.4) did not decrease the viability of Caco-2 cells (Table 6.9). This observation is analogous to the behaviour of HA/CL113 NPs described in chapter 3. However, in contrast to HA/CL113 NPs, CHON/CL113 NPs did not affect the viability of Caco-2 cells even at pH 5 (Fig. 6.27). This implies that, in terms of cytotoxicity, CHON/CL113 NPs are superior to those composed of HA/CL113.

Table 6.9 The viability of Caco-2 cells by MTS assay after 72 hours of exposure to CHON/CL113 NPs in serum-free medium.

TPC [mg/ml]	% of viable cells CHON/CL113 MMR=5	% of viable cells CHON/CL113 MMR=1
2	108.14±11.11	110.11±13.7
1	115.40±9.10	108.83±9.53
0.5	108.64±8.95	114.37±9.32
0.25	110.61±9.93	114.95±6.87

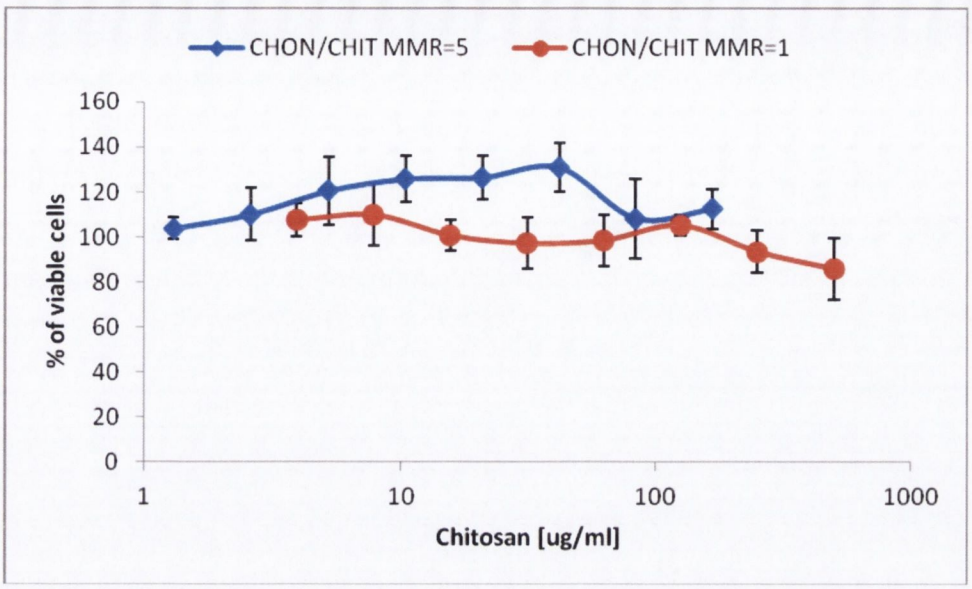

Fig.6.27 The viability of Caco-2 cells by MTS assay after 24-hours of exposure to CHON/CL113 NPs dispersed in serum-free medium pH5 (TPC of the most concentrated samples was of 1 mg/ml).

6.11 Summary and conclusions

An original CHON/sCT nanocomplex was successfully developed and characterised. As a result of the optimisation process, small (100-120 nm), homogenously dispersed CHON/sCT NPs with good colloidal stability were obtained. Moreover, the complexes were characterised by an excellent peptide association efficiency (close to 100%) and a very high sCT loading (~40-70%- the highest described so far).

CHON/CS combination nanocarriers were also prepared and a few important improvements compared to the previously published reports were made. The particle size of the CHON/CS systems was markedly reduced (with the possibility to obtain NPs as small as 77 nm), and new, negatively charged CHON/CS nanoparticles were obtained. Similarly to the previously described HA-based NPs, the manufacture process was very simple and involved mixing of aqueous solutions at room temperature.

CHON/CS NPs did not show any toxic effects in Caco-2 cells. Furthermore, complexation to CHON markedly reduced the toxicity of chitosan. No cytotoxic effects were observed even when pH of the formulation was 5, contrasting with the data presented in Chapter 3.

sCT was successfully loaded into CHON/CL42 NPs, with very high association efficiency (~100%), and a good drug loading (14-33%). CHON/CL24/sCT NPs were small (95-250 m) and had a negative surface charge.

Both, CHON/sCT and CHON/CL24/sCT NPs provided prolonged release of sCT, without premature discharge (less than 40% released within first hour). Incorporation of chitosan decreased slightly the rate of sCT release from NPs. Ionic strength and pH of the medium were found to have a considerable influence on the release of sCT.

In summary, sCT has been successfully combined in one delivery system with CHON. Similarly to HA, CHON NPs appear to be interesting carriers for the delivery and therapeutic applications of sCT.

7. Chondroitin-protamine nanoparticles

7.1 Introduction

In the previous chapters different types of polyelectrolyte complex NPs have been described (Chapters 3, 4, 5 and 6). CHON has been shown to form NPs with good characteristics (i.e. small NP with the size below 200 nm and homogenous size distribution with PDI below 0.25) when complexed to CS, sCT or both macromolecules together (Chapter 6). CHON has also been shown to form polyelectrolyte complexes with other polycations, e.g. lysozyme (Van Damme et al., 1994) and polyethylenimine (Pathak et al., 2009). CHON/CS NPs described in Chapter 6 showed better ability to associate sCT and provided a prolonged release of this peptide, better NP stability in acidic environments and lower toxicity to Caco-2 cells when compared to HA/CS NPs (Chapters 3, 4 and 5).

As stated in Introduction and Chapter 5, protamine is a good candidate to produce polyelectrolyte complex NPs as it is a naturally occurring, reasonably cheap protein already used in drug delivery (Hagedorn, 1937). Moreover, it has been shown to produce very small polyelectrolyte complex NPs (Chapter 5).

To the best of our knowledge, no delivery system comprising CHON and PROT has been developed so far. Due to the outlined earlier (Chapters 1, 5 and 6) interesting properties of CHON (anti-inflammatory and chondroprotective action) and PROT (membrane-translocating activity) such hybrid CHON/PROT NPs may have the potential to form carriers for the delivery of peptides, in particular sCT.

7.2 CHON/PROT NPs

In a first step, initial experiments were performed in order to determine the conditions at which CHON/PROT NPs were likely to be formed. The manufacturing process of CHON/PROT NPs was similar to that of HA/PROT NPs as described in Chapter 5. The concentration of CHON was kept constant and a defined volume of PROT solution with different concentrations varying from 0.4 to 12 mg/ml was used (corresponding to 0.11-3.43 mg/ml of PROT in the final dispersion). Apart from 0.4 and 1.4 mg/ml of CHON, higher concentrations (i.e. 2.1 and 3.6 mg/ml) were also tested due to the molecular weight of CHON being lower and lower viscosity of its solutions, compared to HA.

Different types of CHON/PROT dispersions (i.e. a solution, opalescent or turbid dispersion or phase separation) were observed, depending on the concentration of the protamine solution added. It was observed that for each

concentration of CHON tested systems containing more PROT were generally more turbid. The curves illustrating transmittance as a function of PROT concentration had a sigmoidal shape, being steeper for lower CHON concentrations (0.7 or 1.4 mg/ml) and more extended for higher CHON concentrations (3.6 mg/ml). All systems shown in Fig.7.1 were macroscopically homogenous (i.e. either had the appearance of a solution or were opalescent or turbid), and a further increase in PROT concentration led to a phase separation. The concentrations of PROT, which produced phase separation were higher for CHON/PROT systems, compared to HA/PROT. For the CHON/PROT system, the phase separation occurred at 0.69, 1.26, 1.71 and 3.43 mg/ml of PROT for CHON concentrations of 0.7, 1.4, 2.1 and 3.6 mg/ml, respectively. PROT concentrations of 0.57 and 1.14 mg/ml yielded stable NPs with the concentrations of CHON of 0.7 and 1.4 mg/ml, respectively. When HA was used at the same concentrations (0.7 and 1.4 mg/ml), even lower than the above mentioned concentrations of PROT (i.e. 0.46 and 0.91 mg/ml of PROT for 0.7 and 1.4 mg/ml of HA, respectively) caused phase separation.

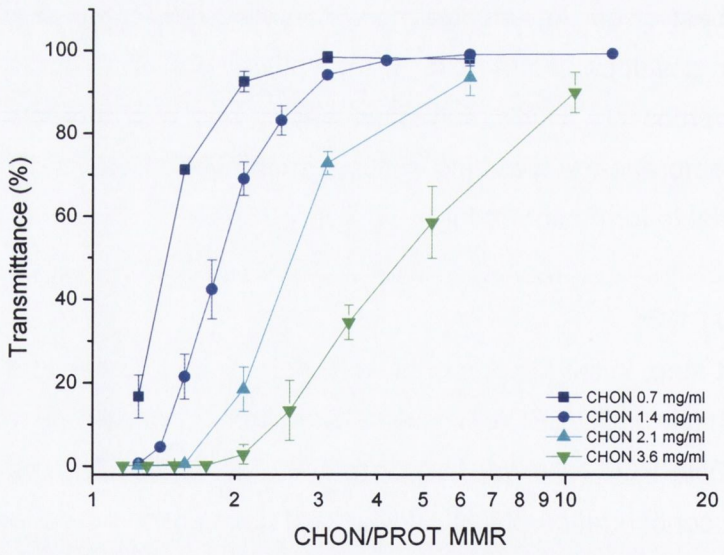

Fig. 7.1 Transmittance of CHON/PROT NPs dispersions.

Fig. 7.2 shows the dynamic viscosity of CHON/PROT systems. It can be observed, that the viscosity decreased correspondingly to an increasing amount of PROT in the formulation. The decrease was more pronounced in the range of lower concentrations of PROT. Also, dispersions with higher concentrations of CHON were more viscous than dispersions with the same concentration of PROT,

but lower CHON concentration, and the difference was statistically significant. However, CHON/PROT dispersions were characterised by a markedly lower viscosity than similar HA/PROT dispersions (Chapter 5).

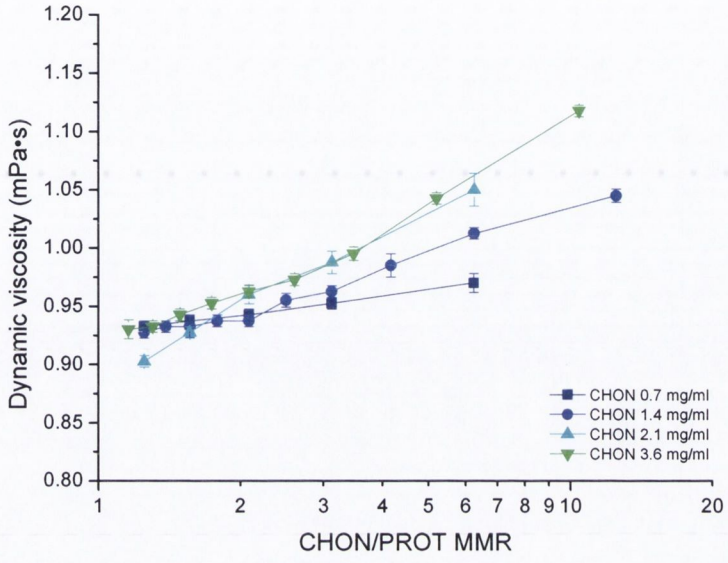

Fig.7.2 Dynamic viscosity of CHON/PROT NPs dispersions.

Fig.7.3 shows the hydrodynamic diameter of CHON/PROT NPs. It can be observed that CHON/PROT NPs were generally small, with the size ranging from 78±3 or 78±12 nm (CHON of 1.4 mg/ml, PROT of 0.46 mg/ml and CHON of 0.7 mg/ml, PROT of 0.22 mg/ml, respectively) to 296±16 nm (CHON of 3.6 mg/ml, PROT of 3.09 mg/ml). The particle size increased with an increasing amount of PROT in the formulation. Similar tendency was observed for HA/PROT NPs. In contrast to HA, the concentration of CHON was found to affect the particle size of CHON/PROT NPs, e.g. CHON of 1.4 mg/ml-based NPs were significantly smaller than CHON of 0.7 mg/ml-based NPs when the concentration of PROT was of 0.34 or 0.45 mg/ml. The size range of CHON/PROT NPs was similar to the previously described (Chapter 6) CHON/CS NPs and both macromolecule combinations yielded the smallest CHON-based NPs described so far.

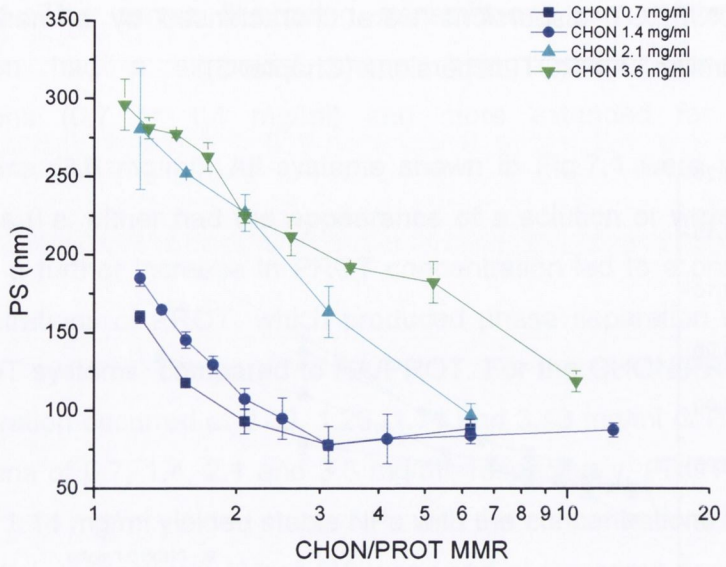

Fig. 7.3 Particle size of CHON/PROT NPs.

Fig. 7.4 presents PDI of CHON/PROT NPs. The PDI values of CHON/PROT NPs varied from 0.105±0.004 (CHON of 1.4 mg/ml and PROT of 1.03 mg/ml) to 0.427±0.019 (CHON of 3.6 mg/ml and PROT of 0.34 mg/ml). It can be seen that the concentration of PROT had a considerable influence on the size distribution of CHON/PROT NPs. The higher the amount of PROT in the dispersion, the more homogenous the size distribution of the particles was. Also, the concentration of CHON was found to affect the PDI values, which were generally increasing accordingly to the increasing concentration of CHON. Most of CHON 0.7 and 1.4 mg/ml-based dispersions were characterised by a homogenous size distribution with PDI values below 0.20 (with the exception of CHON of 0.7 mg/ml, PROT 0.11 mg/ml and CHON of 1.4 and PROT of 0.11 and 0.22 mg/ml).
For 2.1 mg/ml CHON-based NPs, only two dispersions (with PROT of 1.37 and 1.71 mg/ml) were homogenously dispersed with PDI below 0.25, and only the latter had PDI below 0.20. 3.6 mg/ml CHON-based NPs were more heterogeneous with four dispersions with PDI below 0.25 (PROT between 2.06 and 3.09 mg/ml), but none of the PDI values was below 0.2.

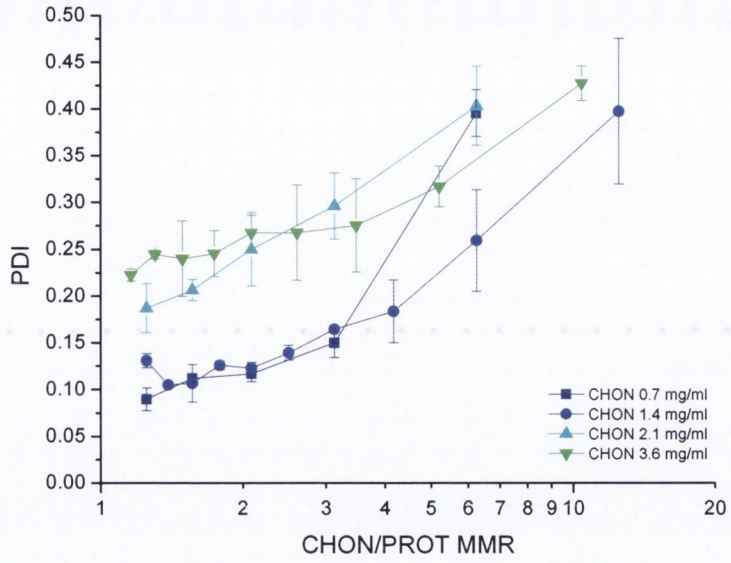

Fig.7.4 Polydispersity index of CHON/PROT NPs.

It can be measured that all stable (i.e. non-sedimenting and non-aggregating) NPs were characterised by a negative surface charge between -27.6±5.99 mV (CHON of 2.1 mg/ml, PROT of 1.71 mg/ml) and -63.1±8.59 mV (CHON of 3.6 mg/ml, PROT of 0.34 mg/ml) (Fig.7.5). The negative zeta potential of these NPs is in agreement with data obtained for HA/PROT NPs. Similarly to HA/PROT NPs, the surface charge of CHON/PROT NPs decreased correspondingly to an increasing quantity of PROT in the dispersions. Also, the concentration of CHON had a considerable impact on zeta potential values-generally the higher amount of CHON in the dispersion, the more negative the surface charge was.

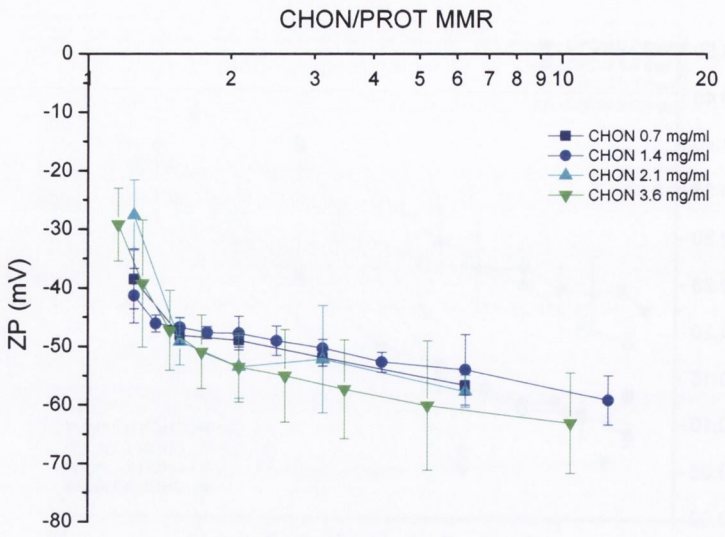

Fig.7.5 Zeta potential of CHON/PROT NPs.

Generally, pH of all CHON/PROT NPs may be considered as similar, as it varied between 6 and 6.5 (Fig.7.6). The pH decreased slightly with the increasing PROT concentration and decreasing CHON concentration.

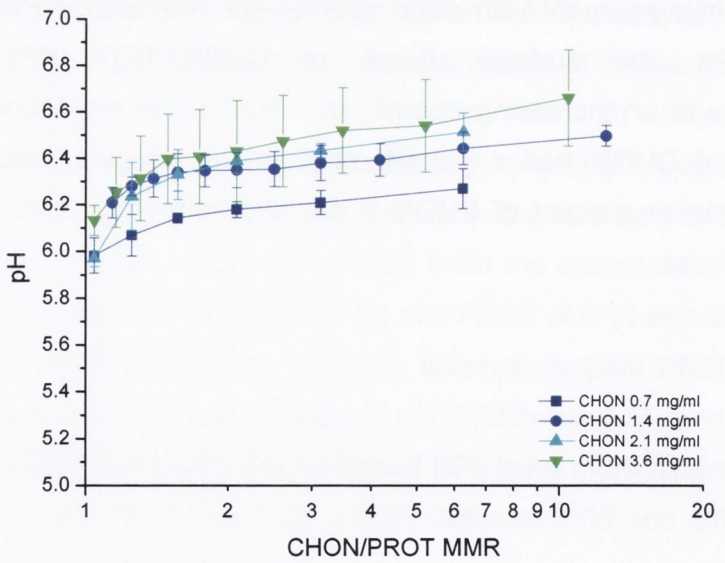

Fig.7.6 pH of CHON/PROT NPs.

CHON/PROT NPs are formed by electrostatic interactions between negatively charge sulphate and carboxylate groups of CHON and positively charged amino acid residues in arginine-rich PROT molecules. Similar mechanism

(i.e. Coulombic interactions) has already been confirmed for other previously described polyelectrolyte complex NPs (previous chapters).

The efforts to obtain stable positively charged HA/PROT NPs were unsuccessful. CHON has a considerably lower molecular weight than HA (chapter 6), and a higher charge density, therefore attempts were made to obtain positively charged CHON/PROT NPs. When CHON solution (0.16 mg/ml) was mixed with PROT solution (0.7 mg/ml) at PROT/CHON MMR of 5, a very homogenously dispersed (PDI of 0.014± 0.01) small (211±6 nm) NPs bearing positive surface charge of 11.6±0.78 mV were obtained. Similarly to HA/PROT NPs, aggregation of the positively charged CHON/PROT NPs was observed after a few hours. This is in agreement with the results shown in Fig.7.7, where the changes in the particle size during storage at room temperature are shown. The size slowly increased within first hours of storage, doubling after 6 hours 45 minutes. Then the particle size increased more and more rapidly, leading to the formation of microparticles and a significant aggregation and sedimentation was observed after 10-12 hours.

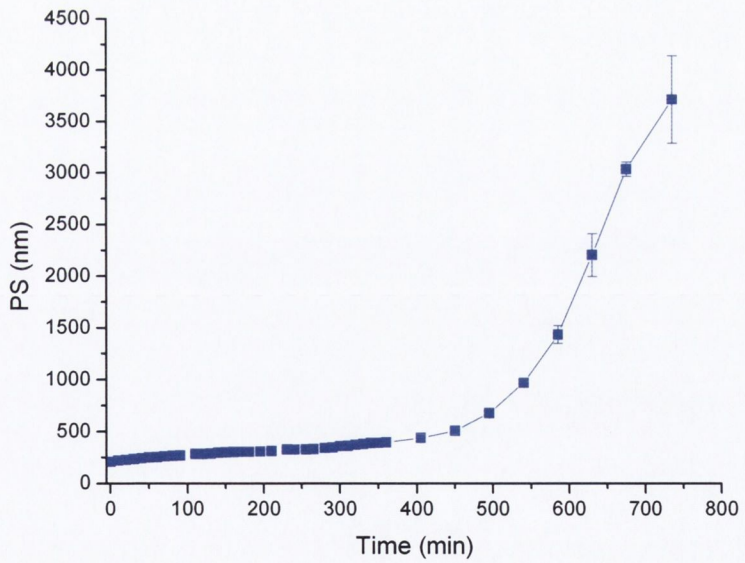

Fig.7.7 Kinetics of change in the particle size of positively charged CHON/PROT NPs (PROT of 0.7 mg/ml, CHON of 0.16 mg/ml).

The increase in PDI values of positively charged CHON/PROT NPs, shown in Fig.7.8, was concurrent to the changes in particle size. PDI increased slowly within first 6 hours to a value of 0.17, and after that a rapid increase was observed; the maximal possible value of 1 was observed after 10.5 hours.

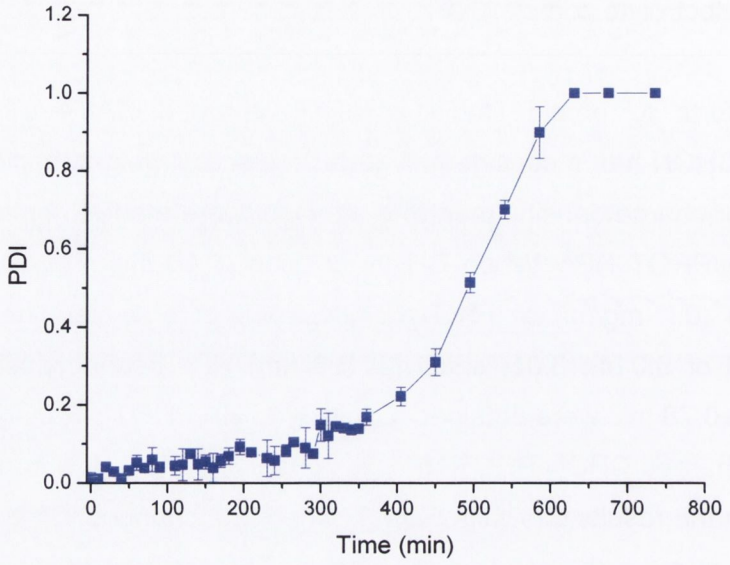

Fig.7.8 Kinetics of change in polydispersity index of positively charged CHON/PROT NPs (PROT of 0.7 mg/ml, CHON of 0.16 mg/ml).

As shown in Fig. 7.9, the zeta potential remained positive and did not change markedly as the final value of 10.1±0.57 mV did not differ significantly (p=0.060) from the initial value.

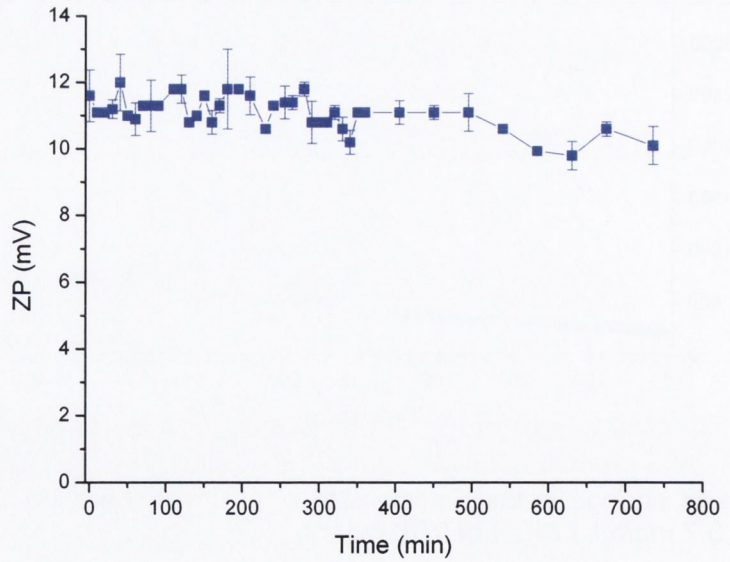

Fig.7.9 Kinetics of change in zeta potential of positively charged CHON/PROT NPs (PROT of 0.7 mg/ml, CHON of 0.16 mg/ml).

Similar results were obtained for positively charged HA/PROT NPs (Chapter 5). The difference between the molecular weight of CHON and PROT is

smaller than for the HA/PROT system, however, the molecular weight of CHON is still approximately 10 times higher than that of PROT.

Table 7.1 illustrates that none of the CHON/PROT or CHON/PROT/sCT NPs tested showed a sign of the isolelectric point after titration with 0.25 M HCl down to pH 1.6-1.7. The only exception was the dispersion containing 0.71 mg/ml of CHON, 0.34 mg/ml of PROT, where the isoelectric point was observed at 1.85±0.08. As CHON/PROT NPs maintained negative surface charge even at acidic pH values, it is likely that the electrostatic interactions between negatively charged CHON in the particles and positively charged associated molecule (sCT) will still be present. Similar results (i.e. no isoelectric point down to 1.6-1.7) were also observed for negatively charged CHON/CS NPs (Chapter 6). However, the surface charge of HA/PROT NPs with similar composition, in contrast to CHON/CS and CHON/PROT NPs, was neutralised at low acidic pH (1.6-2.9; Chapter 5). Therefore CHON-based NPs may be considered as potentially better candidates for oral delivery of sCT and similar macromolecules than HA-based NPs.

Table 7.1. Isoelectric points of CHON/PROT NPs. N/D – not detectable

CHON [mg/ml]	PROT [mg/ml]	sCT [mg/ml]	Isoelectric point
0.714	0.114	-	N/D
0.714	0.114	0.5	N/D
0.714	0.229	-	N/D
1.429	0.229	-	N/D
0.714	0.343	-	1.85±0.08
1.429	0.457	-	N/D

7.3 sCT-loaded CHON/PROT NPs

Three different types of NPs containing the lowest concentrations of CHON (i.e. 0.7, 1.4 and 2.1 mg/ml) were selected to be formulated with sCT. The concentrations of PROT tested were of 0.3, 0.7 and 1.0 mg/ml, however for two of the lowest concentrations of CHON (i.e. 0.7 and 1.4 mg/ml) and sCT of 0.5 mg/ml formulations containing 0.1 mg/ml of PROT were also examined. For 0.7 mg/ml CHON-based samples only 0.5 mg/ml of sCT were tested, as at higher sCT concentrations (i.e. 1 mg/ml) opalescent suspensions were formed even before the addition of PROT solution (Chapter 6).

The success of loading of sCT into CHON/PROT NPs depended on CHON and PROT concentrations and their MMRs. Opalescent or turbid suspension, which can potentially contain NPs with good characteristics (i.e. small and homogenously dispersed), were obtained when the concentration of PROT was up to 0.3, 0.7 and 1.0 mg/ml, for CHON concentrations of 0.7, 1.4 and 2.1, respectively (CHON/PROT MMRs of 2.3, 2 and 2.1). A further increase in PROT concentration and thus a decrease in CHON/PROT MMR values yielded unstable systems, where phase separation and aggregation were observed. The successful loading of sCT into systems with the lowest CHON/PROT MMRs and lowest PROT concentrations may be an evidence that both polycations (sCT and PROT) interact electrostatically with the negatively charged groups of CHON molecules and a competition between sCT and PROT for these binding places occurs. As the negative charge of CHON is neutralised, the nanosuspension becomes unstable and aggregations occurs. Therefore formulations with a low CHON/PROT MMR and a high amount of PROT should be avoided as they are not physically stable.

Fig. 7.10 shows transmittance of sCT-loaded CHON/PROT dispersions. Generally, the incorporation of sCT into the systems resulted in an increased turbidity of the dispersions. However, the decrease in transmittance values was not always statistically significant. For instance, transmittance of CHON of 0.7 mg/ml and PROT of 0.1 mg/ml (MMR=6.2) NPs remained practically the same when 0.5 mg/ml of sCT was incorporated, however incorporation of the same amount of sCT into CHON of 0.7 mg/ml, PROT of 0.3 mg/ml (MMR=2.1) NPs decreased transmittance significantly from 92.5±2.5 to 70.8±5.3% ($p=0.003$). For 1.4 mg/ml CHON-based NPs, the decrease in transmittance after incorporation of 0.5 mg/ml of sCT into the formulation with the lowest concentration of PROT (0.1 mg/ml, MMR=12.5) caused a very small, but statistically significant ($p=0.036$) decrease in transmittance by 1.2%. Nevertheless, when the amount of PROT was increased to 0.3 or 0.7 mg/ml (MMR=4.2 and 2.1), a marked decrease in transmittance values was observed either after incorporation of 0.5 mg/ml of sCT or after a further increase in sCT concentration to 1.0 mg/ml. For 2.1 mg/ml CHON-based formulations, loading of 0.5 mg/ml of sCT did not decrease transmittance significantly, but loading of 1 mg/ml of sCT resulted in significantly more turbid nanosuspensions. With exception of sCT concentration, the turbidity of CHON/PROT/sCT nanosuspensions was also affected by CHON and PROT concentrations and CHON/PROT MMR. The turbidity increased corresponding to a decrease in CHON/PROT MMR. Interestingly, in some formulations where the same concentrations of sCT and PROT were used, formulations based on lower

concentrations of CHON were more turbid than formulations containing higher amounts of CHON. For instance, the formulation containing 0.7 mg/ml of CHON, 0.3 mg/ml of PROT (MMR=2.1) and 0.5 mg/ml of sCT had transmittance of 70.8±5.3%, which was significantly (p=0.002) smaller than 92.4±1.33% for the formulation containing 1.4 mg/ml CHON and 0.3 mg/ml of PROT (MMR=4.2) and 0.5 mg/ml of sCT. In contrast, samples with PROT of 0.3 mg/ml and CHON of 1.4 or 2.1 mg/ml were characterised by similar turbidity.

A decrease in turbidity due to the higher CHON concentration was also observed for CHON/sCT and CHON/PROT NPs and it may be due to the higher solubility of complexes when larger amounts of CHON were used.

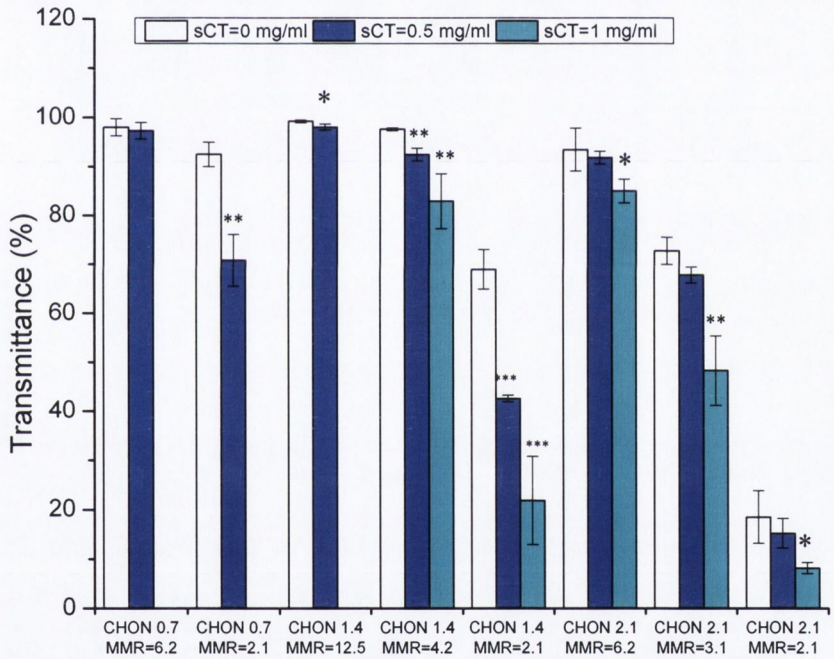

Fig.7.10 Transmittance of sCT-loaded CHON/PROT NPs dispersions. *p<0.05, **p<0.01 and ***p<0.001 versus sCT=0 mg/ml (empty bars)

As shown in Fig.7.11, the dynamic viscosity of CHON/PROT suspensions decreased slightly after loading 0.5 mg/ml sCT. A further increase in sCT concentration to 1.0 mg/ml did not change the viscosity significantly. The viscosity was also observed to increase with the increasing content of CHON in the formulation and CHON/PROT MMR, similarly to CHON/PROT NPs without sCT. Generally, the impact of sCT or PROT content on the dynamic viscosity of CHON/PROT systems was lesser than that observed for HA/PROT systems, probably due to a markedly lower viscosity of CHON when compared to HA.

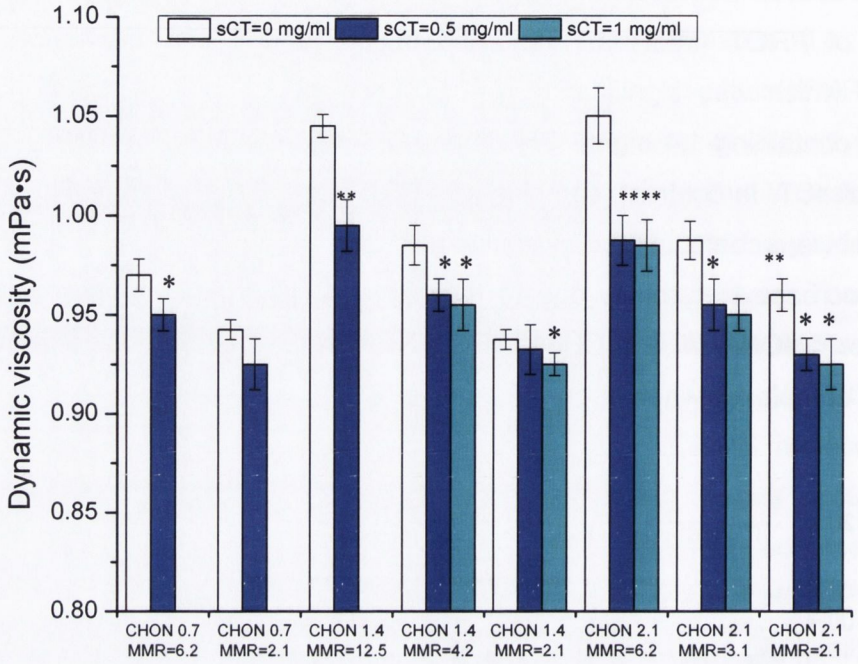

Fig.7.11 Dynamic viscosity of sCT-loaded CHON/PROT NPs suspensions. *p<0.05 and **p<0.01 versus sCT=0 mg/ml (empty bars)

Fig.7.12 shows the particle size of sCT-loaded CHON/PROT NPs. The hydrodynamic diameter of the particles varied between 59.5±6 nm (CHON of 1.4 mg/ml, PROT of 0.3 mg/ml (MMR=4.2) and sCT of 0.5 mg/ml) and 245±33nm (CHON of 2.1 mg/ml, PROT of 1.0 mg/ml (MMR=2.1) and sCT of 1.0 mg/ml). Generally, the incorporation of 0.5 or 1.0 mg/ml of sCT did not change the particle size, but in some cases (i.e. when CHON/PROT MMR was 2.1 and CHON concentration was 0.7 or 1.4 mg/ml) loading of sCT increased the particle size compared to CHON/PROT NPs without sCT (by 50 or 90 nm, respectively). Also, incorporation of 0.5 mg/ml sCT resulted in a decrease in particle size of NPs made of CHON of 0.7 mg/ml and PROT 0.1 mg/ml by 30 nm. Furthermore, formulations with lower concentrations of PROT (0.1 or 0.3 mg/ml) or higher CHON/PROT MMRs (4.2-6.2) were generally characterised by a very small particle size below or close to 100 nm, while NPs with the highest concentration of PROT (1 mg/ml) and CHON/PROT MMR of 2.1 were markedly larger with sizes greater than 200 nm. Therefore using high concentrations of PROT is not advised if very small NPs below 100 nm are to be obtained.

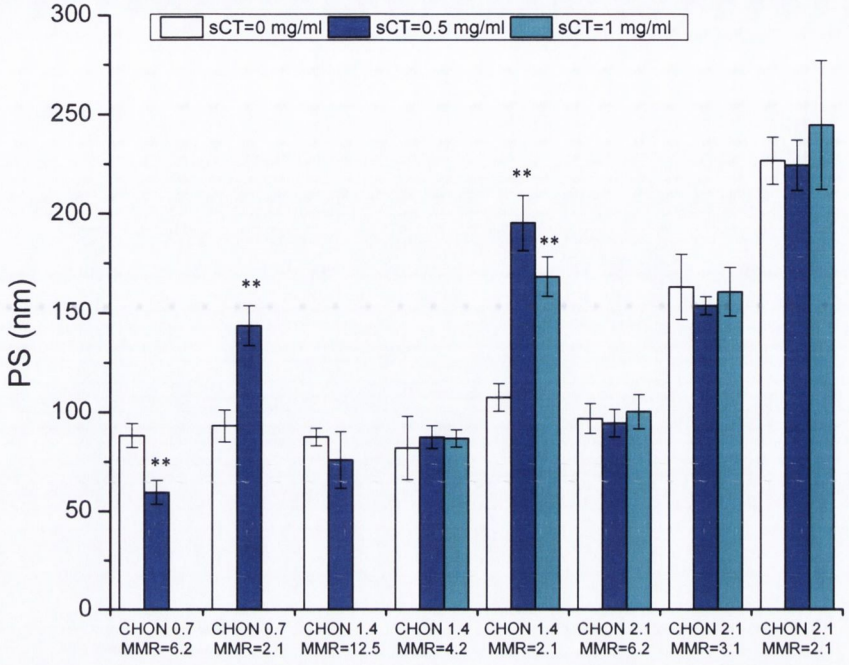

Fig.7.12 Particle size of sCT-loaded CHON/PROT NPs. **p<0.01 versus sCT=0.0 mg/ml (empty bars)

As shown in Fig 7.13, most of sCT-loaded CHON/PROT NPs were characterised by moderate values of PDI (0.25-0.50), and only two formulations were homogenously dispersed (PDI values of 0.234±0.013 and 0.242±0.014 for CHON of 1.4 mg/ml, PROT of 0.3 mg/ml (MMR=4.2), sCT of 1 mg/ml and CHON of 2.1 mg/ml, PROT of 0.3 mg/ml (MMR=6.2), sCT of 1.0 mg/ml, respectively).

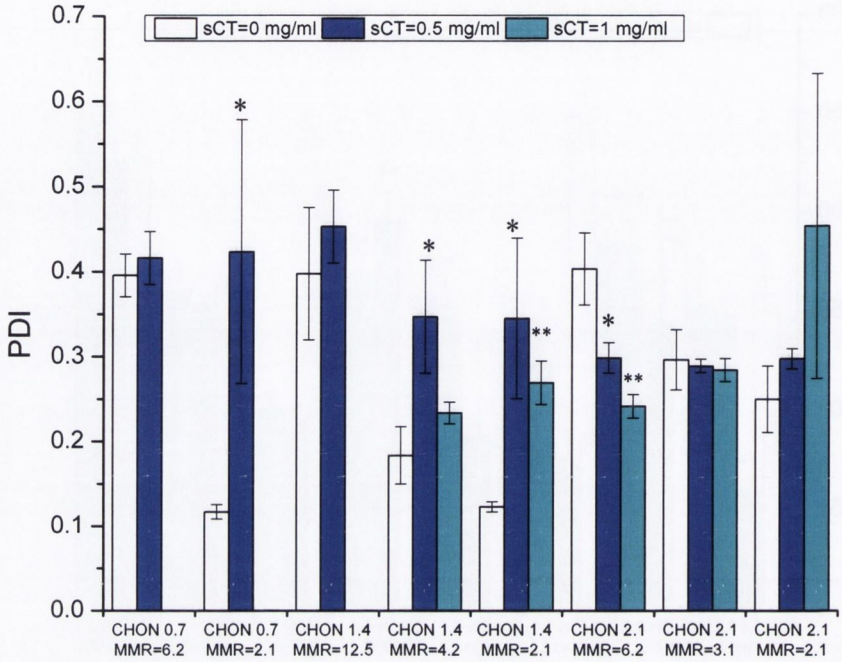

Fig.7.13 Polydispersity index of sCT-loaded CHON/PROT NPs.*$p<0.05$ and **$p<0.01$ versus sCT=0 mg/ml (empty bars).

As illustrated in Fig.7.14, all sCT-loaded CHON/PROT NPs were characterised by a strongly negative surface charge with zeta potential values between -31.3±1.78 mV (CHON of 1.4 mg/ml, PROT of 0.7 mg/ml (MMR=2.1), sCT of 1.0 mg/ml) and -48.2±7.16 mV (CHON of 2.1 mg/ml, PROT of 0.7 mg/ml (MMR=3.1), sCT of 0.5 mg/ml), which indicated their good colloidal stability. Loading of sCT either did not change or significantly decreased (e.g. in case of CHON of 0.7 mg/ml-based formulations) the surface charge of the NPs when compared to CHON/PROT NPs without sCT.

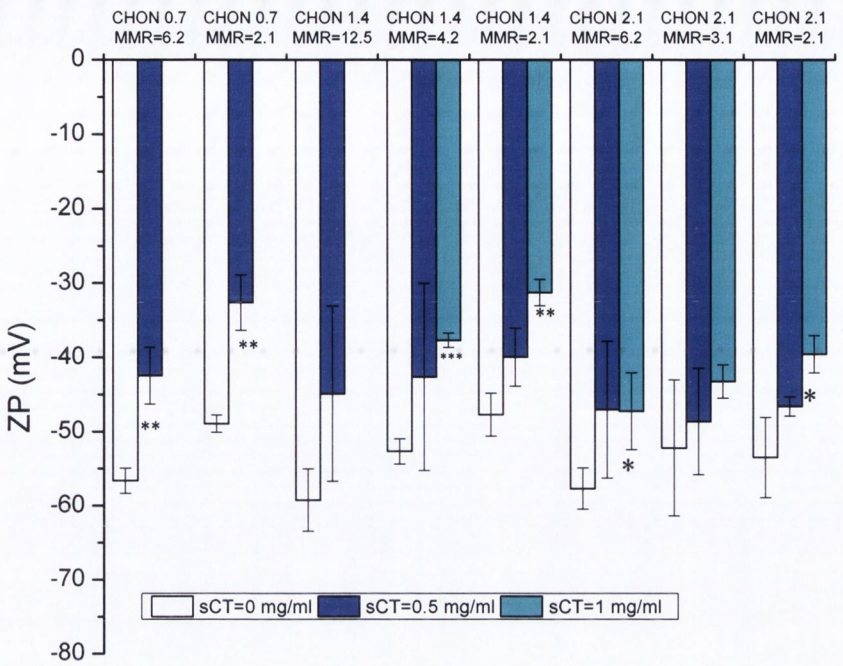

Fig.7.14 Zeta potential of sCT-loaded CHON/PROT NPs. *p<0.05, **p<0.01 and ***p<0.001 versus sCT=0 mg/ml (empty bars)

Loading of 0.5 mg/ml of sCT decreased pH of CHON/PROT nanosuspensions by approximately 1 unit when compared to suspensions without sCT. A further increase in sCT concentration to 1.0 mg/ml decreased the pH by approximately 0.3-0.4 units. This observation is in agreement with the previously described HA or CHON-based NPs containing sCT (Chapters 4, 5 and 6).

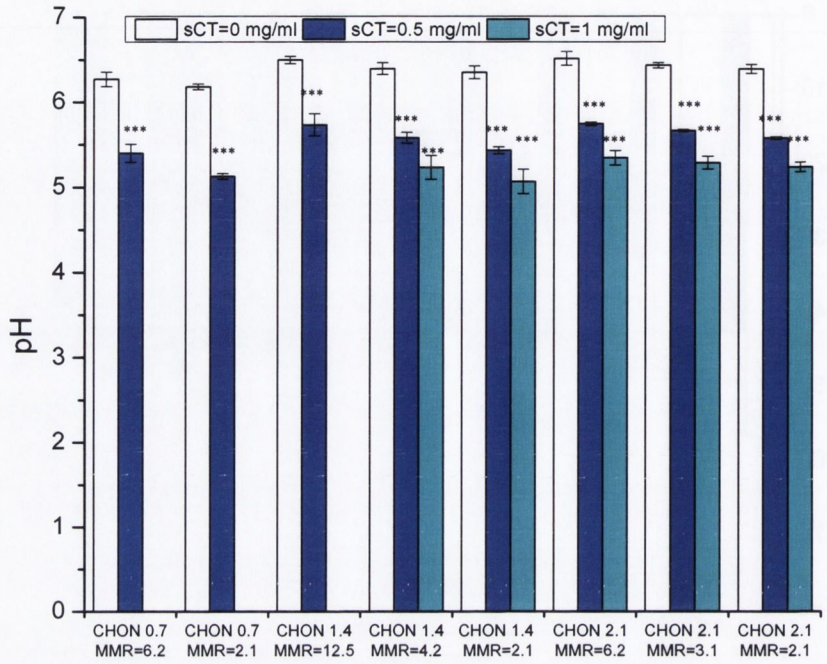

Fig.7.15 pH of CHON/PROT/sCT nano-suspensions. ***p<0.001 versus sCT=0 mg/ml (empty bars).

Table 7.2 shows that CHON/PROT NPs had an excellent ability to associate sCT as the AE values were very high (98.4-99.8%). AEs were slightly higher for formulations containing lower amount of PROT and higher CHON/PROT MMRs, however the differences, although statistically significant, were very small (less than 1.5%). Mass balance was not obtained, as it was impossible to extract all sCT by dilution with 0.0001 M NaOH solution. Similar problems were encountered for other CHON-based NPs described in Chapter 6.

Furthermore, it was possible to obtain very good drug loading between 13.5 and 37.8%. High AE and drug loading are in agreement with the results of other sCT-loaded polyelectrolyte complex NPs described in previous chapters (Chapters 3, 4 and 5).

Table 7.2 Association efficiency and drug loading of CHON/PROT/sCT NPs.

CHON [mg/ml]	PROT [mg/ml]	Initial sCT [mg/ml]	Extracted sCT [%]	AE [%]	Drug loading [%]
2.14	1.03	0.5	54.4±13	98.7±0.25	13.47±0.034
2.14	0.69	0.5	57.0±8.3	99.6±0.11	14.96±0.017
2.14	0.34	0.5	61.9±1.7	99.8±0.11	16.75±0.018
2.14	1.03	1.0	55.0±17.0	98.4±0.10	23.69±0.024
2.14	0.69	1.0	71.3±3.6	99.5±0.07	26.01±0.018
2.14	0.34	1.0	71.4±1.3	99.7±0.06	28.67±0.017
1.43	0.69	0.5	55.2±2.7	98.8±0.33	18.90±0.063
1.43	0.34	0.5	70.5±3.2	99.6±0.09	21.96±0.020
1.43	0.11	0.5	80.7±13.9	99.8±0.08	24.47±0.020
1.43	0.69	1.0	64.0±6.1	98.4±0.26	31.70±0.084
1.43	0.34	1.0	84.5±9.1	99.5±0.08	35.99±0.029
0.71	0.34	0.5	49.3±6.8	98.7±0.46	31.97±0.149
0.71	0.11	0.5	78.7±5.6	99.7±0.10	37.81±0.038

7.4 Stability of CHON/PROT NPs after storage at room temperature.

Three formulations with different concentrations of PROT (0.11, 0.22 and 0.45 mg/ml) and different CHON/PROT MMRs were selected for stability studies. No visual changes or sedimentation were observed even after 4 weeks of storage.

Fig. 7.16 shows changes in transmittance values for CHON/PROT NPs during storage at room temperature. It can be observed that the transmittance of 0.11 mg/ml PROT-based NPs remained unchanged during 28 days. Transmittance of 0.22 mg/ml PROT-based NPs decreased significantly, but the change was small as transmittance after 28 days was only 1.6% smaller than the initial value. A decrease in transmittance observed for 0.45 mg/ml PROT-based NPs was more pronounced, but the change may again be considered as small, as the transmittance after 28 days was only 9% smaller compared with the initial value.

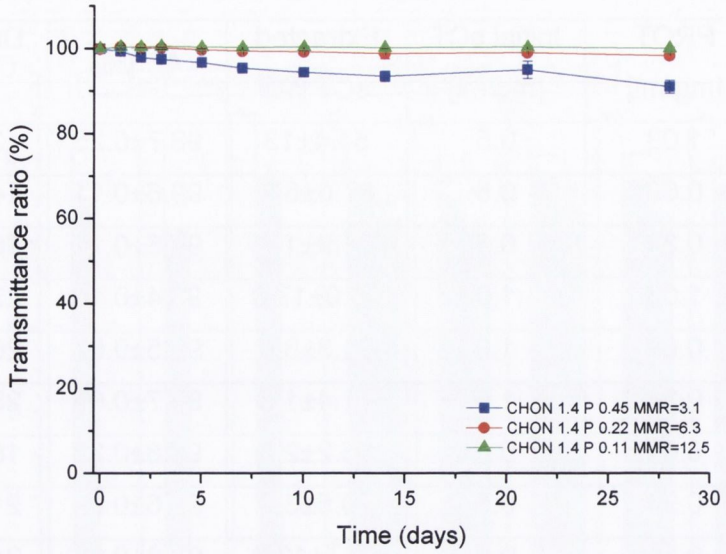

Fig. 7.16 Transmittance ratio of CHON/PROT NPs during storage at RT. P=PROT.

Fig.7.17 illustrates changes in the particle size of CHON/PROT NPs after storage. After first day of storage the particle size of all NPs tested decreased significantly by 28, 27 and 13% for the 0.11, 0.22 and 0.45 mg/ml PROT-based NPs, respectively. This initial decrease in the particle size was followed by a gradual increase during following days of storage. After 4 weeks of storage the particle size of 0.22 and 0.45 mg/ml PROT-based NPs did not differ significantly ($p=0.539$ and 0.054, respectively) from the initial size, however for the formulation with the smallest concentration of PROT (0.11 mg/ml), a pronounced, significant ($p=0.002$) increase in the particle size was observed.

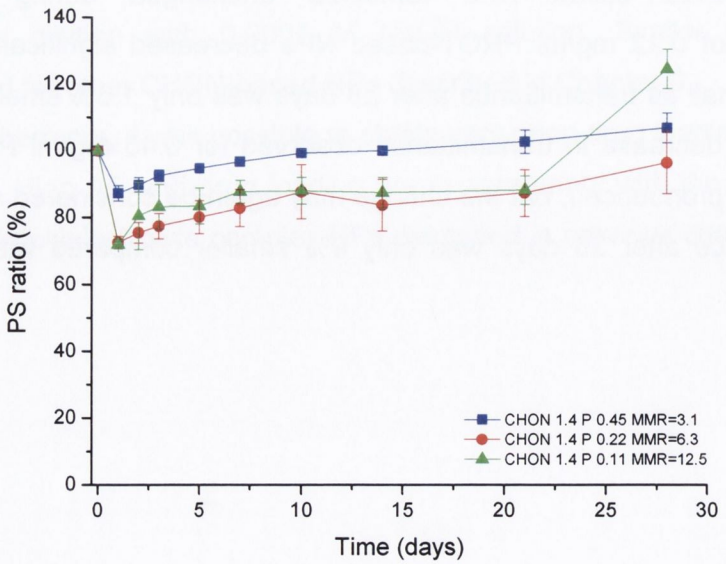

Fig.7.17 Particle size ratio of CHON/PROT NPs during storage at RT. P=PROT.

As shown in Fig.7.18, CHON/PROT NPs became more homogenously dispersed within first two days of storage. Further storage at room temperature did not change the size distribution markedly. Both, PS and PDI results confirm that a reorganisation of the NP structure within the first days after preparation of nanosuspensions occurs.

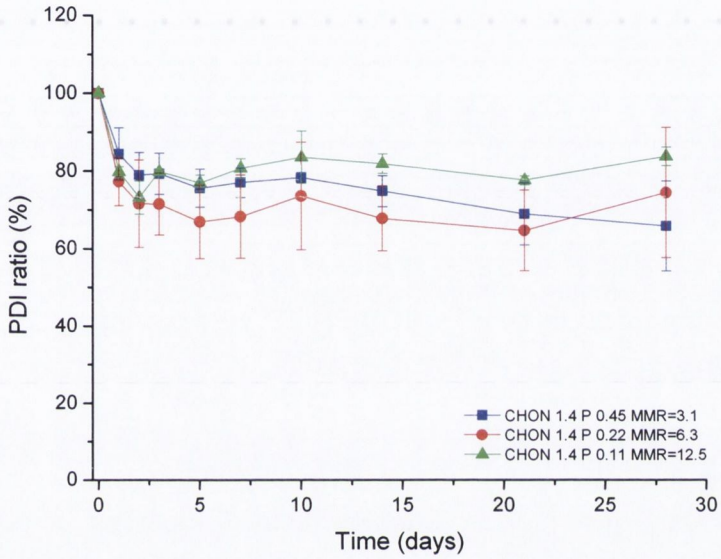

Fig.7.18 Polydispersity ratio of CHON/PROT NPs during storage at room temperature. P=PROT.

As shown in Fig. 7.19, no dramatic changes in zeta potential of CHON/PROT NPs occurred during 4 weeks of storage at room temperature. For the nanosuspension with the highest concentration of protamine (0.45 mg/ml) the surface charge after 4 weeks of storage was significantly ($p=0.001$) higher than the initial value.

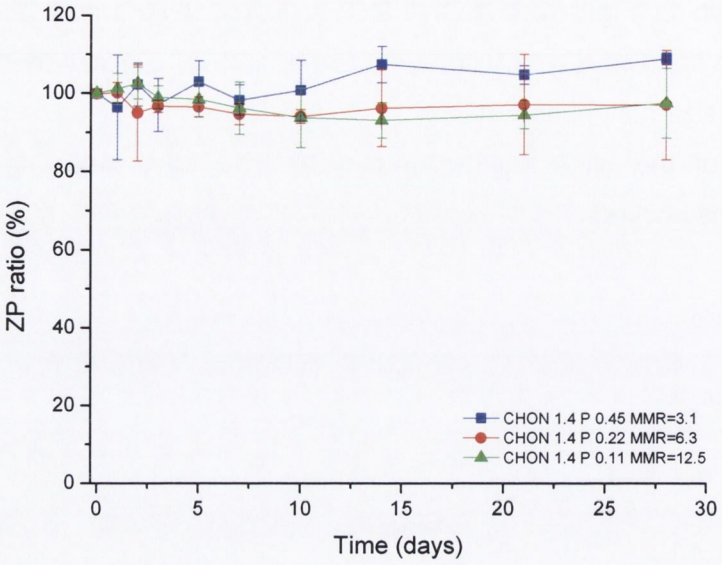

Fig. 7.19 Zeta potential ratio of CHON/PROT NPs during storage at room temperature. P=PROT.

7.5 Stability of CHON/PROT/sCT NPs in different media

As previously described in Chapter 6, the properties of polyelectrolyte complex NPs depend on the properties of the dispersant. Two samples with different CHON/PROT MMRs (6.4 and 4.2) were selected for stability studies. As shown in Fig.7.20, the particle size of NPs made of CHON of 2.1 mg/ml, PROT of 0.33 mg/ml and sCT of 1 mg/ml depended on the composition of the continuous phase. In diluted acetate buffer or diluted PBS the particle size was not different than in water, however with an increasing ionic strength an increase in the particle size was observed. Nevertheless, even in PBS the hydrodynamic diameter of the particles was not significantly different than 200 nm. Moreover, the size did not change within the next 24 hours of storage. In the acidic medium (0.25 M HCl) the particle size increased to 350 nm and, similarly to other media, no significant change occurred within 24 hours.

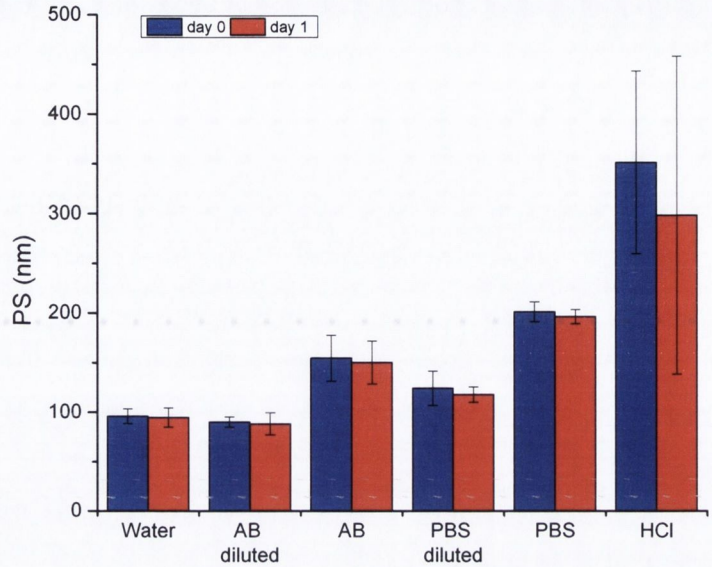

Fig.7.20 Particle size of CHON of 2.1 mg/ml, PROT of 0.33 mg/ml and sCT of 1 mg/ml NPs in different media.

The different types of liquid environment resulted in a significant narrowing the size distribution of the tested NPs compared to water, the only exception being diluted PBS, where no significant change was observed (Fig.7.21). Similarly to the particle size, no significant changes in PDI values were observed after 24 hours.

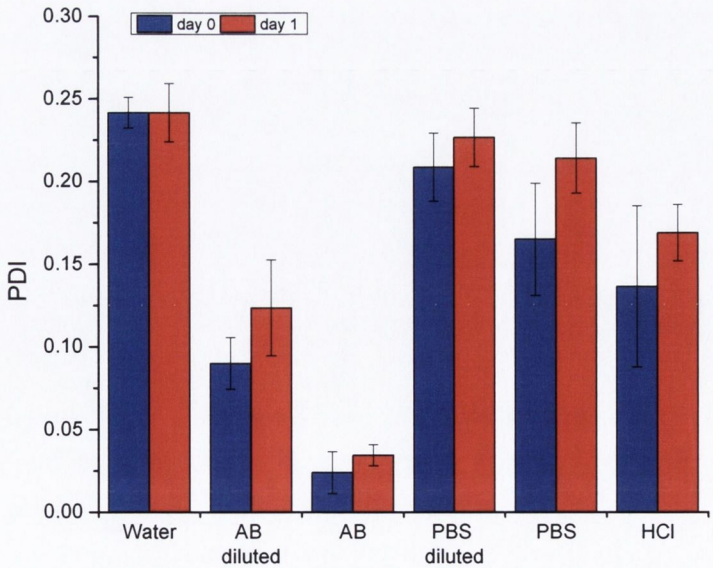

Fig.7.21 Polydispersity index of CHON of 2.1 mg/ml, PROT of 0.33 mg/ml and sCT of 1 mg/ml NPs in different media.

As shown in Fig. 7.22, the different media resulted in a significant decrease in the surface charge. The zeta potential of the tested NPs in water was of-47.3±5.18 mV and was increased by approximately 15 mV in diluted PBS, and by approximately 20 mV in PBS, acetate buffer and diluted acetate buffers. However, the values of zeta potential values were close to -30 mV, therefore the NPs had a strong negative surface charge indicating good colloidal stability. A decrease in pH (HCl solution) led to a decrease in the surface charge to -11.5±0.49 mV. Hence, even at this highly acidic pH (1.2), which could be encountered e.g. in stomach, the particles maintained negative charge, therefore indicating that the Coulombic interactions between positively charged sCT and negatively charged CHON are still present and sCT is likely to be associated with the particles in the whole range of pH of the gastrointestinal tract. Moreover, no significant change of the surface charge was observed after 24 hours.

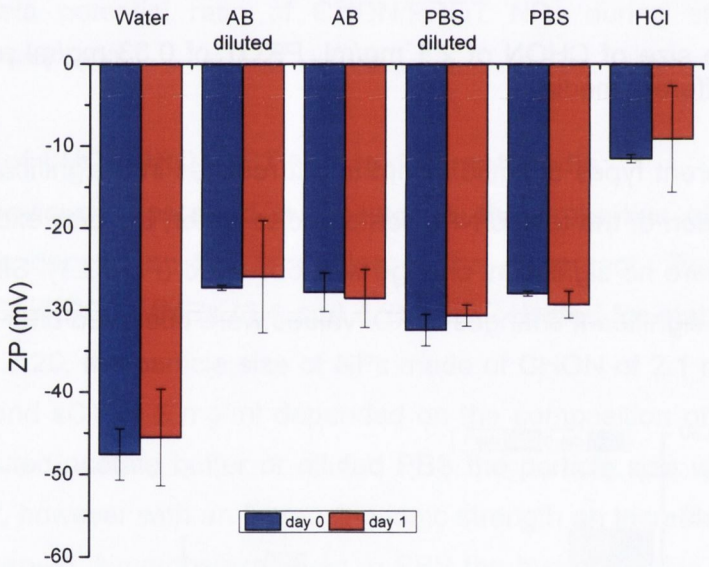

Fig.7.22 Zeta potential of CHON of 2.1 mg/ml, PROT of 0.33 mg/ml and sCT of 1 mg/ml NPs in different media.

Fig. 7.23 shows the particle size of similar, but 1.4 mg/ml CHON-based NPs in different media. The size of these particles in water, PBS, diluted PBS, acetate buffer and diluted acetate buffer did not differ significantly from that of the 2.1 mg/ml CHON-based particles. Also, no significant changes in the particle size were observed after 24 hours. In contrast, in the HCl solution a marked increase in the particle size to 700 nm was observed and after 24 hours a significant decrease in the particle size and precipitation of some of the particles was seen.

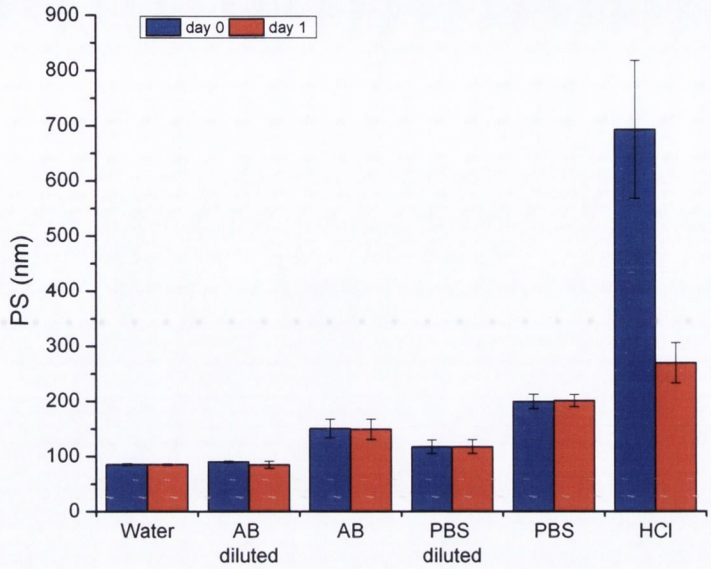

Fig.7.23 Particle size of CHON of 1.4 mg/ml, PROT of 0.33 mg/ml and sCT of 1 mg/ml NPs in different media.

Fig. 7.24 shows PDI values of the 1.4 mg/ml CHON-based NPs. A significant decrease in PDI values for the tested NPs were seen in acetate buffers and PBS solutions compared to water. A significant decrease by 0.03 after 24 hours of storage in PBS occurred and in other media the size distribution remained unchanged. The size distribution of 1.4 mg/ml CHON-based NPs in the HCl solution did not differ significantly compared to water. The size distribution of these NPs was similar to the size distributions of 2.1 mg/ml CHON-based NPs, with the exception of diluted PBS, where 1.4 mg/ml CHON-based NPs were more homogenously dispersed.

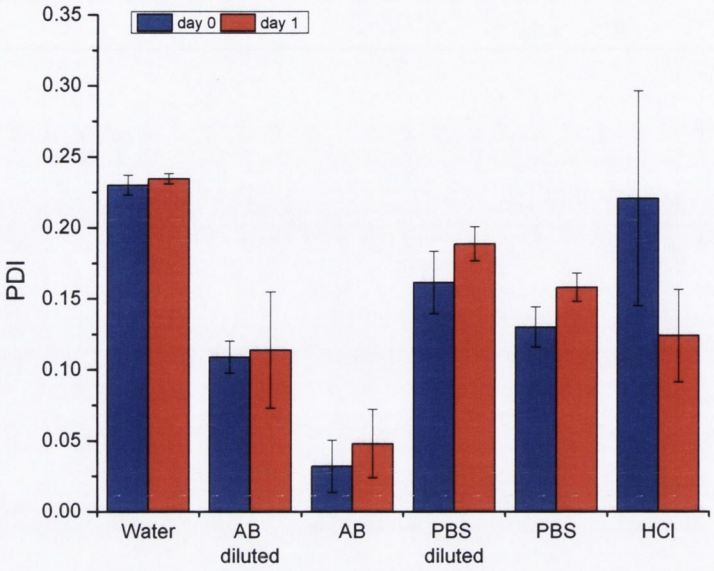

Fig.7.24 Polydispersity index of CHON of 1.4 mg/ml, PROT of 0.33 mg/ml and sCT of 1 mg/ml NPs in different media.

As shown in Fig. 7.25, 1.4 mg/ml CHON-based NPs remained negatively charged in the different media. The surface charge decreased significantly by 10-12 mV in acetate buffers and PBS solutions when compared to water. Apart from the diluted PBS, the surface charge was also significantly smaller when compared to that of 2.1 mg/ml CHON-based NPs. After 24 hours in acetate buffers, the zeta potential of 1.4 mg/ml CHON-based NPs decreased significantly, while after storage in PBS solutions no changes were observed. A pronounced decrease in surface charge to -8.4±0.17 mV was seen in the HCl solution. After 24 hours this surface charge increased significantly by approximately 2 mV.

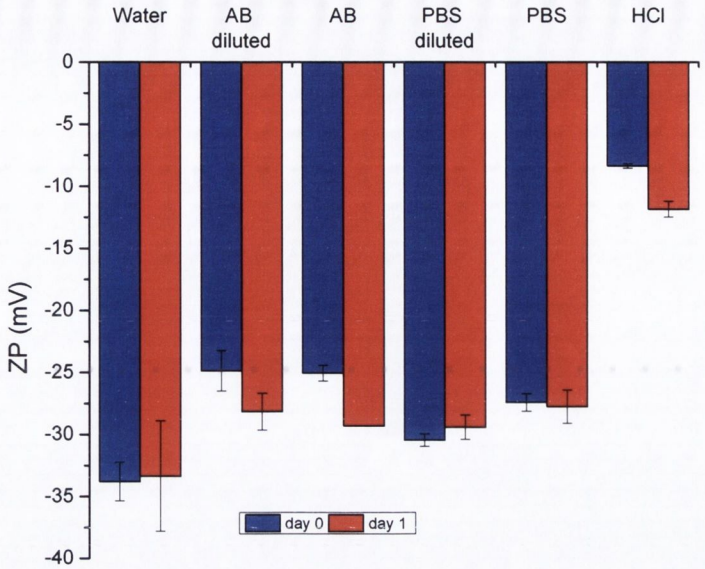

Fig.7.25 Zeta potential of CHON of 1.4 mg/ml, PROT of 0.33 mg/ml and sCT of 1 mg/ml NPs in different media.

7.6 *In vitro* release of sCT

Almost no sCT was released after 6 hours into water or diluted acetate buffer from either 2.1 mg/ml CHON-based NPs (Fig.7.26) or 1.4 mg/ml CHON-based NPs (Fig. 7.27). A very small fraction of sCT (i.e. 5-8%) was initially released into the above media during first hour. The amount of sCT released into HCl solution, PBS or diluted PBS after 6 hours was close to 20-25% for the both formulations tested. 17-18.5% of sCT was released after 6 hours into the acetate buffer and for the 2.1 mg/ml CHON-based formulation this amount was significantly smaller when compared to the HCl solution or diluted PBS. Also, after 2 hours the release of sCT from CHON/PROT/sCT NPs into the acetate buffer decelerated and the release profile became flatter in comparison to that obtained with PBS solutions and the HCl solution.

These release studies concur with the data achieved for sCT release from CHON/sCT or CHON/CL42/sCT NPs as described in Chapter 6. The properties of the release medium (pH and ionic strength) were confirmed to have an important influence on the release of sCT from CHON/PROT/sCT NPs.

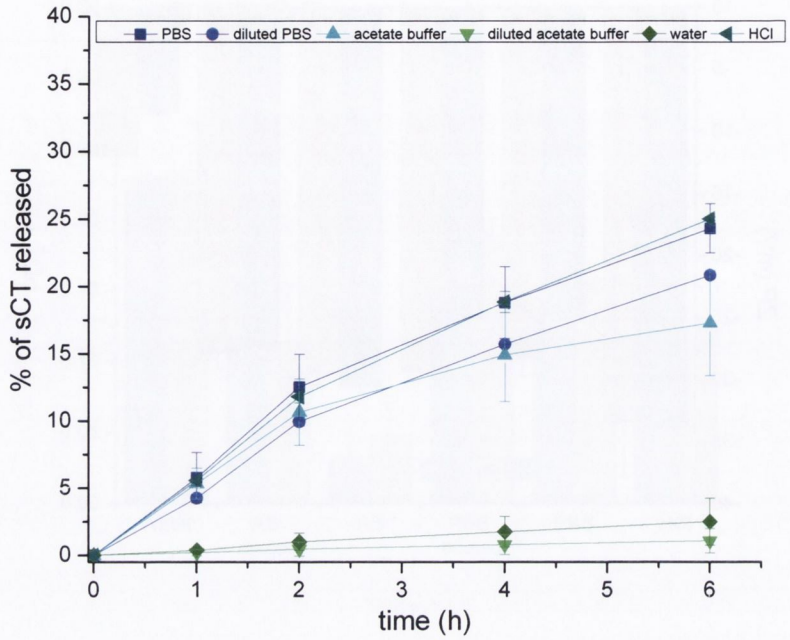

Fig.7.26 Cumulative release of sCT from CHON of 2.1 mg/ml, PROT o 0.33 mg/ml and sCT of 1.0 mg/ml NPs into different media.

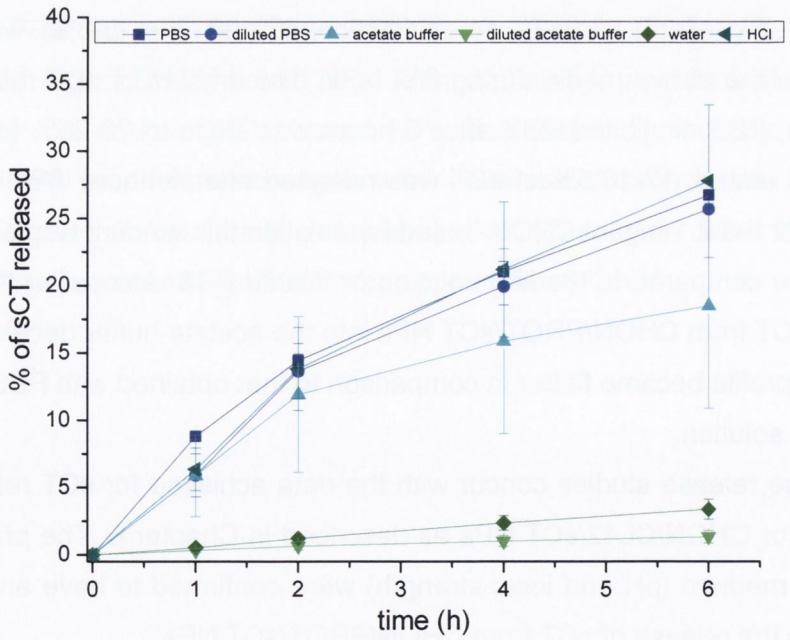

Fig.7.27 Cumulative release of sCT from CHON of 1.4 mg/ml, PROT o 0.33 mg/ml and sCT of 1.0 mg/ml NPs into different media.

The release data was fitted to the first order equation (see Chapter 2, Section 2.2.9, Equation 2.4) for AB, PBS, diluted PBS and the HCl solution. The parameter estimates obtained and related statistics are summarised in Tables 7.3 and 7.4. It can be observed that the amount of sCT released into acetate buffer (pH 5) is smaller compared to PBS or HCl solutions for both CHON/PROT/sCT formulations tested. A similar trend was observed in CHON/CL42 MMR of 5 and CHON/sCT NPs described in Chapter 6. The values of release rate constant (k) of sCT from CHON/PROT NPs were comparable to the previously described CHON/CL42 NPs (Chapter 6) and were markedly lower than HA-based NPs (Chapters 4 and 5).

Table 7.3 Model parameter estimates and related goodness of fit statistics for sCT release from CHON of 1.4 mg/ml, PROT of 0.33 mg/ml and sCT of 1.0 mg/ml NPs data fitted to the first order model.

Buffer/Solution	k [min^{-1}]	W_∞ [µg/mg of NPs]	Red. Chi-Sq.	R Sq.
Acetate buffer	0.3802±0.07442	75±27.0	2.32	0.99387
HCl	0.1918±0.02162	147±21.9	7.01	0.99414
PBS	0.3064±0.01856	114±4.5	3.87	0.99739
PBS diluted	0.2243±0.03522	127±7.2	5.91	0.99556

Table 7.4 Model parameter estimates and related goodness of fit statistics for sCT release from CHON of 2.1 mg/ml, PROT of 0.33 mg/ml and sCT of 1.0 mg/ml NPs data fitted to the first order model.

Buffer/Solution	k [min^{-1}]	W_∞ [µg/mg of NPs]	Red. Chi-Sq.	R Sq.
Acetate buffer	0.3647±0.00056	57±13.0	1.18	0.99597
HCl	0.1672±0.03650	116±15.0	1.55	0.99818
PBS	0.2140±0.10037	103±17.9	3.24	0.99636
PBS diluted	0.1615±0.00219	97±2.2	1.72	0.99703

7.7 Cytotoxicity of CHON/PROT NPs

The cytotoxicity of PROT has been described in Chapter 5. Similarly to the HA/PROT NPs described in the same chapter, CHON/PROT NPs with CHON/PROT MMR of 3.1 were selected for cytotoxicity studies by MTS assay. It appears that PROT nanocomplexed to CHON was significantly less cytotoxic than the same amount of PROT dissolved in serum-free medium. 83.4±4.9% of cells remained alive after 72 hours of exposure to CHON/PROT NPs containing 0.25

mg/ml of PROT, compared to 60.9±10.2% for solution containing an equivalent content of PROT. Moreover, no cytotoxic effects were observed after first 1:1 dilution of the NPs with the serum-free medium (98.4±4.6% of viable Caco-2 cells). At this concentration (0.125 mg/ml) of PROT a significant toxic effect was still observed for PROT dissolved in the medium. Complexation to CHON has also been reported to significantly decrease the cytotoxicity of polyethyleninine in HepG2 and HeLa cells (Pathak et al., 2009). Therefore in can be concluded that by the formation of polyelectrolyte complexes with CHON the toxicity of PROT can be markedly reduced. CHON/PROT NPs may be considered as non-toxic and well tolerated by Caco-2 cells.

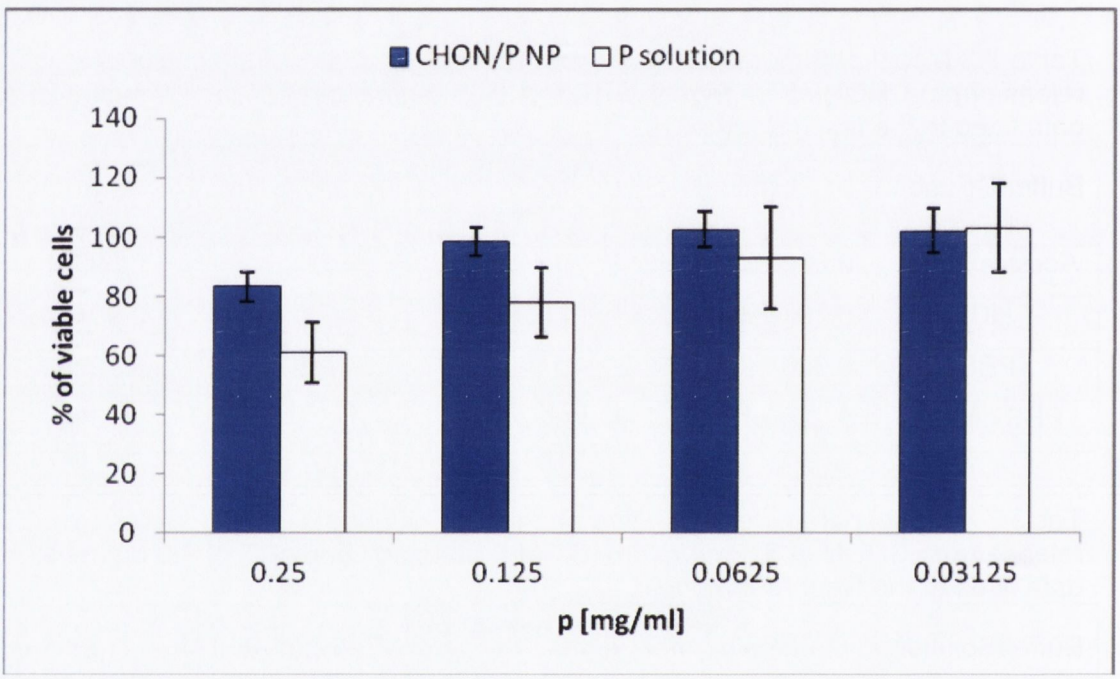

Fig. 7.28 The viability of Caco-2 cells by MTS assay after 72 hours of exposure to CHON/PROT NPs in serum-free medium.

7.8 Summary and conclusions:

A new type of nanocarriers composed of CHON and PROT have been successfully developed and characterised. The formation and properties of CHON/PROT NPs depended on the concentration and MMRs of both components. Positively charged CHON/PROT NPs were not stable after short-term storage at room temperature, while negatively charged particles satisfactorily maintained their characteristics even after 4 weeks. By modulation of formulation conditions it was possible to obtain small (100 nm and less) NPs with a narrow size distribution (PDI below 0.25).

sCT was very efficiently (≈100%) associated with the NPs, and good drug loading (14-38%) was achieved. Some of sCT-loaded CHON/PROT NPs were as

small as 60 nm. CHON/PROT NPs were capable of providing a prolonged release of sCT and less than 10% of the peptide was released in the first hour of the in vitro release studies. CHON/PROT NPs maintained the negative surface charge and were capable to bind sCT even at acidic pH values. Ionic strength and pH of the medium were found to have a considerable influence on the release of sCT from CHON/PROT NPs.

Complexation to CHON markedly reduced the toxic effects exerted by protamine. CHON/PROT NPs were compatible and well tolerated by Caco-2 cells.

8. Freeze-drying of polyelectrolyte complex nanoparticles

8.1. Introduction

In previous chapters of this work formation and properties of the different polyelectrolyte complex nanoparticles have been described. However, as colloidal systems, NPs are thermodynamically unstable and may be susceptible to aggregation after extended periods of storage as a suspension. Long term stability is an important challenge in the development of NPs. Freeze-drying is an attractive approach to achieve the long term stability, as suspensions can be converted into solid state materials with greater physical stability than liquids. Lyophilised formulations also provide easy handling including shipping and storage (Lu et al., 2004). However, stress generated during freeze-drying may adversely impact on the properties of NPs (Zhi-Gang et al., 2009) and incomplete redispersibility may be achieved. Many studies presented that, in order to effectively stabilise the NPs during freeze-drying as well as to ensure their adequate reconstitution, suitable excipients are required (de la Fuente et al., 2008; Zhi-Gang et al., 2009).

Although lyophilisation of various types of NPs have been studied (Abdelwahed et al., 2006), to our best knowledge only de la Fuente et al., (2008) examined lyophilisation of HA and CS-containing NPs. One of the cryoprotectants they tested was glucose, however due to its reducing properties, this sugar as well as other monosaccharides are not good candidates to be used as cryoprotectants in freeze drying with compounds containing amino groups, e.g. peptides, proteins or chitosan. Sugars (e.g. trehalose, sucrose) and sugar alcohols (e.g. mannitol) have been shown to be effective in maintaining the properties of NPs after lyophilisation process (Anhorn et al., 2008; Holzer et al., 2009).

This chapter concentrates on investigations of the effectiveness of freeze drying as a secondary unit process to convert dispersions of NPs into powders with a view to obtain complete NP redispersibilty upon reconstitution. As trehalose is a non-reducing sugar and has been presented to preserve CS/TPP/HA NPs after lyophilisation (de la Fuente et al., 2008), it was selected as the preferred additive, however other molecules as well as lyophilisation without a cryoprotectant were also studied.

8.2 Freeze-drying of HA/CL113 NPs without a cryoprotectant or with mannitol as a cryoprotectant

Given the fact that HA has been described as an efficient cryoprotectant for freeze-drying of liposome formulations (Peer et al., 2003), attempts were made to freeze-dry HA/CL113 NPs (TPC of 1 mg/ml, HA/CL113 MMRs of 2.5 and 5) without any excipients. NPs freeze-dried without trehalose were not successfully redispersed and in the reconstituted suspension aggregates as well as the NPs with the average size 2.8-fold higher (HA/CL113 MMR of 2.5 NPs) than the original were present. Similar, unsuccessful trials to freeze-dry CS/TPP/HA NPs were made by de la Fuente et al., (2008), who attributed this failure to the presence of only a small amount of HA in the suspending medium after the formation of NPs.

Although Anhorn et al., (2008) proved that mannitol can be an effective cryoprotectant for human serum albumin NPs, attempts to use mannitol (at 1, 2, 3 and 5% w/v) as a cryoprotectant for HA/CL113 NPs (TPC of 1 mg/ml, HA/CL113 MMR of 2.5) were unsuccessful. When HA/CL113 NPs were lyophilised with mannitol, a substantial aggregation upon reconstitution was seen in all samples tested.

8.3 Freeze-drying of HA/CL113 NP carriers with trehalose as a cryoprotectant

As previously mentioned, it was impossible to successfully redisperse the NPs and a significant aggregation upon reconstitution was observed. Preliminary experiments were first conducted in order to verify the influence of trehalose concentration on the redispersibility of HA/CL113 NPs. HA/CL113 NPs with the MMR of 2.5 and TPC of 0.75 or 1 mg/ml were freeze-dried in the presence of different concentrations of trehalose and the ratios of the size of the particles after and before freeze-drying (referred to as PS ratios) are presented in Fig. 8.1. The redispersibility was considered as very good, when the particle size did not change more than 20% (i.e. the size ratio was between 0.8-1.2), however NPs with the size ratio higher than 1.2 may be considered as acceptable if aggregation does not occur. For comparison, Zhi-Gang et al., (2009) considered the ratio of 0.7-1.3 appropriate, indicating satisfactory reconstitution.

When NPs were lyophilised with trehalose at a concentration of 1% w/v, the size ratio did not change significantly compared to the previously mentioned sample with no cryoprotectant and only moderate particle aggregation was observed (Fig. 8.1). A further increase in trehalose concentration to 2% w/v

resulted in a decrease in the size ratio to 1.67±0.35 and 1.73±0.23 (TPC of 0.75 and 1 mg/ml, respectively) and, more importantly, only a slight aggregation. A very good redispersibility was achieved when HA/CL113 NPs were freeze-dried at TPC of 0.75 mg/ml with 3, 4 or 5% w/v of trehalose- the size ratio was between 1.17±0.16 (3% w/v trehalose) and 0.96±0.07 (5% w/v trehalose) and aggregation was not seen. However, when TPC was increased to 1 mg/ml, 3% w/v of trehalose produced an acceptable redispersion- no aggregation was observed, but the particle size increased by 36% after freeze-drying. The redispersibility of HA/CL113 MMR of 2.5 NPs at 1 mg/ml was considered to be very good when at least 4% w/v of trehalose was used as the cryoprotectant. When TPC was further increased to 2 mg/ml, a significant aggregation was observed and the particles were not fully redispersible even though the size of the particles remaining in non-aggregated fraction did not change when compared to PS before lyophilisation (the size ratio was 1.07±0.05). When 5% w/v of trehalose was employed, neither the change of the particle size, nor aggregation could be observed, therefore at 5% w/v trehalose act as an effective cryoprotectant for 2 mg/ml HA/CL113 MMR of 2.5 NPs.

Interestingly, when 11% w/v trehalose was used in freeze drying, the particle size of the HA/CL113 NPs with TPC of 2 mg/ml became smaller than before lyophilisation (the size ratio was 0.89±0.02). However this decrease in the particle size did not occur when the same sugar concentration was used to freeze-dry NPs with the TPC of 1 mg/ml. The decrease in particle size could be attributed to compaction of the structure of the NPs (de la Fuente et al., 2008).

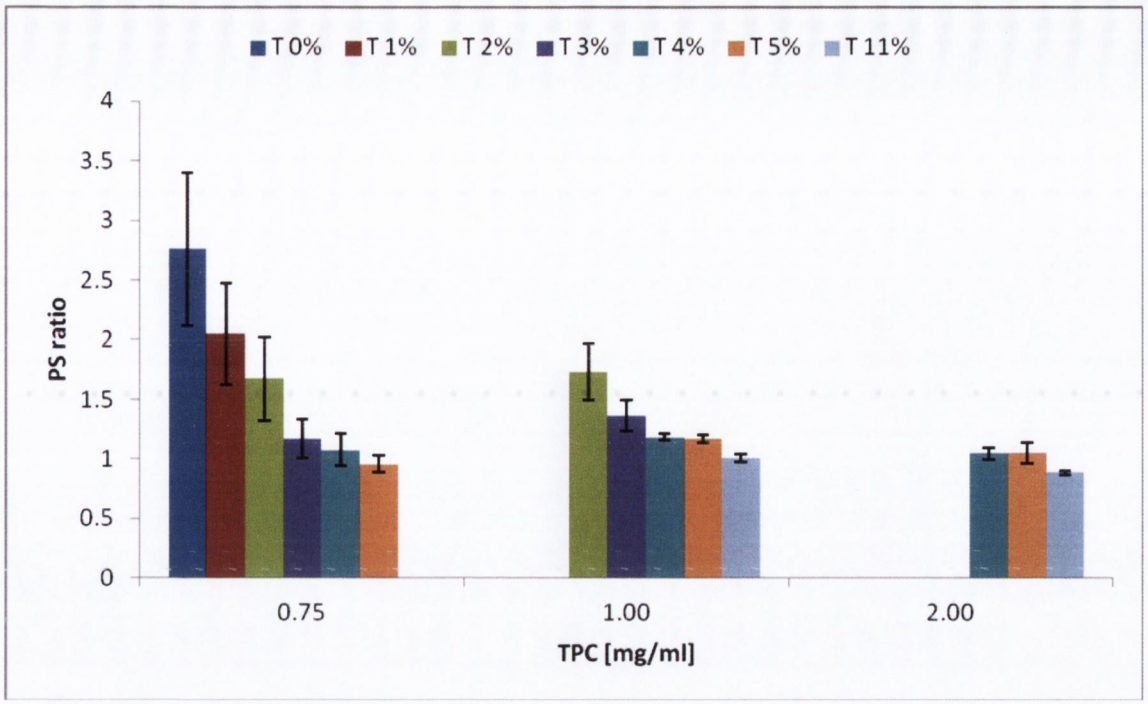

Fig. 8.1 The size ratio (i.e. the ratio of PS after and before freeze-drying) of HA/CL113 MMR of 2.5 NPs freeze-dried with trehalose at different concentrations. TPC of 0.75 mg/ml was obtained by a dilution of 1 mg/ml TPC nano-suspensions with trehalose solution.

Apart from the particle size, other properties of NPs (polydispersity index and zeta potential) were also monitored. Fig. 8.2 shows, on the example of TPC of 0.75 mg/ml HA/CL113 MMR of 2.5 NPs freeze-dried with trehalose, that the changes in the polydispersity index value were similar to changes in the particle size (the ratios of PS after and before freeze-drying did not differ significantly from equivalent ratios of PDI). Zeta potential of the NPs did not change after freeze-drying (zeta potential ratios after and before freeze-drying varied between 0.8-1.2). Therefore in further parts of this chapter only changes to the particle size will be described.

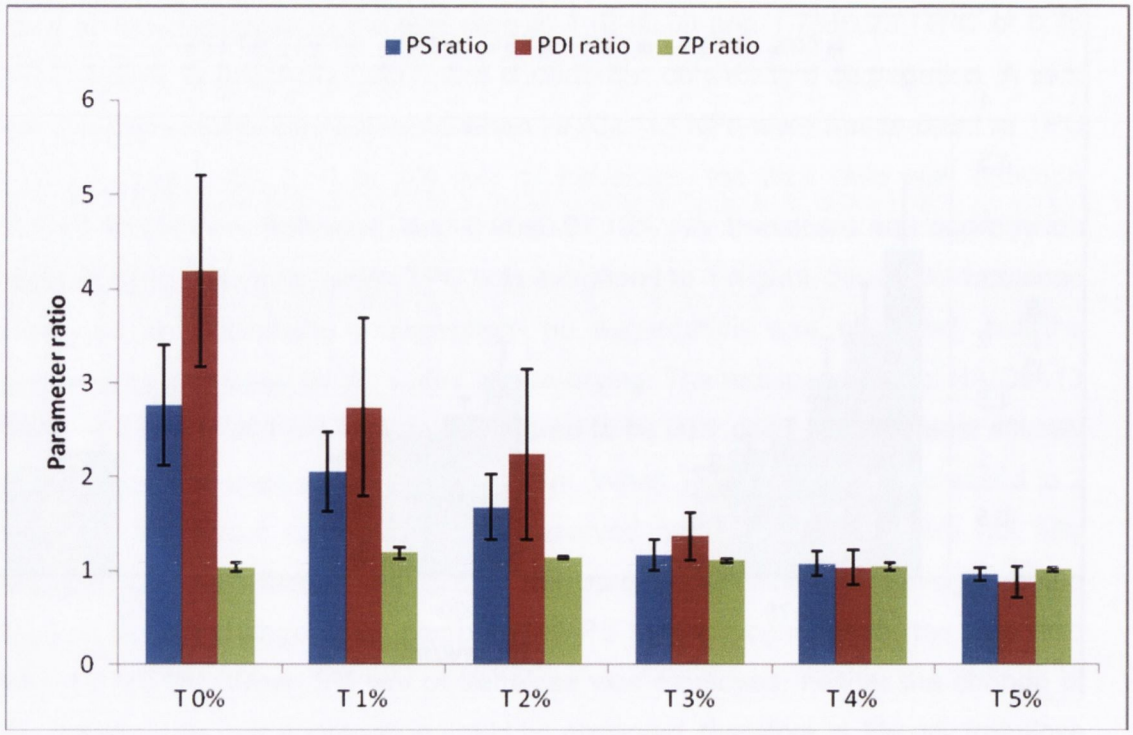

Fig. 8.2 The ratio of particle size, polydispersity index and zeta potential after and before freeze-drying of HA/CL113 MMR of 2.5 NPs (TPC of 0.75 mg/ml) freeze-dried with trehalose at different concentrations (0-5%).

As shown in previous chapters, the composition of the NPs, especially the MMR of the polymers has a considerable influence on their physical properties (i.e. PS, PDI, ZP) and biological (cytotoxicity) properties. Therefore the next step in this study was to verify if the composition of the particles has an influence on their redispersibility after freeze-drying.

HA/CL113 NPs with MMRs of 1 and 5 were initially freeze-dried at TPCs of 1 or 2 mg/ml with 4% w/v trehalose and depending on the result obtained the concentration of the sugar was further increased or decreased in order to determine the lowest concentration at which a good redispersibility could be obtained. Fig. 8.3 illustrates the size ratio after and before freeze-drying of positively charged NPs made of HA/CL113 with the MMR of 1. When the TPC was 2 mg/ml, a significant aggregation was observed with 4% w/v trehalose, but the size ratio was satisfactory (0.93±0.06). Therefore the concentration of trehalose was further increased, and a successful reconstitution without aggregation could be seen at 5, 7 or 11% w/v of this cryoprotectant, with the size ratios close to 1 for 5 and 7% w/v of trehalose and a significant decrease in the particle size after freeze-drying when 11% w/v of trehalose was employed. On the contrary,

HA/CL113 NPs with the MMR of 1 and TPC of 1 mg/ml were successfully reconstituted after freeze-drying with 4% w/v trehalose, with a low size ratio (1.09±0.06) and no aggregation observed. The redispersibility remained very good even when 1% w/v trehalose was used and when the concentration of trehalose was further decreased to 0.5%, a moderate aggregation occurred accompanied by an increase in the particle size by 36%. When the concentration of trehalose was again decreased to 0.2 or 0.1% w/v, a significant aggregation and a 2.3-fold increase in particle size were observed in both cases.

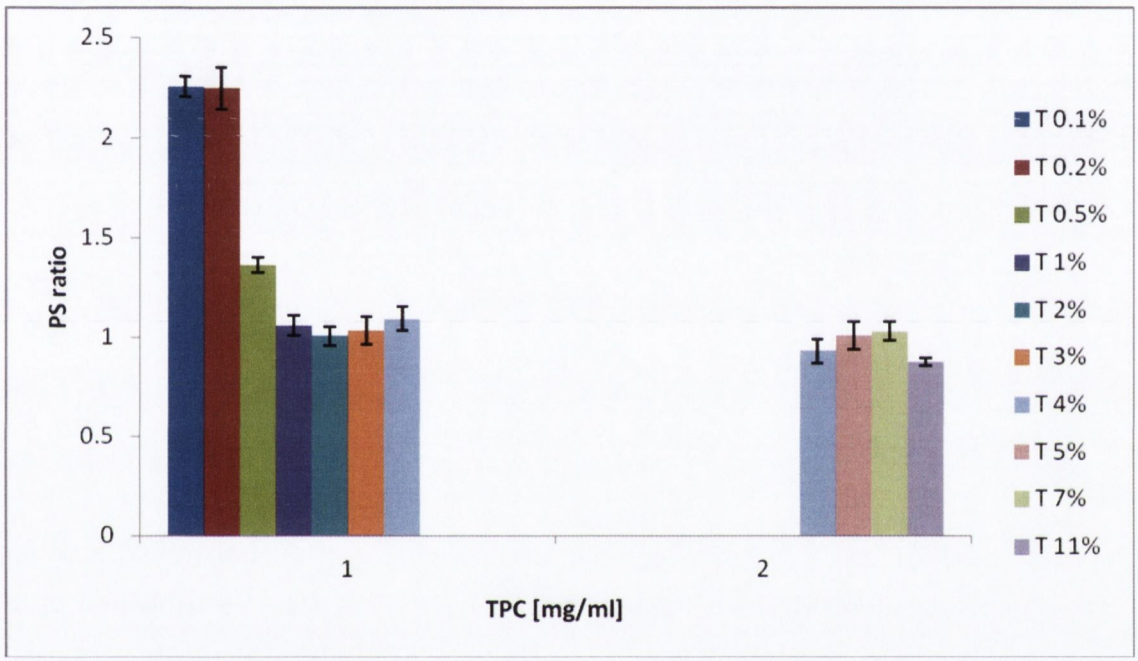

Fig. 8.3 The size ratio of HA/CL113 NPs with the MMR of 1 and TPC of 1 or 2 mg/ml freeze dried with different concentrations of trehalose.

HA/CL113 NPs with the MMR of 5 were satisfactory redispersible at both TPCs (1 and 2 mg/ml) when 4% w/v trehalose was used as the cryoprotectant. No aggregation was observed apart from NPs with the TPC=2 mg/ml freeze-dried with 0.1% w/v trehalose. The size ratios after and before freeze-drying of HA/CL113 NPs with the MMR of 5 are shown in Fig. 8.4. NPs with the TPC of 1 mg/ml were characterised by a very good redispersibility even after lyophilisation with only 0.1% w/v trehalose. The properties of NPs with the TPC of 2 mg/ml were satisfactorily preserved at trehalose concentration down to 0.5% w/v and at 0.2% w/v a significant increase in the particle size after freeze-drying was observed (the size ratio was 1.59±0.01).

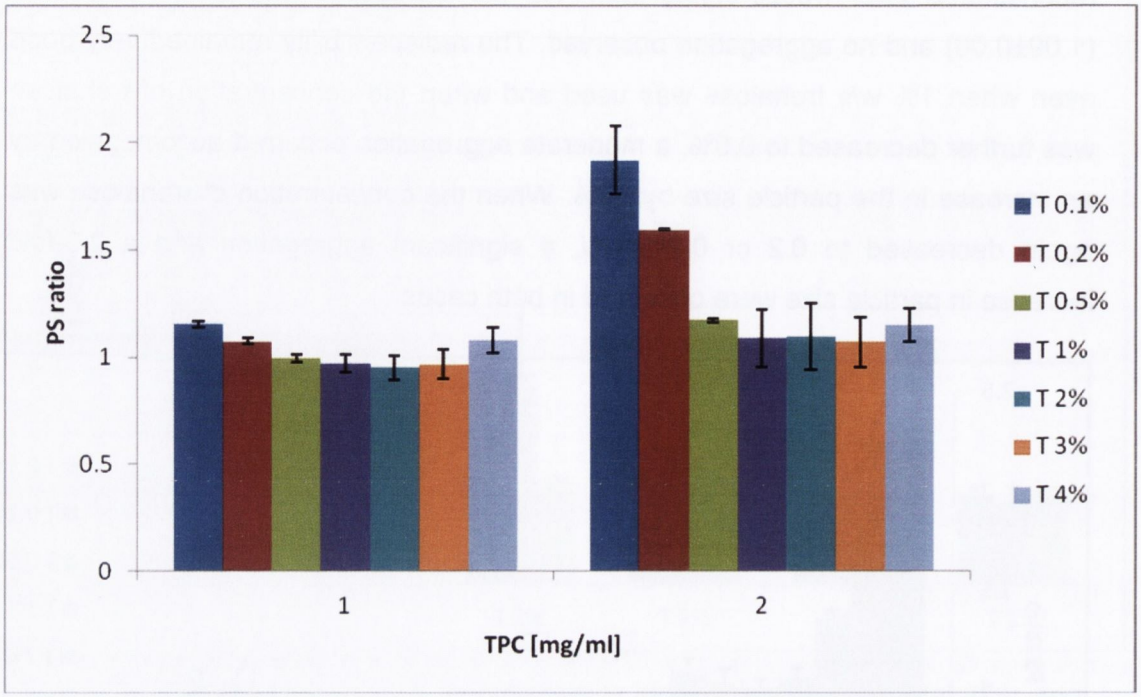

Fig. 8.4 The size ratio of HA/CL113 NPs with the MMR of 5 and TPC of 1 or 2 mg/ml freeze-dried with different concentrations of trehalose.

Hence, HA/CL113 NPs with the MMR of 5 were characterised by a better redispersiblity than NPs with MMRs of 2.5 and 1. This may be explained by a markedly higher content of HA in the former. Also, the corona in NPs with HA/CL113 MMR of 5 is relatively larger than in the case of HA/CL113 MMR of 2.5 NPs, the latter being composed predominantly of a dense core (see Chapter 3). As the corona is characterised by a smaller density than the core, it is possible that the molecules of a cryoprotectant penetrate inside the corona in spaces between HA chains, therefore enabling better preservation of particle properties during exposure to stress associated with the freeze-drying process. In summary, by modifying the composition of the NPs and optimisation of the cryoprotectant concentration, NPs can be successfully redispersed even at the NP to cryoprotectant weight ratio 1:1 (HA/CL113 NPs with the MMR of 5 and TPC of 1 mg/ml freeze-dried with 0.1% w/v trehalose).

The results of freeze-drying of HA/CL113 NPs with trehalose presented here are in agreement with data obtained by de la Fuente et al., (2008), who did not observe important changes in the particle size after freeze-drying CS/TPP/HA NPs with either 5% w/v trehalose or 5% w/v glucose. However, it must be

mentioned that the concentrations of NPs tested (0.075-0.5 mg/ml) where lower than those used here. Also, they did not optimise the concentration of the cryoprotectant, neither they tested the influence of NP composition on their redispersibility. As it is demonstrated here, optimisation of the concentration of cryoprotectant is of vital importance and the NP composition may have a significant influence on redispersibility.

8.4 Freeze-drying of sCT/HA/CL113 NPs with trehalose as a cryoprotectant

Having investigated freeze drying properties of HA/CL113 carriers, sCT-loaded HA/CH113 NPs (TPC of 1 mg/ml, MMR of 5 and sCT of 0.5 mg/ml) were freeze-dried in the presence of trehalose to study the impact of the peptide presence. The size ratios are presented in Fig. 8.5. Although no aggregation was observed when the trehalose concentration used was in the range of 0.1-4%, a significant increase in the particle size after lyophilisation was seen when lower concentrations of trehalose were used. The particle size increased by 36, 63 and 83% for 0.5, 0.2 and 0.1% w/v of the sugar, respectively. Therefore the preservation of particle properties was not as good as for similar HA/CL113 NPs without sCT. Therefore, incorporation of sCT decreases the ability of HA/CL113 NPs to be successfully redispersed. Nevertheless, it is noteworthy that even after 83% of size increase the particles still remain small with sizes well below 400 nm.

As mentioned in the previous chapters, drug loading is a very important property of the particles. The cryoprotectant is very often used at a much higher concentration than the NPs. For instance, de la Fuente et al., (2008) used a cryoprotectant (trehalose or glucose) at 5%, while the concentration of NPs varied between 0.075 and 0.5 mg/ml. Therefore the loading of sCT (or other drugs) in such formulation containing a cryoprotectant will be considerably lower than in the particles. As the addition of a cryoprotectant is required to obtain a redispersible dry form of NPs, the drug loading in the particles must be as high as possible and the concentration of a cryoprotectant as low as possible in order to obtain a solid state formulation with high drug loading. A high content of the drug would be particularly useful if the freeze-dried powder which is to be put into e.g. capsules is intended for oral administration. The sCT loading in samples lyophilised with 0.1, 0.2, 0.5 and 1% w/v trehalose would be approximately 20, 14, 7.7 and 4.3% w/w, respectively. These values can be considered as very high. However a

compromise must be made between the preservation of properties of the particles and the drug loading.

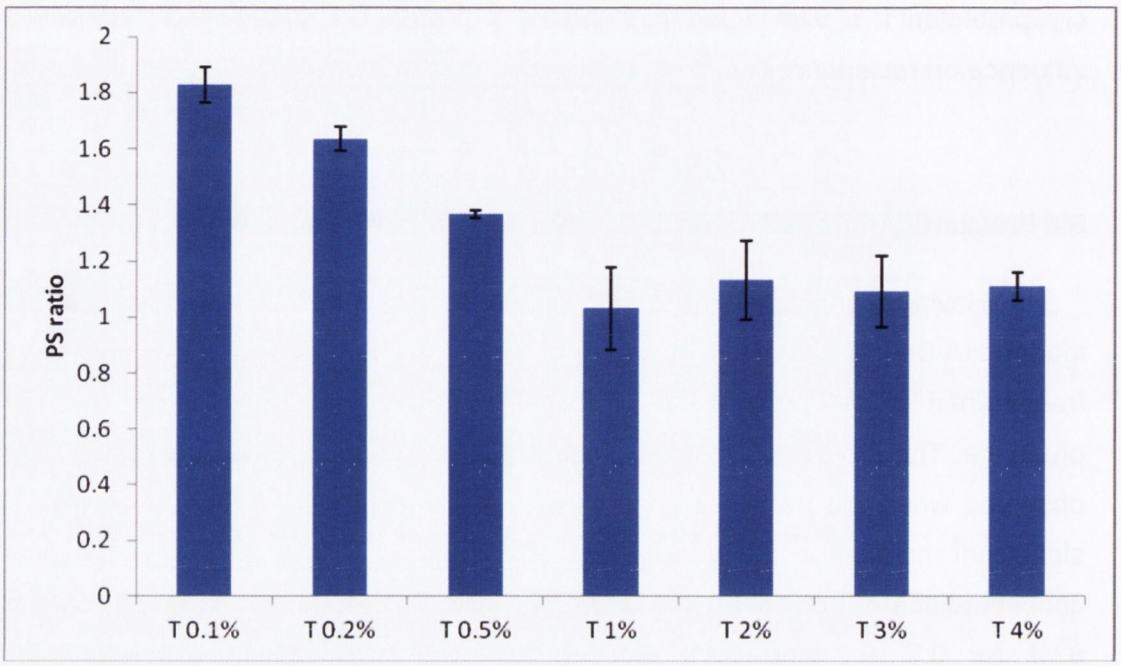

Fig. 8.5 The size ratio of sCT-loaded HA/CL113 MMR of 5 NPs freeze-dried at TPC of 1 mg/ml with trehalose at different concentrations

In order to confirm that no degradation of sCT occurred during the freeze-drying process, separation of non-associated sCT in the reconstituted sample by the previously described ultrafiltration-centrifugation technique was conducted. The sample before freeze-drying was used as a control. Table 8.1 shows the AE and the % of sCT extracted from NPs by dilution with NaOH solution. In can be concluded that sCT was not degraded during lyophilisation, as neither AE not the amount of extracted sCT changed after freeze-drying HA/CL113/sCT NPs with 4% w/v trehalose. The AE values remained very high (99%), and it was possible to extract all sCT from the NPs attaining a very good mass balance.

Table 8.1. The influence of lyophilisation on AE of HA/CL113/sCT NPs.

	AE [%]	sCT extracted [%]
Lyophilised HA/CL113/sCT NPs	98.94±0.27	98.90±1.57
Control	98.92±0.28	96.80±2.19

8.5 Solid state properties of NPs freeze dried with trehalose

The NPs freeze-dried without any cryoprotectant were amorphous (Fig. 8.6) and no clear thermal events were observed in the DSC scans (Fig. 8.7). XRD studies showed that initially crystalline unprocessed trehalose dihydrate became XRD-amorphous after lyophilisation of its aqueous solution (Fig. 8.6). It can be seen that the presence of NPs did not affect the solid state properties of freeze-dried trehalose, which was amorphous.

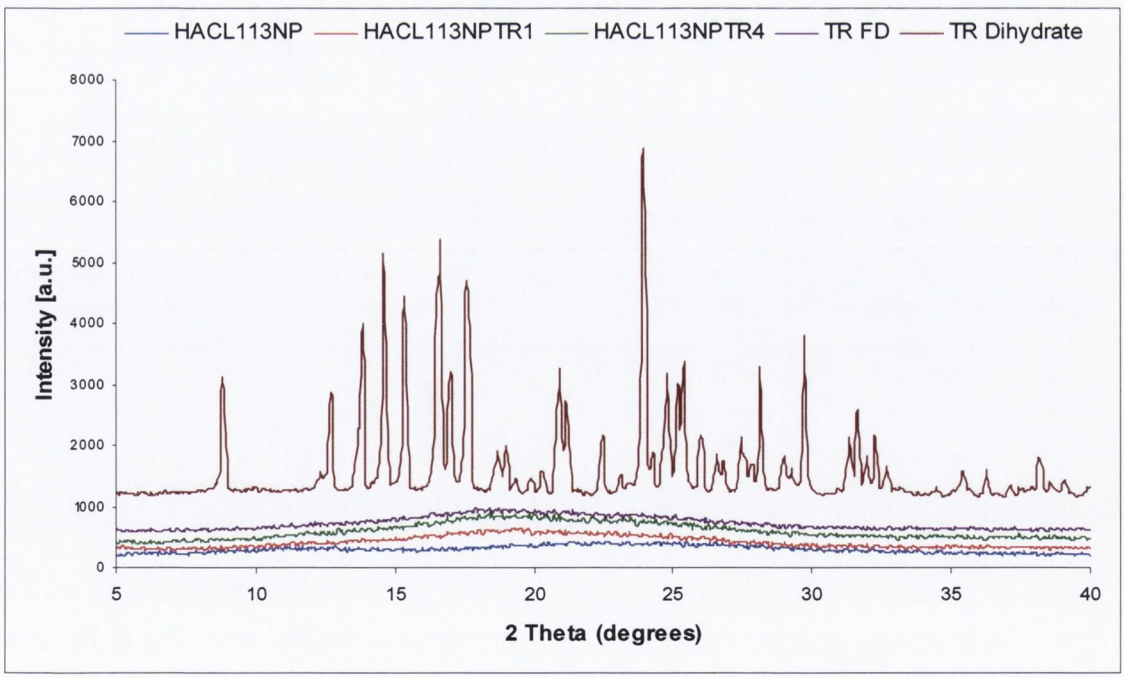

Fig. 8.6 X-ray diffractograms of unprocessed trehalose dihydrate, trehalose freeze-dried from its aqueous solution, and HA/CL113 MMR of 2.5 NPs freeze-dried at TPC of 1 mg/ml without any excipient or in the presence of 1 or 4% trehalose.

As shown in Fig. 8.7, the dehydration of trehalose dihydrate crystal occurs at 97.7 °C, and the anhydrous crystal melts at 211.46 °C, consistent with 97°C and

210 °C, respectively, reported by Ohtake et al., (2010). DSC (Fig. 8.6) confirmed that trehalose was amorphous after freeze drying from aqueous solutions as a glass transition (Tg) had the midpoint at 119.3°C consistent with the Tg of 110-120°C as reported by Ohtake et al., (2010). Similarly, after freeze-drying HA/CL113 NPs with trehalose, the glass transition with a similar midpoint (120.5°C) can be observed, confirming that trehalose was amorphous and addition of the NPs did not affect the thermal properties of lyophilised trehalose.

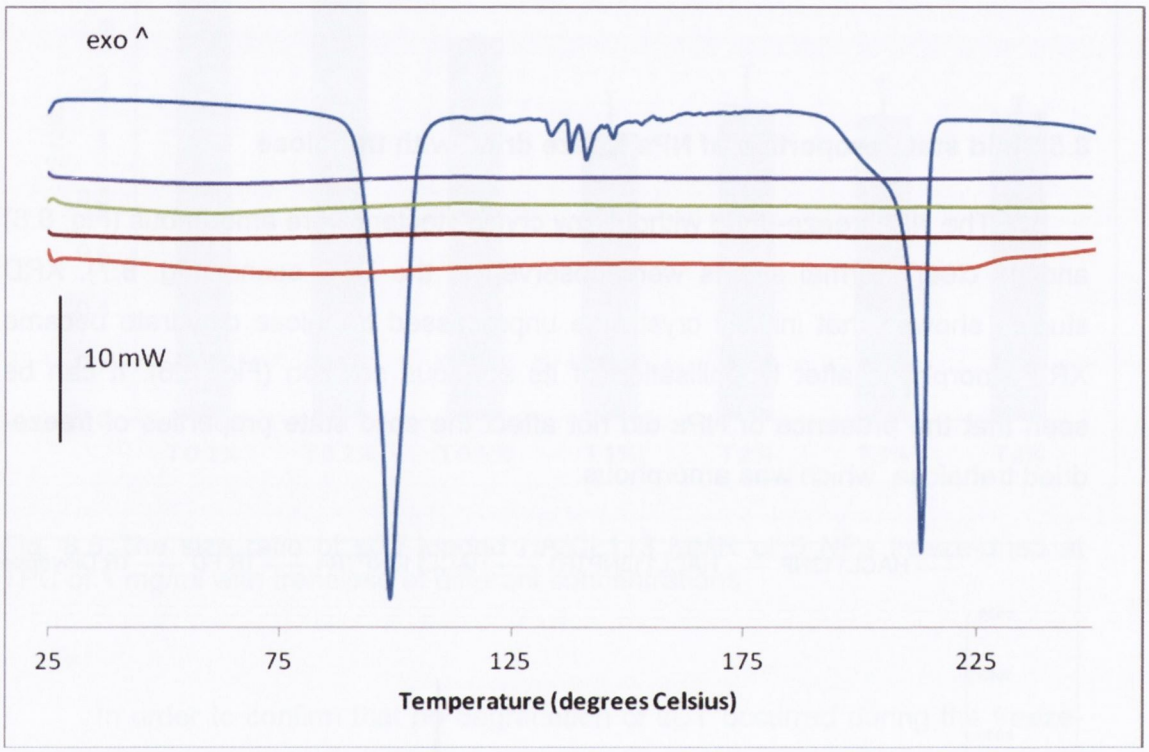

Fig. 8.7 DSC scans of trehalose dihydrate (blue), lyophilised trehalose (brown), HA/CL113 MMR of 2.5 NPs (orange), HA/CL113 MMR of 2.5 NPs lyophilised with trehalose (green) and a 1:1 w/w physical mixture of HA/CL113 MMR of 2.5 NPs with lyophilised trehalose (violet).

8.6 Cytotoxicity of trehalose and freeze-dried HA/CL113 NPs

Cytotoxicity of trehalose was examined, as it would be present in all the freeze-dried nanoparticle samples tested. It can be observed from Fig 8.8 that at 4% w/v (concentration of trehalose in redispersed NPs) it decreases the cells viability by 13%. Trehalose appeared to decrease the viability of Caco-2 cells only at higher concentrations than 2% w/v. It is probably due to the fact that the high concentration of sugar results in hyperosmolar solutions and thus may reduce cells viability unspecifically (Schrieliess, 2011). The IC_{50} of trehalose was 5.8% w/v.

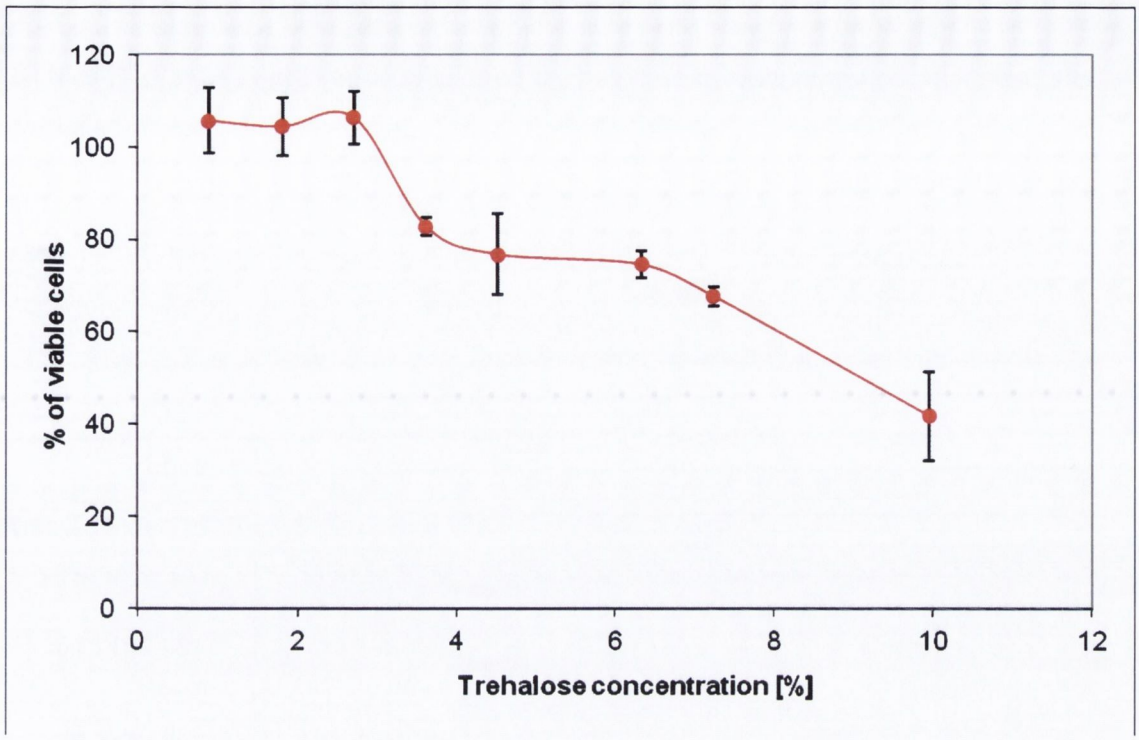

Fig. 8.8 The viability of Caco-2 cells treated with different concentrations of trehalose solution in serum free media for 72 hours.

Table 8.2 shows the cytotoxicity of HA/CL113 NPs. As previously mentioned, at the concentration of 4% w/v (used in the nanoparticle formulations) trehalose can be considered as non-toxic. Although significant, the decrease in cells viability caused by trehalose is small (7% decrease of cell viability compared to control determined by flow cytometry and 13% by MTS assay). The toxicity (by MTS assay) of freeze dried formulations with the HA/CL113 MMR of 1 were comparable to toxicity of trehalose. On the other hand, the MTS assay showed that NPs with the HA/CL113 MMR of 5 were significantly less toxic than 4% w/v solution of trehalose (the viability of the cells after incubation with formulations of TPC of 2 mg/ml and 1 mg/ml were of 89.84±0.87% and 96.56±5.32%, respectively compared to 82.88±1.91% for 4% w/v trehalose solution). The MTS results agreed with those from the flow cytometry assay. HA/CL113 MMR of 5 NPs with TPCs of 1 mg/ml and 2 mg/ml had the amount of viable cells (Annexin V and PI negative) of 90.73±0.49 and 86.35±1.20%, respectively, and TPC of 1 mg/ml NPs were significantly less cytotoxic than the solution of trehalose on its own (84.23±2.20% of viable cells). Nanoparticles with the TPC of 2 mg/ml were significantly more toxic than the control (serum-free medium with 91.29±2.7% of living cells), but the amount of the viable cells after incubation with NPs with TPC of 1 mg/ml did not differ significantly from the control. In conclusion, no toxic effects were observed after the incubation of cells with NPs with the HA/CL113 MMR of 5 moreover, the

TPC of 1 mg/ml NPs seemed to reduce significantly the cytotoxic effects of high concentration of trehalose. Also, it can be concluded from the results of the MTS assay that the decrease in HA/CL113 mixing ratio decreases cell viability slightly, but significantly.

Incorporation of sCT into freeze-dried NPs decreased the viability of cells only slightly (7% decrease by MTS and 9% by flow cytometry), but the difference was statistically significant when compared to similar NPs without sCT (Table 8.2).

Table 8.2 The viability of Caco-2 cells treated with the polymer or cryoprotectant solution or with the dispersion of NPs for 72 hours. N/D – not determined

Sample	Trehalose concentration [%, w/v]	% of viable cells by MTS assay	% of viable cells by flow cytometry
trehalose	4	82.88±1.91	84.23±2.20
2 mg/ml TPCHA/CL113=5	4	89.94±0.87	86.35±1.20
1 mg/ml TPCHA/CL113=5	4	96.56±5.32	90.73±0.49
1 mg/ml TPCHA/CL113=5 sCT 0.5 mg/ml	4	89.70±0.99	81.05±4.60
2 mg/ml TPCHA/CL113=1	4	75.78±8.84	N/D
1 mg/ml TPCHA/CL113=1	4	79.98±8.60	N/D
Serum-free medium (control)	-	100%	91.29±2.70

As TPC of 2 mg/ml, HA/CL113 MMR of 1 NPs were the most toxic from the samples tested (Table 8.2), they were further diluted either with the serum-free medium or with 4% w/v solution of trehalose in the medium, in order to verify if the decrease in the amount of viable cells is caused by trehalose or by NPs. The results are shown in Fig. 8.9. When the NPs were further diluted with 4% w/v solution of trehalose in the serum-free medium after the reconstitution, the viability

of the cells determined by the MTS assay did not increase significantly (75.78±8.84% and 86.23±9.57% of viable cells for TPC of 2 mg/ml and 0.125 mg/ml, respectively). However, when the dilution was performed with the serum-free medium (without trehalose), a significant increase in the number of living cells was observed even at the TPC of 1 mg/ml (107.27±16.23%). Thus, the decrease in cell viability of the formulations containing HA/CL113 NPs with the MMR of 1 may be attributed mainly to the presence of high concentrations of trehalose and the particles themselves appear to be non-toxic even at the TPC of 2 mg/ml. It was not possible to determine the cell viability by flow cytometry for the NP systems with the HA/CL113 MMR of 1 due to the presence of micro-sized aggregates, which caused analysis interferences.

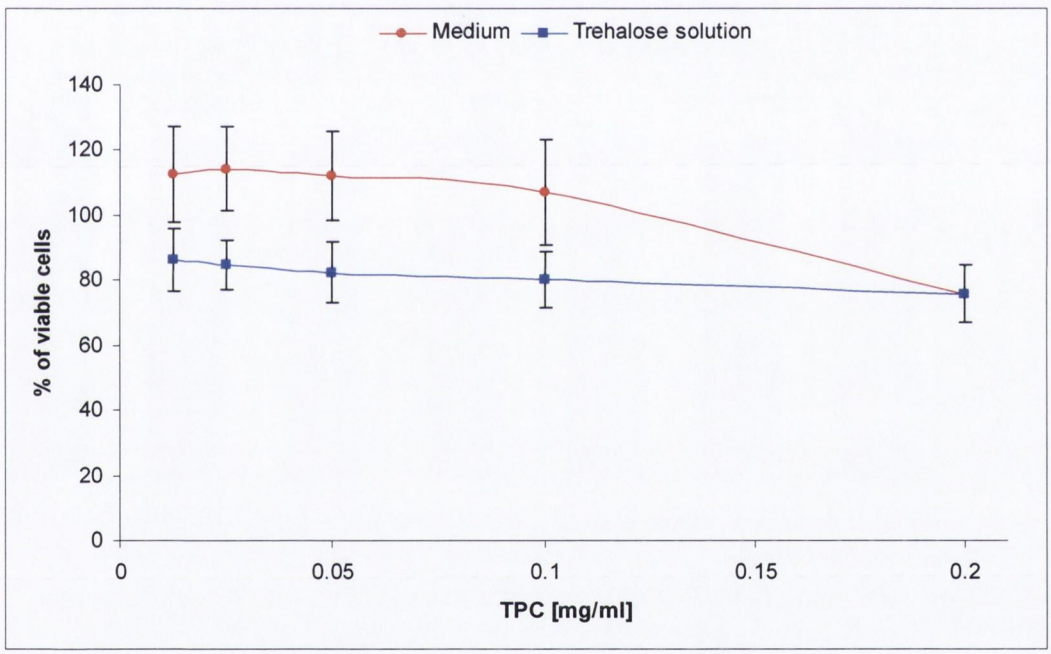

Fig.8.9 The viability of Caco-2 cells treated with different concentrations of NPs with the HA/CL113 MMR of 1 (the starting sample of TPC of 2 mg/ml was diluted either with serum-free medium or with 4% w/v of trehalose in serum-free medium).

8.7 Freeze-drying of HA/PROT, CHON/CS and CHON/PROT NPs with trehalose

Based on the results obtained from freeze-drying of HA/CL113 NPs with trehalose, preliminary experiments were made to examine the redispersibility of NPs described in Chapters 5, 6 and 7.

All HA/PROT NPs tested were successfully redispersed when freeze-dried with 4% w/v trehalose. The size ratios after and before freeze-drying were not

significantly higher than 1.2 (Fig. 8.10) and no aggregation was observed in any of the samples tested. When trehalose concentration was decreased to 1% w/v, no aggregation was observed, but a slight increase in particle size by 27, 34 and 27% was seen for the following samples: HA of 0.7 mg/ml/PROT of 0.3 mg/ml, HA of 1.4 mg/ml/PROT of 0.2 mg/ml and HA of 1.4 mg/ml/PROT of 0.45 mg/ml, respectively. Therefore, even at 1% w/v trehalose an acceptable or a very good redispersion was observed depending on the composition of the sample for all HA/PROT NPs tested. Hence, HA/PROT NPs are characterised by a better redispersibility than HA/CL113 MMR of 2.5 or 1 NPs.

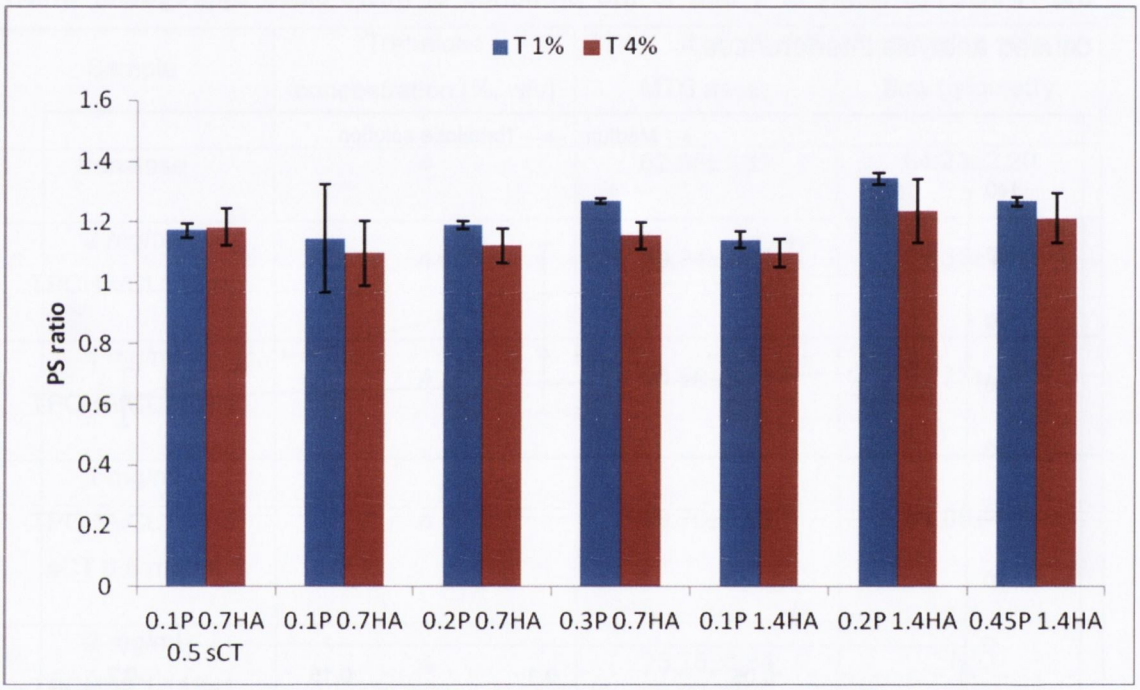

Fig.8.10 The size ratio of HA/PROT NPs freeze-dried with 1 and 4% of trehalose.

Cytotoxicity of freeze dried HA/PROT NPs was tested by MTS assay and flow cytometry, and the results are presented in Table 8.3. It can be observed that the viability of Caco-2 cells was decreased markedly compared to control (serum-free medium). Similarly to protamine (see Chapter 5), the MTS assay was more sensitive than flow cytometry. The viability of the cells decreasing by approximately 10-15% compared to the medium in the apoptosis assay was observed and a 30-50% decrease in the proliferation of the cells was observed by MTS assay. The lyophilised samples contained two ingredients which have been previously shown to decrease the amount of living cells: protamine and high concentration of trehalose. Freeze-dried HA/PROT NPs are markedly more toxic than trehalose, however their toxicity does not differ significantly from protamine at the same concentration. It can be observed that the toxicity increases correspondingly to an

increasing content of protamine in the formulation. For instance, 1.4 mg/ml of HA, 0.46 mg/ml of PROT sample is significantly more toxic that samples containing the same concentration of HA and smaller concentration of PROT (i.e. 0.1 or 0.2 mg/ml). Therefore protamine is probably the ingredient mostly repsonsible for the toxicity of the formulations, but trehalose may also play a role.

Table 8.3 The viability of Caco-2 cells by MTS assay and flow cytometry treated with redispersed HA/PROT NPs freeze-dried with 4% w/v trehalose for 72 hours.

HA [mg/ml]	PROT [mg/ml]	sCT [mg/ml]	% of viable cells by MTS	% of viable cells by flow cytometry
0.714	0.114	0.5	68.79±14.35	80.35±2.00
0.714	0.114	-	65.58±12.98	81.30±2.03
0.714	0.229	-	60.81±9.58	80.28±1.10
0.714	0.343	-	54.15±4.74	77.90±1.05
1.429	0.114	-	67.62±4.14	81.80±0.73
1.429	0.229	-	64.19±2.32	78.35±1.59
1.429	0.457	-	46.80±6.22	75.35±4.46

Formulation containing 1.4 mg/ml of HA and 0.46 mg/ml of PROT, which is the most toxic from freeze-dried HA/PROT NPs tested, was further diluted with the serum free medium, and the number of living cells increased corresponding to a decreasing concentration of all formulation components (Fig 8.11). After the second dilution (i.e. a decrease of the concentration of all components by 4 times) sample was well tolerated by Caco-2 cells with the cell viability of more than 90%.

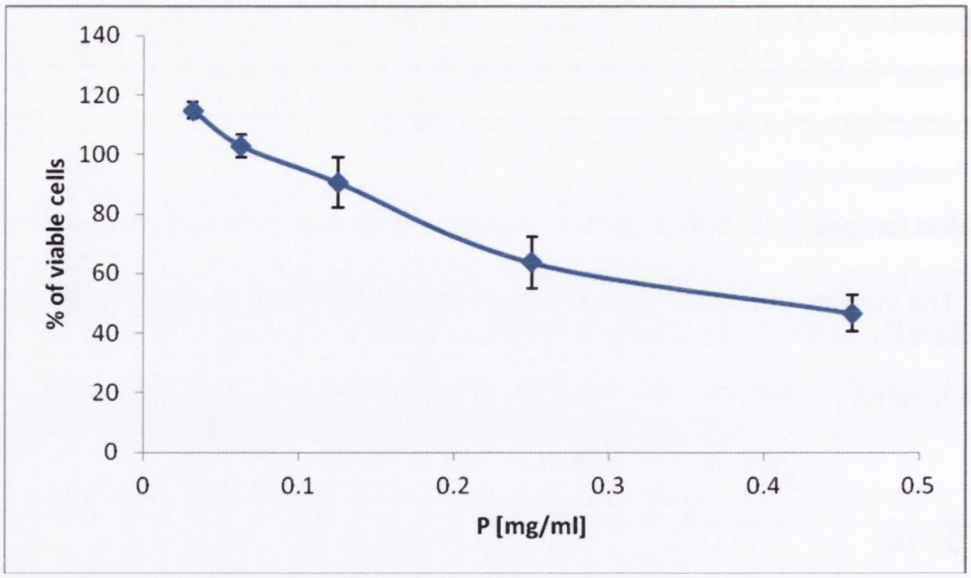

Fig.8.11 The effect of 1.4 mg/ml of HA, 0.46 mg/ml of PROT formulation freeze-dried with 4% of trehalose on Caco-2 cells after 72-hour incubation. The dilutions were performed with the use of serum-free medium and the % of viable cells is presented as a function of PROT concentration in the formulaton.

The redispersibility of CHON-based NPs was also examined in order to verify, if the polyanion (CHON versus HA) has any influence on the properties of reconstituted NPs. As shown in Fig. 8.12, none of the formulations tested were successfully redispersed after lyophilisation with 1% w/v trehalose, apart from the sCT-loaded CHON/CL42 NPs with the MMR of 5 and TPC of 1 mg/ml NPs, where only an acceptable redispersion was achieved with an increase in the particle size by 33%. When the concentration of trehalose was increased to 4% w/v, all formulations with the CHON/CL42 MMR of 5 as well as formulation with TPC of 1 mg/ml, CHON/CL42 MMR of 1 were redispersed with a very good preservation of the particle size. In two formulations with the TPC of 2 mg/ml: CHON/CL42 MMRs of 2.5 and 1, aggregation was observed and the particle size was significantly increased after freeze-drying. Freeze dried CHON/CL42 NPs with the MMR of 2.5 and TPC of 1 mg/ml was satisfactorily redispersed after processing with 4% w/v trehalose, but an increase in the particle size by 27% was observed.

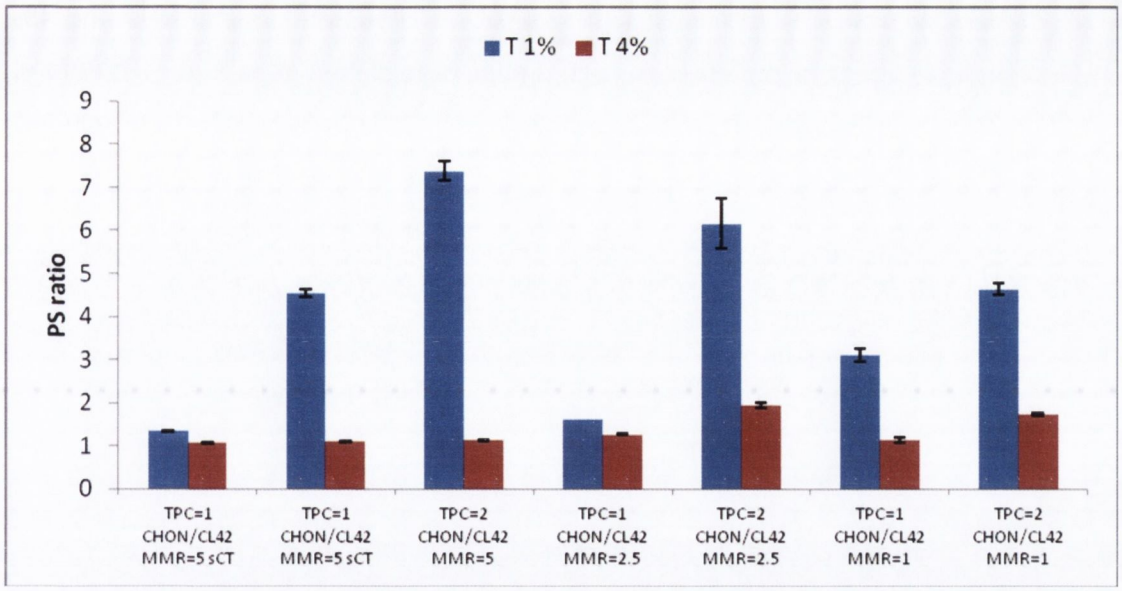

Fig. 8.12 The size ratio of CHON/CL42 NPs freeze-dried with 1 and 4% of trehalose.

The results obtained for CHON/CL42 NPs confirm that the composition of the particles (the MMR of the polymers) and their concentration plays an important role influencing the ability of the NPs to be redispersed. Similarly to HA/CL113 NPs, CHON/CL42 NPs with the MMR of 2.5 were the most difficult to be successfully redispersed and CHON/CL42 NPs with the MMR of 5 NPs were the easiest to fully reconstitute. In contrast to HA-based NPs, incorporation of sCT into CHON-based NPs was seen to improve their redispersibility compared to CHON-based NPs without sCT. Despite the fact that sCT decreased the redispersibility of HA-based NPs, and increased the redispersibility of CHON-based NPs, HA/CL113/sCT NPs can still be considered as easier to redisperse than CHON/CL42/sCT NPs, because after freeze-drying with 1% w/v trehalose their particle size was better preserved. Generally, CHON/CL42 NPs were characterised by worse redispersibility compared to HA-based NPs. Further experiments are necessary to determine the minimal concentration of trehalose at which different types of CHON/CL42 NPs at various concentrations are successfully redispersed.

Table 8.4 shows the effect of freeze-dried CHON/CL113 formulations on Caco-2 cells. All formulations tested were well tolerated by Caco-2 cells. The cytotoxicity of freeze dried samples did not differ significantly from HA/CL113 NPs with equivalent composition. Also, similar effects were observed: incubation with formulations with higher CHON/CL113 MMRs resulted in a higher % of viable cells and a significant increase in the number of living cells after treatment with a

dispersion containing the CHON/CL113 MMR of 5, TPC of 1 mg/ml NPs and 4% w/v trehalose formulation compared to trehalose solution (4% w/v). Therefore, CHON/CL113 NPs also protect Caco-2 cells from the negative effects of osmotic stress caused by trehalose.

Table 8.4. The viability of Caco-2 cells by MTS assay treated with redispersed CHON/CL113 NPs (freeze-dried with 4% trehalose) for 72 hours.

Sample	% of viable cells by MTS assay
2 mg/ml TPC CHON/CL113=5	87.83±6.59
1 mg/ml TPC CHON/CL113=5	98.43±7.92
1 mg/ml TPC CHON/CL113=5 sCT 0.5 mg/ml	86.01±8.76
2 mg/ml TPC CHON/CL113=1	84.39±11.20
1 mg/ml TPC CHON/CL113=1	79.6±8.33

Finally, CHON/PROT NPs were freeze-dried with 1 or 4% w/v trehalose, and the results are shown in Fig. 8.13. Similarly to HA/PROT NPs, no aggregation was observed in any of the samples tested, and all samples were satisfactorily redispersed even after freeze-drying with 1% w/v trehalose. In some samples an increase in the particle size by 30% could be observed, but they did not differ significantly ($p>0.05$) from the size ratio of 1.2. Interestingly, some of the NPs freeze-dried with 4% w/v trehalose were significantly ($p<0.05$) larger than those freeze-dried with 1% w/v trehalose. The formulations composed of 1.4 mg/ml CHON of and 0.1 mg/ml PROT as well as all samples containing 0.7 mg/ml CHON with the exception of the sCT-loaded NPs decreased their size during freeze-drying with 1% w/v trehalose and the size ratios were significantly smaller than 1.

In conclusion, both HA/PROT and CHON/PROT NPs were characterised by a very good redispersibility, which is considerably better than most of the chitosan-containing formulations.

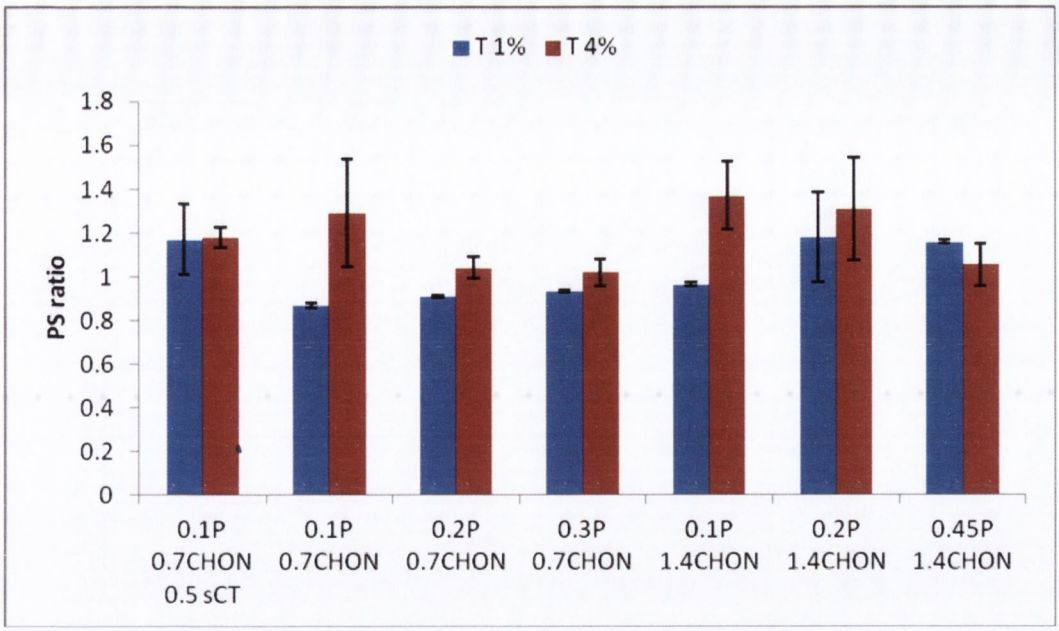

Fig. 8.13 The size ratio of CHON/PROT NPs freeze-dried with 1 and 4% of trehalose.

Table 8.5 shows the cytotoxic effects of lyophilised CHON/PROT formulations on Caco-2 cells. The number of living cells decreased by 20-35%, depending on the composition of the sample. Lyophilised CHON/PROT were generally better tolerated than HA/PROT NPs. Also, they were less toxic than protamine on its own.

Table 8.5 The viability of Caco-2 cells by MTS assay treated with redispersed CHON/PROT NPs freeze-dried with 4% w/v trehalose for 72 hours.

CHON [mg/ml]	PROT [mg/ml]	sCT [mg/ml]	% of viable cells by MTS
0.714	0.114	0.5	76.4±15.18
0.714	0.114	-	80.23±5.19
0.714	0.229	-	74.78±5.91
0.714	0.343	-	72.23±14.12
1.429	0.114	-	75.33±5.40
1.429	0.229	-	74.05±11.39
1.429	0.457	-	64.10±6.40

8.8 Freeze-drying of HA/CL113 NPs with polyethylene glycols as cryoprotectants

Apart from sugars, low molecular weight water soluble polymers could also be used as cryoprotectants. Lee et al., (2009) have shown that 2000 g/mol polyethylene glycol (PEG) successfully performed as a cryoprotectant for naproxen nano-suspension. Therefore in the further phase of this study HA/CL113 NPs with the MMR of 2.5 and TPC of 1 mg/ml were freeze-dried with variable concentrations of different PEGs (2kDa, 4kDa, 10kDa linear PEGs and 10kDa four-arm branched PEG).

Fig. 8.14 shows the size ratios after and before freeze-drying of HA/CL113 NPs with different PEGs. When 0.5% w/v PEG was used, aggregation was observed during reconstitution of the particles, regardless of the type of PEG used. An increase in PEG concentration to 1% w/v resulted in an acceptable redispersibility of the NPs with no aggregation observed and size ratios between 1.25±0.09 and 1.37±0.08 (for PEG 2kDa and branched PEG 10kDa, respectively). A further increase in PEG concentration from 2 to 5% w/v led to a very good redispersibility of the NPs with the increase in particle size during freeze-drying smaller than 20%. Neither the molecular weight nor the structure of PEG molecules were found to have an influence on redispersibility of HA/CL113 NPs. Also, PEGs were found to be more effective cryoprotectants than trehalose, as only 1% w/v

PEGs was needed to obtain acceptable redispersibility of HA/CL113 NPs with the MMR of 2.5 and TPC of 1 mg/ml compared to 3% w/v trehalose and a very good preservation of the size of NPs was achieved at 2% w/v PEG compared to 4% w/v trehalose.

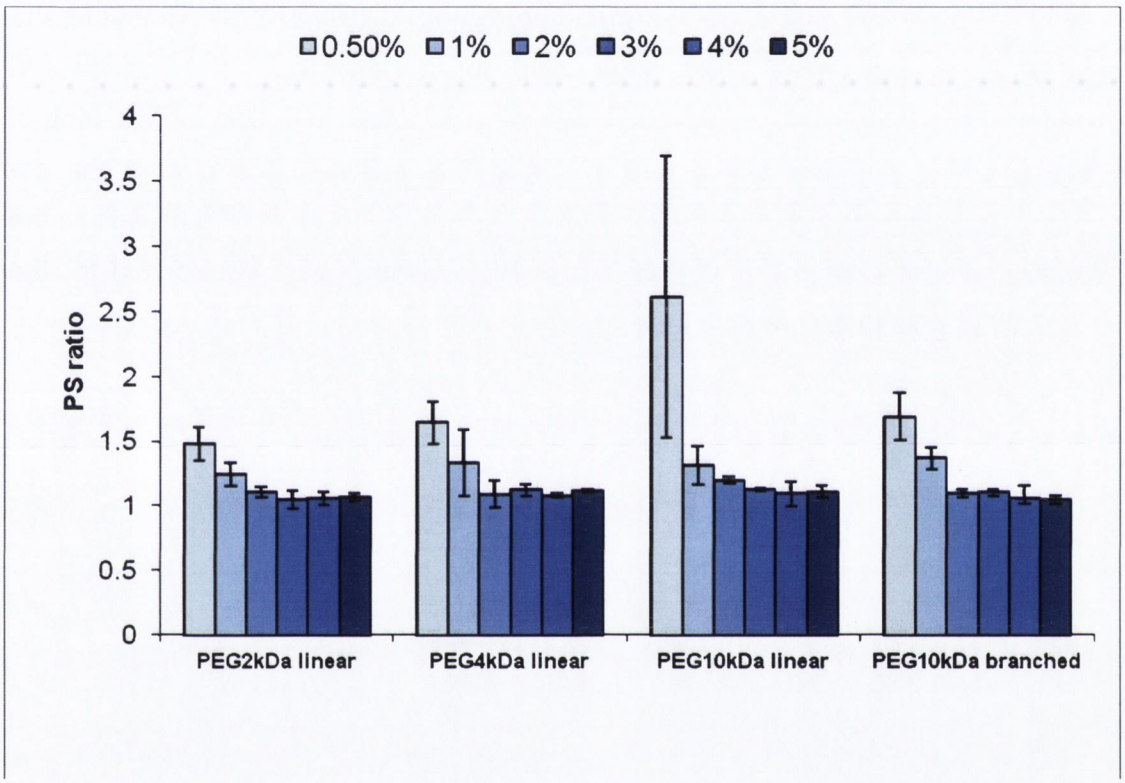

Fig. 8.14 The size ratio of HA/CL113 NPs with the MMR of 2.5 (TPC of 1 mg/ml) freeze-dried with variable concentrations of different PEGs.

X-ray diffractograms (Fig.8.15) and DSC scans (Fig.8.16) show that unprocessed PEG2000 was crystalline. A narrow endotherm with an onset at 52.8°C and peak at 54.3°C could be observed in the DSC thermogram. After freeze-drying PEG preserved its crystallinity, but the onset and peak of melting endotherm appeared at lower temperatures (49.4 and 52.8 °C, respectively) and the endotherm was broader compared to the unprocessed material with a higher ΔH. This may be a result of PEG conformation change. PEG has a helical conformation consisting of seven chemical units and two turns in a fibre identity period of 19.3 Å (Craig, 1995). On melting solid PEGs, the helical structure is lost and a liquid containing random coils is obtained. In aqueous solution the system retains the helical configuration, but in a less ordered form (Craig, 1995). It is possible that due to the rapid decrease in temperature, which takes place during freezing aqueous solution of PEG with the use of liquid nitrogen before the

lyophilisation process, some chain conformation changes occur which affect the thermal behaviour of lyophilised PEG. The crystalline character of PEG was preserved after freeze-drying with HA/CL113 NPs. All peaks present in the XRD diffractograms of the PEG/NP systems were similar to PEG on its own and no extra peaks were seen indicating that no new phase was formed. As the NPs did not show any clear thermal events, the endotherms seen in the DSC thermograms of all PEG/NP systems could be attributed to the melting of PEG. However, the endothermic peaks of PEG/NP systems were broader than that of the unprocessed material and the onsets occurred at lower temperatures. The observed lowering of the onset temperature and widening of the PEG melting endotherm in the co-processed samples may indicate interactions between PEG and NPs as well as the effects of processing. The ΔH values for PEG melting were determined for the PEG/NP freeze dried systems (see Appendix 7).

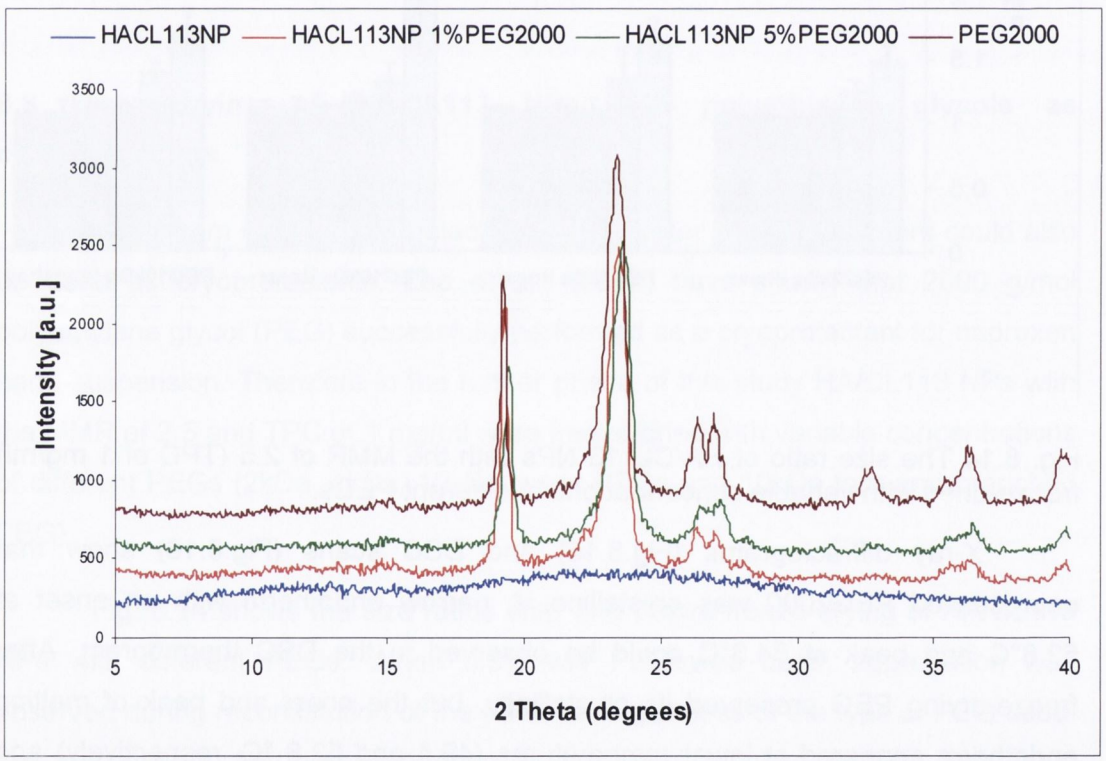

Fig.8.15 X-ray diffractograms of unprocessed PEG2000, HA/CL113 MMR of 2.5 NPs freeze-dried at TPC of 1 mg/ml without any excipient or in the presence of 1 or 5% w/v PEG2000.

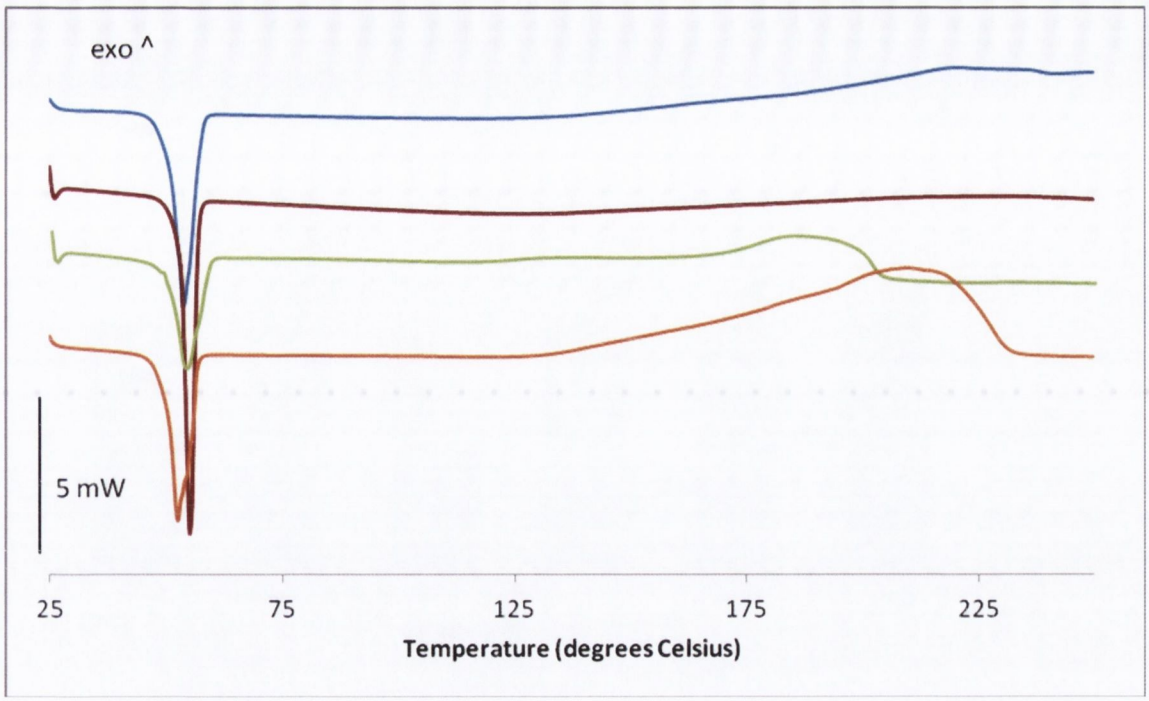

Fig. 8.16 DSC scans of PEG2000 (blue), lyophilised PEG2000 (brown), HA/CL113 MMR of 2.5 NPs lyophilised with PEG2000 (green), and a 1:1 w/w physical mixture of HA/CL113 MMR of 2.5 NPs with lyophilised PEG2000 (orange).

Cytotoxicity of all PEGs (i.e. 2 kDa, 4 kDa, 10 kDa linear and 10 kDa branched PEG) was tested at the same concentration of 5% w/v by MTS assay and flow cytometry in order to compare their toxic effects. The results are shown in Fig. 8.17 and scatter plots from the apoptosis assay are presented in Fig. 8.18. The cytotoxicity of 5% w/v trehalose is also shown in the same figures. It can be observed that, apart from 10kDa linear PEG, other PEGs were well tolerated by Caco-2 cells. MTS assay showed that the proliferation of the cells was slightly increased after incubation with 2 and 4 kDa linear PEGs or 10kDa branched PEG. A statistically significant decrease in the % of viable cells can be observed in the apoptosis assay for all these three PEGs, however the viability was decreased by only approximately 5%. Interestingly, linear 10kDa PEG decreased the viability of Caco-2 cells markedly (40.6±7.5% of viable cells remained by MTS assay).

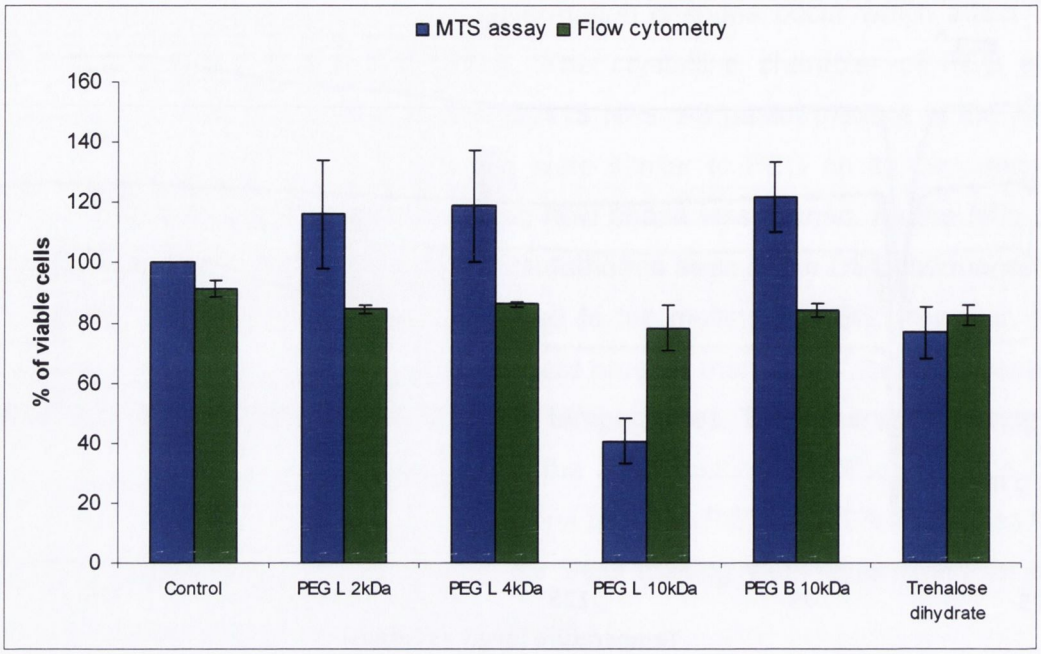

Fig.8.17. The viability of Caco-2 cells after 72-hour exposure to different cryoprotectants at the concentration of 5% w/v.

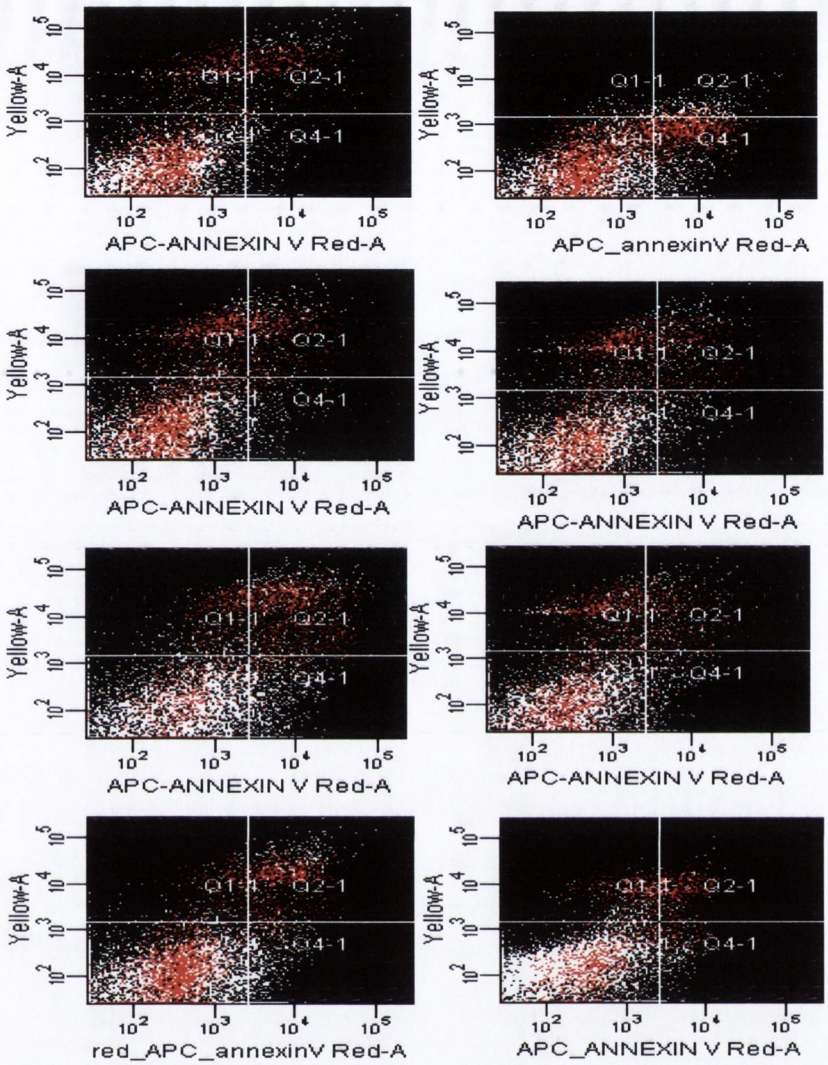

Fig. 8.18 Scatter plots of apoptosis assay: top left: serum-free medium, top right: 5% trehalose dihydrate, second row left: PEG 2kDa, second row right: PEG 4000kDa, third row left: PEG 10kDa linear, third row right: PEG 10kDa branched, bottom left: trehalose dihydrate 4%, bottom right: HA/CS MMR of 5 NPs TPC of 1 mg/ml.

As the linear 10kDa PEG was the most toxic from all cryoprotectants examined, the cytotoxicity of this PEG was also tested at lower concentrations, and the results are shown in Fig. 8.19. At 3 or 4% w/v linear 10kDa PEG remained toxic, however the detrimental effects were markedly reduced at 2% w/v and lower concentrations. The IC_{50} of 10kDa linear PEG was 2.5% w/v, therefore it can be considered as more toxic than trehalose.

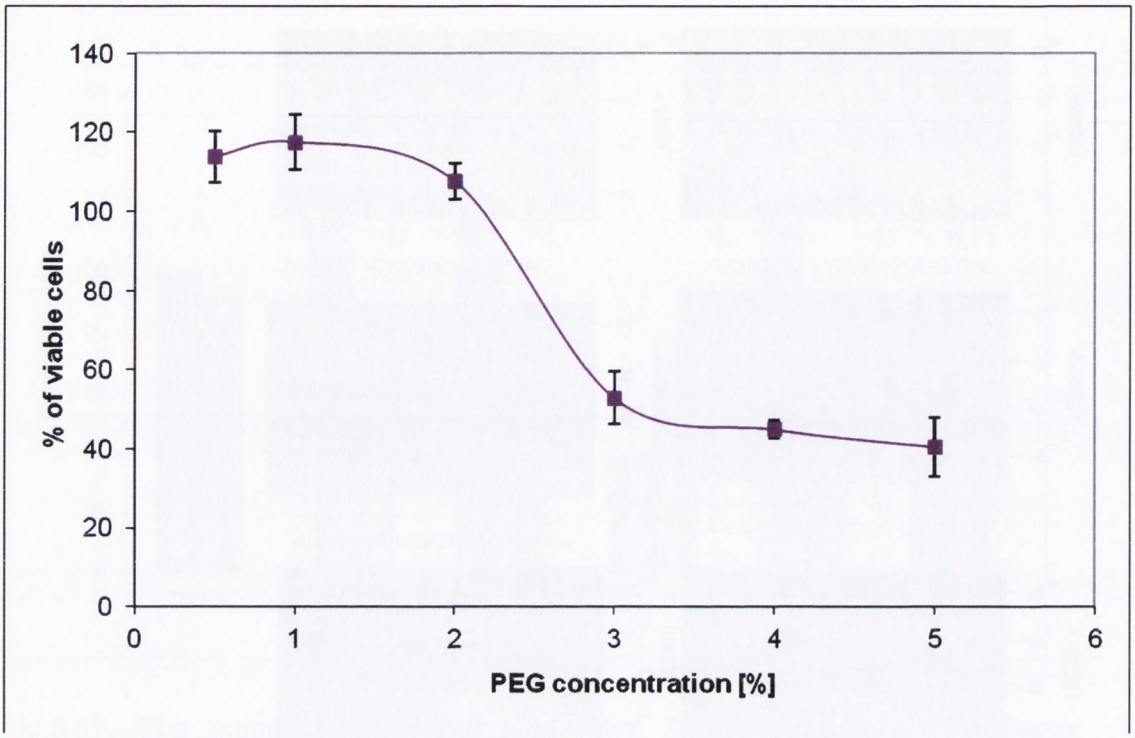

Fig. 8.19 The viability of Caco-2 cells treated with different concentrations of the solution of linear PEG 10 kDa in serum free media for 72 hours.

8.9 Freeze-drying of HA/CL113 NPs with a mixture of trehalose and PEG2000 as cryoprotectants

As PEGs were shown to be more effective cryoprotectants than trehalose, and all PEGs apart from linear 10 kDa PEG were less toxic to Caco-2 cells, attempts were made to decrease the concentration of trehalose required for the successful redispersion of HA/CL113 NPs with the MMR of 2.5 NPs and TPC of 1 mg/ml by freeze drying the nano-suspension with a mixture of cryoprotectants: trehalose and PEG. Also, it was of interest if a combination of these two excipients may have a synergistic effect, i.e. a lower amount of cryoprotectants will be needed for successful redispersion. It has been shown that the viscosity of aqueous PEG solutions increases correspondingly to an increasing molecular weight (González-Telo et al., 1994), therefore PEG with the lowest molecular weight (i.e. 2 kDa) was selected for further co-lyophilisation studies with trehalose. The total concentration of cryoprotectants was kept at 2% w/v, and three systems were tested: 1.5% w/v PEG+0.5% w/v trehalose (3:1), 1% w/v PEG+1% w/v trehalose (1:1) and 0.5% w/v PEG+1.5% w/v trehalose (1:3).

As shown in Fig. 8.20, the size ratio was below 1.2 for all three combinations. More importantly, aggregation was not observed. Therefore it can be concluded, that addition of PEG enabled to decrease the concentration of trehalose required to successfully freeze-dry HA/CL113 MMR of 2.5 NPs.

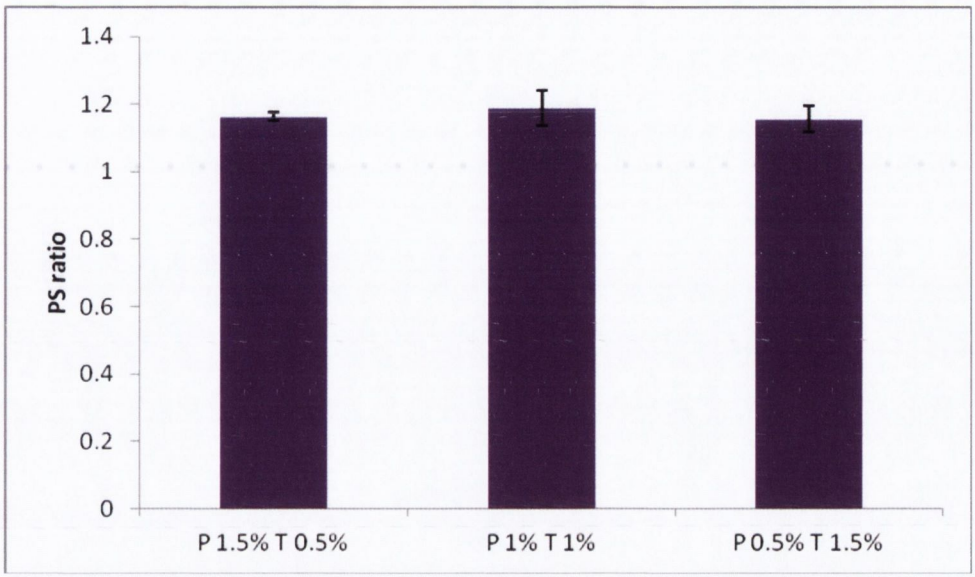

Fig. 8.20 The size ratio of HA/CL113 MMR of 2.5 NPs (TPC of 1 mg/ml) freeze-dried with the mixture of two cryoprotectants:trehalose and PEG 2000.

X-ray diffraction (Fig. 8.21) presented that lyophilisation of HA/CL113 NPs with all PEG/trehalose mixtures tested resulted in the formation of crystalline solid state materials. The peaks characteristic of PEG 2000 at approximately 19 and 23 2theta degrees were seen in all PEG/trehalose/NP diffractograms. Trehalose on its own has been shown to become amorphous after lyophilisation, however, a clear presence of crystalline trehalose dihydrate was noticed for the freeze dried 1 % w/v PEG+ 1% w/v trehalose/NP system and these peaks were more pronounced for the freeze dried 0.5% w/v PEG+ 1.5% w/v trehalose/NP sample. Hence the content of PEG dictates whether the sugar after freeze drying is amorphous or crystalline.

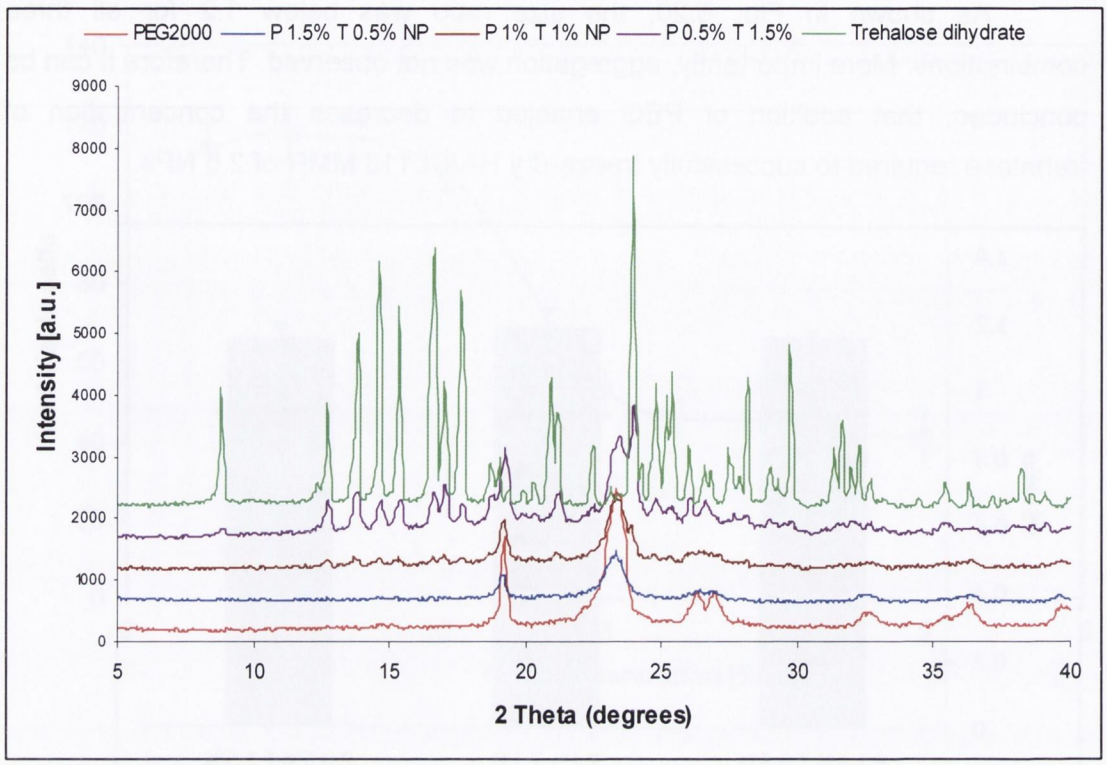

Fig. 8.21 X-ray diffractograms of unprocessed PEG2000, trehalose dihydrate, HA/CL113 MMR of 2.5 NPs freeze-dried at TPC of 1 mg/ml with 1.5% of PEG+0.5% of trehalose, 1% of PEG+1% of trehalose, and 0.5% of PEG+1.5% of trehalose.

DSC scans (Fig. 8.22) show the thermal characteristics of PEG/trehalose/NP systems. In all thermograms an endotherm was seen at approximately 50-55°C, which could be attributed to the melting of PEG. As the theoretical ΔH is lower for the PEG/trehalose 1:1 and 1:3 systems, it is postulated that interactions between PEG and trehalose and/or NPs may be present. For these two systems a Tg of trehalose was also identified, which appeared at a similar temperature (approximately 120°C) compared to that of the trehalose/NP freeze dried systems, but the event was slightly wider, especially for the PEG/trehalose 1:3 system. This Tg is a confirmation of the presence of amorphous trehalose, which was also deducted from XRD data. The Tg was not lowered by the presence of PEG, which excludes the polymer miscibility with the sugar.

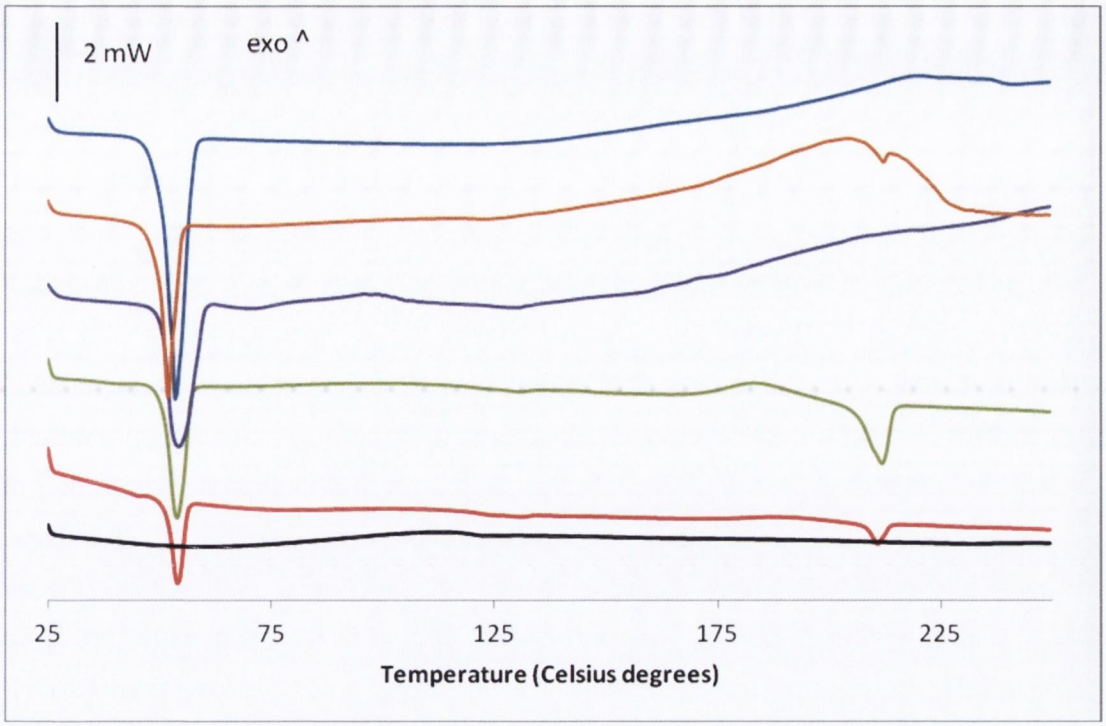

Fig. 8.22 DSC scans of lyophilised PEG 2000 (blue), HA/CL113 MMR of 2.5 NPs lyophilised with the PEG/trehalose weight ratio of 1:3 (brown), 1:1 (green), 3:1 (violet), a physical mixture of HA/CL113 MMR of 2.5 NPs, lyophilised PEG 2000 and lyophilised trehalose (orange) and lyophilised trehalose (black).

Crystallisation and melting of trehalose was visible in the thermograms of the PEG/trehalose 1:1 and 1:3 freeze-dried systems (Fig. 8.22). Crystallisation was characterised by an exotherm with an onset at 170-175°C (1:3 system) followed by an endotherm appearing at 205-208°C for both samples. The crystallisation exotherm was moved to a slightly lower temperature in the system with a smaller amount of trehalose (PEG/trehalose 1:1) and the melting endotherm was broader. A small endotherm of trehalose melting was also present in the physical mix, although this peak overlapped with an event of thermal degradation of sample and its assignment cannot be certain. Interestingly, no crystallisation was observed in the previously described freeze-dried amorphous trehalose. Therefore, it appears that the sugar in the PEG/trehalose freeze-dried 1:1 and 1:3 systems is present in an amorphous and the crystalline, dihydrate form and the crystalline content is driving the amorphous phase to crystallise. Neither crystallisation nor melting of trehalose was observed in the 3:1 system, thus this powder may be considered as physically stable (by DSC).

8.10 Summary and conclusions

Nanoparticles described in the previous chapters have been successfully obtained as solid state formulations with the employment of a lyophilisation process. Freeze-drying of NPs is a complicated process and the type and concentration of a cryoprotectants as well as the composition and concentration of NPs were found to influence the redispersibility of the polyelectrolyte complex NPs. The presence of a cryoprotectant was necessary to achieve a successful reconstitution. The concentration of trehalose, a commonly used cryoprotectant, should be optimised for each type of formulation, as the minimal concentration of cryoprotectant for reconstitution depends on the composition of the NPs. Protamine-based NPs were characterised by an excellent redispersibility, better than CS-based NPs. For the latter, HA-based NPs were found to better preserve their properties after freeze-drying with a lower amount of trehalose than CHON-based NPs. Also, the redispersibility of CS-based NPs depends on the MMR of CS and the type of polyanion (i.e. CHON or HA). Formulations with CHON/CS or HA/CS MMR of 5 were easier to be redispersed than formulations with lower mass mixing ratios.

PEGs were found to be more effective cryoprotectants than trehalose. PEG preserves its crystalline structure after lyophilisation with/without NPs, while trehalose becomes amorphous after freeze-drying. Also, since the freeze dried formulations containing PEGs are crystalline, they should have better storage stability. The addition of PEG enables to reduce the concentration of trehalose and the total concentration of cryoprotectants required for a successful reconstitution of HA/CL113 NPs with the MMR of 2.5 and TPC of 1 mg/ml.

PEGs were found to be well tolerated by Caco-2 cells, with the exception of linear PEG 10kDa. High concentrations of trehalose were also found to decrease the viability of Caco-2 cells. CS-based NPs freeze-dried with trehalose did not have pronounced toxic effects on Caco-2 cells and a slight decrease in the viability of cells was attributed to the high concentrations of trehalose. Moreover, protective effects on cells were observed in some formulations. PROT-based NPs, on the contrary, were found to decrease the viability of Caco-2 cells significantly, probably due to the toxic effects exerted by protamine.

In conclusion, freeze-drying has been demonstrated as a viable drying process that can be utilised in order to convert liquid nano-formulations into solid state forms.

9. *In vitro* and *in vivo* studies of anti-inflammatory effects of HA/CL113/sCT NPs

9.1 Introduction

Prolonged inappropriate local and systemic inflammatory responses contribute to the auto-immune based pathogenesis of rheumatoid arthritis (RA), which affects 0.5-1.0% of adults in the industrialised world (Scott et al., 2010). Persistent joint destruction accompanied by synovial inflammation is present. Disease-modifying anti-rheumatoid drugs (DMARDs) include methotrexate (MTX), leflunomide and TNFα inhibitors as single agents or in combinations (Scott, 2012). Small molecule therapeutics are generally given orally whereas biologics are administered by self-injection for systemic treatment. Anti-inflammatory glucocorticoids can be given orally in short courses to facilitate subsequent lower dose levels of long-acting DMARDS. Steroids are also frequently injected locally via the intra-articular (I.A.) route to specific joints displaying swelling and aggressive flare-up where they can instigate pain relief in RA patients for up to 8 weeks (Hoes et al., 2010).

In contrast, osteoarthritis (OA) is a chronic degenerative joint condition and is more prevalent than RA, affecting 60–70% of people older than 65 years, and 13% of the world's population (Matthews and Hunter, 2011). Knee OA displays degeneration, reflected by loss of articular cartilage components due to an imbalance between extracellular matrix destruction and repair (Ayral et al., 1996; Kuzmanova, 2000), inappropriate osteophyte formation and synovial inflammation (Wieland et al., 2005). Key aspects of cartilage pathogenesis in OA include metabolic signals and degradation driven by cytokine cascades associated with production of inflammatory mediators. The activated synovium releases proteinases and cytokines that accelerate destruction of cartilage. Chondrocytes from OA patients produce increased levels of inflammatory cytokines including IL-1β and TNFα, which, in turn, decrease collagen synthesis and increase degradation proteases, including matrix metalloproteinases (MMPs) (Gerwin et al., 2006). MMPs play a key role in cleavage of cartilage macromolecules including type II collagen and the cartilage proteoglycan, aggrecan. In destructive hip OA, patients displayed significantly elevated MMP-3 and -9 concentrations in synovial cells, synovial fluid, plasma, and sera (Masuhara et al., 2002; Tchetverikov et al., 2005). In contrast to RA, synovial inflammation in OA is mostly confined to local areas adjacent to pathologically damaged cartilage and bone. Although Type-1

cytokine inflammatory pathways mediated by TNFα, IL-1 and IL-6 are major targets for RA and form the basis of effective therapies including etanarcept, rituximab, and abatacept, similar inflammatory targets for OA joints, though likely, have yet to be confirmed (Chevalier et al., 2009; De Ceuninck et al., 2011).

Current treatment options for OA are more limited than for RA and there are no approved disease-modifying drugs. I.A. injections of corticosteroids (Habbib et al., 2010) as well as the viscosupplement, hyaluronic acid (HA) (Bellamy et al., 2006a) are widely used for symptomatic treatment of the knee joint. Effects of I.A. steroids on pain relief are moderate and short-lived, typically lasting for 3 weeks (Bellamy et al., 2006b), while systemic side-effects due to resorption include suppression of the hypothalamic-pituitary adrenal axis for up to 4 days, reduction in serum cortisol and temporary elevation of serum glucose (Habbib, 2010). Effects of a range of I.A.-delivered HA formulations for knee OA ascertained over 10 years in clinical use appear similar to those of I.A. steroids with respect to pain scores, but have less potential side effects and seem to last several weeks longer (Conrizier and Chevalier, 2008). Oral options for symptomatic treatment include paracetamol, NSAIDs, and opioids, however they risk serious side effects with long term use. Unlike RA, which is well relatively well served by a range of therapeutics, OA therefore requires development of new drug formulations that address long term pain relief, the arresting of structural joint degeneration and the sustained reduction of local inflammation. Of the potential candidates to alleviate inflammatory arthritis, sCT, is already approved as a second line nasal and injectable anti-resorptive treatment for osteoporosis (Maricic, 2012). Interest in sCT as a potential treatment for OA has increased due to discovery of beneficial metabolic actions on cartilage and bone turnover (Sondergaard et al., 2006). It inhibits MMP expression and blocks collagen degradation in articular chondrocytes exposed to TNFα/oncostatin M *in vitro* (Esenyel et al., 2012). Intriguingly, while oral formulations of sCT have reached Phase III clinical trials for both osteoporosis and OA (e.g. Karsdal et al., 2011), direct evidence of local anti-inflammatory effects of sCT is limited . An indirect benefit of sCT however was detected in the collagen-induced arthritis (CIA) rat where intra-peritoneal (I.P.) injections of sCT enabled sub-therapeutic doses of prednisolone to achieve adequate reduced paw swelling, thus potentially negating potential systemic side effects associated with prolonged use of high dose steroids (Mancini et al., 2007).

Joint–specific features of OA and RA makes a long-acting I.A. injection an attractive delivery approach as the drug can be retained locally to generate increased efficacy while minimizing systemic side effects at the lower dose levels

used (Gerwin et al., 2006; Burt et al., 2009). A hurdle to translation is that unformulated low molecular weight water soluble drugs are rapidly cleared from the synovial space and have short half-lives following I.A. delivery (Edwards, 2011), thus highlighting the need for novel nanoparticle or hydrogel formulations to provide sustained release over several weeks. Notable examples include I.A. injections of betamethasone in poly(lactic-co-glycolic acid) (PLGA) nanospheres in the antigen-induced rabbit where joint swelling and cell infiltration were reduced (Horisawa et al., 2002b), while methotrexate (MTX) entrapped in PLGA microspheres were also retained longer in rabbit joints compared to MTX solution (Liang et al., 2005). There is considerable debate over the design of the optimal particle composition and diameter for long-lasting retention and targeting to the articular cartilage and this is in part due to the wide range of species and inflammatory arthritis disease induction models used.

There is growing evidence that regulation of an intracellular class of transcription factors, nuclear receptors, plays a fundamental role in maintenance of chronic inflammation (Wang et al., 2008). Expression of the novel nuclear orphan receptor, NURR1 (NR4A2), has been correlated with disease activity in synovial tissue from human arthritic joints, an affect that was reduced by low dose MTX (Ralph, 2005). Furthermore, NR4A-activated genes are rapidly activated by inflammatory mediators in chondrocyte and endothelial cells (Ryan et al., 2009) and NR4A receptors have been identified as intermediate effector molecules for cytokine signalling in macrophages (Ryan et al., 2011). Macrophage exposure to lipopolysaccharide (LPS), cytokines, or oxidized lipids also trigger induction of the NR4A1, 2, and 3 receptors (Pei et al., 2005). There is considerable interest therefore in examining NR4A receptor as potential molecular targets in both RA and local OA: elevated expression is correlated in several inflammatory diseases while reduction in expression is associated with resolution (McMorrow and Murphy, 2011). While increased expression of better-known matrix metalloproteinases (MMPs) have long been associated with RA and OA inflammation and joint destruction (Mengshol et al., 2002), there are no specific inhibitors for either condition, so it is important to target other proteins including NR4A that may be involved in aberrant inflammation.

The aim of this work was to examine whether sCT, HA or HA/CL113/sCT NPs could reduce expression of activated NR4A and MMPs receptors in human chondrocytes and macrophages *in vitro* and evaluate the *in vivo* performance of the NPs after intraarticular delivery to the relatively new acute inflammatory arthritis serum transfer murine model, K/BxN (Monach et al., 2008; Christianson et al.,

2012). Intraarticular injections of HA are approved for OA of the knee joint as a supplement of the viscous properties of the synovial fluid (Bellamy et al., 2006a), however it was of interest to examine if HA also has pharmacological properties which could be useful in the treatment of arthritis, and for that reason HA-based nanoparticles were selected as a carrier for sCT. The HA/CL113/sCT NPs were prepared as described in Chapter 2 (Section 2.2.29.1). The absence of detectable amount of endotoxins was confirmed with the use of E-Toxate ™ kit (Section 2.2.29.2). The *in vitro* studies in chondrocytes and *in vivo* experiments in mice were performed by Dr. Sinead Ryan, currently Dublin Institute of Technology.

9.2 Effects of sCT, HA and HA/CL113/sCT NPs on the expression of NR4As and MMPs in cytokine-treated SW1353, THP-1 and U937 cells

At first primary experiments were conducted in order to verify the influence of different cytokines on the expression of NR4As (NR4A1, NR4A2 and NR4A3) and selected MMPs (MMP-1, MMP-3 and MMP-13). For this purpose, incubation of the following cell lines: SW1353, THP-1 and U397 with cytokines (PGE_2 and IL-1β) was carried out and lasted for 6 hours in order to capture the peak expression of NR4As and MMPs. It was found that MMPs were upregulated by IL-1β in all cell lines tested, while either IL-1β or PGE_2 rapidly and potently induced NR4A2 mRNA in human chondrocyte cells (SW1353) after 1 hour. The expression of NR4A1 and NR4A3 was induced to a smaller extent in case of both cytokines. The peak of expression was achieved after 1 hour.

In further experiments, HA, sCT and HA/CL113/sCT NPs were then assessed for their capacity to down-regulate mRNA expression of inflammation associated with NR4A2 and MMP-13 only in activated human cell lines. PGE_2 (1 μM) induced a 100-fold increase (compared to serum-free medium) in expression of NR4A2 mRNA in SW1353 cells after 1 hour of incubation (Fig. 9.1A). After a further 90 minutes incubation, sCT (100 nM), HA (100 nM) as well as a mixture of the two agents were able to inhibit PGE_2 induced NR4A2 transcript levels by 49%, 41% and 91%, respectively (Fig. 9.1A). The reduction measured with the mixture of sCT and HA was comparable to that attained with dexamethasone (100 nM), which is known to down regulate NR4A, used for the treatment of rheumatoid arthritis and used here as a positive control in all experiments. Similar results on NR4A2 expression was achieved in PGE_2-activated THP-1 (Fig. 9.1B) and in IL-1β-activated (Fig. 9.1C).

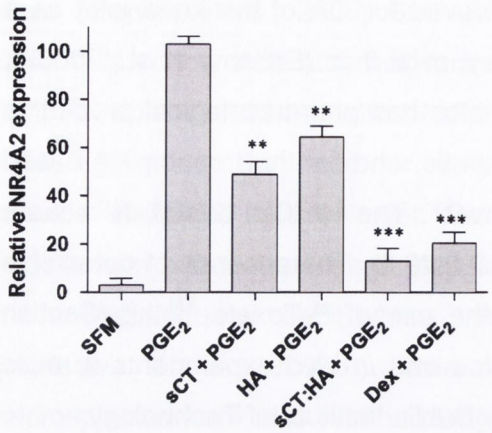

A)

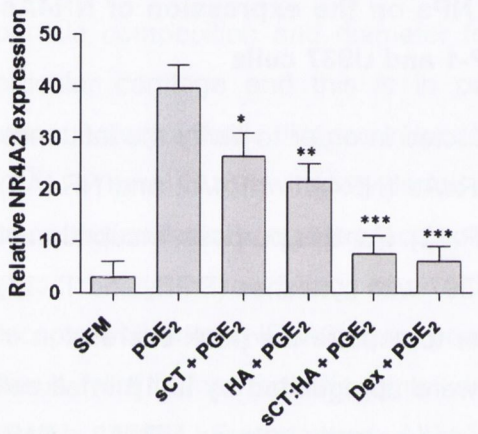

B)

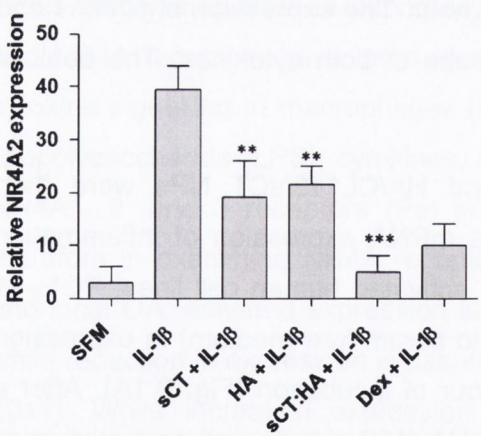

C)

Fig.9.1 Reduction in activated NR4A2 expression by sCT, HA and a mixture thereof. A) SW1353 chondrocytes, B) THP-1 monocytes, C) U937 macrphages. Cells were pre-stimulated with either PGE_2 (1 µM, A, B), or IL-1ß (10 ng/ml, C) followed by sCT (100 nM), HA (100 nM), the mixture of sCT:HA (100 nM each) or dexamethasone (Dex, 100 nM) for 90 min in the presence of the stimulating agents. SFM: Serum-free medium. NR4A2 mRNA levels were normalised to GAPDH. *$p < 0.05$, **$p < 0.01$ and ***$p < 0.001$ versus PGE_2 (A, B) and IL-1β (C), n=3 for each group.

Figure 9.2A shows that IL-1β increased the MMPs mRNA expression dramatically, by approximately a 270-fold for MMP13 in SW1353 cells. The cytokine induced mRNA expression was reduced by 47% by sCT and by 30% by HA. Dexamethasone, used as a positive control, was shown to reduce MMP-13 mRNA expression by 83%, similar to that of HA/sCT (by 87%). Therefore, similarly to NR4A mRNA expression, complexation between HA and sCT reduced the cytokine-induced MMPs expression markedly more than either HA or sCT alone. Figure 9.2B illustrates that in cytokine-treated THP-1 macrophage cells the relative expressions of MMP-13 increased approximately 40-fold compared to serum-free medium. sCT and HA reduced the relative expression of MMP-13 45% for sCT and 50% for HA. A markedly larger decrease in MMP-13 expression was observed after treatment with either dexamethasone (71%) or HA/sCT NPs (81%). In U937 macrophages, IL-1β caused a 45-fold increase in MMP-13 expression compared to serum-free medium. sCT decreased the expression of MMP-13 by 33%, while for HA the reduction was 31%. Again, dexamethasone was more effective in reduction of MMPs expression (76% for MMP-13). The decrease in MMPs mRNA level caused by HA/sCT NPs was again markedly higher (71%) than HA or sCT alone.

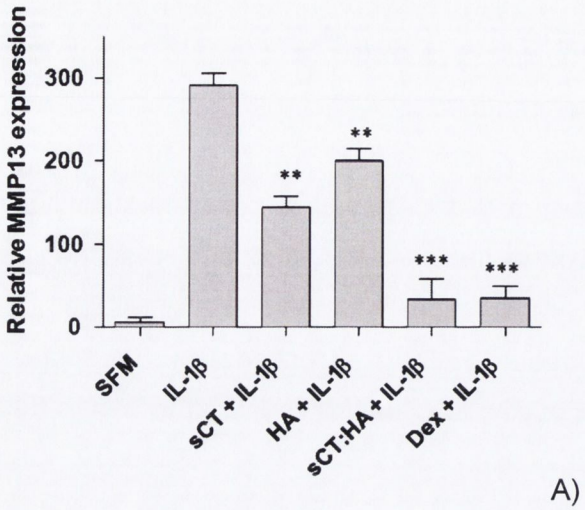

A)

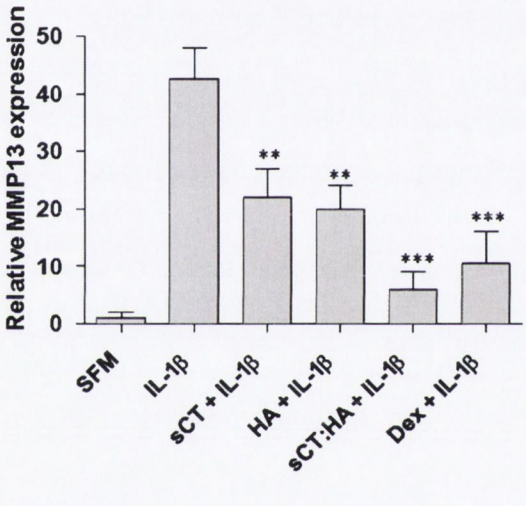

B)

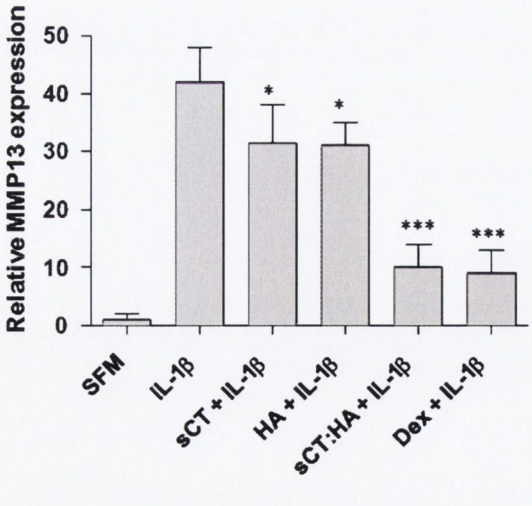

C)

Fig.9.2 Reduction in IL-1β-stimulated MMP13 expression by sCT, HA and a mixture thereof. A) SW1353 chondrocytes, B) THP-1 monocytes, C) U937 macrophages. SFM: Serum-free media control. Concentrations and timings as for Fig. 1XXX. MMP-13 mRNA levels were normalised to GAPDH. *p<0.05, **p<0.01 and ***p<0.001 versus IL-1β, n=3 for each group.

In summary, the above cell culture studies indicate that sCT is involved in the inactivation of the NR4A receptor signaling pathways. Its potency is enhanced when incorporated into HA. As MMPs are downstream biomarkers of inflammation from NR4A pathway, the data confirms that the sCT/HA combination have anti-inflammatory actions at two different sites on the pathway in the cell lines tested. The results clearly show that combinations of HA with sCT give superior effects than either agent alone at the same concentration.

9.3 Effects of I.A. administration to K/BxN mouse model of arthritis

The K/BxN mouse model of arthritis was used to confirm the *in vitro* data and to assess the therapeutic effect (reduction in inflammation in the knee) of intra-articular delivery of the HA/CL113/sCT NPs into the knee.

Mice expressing the KRN T cell receptor transgene and the MHC class II molecule A(g7) (K/BxN mice) develop severe inflammatory arthritis and serum from these mice causes similar arthritis in a wide range of mouse strains, owing to pathogenic autoantibodies to glucose-6-phosphate isomerase (GPI). This model has been useful for the investigation of the development of autoimmunity (K/BxN transgenic mice) and particularly of the mechanisms by which anti-GPI autoantibodies induce joint-specific inflammation (serum transfer model) (Monach et al., 2008).

Passive K/BxN arthritis is an antibody-induced arthritis that is dependent solely on innate immunity, including complement, neutrophils, mast cells, and macrophages. These mice develop an arthritis that is mediated, and transferable, by circulating antibody against GPI. The K/BxN model has distinguishing features: (i) spontaneous disease (24-48 hrs) (ii) ability to transfer disease to a wide range of recipient strains using serum containing the pathogenic autoantibodies; (iii) robust development of arthritis in 100% of transgenic animals and nearly 100% of wild-type mice that have received K/BxN serum; and (iv) inflammation is confined to the 4 paws (Monach et al., 2008).

NR4A mRNA levels were found to be elevated in inflamed ankles from K/BxN mice and I.P. administration of Dex reduced both NR4A2 expression and inflammation. A reduction in paw volume (Fig. 9.3A) and an improvement in overall clinical score (Fig. 9.3B) were observed within 24 h following daily I.P. injections of 30 µg Dex from Day 2–5, compared to untreated K/BxN mice; Improvements in both parameters were sustained to Day 7. Dex significantly reduced NR4A2 mRNA

expression in K/BxN mice compared to mice with untreated inflammation at Day 7 (Fig. 9.3C).

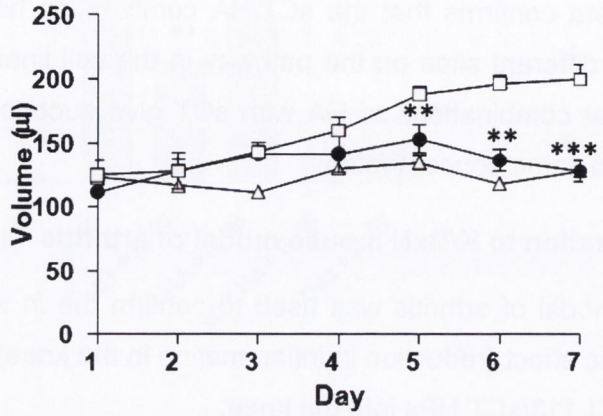

A)

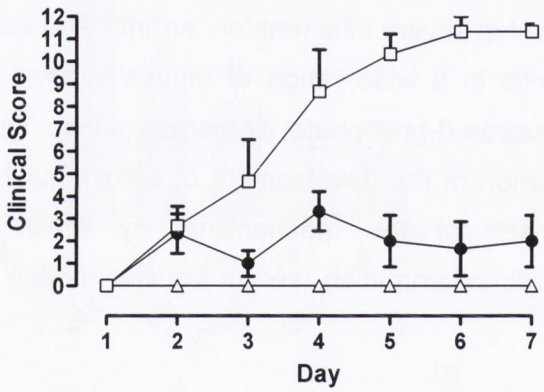

B)

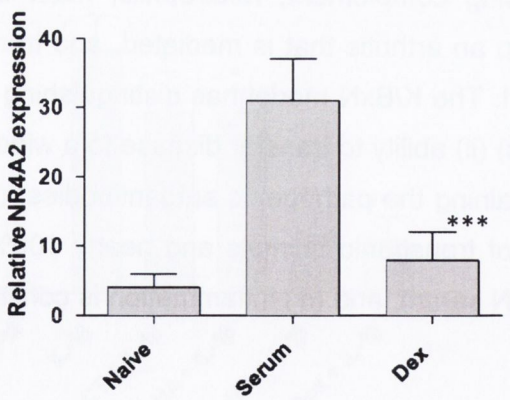

C)

Fig.9.3 Inflammation was induced by K/BxN serum I.P. injection on Day 1 and Day 3. Dex or controls were administered daily by I. P. from Day 2 (arrow) to Day 5. A: Paw volume, B: clinical score. Groups (Mean ± SEM of 5 mice): (•) Dex, 30 µg, (□) serum, (Δ) naïve. Comparison between Dex and serum: *$p < 0.05$, **$p < 0.01$ and ***$p < 0.001$. C: Dex reduced NR4A2 mRNA expression compared to serum control at Day 7. ***$p < 0.001$ versus serum-treated.

The K/BxN mouse model of arthritis was also used to assess reduction in inflammation in the knee following I.A. delivery of sCT/HA NPs. Mice developed a clinical score >1 in at least one paw before treatment. Drug treatments were injected by the I.A. route into the right knee, while PBS (internal control) was injected into the left knee of the same mouse. A reduction in inflammation was seen with the sCT/HA NP treatment compared to PBS in the same mouse (Fig. 9.4). Figure 9.5 depicts the effects of sCT/HA NP delivered by a single injection by the I.A. route on reduced knee diameter over time (Fig. 9.5A) and the clinical score of the ankle joint (Fig. 9.5B) when administered to the K/BxN mice. All formulations reduced knee diameter; comparable reductions in swelling were seen with the NP formulation with that of dexamethasone. Importantly the reduction in diameter seen with the nanoparticles was better than for sCT alone, the overall dose of sCT being the same in both groups. As expected, the overall clinical score was unchanged by any treatment as that refers to all four paws, for which 3 were untreated. Expression of NR4A2 was measured in all test groups (Fig. 9.5C). Anti-inflammatory treatments sCT, sCT-NP and dexamethasone reduced NR4A2 expression however the effect of sCT-NP in reducing NR4A2 expression was superior to sCT.

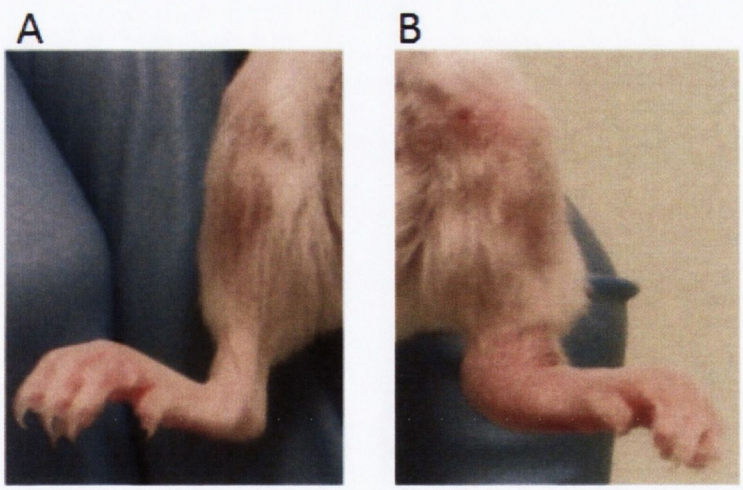

Fig.9.4 I.A. administration in the same mouse A) right hind knee: HA/CL113/sCT NPs; B) left hind knee: PBS

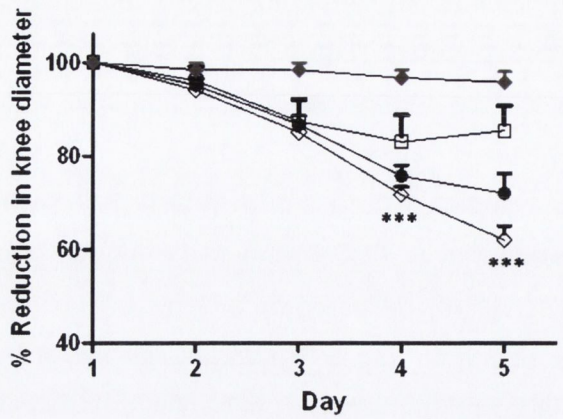

A)

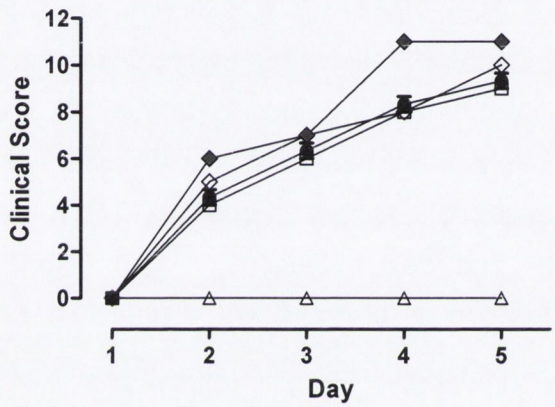

B)

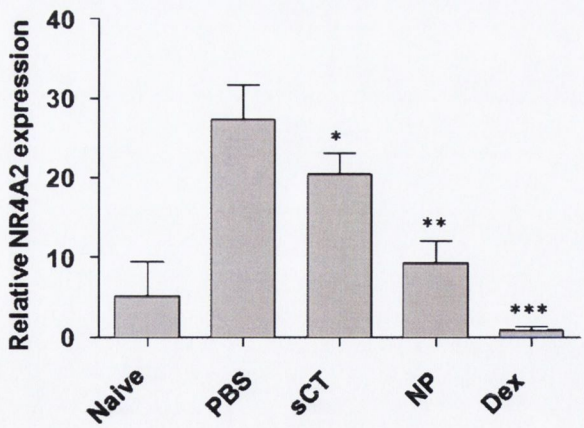

C)

Fig.9.5 Inflammation was induced by I.A. injection of K/BxN serum on Day 1. Treatments were administered once on Day 2. NP delivered by the I.A. route reduced knee diameter and NR4A2 expression in K/BxN mice. A: Knee diameter. ♦PBS, □ sCT (0.2 µg), ◇ NP (0.2 µg), ● dex (0.2 µg). Naïve not included as diameter not increased per se. B: Clinical score. Symbols as for A, but with 'Δ, naïve' included. ***$p < 0.001$ comparing NP to PBS. C: NR4A2 mRNA ankle joint expression at Day 5. *$p < 0.05$, **$p < 0.01$ and ***$p < 0.001$ versus PBS. Mean ± SEM of n= 5 mice in each group.

Figure 9.6A illustrates histological analysis of knee joints from K/BxN mice exposed to different treatment groups. The left panel represents histology analysis of knee joint tissue sections stained with H & E that were injected with PBS by the I.A. route (control). The right panel represents histology analysis of knee joints that received different treatments. The naive group represents a healthy knee, whereas the serum-induced treatment group represents severe cartilage and bone destruction as well as synovitis infiltration. Importantly, preservation of bone architecture was seen with sCT, sCT:HA-NP and dexamethasone. Histology sections of the knee joints were also scored by a blind observer under different categories (i) inflammation (synovitis infiltration and pannus formation), (ii) cartilage erosion and (iii) bone erosion (Fig. 9.6B). sCT:HA-NP preserved bone and cartilage and reduces synovitis infiltration damage compared to controls. In order to take a closer look at cartilage and bone preservation, histology sections of the knee joint were stained with Saffarin O (Fig. 9.7). In comparison to control (Fig.9.7A) and free sCT (Fig. 9.7B), sCT-NP preserved bone and cartilage (orange) and reduced synovitis infiltration damage (Fig. 9.7C). It further shows the effectiveness of the sCT-NP therapy since there is evidence of cartilage regeneration. Importantly the NPs gave greater cartilage protection than sCT showing that formulated into a nanocomplex improves the therapeutic effect and sustained release of sCT showing the I.A. route of delivery has great potential.

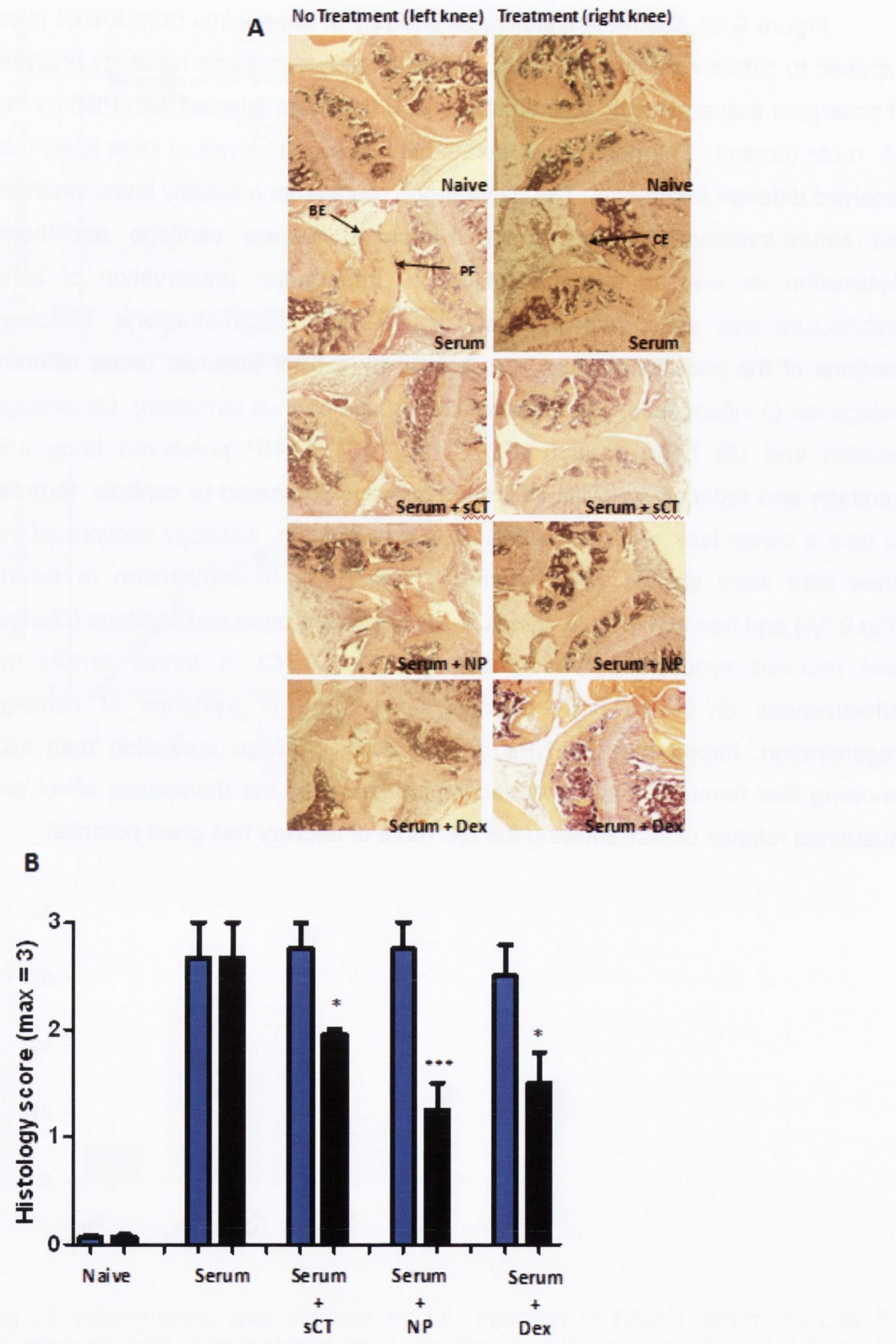

Fig. 9.6 Representative histological sections of knee joints from K/BxN mice were stained with H&E stain. A) represents left knee which was injected by the IA route with saline only (no treatment) and right knee injected intra-articularly with treatment. CE: cartilage erosion, BE: bone erosion and PF: pannus formation. B) Knee joint sections were scored by an observer blinded to treatments. No treatment: (left knee, blue columns). Treatment: (right knee, black columns). The results are mean ± SEM of 5 mice in each group. *$p<0.05$ and ***$p<0.001$.

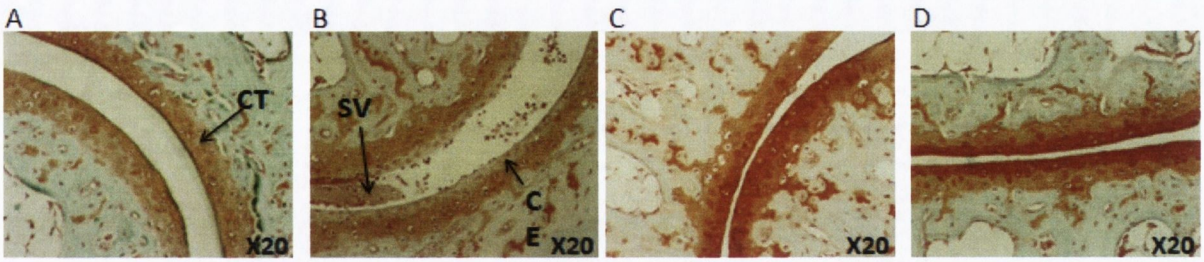

Fig. 9.7 Cartilage analysis of knee joints from K/BxN mice stained with Saffarin O.A) Control B)sCT, C) sCT:HA NP and D) Dex. Cartilage (CT), cartilage erosion (CE) and synovitis and cellular infiltration (SV).

The beneficial effects of formulating sCT and HA into a polymeric nanoparticle when delivered in a single injection by the I.A. route could be seen on reduction of knee diameter over time when administered to the K/BxN mouse model. Importantly the reduction in diameter seen with the nanoparticles was better than for sCT alone, the overall dose of sCT being the same in both groups was superior to free sCT in cartilage and bone preservation, less systemic inflammation and potent when compared to dexamethasone which is one of the current treatments of rheumatoid arthritis. This study suggests that a single I.A. injection of sCT-NPs was a relatively safe and effective treatment in the early phase of inflammatory arthritis in the K/BxN mouse model.

Chitosan was also a component of the NPs, however as the concentration of this polymer is much lower than HA, its relevance to anti-inflammatory and bone preservation effects is unlikely to be very significant. Also, its potential as a microsphere carrier for COX-2 inhibitors for I.A. delivery to rats has already been demonstrated (Thakkar et al., 2004).

9.4 Summary and conclusions

Both, sCT and HA down regulated NR4As and certain MMPs in human chondrocytes and macrophages cell lines. However HA/CL113/sCT NPs produced markedly higher reduction in NR4As and MMPs mRNA expression than HA or sCT, with the efficacy alone comparable to dexamethasone which is used in the treatment of rheumatoid arthritis. The ability of sCT and HA/CL113/sCT NPs to modulate the NR4A2 and MMP inflammatory pathways is novel. Therefore, *in vitro* data suggest that in a localized polymeric conjugate form, sCT could have anti-inflammatory actions in arthritis.

In the K/BxN mouse model of inflammatory arthritis, HA/CL113/sCT NPs delivered by the IA route reduced knee diameter over time. Histology of the knee joint also showed that sCT-loaded HA/CL113 NPs preserved both bone and cartilage and reduced synovitis infiltration damage compared to controls. sCT formulated into a NP was superior to free sCT in cartilage preservation showing that formulation into NPs improved the therapeutic effect and sustained release of sCT demonstrating that IA route of delivery has great potential. HA/CL113/sCT NPs may have potential for either long-acting systemic injection for osteoporosis or for local intra-articular delivery for treatment of osteoarthritis.

10. General discussion

10.1 Introduction

The full market potential for salmon calcitonin (sCT) has not yet been reached due to the low patient compliance associated with the injectable dosage forms (Guggi et el., 2003) and poor bioavailability from the commercial nasal spray, Miacalcin® (Hinchcliffe et al., 2005). Therefore the development of a new, more compliant delivery system for sCT is of a vital importance. Polymeric nanoparticles represent an interesting strategy because of their abilities to entrap macromolecules, protect them against degradation and enhance their transmucosal transport (de la Fuente et al., 2008a).

The studies in this thesis focused on the design and development of new polyelectrolyte complex-based nanoparticulate carriers as potential delivery systems for sCT. At first, the conditions for the formation of sCT-free NPs were determined and the manufacture process of NPs was optimised by examining if the different formulation variables (e.g. the type of polymers used: their molecular weight, charge density, concentration and mixing ratio of the polymers) have an influence on the properties of resulting NPs. sCT was then incorporated into selected formulations and the impact of the peptide on the physicochemical properties of the particles such as size, zeta potential, polydispersity index as well as the association efficiency, drug loading and release was examined. Selected formulations were freeze-dried in order to obtain powdered forms of the nanoparticles intended for long-term storage. Also, cytotoxicity studies of cryoprotectants and selected formulations in the Caco-2 cell line were performed.

10.2 Preparation of polyelectrolyte complex nanoparticles

Recently, considerable efforts have been dedicated towards incorporation of active ingredients into biodegradable nanoparticles (Hamidi et al., 2008). Among polymeric nanoparticles, NPs composed of polyelectrolytes (polyelectrolyte complex nanoparticles) attract particular attention e.g. because of their water-soluble character (Hartig et al., 2007).

Polyelectrolyte complex formation is mainly caused by strong Coulomb interactions between oppositely charged polyelectrolytes, whereby the gain in entropy due to the release of the low molecular counterions initially bound to polyelectrolytes plays a decisive part (Dautzenberg et al., 2002, Schatz et al., 2004). Other inter-macromolecular interactions, e.g. hydrogen bonding, van deer Waals forces, hydrophobic interactions or dipole-charge transfer may also be

involved in the formation of polyelectrolyte complexes (Schatz et al., 2004), nevertheless they are considerably weaker than Coulombic interactions and therefore would have to occur in a great number in order to exert a more significant effect.

At certain conditions, polyelectrolyte complexes can precipitate in the form of colloidal size particles. Usually, there is a narrow window of physicochemical conditions where the complexes are formed and stay in the form of colloidal dispersion (de Kruif et al., 2004). The process of NP formation should be conducted in diluted solutions in order to prevent macroscopic gelation that leads to bulk hydrogels (Oh et al., 2009). The stability of polyelectrolyte complex NPs depends on the repulsion between similarly charged particles. When the charge is neutralised, aggregation occurs. Therefore the net charge of the system must be either strongly positive or strongly negative if the system is to be colloidally stable.

All NPs described in this thesis (i.e. HA/CS, HA/PROT, CHON/CS and CHON/PROT NPs with and without sCT and CHON/sCT NPs) were spontaneously formed using mild conditions of manufacture, by simply mixing aqueous polyelctrolyte solutions at room temperature. Similar methods were used in order to obtain CS/HA/TPP NPs (de la Fuente et al., 2008a,b), HA/polyarginine NPs (Oyarzun-Ampuyero et al., 2011) or CHON/CS NPs (Yeh et al., 2012). Some of the authors encountered problems with precipitation of the complexes and consequently the loss of particles - it was necessary to keep the system at rest for some time (e.g. 24 hours) to allow sedimentation of the larger particles. This type of treatment is described by e.g. Boddohi et al., (2009) (HA/CS NPs) and Fajardo et al., (2011) (CHON/CS NPs). However, as shown by e.g. de la Fuente et al., (2008a, b, c), Yeh et al., (2011) and here, by appropriate optimisation of the formation process it is possible to obtain either HA/CS or CHON/CS NPs in the form of colloidal dispersion without phase separation.

For HA-based NPs, ultrasonication was used in order to reduce the high molecular weight (2882 kDa) of HA (see Chapter 3). However, the sonication process was conducted before incorporation of the active or the formation of NPs, therefore only HA was exposed to ultrasounds. This part of this thesis suggest that if feasible, HA with low (i.e. approximately 500 kDa or lower) molecular weight should used as a starting material to form NPs to avoid the sonication step.

The process of preparation of polyelectrolyte complex does not involve the use of organic solvent or surfactants and a homogenisation step is not needed. This is undoubtedly an advantage over the commonly used polyesters (e.g. PLA

and PLGA), which require the use of organic solvents, surfactants and sometimes high temperature or homogenization (des Rieux et al., 2006).

Also, in the case of drug-loaded NPs the isolation of non-associated cargo molecule is a very important issue. It is essential to point out that the ability to isolate formulations with the use of centrifugation (Oyarzun-Ampuyero et al., 2011) or combined ultrafiltration technique (Prego et al., 2006) circumvents tedious time consuming procedures, such as those performed by Kim et al., (2009), who isolated and purified the NPs by dialysis over 2 days.

10.3 Design of new polyelectrolyte complex-based nanocarriers

10.3.1 Polyelectrolyte components of investigated NPs

Polyelectrolyte complex nanoparticles composed of naturally occurring, biocompatible and biodegradable polymers have been examined recently as they are promising systems for the delivery of macromolecules (e.g. peptides, nucleic acids) (Hartig et al., 2007). Many of the polyelectrolytes used in the production of nanocarriers, e.g. HA and CS have mucoadhesive properties (Wadhwa et al., 2010). In this thesis, two polycations (i.e. chitosan and protamine) and two polyanions (hyaluronic acid and chondroitin sulphate) were examined as candidate components of polyelectrolyte complex NPs. These NP components are characterised by different molecular weights and charge densities. The properties of the polymers used in this thesis are summarised in Table 10.1.

Table 10.1 Summary of the properties of the polymers used for the fabrication of polyelectrolyte complex nanoparticles.

Polyelectrolyte	Mw [kDa]	Strength of acidic/basic groups	Charge density
HA	176-2882	Carboxylic group - weak acid	very low
CHON	59	Sulphonate group - strong acid Carboxylic group - weak acid	low
CS	42-398	Primary amine group - weak base	low
PROT	5.1	Guanidinium group - strong base	high

Protamine was characterised by a markedly smaller molecular weight than other polymers used in the formation of polyelectrolyte complex NPs and had the highest charge density. A few different molecular weights of HA and chitosan were examined in this thesis. As shown in Chapter 3, the use of high molecular weight of HA (more than 590 kDa) was unfavourable, as aggregation of the particles occurred. The use of the chitosans with the highest molecular weights (i.e. G213 - 398 kDa and CL213 - 340 kDa) in the formation of the NPs with HA257 also produced aggregation. Interestingly, HA with the molecular weight of 590 kDa, greater than those of the above chitosan types, produced stable colloidal dispersions with CL113 (110 kDa). Nevertheless, the use of polymers with high molecular weight to form NPs is not recommended.

The molecular weight of the polymer has an important effect on the viscosity of its solutions. As shown in Table 3.2 (Chapter 3) the dynamic viscosity of HA solution dramatically decreases with the decrease in molecular weight of HA. It can be seen (Table 12.5.1, Appendix 5) that the dynamic viscosity of polymer solutions corresponds to the molecular weight of the polymer. For instance, 1 mg/ml solutions of CHON or CL42 have the viscosity of approximately 1.2 mPa*s, CL113 - 1.76 mPa*s and HA257 - 2.14 mPa*s. The viscosity was found to be influenced by the concentration of the polymer (Table 12.5.1, Appendix 5). High viscosity may impair the mixing process and so favour the formation of aggregates/microparticles (Mackay et al., 2006). Therefore polymers with lower molecular weights (e.g. CHON, CL42) may produce NPs even at concentrations 3 or 5 mg/ml, in contrast to higher molecular weight polymers.

The polymers used differed also in terms of their charge sign, charge strength and charge density. CHON and PROT contain strong acid and base groups in their molecules (Table 10.1). Chitosan is a weak base, while HA is a weak acid. Strong polyelectrolyte complexes are generally formed between polymers including anions and cations of strong acids or bases in their structure (Denuziere et al., 1996). In contrast, weak polyelectrolyte complexes are formed between weak acids and bases. Therefore it is expected, that from the pairs of polyelectrolytes tested HA /CS forms the weakest complex, while the strongest complex is obtained for the CHON/PROT combination.

Considering all polyelectrolytes tested, PROT has the highest charge density, CHON and CS have low charge density, while the charge density of HA is very low (Denuziere et al, 1996).

10.3.2 Physicochemical characteristics of investigated NPs

10.3.2.1 Viscosity

Fig. 10.1 compares the viscosity of selected dispersions. It can be observed that the viscosities of CHON-based dispersions were noticeably lower than the viscosity of HA-based dispersions. This trend was observed for both, CS and PROT-based systems. On the other hand, the viscosity values of CS-based dispersions did not differ markedly. However, between the mass ratios of approximately 1.2-2, the viscosities of all systems tested are similar, with the values between 0.89-0.95 mPa*s, regardless of the polyanion used. As explained in Chapter 3, the polymer mixing ratio had a considerable influence on the viscosity of NP suspensions and lower viscosity values were measured for lower charge mixing ratios. Viscosity was also observed to increase with an increase in the concentration of the polymers, but this effect was less pronounced between polyanion/polycation MMR 1.2-2.

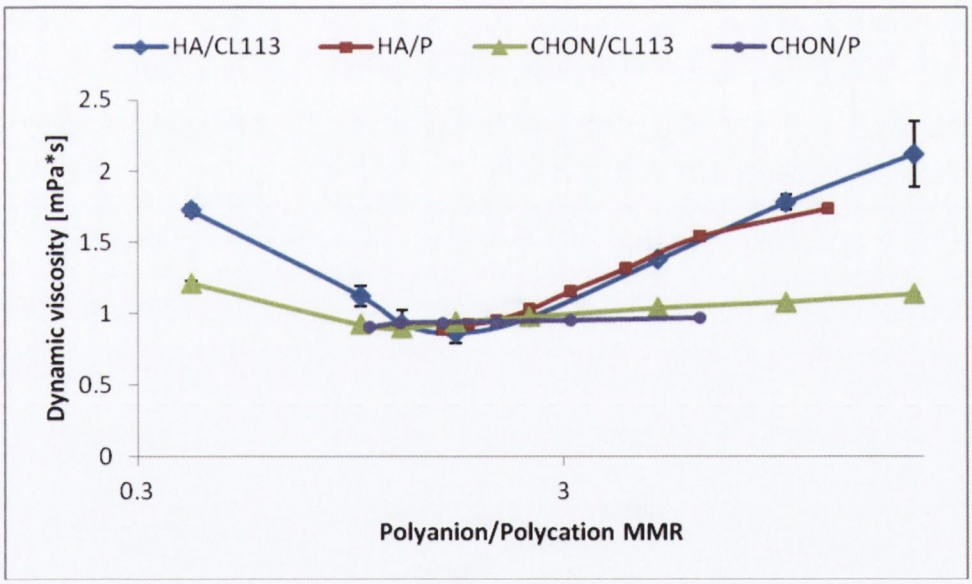

Fig. 10.1 Dynamic viscosity of HA/CL113 and CHON/CL113 (TPC of 1 mg/ml) dispersions as well as HA/PROT and CHON/PROT dispersions (HA and CHON concentrations of 0.7 mg/ml). HA257 was used for HA-based NPs. P=PROT

10.3.2.2 Particle size and size distribution

Fig. 10.2 shows the particle size of selected polyelectrolyte complex NPs. It was possible to obtain small (i.e. below 200 nm or even 100 nm) NPs in the case of all systems tested (i.e. HA/CS, CHON/CS, HA/PROT and CHON/PROT) (Fig. 10.2). HA/CS NPs were generally larger than HA/PROT or CHON-based NPs. In general, HA/CS NPs were the largest. However, at polyanion/polycation MMRs between 1 and 20 CHON/CL113 NPs were characterised by similar particle size.

The reduction in the molecular weight of chitosan caused an important reduction in the particle size. CHON/CL42 NPs were markedly smaller than CHON/CL113 NPs. In general, CHON/PROT NPs had similar size to CHON/CL42 NPs, and they were markedly smaller compared to CHON/CL113 NPs. Similarly, HA/PROT NPs were noticeably smaller than HA/CL113 NPs with the exceptions of the lowest polyanion/polycation MMRs (2.5 and lower). Interestingly, positively charged HA/CL113 NPs with the lowest HA/CL113 MMR (0.4) were large (500 nm) and similar CHON/CL113 NPs were by 300 nm smaller. The sizes of the particles described in this thesis are in agreement with data on other polyelectrolyte-based NPs already published. Generally, polyelectrolyte-based NPs have the size in the range of tens or hundreds nm and the NPs below 100 nm can be considered as very small. HA/PROT NPs were the smallest HA-based NPs described so far, and similarly- CHON/CL42 and CHON/PROT NPs were the smallest CHON-based NPs described when comparing to published reports. HA/CS NPs described by de la Fuente et al., (2008b) were generally smaller than those shown in this thesis (most of them were between 125-200 nm), but the smallest HA/CL113 NPs presented here also are in this range. The incorporation of TPP (cross-linker used by de la Fuente et al. (2008b) may decrease the size of the particles, similarly to a decrease in size caused by sCT (Chapter 4).

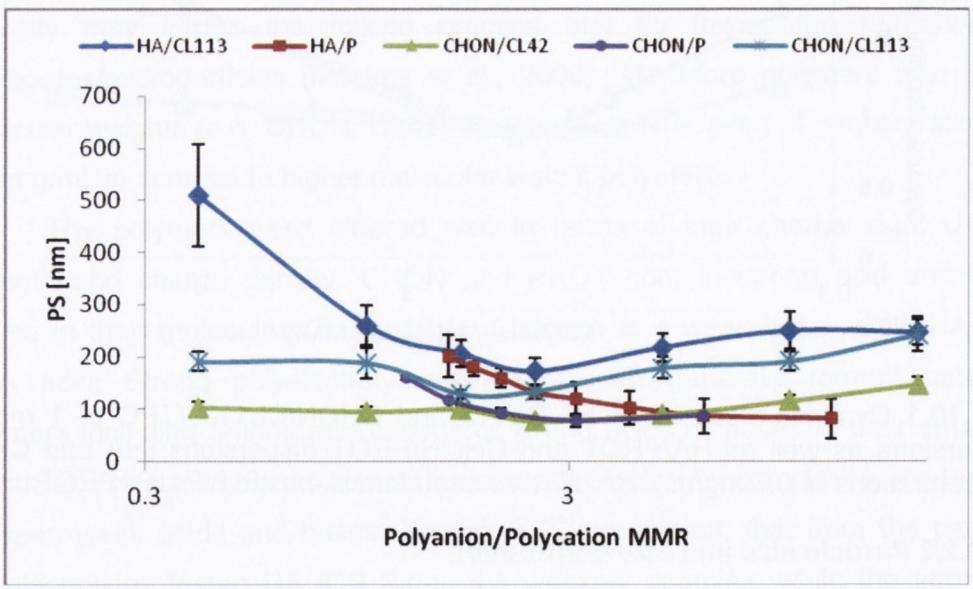

Fig. 10.2 Particle size of HA/CL113, CHON/CL21 and CHON/CL113 (TPC of 1 mg/ml) dispersions as well as HA/PROT and CHON/PROT dispersions (HA and CHON concentrations of 0.7 mg/ml). HA257 was used for HA-based NPs. P=PROT.

Fig. 10.3 shows the size distribution of selected polyelectrolyte complex NPs. Most of the formulations tested had PDI values below 0.25, or even below 0.2, therefore can be considered as homogenously dispersed. Generally all

systems were characterised by a comparable PDI values, apart from CHON/PROT with MMR of 6 and HA/CL113 with MMR of 0.4 NPs, where the size distribution was markedly wider.

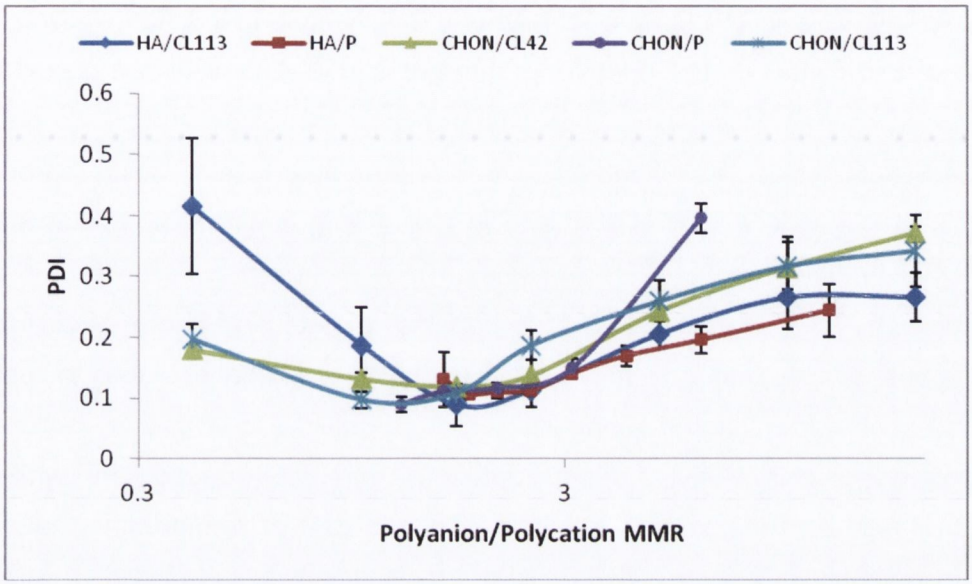

Fig. 10.3 Polydispersity index of HA/CL113, CHON/CL21 and CHON/CL113 (TPC of 1 mg/ml) dispersions as well as HA/PROT and CHON/PROT dispersions (HA and CHON concentrations of 0.7 mg/ml). HA257 was used for HA-based NPs. P=PROT.

10.3.2.3 Zeta potential and isoelectric point

Fig. 10.4 shows the zeta potential of selected polyelectrolyte complex NPs. Surface sign and charge depended on the composition of the NPs. It was possible to obtain both, positively and negatively charged NPs depending on the polyanion and polycation MMR, however for PROT-based NPs only negatively charged formulations were stable. It may be due to the dissimilar molecular weight and charge density of PROT compared to both polyanions. At the highest (i.e. 10-20) and the lowest (0.4-1) polyanion/polycation MMRs HA-based NPs were characterised by a higher surface charge, either negative, or positive. That may be due to the high molecular weight of HA, especially for negatively charged particles. Although HA has a lower charge density than CHON (Denuziere et al., 1996), it has a markedly higher molecular weight (HA- 257 kDa compared to CHON- 59 kDa). Therefore the molecule of HA may have more negatively charged groups than the smaller molecule of CHON. However, HA forms weaker polyelectrolyte complexes than CHON due to lower charge density of the former. At high polyanion/polycation mixing ratios, most of the carboxylic groups of HA are ionised,

as only a small fraction would be neutralised by a polycation, thus if bound to NPs they could be responsible for an increase in the negative surface charge. Therefore, at high polyanion/polycation MMRs the influence of the molecular weight is more pronounced than the effect of charge density or strength of acid groups. At polyanion/polycation MMR of 2.5 or lower, the effect of charge density and strength of acid groups predominates - CHON-based NPs had a lower zeta potential compared to HA. CHON forms stronger polyelectrolyte complexes than HA, as strongly acidic sulphonate groups and weak carboxylic groups are present in the CHON molecule in contrast to HA, where only weakly acidic carboxylic groups are present. Also, CHON has two ionisable groups in each disaccharide unit, while in the molecule of HA a maximum one charge may be present in each disaccharide unit. Therefore CHON is capable to neutralise more basic groups compared to HA. Indeed, for CS-based NPs, aggregation due to charge neutralisation and charge inversion from negative to positive occurs at polyanion/polycation MMR of approximately 1.2 for CHON-based NPs, while HA forms with CS stable, positively charged NPs at this MMR. On the other hand, the charge neutralisation for HA/CL113 NPs occurs at polyanion/polycation MMR of approximately 1.7, while CHON forms stable, negatively charged NPs with CS at this MMR. Also, CHON is capable to neutralise more PROT without destabilising colloidal dispersion. PROT concentrations of 0.57 and 1.14 mg/ml yielded stable NPs with the concentrations of CHON of 0.7 and 1.4 mg/ml, respectively. When HA was used at the same concentrations (0.7 and 1.4 mg/ml), even lower than the above concentrations of PROT (i.e. 0.46 and 0.91 mg/ml of PROT for 0.7 and 1.4 mg/ml of HA, respectively) caused phase separation. However, when considering neutralisation of the particles, more factors have to be taken into account, especially the pH.

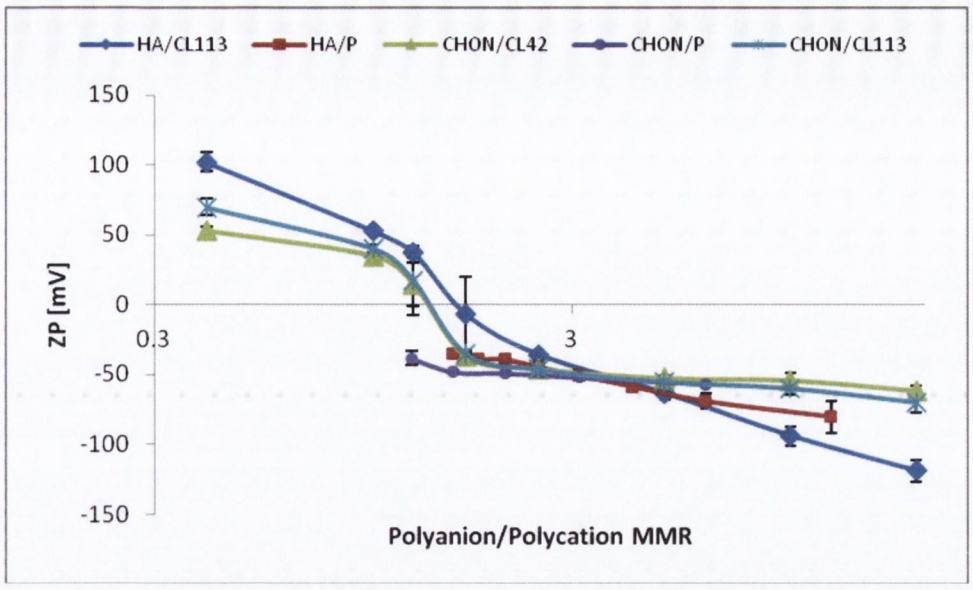

Fig.10.4 Zeta potential of HA/CL113, CHON/CL21 and CHON/CL113 (TPC of 1 mg/ml) dispersions as well as HA/PROT and CHON/PROT dispersions (HA and CHON concentrations of 0.7 mg/ml). HA257 was used for HA-based NPs. P=PROT

In all systems tested, the main factor determining the isoelectric point was the MMR of polyanion and polycation; an increase the content of the polyanion resulted in IEP occurring at lower pH.

Titration studies confirmed that CHON had better ability to maintain the negative surface charge than HA. CHON-based NPs were characterised by IEP values shifted towards more acidic pH compared to HA-based NPs. For instance, CHON/CS MMR of 1 NPs had IEP of 6.19±0.01, compared to 6.98±0.54 for similar HA/CS NPs ($p=0.0667$). While HA/CS MMR of 2.5 and 5 NPs had IEP of 2.83±0.38 and 2.47±0.25, respectively, no IEP was detected in analogical CHON/CS NPs down to pH 1.5-1.7, consistent with stability studies in 0.25M HCl (see Chapter 6). Similarly, most CHON/PROT NPs did not show IEP down to pH of 1.5-1.7, and the IEP of CHON of 0.7 mg/ml, PROT of 0.34 mg/ml of 1.85±0.08 was significantly lower than the IEP of analogical HA-based system (2.90±0.05). HA/PROT NPs were generally characterised by more acidic IEP compared to HA/CSs NPs. CHON-based NPs would therefore be preferred in strongly acidic environments (e.g. stomach juice).

Positively charged CS-based NPs were not stable at pH close to neutral and were stable in an acidic environment. Moreover, at pH 7.4 a charge inversion from positive to negative was observed. Similar results, i.e. isoelectric point at 7.5 and charge inversions from positive to negative above pH of 7.5 were obtained by

López-León et al. (2001). Negatively charged NPs, on the other hand, were stable in neutral and slightly acidic pH (Chapters 3-7).

In summary, the formation and properties of the particles were influenced by the polymers used, concentration and MMR of polycations and polyanions, as well as their molecular weight.

10.3.2.4 Physical stability

Polyelectrolyte complex NPs were also examined in terms their stability upon storage at room temperature for up to 4 weeks. For HA-based NPs sedimentation was observed after 2-3 weeks and for CHON-based NPs - after 3-4 weeks or no sedimentation (CHON/PROT NPs). However, it must be mentioned, that visual indications of sedimentation in many formulations were hardly visible. Positively charged CS-based formulations were less stable when compared to negatively charged. Despite the signs of sedimentation, the characteristics of the particles (i.e. particle size, size distribution and zeta potential) were satisfactorily preserved, apart from HA/PROT NPs and particularly the dispersion composed of 0.7 mg/ml of HA and 0.11 mg/ml of PROT. A slight, systematic decrease in the particle size for the positively charged CS-based NPs may be the result of sedimentation. However, careful observation of the samples is necessary, as in most cases the DLS or LDV data did not show symptoms of sedimentation, especially for the negatively charged formulations. Other minor changes in the parameters may be the result of reorganisation of the structure of the particles, possibly due to Brownian motions and particle interactions in the nano-suspension. The preservation of characteristics of the particles are in agreement with de la Fuente et al., (2008a), who examined the stability of CS/TPP/HA NPs within the period of four weeks and did not observe any major changes.

10.3.3 Cytotoxicity studies

The cytotoxicity of polymers used in the fabrication of polyelectrolyte complex NPs to Caco-2 cells was examined. None of the polysaccharides was toxic to Caco-2 cells at pH 7.4. Protamine was the most toxic from the polyelectrolytes tested - it markedly decreased the viability of Caco-2 cells. The IC_{50} of PROT at pH 7.4 determined by the MTS assay was 240±10 µg/ml, compared to 520±30 µg/ml determined by flow cytometry. This and other examples show that MTS assay was more sensitive than flow cytometry in determination of toxic effects of polymers or NPs.

At pH 5 chitosan decreased the viability of Caco-2 cells in the concentration-dependent manner. The IC_{50} of chitosan at pH 5 was 25.9 μg/ml (serum-free medium with pH 5 was used as a control). Further experiments are necessary to determine the effect of PROT on Caco-2 cells at pH 5. Chitosan was not found to be toxic to Caco-2 cells at pH 7.4.

Neither HA/CS, nor CHON/CS had negative effects on the viability of Caco-2 cells at pH of 7.4. However, when pH was decreased to 5, positively charged HA/CS MMR of 1 NPs decreased the viability of Caco-2 cells in a concentration-dependent way, in contrast to negatively charged HA/CS MMR of 5 NPs, which not only did not have a negative effects on the viability of the cells, but also protected them against the negative effects of lower pH. The IC_{50} of HA/CS MMR of 1 NPs at pH 5 was 83.9 μg of CS/ml (which corresponds to 167.8 μg of NPs/ml), therefore complexation to HA protects the cells against the negative effects of CS. Interestingly, when CS was complexed to CHON in the form of CHON/CS MMR of 1 NPs, the negative effects on cells were minimal and occurred only at the highest concentration (2 mg/ml of NPs, containing 1 mg/ml of CS) used, therefore the calculation of IC_{50} was not applicable. Thus CHON protects the cells against the toxicity of CS even more effectively than HA.

Similarly, Parajó et al., (2010) did not observe toxic effects of HA/CS NPs to C3a cells even at concentration of 1 mg/ml (cell viability was higher than 80%). It has been reported that the presence of hyaluronan in the nanostructure of CS NPs led to a significant reduction in their cytotoxicity, which was probably linked to the excellent biocompatibility profile of the hyaluronan (de la Fuente et al., 2008c).

PROT-based NPs were found to affect negatively the viability of Caco-2 cells even at pH 7.4 as the viability of the cells was decreased by 30% for HA/PROT NPs (HA/PROT MMR of 0.22 and PROT of 0.25 mg/ml) and 17% for analogical CHON/PROT NPs. Complexation to CHON or HA significantly decreased the toxicity of PROT. However, further experiments are necessary to evaluate the toxicity of PROT-based NPs at pH 5. Also, formulations with different polyanion/PROT MMRs should be compared.

The results are consistent with Pathak et al., (2009), who reported that complexation to CHON significantly decreased the cytotoxicity of polyethyleninine in HepG2 and HeLa cells.

10.3.4 Novelty aspects of formed NPs

The NPs composed of HA and CS have already been explored by a few authors (de la Fuente et al., 2008, Boddohi et al., 2009), however this work (as

described in Chapter 3) has introduced a few important improvements to the published methods. In most cases (de la Fuente et al., 2008a, b and c) the NPs contained the cross-linker TPP. If a negatively charged active molecule is to be associated with/incorporated to the HA/CS particles, a negatively charged cross-linker will compete for binding places of positively charged chitosan molecules with negatively charged associated molecule (e.g. nucleic acid) and HA. Therefore such a nanoparticle will contain one positively charged ingredient (CS) and three negatively charged (HA, TPP, active molecule). If the particles are to remain in the form of colloidal dispersion, only a limited amount of each of those ingredients can be used. Therefore, the amount of HA and the negatively charged active molecule to be bound to the nanoparticles will be limited by the presence of TPP and elimination of TPP would increase the loading capacity of NPs for the macromolecule of interest. Moreover, a more complex optimisation studies would be necessary, as the amounts of four ingredients would have to be optimised. Also, it has been shown (Wadhwa et al, 2010), that the presence of high amounts of TPP leads to charge neutralisation and aggregation of particles. Therefore, elimination of TPP from the composition of the particles appears to be beneficial. Although Boddohi et al. (2009) produced cross-linker free particles, they cannot be considered as physically stable as it was seen that it was necessary to leave them overnight in order to remove the aggregated particles. In this work, cross-linker free HA/CS NPs were obtained, stable for at least a few weeks in liquid dispersions. The stability was achieved mainly due to the reduction in the molecular weight of HA, however the use of water instead of a buffer may also have played a role.

Another type of CS-based NPs described in this thesis are CHON/CS NPs (Chapter 6). Although first reports about CHON/CS NPs have already been published (Yeh et al., 2011; da Silva et al., 2012, Hou et al., 2012), they can still be considered as a relatively new subject. Hou et al., (2012) used TPP as a cross-linker, while cross-linker free chitosan/TPP NPs were obtained in the course of these studies. Also, to our best knowledge, no negatively charged chondroitin/chitosan nanoparticles have been described so far. Such nanocarriers would be ideal candidates for the association of positively charged molecules.

Moreover, within this project two new types of polyelectrolyte complex nanoparticles with protamine have successfully been developed (presented in Chapter 5 and 7). The HA/PROT and CHON/PROT nanoparticles have not been described so far.

10.3.5 Association of sCT with polyelectrolyte complex NPs

Biomacromolecules (i.e. peptides and nucleic acids) are characterised by different physicochemical properties in comparison to conventional, low molecular weight compounds. They differ considerably in terms of hydrophilicity, solubility, molecular weight, charge strength and density. Moreover, some of these properties, e.g. charge density depend on the environment, e.g. pH. Therefore it is expected that various macromolecules will differently interact with NPs, especially polyelectrolyte complex-based. Consequently, none of the macromolecules can be considered as a model compound. Many authors have encapsulated or associated different proteins with the NPs, however many of them (e.g. BSA- bovine serum albumin) do not have any important therapeutic applications. Although these studies may be helpful in understanding the mechanisms of NP formation and the mechanisms of association of macromolecules, it may not be possible to simply replace one macromolecule by another, and as a result new optimisation studies should be carried out.

Due to its many applications in therapy and lack of commercially available forms other than injections and nasal spray, salmon calcitonin was selected to be associated with the nanoparticles, as there is a pressing need for a new, more compliant delivery system of this peptide (Patton, 2000). To the best of knowledge, it is the first time that sCT has been comprised in one delivery system with HA or CHON. As shown in Chapter 9, the combination of HA and sCT resulted in the reduction of inflammatory biomarkers (NR4As and MMPs) as well as the reduction of inflammation in K/BxN mouse model of inflammatory arthritis, an effect that was significantly better than sCT on its own. Therefore it appears that the HA/sCT combination has also a therapeutic merit and it is not only required from the peptide delivery system design point of view.

As the isoelectric point of sCT is of 10.4, it is expected to carry a positive surface charge at acidic and neutral pH. Hence, only negatively charged formulations were selected as candidates for the carriers for sCT. As positively charged sCT is expected to interact mainly with the polyanions, the possibility of formation of the HA/sCT or CHON/sCT NPs was also examined. Although UV and viscosity results confirmed, that sCT interacts with HA, the samples were not suitable for DLS analysis and no particles with acceptable quality were formed. In contrast to HA, complexation to CHON yielded small (PS below 200 nm), homogenously dispersed (PDI below 0.2) NPs. sCT has low molecular weight (3.4 kDa), and is a weak base, therefore its interactions with HA may not produce complexes strong enough to precipitate in the form of NPs. CHON, on the other

hand, contains strong acid groups, and forms stronger complexes than HA, therefore CHON is able to form NPs even with weakly basic, small molecular weight sCT.

Indeed, as shown in Chapters 4-7, sCT was very efficiently associated either with HA-based, or with CHON-based NPs. Almost all polyelectrolyte complex NPs examined had the association efficiency values higher than 90%. Generally, CHON-based NPs were characterised by slightly higher AE values (99-100%) compared to HA NPs (90-100%). AE decreased slightly with the increase of the amount of polycation (i.e. PROT or CS) in the formulation, especially in HA-based NPs. Moreover, very high drug loading (30% and more) was achieved. The highest drug loading was achieved for CHON/sCT NPs (up to 73%).

Different AE values were reported for sCT NPs. For instance Cetin et al., (2012) stated that the AE was approximately 70% in Eudragit® and Eudragit®/PLGA NPs, Glowka et al., (2010) reported 80% AE of sCT in PLGA NPs, Yang et al., (2012)- 97% in PLGA NPs, however most of them had very low drug loading (e.g. Glowka et al. (2010) - 0.2% with the highest reported for Cetin et al.,(2012) - 9.9%). Therefore, in this thesis an important improvement has been made in terms of achievement of very high sCT loading in NPs.

The release studies confirmed that interactions between CHON and sCT are stronger than between HA and sCT. CHON-based NPs were capable to provide slower release than HA-based NPs, with markedly smaller amount of sCT released within the first hour. The influence of polycation (PROT versus CS) on the release of sCT was markedly smaller than the influence of the polyanion (HA versus CHON). Kamiya et al., (2003), who examined the release of lysozyme from its complexes with different polyanions proved that the rate of lysosyme release was controlled by the nature of the polyanion, decreasing upon increase in its linear charge density, length and hydrophobicity.

However due to recently realised fact that calcitonin-containing medicines slightly increase the risk of cancer as a result of their long-term use, sCT should no longer be used in the treatment of osteoporosis, and is only authorised for a short-term use in Paget's disease, acute bone loss due to sudden immobilisation and hypercalcemia caused by cancer (EMA/476001/2012). Therefore the interest in development new sCT-containing delivery systems intended for long-term use may decrease in the nearest future.

10.3.6 Freeze-drying of polyelectrolyte complex NPs

Attempts were made to obtain solid state form of HA and CHON-based polyelectrolyte complex NPs with the employment of a lyophilisation process. The presence of a cryoprotectant was necessary to achieve a successful reconstitution. This is in agreement with de la Fuente et al., (2008a), who were unable to successfully redisperse CS/HA/TPP NPs freeze-dried without a cryoprotective agent. Trehalose, already used as a cryoprotectant for freeze-drying of CS/HA/TPP NPs (de la Fuente et al., 2008a), was selected for freeze-drying of HA/CS NPs. Freeze-drying of NPs was found to be a complicated process and the type and concentration of a cryoprotectant as well as the composition and concentration of NPs were found to influence the redispersibility of the polyelectrolyte complex NPs. The concentration of trehalose, a commonly used cryoprotectant, should be optimised for each type of formulation, as the minimal concentration of cryoprotectant for reconstitution depends on the composition of the NPs. Protamine-based NPs were characterised by an excellent redispersibility, better than CS-based NPs. For the latter, HA-based NPs were found to better preserve their properties after freeze-drying with a lower amount of trehalose than CHON-based NPs. Also, the redispersibility of CS-based NPs depends on the MMR of CS and polyanion (i.e. CHON or HA). Formulations with CHON/CS or HA/CS MMR of 5 were easier to be redispersed than formulations with lower mass mixing ratios. sCT was found to decrease the redispersibility of HA/CS NPs, and improved the redispersibility of CHON/CS NPs.

In this work important improvements have been made in the design of freeze-drying of polyelectrolyte complex NPs. Although de la Fuente et al., (2008a) presented that trehalose can be an effective cryoprotectant for CS/HA/TPP NPs, they did not optimise the concentration of the cryoprotectant. The influence of the concentration of NPs on the freeze-drying process was evaluated, but the use of a cryoprotectant at 5% w/v with NPs at 0.075-0.5 mg/ml would provide NP loading of approximately 0.15-1% w/w, therefore the loading of the drug in the formulation would be even smaller. The decrease in a cryoprotectant concentration would provide an important advantage in terms of increasing the peptide content. Also, de la Fuente et al., (2008a) did not examine the influence of the composition of the NPs on their redispersibility. As shown in this thesis, the NP composition has an important effect on redispersibility of the NPs, and this may be one of the most important criteria for the selection of formulation with optimal properties. Indeed, by optimisation of process parameters it was possible to successfully redisperse HA/CL113/sCT NPs (PS ratio after and before freeze-drying below 1.2) with the

loading of NPs of approximately 13% w/w and sCT loading of approximately 4% w/w.

PEGs were found to be more effective cryoprotectants than trehalose. PEG employed as a cryoprotectant at 2% w/v enabled successful reconstitution of HA/CL113 MMR of 2.5 NPs freeze-dried at the concentration of 1 mg/ml, while it was necessary to use 4% w/v trehalose to achieve a similar effect. Moreover, the addition of PEG enables to reduce the concentration of trehalose and the total concentration of cryoprotectants required for a successful reconstitution of HA/CL113 NPs with the MMR of 2.5 and TPC of 1 mg/ml. However, further studies on lyophilisation with PEGs are necessary in order to verify the influence of the composition and concentration of NPs on their redispersibility after lyophilisation with PEGs.

PEGs (apart from 10 kDa linear PEG) were found to be superior to trehalose in terms of toxicity to Caco-2 cells. At high concentrations linear 10 kDa PEG and trehalose decreased the viability of Caco-2 cells markedly (IC_{50} values of 2.5 and 6.8% w/v, respectively). Other PEGs (i.e., 2 kDa, 4 kDa liner PEGs and 10 kDa branched PEG) were very well tolerated by Caco-2 cells.

10.4 Conclusions: summary of criteria for the selection of NPs with optimal properties

In this work many NP formulations were tested. It is important to define the criteria for the selection of nano-formulations with the most favourable properties. Many criteria should be taken into account, e.g.: AE, DL and release of associated macromolecule; physical properties (size, size distribution, zeta potential), isoelectric point, stability upon storage and in different buffers, the ability to obtain solid state form and its redispersibility as well as cytotoxicity. Also, the potential biological properties of the components of the carriers may be important, as shown in Chapter 9.

It has been confirmed for all types of NPs tested (i.e. HA/CS, HA/PROT, CHON/CS and CHON/PROT) formulations containing more polyanions and higher polyanion/polycation MMRs were capable to associate more sCT. On the other hand, the presence of polycation (i.e. CS or PROT) was necessary in order to obtain sCT-loaded HA-based NP. Therefore NPs with a low polycation concentration seem to be the most optimal carrier for sCT.

The Coulombic interactions of CHON with sCT are stronger than HA-sCT interactions as CHON has a stronger charge and a higher charge density. CHON-

based NPs were capable to provide slower and more sustained release of sCT compared to HA-based NPs. Also, the initial quick release of sCT was markedly more pronounced in HA-based NPs than in CHON-based NPs. CHON has a stronger charge and higher charge density than HA, and it have been shown that its interactions of sCT with CHON were stronger than with HA (chapter 4 and 6). On the other hand, HA has a higher molecular weight than CHON. The release studies results are consistent with the view that the stronger polyanion-sCT complex (due to electrostatic interactions), the slower is the rate of sCT release.

sCT-loaded CHON-based NPs were generally smaller than HA-based sCT-loaded NPs. CHON-based NPs were characterised by an isoelectric point at lower pH compared to HA NPs, so they are recommended for acidic pH and make a more attractive candidate for oral delivery of sCT. Negatively charged HA-based NPs were characterised by an isoelectric point close to 2 or 3, thus they aggregate at pH encountered e.g. in stomach. Negatively charged CHON-based NPs on the other hand were capable to maintain the negative charge even at pH of 1.2, and as showed by release studies, even at such a low pH CHON-based NPs were able to efficiently bind sCT. The properties of NPs in buffers (Chapter 6 and 7) were slightly different compared to water. The properties of polylelctrolyte complex NPs depend on many parameters, among them on pH and ionic strength of the medium (Boddohi et al., 2009). López-León et al., (2005) showed that CS/TPP NPs exhibited volume phase transitions (swelling/shrinking processes) as a result of change of the physicochemical conditions of the medium. CHON/PROT/sCT NPs were characterised by a better stability in buffers than CHON/CS/sCT NPs, especially in PBS as the size was small (200 nm) and it did not change significantly over 24 hours. CS tends to form ion pairs with non-monovalent anions. This ability is commonly used in ionic gelation processes with cross-linking molecules, e.g. TPP (Calvo et al., 1997; Janes et al., 2001, Vila et al., 2002) or sulphate (Berthold et al., 1996; Van der Luben et al., 2001). Therefore, the presence of phosphate anions (PBS) may also affect chitosan properties (López-León et al., 2005).

Another very important parameter which must be taken into account during selection of nano-formulations is the possibility to obtain solid state form and redispersibility of the NPs. Cryoprotectants, which are necessary to successfully freeze-dry polyelctrolyte complex NPs, are usually employed at much higher concentrations than NPs. Consequently, after the use of a cryoprotectant the DL will be markedly lower. Therefore it is necessary to decrease the concentration of a cryoprotectant to the lowest amount possible, and use NPs with high DL in order to obtain formulation with a satisfactory DL. PROT-based NPs were characterised by

a better redispersibility compared to CS-based NPs and HA/CS NPs were capable to be successfully redispersed with the use of lower concentrations of trehalose than CHON/CS NPs. However, at the highest concentration tested PROT-based NPs exert a slightly cytotoxic effect on Caco-2 cells, while CS-based NPs were very well tolerated by Caco-2 cells at pH 7.4. CHON-based NPs were found to be less cytotoxic compared to HA-based NPs, probably due to stronger interactions between CHON and the polycation when compared to HA.

10.5 Main findings

- Polyelectrolyte complex NPs can be successfully formed for the following polyelectrolytes: HA/CS, HA/PROT, CHON/CS and CHON/PROT
- The formation and properties of the above polyelectrolyte complex NPs depended on many process variables, e.g. the type and molecular weight of the polyelectrolytes, the mixing ratio and concentrations of the polymers and the counterion type in the polymer salts
- CS formed with HA and CHON stable positively and negatively charged NPs, while only negatively charged PROT-based NPs were stable
- The isoelectric point of the NPs was governed mainly by the mixing ratio of the polyelectrolytes and an inversion of the sign of the charge of the particles may occur as a result of pH change
- Most of the NP tested satisfactorily preserved their properties (particle size, polydispersity index and zeta potential) after short term storage, however after 2-4 weeks first signs of sedimentation were observed
- sCT interacts with HA and CHON by electrostatic forces; in case of CHON/sCT system it was possible to obtain polyelectrolyte complex NPs
- sCT was very efficiently associated with HA and CHON-based NPs, and a high peptide loading was achieved
- CHON-based NPs released sCT at a lower rate than HA-based NPs
- The release of sCT from CHON-based NPs was affected by the composition of the dispersant
- At pH 7.4, HA, CHON and CS were well tolerated by Caco-2 cells, while PROT affected the viability of the cells markedly
- The cytotoxicity of the particles depended on the composition of the particles with PROT-based NPs being more toxic that CS-based NPs
- pH affected the cytotoxicity of positively charged CS NPs

- Complexation to polyanions had a protective effect against toxicity of polycations in Caco-2 cells
- NPs could be successfully obtained in the solid state dry form by freeze-drying
- Redispersibility of polyelectrolyte complex NPs was found to depend on the composition and concentration of the particles as well as the type and concentration of the cryoprotectant used
- 2 kDa, 4 kDa linear PEGs and 10 kDa branched PEG were very well tolerated by Caco-2 cells, while linear 10 kDa PEG and trehalose decreased the viability of Caco-2 cells at higher concentrations
- HA/CL113/sCT NPs produced reduction in mRNA of inflammatory biomarkers (NR4As and MMPs) comparable to dexamethasone and markedly higher than sCT or HA on its own
- HA/CL113/sCT NPs reduced inflammation and preserved bone and cartilage structure in the K/BxN mouse following I.A. injection and down-regulated expression of NR4A in ankle joints

10.6 Future work:

- *in vitro* cell culture transport studies (e.g. in Caco-2 monolayers) for the oral uptake of the nanoparticles
- *in vivo* animal studies on oral administration of sCT from the NPs
- *in vitro* cell culture studies of the anti-inflammatory properties of CHON-based NPs, followed by possible *in vivo* studies
- A further optimisation of the freeze-drying process (especially with the use of PEG as a cryprotectant) and *in vitro* cytotoxicity studies of NPs freeze-dried with PEG
- FTIR studies of molecular interactions between HA and sCT as well as CHON and sCT
- Stability of HA-based NPs in different media (pH and ionic strength)
- Morphology studies (e.g. TEM, SEM and AFM) of CHON-based NPs
- Evaluation of mucoadhesive properties of the NPs and their interactions with membranes e.g. *in vitro* with the use of quartz crystal microbalance

11. References

Afzal, A., Afzal, M., Jones, A., Armstrong, D., Rapid determination of glutamate using HPLC technology. Methods in Molecular Biology 2002; 186: 111-115.

Agnihotri, S.A., Mallikarjuna, N.N., Aminabhavi, T.M., Recent advances on chitosan-based micro- and nanoparticles in drug delivery. Journal of Controlled Release 2004;100: 5-28.

Aktaş Y., Andrieux K., Alonso M., Calvo P., Gürsoy R., Couvreur P., Çapan Y., Preparation and in vitro evaluation of chitosan nanoparticles containing a caspase inhibitor. International Journal of Pharmaceutics 2005; 298: 378-383

Alkrad, J.A., Mrestani, Y., Stroehl, D., Wartewig, S., Neubert, R., Characterization of enzymatically digested hyaluronic acid using NMR, Raman, IR, and UV-Vis spectroscopies. Journal of Pharmaceutical and Biomedical Analysis 2003; 31: 545-550.

Allèmann E., Leroux J., Gurny R., Polymeric nano- and microparticles for the oral delivery of peptides and peptidomimetics. Advanced Drug Delivery Reviews 1998; 34: 171-189

Alonso, M.J., Nanomedicines for overcoming biological barriers; Biomedicine and Pharmacotherapy 2004; 58: 168-172

Andrews, G.P., Laverty, T.P., Jones, D.S., Mucoadhesive polymeric platforms for controlled drug delivery. European Journal of Pharmaceutics and Biopharmaceutics 2009; 71: 505-518

Anhorn, M., Maher, H.C., Langer, C., Freeze-drying of human serum albumin (HSA) nanoparticles with different excipients. International Journal of Pharmaceutics 2008; 363: 162-169

Arturrson, P., Palm, K., Luthman, K., Caco-2 monolayers in experimental and theoretical predictions of drug transport. Advanced Drug Delivery Reviews 2001; 46: 27-43

Ayral, X., Dougados, M., Listrat, V., Bonvarlet, J.p., Simmonet, J., Amor, B., Arthroscopic evaluation of chondropathy in osteoarthritis of the knee. The Journal of Rheumatology 1996; 23: 698-706

Bansil, R., Turner, B.S., Mucin structure, aggregation, physiological functions and biomedical applications. Current Opinion in Colloid & Interface Science 2006; 11: 164-170

Bayat A., Larijani B., Ahmadian S., Jungingen H., Rafiee-Tehrani M., Preparation and characterisation of insulin nanoparticles using chitosan and its quarenized derivatives. Nanomedicine: Nanotechnology, Biology and Medicine 2008; 4: 115-120

Bellamy, N., Campbell, J., Robinson V., Gee, T., Bourne, R., Wells, G., Viscosupplementation for the treatment of osteoarthritis of the knee. Cochrane Database of Systematic Reviews 2006a; 19: CD005321

Bellamy, N., Campbell, J., Robinson,V., Gee, T.,Bourne, R., Wells, G., Intraarticular corticosteroid for treatment of osteoarthritis of the knee. Cochrane Database of Systematic Reviews 2006b; 2:CD005328

Berthold, A., Cremer, K., Kreuter, J., Preparation and characterization of chitosan microspheres as drug carrier for prednisolone sodium phosphate as model for anti-inflammatory drugs. Journal of Controlled Release 1996; 39: 17-25

Bezakova, Z., Hermannova, M., Drimalova, E. , Malovikova, A., Ebringerova, A. , Velebny, V., Effect of microwave irradiation on the molecular and structural properties of hyaluronan. Carbohydrate Polymers 2008; 73: 640-646.

Bilati, U., Alleman, E., Doelker, E., Development of a nanoprecipitation method intended for the entrapment of hydrophilic drugs into nanoparticles. European Journal of Pharmaceutical Sciences 2005; 24: 67-75

Blanco, M.D., Alonso, M.J., Development and characterization of protein-loaded poly(lactide-co-glycolide) nanospheres. European Journal of Pharmaceutics and Biopharmaceutics 1997; 43: 287-294

Boddohi, S., Kipper, M.J., Engineering nanoassemblies of polysaccharides. Advanced Materials 2010; 22: 2998-3016

Boddohi, S., Moore, N., Johnson, P., Kipper, M., Polysaccharide-based polyelectrolyte complex nanoparticles from chitosan, heparin and hyaluronan. Biomacromolecules 2009; 10: 1402-1409

Bodmeier, R., McGinity, J.W., The preparation and evaluation of drug-containing poly(dl-lactide) microspheres formed by the solvent evaporation method. Pharmaceutical Research 1987; 4: 465-471

Bonta, P.I., van Tiel, C.M., Vos, M., Pols, T.W.H., van Thienen, J.V., Ferreira, V., Arkenbout, E.K., Seppen, J., Speck, C.A., van der Poll, T., Pannekoek, H, de Vries C.J.M., Nuclear receptors Nur77, Nurr1, and NOR-1 expressed in atherosclerotic lesion macrophages reduce lipid loading and inflammatory responses. Arteriosclerosis, Thrombosis and Vascular Biology 2006; 26: 2288-2294

Borges O., Borchard G., Verhoef, J.C., De Sousa, A., Junginger, H.E., Preparation of coated nanoparticles for a new mucosal vaccine delivery system; International Journal of Pharmaceutics 2005; 299: 155-166

Boryniec, S., Strobin, G., Struszczyk, H., Niekraszewicz, A., Kucharska, M., GPC studies of chitosan degradation. International Journal of Polymer Analysis and Characterization 1997; 3: 359-368.

Burt, H.M., Tsallas, A., Gilchrist, S., Liang, L.S., Intra-articular drug delivery systems: Overcoing the shortcomings of joint disease therapy. Expert Opinion on drug Delivery 2009; 6: 17-26

Calis, S., Yeyanthi, R., Tsai, T., Metha, R.C., Deluca, P.P., Adsorption of salmon calcitonin to PLGA microspheres. Pharmaceutical Research 1995; 12:1072-1076

Calvo, P., Remuñán-López, Vila-Jato, J.L., Alonso, M.J., Novel hydrophilic chitosan-polyethylene oxide nanoparticles as protein carriers. Journal of Applied Polymer Science 1997; 63: 125-132

Cetin, M., Aktas, M.S., Vural, I., Ozturk, M., Salmon calcitonin-loaded Eudragit® and Eudragit®-PLGA nanoparticles: in vitro and in vivo evaluation. Journal of Microencapsulation 2012; 29: 156-166

Chalasani K., Russel-Jones G., Jain A., Divan P., Jain S., Effective oral delivery of insulin in animal models using vitamin B12-coated dextran nanoparticles. Journal of Controlled Release 2007; 122: 141-150

Chevalier, X., Goupille, P., Beaulieu, A.D., Burch, F.X., Bensen, W.G., Conrozier, T., Loueille, D., Kivitz, A.J., Silver, D., Appleton, B.E., Intra-articlar injection of anakinra in osteoarthritis of the knee: a mulitcenter, randomized, double-blind, placebo-controlled study. Arthritis & Rheumatism 2009; 61: 344-352

Choi, K.Y., Chung, H., Min, K.H., Yoon, H.Y., Kim, K., Park, J.H., Kwon, I.C., Jeong, S.Y., Self assembled hyaluronic acid nanoparticles for active tumor targeting. Biomaterials 2010; 31: 106-114.

Christianson, C.A., Corr, M., Yaksh, T. L., Svensson, C. I., K/BxN serum transfer arthritis as a model of inflammatory joint pain. In: Pain Research: Methods and Protocols, Methods in Molecular Biology, 2012; 851; 249-260. Ed. Luo, D. Z. Springer, New York.

Conrozier, T., Chevalier, X.,Long-term experience with Hylan® GF-20 in the treatment of knee osteoarthritis. Expert Opinion on Pharmacotherapy 2008; 9: 1797-1804

Cooper, C.L., Dubin, P.L., Kayimazer, A.B., Turksen, S., Polyelectrolyte-protein complexes. Current Opinion in Colloid & Interface Science 2005; 10: 52-78

Corrigan, D.O., Healy, A.M., Corrigan, O.I., Preparation and release of salbutamol from chitosan and chitosan co-spray dried compacts and multiparticulates. European Journal of Pharmaceutics and Biopharmaceutics 2006; 62: 295-305

Corrigan, O.I., Li, X., Quantifying drug release from PLGA nanoparticulates. European Journal of Pharmaceutical Sciences 2009; 37: 477-485

Craig, D.Q.M., A review of thermal methods used for the analysis of the crystal form, solution thermodynamics and glass transition behaviour of polyethylene glycols. Thermochimica Acta 1995; 248: 189-203

da Silva. L.C., Garcia, T., Mori, M., Sandri, G., Bonferoni, M.C., Finotelli, P.V., Cinelli, L.P., Caramella, C., Cabral, L.M., Preparation and characterization of

polysaccharide-based nanoparticles with anticoagulant activity. International Journal of Nanomedicine 2012; 7: 2975-2986

Damgé, C., Michel, C., Aprahamian, M., Couvreur, P., New approach for oral administration of insulin with polyalkylcyanoacrylate nanocapsules as drug carrier. Diabetes 1988; 37: 246-251

Dautzenberg, H., Jaeger, W., Effect of charge density on the formation and salt stability of polyelectrolyte complexes. Macromolecular Chemistry and Physics 2002; 203: 2095-2102

de Campos, A.M., Sanchez, A., Gref, R., Calvo, P., Alonso, M.J., The effect of a PEG versus a chitosan coating on the interaction of drug colloidal carriers with the ocular mucosa. European Journal of Pharmaceutical Sciences 2003; 20: 73-81

de Ceunick, F., Sabatini, M., Pastoureau, P., Recent progress toward biomarker identification for osteoarthritis. Drug Discovery Today 2011; 16: 443-449

de Kruif, C.G., Weinbreck, F., de Vries, R., Complex coacervation of proteins and anionic polysaccharides. Current opinion in Colloid & Interface Science 2004 ; 9 : 340-349

de la Fuente, M., Seijo, B., Alonso, M.J., Novel hyaluronan-based nanocarriers for transmucosal delivery of macromolecules. Macromolecular Bioscience 2008a; 8: 441-450

de la Fuente, M., Seijo, B., Alonso, M.J., Novel hyaluronic acid-chitosan nanoparticles for ocular gene therapy. Investigative Ophthalmology & Visual Science 2008b ; 49: 2016-2024.

de la Fuente M, Seijo B, Alonso MJ., Design of novel polysaccharidic nanostructures for gene delivery. Nanotechnology 2008c; 19: 075105-075114

Denuziere, A., Ferrier, D., Domard, A., Chitosan- chondroitin sulfate and chitosan-hyaluronate polyelectrolyte complexes. Physico-chemical aspects. Carbohydrate Polymers 1996; 29: 317-323

des Rieux, A., Fievez, V., Garinot, M., Schneider, Y.-J., Préat, V., Nanoparticles as potential oral delivery systems of proteins and vaccines: A mechanistic approach. Journal of Controlled Release 2006; 116: 1-27

Desai, M.P., Labhasetwar, V., Amidon, G.L., Levy, R.J., Gastrointestinal uptake of biodegradable microparticles: effect of particle size. Pharmaceutical Research 1996; 13: 1838-1845

Drimalova, E., Velebny, V., Sasinkova, V., Hromadkova, Z., Ebringerova, A., Degradation of hyaluronan by ultrasonication in comparison to microwave and conventional heating. Carbohydrate Polymers 2005; 61: 420-426.

du Souich, P., Immunomodulatory and anti-inflammatory effects of chondroitin sulphate. Osteoarthritis 2009; 8-10

Edsman, K., Hagerstrom, H., Pharmaceutical applications of mucoadhesion for the non-oral routes. Journal of Pharmacy and Pharmacology 2005; 57: 3-22

Edwards, S.H.R., Intra-articular drug delivery: the challenge to extend drug residence time within the joint. Veterinary Journal 2011; 190: 15-21

EMEA website, EMA/476001/2012; EMEA/H/A-31/1291, Questions and answers on the review of calcitonin-containing medicines. http://www.ema.europa.eu/docs/en_GB/document_library/Referrals_document/Calcitonin_31/WC500130149.pdf

Emerich, D.F., Thanos, C.G., Nanotechnology and medicine. Expert Opinion on Biological Therapy 2003; 3: 655-663

Epand, R.M., Epand, R.F., Orlowski, R.C., Schlueter, R.J., Boni, L.T., Hui, S.W., Amphipatic helix and its relationship to the interaction of calcitonin with phospholipids. Biochemistry 1983; 22: 5074-5084

Fessi, H., Puisieux, F., Devissaguet, J.P., Ammoury, N., Benita, S., Nanocapsule formation by interfacial polymer deposition following solvent displacement. International Journal of Pharmaceutics 1989; 55: R1-R4

Florence, A.T., The oral absorption of micro- and nanoparticulates: neither exceptional nor unusual. Pharmaceutical Research 1997; 14: 259-266

Ganzevles, R.A., Kosters, H., van Vliet, T., Cohen Stuart, M.A., de Jongh, H.H.J., Polysaccharide charge density regulating protein adsorption to air/water interfaces by protein/polysaccharide complex formation. Journal of Physical Chemistry B 2007; 111: 12969-12976

Garcia-Fuentes, M., Torres, D., Alonso, M.J., New surface-modified lipid nanoparticles as delivery vehicles for salmon calcitonin. Pharmaceutical Nanotechnology 2005; 296: 122-132

Gerwin, N., Hops, C., Lucke, A., Intraarticular drug delivery in osteoarthritis. Advanced Drug Delivery Reviews 2006; 58: 226-242

Glowka, E., Sapin-Minet, A., Leroy, P., Lulek, J., Maincent, P., Preparation and *in-vitro- in vivo* evaluation of salmon calcitonin loaded polymeric nanoparticles. Journal of Microencapsulation 2010; 27: 25-36

Goutelle, S., Maurin, M., Rougier, F., Barbaut, X., Bourguignon, L., Ducher, M., Maire, P., The Hill equation : a review of its capabilities in pharmacological modelling. Fundamental & Clinical Pharmacology 2008; 22: 633-648

Govender, T., Stolnik, S., Garnett, M.C., Illum, L., Davis, S.S., PLGA nanoparticles prepared by nanoprecipitation: drug loading and release studies of a water soluble drug. Journal of Controlled Release 1999; 57: 171-185

Grabnar, P.A., Kristl, J., The manufacturing techniques of drug-loaded polymeric nanoparticles from preformed polymers. Journal of Microencapsulation 2011; 28: 323-335

Grabovac, V., Guggi, D., Bernkop-Schnurch, A., Comparison of the mucoadhesive properties of various polymers. Advanced Drug Delivery Reviews 2005; 57: 1713-1723 Guggi, D., Kast, C.E., Bernkop-Schnürch, A., *In vivo* evaluation of an oral salmon-calcitonin delivery system based on a thiolated chitosan carrier matrix. Pharmaceutical Research 2003; 20: 1989-1994

Habbib, G.S., Haliba, W., Nashashibi, M., Local effects of intraarticular corticosteroids. Clinical Rheumatology 2010; 29: 347-356

Habbib,G.S., Systemic effects of intra-articular corticosteroids. Clinical Rheumatology 2010; 28: 749-756

Hagedorn, H.C., Protamine Insulinate. Proceedings of the Royal Society of Medicine 1937; 30: 805-814

Hahn, S.K., Hoffman, A.S., Preparation and characterization of biocompatible polyelectrolyte complex multilayer of hyaluronic acid and poly-L-lysine. International Journal of Biological Macromolecules 2005; 37: 227-231

Hamidi, M., Azadi, A., Rafiei, P., Hydrogel nanoparticles In drug delivery. Advanced Drug Delivery Reviews 2008; 60: 1638-1649

Hartig, S.M., Greene, R.R., Dikov, M.M., Prokop, A., Davidson, J.M., Multifunctional nanoparticulate polyelectrolyte complexes. Pharmaceutical Research 2007; 24: 2353-2369

Herrmann, J., Bodmeier, R., Somatostatin containing biodegradable microspheres prepared by a modified solvent evaporation method based on W/O/W- multiple emulsions. International Journal of pharmaceutics 1995; 126: 129-138

Hillery A., Toth I., Florence A., Co-polymerised peptide particles II: oral uptake of a novel co-polymeric nanoparticulate delivery system for peptides, Journal of Controlled Release 1996a; 42: 65-73

Hillery A., Toth I., Shaw A., Florence A., Co-polymerised peptide particles (CPP) I: synthesis, characterisation and in vitro studies on a novel oral nanoparticulate delivery system. Journal of Controlled Release 1996b; 41: 271-281

Hinchcliffe, M., Jabbal-Gill, I., Smith, A., Effect of chitosan on the intranasal absorption of salmon calcitonin in sheep. Journal of Pharmacy and Pharmacology 2005; 57: 681-687

Hirai, A., Odani, H., Nakajima, A., Determination of degree of deacetylation of chitosan by ^{1}H NMR spectroscopy. Polymer Bulletin 1991; 26: 87-94.

Hoes, J. N., Jacobs, J. W., Buttgereit ,F., Bijlsma, J. W., Current view of glucocorticoid co-therapy with DMARDs in rheumatoid arthritis. Nature Reviews Rheumatology 2010; 6: 693-702.

Holzer, M., Vogel, V., Mäntele, W., Schwartz, D., Haase, W., Langer, K., Physico-chemical characterisation of PLGA nanoparticles after freeze-drying and

storage. European Journal of Pharmaceutics and Biopharmaceutics 2009; 72: 428-437

Hopwood, D., Use of isoelectric focusing to determine the isoelectric point of bovine serum albumin after treatment with various common fixatives. Histochemical Journal 1970; 3: 201-205

Horisawa, E., Kubota, K., Tuboi, I., Sato, K., Yamamoto, H., Takeuchi, H., Kawashima, Y., Size-dependency of DL-lactide/glycolide copolymer particulates for intra-articular delivery system on phagocytosis in rat synovium. Pharmaceutical Research 2002a; 132-139

Horisawa, T.H.E., Kawazoe, S., Yamada, J., Yamamoto H., Takeuchi, H., kawashima, Y., Prolonged anti-inflammatory action of DL-lactide/glycolide copolymer nanospheres containing betamethasone sodium phosphate for an intraarticular delivery system in antigen-induced arthritic rabbit. Pharmaceutical Research 2002b; 4: 403-410

Hou, Y., Hu, J., Park, H., Lee, M., Chitosan-based nanoparticles as a sustained protein release carrier for tissue engineering applications. Journal of Biomedical Material Research P2012; 100A: 939-947

Huang, T.-L., Hsu, H.-C., Yao, C.-H., Chen, Y.-S., Wang, J., Anti-inflammatory and structure-protective effects of hyaluronans: Are these effects molecular weight dependent? Biomedical Engineering- Applications Basis Communications 2011; 23: 13-20; DOI: 10.4015/51016237211002323

ICH guideline Q8(R2) "Pharmaceutical development", August 2009:

Ikada, Y., Tsuji, H., Biodegradable polyesters for medical and ecological applications. Macromolecular Rapid Communications 2000; 21: 117-132

Imada, K., Oka, H., Kawasaki, D., Miura, N., Sato, T., Ito, A., Anti-arthritic action mechanisms of natural chondroitin sulfate in human articular chondrocytes and synovial fibroblasts. Biological and Pharmaceutical Bulletin 2010; 33: 410-414

Isakovic, A., Markovic, Z., Todorovic-Markovic, B., Nikolic, N., Vranjes-Djuric, S., Mirkovic, M., Dramicanin, M., Harhaji, L., Raicevic, N., Nikolic, Z., Trajkovic, V., Distinct cytotoxic mechanisms of pristine versus hydroxylated fullerene. Toxological Sciences 2006; 91: 173-183

Jain, A.K., Mehra, N.K., Lodhi, N., Dubey, V., Mishra, D.K., Jain, P.K., Jain, N.K., Carbon nanotubes and their cytotoxicity. Nanotoxicology 2007; 1: 167-197

Janes, K.A., Calvo, P., Alonso, M.J., Polysaccharide colloidal particles as delivery systems for macromolecules. Advanced Drug Delivery Reviews 2001; 47: 83-97.

Jeyanthi, R., Thanoo, B.C., Metha, R.C., DeLuca, P.P., Effect of solvent removal technique on the matrix characteristics of polylactate/glycolide microspheres for peptide delivery. Journal of Controlled Release 1996; 38: 235-244

Jung, T.-S., Kwon, B.-S., Lee, H.-E., Kim, A.-Y., Lee, M.-J., Park, C.-R., Kang, H.-K., Kim, Y.-D., Lee, S.-K., Kang, J.-S., Choi, G.-J., Enhanced oral absorption of salmon calcitonin-encapsulated PLGA nanoparticles by adding organic substances. Korean Journal of Chemical Engineering 2009; 26: 131-135

Junghans, M., Kreuter, J., Zimmer, A., Antisense delivery using protamine-oligonucleotide particles. Nucleic Acids Research 2000; 28(10) e45

Kamiya, N., Klibanov, A.M., Controlling the rate of protein release from polyelectrolyte complexes. Biotechnology and Bioengineering 2002; 82: 590-594

Karsdal, M.A., Henriksen, K., Bay-Jensen, A.C., Molly, B., Arnold, M., John, M.R., Byrjalsen, I., Azria, M., Riis, B.J., Qvist, P., Christiansen, C., Lessons learned from the development of oral calcitonin: The first tablet formulation of a protein in phase III clinical trials. Journal of Clinical Pharmacology 2011; 51: 460-471

Kaszuba, M., McKnight, D., Connah, M.T., McNeil-Watson, F.K., Nobbmann, U., Measuring sub nanometre sizes using dynamic light scattering. Journal of Nanoparticle Research 2008; 10: 823–829.

Kawasaki, K., Ochi, M., Uchio, Y., Adachi, N., Matsusaki, M., Hyaluronic acid enhances proliferation and chondroitin sulfate synthesis in cultured chondrocytes embedded in collagen gels. Journal of Cellular Physiology 1999; 179: 142-148.

Kawashima, Y., Yamamoto, H., Takeuchi, H., Kuno, Y., Mucoadhesive DL-lactide/glycolide copolymer nanospheres coated with chitosan to improve oral delivery of elcatonin. Pharmaceutical Development and Technology 2000; 5: 77-85

Kim, E.-J., Shim, G., Kim, K., Kwon, I.C., Oh, Y.-K., Shim, C.-K., Hyaluronic acid complexed to biodegradable poly L-agrinine for targeted delivery of siRNAs. The Journal of Gene Medicine 2009; 11: 791-803

Knudson, W., Chow, G., Knudson, C.B., CD44-mediated uptake and degradation of hyaluronan. Matrix Biology 2002; 21: 15-23

Koshy, P. J., Lundy, C. J., Rowan, A. D., Porter, S., Edwards, D. R., Hogan, A., Clark, I. M., Cawston, T. E., The modulation of matrix metalloproteinase and ADAM gene expression in human chondrocytes by interleukin-1 and oncostatin M: a time-course study using real-time quantitative reverse transcription-polymerase chain reaction. Arthritis & Rheumatism 2002; 46: 961–967

Kudsiova, L., Lawrence, M.J., A comparison of the effect of chitosan and chitosan-coated vesicles on monolayer integrity and permeability across Caco-2 and 16HBE14o-cells. Journal of Pharmaceutical Sciences 2008; 97: 3998-4010.

Kuzmanova, S.I., Arthroscopic evaluation of chondropathy in knee osteoarthritis. Folia Medica 2000; 42: 16-18

Lapčík L. Jr., Lapčík, L., de Smedt, S., Demeester, J., Chabreček, P., Hyaluronan: preparation, structure, properties and applications. Chemical Reviews 1998; 98: 2664-2683.

Lawrie, G., Keen, I., Drew, B., Chandler-Temple, A., Rintoul, L., Fredericks, P., Grøndahl, L., Interactions between alginate and chitosan biopolymers characterized using FTIR and XPS. Biomacromolecules 2007; 8: 2533-2541.

Leane, M.M., Nankervis, R., Smith, A., Illum, L., Use of ninhydrin assay to measure the release of chitosan from oral solid dosage forms. International Journal of Pharmaceutics 2004; 271: 241-249

Lee W., Park J.Y., Jung S., Yang C., Kim W., Kim A., Park J.H., Park J.S., Preparation and characterisation of biodegradable nanoparticles entrapping immunodominant peptide conjugated with PEG for oral tolerance induction. Journal of Controlled Release 2005; 105: 77-88

Lee, H.-E., Lee, M.-J., Park, C.-R., Kim, A.Y., Chun, K.-H., Hwang, H.-J., Oh, D.-H., Jeon, S.-O., Kang, J.-S., Jung, T.-S., Choi, G.-J., Lee, S., Preparation

and characterisation of salmon calcitonin-sodium triphosphate ionic complex for oral delivery. Journal of Controlled Release 2010; 143: 251-257

Lee, M.K., Kim, M.Y., Kim, S., Lee, J., Cryoprotectants for freeze-drying of drug nano-suspensions: effect of freezing rate. Journal of Pharmaceutical Sciences 2009; 98: 4808-4817

Leo, E., Vandelli, M.A., Cameroni, R., Forni, F., Doxorubicin-loaded gelatine nanoparticles stabilized by glutaraldehyde- involvement of the drug in the cross-linking process; International Journal of Pharmaceutics 1997; 155: 75-82

Liang, L.S., Wong, W., Burt, H.M., Pharmacokinetic study of methotrexate following intra-articular injection of methotrexate-loaded poly(L-lactic acid) microspheres in rabbits. Journal of Pharmaceutical Sciences 2005; 94: 1204-1215

Liu, Z., Jiao, Y., Wang, Y., Zhou, C., Zhang, Z., Polysaccharide-based nanoparticles as drug delivery systems. Advanced Drug Delivery Reviews 2008; 60: 1650-1662

Lochmann, D., Weyermann, J., Georgens, C., Prassl, R., Zimmer, A., Albumin-protamine-oligonucleotide nanoparticles as a new antisense delivery system. Part 1: Physicochemical characterization. European Journal of Pharmaceutics and Biopharmaceutics 2005; 59: 419-429

Loretz, B., Bernkop-Schnürch, A., In vitro cytotoxicity testing of non-thiolated and thiolated chitosan nanoparticles for oral gene delivery. Nanotoxicology 2007; 1: 139-148.

Lowe, P.J., Temple, C.S., Calcitonin and insulin in isobutylocyanoacrylate nanocapsules: protection against proteases and effect on intestinal absorption in rats. Journal of Pharmacy and Pharmacology 1994; 46: 547-552

Lu, X., Pikal, M., Freeze-drying of mannitol-trehalose-sodium chloride-based formulations: the impact of annealing on dry layer resistance to mass transfer and cake structure. Pharmaceutical Development and Technology 2004; 9: 85-95

Lu, X.-Y., Wu, D.-C., Li, Z.-J., Chen, G.-Q., Nanobiotechnology and personalized medicine. In: Nanoparticles in Translational Science and Medicine 2011; First Edition (Editors: A.Villaverde). ISBN: 9780124160200

Mackay, M.E., Tuteja, A., Duxbury, P.M., Hawker, C.J., van Horn, B., Guan, Z., Chen, G., Krishnan, R.S., General strategies for nanoparticle dispersion. Science 2006; 311: 1740-1743.

Madsen ,F., Eberth, K., Smart, J.D., A rheological assessment of the nature of interactions between mucoadhesive polymers and a homogenised mucus gel. Biomaterials 1998; 19: 1083-1092

Maier, R., Brugger, M., Brückner, H., Kamber, B., Riniker, B., Rittel, W., Analogues of human calcitonin. Acta Endocrinologica 1977; 85: 102-108

Mainardes, R.M., Evangelista, R.C., PLGA nanoparticles containing praziquantel : effect of formulation variables on size distribution. International Journal of Pharmaceutics 2005 ; 290: 137-144

Makhlof, A., Werle, M., Tozuka, Y., Takeuchi, H., Nanoparticles of glycol chitosan and its thiolated derivative significantly improved the pulmonary delivery of calcitonin. International Journal of Pharmaceutics 2010; 397: 92-95

Mancini L., Pau-Clark, M.J., Rosignoli, G., Hannon, R., Martin, J.E., Macintyre, I., Perretti, M., Calcitonin and prednisone display antagonistic actions on bone and have synergistic effects in experimental arthritis. American Journal of Pathology 2007; 170: 1018-1027

Manicourt, D.-H., Devogelaer. J.-P., Azria, M., Silverman, S., Rationale for the potential use of calcitonin in osteoarthritis. Journal of Musculosceletal Neuronal Interactions 2005; 5:285-293

Masuhara, K., Nakai, T., Yamaguchi,K., Yamasaki, S., Sasaguri, Y., Significant increases in serum and plasmaconcentrations of matrix metalloproteinases 3 and 9 in patients with rapidly destructive osteoarthritis of the hip. Arthritis & Rheumatism 2002; 46: 2625-2631

Matthews, G.L., Hunter, D.J., Emerging drugs for orteoarthritis. Expert Opinion on Emerging Drugs 2011; 16: 479-491

Mayer, G., Vogel, V., Weyermann, J., Lochmann, D., van den Broek, J.A., Tziatzios, C., Haase, W., Wouters, D., Schubert, U., Zimmer, A., Kreuter, J., Schubert, D., Oligonucleotide-protamine-albumin nanoparticles: protamine sulfate causes drastic size reduction. Journal of Controlled Release 2005; 106: 181-187

McCarron, P.A., Donnelly, R.F., Marouf, W., Celecoxib-loaded poly(D,L,-lactide-co-glycolide) nanoparticles prepared using a novel and controllable combination of diffusion and emulsification steps as part of the salting-out procedure. Journal of Microencapsulation 2006; 23: 480-498

McMorrow, J., Murphy, E.P., Inflammation: a role for NR4A receptors. Biochemical Society Transactions 2011; 39: 688-693

Medina, C., Santos-Martinez, M.J., Radomski, A., Corrigan, O.I., Radomski, M.W., Nanoparticles: pharmacological and toxicological significance. British Journal of Pharmacology 2007; 150: 552-558

Mengshol J.A., Mix, S.K, Brinckerhoff, C.E., Matrix metalloproteinases as therapeutic agents in arthritic diseases: Bull's-eye or missing the mark? Athritis and Rheumatism 2002; 46: 13-20

Metha, R.C., Jeyanthi, R., Calis, S., Thanoo, B.C., Burton, K.W., DeLuca, P.P. Biodegradable microspheres as depot for parenteral delivery of peptide drugs. Journal of Controlled Release 1994; 29: 375-384

Miyazaki, T., Yomota, C., Okada, S., Ultrasonic depolymerization of hyaluronic acid. Polymer Degradation and Stability 2001; 74: 77-85.

Mok, H., Park, J.W., Park, T.G., Antisense oligodeoxynucleotide-conjugated hyaluronic acid/protamine nanocomplexes for intracellular gene inhibition. Bioconjugate Chemistry 2007; 18: 1483-1489

Molyneux, P., Frank, H.P., The interaction of polyvinylpyrrolidone with aromatic compounds in aqueous solution. Part II. The effect of the interaction on the molecular size of the polymer. Journal of the American chemical Society 1961; 83: 3175-3180

Monach P.A., Nigrovic P.A., Chen M., Hock H., Lee D.M., Benoist C., Mathis D., Neutrophils in a mouse model of autoantibody-mediated arthritis: critical producers of Fc receptor gamma, the receptor for C5a, and lymphocyte function-associated antigen 1. Arthritis & Rheumatism 2010; 62: 753-64.

Monach, P.A., Mathis, D., Benoist, C., Animal models for autoimmune and inflammatory disease. Current Protocols in Immunology 2008; Suppl. 81 15.22.1-15.22.12.

Montfort, J., Pelletier, J.-P., Garcia-Giralt, N., Martel-Pelletier, J., Biochemical basis of the effect of chondroitin sulphate on osteoarthritis articular tissues. Annals of the Rheumatic Diseases 2008; 67: 735-740

Morfin, I., Buhler, E., Cousin, F., Grillo, I., Boué, F., Rodlike complexes of a polyelectrolyte (hyaluronan) and a protein (lysozyme) observed by SANS. Biomacromolecules 2011; 12: 859-870

Morgen, M., Tung, D., Boras, B., Miller, W., Malfait, A.-M., Tortorella, M., Nanoparticles for improved local retention after intra-articular injection into the knee joint. Pharmaceutical Research 2013; 30: 257-268

Mori, Y., Nakamura, S., Kishimoto, S., Kawakami, M., Suzuki, S., Matsui, T., Ishihara, M., Preparation and characterization of low-molecular-weight heparin/protamine nanoparticles (LMW-H/P NPs) as FGF-2 carrier. International Journal of Nanomedicine 2010; 5: 147-155

Müller, R.H., Lherm, C., Herbort, J., Blunk, T., Couvreur, P., Alkylcyanoacrylate drug carriers: I. Physicochemical characterization of nanoparticles with different alkyl chain length. International Journal of Pharmaceutics 1992; 84:1-11

Nasti, A., Zaki, N.M., de Leonardis, P., Ungphaiboon, S., Sansongsak, P., Rimoli, M.G., Tirelli, N., Chitosan/TPP and chitosan/TPP- hyaluronic acid nanoparticles : systematic optimisation of the preparative process and preliminary biological evaluation. Pharmaceutical Research 2009; 26: 1918-1930

Nizri, G., Magdassi, S., Schmidt, J., Cohen, Y., Talmon, Y., 2004. Microstructural characterization of micro- and nanoparticles formed by polymer-surfactant interactions. Langmuir 20, 4380-4385.

O'Donnell, P.B., McGinity, J.W., preparation of microspheres by the solvent evaporation technique. Advanced Drug Delivery Reviews 1997; 28: 25-42

Oh, J.K., Lee, D.I., Park, J.M., Biopolymer-based microgels/nanogels for drug delivery applications. Progress in Polymer Science 2009; 34: 1261-1282

Ohtake, S., Wang, Y.J., Trehalose:current use and future applications. Journal of Pharmaceutical Sciences 2011; 100: 2020-2053

Oyarzun-Ampuero, F.A, Brea, J., Loza, M.I., Torres, D., Alonso, M.J., Chitosan-hyaluronic acid nanoparticles loaded with heparin for the treatment of asthma. International Journal of Pharmaceutics 2009; 381: 122-129

Oyarzun-Ampuero, F.A., Goycoolea, F.M., Torres, D., Alonso, M.J., A new drug nanocarrier consisting of polyarginine and hyaluronic acid. European Journal of Pharmaceutics and Biopharmaceutics 2011; 79: 54-57

Ozoran, K., Yildirim, M., Önder, M., Sivas, F., Inanir, A., The bone mineral density effects of calcitonin and alendronate combined therapy in patients with rheumatoid arthritis. APLAR Journal of Rheumatology 2007; 10: 17-22

Paluch, K.J., Tajber, L., McCabe, T., O'Brien, J.E., Corrigan, O.I., Healy, A.M., Preparation and solid state characterisation of chlorothiazide sodium intermolecular self-assembly suprastructure. European Journal of Pharmaceutical Sciences 2010; 41, 603-611.

Parajó, Y., d'Angelo, I., Welle, A., Garcia-Fuentes, M., Alonso, M.J., Hyaluronic acid/chitosan nanoparticles as delivery vehicles for VEGF and PDGF-BB. Drug Delivery 2010; 17: 596-604

Parojčić, J., Stojković, A., Tajber, L., Grbić, S., Paluch, K.J., Djurić, Z., Corrigan, O.I., Biopharmaceutical characterization of ciprofloxacin HCl-ferrous sulfate interaction. Journal of Pharmaceutical Sciences 2011; 100: 5174-5184.

Pathak, A., Kumar, P., Chuttani, K., Jain, S., Mishra, A., Vyas, S.P., Gupta, K.C., Gene expression, biodistribution and pharmacoscintigraphic evaluation of chondroitin sulphate-PEI nanoconstructs mediated tumor gene therapy. ACS Nano 2009; 3: 1493-1505

Patton, J., Pulmonary delivery of drugs for bone disorders. Advanced Drug Delivery Reviews 2000; 42: 239-248

Peer, D., Florentin, A., Margalit, R., Hyaluronan is a key component in cryoprotection and formulation of targeted unilamellar liposomes. Biochimica et Bipohysica Acta 2003; 1612: 76-82

Pelley, J.L., Daar, A.S., Saner, M., State of academic knowledge on toxicity and biological fate of quantum dots. Toxological Sciences 2009; 112: 276-296

Pei, L., Castrillo, A., Chen, M., Hoffmann, A., Tontonoz, P., Induction of NR4A orphan nuclear receptor expression in macrophages in response to inflammatory stimuli. Journal of Biological Chemistry 2005; 280: 29256-29262

Peniche, C., Fernández, M., Rodríguez, G., Parra, J., Jimenez, J., Bravo, A.L., Gómez, D., San Román, J., Cell supports of chitosan/hyaluronic acid and chondroitin sulphate systems. Morphology and biological behaviour, Journal of Materials Science: Materials in Medicine 2007; 18: 1719-1726.

Philipp, B., Dautzenberg, H., Linow, K.J., Kötz, J., Dawydoff, W., Polyelectrolyte complexes- recent developments and open problems. Progress in Polymer science 1989; 14: 91-172

Pisal, D.S., Kosloski, M.P., Balu-Iyer, S.V., Delivery of therapeutic proteins. Journal of Pharmaceutical Sciences 2010; 99: 2557-2575

Prego, C., Garcia-Fuentes, M., Torres, D., Alonso, M.J., Transmucosal macromolecular drug delivery. Journal of Controlled Release 2005; 101: 151-162

Prego, C., Torres, D., Fernandez-Megia, E., Novoa-Carballal, R., Quiñoá, E., Alonso, M.J., Chitosan-PEG nanocapsules as new carriers for oral peptide delivery. Effect of chitosan pegylation degree. Journall of controlled Release 2006; 111: 299-308

Quintanar-Guerrero, D., Fessi, H., Allémann, E., Doelker, E., Influence of stabilizing agents and preparative variables on the formation of poly(D,L-lactic acid) nanoparticles by an emulsification-diffusion technique. International Journal of Pharmaceutics 1996; 143: 133-141

Radziwon-Balicka, A., Medina, C., O'Driscoll, L., Treumann, A., Bazou, D., Inkielewicz-Stepniak, I., Radomski, A., Jow, H., Radomski, M.W., Platelets increase survival of adenocarcinoma cells challenged with anticancer drugs: mechanisms and implications for chemoresistance. British Journal of Pharmacology 2012; 167: 787-804

Ralph, J.A., McEvoy, A.N., Kane, D., Bresniham, B., Fitzgerald, O., Murphy, E.P., Modulation of orphan nuclear receptor, NURR1, expression by methotrexate in human inflammatory joint disease involved adenosine A2A receptor-mediated resposes. Journal of Immunology 2005; 175: 555-565

Reynolds, F., Weissleder, R., Josephson, L., Protamine as an efficient membrane-translocating peptide. Bioconjugate Chemistry 2005; 16: 1240-1245

Rosca, I.D., Watari, F., Uo, M., Microparticle formation and its mechanism in single and double emulsion solvent evaporation. Journal of Controlled Release 2004; 99: 271-280

Ryan, S.M., Frias, J.M., Wang, X., Sayers, C.T., Haddleton, D.M., Brayden, D.J., PK/PD modelling of comb-shaped PEGylated salmon calcitonin conjugates of differing molecular weights. Journal of Controlled Release 2011; 149: 126-132

Ryan, S.M., Wang, X., Mantovani, G., Sayers, C.T., Haddleton, D.M., Brayden, D.J., Conjugation of salmon calcitonin to a combed-shaped end functionalized poly(poly(ethyleneglycol) methyl ether methacrylate) yields a bioactive stable conjugate. Journal of Controlled Release 2009; 135: 51-59

Sabbisetti, V.S., Chirugupati, S., Thomas, S., Vaidya, K.S., Reardon, D., Chiriva-Internati, M., Iczkowski, K.A., Shah, G.V., Calcitonin increases invasiveness of prostate cancer cell: role for cyclic AMP-dependent protein kinase A in calcitonin action. International Journal of Cancer 2005; 117: 551-560

Sánchez, A., Tobio., M., Gonzalez, M., Fabra, A., Alonso, M.J., Biodegradable micro- and nanoparticles as long-term delivery vehicles for interferon-alpha. European Journal of Pharmaceutical Science 2003; 8: 221-229

Schatz, C., Domard, A., Viton, C., Pichnot, C., Delair, T., Versatile and efficient formation of colloids of biopolymer-based polyelectrolyte complexes. Biomacromolecules 2004; 5: 1882-1892

Schipper, N.G., Vårum, K.M., Artursson, P., Chitosans as absorption enhancers for poorly absorbable drugs. 1: Influence of molecular weight and degree of acetylation on drug transport across human intestinal epithelial (Caco-2) cells. Pharm. Res. 1996; 13: 1686-1692.

Schrand, A.M., Rahman, M.F., Hussain, S.M., Schlager, J.J., Smith, D.A., Syed, A.F., Metal-based nanoparticles and their toxicity assessment. Wiley Interdisciplinary Reviews- Nanomedicine and Nanobiotechnology 2010; 2: 544-568

Schroeder K., Sommerfeld P., Sabel B., Efficacy of oral dalargin-loaded nanoparticle delivery across the blood-brain barrier, Peptides 1998; 19: 778-780

Scott, D.L. , Wolfe, F., Huizinga, T.W., Rheumatoid arthritis. Lancet 2010; 376: 1094-1108.

Sondergaard, B.C., Wulf, H., Henriksen, K., Schaller, S., Oestergaard, S., Qvist P., Tanko, I.B., Bagger, Y.Z., Christiansen, C., Karsdal, M.A., Calcitonin directly attenuates collagen type II degradation by inhibition of matrix metalloptoteinase expression and activity in article chondrocytes. Osteoarthritis Cartilage 2006; 14: 759-768

Soppimath, K.S., Aminabhavi, T.M., Kulkarni, A.R., Rudzinski, W.E., Biodegradable polymeric nanoparticles as drug delivery devices. Journal of Controlled Release 2001; 70: 1-20

Stahl, P.H., Wermuth, C.G., 2008, Handbook of pharmaceutical salts properties, selection and use. Wiley-VCH.

Stern, R., Asari, A.A., Sugahara, K.N., Hyaluronan fragments: an information reach system. European Journal of Cell Biology 2006; 85: 699-715.

Sundar, S., Kundu, J., Kundu, S.C., Biopolymeric nanoparticles. Science and Technology for Advanced Materials 20110; 11/ 014104 (13pp)

Tajber, L., Corrigan, D.O., Corrigan, O.I, Healy, A.M., Spray drying of budesonide, formoterol fumarate and their composites I. Physicochemical characterisation. International Journal of Pharmaceutics 2009; 367, 79-85.

Tchetverikov, I., Lohmander,L.S., Verzjil, N., Huizngа, T.W., TeKoppele, J.M., Hanemaaijer, R., DeGroot, J., MMP protein and activity levels in synoval fluid from patients with joint injury, inflammatory arthritis, and osteoarthritis. Annals of the Rheumatic Diseases 2005; 64: 694-698

Thakkar., H., Sharma, R.K., Mishra, A.K., Chuttani, K., Murthy, R.S., Celecoxib-incorporated chitosan microspheres: in vitro and in vivo evaluation. Journal of drug Targeting 2004; 12: 549-557

Tobio, M., Gref, R., Sánchez, A., Langer, R., Alonso, M.J., Stealth PLA-PEG nanoparticles as protein carriers for nasal administration. Pharmaceutical Research 1998; 15: 270-275

Tobio, M., Sánchez, A., Vila, A., Soriano, I., Evora, C., Vila-Jato, J.L., Alonso, M.J., The role of PEG on the stability in digestive fluids and in vivo fate of PEG-PLA nanoparticles following oral administration. Colloids and Surfaces B 2000; 18: 315-323

Torres-Lugo, M., Peppas, N.A., Transmucosal delivery systems fo calcitonin: a review. Biomaterials 2000; 21: 1191-1196

Tsai, H.-Y., Chiu, C.-C., Lin, P.-C., Chen, S.-H., Huang, S.-J., Wang, L.-F., Antitumor efficacy of doxorubicin released form crosslinked nanoparticulate chondroitin sulphate/chitosan polyelectrolyte complexes. Macromolecular Bioscience 2011; 11: 680-688

van Damme, M.-P. I., Moss, J.M., Murphy, W.H., Preston, B.N., Binding properties of glycosaminoglycans to lysozyme- effect of salt and molecular weight. Archives of Biochemistry and Biophysics 1994; 310: 16-24

van der Lubben, I.M., Verhoef, J.C., van Aelst, A.C., Borchard, G., Junginger, H.E., Chitosan microparticles for oral vaccination: preparation, characterization and preliminary *in vivo* uptake studies in murine Peyer's patches. Biomaterials 2001; 22: 687-694

Varian, Inc. PL aquagel-OH Mixed Data Sheet http://www.varianinc.com/image/vimage/docs/products/consum/gpc-sec/gpcseccolumns/aqueous/shared/pl_aquagel-oh_mixed_ds.pdf accessed on 09/05/2012

Vila, A., Sanchez, A., Tobio, M., Calvo, P., Alonso, M.J., design of biodegradable particles for protein delivery. Journal of Controlled Release 2002; 78: 15-24

Vogel, V., Lochmann, D., Weyermann, Y., Mayer, G., Tziatzios, C., Van den Broek, J.A., Haase, W., Wouters, D., Schubert, U.S., Kreuter, J., Zimmer, A., Schubert, D., Oligonucleotide-protamine-albumin nanoparticles: preparation, physical properties, and intracellular distribution. Journal of Controlled Release 2005; 103: 99-111

Volpi, N., Oral absorption and bioavailability of ichthyic origin chondroitin sulphate in healthy male volunteers. Osteoarthritis and Cartilage 2003; 11: 433-441

Volpi, N., Oral bioavailability of chondroitin sulfate (Condrosulf®) and its constituents in healthy men volunteers. Osteoarthritis and Cartilage 2002; 10: 768-777

Vranckx, H., Demoustrier, M., Deleers, M., A new nanocapsule formulation with hydrophilic core: application to the oral administration of salmon calcitonin. European Journal of Pharmaceutics and Biopharmaceutics 1996; 42: 345-347

Wadhwa, S., Paliwal, R., Paliwal, S.R., Vyas, S.P., Hyaluronic acid modified chitosan nanoprticles for effective manageent of glaucoma: development, characterization and evaluation. Journal of Drug Targetting 2009; 18: 29-302

Wang, K., Wan, Y.-J., Nuclear receptors and inflammatory diseases. Experimental Biology and Medicine 2008; 233: 496-506

Wieland, H.A., Michaelis, M., Kirschbaum, BJ., Rudolphi, k.A., Osteoarthritis- an untreatable disease? Nature Reviews Drug Discovery 2005; 4: 331-344

Windish, V., de Luccia, F., Dahau, L., Herman, F., Mencel, J.J., Tang, S.-Y., Vuilhorgne, M., Degradation pathways of salmon calcitonin in aqueous solution. Journal of Pharmaceutical Sciences 1997; 86: 359-364

Wyatt, C. A., Coon, C. I., Gibson, J. J., and Brinckerhoff, C. E., Potential for the 2G single nucleotide polymorphism in the promoter of matrix metalloproteinase to enhance gene expression in normal stromal cells. Cancer Research 2002; 62: 7200-7202

Yang, M., Yamamoto, H., Kurashima, H., Takeuchi, H., Yokoyama, T., Tsujimoto, H., Kawashima, Y., Design and evaluation of poly(DL-lactic-co-glycolic acid) nanocomposite particles containing salmon calcitonin for inhalation. European Journal of Pharmaceutical Sciences 2012; 46: 374-380

Yeh, M.-K., Cheng. K.-M., Hu, C.S., Huang, Y.-H., Yong, J.-J., Novel protein-loaded chondrotin sulfate-chitosan nanoparticles: Preparation and characterization. Acta Biomaterialia 2011; 7: 3804-3812

Yogasundaram, H., Bahniuk, M.S., Singh, H.-D., Aliabadi, H.M., Uludağ, H., Unsworth, L.D., BSA nanoparticles for siRNA delivery: Coating effects on

nanoparticle properties, plasma protein adsorption, and *in vitro* siRNA delivery. International Journal of Biomaterials 2012; doi: 10.1155/2012/584060

Zambaux, M.F., Bonneaux, F., Gref, R., Maincent, P., Dellacherie, E., Alonso, M.J., Labrude, P., Vigneron, C., Influence of experimental parameters on the characteristics of poly(lactic acid) nanoparticles prepared by a double emulsion method. Journal of Controlled Release 1998; 50: 31-40

Zhi-Gang, F., Ping, P., Zhi-Qiang, Y., Ya-Gen, C., Jian-Kang, Z., Miao, W., Xue-Nong, Z., Qiang, Z., Two novel freeze-dried pH-sensitive cyclosporine A nanoparticles: preparation, *in vitro* drug release, and *in vivo* absorption enhancement effects. Current Nanoscience 2009; 5: 449-456

Zille, H., Paquet, J., Henrionnet, C.J., Scala-Bertola, J.G., Leonard, M.J., Six, J.L., Deschamp, F., Netter, P., Verges, J., Gillet, P., Grossin, L., Evaluation of intra-articular delivery of hyaluronic acid functionalized biopolymeric nanoparticles in healthy rat knees. Bio-medical Materials and Engineering 2010; 20: 235-242

Appendix 1

Isolation of non-associated sCT from HA/CL113/sCT NPs and extraction of associated sCT from the nanocomplexes

The characteristics of nanoparticles (i.e. particle size, PDI, zeta potential and transmittance) after the ultrafiltration-centrifugation process were examined and compared to those obtained for equivalent particles before the process. The ratio of the transmittance values after and before ultrafiltration-centrifugation of TPC of 1 mg/ml-based formulations varied between 90.4±11.1 and 107.4±4.1 %, therefore the turbidity did not change during this process (Fig. 12.1.1). The only exception was the HA/CL113 MMR of 2.5, sCT of 0.35 mg/ml formulation, where the transmittance increased significantly after the ultrafiltration-centrifugation process. This may be attributed to aggregation of particles and possibly adsorption on centrifugation tubes. Indeed, the presence of a small amount of aggregates, which could not be resuspended, was observed.

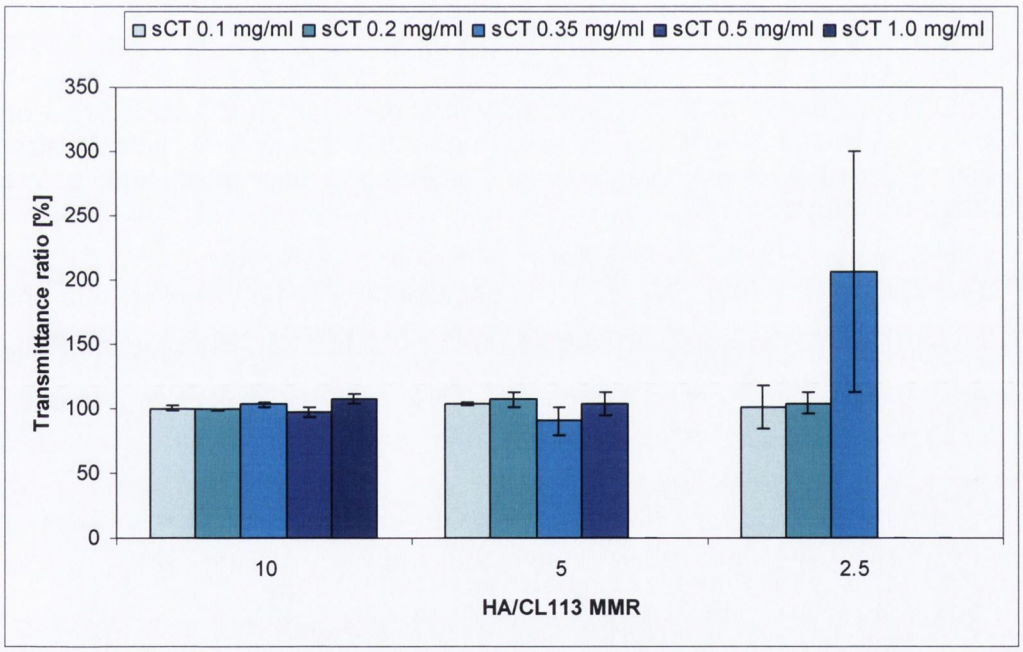

Fig. 12.1.1 The influence of a combined ultrafiltration-centrifugation technique on the characteristics of sCT-loaded TPC of 1 mg/ml HA/CL113 NPs: transmittance. The changes in transmittance are presented as percentage ratio after and before ultrafiltration-centrifugation.

The particle size of TPC of 1 mg/ml formulations did not change significantly after the centrifugation-ultrafiltration process and the particle size ratio was close to 100% in most cases (Fig. 12.1.2). Only for some formulations containing lower concentrations of sCT (all formulations with 0.1 mg/ml and one

with 0.2 mg/ml of sCT) the particle size increased by 20-48%. It may be due to reorganisation of the particle structure due to the forces to which particles were exposed during centrifugation.

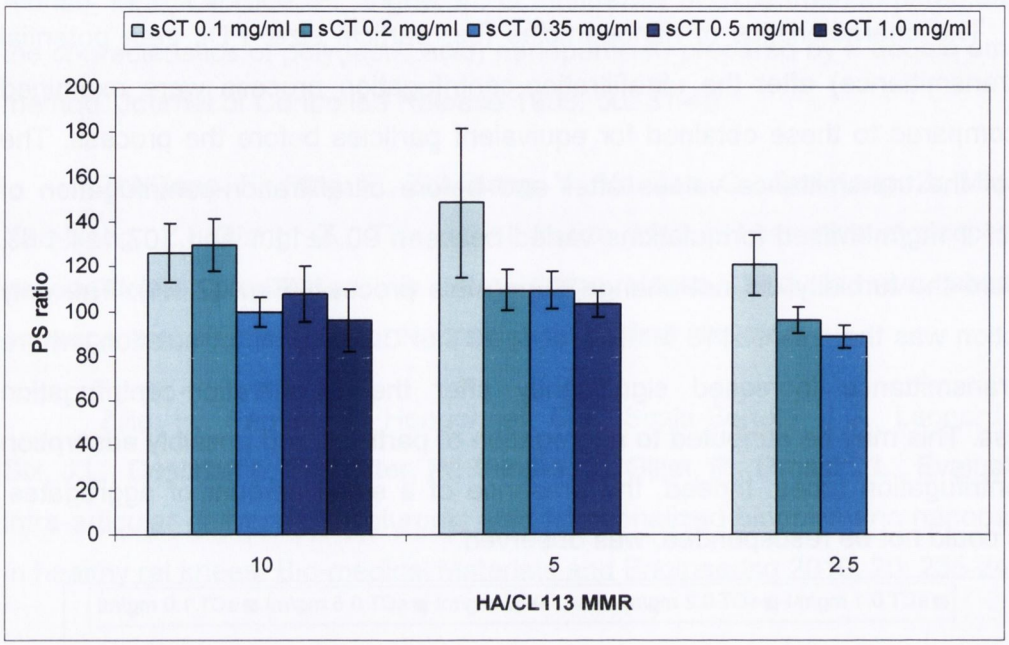

Fig. 12.1.2 The influence of a combined ultrafiltration-centrifugation technique on the characteristics of sCT-loaded TPC of 1 mg/ml HA/CL113 NPs: particle size. The changes in PS are presented as percentage ratio after and before ultrafiltration-centrifugation.

The particle size (Fig.12.1.3) and transmittance (Fig.12.1.4) of HA590 and HA257-based formulations did not change during ultrafiltration-centrifugation, the change was smaller than 15 % for either particle size or transmittance.

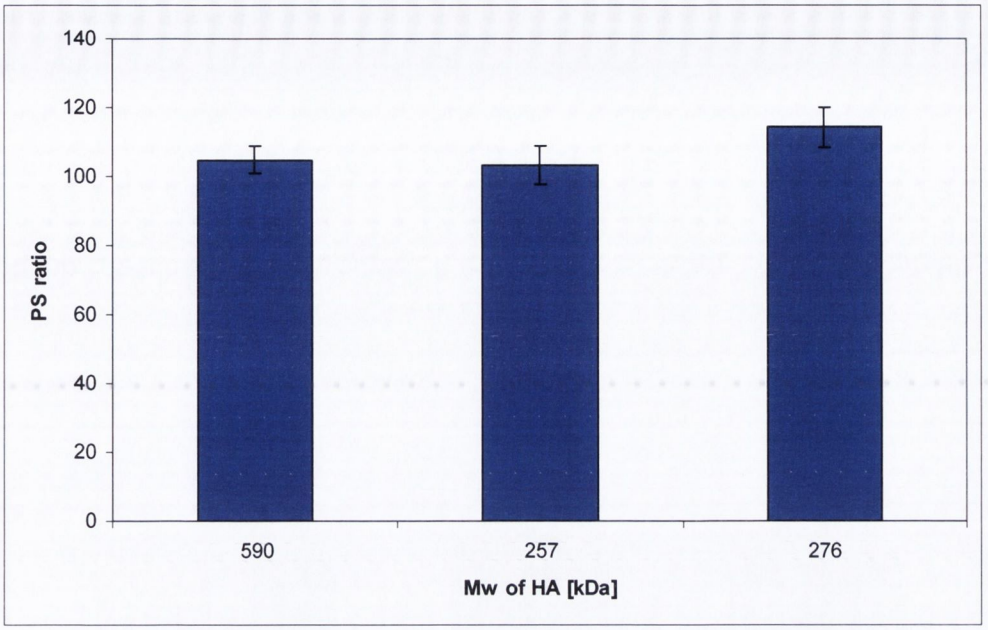

Fig. 12.1.3 The influence of a combined ultrafiltration-centrifugation technique on the characteristics of sCT-loaded TPC of 1 mg/ml HA/CL113 NPs: particle size. The changes in PS are presented as percentage ratio after and before ultrafiltration-centrifugation.

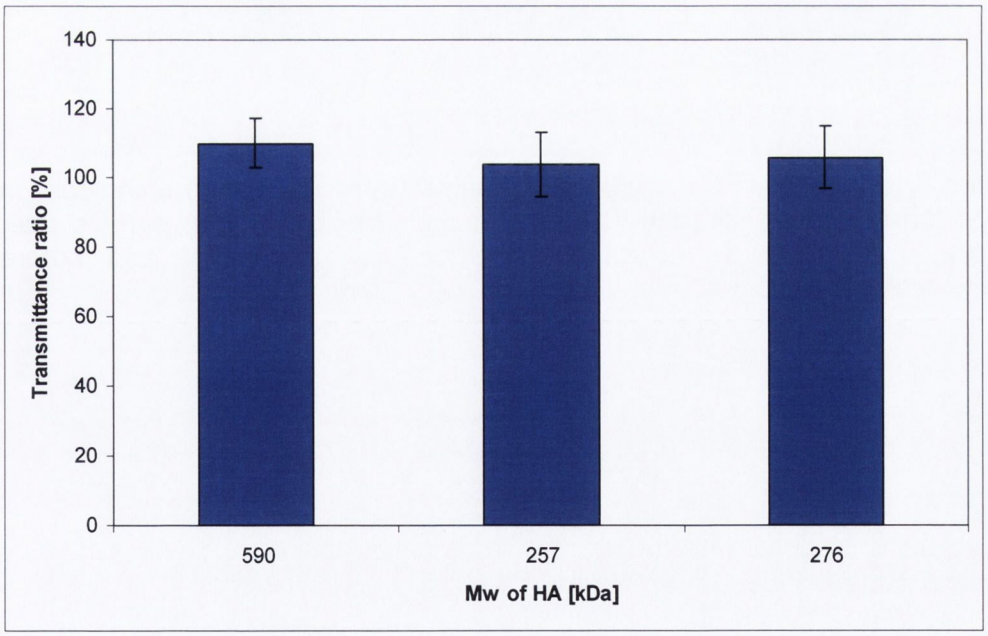

Fig. 12.1.4 The influence of a combined ultrafiltration-centrifugation technique on the characteristics of sCT-loaded TPC of 1 mg/ml HA/CL113 NPs: transmittance. The changes in transmittance are presented as percentage ratio after and before ultrafiltration-centrifugation.

Although the particle size of the TPC of 2 mg/ml-based formulations did not change upon isolation of non-associated sCT (Fig.12.1.5), a substantial increase in

transmittance values was observed (Fig. 12.1.6). The lower HA/CL113 MMR, the larger was the increase in transparency of the samples. That again may be attributed to sedimentation of larger particles and difficulties in their resuspending. As water is being removed during the process, the particles become more concentrated and therefore interactions between the particles may be stronger. This, together with the forces to which the particles are exposed during centrifugation process, may lead to aggregation of some of the particles.

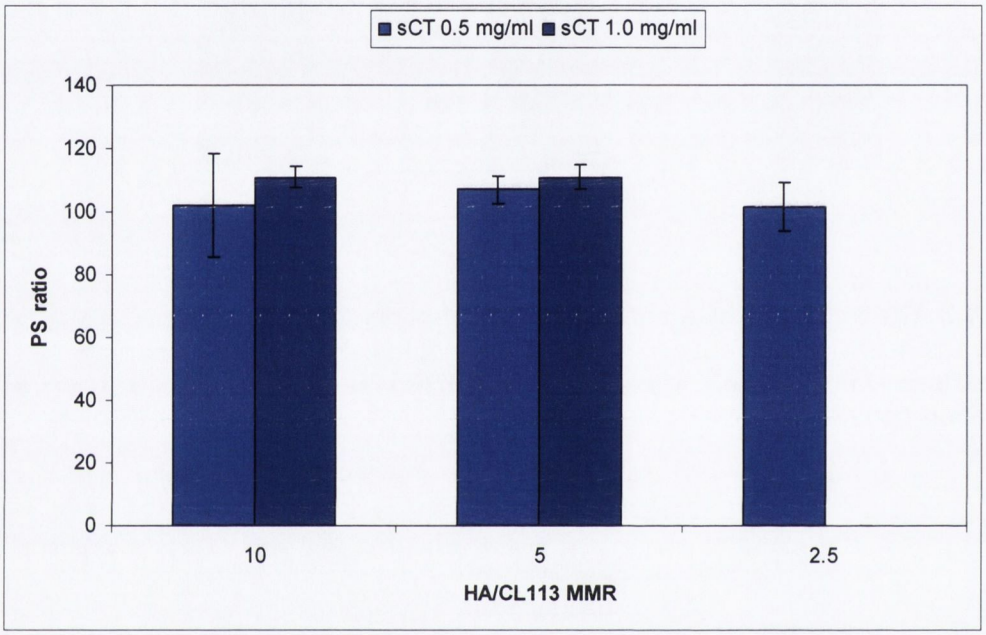

Fig. 12.1.5 The influence of a combined ultrafiltration-centrifugation technique on the characteristics of sCT-loaded TPC of 2 mg/ml HA/CL113 NPs: particle size. The changes in PS are presented as percentage ratio after and before ultrafiltration-centrifugation.

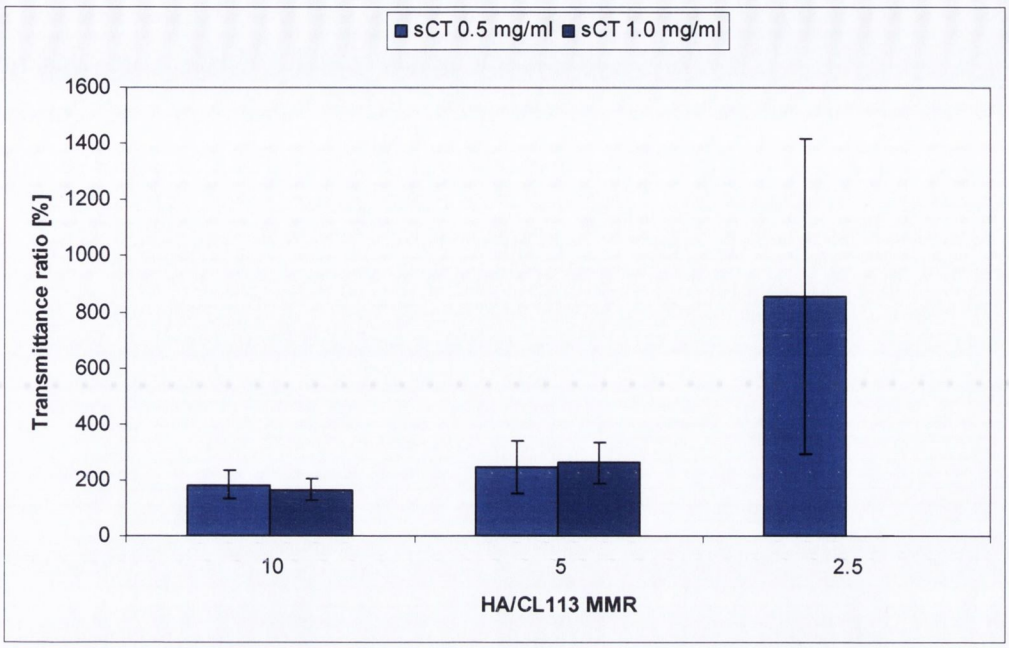

Fig. 12.1.6 The influence of a combined ultrafiltration-centrifugation technique on the characteristics of sCT-loaded TPC of 2 mg/ml HA/CL113 NPs: transmittance. The changes in transmittance are presented as percentage ratio after and before ultrafiltration-centrifugation.

The PDI of the formulations with TPC of 1 mg/ml did not change after ultrafiltration-centrifugation (Fig.12.1.7).

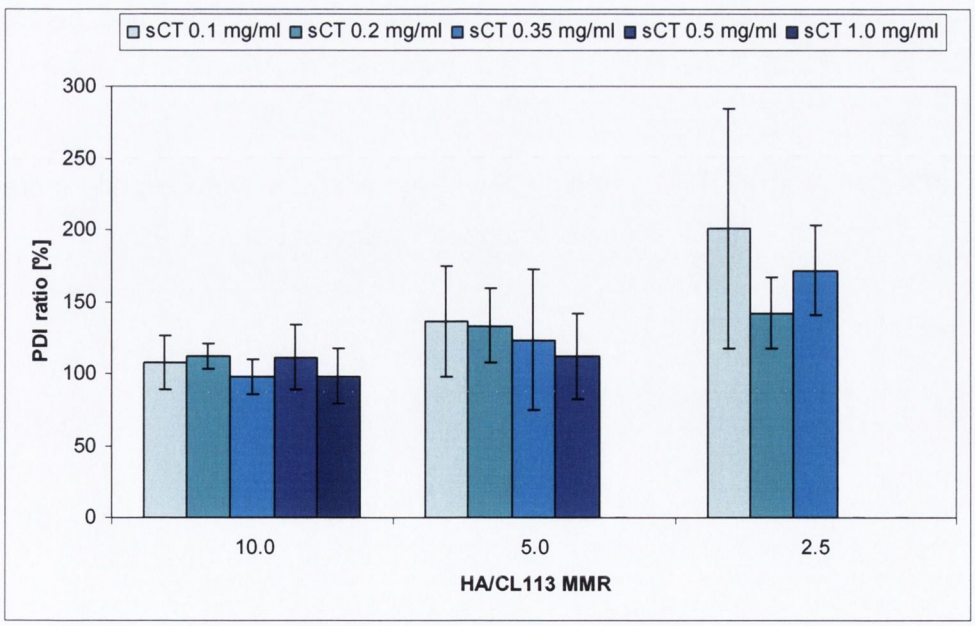

Fig. 12.1.7 The influence of a combined ultrafiltration-centrifugation technique on the characteristics of sCT-loaded TPC of 1 mg/ml HA/CL113 NPs: polydispersity index. The changes in PDI are presented as percentage ratio after and before ultrafiltration-centrifugation.

Similarly, for all NPs with different molecular weight of HA there was no considerable change in the size of the NPs with TPC of 1 mg/ml and sCT of 0.5 mg/ml (Fig. 12.1.8). However NPs with TPC 1 mg/ml, HA/CL113 MMR of 2.5 became more heterogeneously dispersed after the isolation process (Fig.12.1.7).

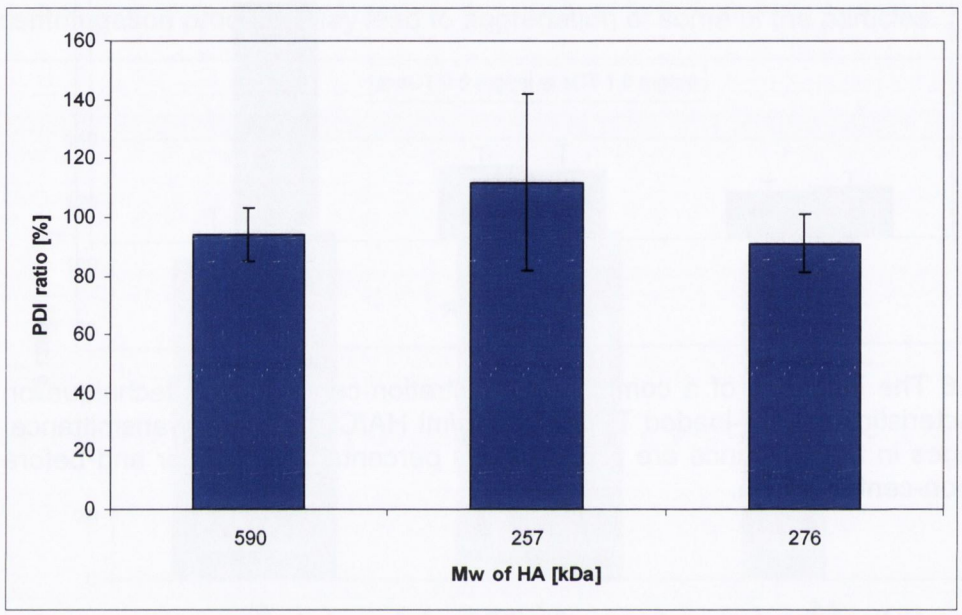

Fig. 12.1.8 The influence of a combined ultrafiltration-centrifugation technique on the characteristics of sCT-loaded TPC of 1 mg/ml HA/CL113 NPs: polydispersity index. The changes in PDI are presented as percentage ratio after and before ultrafiltration-centrifugation.

On the contrary, all TPC 2 mg/ml-based formulations were slightly more monodispersed after the ultrafiltration-centrifugation process (Fig.12.1.9).

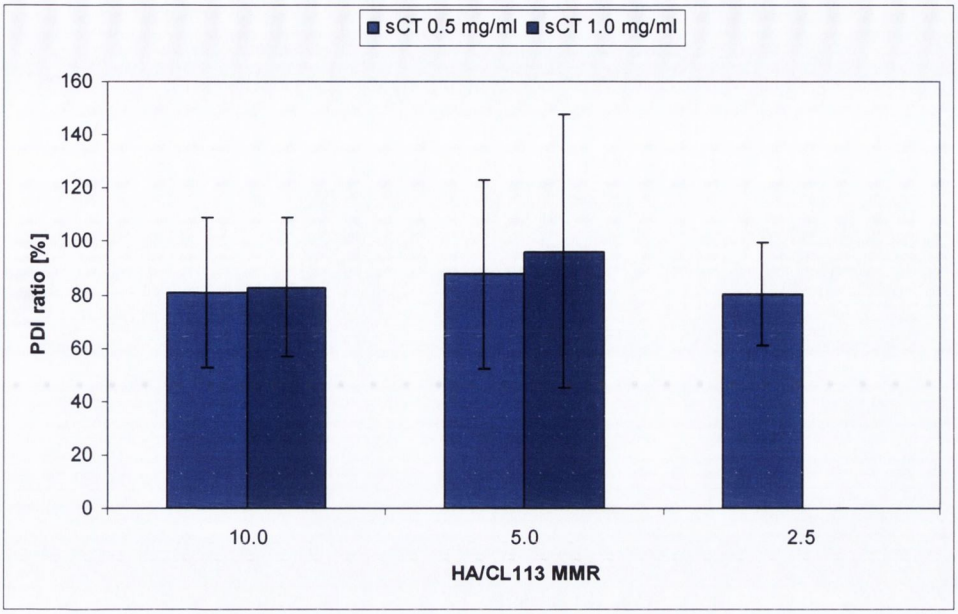

Fig. 12.1.9 The influence of a combined ultrafiltration-centrifugation technique on the characteristics of sCT-loaded TPC of 2 mg/ml HA/CL113 NPs: polydispersity index. The changes in PDI are presented as percentage ratio after and before ultrafiltration-centrifugation.

There were no considerable changes in zeta potential values after the isolation process for any formulations tested (Fig. 12.1.10-12.1.12).

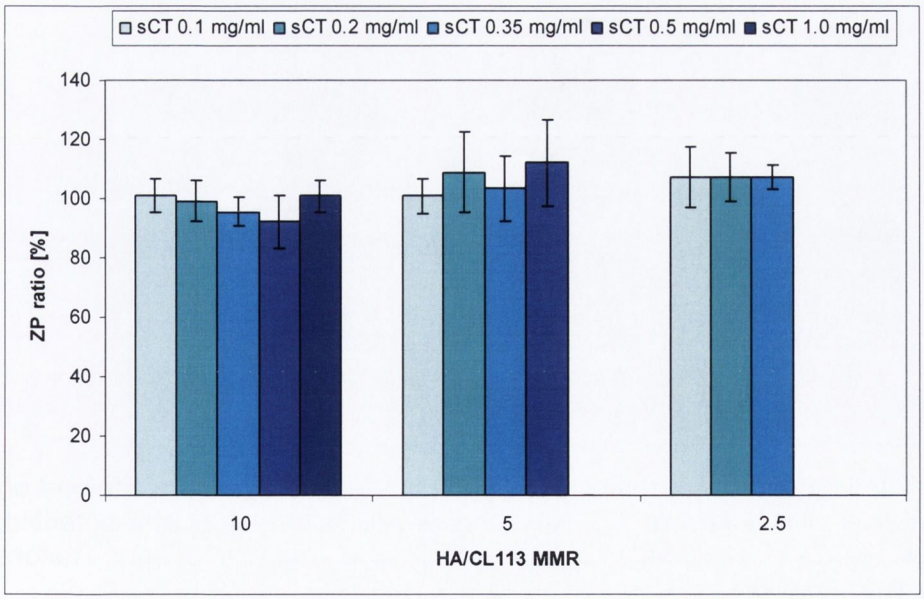

Fig. 12.1.10 The influence of a combined ultrafiltration-centrifugation technique on the characteristics of sCT-loaded TPC of 1 mg/ml HA/CL113 NPs: zeta potential. The changes in ZP are presented as percentage ratio after and before ultrafiltration-centrifugation.

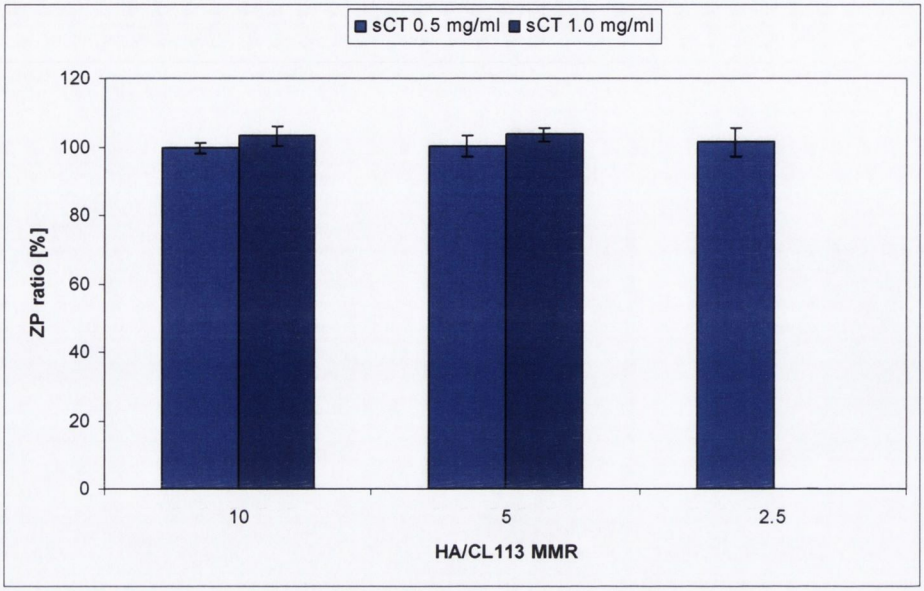

Fig. 12.1.11 The influence of a combined ultrafiltration-centrifugation technique on the characteristics of sCT-loaded TPC of 2 mg/ml HA/CL113 NPs: zeta potential. The changes in ZP are presented as percentage ratio after and before ultrafiltration-centrifugation.

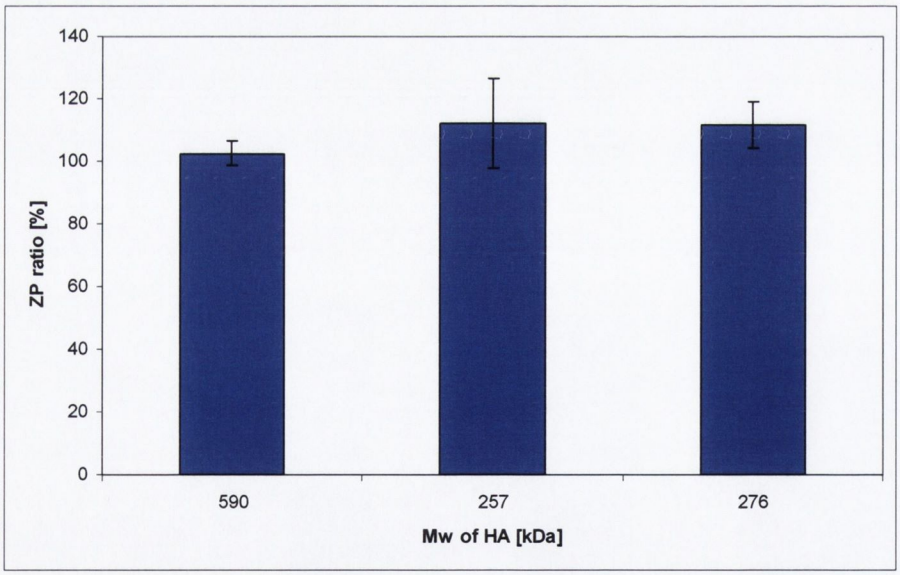

Fig. 12.1.12 The influence of a combined ultrafiltration-centrifugation technique on the characteristics of sCT-loaded TPC of 1 mg/ml HA/CL113 NPs: zeta potential. The changes in ZP are presented as percentage ratio after and before ultrafiltration-centrifugation.

As sCT is likely to interact with HA via electrostatic forces, attempts were made to release sCT from its complex with HA by controlling the pH of the environment. 0.0001 M NaOH solution was used for the extraction of sCT, as at this basic pH values, close to IEP of sCT, the peptide has a net charge close to 0 and thus is expected to dissociate from its complex with HA and NPs. More concentrated NaOH solutions were not used due to the chemical degradation of sCT as it is known that the acid- or base- catalysed hydrolysis of amides may occur at extreme pH values (Windisch et al., 1997). It was possible to recover 97.7±0.13 % of sCT after mixing aqueous solution of sCT with 0.0001 M NaOH, however when 0.001 M NaOH solution was used, only 90.6±0.16 % of sCT was recovered, consistent with possible degradation sCT. When associated sCT was extracted from particles after isolation by ultrafiltration-centrifugation with the use of 0.0001 M NaOH, in all cases the mass balance was obtained (90-100% of sCT was recovered). Other authors (Lee at al., 2010) also managed to dissociate sCT from its ionic complex with TPP by controlling environmental pH with the use of PBS with pH=3.

Appendix 2
Model parameter estimates and related goodness of fit statistics for sCT release data from HA/CL113 NPs fitted to the first order model

Symbols:

Winf: weight released at infinity

k: release rate constant

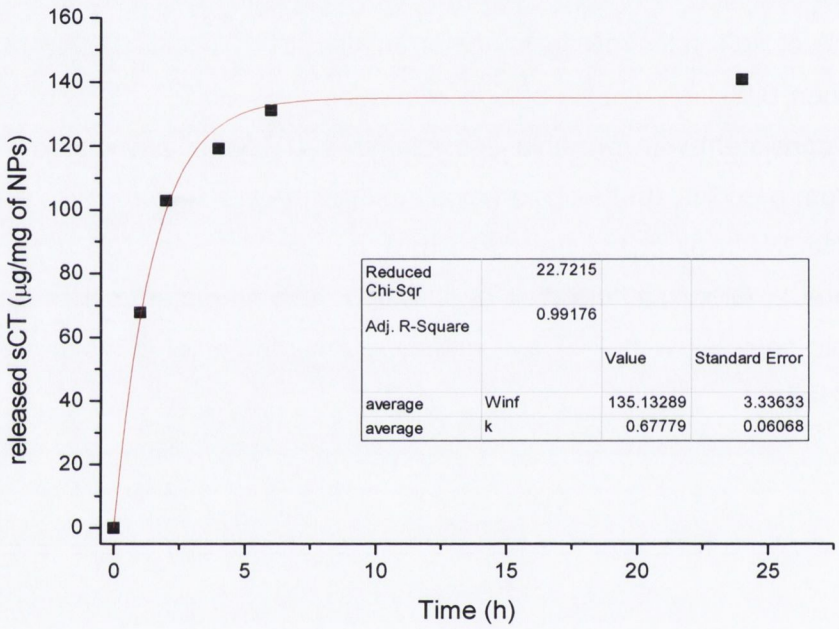

Fig.12.2.1 Model parameter estimates and related goodness of fit statistics for sCT release data from HA/CL113 NPs (sample 5- see Table 4.4, chapter 4) fitted to the first order model.

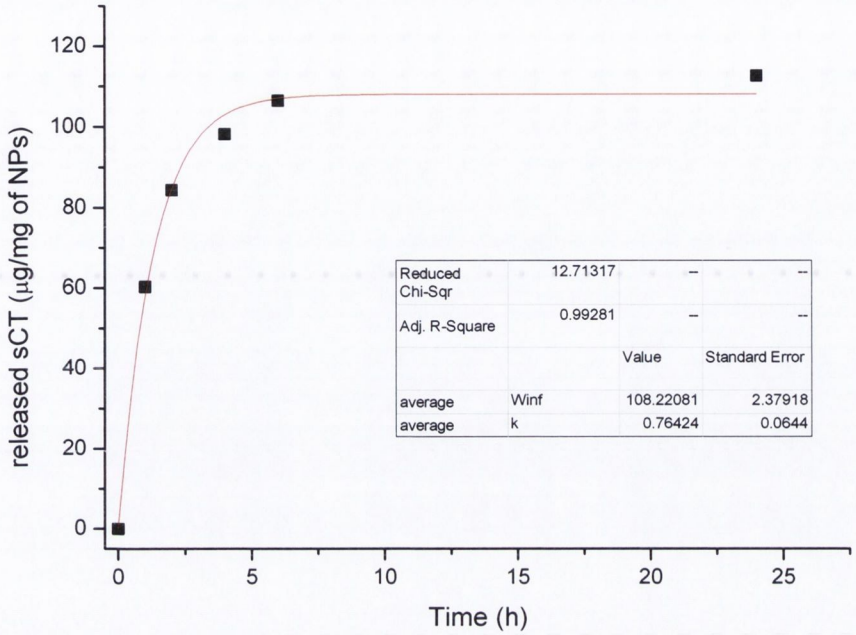

Fig.12.2.2 Model parameter estimates and related goodness of fit statistics for sCT release data from HA/CL113 NPs (sample 9- see Table 4.4, chapter 4) fitted to the first order model.

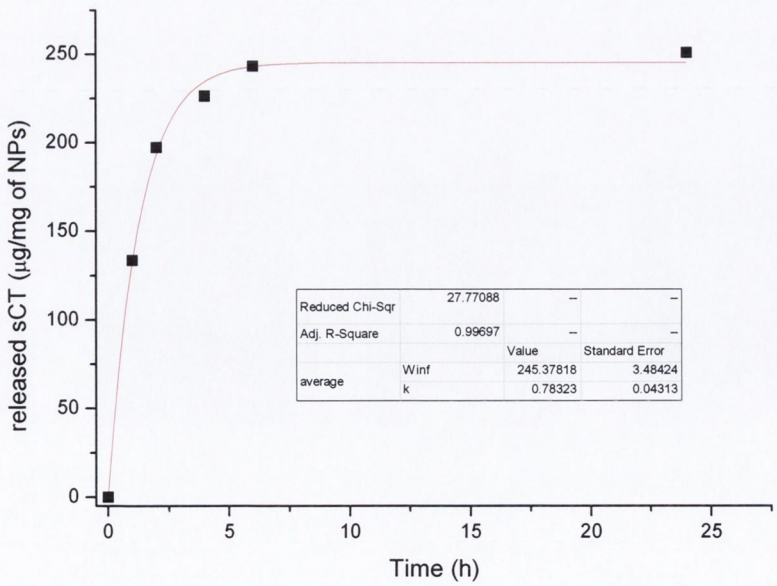

Fig.12.2.3 Model parameter estimates and related goodness of fit statistics for sCT release data from HA/CL113 NPs (sample 11- see Table 4.4, chapter 4) fitted to the first order model.

Appendix 3
Stability studies of sCT in water, aqueous solutions of HA, CL113 and in HA/CL113 NPs.

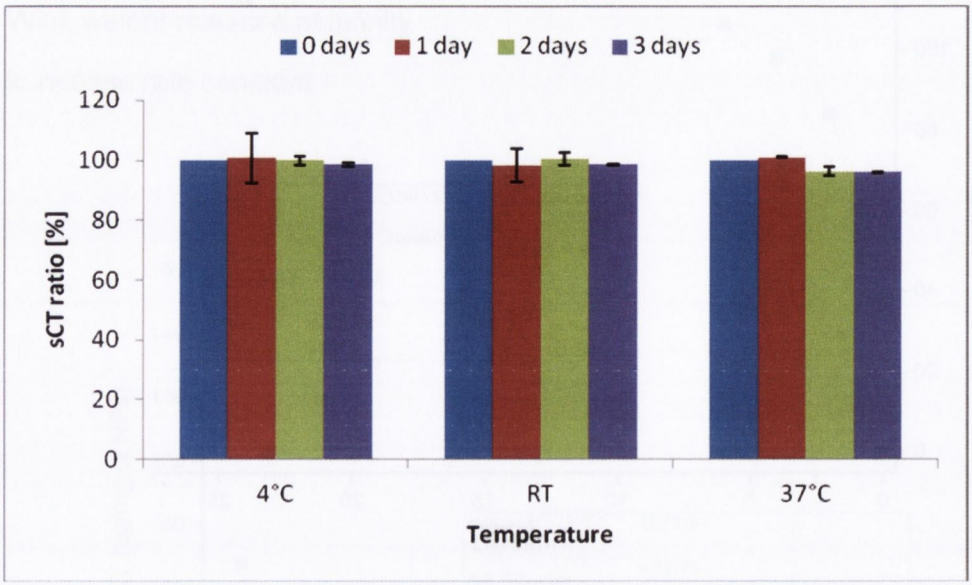

Fig.12.3.1 Stability of sCT associated with HA/CL113 NPs upon storage at 4 °C, room temperature and 37 °C for 3 days. The changes are presented as percentage ratio after storage in relation an initial value treated as 100%.

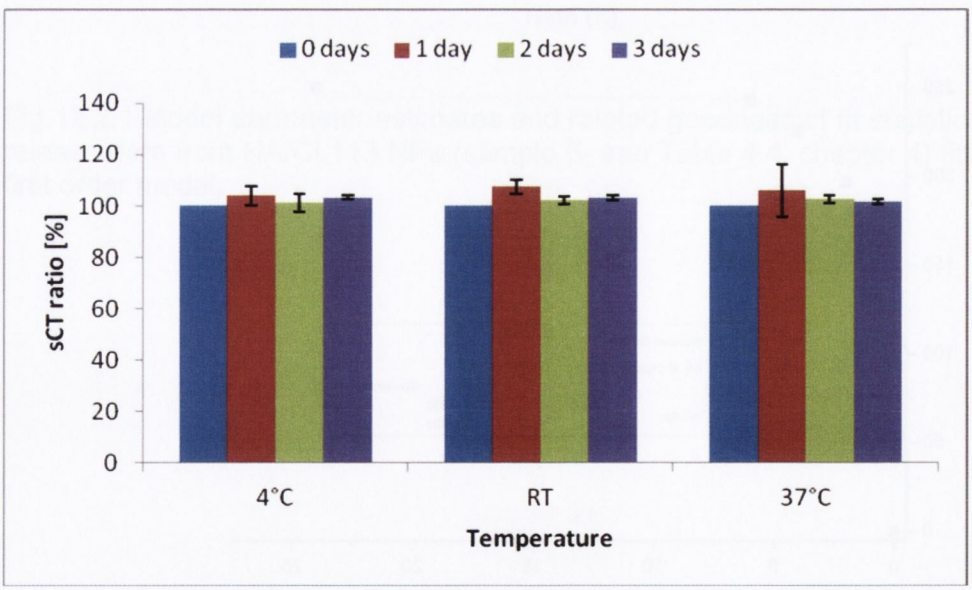

Fig.12.3.2 Stability of sCT in aqueous solution of HA upon storage at 4 °C, room temperature and 37 °C for 3 days. The changes are presented as percentage ratio after storage in relation an initial value treated as 100%.

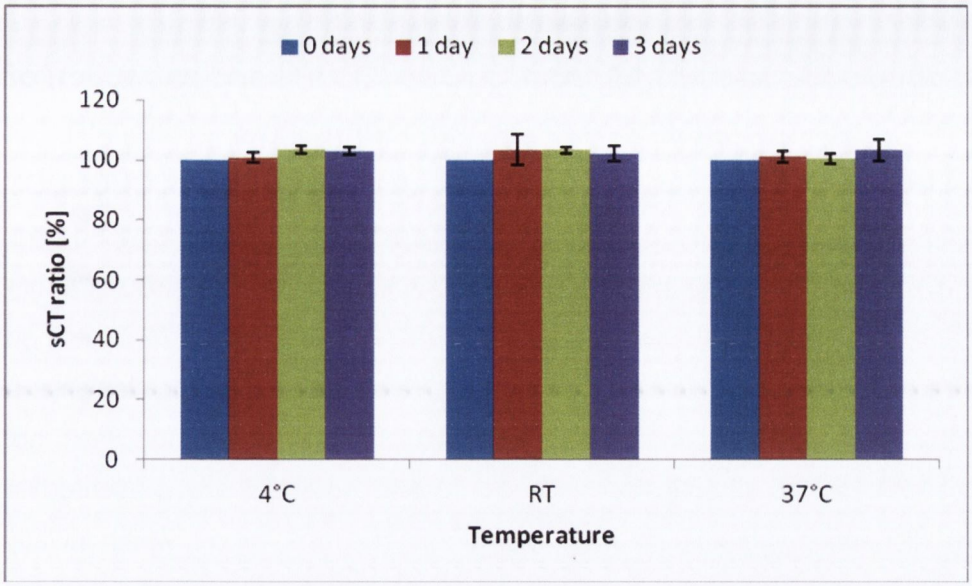

Fig.12.3.3 Stability of sCT in aqueous solution of CL113 upon storage at 4 °C, room temperature and 37 °C for 3 days. The changes are presented as percentage ratio after storage in relation an initial value treated as 100%.

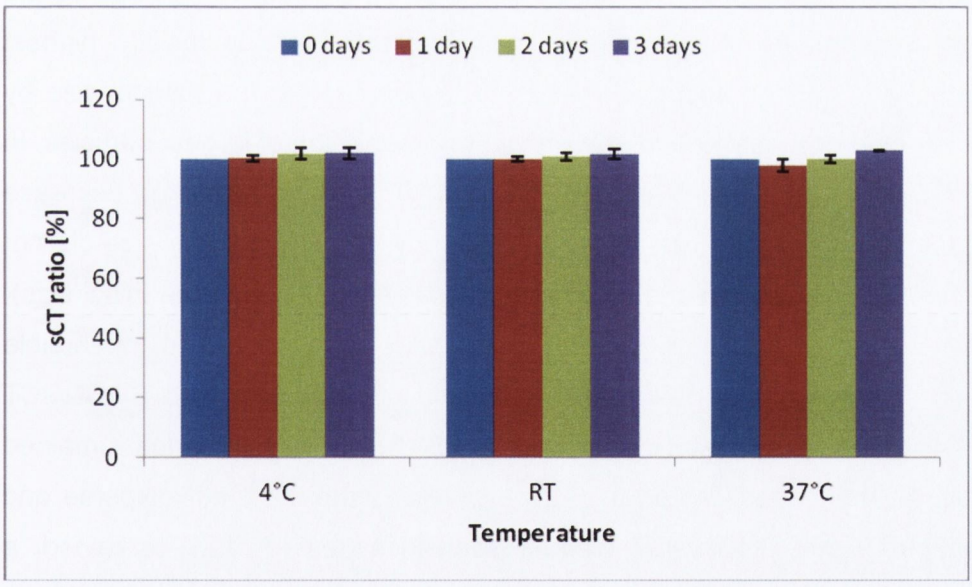

Fig.12.3.4 Stability of sCT in water upon storage at 4 °C, room temperature and 37 °C for 3 days. The changes are presented as percentage ratio after storage in relation an initial value treated as 100%.

Appendix 4

Isolation of non-associated sCT from CHON/sCT NPs and extraction of associated sCT from the nanocomplexes

The influence of ultrafiltration-centrifugation on the properties of CHON/sCT particles depended on the composition of the dispersion. Figures 12.4.1-12.4.2 show the changes in the properties of the nano-suspensions after ultrafiltration-centrifugation process. The suspension with CHON/sCT MMR of 0.175 contained large aggregates, most of which sedimented upon centrifugation leaving a transparent supernatant (transmittance of 99.3±0.7%). As the sample was not suitable for DLS analysis, only the changes in zeta potential are presented in 12.4.4. The dispersion with CHON of 0.7 mg/ml and sCT of 2 mg/ml, which initially was the most turbid system (transmittance of 0.35 %), also became markedly more transparent after centrifugation (the transmittance increased to 61±19 %). As the decrease in transmittance was dramatic, this sample is not shown in Fig. 12.4.2. The changes in transmittance values were due to the aggregation of the nanoparticles upon ultrafiltration-centrifugation and this was visually assessed. This aggregation process was irreversible and it was impossible to redisperse the aggregated fraction. As this dispersion was characterised by initially highest particle size from all nano-suspensions tested, a decrease in the particle size by half was observed probably due to irreversible sedimentation of largest particles. In the case of another dispersion with CHON/sCT MMR of 0.35, a marked decrease of transmittance by a 3-fold was also observed, however the particle size did not change after the ultrafiltration-centrifugation process (115±27 % of the initial size). A decrease in transmittance in this case can also be attributed to irreversible aggregation of some of the particles. In the case of dispersion with CHON/sCT MMR of 1.4, the initial size was decreased by ~50%, but transmittance remained unchanged. As mentioned earlier, this dispersion was the most polydisperse and transparent from all CHON/sCT nano-suspensions tested and contained a relatively high excess of CHON to sCT. It is possible, that due to forces applied to particles during centrifugation and also due to an increase in concentration of both polymers as the water was being removed by the filtration process, a reorganisation in the structure of particles occurred, leading to the formation of smaller, more homogenously dispersed nanoparticles (PDI decreased by ~40% upon ultrafiltration-centrifugation). The particle size of dispersion containing CHON of 0.7 mg/ml and sCT of 1.0 mg/ml increased by 60%, however neither a change in transmittance nor sedimentation was observed. Thus a reorganisation in the

structure of the particles is likely to occur leading to the formation of a smaller amount of larger particles, probably due to the fusion of smaller particles, which results in a decrease in PDI by 20 %, consequently suggesting a more homogenous size distribution. The dispersion containing 1.4 mg/ml of CHON and 2.0 mg/ml of sCT appeared not to be affected markedly by ultrafiltration-centrifugation. The increase in the particle size and transmittance was small (13 and 18%, respectively). PDI increased by 35%, however the size distribution can be still considered as homogenous, because the PDI value after centrifugation is smaller than 0.250 (0.182±0.008). It can be seen (Fig. 12.4.4) that there were no considerable changes in zeta potential during the ultrafiltration-centrifugation process in the nano-suspenions tested. In summary, the samples with CHON/sCT MMR of 0.7 preserved their physical properties after the application of ultrafiltration-centrifugation technique markedly better than CHON/sCT NPs with lower CHON/sCT MMRs.

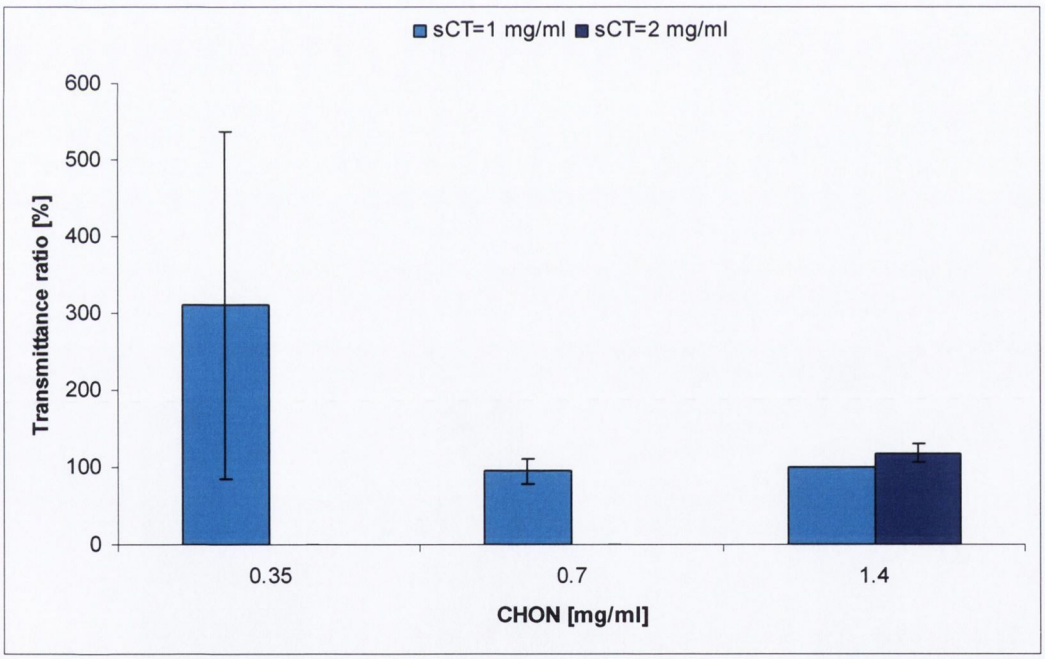

Fig. 12.4.1 The influence of a combined ultrafiltration-centrifugation technique on the characteristics of CHON/sCT nanoparticles: transmittance. The changes in transmittance are presented as a percentage ratio after and before ultrafiltration-centrifugation.

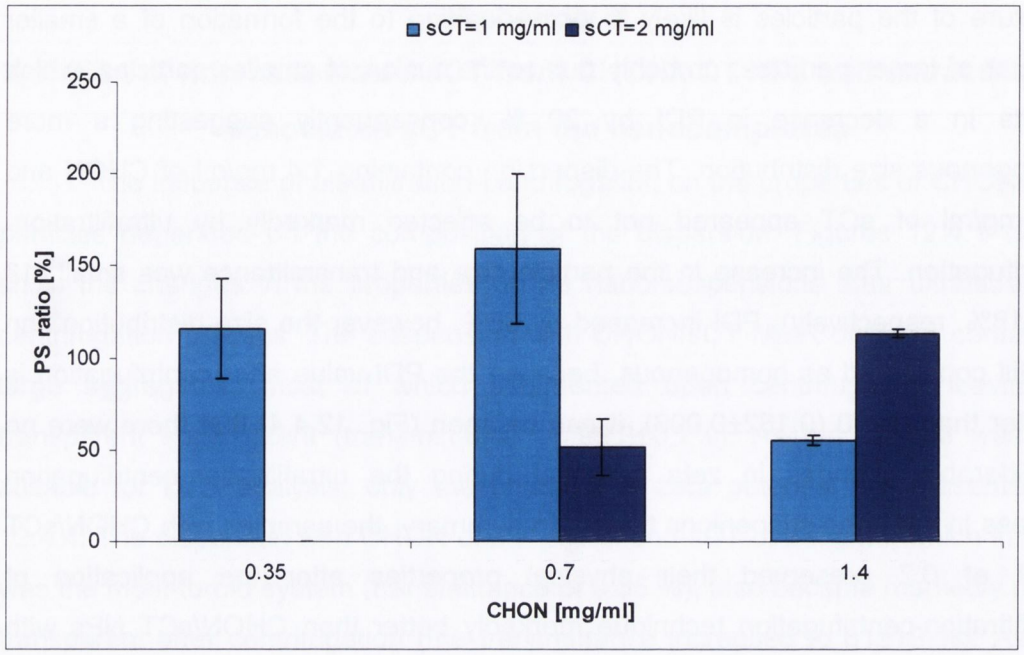

Fig. 12.4.2 The influence of a combined ultrafiltration-centrifugation technique on the characteristics of CHON/sCT nanoparticles: particle size. The changes in PS are presented as a percentage ratio after and before ultrafiltration-centrifugation.

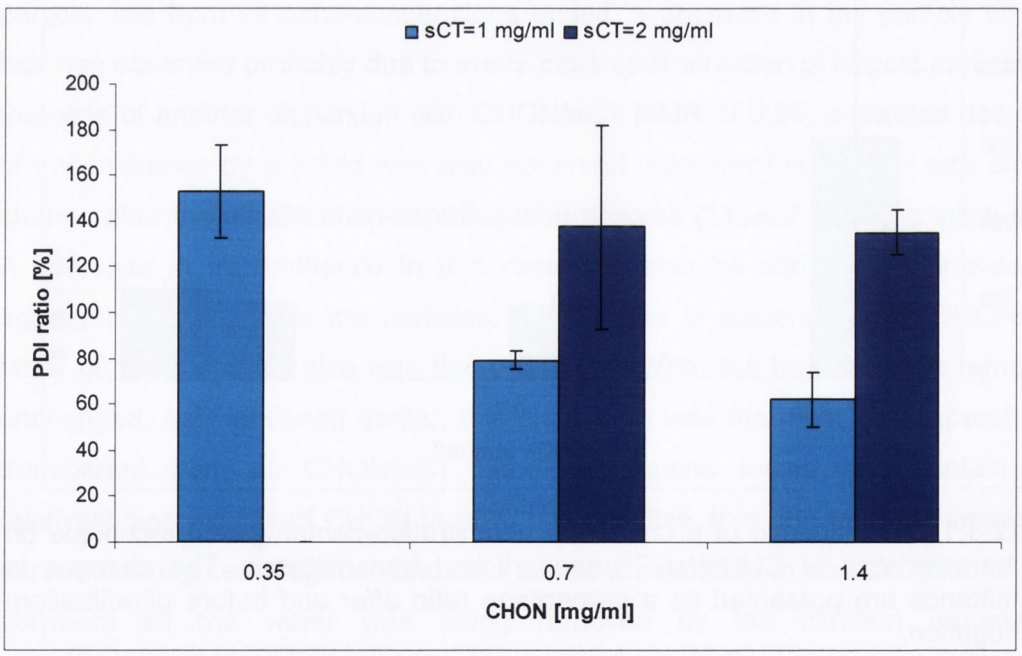

Fig. 12.4.3 The influence of a combined ultrafiltration-centrifugation technique on the characteristics of CHON/sCT nanoparticles: polydispersity index. The changes in PDI are presented as a percentage ratio after and before ultrafiltration-centrifugation.

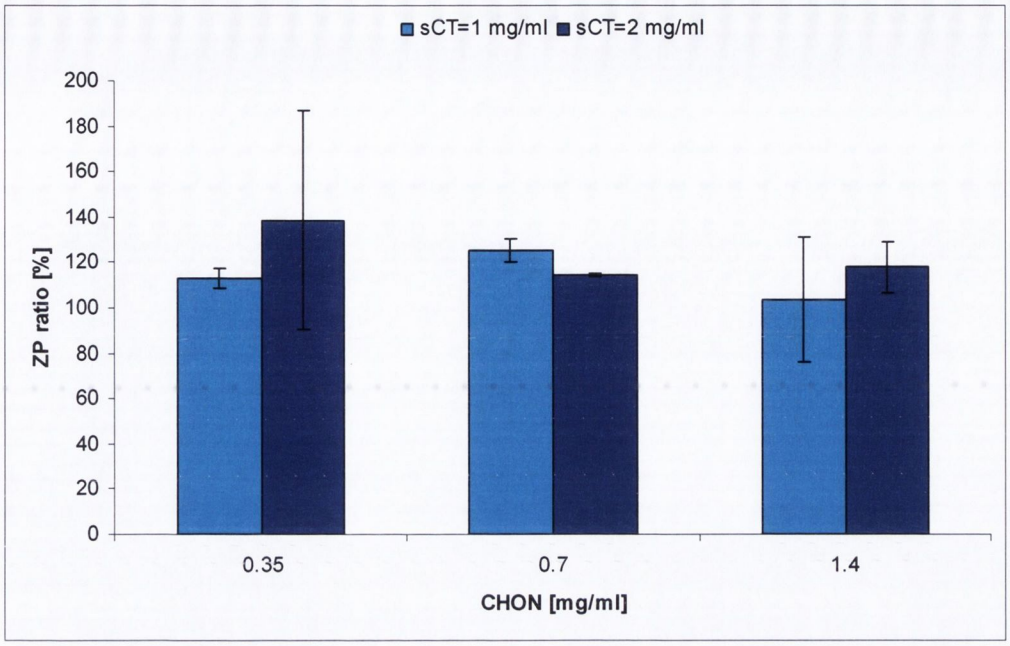

Fig. 12.4.4 The influence of a combined ultrafiltration-centrifugation technique on the characteristics of CHON/sCT nanoparticles: zeta potential. The changes in ZP are presented as a percentage ratio after and before ultrafiltration-centrifugation.

Appendix 5
Dynamic viscosities of polysaccharide solutions

Table 12.5.1 Dynamic viscosities of polysaccharide solutions

Polysaccharide	Concentration [mg/ml]	Dynamic viscosity [mPa*s]
HA257	2	3.37±0.638
HA257	1	2.14±0.162
CHON	5	1.59±0.013
CHON	3	1.39±0.010
CHON	2	1.32±0.030
CHON	1	1.16±0.013
CL113	2	2.21±0.090
CL113	1	1.76±0.22
CL42	5	1.99±0.032
CL42	3	1.80±0.008
CL42	2	1.51±0.005
CL42	1	1.20±0.013

Appendix 6
Isolation of non-associated sCT from CHON/CL42/sCT NPs and extraction of associated sCT from the nanocomlexes

The influence of centrifugation on the characteristics of CHON/CL42/sCT NPs is shown in Figures 12.6.1-12.6.4. The changes in transmittance after ultrafiltration-cetrfugation process of most of the nanoformulations tested can be considered as negligible (Fig.12.6.1). The transmittance ratio after and before ultrafiltration-centrifugation is close to 100-120% in all TPC of 1 or 2 mg/ml formulations and TPC of 3 mg/ml CHON/CL42 MMR of 10. A slight increase of transmittance by ~30% was observed in formulations with TPC of 3 mg/ml, CHON/CL42 MMR of 5. Samples with TPC of 3 mg/ml and CHON/CL42 MMR of 2.5 became markedly less turbid upon ultrafiltration-centrifugation process, and the presence of large, non-redispersable aggregates was observed.

No marked differences in particle size, PDI or zeta potential were observed after ultrafiltration-centrifugation of CHON/CL42/sCT NPs- the ratio of those parameters after and before this process remained between 90-120% (Fig.12.6.2-12.6.4). Therefore only formulations with TPC of 3 mg/ml, CHON/CL42 MMR of 2.5 are unsuitable for use after centrifugation.

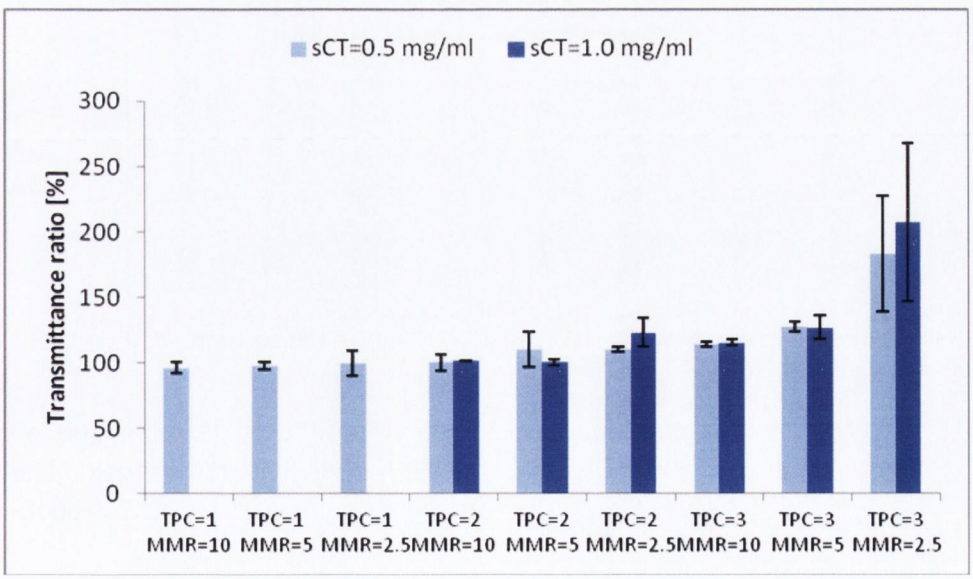

Fig.12.6.1 The influence of a combined ultrafiltration-centrifugation technique on the characteristics of sCT-loaded CHON/CL42 NPs: transmittance. The changes in transmittance are presented as percentage ratio after and before ultrafiltration-centrifugation.

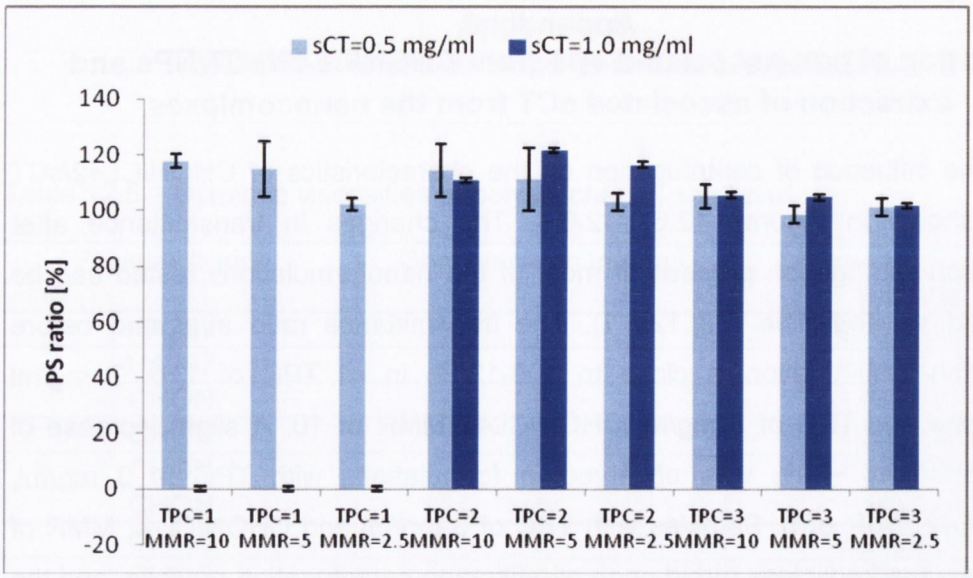

Fig.12.6.2 The influence of a combined ultrafiltration-centrifugation technique on the characteristics of sCT-loaded CHON/CL42 NPs: particle size. The changes in PS are presented as percentage ratio after and before ultrafiltration-centrifugation.

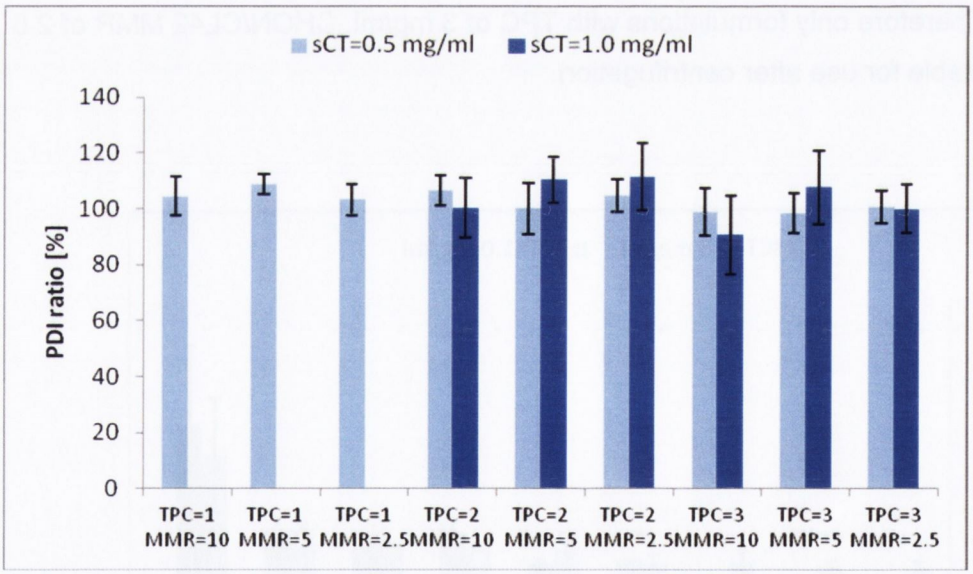

Fig.12.6.3 The influence of a combined ultrafiltration-centrifugation technique on the characteristics of sCT-loaded CHON/CL42 NPs: polydispersity index. The changes in PDI are presented as percentage ratio after and before ultrafiltration-centrifugation.

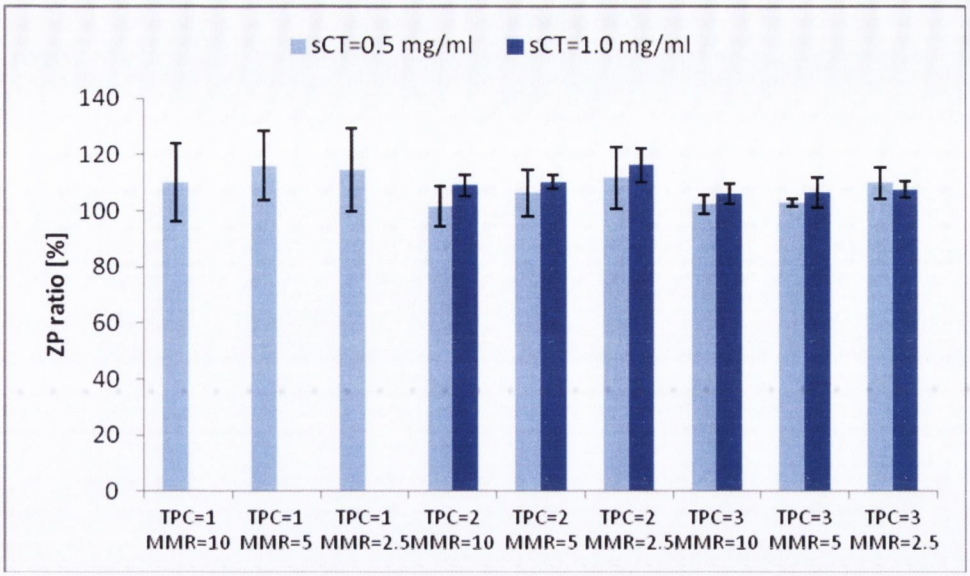

Fig.12.6.1 The influence of a combined ultrafiltration-centrifugation technique on the characteristics of sCT-loaded CHON/CL42 NPs: zeta potential. The changes in ZP are presented as percentage ratio after and before ultrafiltration-centrifugation.

Appendix 7
Thermal properties of cryoprotentants and lyophilised solid state form of NPs.

Table 12.7.1 The thermal characteristics of HA/CL113 MMR of 2.5 NPs (TPC of 1 mg/ml) freeze-dried with variable concentrations PEG2000.

	Onset [°C]	ΔH [J/g]
PEG raw material	52.77	-177.72
PEG lyophilised	49.35	-189.16
0.5% w/w PEG+NP	49.65	-135.29
PEG lyophilised +NP physical mixture 1:1 w/w	49.61	-164.28

Table 12.7.2 Thermal events in HA/CL113 MMR of 2.5 NPs freeze-dried at TPC of 1 mg/ml with the following mixture of cryoprotectants: 1.5% of PEG+ 0.5% of trehalose (T), 1% of PEG+ 1% of trehalose, and 0.5% of PEG+ 1.5% of trehalose.

	First endotherm	Glass transition	Exotherm	Second endotherm
NP+PEG/T 3:1	ΔH -136.37 J/g Onset 50.47°C Peak 53.98°C	-	-	-
NP+PEG/T 1:1	ΔH -82.99J/g Onset 50.68°C Peak 53.45°C	Onset 116.99°C Midpoint 119.54°C	ΔH 33.64J/g Onset 170.39°C Peak 183.40°C	ΔH -48.86J/g Onset 205.61°C Peak 211.40°C
NP+PEG/T 1:3	ΔH -39.12J/g Onset 51.48°C Peak 53.88°C	Onset 116.94°C Midpoint 120.31°C	ΔH 11.01J/g Onset 174.45°C Peak 190.24°C	ΔH -10.03J/g Onset 207.93°C Peak 210.64°C
Physical mixture	ΔH -93.69J/g Onset 49.46°C Peak 51.53°C	-	-	-